DISSERTATION ZUR ERLANGUNG DES DOKTORGRADES
DER FAKULTÄT FÜR CHEMIE UND PHARMAZIE
DER LUDWIG-MAXIMILIANS-UNIVERSITÄT MÜNCHEN

Synthesis, Characterization, and Investigation of Energetic Oxetane Derivatives and Polymers thereof

Maximilian Manfried Born
aus
Memmingen, Deutschland
2022

Erklärung:
Diese Dissertation wurde im Sinne von § 7 der Promotionsordnung vom 28. November 2011 von Herrn Professor Dr. Thomas M. Klapötke betreut.

Eidesstattliche Versicherung:
Diese Dissertation wurde eigenständig und ohne unerlaubte Hilfe erarbeitet.

München, 08.05.2022

Maximilian Born

Dissertation eingereicht am: 10.05.2022

1. Gutachter: Prof. Dr. Thomas M. Klapötke
2. Gutachter: Prof. Dr. Konstantin Karaghiosoff

Mündliche Prüfung am: 05.07.2022

Danksagung

Mein besonderer Dank gilt Herrn **Prof. Dr. Thomas M. Klapötke**, welcher das Prädikat „Doktorvater“ sicherlich mehr als verdient. Er gab mir mehrfach die Möglichkeit in seinem Arbeitskreis zu forschen und so meiner Leidenschaft für energetische Materialien nachzukommen. Ganz besonders möchte ich mich für sein Vertrauen in meine Fähigkeiten bedanken, als er mich nicht nur zur Promotion annahm, sondern mir mein Thema auf einem Notizzettel überreichte, welcher einen Oxetanring zeigte. Daraufhin gewährte er mir frei zu forschen, was für einen Wissenschaftler ein äußerst wertvolles Gut darstellt. Ich möchte auch dafür danken, dass er mir immer mit Rat und Tat zur Seite stand, sich stets Zeit für mich nahm und es mir ermöglichte, eine vielfältige Expertise im Bereich energetischer Materialien zu entwickeln. Ich hoffe, dass er der Wissenschaft noch lange erhalten bleibt, da er die Faszination energetischer Materialien wie kein anderer zu vermitteln versteht und so zum Erhalt und zur Verbreitung dieses spezifischen Wissens in unersetzbarer und unschätzbarer Weise beiträgt.

Herrn **Prof. Dr. Karaghiosoff** möchte ich für die Übernahme des Zweitgutachtens meiner Dissertation danken, sowie für etliche NMR-Messungen, vielmehr jedoch für seinen bewundernswerten Elan als Kristallograph. Dank ihm wird die Welt beständig reicher an Einblicken in die Strukturen der untersuchten Verbindungen. Er ist ein Mensch, der sich bis zur Selbstaufgabe Zeit für Studenten, Doktoranden und Kollegen nimmt und mit seiner offenen, herzlichen und kümmernden Art ein wunderbares Forschungsklima ermöglicht. Er fand selbst spät in der Nacht noch aufmunternde Worte, wenn das einzige Reaktionsprodukt „Frust“ hieß und stellt so eine Ausnahmeerscheinung dar.

Der Prüfungskommision, bestehend aus **Prof. Dr. Thomas M. Klapötke**, **Prof. Dr. Konstatin Karaghiosoff**, **Prof. Dr. Hans-Christian Böttcher**, **Prof. Dr. Andreas Kornath**, **Prof. Dr. Ivana Ivanović-Burmazović** und **Prof. Dr. Oliver Trapp** danke ich für das Lesen meiner Dissertation und die Bereitschaft meiner Verteidigung beizuwohnen.

Meinen außerordentlichen Dank möchte ich dem Unternehmen Spirochem AG Basel, jedoch insbesondere Herrn **Dr. Thomas C. Fessard** (CEO) aussprechen. Obwohl sein Interesse der pharmazeutischen Chemie gilt, fasste er rasch Vertrauen zur Chemie der Münchener „Bombenbastler“ und unterstützte meine Forschung maßgeblich durch das stets großzügige Bereitstellen interessanter und oft auch kostspieliger Oxetanderivate. Auf diese Weise konnten in meinen Rundkolben viele spannende Verbindungen und anschließend gemeinsame Publikationen entstehen – getreu seinem Motto „Do the compounds that you should, not the ones that you could“. An dieser Stelle sei auch **Lucas Göttemann** gedankt, welcher mit der Synthese all dieser Vorstufen betraut war und sicherlich viele Lebensstunden beim Säulen vertröpfeln ließ.

Herrn **Dr. Burkhard Krumm** danke ich neben der Messung vieler NMR-Spektren für die Laborsicherheit, denn die Auslegung von „Sicherheit“ kann angesichts unzähliger Mitarbeiter nicht nur deutlich variieren, sondern deren Aufrechterhaltung schnell zur mühsamen Sisyphos-

Aufgabe ausarten. Ferner bedanke ich mich für die kurzweiligen Intermezzi im Rahmen des AC3-Praktikums, durch welche mir die Entschlüsselung seines einzigartigen Humors gelang.

Herrn **Dr. Jörg Stierstorfer** möchte ich für seinen unentwegten Einsatz für den Arbeitskreis im Allgemeinen danken. Er nimmt sich immer Zeit für den „chemischen Nachwuchs“ und verfügt über eine bemerkenswerte Expertise im Bereich der Azide und stickstoffreichen Heterozyklen, mit welcher er mir jederzeit zur Seite stand. Man könnte buchstäblich sagen, er sorge für die richtige „N-ergy“ in unserer Forschungsgruppe.

Frau **Irene Susanne Scheckenbach**, kurz „ISS“, möchte ich für ihren unvergleichlichen und unermüdlichen Einsatz für den Arbeitskreis und ihr organisatorisches sowie verwaltungstechnisches Geschick danken. Hierdurch hält Sie nicht nur den Arbeitskreis zusammen, sondern bewahrte auch meine Nerven angesichts mancher bürokratischer Hürde in „Zettelland Deutschland“ vor dem Zusammenbruch. Sie trägt das Herz am rechten Fleck und ihre Katzen dienen als Indikator, denn frei nach Goethe „weiß die Katze wohl, wem sie den Bart leckt“.

Großer Dank gilt auch **Stefan „Hubsi“ Huber** für die Bestimmung der Sensitivität zahlreicher Proben. Vielmehr danke ich jedoch für die hervorragenden, erheiternden und humorvollen Gespräche während dieser Messungen. Zudem für seinen „nivellierenden Effekt“, denn er kann Doktoranden im Nebensatz aufbauen, von Höhenflügen zurückholen oder manches Ärgernis klein erscheinen lassen. Er ist von unschätzbarem Wert, wenn verschollene Materialien aufzutreiben sind oder Probleme „unbürokratisch“ gelöst werden müssen. Ohne diese gute Seele wäre der Arbeitskreis nicht das, was er ist.

Dank schulde ich meinen ehemaligen Praktikanntinnen und Praktikannten **Michael Voggenreiter**, **Tessa Kustermann**, **Johannes Korber**, **Claudia Gines**, **Larissa Lehnert**, **Konstantin Kublik** und **Jakob Plank**, welche maßgeblich dazu beigetragen haben, das Gebiet energetischer Oxetane zu erschließen. Ihr habt großartige Arbeit geleistet und zudem für eine sehr gute und freundschaftliche Arbeitsatmosphäre gesorgt. Besonders erwähnt sei Jakob Plank. Ohne seinen unermüdlichen Einsatz und seine Ataraxie wäre mancher Erfolg nicht verzeichnet worden. Ich bin mir sicher, dass er seinen Weg in der Chemie und Wissenschaft mit Leichtigkeit finden wird.

All meinen Kollegen möchte ich für die durchweg gute Zeit danken, welche von vielen lustigen, fröhlichen und geselligen Momenten geprägt war. Hierbei möchte ich insbesondere meinen Mitstreitern aus der Gefahrenzone „Labor D3.110“ danken – **Dr. Marc Bölter**, **Dr. Mohammed „Moham“ Abdel-Ghany**, **Alexander Harter** und **Jelena „Jelly“ Reinhardt**, welche in besonderem Maße für eine großartige Laboratmosphäre gesorgt hat (menschlich und chemisch). Mit ihnen ist die Promotion wie im Flug vergangen und ich hoffe, dass das Labor mit ihnen weiter seinen einzigartigen „Irrenhaus-Charme“ behalten wird.

Auch wenn es zeitlich etwas zurückliegt, möchte ich mich bei meinen damaligen Gymnasiallehrern Herrn **Dr. Hans-Martin Steiger** (Chemie, Biologie) und Herrn **Andreas Kellerer** (Mathematik, Physik, Astronomie) sehr herzlich bedanken. Sie stellen Ausnahmelehrkräfte dar, welche es verstehen, Generationen von Schülern für die Naturwissenschaften zu begeistern. Sie haben meine wissenschaftliche Neugier immer befeuert, mich zur Teilnahme an wissenschaftlichen Wettbewerben ermutigt und das Fundament für meinen Werdegang gelegt.

Meinen Freunden, dem „Kuriositätenkabinett“, danke ich, da sie mich in den letzten Jahren nicht nur begleitet haben, sondern durch ihre „individuellen Webfehler“ im Teppich das Leben fernab der Chemie sehr bunt machten und mich so erdeten. Die Nicht-Wissenschaftler unter ihnen sahen mir manche Chemikermarotte nach oder bemühten sich sogar um Spitznamen wie „ShelDude“ (Sabrina) um mein Wesen zu beschreiben. Eine besondere Nennung verdient meine „Erst-Ehefrau“ und „Sekretärin“ **Dominik Dosch** alias DoDo (mittlerweile Doktor Dominik Dosch oder „Tri-Do“). Nachdem er am ersten Unitag mein damaliges MacBook auf das Äußerste beleidigte, wurde auch direkt darauf der studentische Grill befeuert, ein „Gustl“ geköpft und eine tiefe und besondere Freundschaft nahm ihren Anfang.

Mein allergrößter Dank gilt meiner lieben Verlobten **Marie-Louise Köhler**, welche mir nun seit vielen Jahren mit ihrer uferlosen Liebe zur Seite steht und dies vor allem in guten wie in schlechten Zeiten. Sie ist ein wahrlicher Tausendsassa und ich durfte fernab der Chemie viel von ihr lernen. Durch ihre liebevolle, verständnisvolle, lebensfrohe, aber auch resiliente Art, half sie mir Durststrecken bestens zu überstehen. Sie gab mir immer die Kraft weiterzumachen und die Motivation sowie den richtigen Fokus nicht zu verlieren. Wenn die Leidenschaft Chemie wieder einmal buchstäblich Leiden schaffte, zauberte sie mir mit ihren exzellenten Kochkünsten wieder ein Lächeln auf das frustrierte Gesicht. Sie brachte selbst dann Verständnis auf, wenn ich an manchem Tag angefressen aus dem Labor kam und mein Gehirn auch in der Freizeit noch unablässig und teils lautstark ratternd nach chemischen Lösungen suchte. Ein geflügeltes Wort besagt, hinter jedem erfolgreichen Mann stehe eine starke Frau (und eine Katze). Ich kann dem nur beipflichten und sagen, dass ohne sie manche Herausforderung nicht gemeistert worden wäre.

Nicht weniger dankbar bin ich meiner Familie. Hierbei sei besonders mein Vater **Rainer Karl** erwähnt, welcher als Ingenieur meine Faszination für Blitz, Knall und Rauch wohl nicht ganz nachvollziehen konnte, aber mit pragmatischen Sprüchen wie „Helm auf und durch“ moralischen Beistand leistete und manches Lamento mit der Erinnerung quittierte, ich hätte mir das schließlich selbst ausgesucht. Meine größte Dankbarkeit gilt jedoch meiner Mutter, **Virgilia**, welche meinen Werdegang von Kindesbeinen an unterstützte und die Anschaffung mehrerer Chemiebaukästen selbst dann nicht bereute, als diese zu einem Heimlabor expandierten, in welchem allerhand Schindluder getrieben wurde und mancher Knall sie unsanft aus dem Mittagsschlaf holte. Viele weitere Anekdoten ließen sich erzählen, jedoch möchte ich mich auch für ihre beständige ideelle und auch pekuniäre Unterstützung bedanken, wenn München den studentischen Geldbeutel nicht verschonte. Ohne sie wäre mein Weg sicherlich sehr viel beschwerlicher gewesen.

Table of Contents

1 Introduction

Since the discovery of black powder, high energy density materials (HEDMs) have been a subject of intense research and are developed further in numerous research groups all around the world. In a continuous, often iterative research process, new compounds with even more tailored properties for a certain application are constantly created, characterized, and investigated. Even though many of the energetic materials available today were developed in a military context and are therefore not always connotated positively, the predominant amount is used in times of peace and for civil applications. One could even argue that our modern world is unimaginable without these materials. Typical applications are mining, quarrying, tunneling, or the demolition of buildings, in addition to rockets that transport payloads into space, or applications in the automotive industry such as gas generators for airbags or seatbelt tensioners. Also, pyrotechnics starting from simple emergency signaling devices to large-scale fireworks, are noteworthy. In this respect, modern communication, space travel, or even the acquisition of raw materials for construction projects in the quantities required nowadays would be impossible without energetic materials. According to the generally accepted definition of the American Society for Testing and Materials (ASTM), energetic materials are compounds or mixtures of substances that contain both a fuel and an oxidizer and react readily to release energy and gas.[1] Depending on their properties and the resulting application, they can be roughly subdivided into five larger categories – primary, secondary, and tertiary explosives, propellants, and pyrotechnics.[1] For a more precise classification according to their use, some categories are further subdivided, as shown in Figure 1.[1]

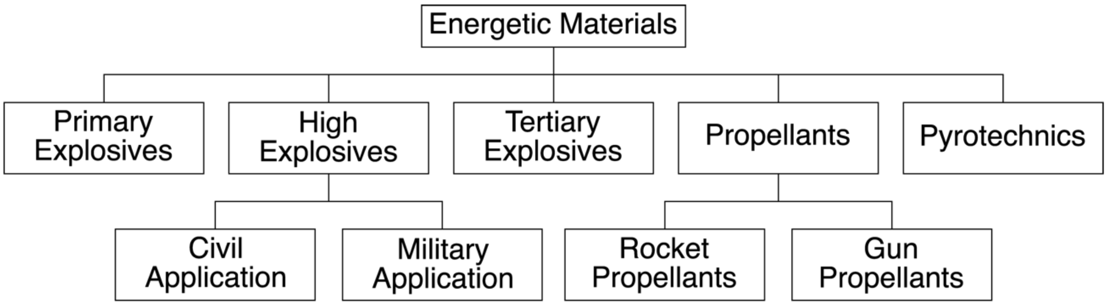

Figure 1.1. Classification of energetic materials.

To render the characteristics of these categories and the differentiation more comprehensible, the five main categories are defined below.

1.1 Classification of Energetic Materials

Primary explosives are energetic materials characterized by a considerable sensitivity toward external stimuli (e.g., shock, friction, heat, electrostatic discharge) and their ability to undergo a rapid combustion- or deflagration to detonation transition (DDT) – sometimes referred to as acceleration.[1,2] Most commonly, they detonate without confinement and even in very small quantities. As a result, they provide heat and a shockwave which allows the initiation of less sensitive materials like booster charges, secondary explosives, or propellants.[1,2] In general, they show much lower performance than secondary explosives.[1] The most prominent and widely used primary explosives are lead azide and lead styphnate.[1] Due to their adverse environmental impact, heavy metal-free "green" alternatives (e.g., K_2DNABT) are constantly investigated and developed.[3]

Secondary explosives or "high explosives" are significantly less sensitive to the aforementioned, external stimuli. For instance, exposure to heat only causes them to combust or deflagrate when unconfined and their detonation requires initiation by a strong shock as provided by primary explosives. Contrary to these, they offer notably higher performance and are used as booster explosives or as main charges. PETN, TNT, RDX, or HMX represent typical and currently used compounds of this class. In this context, PETN is considered a benchmark explosive, as substances of lower sensitivity than PETN are usually classified as primary explosives.[1,4,5] Contemporary research in this field is focused on high-performance explosives, heat resistant explosives, low sensitivity explosives for insensitive munitions, and compounds of improved environmental friendliness.[1,5] Regardless of these sub-areas, combining high performance with high thermostability and insensitivity is a constant challenge for chemists in the field of HEDMs.

Tertiary explosives or "blasting agents" are characterized by their very high insensitivity toward external stimuli like shock, friction, or heat. Being even more insensitive than high explosives, they require an intermediate charge (booster) for their initiation.[1,4] These explosives often feature a rather large critical diameter and are therefore unsuitable for use in small charges.[4] Hence, they are used predominantly for civil applications such as mining and demolition. Typical examples are ANFO-explosives (ammonium nitrate fuel oil) or slurry explosives.[1,4,6]

Propellants are either used for the acceleration of ammunition (gun propellants) or to provide thrust for rockets (rocket propellants) next to their application as gas generators (e.g., airbags). They are thus designed to generate hot gases by a controlled deflagration, whereas detonation is to be avoided.[1,4,7]

Pyrotechnics are commonly compositions of substances to produce certain effects such as light, smoke, noise, gas, or heat, or a combination of these through a self-sustaining exothermic (non-detonative) reaction. In general, the underlying reaction is independent of external (atmospheric) oxygen. Usually, pyrotechnics are characterized by exothermic reactions in the subsonic range, but can also detonate under certain circumstances.[1,4,5]

Energetic polymers are energetic materials composed of macromolecules. By definition, a macromolecule is "a molecule of high relative molecular mass, the structure of which essentially comprises the multiple repetition of units derived, actually or conceptually, from molecules of low relative molecular mass".[8] In the case of energetic polymers, these units are designated by the presence of explosophoric groups (e.g., $-N_3$, $-NO_2$, $-ONO_2$) which allow the material to release chemical energy upon an external stimulus like shock, friction, or heat. Energetic polymers are primarily used as binders in explosive and propellants formulations.[1,9] Among others, they fulfill tasks like the prevention of segregation and the prevention of crack formation due to cyclic thermal stresses while they reduce the overall sensitivity of a formulation to allow safe handling. The most well-known and probably most widely used energetic polymers are nitrocellulose (NC) and the glycidyl azide polymer (GAP).[9] Energetic polymers can be regarded as an additional, sixth category (Figure 1) or simply as materials that can in principle be applied to any of the categories described.

1.2 A Brief History of Energetic Materials

In general, energetic materials can look back on a rich and, above all, long history of development. Their era begins rather early with the accidental discovery of black powder (**BP**) in China around 200 BC.[1] In this respect, it is impossible to give a full account of their history within a thesis. Nevertheless, the overall development can be represented by a few important milestones (Figure 2). For example, the aforementioned black powder remained unknown in Europe until the 13th and 14th centuries, when it was further investigated by the English monk Roger Bacon (1249) and the German monk Berthold Schwarz (1320).[1] First used by the military at the end of the 13th century, an improved manufacturing process developed by Corning (1425) rendered it useful as a propellant charge in small and large caliber guns.[1] Although no adequate use was found for a long time, mercury fulminate (**MF**), independently discovered by the Dutch Cornelius Drebbel and the German Johannes Kunkel von Löwenstern in the 17th century, was an important milestone.[2] It represents the first primary explosive to be used by Alfred Nobel in first detonators to initiate nitroglycerin (**NG**).[2] NG itself was discovered by the Italian chemist Ascanio Sobrero in the year 1846, in which nitrocellulose (**NC**) had also been independently discovered as another nitrate ester by the Swiss Christian Friedrich Schönbein and the German Rudolf Christian Böttger.[10] NC represents the first energetic polymer and is still widely used today as a propellant.[9,11] A few years later, Alfred Nobel achieved a significant milestone by desensitizing NG with Kieselguhr thereby inventing Dynamite, which he patented in 1867.[1] Furthermore, he realized that a mixture of NC and NG forms a powerful gel which became known as blasting gelatin and further refinement led to the first smokeless powder (ballistite) in 1888.[1] Picric acid (**PA**), which was already reported by Glauber in 1742, soon replaced black powder among the military in the late 19th century (1885–1888) and was used in grenades and mines.[1,12] Unfortunately, PA tends to form highly sensitive metal salts upon direct contact with shell walls opposing a safe application upon prolonged ammunition storage.[1] Therefore, it was replaced by trinitrotoluene (**TNT**) which was first prepared in 1863 by the German Julius Wilbrand.[13] Pure 2,4,6-trinitrotoluene was obtained by Hepp in 1880.[12] In TNT, the hydroxy group of PA is formally replaced by a methyl group to avoid salt formation. Due to advantageous properties such as chemical stability, low sensitivity and production cost, melt castability, compatibility with other explosives, and good performance, it has been used before World War I and is still used today substantiating its milestone character.[12] Another polynitroarylene explosive and the first of the nitramino-type, **tetryl**, was synthesized by Mertens in 1877 – used since 1906, it was applied as a blasting cap base charge and as a component of explosive mixtures.[1,12] However, with the development of the powerful **PETN** by Bruno Thieme in 1894, it was largely replaced by the latter.[14] In 1899, **RDX** was prepared by Henning and soon (1920) Herz pioneered preparing it from inexpensive hexamethylenetetramine. With further improvements by Hale, it became the high explosive of choice during World War II.[1,12] Decades later (~1943), the analog **HMX** became available which is a side product of the Bachmann process used for the production of RDX.[1,5] It shows physicochemical properties comparable to RDX at higher performance.[1,15,16] After the war, explosives of especially high thermostability and insensitivity became a matter of interest leading to the development of hexanitrostilbene (**HNS**) in 1964 by Shipp and the availability of triaminotrinitrobenzene (**TATB**).[1,17] Although first prepared in 1888 by Jackson and Wing, TATB did not become commercially available until 1978.[1,12,18] Due to their high thermostability, both compounds are well-suited for applications such as hot deep oil drilling and especially HNS found use in the oil industry.[1,17] Having the need for high thermostability essentially fulfilled, the research focus shifted toward high-performing compounds surpassing RDX and HMX. The continued research into nitramino explosives soon led to **CL20** prepared by Nielsen in 1988.[19] Another benchmark compound and milestone followed with the synthesis of the structurally appealing compound octanitrocubane (**ONC**) by Eaton in 2000 which features an oxygen balance (CO_2) of exactly 0.[20] CL20 and ONC belong to the most powerful compounds ever prepared. Unfortunately, its polymorphism and price largely exclude CL20 from application, while ONC is too costly due to its complicated synthesis. In the last two decades, a wide variety of synthesis concepts have been applied to achieve an improved interplay of performance, thermostability, insensitivity, and also environmental friendliness. In this context, nitrogen-rich compounds play a key role. For example, **TKX-50** developed in 2012 by Klapötke et al. is one of the most promising compounds of recent years. Its energetic performance is comparable to Cl20 and ONC while it offers a more cost-efficient synthesis and essentially fulfills the requirements for an RDX replacement while offering low toxicity.[21,22] Soon (2016) **TKX-55** followed as a promising replacement for HNS due to its high thermal stability and performance.[23]

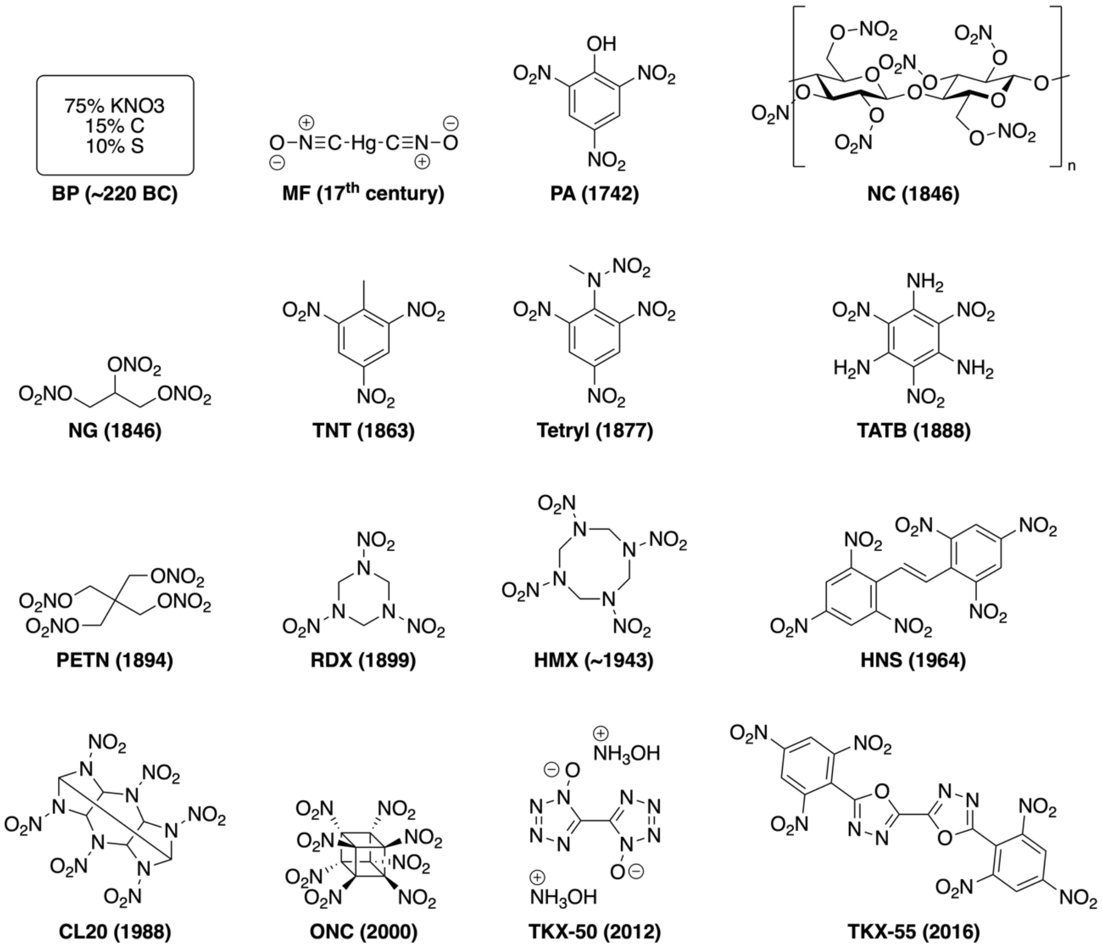

Figure 1.2. Important milestones in the discovery and development of energetic materials.

Unfortunately, benchmark compounds such as CL20, ONC, or TKX-50 strongly indicate that a "chemical performance limit" has been reached, and pushing this limit even further seems only possible by a disproportionate synthetic effort. Therefore, future compounds should be designed to offer comparable performance at reduced cost, higher environmental friendliness, and improved insensitivity as well as thermostability to offer safe handling.

Next to the further development of inherently insensitive compounds, another strategy that emerged in the 1950s is to desensitize propellants and explosives by embedding them in an elastic polymer matrix that absorbs mechanical forces acting upon the formulation (e.g., bullet or shrapnel impact, shaped charge jets). Such polymer-bonded explosives (PBX) allow the manufacturing of particularly resistant insensitive munitions (IM).[1,9] In a first generation, inert polymers were used for this purpose, but they reduce the overall performance and were thus replaced by energetic binders in the course of continuous development.

However, since energetic binders are added to formulations in non-negligible amounts while their performance is currently still way inferior to TNT, the development of new monomers and corresponding polymeric binders offers significant room for improvement regarding the performance and safety characteristics of modern ammunition. In the following section, the historical and chemical development of binder polymers will be described in more detail.

1.3 Polymers in HEDM chemistry

1.3.1 Development of Inert Polymers

Since the discovery of the semi-synthetic nitrocellulose in 1846, which is considered to be the first energetic polymer, both inert and energetic polymers have contributed massively to advances in explosives and propellant technology.[9] In this context, they have been primarily used as binders in energetic formulations to fulfill various technical tasks. For example, these tasks include the prevention of segregation in composite propellants and composite explosives, the prevention of crack formation due to cycles of thermal expansion and contraction, the improvement of processability and mechanical properties, and the reduction of the sensitivity of a formulation to mechanical stimuli.[1,9] Their history is thus closely interwoven with the general development of energetic materials and ammunitions and their development shall be outlined in more detail.

As the only energetic polymer available, nitrocellulose continued to dominate research and development for a long time. It was first used as a binder in the course of the first smokeless (single-base) powder (Poudre B) as invented by Vieille in 1884.[9] NC was also used as a binder for nitroglycerin as it thickens the liquid explosive to form a moldable semi-solid of reduced sensitivity, which can be used as double-base propellant.[1,24] For example, NC-based propellants found application in barrage rockets during World War II.[25]

Apart from NC, the actual history of sophisticated polymers as binders probably began in 1926 with the synthesis of **polysulfide** from ethylene dichloride and sodium polysulfide by Joseph C. Patrick (Figure 3).[26,27] He named it Thiokol and founded the famous Thiokol Corporation in 1928 to market it. Like today's energetic polymers, the elastomer was curable, which was achieved via oxidative coupling to form disulfide bridges, and it was first applied in a solid composite propellant in 1945.[26] When aluminum became an ingredient to high-performance propellant formulations in 1955, polysulfide turned out to be highly incompatible as it reacted with aluminum to cause explosions of the propellant upon storage – as a consequence, polybutadiene-based binders were developed as a replacement by the Thiokol Corporation.[9] The first polymer of this class was **PBAA**, a copolymer of butadiene and acrylic acid developed in 1954.[9] Unfortunately, PBAA showed a random distribution of the functional groups owing to its preparation by radical polymerization resulting in an adverse, poor reproducibility of its mechanical properties.[25] Thus, PBAA was replaced by **PBAN**, a terpolymer of butadiene, acrylonitrile, and acrylic acid which could be prepared at low cost and offered improved mechanical properties as acrylonitrile added additional space between the acrylic acid crosslinking sites.[25] Nevertheless, another binder polymer was developed in the late 1950s by Thiokol – carboxyl terminated polybutadiene (**CTPB**).[9] With CTPB, the same curing agents (e.g., epoxides (Epon X-801^{TM}) or aziridines (Mapo^{TM})) as in the case of PBAA and PBAN can be used while the polymer offers improved mechanical properties at low temperatures whereas characteristics like the density, solids loading or the specific impulse stayed the same.[9,28] CTPB rubbers were used in propellant formulations since the 1960s and were for instance employed in the Star 37 deceleration rocket motor of the first Surveyor lunar landing modules.[29] A different approach was pursued by the Aerojet General Corporation as a competitor to Thiokol. Aerojet developed **polyurethane** binders based on high-molecular difunctional glycols and isocyanates in the mid-1950s.[30] These were characterized by a shrink-free, homogeneous curing at low temperature and the advantage that the polymer backbone contained notable amounts of oxygen.[9] Despite this, polybutadiene binders gained greater popularity.[9] Finally, the different approaches were combined at Aerojet GenCorp by the development of hydroxy-terminated polybutadiene (**HTPB**) by Klager in 1961.[25] HTPB can be crosslinked by isocyanates leading to polyurethane linkages. HTPB began to push CTPB out of place as it exhibits improved properties with regard to aging and elongation at low temperatures and replaced CTPB in various solid rocket motors as employed in Maverick, Stinger, and Sidewinder rockets.[9,25] First used in a rocket motor in 1972, HTPB has become the most widely used polymer in solid propellant formulations with enhanced insensitivity.[9,31] In addition to their use as propellant binders, polymers have also been considered as binders for high explosives to replace former desensitizing agents such as natural or synthetic waxes.[9,32-34]

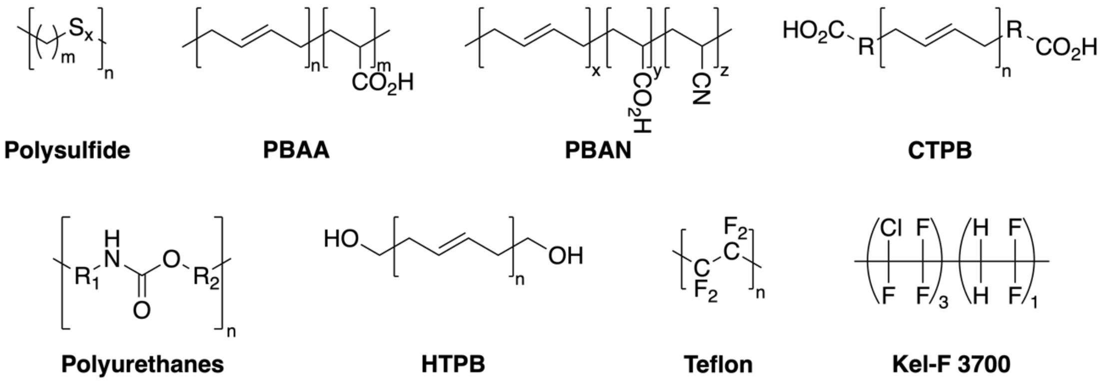

Figure 1.3. Typical inert binders for propellants and explosives.

The development of such polymer-bonded explosives (PBX), in which a crystalline explosive is embedded in an elastic polymer matrix, began at the Los Alamos Scientific Laboratory in 1952.[9] The first PBX composition contained RDX in a polystyrene matrix which was plasticized by dioctyl phthalate.[9] PBX were found to offer better processability and insensitivity than waxed explosives.[35] However, as the fillers in the formulations themselves became more insensitive, polymers served soon more to provide structural integrity than to reduce sensitivity.[9] Therefore, in addition to soft, rubbery binders, hard polymers with high modulus, such as **Teflon** or **Kel-F 3700**, were used.[9] A very prominent PBX is Semtex developed in 1966 by

Stanislav Brebera in the suburb Semtin (Czech Republic) which gave it its name.[1] It comprises varying rations of PETN or RDX embedded in a polyisobutylene polymer matrix and phthalic acid *n*-ocytylester as plasticizer.[1]

1.3.2 Development of Energetic Polymers

With the use of non-energetic polymers as binders in propellant and explosive formulations, the associated drawbacks became increasingly apparent. For instance, their admixture leads to a decreased performance of the formulation as they "dilute" the mixture to result in a decreased energy density. This is due to the fact that inert binders themselves provide no energetic contribution and, in the worst case, even withdraw energy from the combustion or explosion.[36] Moreover, inert binders represent fuels and require an increased oxidizer loading to maintain the overall performance and oxygen balance. The fact that complete combustion of HTPB requires a theoretical loading of 92 wt.% ammonium perchlorate illustrates their adverse effect and adding insult to injury, a binder admixture of 15–20 wt.% is necessary to obtain a processable propellant formulation.[24] To address the underlying problem, two strategies emerged. One was to change the processing technique as both extrusion and pressing allow to reduce the amount of binder in comparison to the cast-cure process.[24] A more radical but quite obvious strategy was the development of energetic polymers that would exhibit explosophoric side-groups along the polymer backbone thereby enhancing the internal energy and oxygen balance of the respective formulation (Figure 4, p.10).[24] As the use of binders essentially emerged from propellant technology, in which a high oxygen content of the formulation is of utmost importance, the first development in this direction was based on an oxygen-rich organic nitrate, polyglycidyl nitrate (**PGN**), which was developed in the 1950s at the Naval Air Warfare Center (NSWC) by Thelen et al.[9] Unfortunately, the corresponding monomer glycidyl nitrate (GN) was at that time prepared via nitration of glycidol using a mixture of 100% nitric acid and acetic anhydride.[9] This made a cumbersome purification of the monomer necessary as the dangerous nitrating agent acetyl nitrate and other contaminants had to be removed quantitatively prior to cationic ring-opening polymerization.[9] Hence, PGN did not become successful until the 1990s, when GN was prepared by the British Defense Research Agency (DRA) in a flow process using dinitrogen pentoxide as nitrating agent.[9,37] Probably the most remarkable milestone in energetic binder research to date was achieved by Vandenberg in 1970 at Hercules Incorporated when he first prepared **GAP** (glycidyl azide polymer) via azidation of poly(epichlorohydrin) with sodium azide in DMF,[38] which was closely followed by the preparation of GAP-triol in 1976 by Frankel and co-workers at Rocketdyne.[39] Despite its notable energetic character and sensitivity toward impact and friction (Table 1), studies by Radwan[40] demonstrated its remarkable desensitizing effect on RDX-based PBX compositions. A formulation containing 15% GAP reduces the impact sensitivity of RDX by 100% while an admixture of 21% even causes an astonishing decrease of 211%. In the case of a composite comprising 73% RDX, 15% aluminum, and either 12% GAP or HTPB, the formulation containing GAP even shows a significantly lower impact sensitivity (35.8 J) when compared to the formulation containing HTPB as a fully inert binder (21.6 J) thereby demonstrating GAP's superiority.[40]

Table 1.1. Physicochemical and energetic properties of GAP-diol.

General		**EXPLO5 V6.04**[41]		**Specific properties**	
Formula	$(C_3H_5N_3O)_n$	$-\Delta_EU^{\circ}$[g] [kJ·kg^{-1}]	3668	Appearance	Amber liquid[42]
FW [g·mol^{-1}]	99.09	$T_{C\text{-}J}$[h] [K]	2399	Viscosity (cP)	4280[5], 12.000[42], 15.000[43]
IS[a] [J]	8	$p_{C\text{-}J}$[i] [GPa]	12.6	Vapor pressure	negligible[43]
FS[b] [N]	360	$D_{C\text{-}J}$[j] [m·s^{-1}]	6536	Solubility (water)	negligible[43]
Ω[c] [%]	−72.2	V_0[k] [dm^3·kg^{-1}]	791	Suitable solvents	DCM, $CHCl_3$, THF, 1,4-Dioxan, DMF, DMSO
T_g, T_{dec}[d] [°C]	−47.9, 213	Spec. IM [l]		LD50 (rat, oral) [mg/kg]	> 5000[43]
ρ[e] [g·cm^{-3}]	1.30			M_n [g/mol] [m]	1700 ± 300[24], 2000[5]
ΔH_f°[f] [kJ·mol^{-1}]	116.1[24], 116.7[5], 125.3, 490[9]			Functionality	~ 2

[a] Impact sensitivity (BAM drop hammer, method 1 of 6). [b] Friction sensitivity (BAM friction apparatus, method 1 of 6). [c] Oxygen balance based on CO formation. [d] Glass transition and decomposition temperature (DSC, β = 5 °C·min^{-1}). [e] Density at 298 K (weighing of 100 µL). [f] Standard molar enthalpy of formation. [g] Detonation energy. [h] Detonation temperature. [i] Detonation pressure. [j] Detonation velocity. [k] Volume of detonation gases at standard temperature and pressure. [l] Specific impuls (neat compound). [m] Number average molecular mass.

Today, GAP is the most well-investigated, most widely used, and most readily available energetic polymer on the market.[9,24,44] This may be attributed to the excellent polymerizability of epichlorohydrin, its low price, good binder properties[24], and last but not least its comparatively high performance arising from a fairly high density in combination with a high, positive heat of formation.[9,45]

As a result of its success, the curable prepolymer became commercialized by various companies – for example by 3M under the trademark "GAP 5527 Polyol" or as "GAP Diol" by Eurenco Bofors.[42,46] Although the polyoxiranes PGN and GAP provided a relatively oxygen-rich as well as a nitrogen-rich binder, the development of energetic polyoxetanes as binders followed quickly. However, since energetic oxetanes and polymers thereof represent the main focus of the thesis at hand, the class of energetic polyoxetanes will be addressed separately in the next section. The most recent advance in the field of energetic binders are hybridic, inorganic-organic **polyphosphazenes** that have been developed in 2001 by the British Atomic Weapons Establishment and became first known to the energetic materials community in 2004.[47,48] Their backbone structure can be described by the general formula (NPR^1R^2)$_n$. The side groups (R) can be halogeno or organo units, and a chemical replacement of these by explosophoric groups renders the polymers energetic.[9]

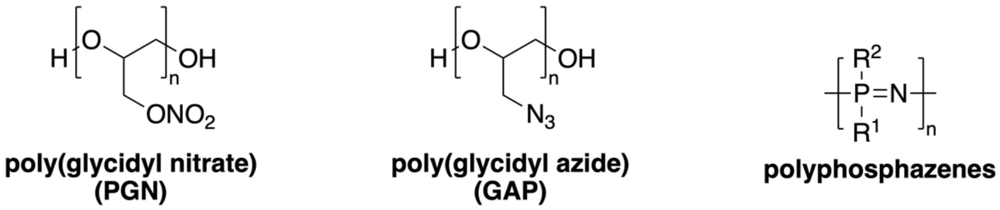

poly(glycidyl nitrate) (PGN)

poly(glycidyl azide) (GAP)

polyphosphazenes

Figure 1.4. Major steps in the development of energetic binders.

Although they are considered promising candidates due to their nitrogen-rich backbone and their functionalization potential, they have been little studied and have not yet gained popularity or found practical application.[49] This may be justified by the fact that they cannot be cured by conventional means like hydroxy-terminated polyethers.[50] Hence, additional chemical modification steps will be required. It is also not currently foreseeable whether the phosphorus present will have any adverse effect. Therefore, it simply remains to be seen whether polyphosphazenes can prevail over existing polyether polymers in the future.

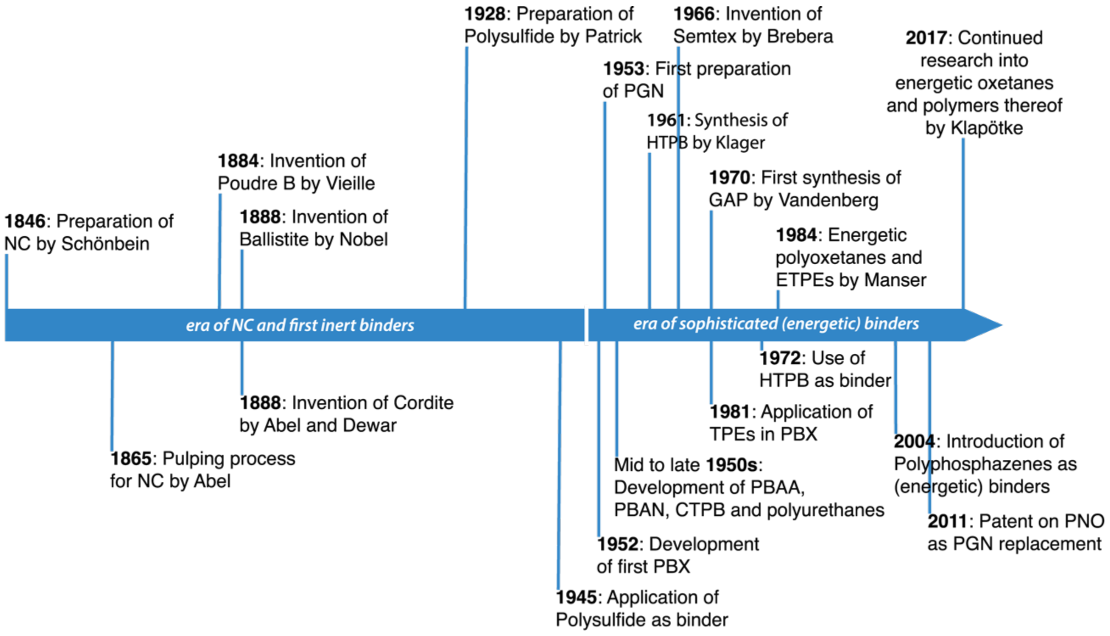

Figure 1.5. Historical development of non-energetic and energetic binders.

1.3.3 Polyoxetanes as Energetic Binders

Continued binder research at Aerojet led to the development of energetic polyoxetanes by G. E. Manser who prepared copolymers via cationic ring-opening polymerization in 1984 on the basis of 3,3-bis(azidomethyl)oxtane (BAMO) and 3-azidomethyl-3-methyloxetane (AMMO).[9,51] Only a few years later, in 1993, Manser and co-workers developed 3-nitratomethyl-3-methyloxetane (NIMMO) and reported its polymer.[9,52] A common feature of **poly(AMMO)**, **poly(BAMO)**, and **poly(NIMMO)** is their low viscosity and good mechanical properties after curing, as well as the simple synthesis of the respective monomers (Scheme 1).[9] BAMO, first prepared by Carpenter in 1964, can be obtained with ease via azidation of 3,3-bis(chloromethyl)oxetane (BCMO) using sodium azide in DMF.[53,54] AMMO and NIMMO can be prepared from the precursor 3-hydroxymethyl-3-methyloxetane (HMMO). The former is obtained via tosylation of HMMO to give TMMO and subsequent azidation, while NIMMO was first prepared via nitration using acetyl nitrate.[9] As acetyl nitrate was considered problematic, once again a flow synthesis using dinitrogen pentoxide was developed by the British DRA as in the case of glycidyl nitrate.[55]

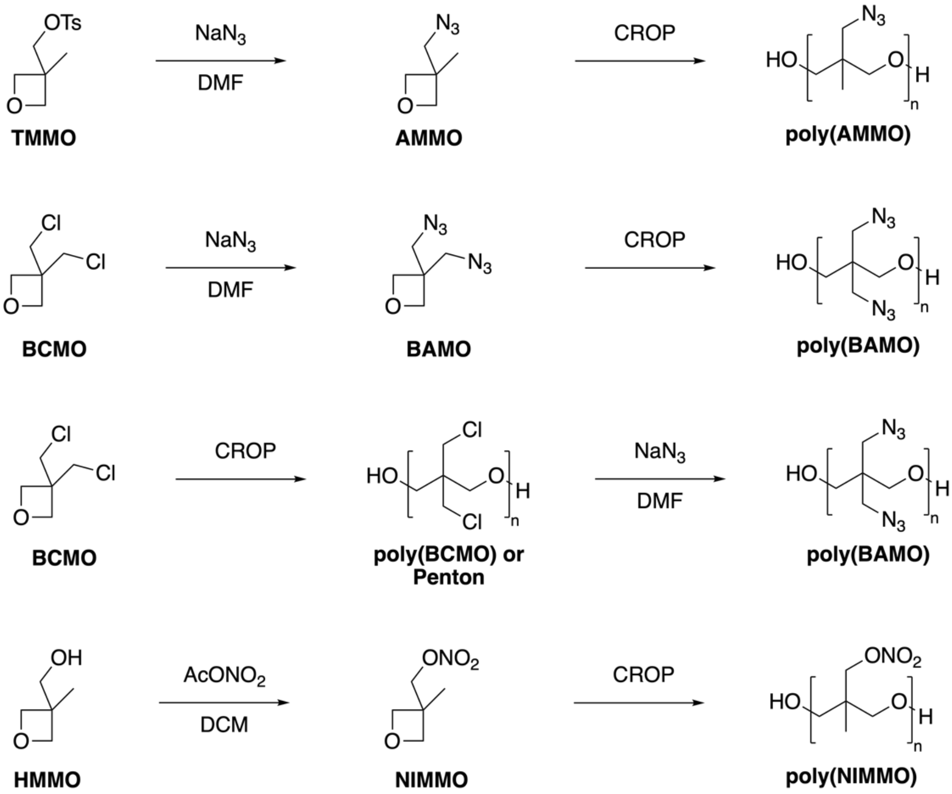

Scheme 1.1. Common synthetic procedures toward AMMO, BAMO, NIMMO and their homopolymers making use of cationic ring-opening polymerization (CROP).

Unfortunately, the homopolymers of AMMO, BAMO, and NIMMO all suffer from specific shortcomings. Poly(NIMMO) as an organic nitrate offers a very limited thermostability of only

187 °C and suffers from chemical changes at considerably lower temperatures due to scission of the nitrate ester bond to form radicals ($CH_2O\cdot$, $NO_2\cdot$) which initiate auto-oxidation that ultimately results in a scission of the polyether backbone.[24] Furthermore, it exhibits a glass transition temperature (T_G) of only −25 °C and thus needs to be copolymerized with other monomers to obtain a T_G in the range of modern requirements.[55] Poly(BAMO) is rather sensitive (IS 5 J, FS 288 N)[5] and exhibits a symmetric structure causing it to be highly crystalline next to an insufficient glass transition temperature (−41 °C).[56] Thus, BAMO also requires copolymerization with other monomers to afford useful binders. The lowest T_G of −42 °C is offered by poly(AMMO).[9] However, it features the worst oxygen balance of all homopolymers and also the lowest density, which further diminishes its performance.

However, as energetic thermoplastic elastomers (ETPEs) have been increasingly investigated and used since the 1980s, virtue has been made out of the necessity for copolymerization. TPEs are made up of alternating segments of soft, amorphous polymers and hard, crystalline polymers. Consequently, this arrangement can be either obtained by linking corresponding polymer blocks with curing agents or by sequential polymerization.[9] As a result of their structure, they behave like elastomers at deep temperatures and become soft at elevated temperatures, which is linked to significant advantages: For example, TPEs can be processed by common techniques like extrusion or injection molding allowing the solvent-free manufacture of energetic composites.[9] Beyond, TPE binders can be recovered and recycled providing an even higher environmental friendliness.[9] First energetic TPEs (ETPEs) were developed at the Thiokol Corporation.[9,57] Prominent examples are copolymers of crystalline polymers such as poly(BAMO) and less crystalline or amorphous polymers such as poly(NIMMO), poly(AMMO) or GAP (Figure 6).[9]

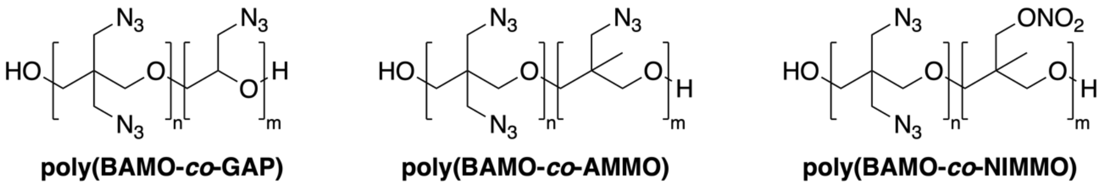

Figure 1.6. Energetic thermoplastic copolymers based on state-of-the-art monomers.

To date, the literature on energetic binders is mostly dominated by copolymers of this type. On the one hand, copolymers allow a special fine-tuning of the polymer properties, and on the other hand, they represent a strategy to come close to meeting the long list of criteria that modern binders should fulfil:

- Decomposition temperature above 200 °C
- Glass transition temperature below −50 °C
- Higher performance than state-of-the-art binders
- Improved oxygen balance compared to available energetic binders
- Lower sensitivity toward impact and friction than prior art binders

- Compatibility with common fillers for explosive and propellant formulations
- Sufficient interaction with typical plasticizers
- Low viscosity to offer a facile processing and high filler loadings
- Long-term stability (shelf-life)
- Mechanical properties superior to the prior art
- Facile, low-costs synthesis of the respective monomers
- Scalabe monomer and polymer preparation
- Telechelic nature, end-group functionality ≥ 2
- Curable with established curing agents
- High environmental friendliness

Besides the aforementioned oxetane species, several other interesting oxetane monomers have been described in the literature. Almost concurrently with Manser's work, several energetic oxetanes were developed in 1983 by Kurt Baum and co-workers at Fluorochem Incorporated. These include **3-azidooxetane**, the constitution isomer of glycidyl azide, next to **3-nitrooxetane** and **3,3-dinitrooxetane**. Very surprisingly, only the homopolymers of the azide and the geminal dinitro-compound were reported.[58,59] Although interesting as nitrogen- (azide) and oxygen-rich compounds, these derivatives and their homopolymers have not attained technical relevance to date. This is probably due to the cumbersome synthetic protocol starting from oxetan-3-ol and the fact that the latter was commercially unavailable at that time and also had to be prepared via a laborious multi-step synthesis (Scheme 2).[58,60]

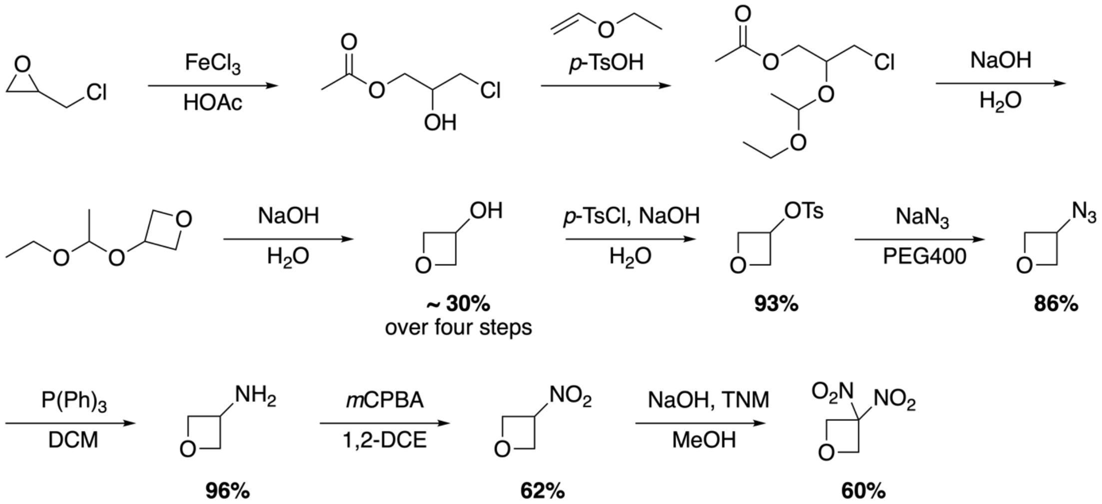

Scheme 1.2. Preparation of oxetan-3-ol starting from epichlorohydrin and subsequent steps toward the energetic monomers 3-azidooxetane, 3-nitroxetane and 3,3-dinitrooxetane.

A particularly oxygen-rich oxetane species, 3,3-bis(nitratomethyl)oxetane (**BNMO**) was already prepared in 1953 by Elrick in the course of a study on pentaerythritol trinitrate halides under the supervision of Hercules Incorporated (Figure 7).[61] However, the compound and its homopolymer failed to gain importance in the field of energetic binders. This can be attributed to the fact that BNMO is most easily prepared by nitration of the corresponding alcohol. However, 3,3-bis(hydroxymethyl)oxetane can be only obtained with difficulty and in low yields starting from pentaerythritol. Among others, bromination of pentaerythritol is a popular route but requires separation of the monobrominated species from the multibrominated species by fractional crystallization or column chromatography.[62] Subsequent cyclization of the bromohydrin via Williamson ether synthesis is linked to further losses. In a dissertation thesis, an overall yield of only 2.5% is reported.[63] Adding insult to injury, BNMO as organic nitrate features a low decomposition temperature and corresponding copolymers decompose early at roughly 150 °C.[62] Due to its symmetrical structure analogous to BAMO, poly(BNMO) is also too crystalline to find application as a homopolymer.

Later, in 1995, a patent was filed by Aerojet in which Manser disclosed 3-azidomethyl-3-nitratomethyloxetane (**AMNMO**) as the key compound of the invention (Figure 7).[64] The preparation of its homopolymer was reported and AMNMO was claimed to yield amorphous, elastomeric binders upon copolymerization with known energetic oxetanes. For instance, AMHMO was envisaged to provide useful (amorphous) binders even when small amounts of AMNMO (5–20%) are copolymerized with oxetanes like BAMO or BNMO which would otherwise afford too highly crystalline polymers. At the same time, AMNMO should offer more performance than other asymmetric oxetanes such as AMMO or NIMMO. However, it has not been able to establish itself on the market these days, and investigations by Klapötke et al. (chapter 11) showed that poly(AMNMO) itself exhibits only a moderately low glass transition temperature of −31 °C.[65] Accordingly, it offers advantages only in terms of performance and must be copolymerized with other cyclic ethers to achieve sufficiently low glass transition temperatures.

Although poly(glycidyl nitrate) has been able to establish itself as a high-performing and oxygen-rich binder for propellants, a study found isocyanate-cured PGN to undergo cure reversion upon aging thereby limiting its usefulness.[66] The effect was attributed to interactions of the urethane linkages with hydrogen atoms adjacent to the nitrato group. A solution was developed by Baum and Willer by making use of its constitution isomer 3-nitratooxetane (**3NO**) and its homopolymer poly(3-nitratooxetane) (**PNO**) (Figure 7). A corresponding patent was filed in 2011 by Fluorochem Incorporated, covering the synthesis of 3NO via nitration of oxetan-3-ol and the preparation of PNO.[67] Due to the similar structure, PNO is a first-rate alternative to PGN with high chances of a near-term application. This is further supported by the circumstance that PNO, in contrast to PGN, is terminated exclusively by primary hydroxy groups to offer improved curing results.[68] So far, however, the actual use of PNO has been a long time coming.

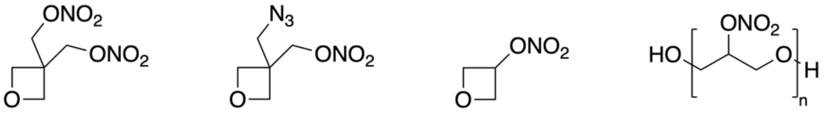

BNMO **AMNMO** **3NO** **PNO**

Figure 1.7. Energetic oxetane monomers and polymers, which have not yet gained importance.

Given that the number of available energetic oxetanes is currently extremely limited and that many shortcomings of existing binders have not yet been overcome or have perhaps not yet emerged, the development of new oxetane monomers represents an important and promising field of activity. The following section is therefore dedicated to various aspects regarding the history, chemistry, and use of oxetanes.

1.4 Oxetanes – A Brief Overview

Taking a closer look at the state of the art in the field of energetic polymers, it becomes evident that a wide variety of polymer classes have been investigated for a potential binder application. These include polyformals, polyurethanes, acrylic-based binders, nitrated polybutadienes, nitrated polystyrenes, energetic vinyl polymers such as poly(vinyl nitrate) or poly(vinyl tetrazole), polynitrophenylenes, and polyphosphazenes to name just a few.[24,55] Despite the extensive studies, however, essentially only energetic polyether polymers have found their way into practice. The most important and successful polymers are the polyoxiranes PGN and GAP, along with the polyoxetanes poly(AMMO), poly(BAMO) as well as poly(NIMMO), and copolymers based on these. Thus, polyoxetanes form the vast majority. This is also reflected by a growing number of patents claiming protection for polymer-bonded explosives and propellant formulations containing these oxetane-based polymers.[36,69,70] Various circumstances have certainly contributed to their particular success.

One circumstance is probably the fact that the polymer backbone itself already contains oxygen and is usually characterized by high thermostability and chemical stability. Furthermore, polyethers represent technically and industrially relevant polymers, for which reason the corresponding polymerization processes are well studied.[71] For example, cationic ring-opening polymerization allows the synthesis of so-called telechelic polymers which feature a relatively low molecular weight next to an end-capping of their chains with functional groups allowing a subsequent crosslinking via curing agents.[72] This is linked to advantages in terms of the processing of energetic materials. Such low-molecular-weight and low-viscosity energetic binder polymers can be easily and homogeneously mixed with energetic fillers to subsequently embed them in an elastic polymer matrix formed upon curing. Solvents or wetting agents can be bypassed, which are otherwise difficult to remove from the formulation. The question of why oxetanes prevailed over oxiranes or tetrahydrofuran derivatives may also be answered – oxetanes offer a ring strain comparable to the smallest cyclic ether (oxirane) and therefore show a similarly high polymerizability, while the ring strain drops significantly toward the five-membered homolog THF (Figure 8).[73]

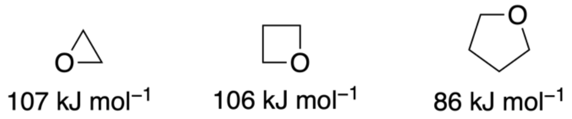

Figure 1.8. Ring strain comparison for the cyclic ethers oxirane, oxetane and tetrahydrofuran.

In addition, oxetanes offer higher chemical stability than oxiranes under a wide range of reaction conditions allowing a more facile and more extensive functionalization. For example, oxetanes are very stable toward bases, and while monosubstituted oxetanes are known to be stable above pH 1 under acidic conditions, some 3,3-disubstituted oxetanes are even stable at pH 1.[74,75] In this respect, oxetanes provide an optimum of chemical functionalization possibilities and polymerizability in addition to the least possible carbon-hydrogen ballast apart from the generally less stable and less suitable oxiranes. In view of their success in the field of energetic binders and recent developments in the field of oxetanes, these will be addressed in more detail below.

1.4.1 Oxetane – The Parent Compound

Unsubstituted oxetane, the formal parent compound of all oxetane derivatives, is a colorless liquid with a boiling point of 47.8 °C.[76] It was first isolated in 1858 and first prepared in 1878 by Reboul via cyclization of 1-Chloro-3-hydroxypropane using aqueous base.[77] Although oxetanes were thus known quite early, they remained a little-studied niche motif until the 1950s – since then, they are facing an ever-increasing interest. Despite this, the crystal structure of oxetane was elucidated much later in 1984 by Luger and Buschmann (Figure 9).[78]

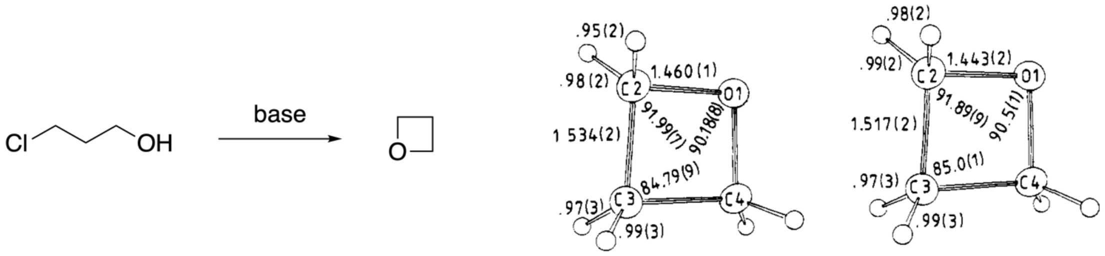

Figure 1.9. First preparation of oxetane by Reboul (left); Determined bond length and valence angles for unsubstituted oxetane at 90 K (left) and 140 K (right) as depicted in the work of Luger and Buschmann.

Contrary to early studies on the ring geometry at ambient conditions by microwave-spectroscopy, which indicated an essentially planar structure (puckering angle < 0.33°)[79], the crystallographic study revealed a slightly puckered structure with a puckering angle of 8.7(2)° at 90 K and 10.7(1)° at 140 K. Furthermore, the endocyclic C2–O1 bond was found to be rather large for a carbon-oxygen single bond with a length of 1.46 Å at 90 K.[78]

The relatively small puckering angle may seem perplexing compared to the analogous cyclobutane, which exhibits a puckering angle of roughly 30°.[80] However, the formal exchange of a methylene group with an oxygen atom minimizes the unfavorable eclipsing interactions, which are minimized in cyclobutane by the strong out-of-plane distortion. The more planar structure also reduces the ring strain by 6.3 kJ mol^{-1} to 106.3 kJ mol^{-1}[81] in comparison to cyclobutane, which features a ring strain of 112.6 kJ mol^{-1}.[82]

However, unfavorable eclipsing interactions can be increased by the introduction of substituents to the ring, resulting in larger puckering angles. The highly strained C–O–C bond angle results in an exposure of the oxygen atom lone pairs rendering oxetane an excellent Lewis base and hydrogen-bond acceptor.[83] However, this effect is counteracted to a certain extent by the hybridization of the oxygen atom. In small rings, the p-character of the endocyclic bonds is increased, leading to a correspondingly increased s-character of the oxygen atom's lone pairs. This causes a reduced ability to engage in hydrogen bonding next to increased bond angles of exocyclic substituents.[80,84] However, studies suggest that the change in hybridization is only significant in the case of oxiranes.[84,85] Thus, it is likely that oxetanes even feature the most Lewis-basic oxygen atom among cyclic ethers.[86] This is of great advantage for the cationic ring-opening polymerization of oxetanes as their polymerizability depends primarily on the monomer basicity and ring strain.[76]

1.4.2 Natural Occurrence of Oxetanes

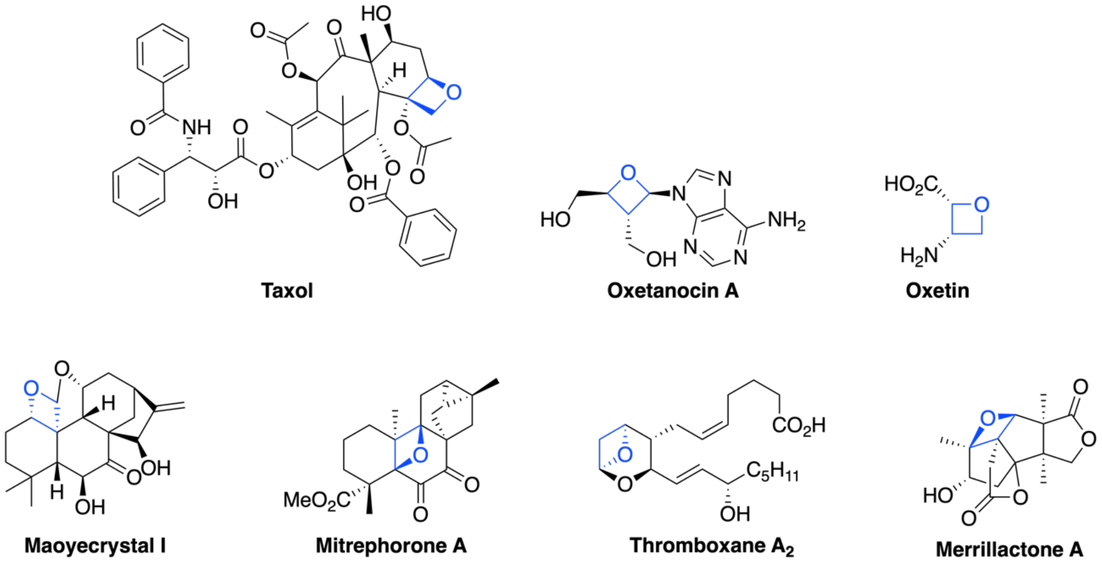
Taxol **Oxetanocin A** **Oxetin**

Maoyecrystal I **Mitrephorone A** **Thromboxane A$_2$** **Merrillactone A**

Figure 1.10. Selection of natural oxetane-containing compounds (OCCs).

Various compounds that contain an oxetane motif (Figure 10) have been isolated from natural sources – these are not particularly numerous, but the compounds have in common that the presence of the oxetane ring is always linked to a biological activity, which apparently depends on it.[80] The most prominent of these naturally-occurring oxetanes is Taxol, isolated in 1971 from the western yew, which is used in cancer chemotherapy.[87] A compound to inhibit the *in vivo* replication of the HI virus called Oxetanocin A was isolated from the soil bacterium *Bacillus megaterium*.[80] A far less complex structure, oxetin, was found in the gram-positive bacteria

Streptomyces sp OM-2317 and exhibits an antibacterial and herbicidal effect.[80,88] Many other isolated compounds also show a biological activity. For instance, maoyecrystal I and mitrephorone A show cytotoxic effects[84], while Thromboxane A_2 turned out as a prothrombotic compound giving it its name.[80] Merrilactone A, isolated in 2000 from the plant *Illicium merrilanium*, a special star anise genus, was found to stimulate neuron growth in rats.[89] A long continuation of this sequence can be assumed, as more than 600 natural oxetane-containing compounds (OCCs) became known till the end of 2018.[90] A correspondingly large interest of the pharmaceutical industry in the oxetane motif has thus been triggered.

1.4.3 Pharmaceutical Application of Oxetanes

The exploration and exploitation of the oxetane motif in medicinal chemistry are strongly associated with the work of Carreira and collaborators. A very influential publication was brought forward in 2006 when Carreira, Roger-Evans, and co-workers propagated 3,3-disubstituted oxetanes as a potential replacement for geminal dimethyl groups.[91] These are used to protect metabolically vulnerable methylene sites. Unfortunately, *gem*-dimethyl groups cause increased lipophilicity, which may also result in adverse effects regarding the pharmacokinetic properties of a certain compound.[80] Contrary to this, the alternative use of the oxetane motif leads to reduced lipophilicity and metabolic liability (Figure 11).[80,91]

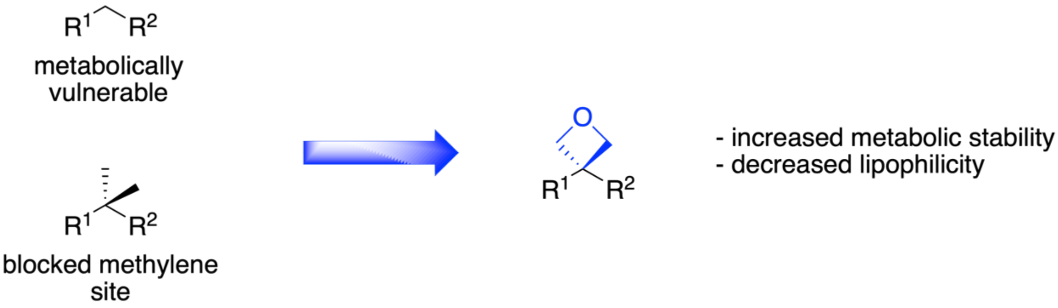

Figure 1.11. The oxetane motif as replacement for geminal dimethyl groups.

Several other publications by Carreira and co-workers investigated oxetanes as a potential replacement for carbonyl groups.[75,84,92,93] This is mainly due to the fact that oxetanes have a comparable dipole character as well as similar H-bonding properties.[93] While carbonyl groups are susceptible to enzymatic attacks and *alpha*-deprotonation, oxetanes are stable concerning these influences.[80] The largest and most significant difference between carbonyl groups and the oxetane motif is the length of the group, which increases from 1.2 Å to 2.1 Å (Figure 12).[80]

Figure 1.12. The oxetane motif as a carbonyl replacement and change of group dimensions.

In the corresponding studies, the physicochemical and biological properties of certain carbonyls were compared to those of the respective oxetane analogs (Figure 13). The introduction of the oxetane ring resulted in reduced aqueous solubility of the investigated compound pairs, while inconclusive effects on the lipophilicity were found.[80] However, improved metabolic stability was found in the case of certain oxetane analogs.[80,93]

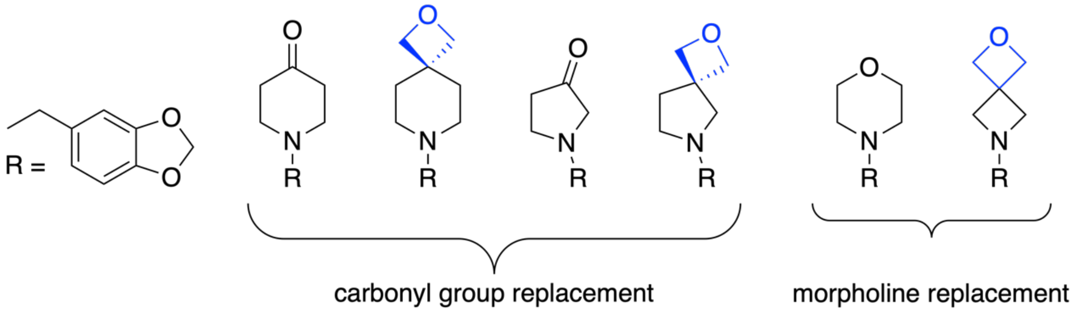

Figure 1.13. Compounds used to investigate the suitability of the oxetane motif to replace carbonyl groups and the morpholine motif.

Furthermore, spirocyclic oxetane derivatives were envisioned as a surrogate for morpholine moieties (Figure 13) which increase the aqueous solubility of drug scaffolds.[80] Unfortunately, the morpholine structure is prone to oxidative metabolic attacks.[84] Fortunately, it was successfully demonstrated that the replacement of a morpholine structure by a structurally related oxetane motif is linked to improved aqueous solubility, reduced lipophilicity, and increased stability toward oxidation.[80,93] Thus, the enormous potential of the four-membered cyclic ether was repeatedly and impressively demonstrated. Next to its use as a bioisoster, many other problems in medicinal chemistry were successfully addressed by making use of the oxetane scaffold. However, due to the extensive scope of this topic, the interested reader is referred to the numerous reviews available in the literature.[80,84,94,95]

1.4.4 Preparation of Oxetanes

Until their great revival due to the findings in the field of medicinal chemistry, oxetanes only had a niche existence and essentially still suffer from a rather subordinate role in chemistry. Despite this, a wide variety of synthetic methods have been developed for their synthesis. However, the methods repeatedly found in the literature are essentially limited to Williamson ether synthesis, the Paternó-Büchi reaction, and the addition of sulfur ylides to aldehydes (Scheme 3).[86]

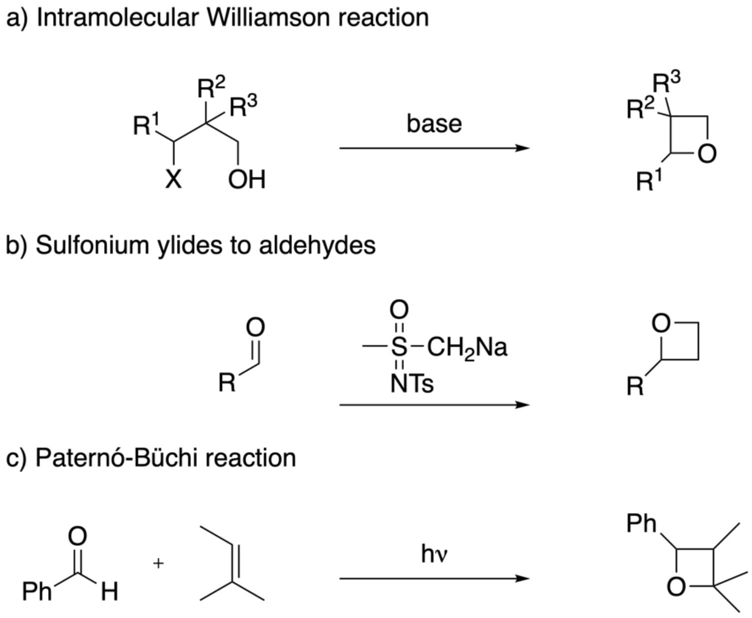

Scheme 1.3. Common methods for the preparation of oxetanes.

Among these, the Williamson reaction is the most widespread[96] despite the difficult ring closure. Studies have shown that the rate of closure is very much different for β- and γ-chlorohydrins.[97] Hereby, epoxide formation from β-chlorohydrins is favored by a magnitude of two over the γ-homolog to form an oxetane ring.[97] Major drawbacks of the Williamson ether reaction are side reactions which may lower the yield considerably. These side reactions include the Grob fragmentation of the γ-haloalcoxide to result in the formation of an alkene and an aldehyde next to the undesired and uncontrolled formation of polyethers via intermolecular reactions of the halohydrin (Scheme 4).[74,86,98]

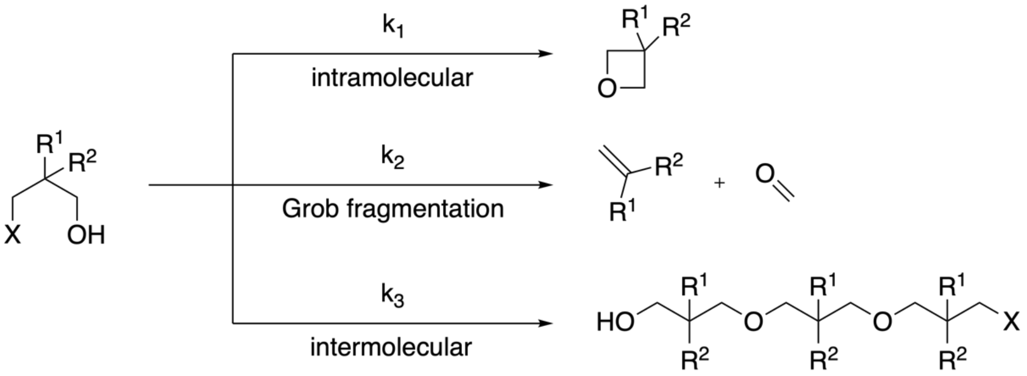

Scheme 1.4. Side reactions during the preparation of oxetanes using the Williamson ether synthesis.

The Paternó-Büchi reaction is a UV light-mediated reaction to form the oxetane ring from a light-absorbing carbonyl species and an alkene. This particular reaction was discovered by Paternó in 1909, re-examined by Büchi in 1954, and provides access to oxetanes of various substitution patterns.[99,100] It was the first reaction to furnish 3,3-diarlyoxetanes in 2001, which were not accessible by other methods until then.[80,101]

Another synthetic route toward oxetanes is given by the one-pot reaction of carbonyl compounds with sulfoxonium ylides.[102] The reaction is thought to proceed via an epoxide intermediate which is ring-opened by another equivalent of ylide to give an γ-alkoxy sulfonium ylide. The latter performs an intramolecular displacement reaction to result in a 2-substituted oxetane.[86] Since substituents at the 2- and 4-position of the oxetane ring may cause a steric inhibition of an intended polymerization[76], only 3-substituted and 3,3-disubstituted oxetanes are relevant for the preparation of energetic binders, rendering the latter synthetic methods of very limited use in HEDM chemistry.

In this context, however, it should also be mentioned to what extent the chemistry of energetic oxetanes can benefit from the increased interest of medicinal and pharmaceutical chemistry in the oxetane motif. For instance, this increased interest has led to a considerably improved understanding of the specific chemistry of oxetanes in general. Methods for their synthesis and derivatization are now being researched and further developed with great effort. As a result, more and more oxetane building blocks become commercially available, which in turn stimulates further research in the field of the associated drug discovery and oxetanes in general. Through this self-amplifying development, an ever-increasing number of 3-substituted and 3,3-disubstituted oxetane derivatives that are suitable for the synthesis of new powerful energetic oxetane monomers are becoming commercially available. As prices for the corresponding starting materials continue to drop, the need to synthesize oxetane building blocks is increasingly eliminated. For example, Spirochem AG, a swiss company specialized in the synthesis of oxetanes, currently offers 392 oxetanes on a milligram to kilogram scale.[103] Many of the compounds offered can be directly converted into energetic oxetanes in one-step reactions or in few successive steps, as synthetically versatile functional groups are available. For instance, alcohols and amines (**1**–**5**) provide access to nitrate esters and nitramines. Classical C-nitro compounds can be obtained via oxidation of the amino groups. Olefins and carbonyl compounds (**6**, **7**) allow the preparation of energetic monomers via addition reactions, and oxetanes bearing leaving groups (**8**) enable a fast-forward monomer synthesis via nucleophilic substitution reactions using energetic nucleophiles. An exemplary selection of such available and useful compounds is shown in Figure 14.

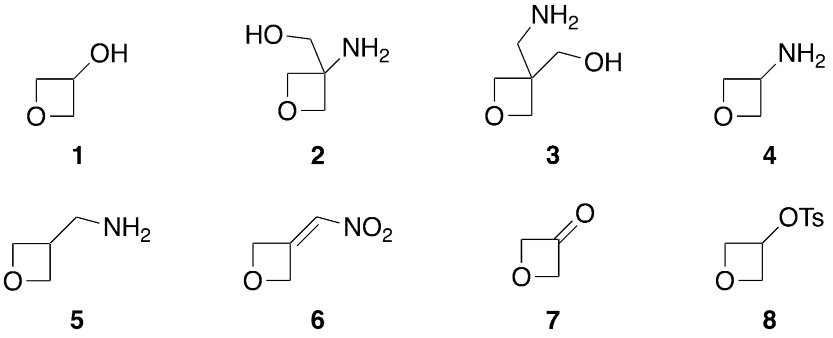

Figure 1.14. Useful and commercially available oxetanes for the preparation of energetic oxetane monomers.

While drug development often requires the multi-step synthesis of complex structures using a wide variety of often expensive reagents and specialty chemicals, HEDM chemistry focuses on inexpensive, preferably easily functionalizable starting materials capable of providing compounds suitable for a certain application with the least possible number of steps and the highest possible overall yield. Expensive reagents and non-scalable techniques need to be avoided to increase the chance of a practical application. Given these contrasting chemical approaches, it remains to be seen to what extent pharmaceutical chemistry will also benefit from the continued research into energetic oxetanes.

1.4.5 Ring-Opening Polymerization of Oxetanes

General aspects

Next to chain polymerization (ionic or radical) and condensation polymerization, ring-opening polymerization (ROP) is one of the major pathways to polymers that are important to today's society.[71] Many polymers of technical and industrial importance are prepared via ROP, including polycyclooctene, polynorbornene, polysiloxane, polyphosphazene, and propylene oxide, among others.[71] In purely quantitative terms, however, polyoxymethylenes (POMs), nylon 6, and polyurethanes produced from polyether diols belong to the most important polymers.[71] In addition to insertion polymerization, free-radical, anionic, and cationic ring-opening polymerization (CROP) represent typical polymerization processes – the latter being the most widespread and predominantly used technique.[76] The first oxetane derivative polymerized via CROP was poly[3,3-bis(chloromethyl)oxetane] (PBCMO), which was obtained by Farthing and coworkers in 1954 and subsequently marketed by Hercules Incorporated as Penton®.[76,104] Nowadays, it is used to prepare the energetic binder poly(BAMO) via polymer-analogous transformation (PAT). CROP is also the weapon of choice for the polymerization of energetic cyclic ethers such as energetic oxiranes or oxetanes. This can be mainly attributed to the fact that many explosophoric groups would otherwise be unstable under the applied polymerization conditions. For example, organic azides, which are very attractive for the synthesis of energetic binders, cannot be polymerized via free radical polymerization techniques as the azido groups would decompose.[56] Moreover, as the azide ion is only moderately nucleophilic, strong bases in the case of anionic polymerization methods may provoke undesired nucleophilic displacement reactions.[56] The same applies to nitro or nitrato groups which can act as leaving groups upon contact to bases, and primary nitramines that are very prone to salt formation. The unsubstituted parent compound oxetane, which is also known as trimethylene oxide, oxacyclobutane, or 1,3-epoxypropane, polymerizes readily as probably the most basic of all cyclic ethers with a remarkable ring strain of roughly 106 kJ mol^{-1}.[76,96] In general, a wide variety of oxetanes can be polymerized, and quantitative conversion toward the polymer can be achieved provided that sufficiently pure materials are ring-opened under suitable conditions with suitable initiators.[76,105] In addition to basicity and ring strain, structural factors are also important for the polymerizability of oxetanes. In the case of CROP, electron-donating substituents such as hydroxy, amino, or carboxyl groups can completely inhibit polymerization or terminate it after a few propagation steps.[76] Moreover, electron-withdrawing substituents can oppose the formation of a stable oxonium ion, which is necessary for a successful polymerization, and bulky substituents at the 2 and 4 position of the ring may lead to steric inhibition.[76] Thus, 3-substituted and 3,3-disubstituted oxetanes are favorable, provided that they match the abovementioned design criteria. However, the choice of a suitable initiator is also crucial, and initiators common in the case of CROP will be discussed in the following paragraph.

Initiators

A prerequisite to a successful cationic ring-opening polymerization is a reagent that provides the propagating tertiary oxonium ion (Figure 15), and numerous initiators have been developed and can be employed.[76]


1 2

Figure 1.15. Tertiary (1) and secondary (2) oxonium ion to initiate propagation.

The most prevalent initiators to polymerize oxetanes in a cationic manner include Brønsted acids, carbenium-, acyl- and onium ions, Lewis acids, as well as alkyl esters of strong organic acids such as sulfonic acids and aluminum alkyls.[76,106] Some of the most important representatives are briefly outlined below.

Brønsted acids. "Dry" acids such as neat perchloric acid, hydrogen chloride, sulfuric acid, or strong sulfonic acids such as trifluoromethane sulfonic acid are often used as Brønsted acids.[71] However, these are linked to several and major disadvantages. One is the formation of a secondary oxonium (Figure 15 (2)) ion, which is less reactive compared to the tertiary oxonium species[76], another is the fact that the CROP of oxetanes with such acids is often characterized by an induction period which complicates the control of the polymerization.[71]

Trialkyl oxonium salts. In contrast, initiation by strong alkylating agents such as trialkyl oxonium salts is more advantageous. Typical examples are trimethyloxonium tetrafluoroborate or the related triethyloxonium species.[76] In addition to tetrafluoroborate, hexafluorophosphate and hexafluoroantimonate are suitable counterions to ensure a stable oxonium ion and to avoid termination at an early stage due to a counterion collapse.[71,76] Here, the tertiary oxonium ion required for the propagation of the polymerization is formed by the transfer of an alkyl group (Scheme 5).

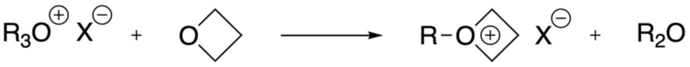

Scheme 1.5. Initiation of CROP via trialkyl oxonium salts.

Acylium ion salts. A very similar approach is given by the use of acylium ion salts, which feature the aforementioned, non-nucleophilic counterions. They are comparably reactive to trialkyl oxonium salts.[76] The main difference to trialkyl oxonium species is that the propagating tertiary oxonium ion is formed by formal addition, and thus no ether (R_2O) is split off (Scheme 6).

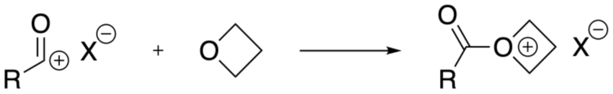

Scheme 1.6. Initiation of CROP using acylium salts.

Lewis Acids. As outlined above, Brønsted acids act as initiators but are also linked to drawbacks limiting their usefulness. Although being excellent initiators, alkyl oxonium salts and acylium ion salts are rather unsuitable for the preparation of energetic polyoxetane binders. This is due to the fact that polymers with a partially unreactive end-capping are form that oppose curing by crosslinkers such as isocyanates. Lewis acids offer a solution to this problem and have therefore become established as initiators in the field of energetic binders. The most commonly used Lewis acid is boron trifluoride or its diethyl ether adduct $BF_3{\cdot}Et_2O$.[71]

However, BF_3 alone is not capable to polymerize pure (dry) oxetanes and requires the presence of water or an alcohol leading to BF_3OH^- or BF_3OR^- counterions.[76,104] Most commonly, butane-1,4-diol (BDO) is used as studies by Biedron et al. state that the application of BDO leads to the formation of less cyclic oligomers compared to its homolog ethylene glycol, which is also common.[107,108] Lewis acids such as PF_5 and SbF_5 are able to self-initiate without the necessity for co-initiators.[76] However, they are rarely used for the polymerization of energetic oxetanes.

Aluminum alkyls. Another potent initiator is given by trialkyl aluminum species. To act as initiators, these have to be chemically modified in an inert solvent by the addition of roughly 0.5–1.0 equivalents of water.[76] For instance, various kinds of activated aluminum alkyls have been employed by Vandenberg, the inventor of GAP, to gain high-molecular-weight polyepoxides.[109] A species that found widespread use is triisobutylaluminum (TIBA) with varying equivalents of water.[110,111] An accepted mechanism explains the CROP initiation through the formation of a highly acidic complex between TIBA and water. Then, a proton adds to the monomer to result in an ion pair. Subsequently, the carbocation reacts with further monomers to enable propagation. Thus, the growing chain is always terminated by the carbocation and the initially formed counter ion.[110] In general, the TIBA-water initiating system is known to provide polyoxetanes of very high molecular mass.[110,111]

Mechanistic considerations

Cationic ring-opening polymerization can proceed by two mechanisms - the "active chain end" mechanism (ACE or ACEM) and the "activated monomer" mechanism (AMM).[71,112] The mechanisms essentially differ in the mode of chain propagation, and the preference for one of the mechanisms significantly affects the nature and properties of the final polymer. Therefore, both mechanisms will be directly compared to each other using the example of the widely used boron trifluoride etherate-diol system.

Regardless of the actual mechanism, the added alcohol (butane-1,4-diol, R = $(CH_2)_4$) first reacts with the boron trifluoride diethyl ether adduct to form an initial ion pair. The oxonium ion formed subsequently protonates the highly basic oxygen atom of an oxetane monomer, leading to the formation of a secondary oxonium ion. The nucleophilic attack of an available monomer on this ion finally leads to the formation of the propagating chain, which is characterized by a terminal tertiary oxonium ion and the previously formed counterion (Scheme 7).

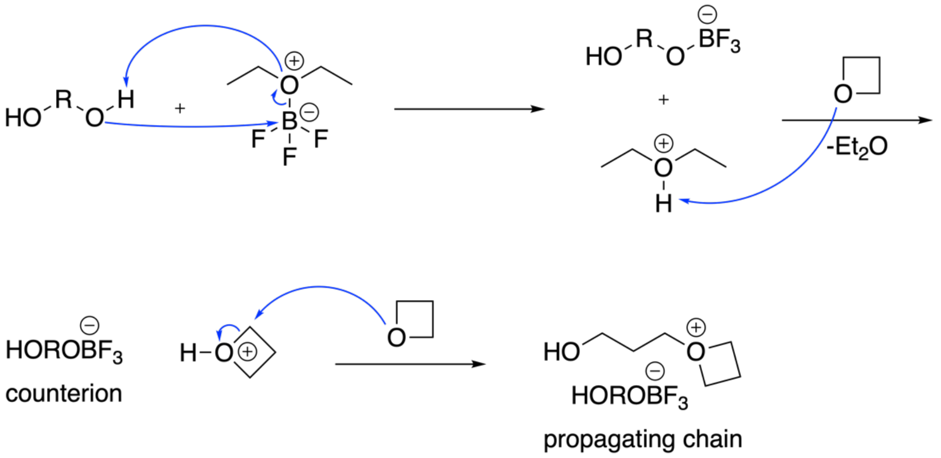

Scheme 1.7. Formation of the propagating chain using boron trifluoride etherate and butane-1,4-diol.

Subsequently, the remaining monomers present in the reaction system add via an S_N1 or S_N2 mechanism (Scheme 8). Here, the prevailing mechanism is determined by the stability of the acyclic cationic species – in the case of unsubstituted cyclic ethers, which cannot stabilize the charge via suitable neighboring substituents, a predominant S_N2 mechanism can be assumed.[106] Hereby, the oxygen lone pair of an approaching monomer attacks one of the α-carbon atoms of the oxetane ring. Depending on whether the attack occurs at both or only at one α-carbon atom, polymers with a microstructure can be formed in the case of unsymmetrically substituted oxetanes, whereas this is not the case for 3-substituted oxetanes.[76]

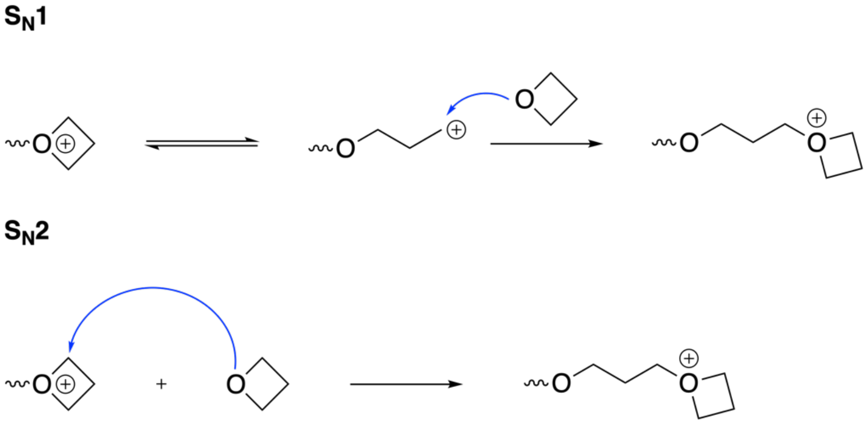

Scheme 1.8. Chain propagation via an S_N1 or S_N2 mechanism.

A problem arises from the fact that all oxygen atoms of the growing polyether backbone or oxygen atoms in side chains are also reactive and may cause undesired side reactions. For instance, the attack of a main chain oxygen atom at the electrophilic chain end (back-biting) leads to the formation of cyclic oligomers and macrocycles due to subsequent ring-elimination.[76,113] In addition, the collapse of the counterion is a detrimental side reaction (Scheme 9).[71]

Back-biting

Ring elimination

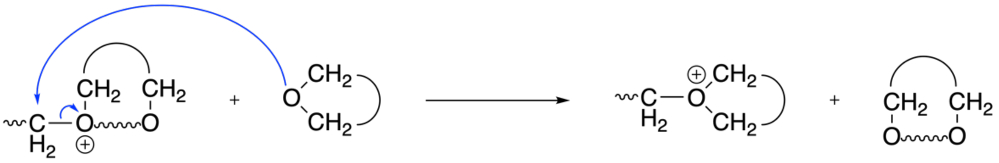

Counterion collapse

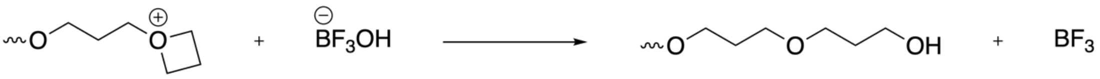

Scheme 1.9. Problematic side reactions during cationic ring-opening polymerization.

Depolymerization can occur if the attack results from the penultimate oxygen atom. However, this process is rather insignificant among oxetanes as it requires the energetically unfavored formation of a highly strained ring.[76] As far as sterically possible, intermolecular reactions can occur between the tertiary oxonium ion of a growing chain and a backbone oxygen atom of another chain, resulting in polymeric acyclic oxonium ions.[76] Apart from these undesired side reactions, quenching of the CROP with water ideally leads to the desired polymeric diol. (Scheme 10).

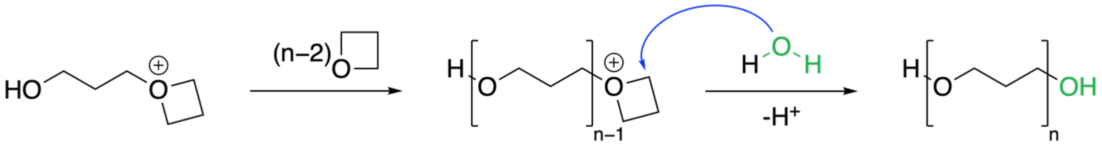

Scheme 1.10. Quenching of the reaction with water to result in a hydroxy-terminated polymer.

The extent of such side reactions and associated by-products largely depends on structural features of the cyclic ether to be polymerized, the employed reactions conditions, and the rate of these reactions in comparison to the rate of chain propagation.[107,114] For instance, the polymerization of THF proceeds smoothly with negligible amounts of side products, while the polymerization of oxiranes may yield considerable amounts of cyclic oligomers, which can even become the main product under inappropriate conditions.[115,116]

Due to the disadvantages linked to the ACEM, CROP is performed mainly in the presence of a diol or polyol under monomer starving conditions.[107,114] In this case, the instantaneous concentration of the monomer is kept low, which is then present in the protonated state. As a consequence, the polymerization may predominantly proceed via the AMM. Contrary to the ACEM, propagation then proceeds through the nucleophilic attack of a hydroxy-terminated chain end on a protonated monomer.[107] Thereby, the polymer chains grow in an uncharged state, avoiding the adverse termination reactions resulting from the ACEM (Scheme 11).[117]

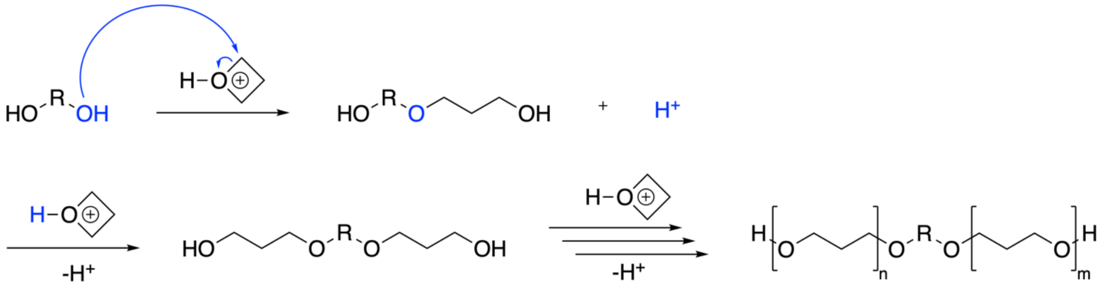

Scheme 1.11. Chain propagation in case of the activated monomer mechanism.

With the AMM, the number of terminating hydroxy groups of each polymer chain corresponds to the number of hydroxy groups of the alcohol (quenching with water), as these represent the starting point of chain growth.[24,117] Thus, the employed alcohol is ultimately incorporated into the polymer backbone. For example, tri-hydroxy-terminated polymers can be obtained using a triol such as glycerin – for instance, GAP-triol is prepared in this way.[24] Unfortunately, however, CROP does not proceed solely according to the AMM, and a competition between the two mechanisms takes place.[117] Luckily, the rate of ACEM is proportional to the concentration of non-protonated monomers, whereas the rate of AMM depends on the concentration of hydroxy groups and "activated" (protonated) monomers.[118] Hence, a favoring of the AMM can be accomplished by keeping the monomer concentration as low as possible during the entire polymerization (starving conditions).[107,116] In practice, this is achieved through a very slow, dropwise monomer addition using a syringe pump – ideally leading to a state in which the monomer consumption is faster than the addition. With increased AMM participation, the living character of the CROP increases, resulting in less cyclics, improved molecular weight control, and narrower polydispersities.[119,120] However, as it is almost impossible to avoid a certain ACEM involvement in practice, the formation of cyclic by-products will often lead to a decreased end-group functionality to complicate the curing of telechelic polyethers.

Therefore, just like the development of energetic binders with tailored properties for a specific application, the optimization and fine-tuning of polymerization conditions to achieve the best possible result will remain a necessary, iterative, and laborious task in the future.

References

[1] Klapötke, T. M. *Chemistry of High-Energy Materials*; 5th ed.; DeGruyter: Boston, **2019**.

[2] Matyáš, R.; Pachman, J. *Primary Explosives*; Springer: Berlin, Heidelberg, **2013**.

[3] Fischer, D.; Klapötke, T. M.; Stierstorfer, J. Potassium 1,1′-Dinitramino-5,5′-bistetrazolate: A Primary Explosive with Fast Detonation and High Initiation Power. *Angew. Chem. Int. Ed.* **2014**, *53*, 8172-8175.

[4] Agrawal, J. P. *High Energy Materials*; Wiley-VCH: Weinheim, **2010**, pp 1-67.

[5] Köhler, J.; Meyer, R.; Homburg, A. *Explosives*; 10th ed.; Wiley-VCH: Weinheim, **2008**.

[6] Mahadevan, E. G. *Ammonium Nitrate Explosives for Civil Applications: Slurries, Emulsions and Ammonium Nitrate Fuel Oils*; Wiley-VCH: Weinheim, **2013**, pp 15-30.

[7] Hafstrand, A.; Sandstrom, J.; Sjoberg, P. Airbag device and propellant for airbags. US 6 713 3696, **1997**.

[8] Jenkins, A. D.; Kratochvíl, P.; Stepto, R. F. T.; Suter, U. W. Glossary of basic terms in polymer science (IUPAC Recommendations 1996). *Pure and Appl. Chem.* **1996**, *68*, 2287-2311.

[9] Ang, H. G.; Pisharath, S. *Energetic Polymers: Binders and Plasticizers for Enhancing Performance*; Wiley-VCH: Weinheim, **2012**.

[10] Davis, T. L. *The Chemistry of Powder and Explosives*; Angriff Press: Hollywood, CA, **1972**.

[11] Agrawal, J. P. *High Energy Materials*; Wiley-VCH: Weinheim, **2010**, pp 209-330.

[12] Akhavan, J. *The Chemistry of Explosives*; 2nd ed.; RSC Publishing: Cambridge, UK, **2004**.

[13] Wilbrand, J. Notiz über Trinitrotoluol. *Liebigs Ann. Chem.* **1863**, *128*, 178-179.

[14] Thieme, B. Process of making nitropentaerythrit. US 541 899, **1895**.

[15] Agrawal, J.; Hodgson, R. *Organic Chemistry of Explosives*, John Wiley & Sons Ltd.: Hoboken, New Jersey, **2006**, pp 191-261.

[16] Urbanski, T. *Chemie und Technologie der Explosivstoffe*; Vol. 3; VEB Dt. Verl. f. Grundstoffindustrie: Leipzig, **1964**.

[17] Shipp, K. G. Reactions of α-Substituted Polynitrotoluenes. I. Synthesis of 2,2',4,4',6,6'-Hexanitrostilbene. *J. Org. Chem.* **1964**, *29*, 2620-2623.

[18] Dobratz, B. M. *The insensitive high explosive triaminotrinitrobenzene (TATB): Development and characterization, 1888 to 1994*; LA-13014-H; U.S. Department of Education, Lawrence Livermoore National Laboratory (LANL): Los Alamos, NM, **1995**. DOI: 10.2172/90370

[19] Nielsen, A. T. Caged Polynitramine Compound. US 5 693 794, **1997**.

[20] Zhang, M.-X.; Eaton, P. E.; Gilardi, R. Hepta- and Octanitrocubanes. *Angew. Chem. Int. Ed.* **2000**, *39*, 401-404.

[21] Fischer, N.; Fischer, D.; Klapötke, T. M.; Piercey, D. G.; Stierstorfer, J. Pushing the limits of energetic materials – the synthesis and characterization of dihydroxylammonium 5,5′-bistetrazole-1,1′-diolate. *J. Mater. Chem.* **2012**, *22*, 20418-20422.

[22] Fischer, D. High Performing and Nitrogen-rich High Energy Density Materials. Ph. D. Dissertation, Ludwig-Maximilian University (LMU) Munich, Munich, Germany, **2016**.

[23] Klapötke, T. M.; Witkowski, T. G. 5,5′-Bis(2,4,6-trinitrophenyl)-2,2′-bi(1,3,4-oxadiazole) (TKX-55): Thermally Stable Explosive with Outstanding Properties. *ChemPlusChem* **2016**, *81*, 357-360.

[24] Provatas, A. *Energetic Polymers and Plasticizers for Explosive Formulations – A Review of Recent Advances*; DSTO-TR-0966; Defence Science & Technology Organisation (Department of Defence), Aeronautical and Maritime Research Laboratory: Melbourne, Victoria, **2000**.

[25] Mason, B. P.; Roland, C. M. SOLID PROPELLANTS. *Rubber Chemistry and Technology – Rubber Reviews*, **2019**, *92*, 1-24. DOI: 10.5254/rct.19.80456

[26] Sutton, E. Prom polymers to propellants to rockets – A history of Thiokol. In *35th Joint Propulsion Conference and Exhibit of the American Institute of Aeronautics and Astronautics*, Los Angeles, CA, U.S.A, June 20–24 ,**1999**.

[27] Patrick, J. C. Rubber composition. US 281 376 28, **1932**.

[28] Sutton, E. From polysulfides to CTPB binders – A major transition in solid propellant binder chemistry. In *20th Joint Propulsion Conference and Exhibit of the American Institute of Aeronautics and Astronautics*, Los Angeles, CA, U.S.A, June 11–13, **1984**.

[29] Moore, T.; Rohrbaugh, E. CTPB Propellants for Soace Appliations. In *38th AIAA/ASME/SAE/ASEE Joint Propulsion Conference and Exhibit of the American Institute of Aeronautics and Astronautics*, Indianapolis, IN, U.S.A, July 07–10, **2002**.

[30] Pisharath, S.; Ang, H. G. Synthesis and thermal decomposition of GAP–Poly(BAMO) copolymer. *Polym. Degrad. Stab.* **2007**, *92*, 1365-1377.

[31] Daniel, M. A. *Polyurethane Binder Systems for Polymer Bonded Explosives*; DSTO-GD-0492; Defence Science & Technology Organisation (Department of Defence), Weapons Systems Division: Edinburgh, South Australia, **2006**.

[32] Copp, J. L.; Ubbelohde, A. R. Part III. (1) The Grit Sensitiveness of High Explosives. *Philos. Trans. R. Soc. London. Series A. Math. Phy. Sci.* **1948**, *241*, 248-265.

[33] Kosowski, B. M.; Taylor, R. C. Method and composition for melt cast explosives, propellants and pyrotechnics. US 5 431 756 A, **1995**.

[34] Linder, P. W. Desensitization of explosives. *Trans. of the Faraday Soc.* **1961**, *57*, 1024-1030.

[35] Kneisl, P. Hi-temp explosive binder. US 6 989 064 B2, **2006**.

[36] Auer, M.; Clement, D.; Hahma, A.; Licha, J.; Pham, O. Compressible insensitive explosive mixture comprises a sensitive first explosive, a polymer as binder and an insensitive second explosive. DE 10 2010 005 923 A1, **2011**.

[37] Desai, H. J.; Cunliffe, A. V.; Lewis, T.; Millar, R. W.; Paul, N. C.; Stewart, M. J.; Amass, A. J. Synthesis of narrow molecular weight α,ω-hydroxy telechelic poly(glycidyl nitrate) and estimation of theoretical heat of explosion. *Polymer* **1996**, *37*, 3471-3476.

[38] Vandenberg, E. J. Polyethers containing azidomethyl side chains. US 3 645 917, **1972**.

[39] Frankel, M.; Grant, L.; Flanagan, J. Historical Development of GAP. In *25th Joint Propulsion Conference of the American Institute of Aeronautics and Astronautics*, Monterey, CA, U.S.A., July 12–16, **1989**.

[40] Radwan, M. A.; Seleet, M. M.; Zaki, M. G. Effect of different binders on the performance of some advanced plastic bonded explosives. In *3rd International Conference On Chemical & Environmental Engineering*, Military Technical College Cairo, Cairo, Egypt, May 16–18, **2006**.

[41] Sućeska, M., EXPLO5, Version 6.04, Brodarski Institute Zagreb, **2017**.

[42] 3M™ Glycidyl Azide Polymer GAP-5527 Polyol; Product Information; 3M Specialty Materials: St. Paul, MN, **2000**. https://www.machichemicals.com/pdf/3M_GAP-5527.pdf (accessed 2021-09-01).

[43] 3M™ Glycidyl Azide Polymer GAP-5527 Polyol; Safety Data Sheet; 3M Specialty Materials: St. Paul, MN, **2000**. https://multimedia.3m.com/mws/mediawebserver?SSSSSuUn_zu8l00xl82948_BMv70k17zHvu9lxtD7SSSSSS-- (accessed 2022-03-15)

[44] Fruci, S.; Lamia, P.; Cappello, M.; Filippi, S.; Polacco, G. Synthesis of GAP and PAMMO Homopolymers from Mesylate Polymeric Precursors AU - Mura, Claudio. *J. Energ. Mater.* **2016**, *34*, 216-233.

[45] Murali Mohan, Y.; Mohana Raju, K.; Sreedhar, B. Synthesis and Characterization of Glycidyl Azide Polymer with Enhanced Azide Content. *Int. J. Polym. Mater. Polym. Biomater.* **2006**, *55*, 441-455.

[46] Eurenco GAP Diol; Eurenco Product catalogue; Eurenco: Sorgues, France, 2021. https://eurenco.com/wp-content/uploads/2021/04/EURENCO-Product-Catalogue.pdf (accessed 2022-01-21).

[47] Golding, P.; Contini, A.; Kay, J. A.; Clubb, J. W. *Novel Energetic Phosphazene Polymer Binder Systems for Environmentally Friendly Rocket Motor Propellants*; SERDP WP-2141; Naval Air Warfare Center Weapons Division, Naval Air Systems Command: China Lake, CA, **2015**.

[48] Golding, P.; Trussell, S. J. Energetic polyphosphazenes – a new category of binders for energetic formulations. In *NDIA Insensitive Munitions and Energetic Materials Technology Symposium*, San Francisco, CA, U.S.A., November 15–17, **2004**.

[49] Cheng, T. Review of novel energetic polymers and binders – high energy propellant ingredients for the new space race. *Des. Monomers Polym.* **2019**, *22*, 54-65.

[50] Bolton, P. R.; Golding, P.; Murray, C. B.; Till, M. K.; Trussell, S. J. *Enhanced Energetic Polyphosphazenes*; Atomic Weapons Establishment: Aldermaston, Reading, Berkshire, RG7 4PR, UK, **2006**. https://imemg.org/wp-content/uploads/IMEMTS%202006_Golding_paper9B.pdf (accessed 2022-03-12).

[51] Manser, G. E. Energetic Copolymers and method of making same. US 4 483 978, **1984**.

[52] Manser, G. E.; Hajik R. M. Method of synthesizing nitrato alkyl oxetanes. US 5 214 166, **1993**.

[53] Carpenter, W. R. Process for synthesis of various tetrazoles. US 3 138 609, **1964**.

[54] Frankel, M. B.; Wilson, E. R. Energetic azido monomers. *J. Chem. Eng. Data* **1981**, *26*, 219-219.

[55] Colclough, M. E.; Desai, H.; Millar, R. W.; Paul, N. C.; Stewart, M. J.; Golding, P. Energetic polymers as binders in composite propellants and explosives. *Polym. Adv. Technol.* **1994**, *5*, 554-560.

[56] Cheradame, H.; Andreolety, J. P.; Rousset, E. Synthesis of polymers containing pseudohalide groups by cationic polymerization, 1. Homopolymerization of 3,3-bis(azidomethyl)oxetane and its copolymerization with 3-chloromethyl-3-(2,5,8-trioxadecyl)oxetane. *Makromol. Chem.* **1991**, *192*, 901-918.

[57] Manser, G. E.; Miller, R. S. Thermoplastic elastomers having alternate crystalline structure for us as high energy binders. US 5 210 153, **1993**.

[58] Baum, K.; Berkowitz, P. T.; Grakauskas, V.; Archibald, T. G. Synthesis of electron-deficient oxetanes. 3-Azidooxetane, 3-nitrooxetane, and 3,3-dinitrooxetane. *J. Org. Chem.* **1983**, *48*, 2953-2956.

[59] Grakauskas, V.; Berkowitz, P. T.; Baum, K. Synthesis and polymerization of 3-azidooxetane. US 4 414 384, **1983**.

[60] Wojtowicz, J. A.; Polak, R. J. 3-Substituted oxetanes. *J. Org. Chem.* **1973**, *38*, 2061-2066.

[61] Elrick, D. E.; Gardner, W. H.; Marans, N. S.; Preckel, R. F. Preparation of Halides of Pentaerythritol Trinitrate1. *J. Am. Chem. Soc.* **1954**, *76*, 1374-1375.

[62] Mukhametshin, T. I.; Sharipov, R. I.; Petrov, V. A.; Kostochko, A. V.; Vinogradov, D. B.; Bulatov, P. V. Energy-Intensive Random Block Copolymers of 3,3-Bis(nitratomethyl)oxetane and 3-Azidomethyl-3-Methyloxetane. *Propellants, Explos. Pyrotech.* **2018**, *43*, 1115-1121.

[63] Carolan, S. Routes to simple 3-substituted oxetanes. Ph. D. Dissertation, University of Salford, Salford, United Kingdom, **1992**.

[64] Manser, G. E.; Malik, A. A.; Archibald, T. G. 3-Azidomethyl-3-Nitratomethyloxetane, US 5 489 700, **1996**.

[65] Born, M.; Plank, J.; Klapötke, T. M. Energetic Polymers: A Chance for Lightweight Reactive Structure Materials? *Propellants, Explos. Pyrotech.* **2022**, *47*, e202100368.

[66] Leeming, W.; Marshall, E.; Bull, H.; Rodgers, M.; Paul, N. An investigation into polyGLYN cure stability. In *25th International Annual Conference of the Fraunhofer ICT, Energetic Materials – Past, Present and Future,* Karlsruhe, Germany, June 25–28, **1996**.

[67] Baum, K.; Lin, W. H.; Willer, R. L. Synthesis of poly-(3-nitratooxetane). US 8 030 440 B1, **2011**.

[68] Born, M.; Karaghiosoff, K.; Klapötke, T. M. A GAP Replacement: Improved Synthesis of 3-Azidooxetane and Its Homopolymer Based on Sulfonic Acid Esters of Oxetan-3-ol. *J. Org. Chem.* **2021**, *86*, 12607-12614.

[69] Ampleman, G.; Brousseau, P.; Thiboutot, S.; Dubois, C.; Diaz, E. Insensitive melt cast explosive compositions containig energetic thermoplastic elastomers. EP 1167324 B1, **2002**.

[70] Hamilton, S. R.; Hatch, R. L.; Lund, G. K.; Wardle, R. B. BAMO/AMMO propellant formulations. WO 001 995 009 824 A1, **1995**.

[71] Nuyken, O.; Pask, S. D. Ring-Opening Polymerization—An Introductory Review. *Polymers* **2013**, *5*, 361-403.

[72] Horie, K.; Barón, M.; Fox, R. B.; He, J.; Hess, M.; Kahovec, J.; Kitayama, T.; Kubisa, P.; Maréchal, E.; Mormann, W.; Stepto, R. F. T.; Tabak, D.; Vohlídal, J.; Wilks, E. S.; Work, W. J. Definitions of terms relating to reactions of polymers and to functional polymeric materials (IUPAC Recommendations 2003). *Pure Appl. Chem.* **2004**, *76*, 889-906.

[73] Searles, S. Oxetanes and Oxetenes. In *Comprehensive Heterocyclic Chemistry*; Katritzky, A. R., Rees, C. W., Eds.; Vol. 7; Pergamon: Oxford, **1984**; pp 363-402.

[74] Thompson, J. Oxetane - Drug Development, Synthesis & Applications. Dong Group Literature Seminar, September 24, **2014**.
http://gbdong.cm.utexas.edu/seminar/old/Oxetane%20Presentation.pdf (accessed 2022-03-18)

[75] Wuitschik, G.; Carreira, E. M.; Wagner, B.; Fischer, H.; Parrilla, I.; Schuler, F.; Rogers-Evans, M.; Müller, K. Oxetanes in Drug Discovery: Structural and Synthetic Insights. *J. Med. Chem.* **2010**, *53*, 3227-3246.

[76] Dreyfuss, M. P.; Dreyfuss, P. Oxetane Polymers. In *Encyclopedia of Polymer Science and Technology*, (Ed.), John Wiley & Sons: Hoboken, New Jersey, **2011**. DOI 10.1002/0471440264.pst520

[77] Reboul, M. Oxede de Propylene Normal et Poluoxypropylenes. *Ann. Chim. (Paris)* **1878**, *14*, 495–497.

[78] Luger, P.; Buschmann, J. Oxetane: the first x-ray analysis of a nonsubstituted four-membered ring. *J. Am. Chem. Soc.* **1984**, *106*, 7118-7121.

[79] Fernandez, J.; Myers, R. J.; Gwinn, W. D. Microwave Spectrum and Planarity of the Ring of Trimethylene Oxide. *J. Chem. Phys.* **1955**, *23*, 758-759.

[80] Bull, J. A.; Croft, R. A.; Davis, O. A.; Doran, R.; Morgan, K. F. Oxetanes: Recent Advances in Synthesis, Reactivity, and Medicinal Chemistry. *Chem. Rev.* **2016**, *116*, 12150-12233.

[81] Searles Jr., S. Oxetanes In *Chemistry of Heterocyclic Compounds*; Weissberger, A., Ed.; John Wiley & Sons: Hoboken, New Jersey, **1964**; pp 983-1068.

[82] Schleyer, P. v. R.; Williams, J. E.; Blanchard, K. R. Evaluation of strain in hydrocarbons. The strain in adamantane and its origin. *J. Am. Chem. Soc.* **1970**, *92*, 2377-2386.

[83] Searles, S.; Tamres, M. Hydrogen Bond Formation with Saturated Cyclic Ethers[1]. *J. Am. Chem. Soc.* **1951**, *73*, 3704-3706.

[84] Burkhard, J. A.; Wuitschik, G.; Rogers-Evans, M.; Müller, K.; Carreira, E. M. Oxetanes as Versatile Elements in Drug Discovery and Synthesis. *Angew. Chem. Int. Ed.* **2010**, *49*, 9052-9067.

[85] West, R.; Powell, D. L.; Lee, M. K. T.; Whatley, L. S. Hydrogen Bonding Studies. IX. The Thermodynamics of Hydrogen Bonding of Phenol to Ethers and Related Compounds. *J. Am. Chem. Soc.* **1964**, *86*, 3227-3229.

[86] Wuitschik, G. Oxetanes in Drug Discovery. Ph. D. Dissertation, Swiss Federal Institute of Technology (ETH) Zürich, Zürich, Switzerland, **2008**.

[87] Wani, M. C.; Taylor, H. L.; Wall, M. E.; Coggon, P.; McPhail, A. T. Plant antitumor agents. VI. Isolation and structure of taxol, a novel antileukemic and antitumor agent from Taxus brevifolia. *J. Am. Chem. Soc.* **1971**, *93*, 2325-2327.

[88] Omura, S.; Murata, M.; Imamura, N.; Iwai, Y.; Tanaka, H.; Furusaki, A.; Matsumoto, T. Oxetin, a New Antimetabolite from an Actinomycete. Fermentation, Isolation, Structure and Biological Activity. *J. Antibiot.* **1984**, *37*, 1324-1332.

[89] Huang, J.-m.; Yokoyama, R.; Yang, C.-s.; Fukuyama, Y. Merrilactone A, a novel neurotrophic sesquiterpene dilactone from Illicium merrillianum. *Tetrahedron Lett.* **2000**, *41*, 6111-6114.

[90] Vil, V.; Terent'ev, A. O.; Al Quntar, A. A. A.; Gloriozova, T. A.; Savidov, N.; Dembitsky, V. M. Oxetane-containing metabolites: origin, structures, and biological activities. *Appl. Microbiol. Biotechnol.* **2019**, *103*, 2449-2467.

[91] Wuitschik, G.; Rogers-Evans, M.; Müller, K.; Fischer, H.; Wagner, B.; Schuler, F.; Polonchuk, L.; Carreira, E. M. Oxetanes as Promising Modules in Drug Discovery. *Angew. Chem. Int. Ed.* **2006**, *45*, 7736-7739.

[92] Carreira, E. M.; Fessard, T. C. Four-Membered Ring-Containing Spirocycles: Synthetic Strategies and Opportunities. *Chem. Rev.* **2014**, *114*, 8257-8322.

[93] Wuitschik, G.; Rogers-Evans, M.; Buckl, A.; Bernasconi, M.; Märki, M.; Godel, T.; Fischer, H.; Wagner, B.; Parrilla, I.; Schuler, F.; Schneider, J.; Alker, A.; Schweizer, W. B.; Müller, K.; Carreira, E. M. Spirocyclic Oxetanes: Synthesis and Properties. *Angew. Chem. Int. Ed.* **2008**, *47*, 4512-4515.

[94] Burkhard, J. A.; Wuitschik, G.; Evans, M. R.; Müller, K.; Carreira, E. M. Oxetanes as Unique Building Blocks in Medicinal Chemistry. *Medchem news* **2012**, *22*, 8-15.

[95] Mahal, A. Oxetanes as versatile building blocks in the total synthesis of natural products: An overview. *Eur. J. Chem.* **2015**, *6*, 357-366.

[96] Searles Jr., S. Oxetanes In Chemistry of Heterocyclic Compounds; Weissberger, A., Ed.; John Wiley & Sons: Hoboken, New Jersey, 2008; Vol. 19; pp 983-1068. DOI 10.1002/9780470239704.ch9

[97] Forsberg, G. Rate Constants and Reaction Products of the Alkaline Hydrolysis of Ethylene and Trimethylene Chlorohydrins with Alkyl Substituents. *Acta Chem. Scand.* **1954**, *8*, 135–136.

[98] Fischer, W.; Grob, C. A. Competing Fragmentation, Substitution and Elimination in the Solvolysis of Alkylated 3-Chloropropanols and their Ethers. Fragmentation reactions no. 28. *Helv. Chim. Acta* **1978**, *61*, 2336-2350.

[99] Paterno, E. Sintesi in chimica organica per mezzo della luce. Nota II. Composti degli idrocarburi non saturi con aldeidi e chetoni. *Gazz. Chim. Ital.* **1909**, *39*, 341.

[100] Büchi, G.; Inman, C. G.; Lipinsky, E. S. Light-catalyzed Organic Reactions. I. The Reaction of Carbonyl Compounds with 2-Methyl-2-butene in the Presence of Ultraviolet Light. *J. Am. Chem. Soc.* **1954**, *76*, 4327-4331.

[101] Xue, J.; Zhang, Y.; Wu, T.; Fun, H.-K.; Xu, J.-H. Photoinduced [2 + 2] cycloadditions (the Paterno–Büchi reaction) of 1H-1-acetylindole-2,3-dione with alkenes. *J. Chem. Soc. Perkin Trans. 1* **2001**, 183-191.

[102] Welch, S. C.; Rao, A. S. C. P. A convenient one-step synthesis of 2,2-disubstituted oxetanes from ketones. *J. Am. Chem. Soc.* **1979**, *101*, 6135-6136.

[103] https://spirochem.com/catalog/oxetanes.html (accessed 2022-03-05)

[104] Farthing, A. C.; Reynolds, R. J. W. Synthesis and properties of a new polyether: Poly-3,3-bis(chloromethyl)-1-oxabutene. *J. Polym. Sci.* **1954**, *12*, 503-507.

[105] Dreyfuss, M. P.; Dreyfuss, P. p-Chlorophenyldiazonium hexafluorophosphate as a catalyst in the polymerization of tetrahydrofuran and other cyclic ethers. *J Polym. Sci. A1: Polym. Chem.* **1966**, *4*, 2179-2200.

[106] Endo, T. General Mechanisms in Ring-Opening Polymerization. In *Handbook of Ring-Opening Polymerization*; Dubois P.; Coulembier, O.; Raquez, J.-M., Eds.; Wiley-VCH: Weinheim, **2009**; pp 53-63.

[107] Hafner, S. Internal plasticized glycidyl azide copolymers for energetic solid propellant binders. Ph. D. Dissertation, Ludwig-Maximilian University (LMU) Munich, Munich, Germany, **2019**.

[108] Biedron, T.; Kubisa, P.; Penczek, S. Polyepichlorohydrin diols free of cyclics: Synthesis and characterization. *J. Polym. Sci.* **1991**, *29*, 619-628.

[109] Vandenberg, E. J. Epoxide polymers: Synthesis, stereochemistry, structure, and mechanism. *J Polym. Sci. A1: Polym. Chem.* **1969**, *7*, 525-567.

[110] Garaev, I. K.; Kostochko, A. V.; Petrov, A. I.; Ibragimov, E. N.; Golubev, A. E. Synthesis of azidooxetane statistical polymers and copolymers. *Russ. J. Gen. Chem.* **2016**, *86*, 1459-1468.

[111] Mukhametshin, T. I.; Petrov, A. I.; Kuznetsova, N. V.; Petrov, V. A.; Averianova, N. V.; Garaev, I. K.; Kostochko, A. V.; Gubaidullin, A. T.; Vinogradov, D. B.; Bulatov, P. V. Synthesis and copolymerization of azidomethyl-substituted oxetanes: the morphology of statistical block copolymers. *Chem. Heterocycl. Compd.* **2017**, *53*, 811-821.

[112] Kawamoto, A. M.; Diniz, M. F.; Lourenco, V. L.; Takahashi, M. F.; Keicher, T.; Krause, H.; Menke, K.; Kempa, P. B. Synthesis and characterization of GAP/BAMO copolymers applied at high energetic composite propellants. *J. Aerosp. Technol.* **2010** *2*, 307-322.

[113] Goethals, E. J. Cyclic Oligomers in the Cationic Polymerization of Heterocycles. *Pure Appl. Chem.* **1976**, *48*, 335-341.

[114] Penczek, S.; Cypryk, M.; Duda, A.; Kubisa, P.; Słomkowski, S. Living ring-opening polymerizations of heterocyclic monomers. *Prog. Polym. Sci.* **2007**, *32*, 247-282.

[115] Penczek, S.; Kubisa, P.; Matyjaszewski, K. *Cationic Ring-Opening Polymerization: 2. Synthetic Applications*; Springer: Berlin, Heidelberg, **1985**.

[116] Duda, A.; Kowalski, A. Thermodynamics and Kinetics of Ring-Opening Polymerization. In *Handbook of Ring-Opening Polymerization*; Dubois P.; Coulembier, O.; Raquez, J.-M., Eds.; Wiley-VCH: Weinheim, 2009; pp 1-51.

[117] Barbieri, U.; Keicher, T.; Polacco, G. Homo- and copolymers of 3-tosyloxymethyl-3-methyloxetane (TMMO) as precursors to energetic azido polymers. *e-Polymers* **2009**, *9*, 565.

[118] Kubisa, P.; Penczek, S. Cationic activated monomer polymerization of heterocyclic monomers. *Prog. Polym. Sci.* **1999**, *24*, 1409-1437.

[119] Kubisa, P.; Bednarek, M.; Biedroń, T.; Biela, T.; Penczek, S. Progress in activated monomer polymerization. Kinetics of AM polymerization. *Macromol. Symp.* **2000**, *153*, 217-226.

[120] Penczek, S. Cationic ring-opening polymerization (CROP) major mechanistic phenomena. *J. Polym. Sci.* **2000**, *38*, 1919-1933.

2 Motivation, Objectives, and Strategies

The main objective of this thesis was the synthesis, characterization, and investigation of new and high-performing oxetane derivatives and the preparation of energetic polyether polymers thereof. Besides new compounds, another important focus was the synthesis optimization of literature known oxetane species, which appear promising for further derivatization or direct preparation of energetic polymers as well as precursor polymers. The necessity and need for this task can be directly derived from the available literature on energetic materials in general and especially on available energetic binders:

A closer look at the state of the art quickly reveals that the field is dominated by only five key polymers, including PGN, GAP, poly(AMMO), poly(BAMO), and poly(NIMMO), as well as thermoplastic copolymers derived from these, such as poly(BAMO-*co*-THF). While PGN was already developed in 1953 in the course of the first PBX and GAP in 1970, the latter energetic polyoxetanes originate from the 1980s and early 1990s. Since then, the development of new monomers and binders has largely stagnated, which is problematic considering their properties. Chemically, the corresponding monomers can be subdivided into a group of azides, which exhibit a disadvantageous oxygen balance together with an acceptable thermostability (> 200 °C), and a group of nitrate esters, which offer a better oxygen balance at the price of low thermostability (<< 200 °C). According to EXPLO5 calculations (Table 1), one common feature is their low performance, which barely approaches that of TNT as an almost outdated secondary explosive.

Table 2.1. Calculated performance of the most important prior art monomers in comparison to TNT.

	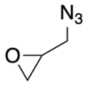	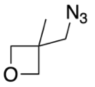	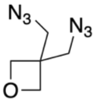	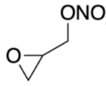	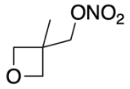	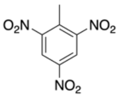
Acronym	**GA**	**AMMO**	**BAMO**	**GLYN**	**NIMMO**	**TNT**
Formula	$C_3H_5N_3O$	$C_5H_9N_3O$	$C_5H_8N_6O$	$C_3H_5NO_4$	$C_5H_9NO_4$	$C_7H_5N_3O_6$
Ω [CO][a] [%]	−72.7	−107.0	−76.1	−60.5	−76.1	−25.3
$T_{dec.}$[b] [°C]	213	210	207	-	170	290
$-\Delta_E U°$[c] [kJ·kg^{-1}]	4445	3411	4479	4852	3949	4380
$T_{C\text{-}J}$[d] [K]	2794	2086	2786	3279	2507	3190
$p_{C\text{-}J}$[e] [GPa]	10.6	7.69	12.4	15.8	10.6	18.7
$D_{C\text{-}J}$[f] [m·s^{-1}]	6129	5544	6548	6664	5906	6809
V_0[g] [dm^3·kg^{-1}]	828	803	797	829	827	640

[a] Oxygen balance based on CO formation. [b] Decomposition temperature (DSC, β = 5 °C·min^{-1}). [c] Detonation energy. [d] Detonation temperature. [e] Detonation pressure. [f] Detonation velocity. [g] Volume of detonation gases at standard temperature and pressure.

Their respective polymers were originally designed to replace inert binders, as their addition to formulations was too detrimental to the overall performance. However, research into energetic materials in recent decades has ostensibly been aimed at higher performance of propellants and explosives. In this respect, there is an ever-increasing performance gap between modern developments and existing binders. Since higher performance is generally accompanied by higher sensitivity, a need arises for higher-performing and more insensitive polymer binders. Therefore, it is of the utmost importance to first and foremost lessen the lack of suitable monomers by developing monomers with an improved balance between performance, thermostability, insensitivity, and oxygen balance.

However, to render new compounds attractive for an application in the HEDM sector, it is often not enough to achieve the properties in demand. It is equally significant that they are cost-effective, so expensive reagents and poorly scalable purification methods should be avoided. Likewise, multi-step syntheses should be avoided as far as possible, or the individual steps should be characterized by a high yield and selectivity. For this reason, the present work made mainly use of commercially available oxetane building blocks (**1**–**5**) or compounds that can be prepared at low cost in a scalable fashion on the laboratory scale (**4**–**6**) (Figure 1). This contributes significantly to a high availability of the required starting materials for the prepared target compounds and facilitates their scale-up.

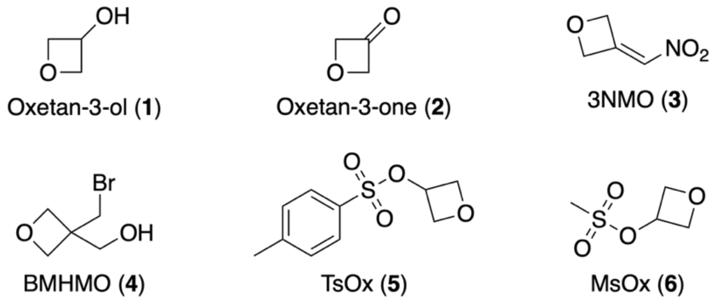

Figure 2.1. Well-suited oxetane building blocks for the preparation of new energetic monomers.

As a major objective of the present work was to explore the feasible performance limits of oxetane monomers and to surpass the state of the art in this regard, the oxetane ring itself posed a major challenge. The oxetane ring introduces a high carbon-hydrogen ballast which has a strong "diluting" effect on the overall performance, while the energetic contribution of its ring strain is almost negligible. For instance, the ring motif of a 3-substituted oxetane (C_3H_5O) requires 3.75 equivalents of oxygen (O_2) for complete combustion.

Therefore, 3,3-disubstituted oxetanes appear beneficial as they allow a higher loading of the scaffold with explosophoric groups to compensate for this influence. Unfortunately, as these are mostly electron-withdrawing, a direct attachment at C3 of the ring leads to reduced basicity of the ring oxygen atom and thus reduced polymerizability. Hence, methylene groups are often used as spacers (compound **4**), which in turn increase the adverse carbon-hydrogen ballast. Therefore, a novel concept was implemented – the use of larger, energetic structural motifs as substituents to shift the structural weighting on these, mitigating the oxetane ring's influence, which at best offers a certain combustion potential. For example, classical nitroaromatics (**A**) or nitrogen-rich heterocycles were used (**B**, **C**, **D**), as depicted in Figure 2. Desirably high performance was achieved in this way, meeting the described objective and the use of well-investigated explosives as substituents renders the compounds very scalable. In addition, and albeit based on a different synthesis strategy, compound **E** established a new performance benchmark in the field of energetic oxetanes.

Another objective was to take first steps toward polymerizable primary explosives. In this context, compound **C** is characterized by a fast DDT, which is otherwise common for primary explosives, and a low impact sensitivity (2–3 J) just like compound **E** (IS: < 1 J), which is also extremely sensitive to friction (FS: 1 N). However, compound **E** responds to mechanical or thermal stimuli only with deflagration.

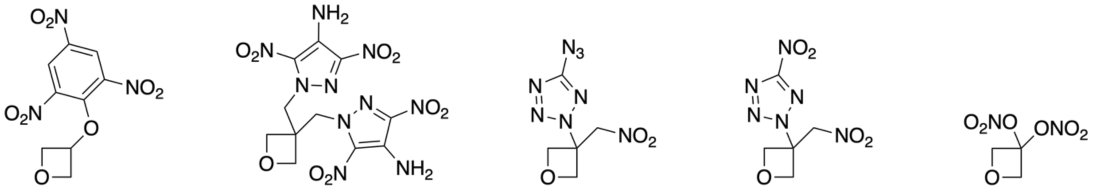

TNPO (**A**)
VoD: 6891ms^{-1}
$p_{C\text{-}J}$: 19.5 GPa

B
VoD: 7335 ms^{-1}
$p_{C\text{-}J}$: 20.9 GPa

C
VoD: 7159 ms^{-1}
$p_{C\text{-}J}$: 18.7 GPa

D
VoD: 7686 ms^{-1}
$p_{C\text{-}J}$: 23.5 GPa

E
VoD: 8275 ms^{-1}
$p_{C\text{-}J}$: 29.7 GPa

Figure 2.2. Selection of prepared monomers with improved energetic performance compared to prior art energetic oxetanes.

Regarding the polymer-chemical part of this thesis, it must be stated that GAP has prevailed over all other energetic binders due to its advantageous properties and is commercially available nowadays. Since GAP was patented in 1972, the industry has adapted to the production and application of GAP as a binder, especially since it meets all technical requirements in the best possible way. For 50 years, no other binder has accomplished to "beat" GAP. Therefore, it seemed promising to identify a polymer that is very similar but offers superior properties. Hence, another major focus was to render the constitutional isomer, 3-azidooxetane, more accessible and to compare its properties with those of glycidyl azide. This seemed overdue, as only the polymer (GAP) was found to be adequately described in the literature. In addition, poly(3-azidooxetane) was prepared via cationic ring-opening polymerization and thoroughly investigated as a potential, industry-friendly surrogate for GAP due to its similar physico-chemical properties in combination with advantages like a uniform termination with primary hydroxy groups to provide improved curing results.

As first studies (chapter 9) indicated the suitability of poly(3-azidooxetane), a linked objective was to obtain the polymer via polymer-analogous transformation in higher yield and with enhanced safety by avoiding manipulation of the rather sensitive 3-azidooxetane. For this purpose, the new polymers poly(3-mesyloxyoxetane) and poly(3-tosyloxyoxetane) were prepared, as they do not only afford poly(3-azidooxetane) upon azidation but can also be utilized for the synthesis of various energetic binders via nucleophilic displacement reactions. Ultimately, poly(3-azidooxetane) turned out as a very promising if not fully adequate GAP replacement.

Another research topic was to break new ground in the field of energetic polymers. These have so far only been considered as binders but also represent an interesting alternative to metal-based reactive structural materials. While the latter are heavy, require atmospheric oxygen, and offer little performance, this does not apply to energetic polymers. Therefore, they hold the potential of considerable weight savings together with increased operational ranges and enhanced performance of various weapon systems. However, completely different monomer structures than currently available are required to achieve glass transition temperatures above operational temperatures and mechanically durable materials. In terms of an initial feasibility study, a monomer of suitable structure (TPNO, **A**) was copolymerized with known energetic oxetanes. Here, the glass transition temperature increasing character of the TNPO repeating unit on the obtained copolymers was impressively demonstrated, and a performance in the range of TNT was obtained even under non-optimized conditions, underlining the general potential of polymeric RSMs.

Last but not least, the continuous research into energetic materials constantly provides new compounds, causing a need for methods that allow their characterization in small quantities for safety and cost reasons. One method that allows quite far-reaching conclusions to be drawn about the sensitivity of compounds based on their crystal structure is the Hirshfeld Surface Analysis (HSA) in combination with the 2D fingerprinting method. For this reason, a side-objective was to apply the method to the prepared monomers to evaluate its usefulness accordingly. This is an important task because a deeper understanding of structure-property relationships of energetic materials and a refinement of the HSA can contribute substantially to an improved design of future energetic materials.

3 Summary and Conclusion

Chapters 4–11 have been published in peer-reviewed scientific journals. The content of each chapter is consistent with the respective publication. However, the layout of the articles has been modified to provide a consistent layout of the thesis. In this chapter, a brief summary of the respective results is presented.

3.1 Chapter 4: Investigation of Structure–Property Relationships of Three Nitroaromatic Compounds: 1-Fluoro-2,4,6-trinitrobenzene, 2,4,6-Trinitrophenyl Methanesulfonate, and 2,4,6-Trinitrobenzaldehyde

Improved synthetic protocols were used for the preparation of 1-fluoro-2,4,6-trinitrobenzene (**1**), 2,4,6-trinitrophenyl methanesulfonate (**2**), and 2,4,6-trinitrobenzaldehyde (**3**) which form a group of trinitrobenzene derivatives. The compounds were intensively characterized, and their structures were elucidated via single-crystal X-ray diffraction (Figure 1).

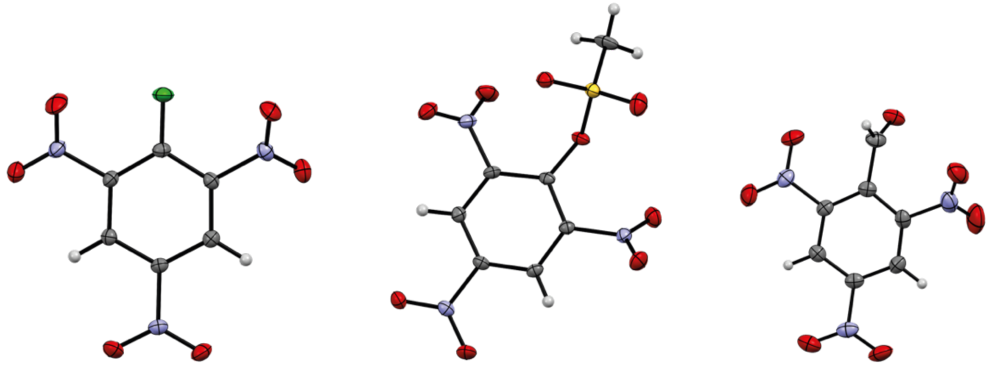

Figure 3.1. Molecular structure of compounds **1**–**3** in the crystal. Ellipsoids drawn at the 50% probability level.

The results presented in chapter 4 provide an improved insight into the structure-property relationships of compounds **1**–**3**. A key finding is that very few but strong, stabilizing interactions in the crystal may provide the same extent of stability and insensitivity as far more numerous but weaker stabilizing interactions. Thus, a compensatory effect exists.

This confirmed the postulated trends between the distribution of stabilizing and destabilizing close-contact interactions in the crystal and the sensitivity of an energetic material found in other publications dealing with Hirshfeld Surface Analysis. The prepared compounds were classified as secondary explosives comparable to 2,4,6-trinitrotoluene (TNT) regarding their performance. According to EXPLO5 calculations, the latter decreases from **1** over **3** to **2**. In general, due to the leaving groups present, compounds **1** and **2** can be utilized to prepare corresponding trinitrobenzene derivatives via nucleophilic aromatic substitution reactions.

3.2 Chapter 5: Improved Preparation of 3-Oximinooxetane – An Important Precursor to Energetic Oxetanes

An improved, fast and cost-efficient synthesis of 3-oximinooxetane (**1**) is presented. While the compound was scarcely and insufficiently described in the literature, it has now been characterized in great detail – also with regard to its energetic properties. Furthermore, the structure of 3-oximinooxetane was elucidated by single-crystal X-ray diffraction (Scheme 1).

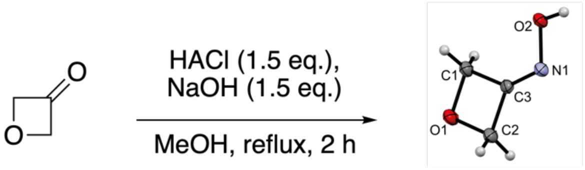

1 (92%)

Scheme 3.1. Improved preparation of 3-oximinooxetane and molecular structure in the crystal. Ellipsoids drawn at the 50% probability level.

Starting from oxetan-3-one, oxime **1** can be prepared in high yield and purity using commercially available materials. Calculations using the EXPLO5 V6.04 thermochemical code showed that the oxime exhibits a notable energetic performance which is in the range of literature-known energetic oxetane monomers such as NIMMO or BAMO.

The results of chapter 5 do not only show that 3-oximinooxetane can be easily obtained in a more straightforward procedure than before, but its high insensitivity (IS: 40 J, FS: 360 N) also allows very safe handling. This renders oxime **1** a suitable and versatile precursor for the synthesis of 3-aminooxetane, 3-nitrooxetane, and 3,3-dinitrooxetane via known single-step reactions for the transformation of the oximino group. These represent valuable monomers for the preparation of energetic polymers.

3.3 Chapter 6: 3,3-Dinitratooxetane – An Important Leap Towards Energetic Oxygen-Rich Monomers and Polymers

A series of simple but highly oxygen-rich oxetane monomers is presented comprising 3-nitratomethyl-3-methyloxetane (**3**), 3-nitratooxetan (**2**), and 3,3-dinitratooxetan (**1**). Having nitrato groups as an oxygen source in common, the oxygen balance (Ω_{CO}) of these compounds increases stepwise from −42.1% over −20.1% to +17.8%, rendering 3,3-dinitratooxetan (DNO, **1**) the most oxygen-rich oxetane species known today. With a calculated (EXPLO5 V6.04) detonation velocity of 8275 ms^{-1} and a detonation pressure of 29.7 GPa, DNO also represents the currently most powerful oxetane derivative.

The geminal nitrate **1** was obtained via addition of dinitrogen pentoxide to oxetan-3-one. In contrast, the organic nitrates **2** and **3** were obtained by esterification of the corresponding alcohols using acetyl nitrate and dinitrogen pentoxide, respectively (Scheme 2). All compounds were intensively characterized and single-crystals of DNO allowed the determination of its crystal structure through X-ray diffraction.

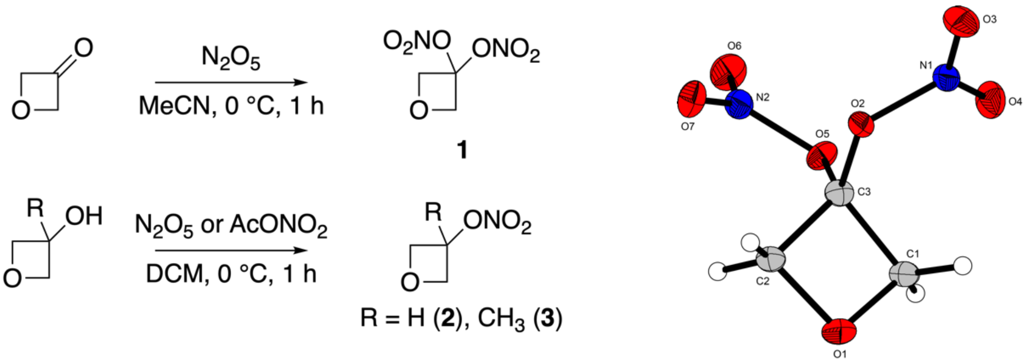

Scheme 3.2. Preparation of compounds **1**–**3** and molecular structure of compound **1** in the crystal (ellipsoids drawn at the 50% probability level).

Contrary to expectation, the obtained data indicates no particular correlation between the substitution at C3 of compounds **1**–**3** and their sensitivity as well as thermal stability.

Due to the most advantageous combination of cost, insensitivity, thermostability, and performance, compound **2** represents the most attractive monomer for the preparation of energetic binders. As a constitutional isomer to glycidyl nitrate (GLYN), it can serve as a potential, advantageous surrogate. However, the low thermostability of compounds **1** and **3** is likely to exclude them from practical applications. Nevertheless, compound **1** represents a new benchmark in terms of oxygen content and performance to stimulate further research. In addition, its high friction and impact sensitivity (IS: < 1 J, FS: 1 N) suggests the general feasibility of polymerizable primary explosives.

3.4 Chapter 7: Oxetane Monomers Based On the Powerful Explosive LLM-116: Improved Performance, Insensitivity, and Thermostability.

The field of energetic binders is essentially defined by the polyethers GAP, poly(AMMO), poly(BAMO), poly(NIMMO), and poly(GLYN). Unfortunately, their energetic contribution in formulations is very limited, as they exhibit performances even far below TNT as an almost outdated secondary explosive. Further, their sensitivity toward impact is rather high (< 8 J). The corresponding organic nitrate monomers (GLYN, NIMMO) lack thermostability, while the azides (AMMO, BAMO) offer a poor oxygen balance. Thus, monomers with an improved interplay of aforementioned key aspects are highly desirable. In chapter 7, a new synthetic concept addressed this problem – the functionalization of a suitable oxetane scaffold with secondary explosives.

For this purpose, 3-bromomethyl-3-hydroxymetyloxetane (BMHMO) was chosen as inexpensive, scalable starting material and its synthesis has been significantly optimized.

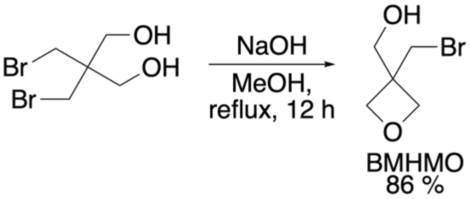

Scheme 3.3. Improved preparation of the starting material BMHMO.

Due to its high performance and scalability (pilot plant scale), LLM-116 (4-amino-3,5-dinitro-1*H*-pyrazole) was chosen for the functionalization of BMHMO and four LLM-116 derivatives were synthesized, intensively characterized and their structures elucidated by single-crystal X-ray diffraction.

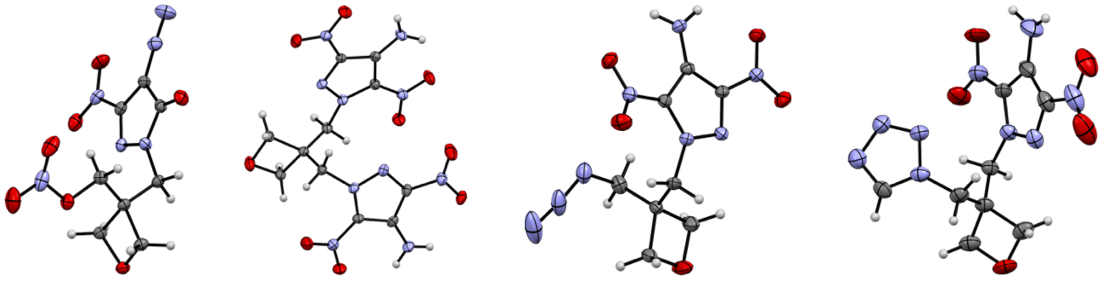

4 **7** **8** **9A**

Figure 3.2. Molecular structures of compound **4** and **7**–**9** in the crystal. Ellipsoids drawn at the 50% probability level.

The results of chapter 7 allow to conclude that the aforementioned concept can furnish monomers with substantially enhanced properties. With the exception of compound **4**, all monomers prepared are characterized by a superior thermostability (> 230 °C) and a great insensitivity toward mechanical stimuli (FS: > 360 N, IS: > 40 J) compared to the prior art. Their insensitivity was impressively demonstrated by initiation tests and SSRT tests. The performance of the presented compounds is comparable to TNT (**8**, **9**B) or even notably higher (**4**, **7**, **9**A). Due to their properties, monomers **7**–**9** are especially suitable for preparing insensitive polymers for application in low-vulnerability ammunitions.

Table 3.1. Brief comparison of compound **7** with the state-of-the-art monomer **NIMMO** with regard to performance (calculated, EXPLO5 V6.04) and oxygen balance.

	7	**NIMMO**
VoD [ms^{-1}]	7335	5906
$p_{C\text{-}J}$ [GPa]	20.9	10.6
$T_{dec.}$ [°C]	246	170
Ω [CO] [%]	−29.9	−59.8

3.5 Chapter 8: 3-Nitromethyleneoxetane: A Very Versatile and Promising Building Block for Energetic Oxetane Based Monomers

Energetic binders are vastly used in propellant and explosive formulations. While the performance of energetic fillers is constantly increasing, state-of-the-art binders have already been developed in the 1970s and 1980s and show comparatively poor performances. Therefore, the development of new high-performing monomers is a necessary and overdue task. Although tetrazoles have proven to be excellent motifs for the synthesis of powerful compounds, corresponding oxetane derivatives are essentially unknown. In this context, 3-(nitromethylene)oxetane (NMO), which has recently become commercially available, was identified as a promising platform for the preparation of such derivatives in elegant one-step reactions, making use of the Aza-Michael addition.

1*H*-Tetrazole and 1*H*-tetrazole-5-amine were chosen as inexpensive, commercially available Michael-donors, while the rather exotic tetrazole derivatives 5-azido-1*H*-tetrazole and 5-nitro-2*H*-tetrazole were selected to achieve exceptional performance.

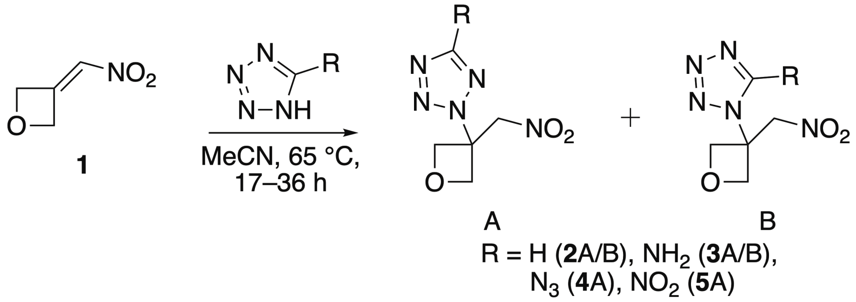

Scheme 3.4. Preparation of highly energetic tetrazole-based oxetane monomers via conjugate addition.

The respective products were intensively characterized and further investigated through computational methods and several practical tests. Their structures were determined by single-crystal X-ray diffraction.

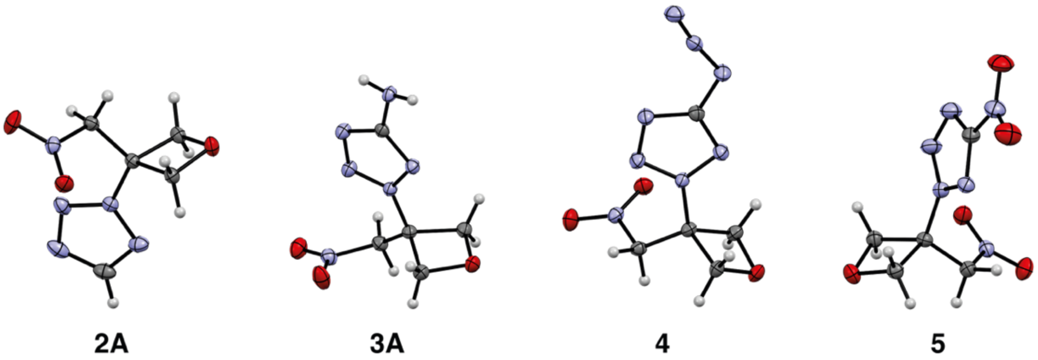

Figure 3.3. Molecular structures of compounds **2**–**5** in the crystal. Ellipsoids drawn at the 50% probability level.

The results confirm that NMO can indeed furnish high-performing monomers in simple synthetic procedures using suitable Michael-Donors such as azoles. The performance of compounds **2** and **3** is comparable to TNT, while compounds **4** and **5** outperform TNT, placing them among the most powerful oxetanes known. Considering the parent compounds, surprisingly low sensitivities were found for compounds **4** and **5**. However, these could be explained by the extent of stabilizing interactions in the crystal, as revealed by Hirshfeld Surface Analysis. This demonstrates that even very sensitive materials can be used to synthesize useful energetic compounds, as long as the target compound's design allows sufficient stabilization through beneficial interactions in the crystal. Apart from that, compound **4** partially exhibits properties typical of primary explosives such as a fast DDT. Thus, it strongly indicates the feasibility of energetic oxetanes leading to polymeric primary explosives (covalent) as a new substance class in the near future.

3.6 Chapter 9: A GAP Replacement: Improved Synthesis of 3-Azidooxetane and Its Homo-polymer Based on Sulfonic Acid Esters of Oxetan-3-ol

Since literature methods largely failed to provide 3-azidooxetane in acceptable yield and purity, an improved preparation method was developed. Here, the azide (**3**) is obtained via a nucleophilic substitution reaction between the sulfonic acid ester 3-tosyloxyoxetane (**1**) or 3-mesyloxyoxetane (**2**) and sodium azide using DMSO as an environmentally benign solvent.

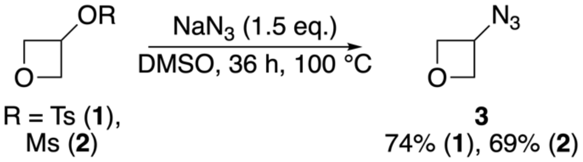

Scheme 3.5. Improved preparation of 3-azidooxetane starting from 3-tosyloxyoxetane (**1**) or 3-mesyloxyoxetane (**2**).

To facilitate the complete removal of DMSO by liquid-liquid extraction, its total amount was minimized by utilizing the molten sulfonic acid esters as both reactant and solvent. Ultimately, 3-azidooxetane was compared to its constitution isomer glycidyl azide with regard to physicochemical and energetic properties, and poly(3-azidooxetane) was prepared by cationic ring-opening polymerization.

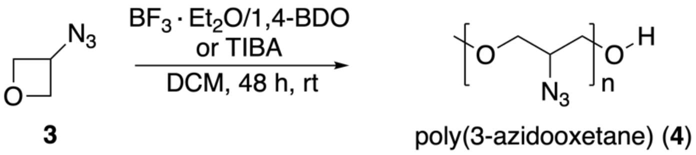

Scheme 3.6. Polymerization of 3-azidooxtane toward poly(3-azidooxetane).

In addition, the syntheses of compounds **1** and **2** were significantly improved compared to literature methods starting from commercially available oxetan-3-ol, and their molecular structures were elucidated by single-crystal X-ray diffraction.

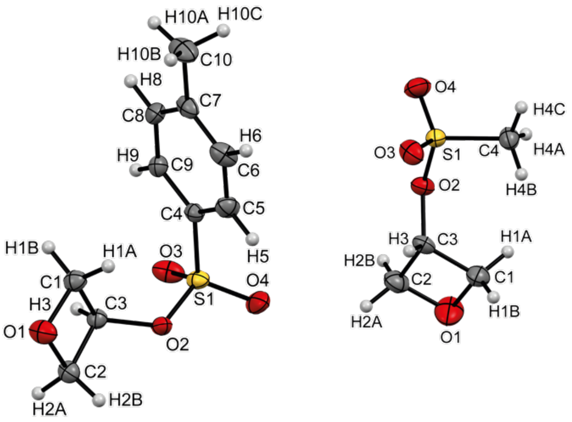

Figure 3.4. Molecular structures of compounds **1** and **2** in the crystal. Ellipsoids drawn at the 50% probability level.

From the investigations outlined in this chapter, it can be concluded that 3-azidooxetane offers a slightly higher energetic performance than glycidyl azide and polymerizes readily, while the direct polymerization of glycidyl azide is impossible due to its lack of reactivity. In terms of glass transition temperature, performance, thermostability, and sensitivity, poly(3-azidooxetane) was found to be fully equal to the market-dominating glycidyl azide polymer (GAP). In addition, it has the potential to provide improved curing results as it is only terminated by the more reactive primary hydroxy groups, contrary to GAP, which also features less reactive secondary hydroxy groups. Thus, poly(3-azidooxetane) turned out as a first-rate alternative to GAP. Moreover, 3-azidooxetane is a very promising candidate for the synthesis of energetic copolymers due to its excellent polymerizability, high enthalpy of formation (225.6 kJ mol^{-1}), and associated, high performance (VoD: 6307 ms^{-1}, $p_{\text{C-J}}$: 11.5 GPa) next to a nitrogen content of 42.4%. Last but not least, both sulfonic acid esters (**1**, **2**) represent excellent building blocks for both energetic and non-energetic oxetanes via nucleophilic substitution reactions.

3.7 Chapter 10: A GAP Replacement, Part 2: Preparation of Poly(3-azidooxetane) via Azidation of Poly(3-tosyloxyoxetane) and Poly(3-mesyloxyoxetane)

The synthesis of the new polymers poly(3-tosyloxyoxetane) and poly(3-mesyloxyoxetane) is reported next to their intensive characterization. As different catalysts have been employed for the polymerization of the corresponding monomers, both a low- (LMW) and a high-molecular-weight (HMW) species were obtained in each case (Scheme 7).

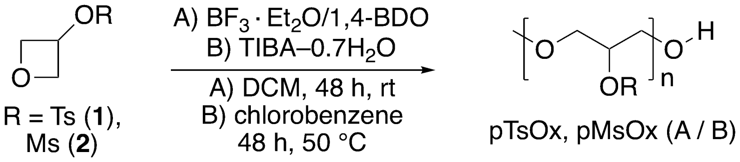

Scheme 3.7. Polymerization of 3-tosyloxyoxetane (**1**) and 3-mesyloxyoxetane (**2**) toward the corresponding homopolymers.

Owing to their excellent leaving groups, all precursor polymers allow a facile preparation of various energetic or non-energetic polyoxetanes via polymer-analogous transformation (PAT) reactions. In the presented study, however, all sulfonic acid ester polymers were azidated to provide the pendant LMW- and HMW-species of poly(3-azidooxetane) – the latter being described for the first time.

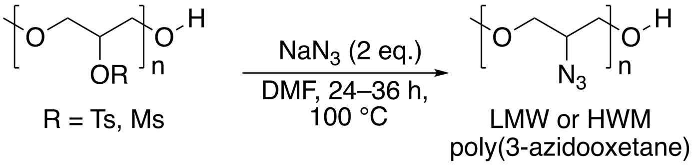

Scheme 3.8. Azidation of the prepared precursor polymers toward LMW and HMW poly(3-azidooxetane).

In this context, PAT offers significant advantages over the previously described direct polymerization of 3-azidooxetane, as the handling of the rather sensitive 3-azidooxetane (IS: 3 J, FS > 192 N) is bypassed, and the precursor polymers can be up-scaled without any risk. Furthermore, the overall yield regarding poly(3-azidooxetane) was more than doubled (86% instead of 39%) using the developed synthetic route.

To further substantiate its suitability as a substitute for GAP, poly(3-azidooxetane) was compared with it in great detail. It was found to offer higher performance and lower impact sensitivity at comparable thermostability.

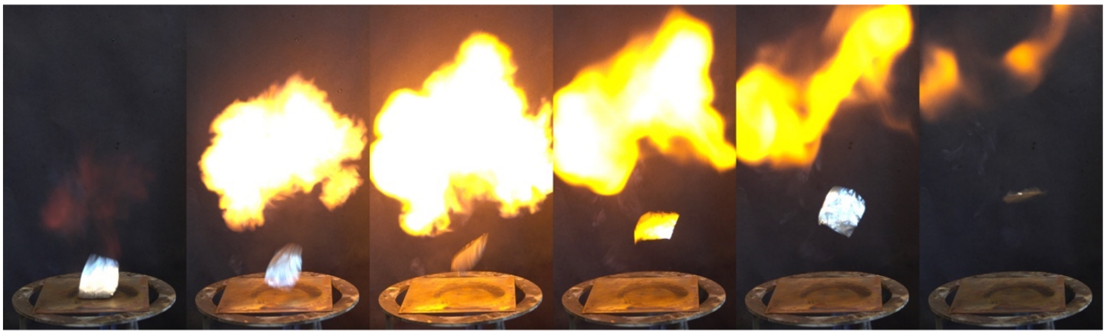

Figure 3.5. Violent deflagration of 50 mg poly(3-azidooxetane).

It was also found to be compatible with typical azido-plasticizers and curable with common isocyanates such as TDI. In addition, an aquatic toxicity assessment showed that poly(3-azidooxetane) can be prepared in a more environmentally friendly manner than GAP starting from 3-tosyloxyoxetane. Overall, light was shed on various application-related aspects of poly(3-azidooxetane), further demonstrating its suitability as a first-rate GAP replacement with high chances of a near-term application.

3.8 Chapter 11: Energetic polymers: A Chance for Lightweight Reactive Structure Materials?

Today, ammunition still consists of roughly 70 wt% non-energetic structure-providing materials causing a significant deadweight. A possible solution is provided by energetic reactive structure materials (RSMs) which currently rely on heavy, metal-based materials (e.g., alloys, thermites). In contrast, energetic polymers may provide especially lightweight RSMs. Unfortunately, available oxetane monomers are unsuitable for their preparation as these were originally designed to provide elastic binders of the lowest possible glass transition temperature (T_G). For a polymeric RSM, exactly the opposite is required. Hence, a new and different approach was followed with the synthesis of (2,4,6-trinitrophenoxy)oxetane (TNPO) – an insensitive but performant monomer to potentially provide rigid polymers of high T_G. In chapter 11, its homopolymer was prepared and characterized.

Scheme 3.9. Polymerization of TNPO.

Furthermore, TNPO was copolymerized with several prior art energetic oxetanes to study its effect on the glass transition temperature in detail. In addition, the performance of all polymers was assessed to estimate the potential performance range of polyoxetane-based RSMs.

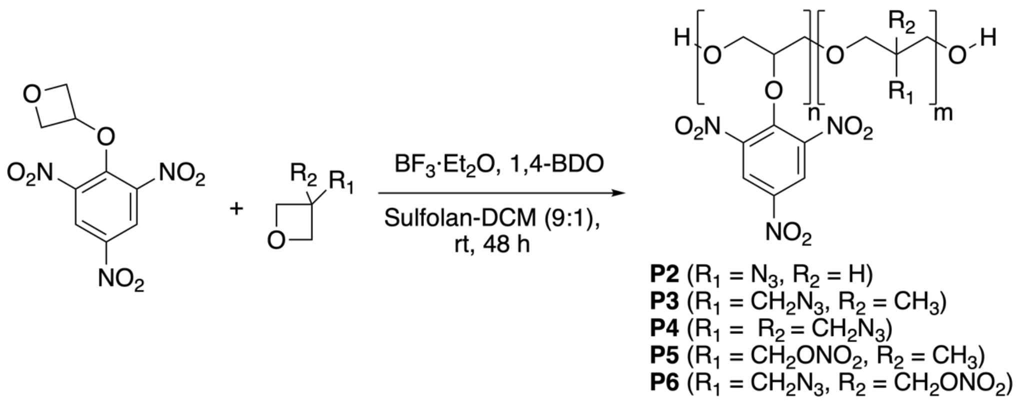

P2 ($R_1 = N_3$, $R_2 = H$)
P3 ($R_1 = CH_2N_3$, $R_2 = CH_3$)
P4 ($R_1 = R_2 = CH_2N_3$)
P5 ($R_1 = CH_2ONO_2$, $R_2 = CH_3$)
P6 ($R_1 = CH_2N_3$, $R_2 = CH_2ONO_2$)

Scheme 3.10. Copolymerization of TNPO with prior art energetic oxetanes.

Based on the results, it can be concluded that even moderately bulky motifs, as in the case of TNPO, can provide notably high glass transition temperatures. A very dominant effect of the TNPO repeating unit on the investigated copolymers was found. Other bulky structural motifs (e.g., energetic heterocycles) could thus substantially contribute to the development of suitable monomers and polymers. In terms of performance, all studied polymers show a performance in the range of TNT. Thus, energetic polymers as RSMs could contribute positively to an increased blast effect next to beneficial effects such as weight reduction and independence from atmospheric oxygen. Based on the current state of research, the development of such materials appears very challenging but worthwhile.

4 Investigation of Structure-Property Relationships of Three Nitroaromatic Compounds: 1-Fluoro-2,4,6-trinitrobenzene, 2,4,6-Trinitrophenyl Methanesulfonate, and 2,4,6-Trinitrobenzaldehyde

by
Max Born, Dominik E. Dosch, Konstantin Karaghiosoff, Marco Reichel and Thomas M. Klapötke

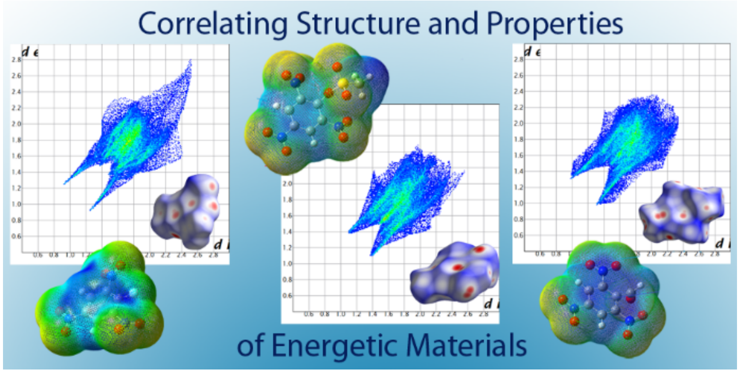

as published in
Crystal Growth & Design **2021**, *21*, 243–248
(doi:10.1021/acs.cgd.0c01049)

Abstract

Recently, the investigation of the correlation between the crystal structure and important properties like sensitivity and thermostability of energetic materials has gained more and more interest among experts in the field. To contribute to this development, several models for the sensitivity prediction of energetic materials have been applied to the title compounds. Very often, older models that focus on bond dissociation enthalpy or electrostatic potential result in values that differ significantly from values of actual measurements. However, more recent models like Hirshfeld surface analysis or Fingerprint plot analysis offer an improved correlation between prediction and practical tests. We compared these methods with the mentioned older models and gained further insight into structure-property relationships of energetic materials. The accuracy of predictions of structure-property relationships, which can be deduced from a crystal structure, increases with the sample size over time. Therefore, this method should be pursued and applied to different energetic materials in the future for a better understanding of those relationships.

4.1 Introduction

In 1997, Spackman communicated a novel concept for the definition and visualization of a molecule in a crystal based on Hirshfelds Stockholder partitioning scheme.[1-2] This method for crystal analysis and crystal engineering was further refined and became famous as the Hirshfeld surface in 1998.[3] In 2002, McKinnon and Spackman complemented their method with 2D Fingerprint plot analysis for an improved visualization of intermolecular close contacts in a crystal.[4] This work was followed by the initial development of the CrystalExplorer software in 2004 and 2005, which has been continuously improved since then.[5] With the current version of CrystalExplorer, various interactions in the crystal can be easily visualized and quantified including features like crystal surface mapping and close contact analysis, which makes it a valuable tool for crystal engineering and material design.[6] In 2014, Hirshfeld surface and Fingerprint plot analysis found their way into the analysis and development of energetic materials for the first time.[7] Since then, various authors like Gozin[8], Klapötke[9], and Shreeve[10] have utilized this methodology and the CrystalExplorer software for the investigation and design of new energetic materials with the goal to achieve a deeper insight into structure-property relationships, especially with regard to sensitivity and thermal stability. Regarding synthesis and design of new energetic materials, the insensitivity toward external stimuli is one of the most important requirements among other characteristics like improved environmental compatibility, higher density, and thermal stability as well as increased detonation velocity and pressure.[11-12] One strategy to achieve an increased performance of HEDMs is to use compounds with a high heat of formation, but this is often related to a higher sensitivity toward external stimuli.[13] Due to this contrary behavior,[13-15] the molecular design as well as the crystallographic design have to be considered when creating new materials to achieve a suitable balance between safety and performance.[10] For this purpose, we applied a combination of various methods to all title compounds, which form a group of 1-substituted derivatives of 2,4,6-trinitrobenzene. Those molecules are interesting building blocks for the synthesis of more sophisticated energetic materials and serve as model compounds for the analysis of structure-property relationships. The applied set of methods comprises both preceding predictive models like the computation of BDE- and ESP values – as well as newer methods like Hirshfeld surface- and Fingerprint plot analysis.[7-10,16] By comparing the results of different prediction models with experimental values, we hope to achieve a better understanding of the energetic behavior regarding the aforementioned compounds and also a deeper insight into structure-property relationships of energetic materials in general.

4.2 Results and Discussion

4.2.1 Spectroscopic Characterization

The three title compounds were prepared by utilizing modified and optimized methods and intensively characterized by multinuclear NMR spectroscopy, vibrational spectroscopy (IR, Raman), elemental analysis as well as single-crystal X-ray diffraction. Found ^{1}H NMR chemical shifts of aromatic protons (**1**: 9.20, **2**: 9.24; **3**: 9.16) are in good agreement with other known 1-substituted trinitrobenzene derivatives like TNT (8.8 ppm) or picric acid (9.0 ppm).[17-18] The ^{13}C{^{1}H} NMR spectra reveal the corresponding chemical shifts between 120 ppm and 190 ppm. Compound **1** shows two distinct signals for the nitro groups in *ortho* and *para* position in the ^{14}N NMR spectrum. In the case of molecules **2** and **3**, no distinct signals for the nitro groups were found due to the rather large signal width of 440 Hz and 500 Hz. Typical Raman- and infrared vibration modes were found in the corresponding spectra and assigned according to available literature (Table 1).[19]

Table 4.1. Characteristic vibration modes of **1**, **2**, and **3**.

	1		**2**		**3**	
	IR	Raman	IR	Raman	IR	Raman
ν (C–H)	3063	3063	3095	3097	3096	3104
ν_{as} (NO_2)	1541	1548	1543	1547	1554	1553
ν_{s} (NO_2)	1342	1364	1343	1363	1343	1351
ν (C–N)	923	940	919	1089	919	938
δ (NO_2)	737	817	730	823	729	826

$\nu_{as/s}$: asymmetric / symmetric vibration mode δ: deformation vibration

All three compounds show very similar values for the symmetric, asymmetric, and deformation modes of the nitro groups. The same applies to the C-H and C-N modes of the three title compounds, with the exception of the Raman C-N mode of compound **2**. It has been previously shown by other researchers that the bond dissociation enthalpy (BDE) can be directly linked to the sensitivity of energetic materials.[20-21] All three compounds are expected to have very similar BDE values and therefore similar sensitivities toward external stimuli using this particular model. In this work, the BDEs were calculated based on the respective crystal structure data and the B3LYP/6-311G+(d,p) method. According to various studies, the BDEs of a molecule can be considered as the most important factor in pyrogenic decomposition. The BDE correlates to a trigger bond which is first to break and can therefore be utilized to assess the sensitivity of a material.[10]

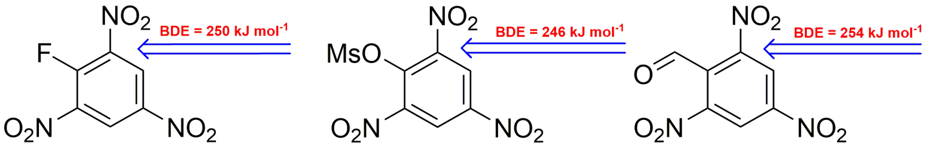

Figure 4.1. Calculated BDE values of the weakest bond in molecules **1**–**3** considering all X-C bonds (X: C, O, N, F)

The C-N bond of the *ortho* nitro group was identified as the weakest bond in all investigated compounds. All BDE values of compounds **1**, **2**, and **3** fall in a range between RDX (161 kJ mol^{-1}) and TATB (355 kJ mol^{-1}), which is the reason for categorizing them as sensitive.[15,22-28] The calculation-based trend of BDEs is **2** < **1** < **3**, but the relative difference is very small (< 10 kJ mol^{-1}). Based on this model, very similar sensitivity values would be expected. The electrostatic potential (ESP) can be utilized for the visualization of the bond strength inside a molecule and therefore as an indicator for the potential sensitivity.[11] In addition, the calculation of h_{50} values or the acquisition of volume-based sensitivities based on ESP is possible.[11]

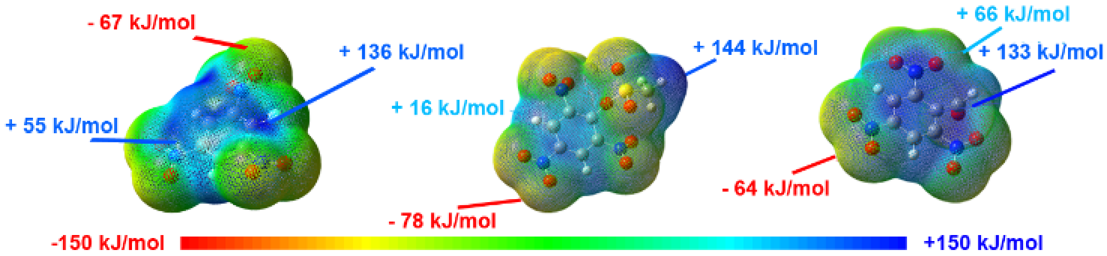

Figure 4.2. ESP of **1** (left), **2** (center), and **3** (right), calculated on the 0.02 electron bohr^{-3} hypersurface.

Regarding the ESP, all compounds show a significantly larger surface area in the positive range and the corresponding values are more pronounced in comparison to peak values of negative areas. This distribution and the strongly positive center of the investigated compounds is a typical indicator for sensitive materials.[26-28] The difference between the peak positive spot and the peak negative spot (**1**: +69 kJ mol^{-1}, **2**: +66 kJ mol^{-1}, **3**: +69 kJ mol^{-1}) is very similar for all three compounds. Therefore, a similar behavior toward external stimuli is expected.

4.2.2 Structure-Property Relationship

Impact and friction resemble external mechanical stimuli which can cause the displacement of stabilizing layers in the crystal and therefore lead to internal strains. If the strain energy is below the lowest BDE, the integrity of the molecule is not affected. On the contrary, if the strain energy surpasses the energy necessary to break the weakest bond, the compound will decompose.[7] Besides the stacking and gearings of the individual layers, the strain caused by an interlayer slide also depends on other stabilizing interactions in the crystal, i.e. hydrogen bridges.[29] All three isolated molecules a, b and c show an almost planar benzene ring. When comparing the largest torsion angles of the *ortho* nitro groups (**1**: 41°, **2**: 45°, **3**: 41°), a very similar twisting behavior can be identified. This can be explained by sterical effects as well as by electronic repulsion between the substituents at the 1-position and the neighboring nitro groups. Despite those similarities, each compound exhibits a unique packing behavior in the unit-cell of the crystal (d, e, f) and therefore a difference in the gearing of the individual layers. Compound **1** exhibits a wave-like pattern with a moderate gearing between each layer. Compound **3** exhibits a wave-like pattern with a higher gearing of the individual layers and compound **2** shows a layered structure with the lowest gearing of all investigated materials. For compound **3,** the strain energy arising from mechanical stimuli is assumed to be the highest due to the high interlayer gearing and therefore the highest sensitivity is expected. Compound **2** exhibits the highest interlayer distance and therefore this material is expected to be the least sensitive toward mechanical stimuli, as it allows an easier sliding of adjacent layers without negative oxygen-oxygen repulsions or other detrimental interactions.

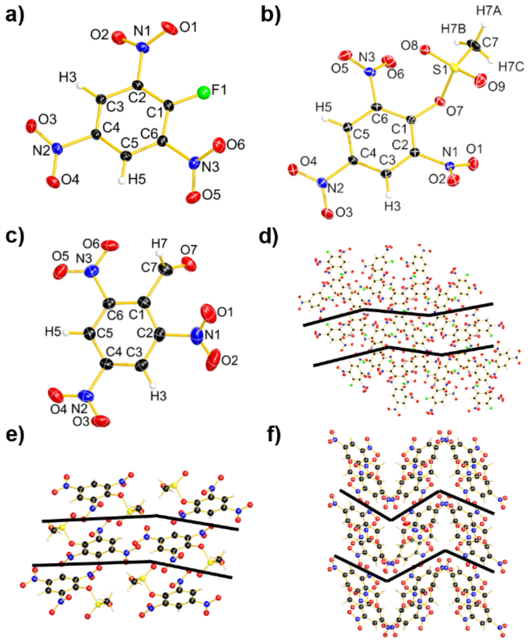

Figure 4.3. Single-crystal X-ray structure of **1** (a), **2** (b), and **3** (c) and the crystal packing of **1** (d), **2** (e), and **3** (f).

When this effect is very pronounced, the slip barrier can be reduced significantly enough to become smaller than the bond dissociation energy.[7] Next to crystal packing, a significant contribution to the extent of the slide barrier is made up by intermolecular interactions which therefore directly correlate with the sensitivity of a compound toward mechanical stimuli. In general, insensitive molecules exhibit a Hirshfeld surface in which the plane features the most red dots representing close contacts and fewer red dots between the individual layers.[29] Compounds **1**–**3** exhibit red dots and therefore close contacts which point out of the molecular plane (Figure 4) and can therefore be considered sensitive. Because none of these close contacts is arranged in a slidable plane, interlayer repulsion results from external stimuli, which is characteristic for sensitive materials.

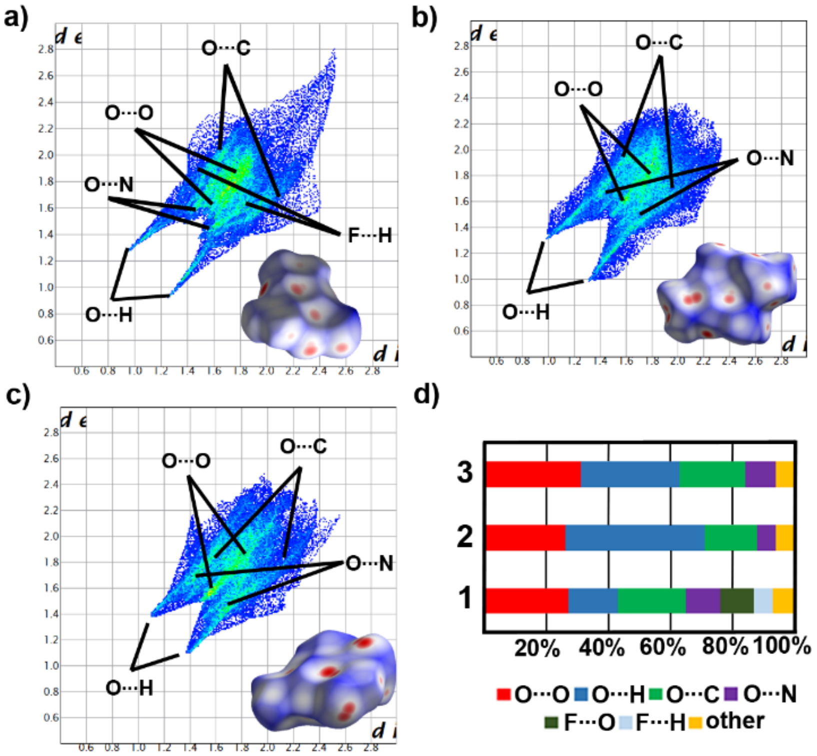

Figure 4.4. Two-dimensional Fingerprint plot in crystal stacking as well as the corresponding Hirshfeld surface (bottom right in the 2D plot) of **1** (a), **2** (b), and **3** (c). Color coding: white, distance *d* equals VDW distance; blue, *d* exceeds VDW distance; red, distance *d* is smaller than the VDW distance. Population of close contacts of **1**–**3** in crystal stacking (d).

The experimental sensitivity values for compounds **1**–**3** (IS: 9–10 J, FS: > 360 N, ESD: 50–160 mJ) are very similar and the same would be expected for the distribution and intensity of stabilizing and destabilizing close-contacts in the Hirshfeld surface and Fingerprint plot analysis of the crystal structures. The compounds show a 3D network with regard to their close contacts, represented by red dots on the surface in all three dimensions, which is typical for sensitive materials. The analysis of the 2D Fingerprint plots shows very interesting results as the distribution and intensity of the close contacts in the model compounds are very different. Less sensitive energetic materials are often designated by numerous and/or strong O···H and N···H interactions as they facilitate more rigid interlayers, which absorb energy more easily and are hence less likely to cause a detrimental sliding of the planes that induces a repulsion of these layers.[10] Compound **1** shows very few O···H contacts (22%) when compared to compound **2** (45%) and **3** (32%), but the number of strong O···H contacts (< 2.5 Å) is significantly higher for compound **1**. Apparently, very few but strong O···H close contacts in compound **1** are capable of stabilizing the molecule to the same extent as significantly more but weaker interactions in compounds **2** and **3**, as they show very similar sensitivities toward external stimuli. The stabilizing N···H close-contacts can be neglected in all three cases as their occurrence is low (0–0.9%) and they can be regarded as weak (> 3 Å). The same is true for the stabilizing F···H interactions (1.3%) in compound **1**. The O···O interaction is a particularly important close contact interaction, as a high occurrence of O···O contacts implies a high sensitivity. An increased exposure of nitro groups on the molecular surface causes the risk of explosion to rise due to the increased repulsion in the case of interlayer sliding.[7,10,15,29] The title compounds show significant amounts of O···O close-contacts (26–32%) and can therefore be considered sensitive. All O···N and C···N contacts are very weak (> 3 Å), which is typical for sensitive materials.[29] The 2D Fingerprint plots exhibit two pronounced spikes that indicate strong O···H bonding in all investigated compounds.[10] With respect to $d_i + d_e$ (d_i, distance between the Hirshfeld surface to the nearest atom interior; d_e, distance from the Hirshfeld surface to the nearest atom exterior), the trend for the amount of hydrogen bonds is **2** > **3** > **1**, but an inverse trend is found for the relative strength of the H-bonds. These results indicate that not only the quantity but also the relative bond strength for stabilizing interactions must be considered when utilizing Hirshfeld surface and Fingerprint plot analysis for the sensitivity assessment of energetic materials.

4.2.3 Heat of Formation and Detonation Parameters

The performance of an energetic material depends directly on its density, which therefore is not only a decisive factor, but most interestingly results from the packing behavior within the crystal. We observed the crystal densities of **1**, **2**, and **3** to be 1.89, 1.84, and 1.76 g cm^{-3} at 145 K. Hence, the calculated densities under ambient conditions are 1.84, 1.80, and 1.72 g cm^{-3}. To calculate the heat of formation (HOF), extremely precise theoretical methods must be applied since experimental values are often inaccurate.[10] The calculation of the HOF was therefore performed using *ab-initio* calculations which make use of the optimized molecule geometry obtained by refining the obtained geometry from the X-ray diffraction experiment. According to Trouton's Rule, the HOF was determined by the subtraction of the sublimation enthalpy from the HOF of the corresponding gas-phase species.[11] To obtain the HOF of the corresponding gas-phase species, the atomization energies were subtracted from the total enthalpy of the molecules.[30-31] All calculations were carried out on a CBS-4M level of theory in combination, starting from the respective crystal structures. Applying the specific densities and the EXPLO5 (V6.05)[32] thermochemical code, the detonation properties of **1**, **2**, and **3** were determined and are given in Table 2. They were calculated at the Chapman–Jouguet point with the help of the stationary detonation model using a modified Becker–Kistiakowski–Wilson state equation for the system. The C–J point was found by the Hugoniot curve of the system by its first derivative.[32-33]

Table 4.2. Physical and calculated detonation parameters of compounds **1**–**3** using the EXPLO5 computer code.

	1	**2**	**3**
Formula	$C_6H_2N_3O_6F_1$	$C_7H_5N_3O_9S_1$	$C_7H_3N_3O_7$
MW [g mol^{-1}]	231.09	307.19	241.11
IS[a] [J]	10	9	10
FS[b] [N]	>360	>360	>360
ESD [mJ]	160	50	120
N[c] [%]	18.18	13.68	17.43
N + O[d] [%]	59.72	60.55	63.88
$\Omega[CO_2]$[e] [%]	−48.5	−39.1	−56.4
T_{melt}[f] [°C]	126.7	139.4	101.6
T_{dec}[g] [°C]	350.6	237.4	185.1
$\rho_{25°C}$[h] [g cm^{-3}]	1.837	1.795	1.721
ΔH_f°[i] [kJ mol^{-1}]	-532.8	−386.1	−163.2
	EXPLO5 V6.05		
ΔU_f°[j] [kJ kg^{-1}]	−4070	−3904	−4391
$T_{C\text{-}J}$[k] [K]	3301	2240	3361
$P_{C\text{-}J}$[l] [GPa]	23.8	12.6	20.4
V_{det}[m] [ms^{-1}]	7376	5863	7062
V_o[n] [dm^3 kg^{-1}]	606.9	383.9	616.1

[a] Impact sensitivity.[22] [b] Friction sensitivity.[23] [c] Nitrogen content. [d] Combined nitrogen and oxygen content. [e] Absolute oxygen balance assuming the formation of CO or CO_2. [f] Melting point from DTA. [g] Decomposition from DTA. [h] Calculated room temperature density. [i] Heat of formation calculated at the CBS-4M level of theory for FMN, experimentally determined for MN. [j] Detonation energy. [k] Detonation temperature. [l] Detonation pressure. [m] Detonation velocity. [n] Volume of detonation gases at standard temperature and pressure conditions.

The HOF of the compounds can be ordered **3** > **1** > **2** whilst the densities are ordered **1** > **2** > **3**. According to these results, similar values for the detonation pressure and the detonation velocity can be expected. However, the mesyl substituent in compound **2** leads to a significantly lowered oxygen balance when compared to the other two compounds. It also exhibits significantly lower values for V_{det} and P_{C-J}. Regarding these values, compounds **1** and **3** slightly exceed TNT (6881 ms^{-1}, 18.9 GPa), whilst molecule **2** is unable to compete.[26-28]

4.3 Conclusions

1-Fluoro-2,4,6-trinitrobenzene, 2,4,6-trinitrophenyl methanesulfonate, and 2,4,6-trinitrobenzaldehyde have been prepared and intensively characterized. The molecular structures of all aforementioned compounds were elucidated by single-crystal X-ray diffraction. Older methods for the prediction of an energetic materials sensitivity (BDE, ESP) were compared with newer, current methods which are based on the crystal structure of a compound (Hirshfeld surface & Fingerprint plot analysis). We found that a combination of very few but strong stabilizing interactions in a crystal may result in the same sensitivity as numerous but significantly weaker stabilizing interactions. Another key result is the fact that all investigated energetic materials had at least 25% of destabilizing O···O interactions as well as close contacts between the individual layers. The broader application of Hirshfeld surface analysis could lead to deeper insight and understanding of the relationship between structure and sensitivity of an energetic material. Sensitivity values could be predicted or even determined without the need to prepare large amounts of energetic material. This is not only environmentally friendly but also leads to a significant safety increase. The calculation using the EXPLO5 code showed that the performance of the investigated compounds decreases from **1** over **3** to **2**. Except for the latter compound, the values are comparable to TNT.

4.4 Experimental Section

General Information. 1-Fluoro-2,4-dinitrobenzene, pyridine, iodine *N*,*N*-dimethyl-*p*-nitrosoaniline, methanesulfonic anhydride, perchloric acid, nitric acid, sulfuric acid, oleum, and potassium nitrate are commercially available. Potassium picrate and TNT were used from a group internal stockpile.

For NMR spectroscopy the solvent DMSO-d_6 was dried using 3 Å molecular sieves. Spectra were recorded on a Bruker Avance III spectrometer operating at 400.1 MHz (^1H), 100.6 MHz (^{13}C), and 28.9 MHz (^{14}N). Chemical shifts are referred to TMS (^1H, ^{13}C) and $MeNO_2$ (^{14}N). Raman spectra were recorded with a Bruker MultiRam FT Raman spectrometer using a neodymium-doped yttrium aluminum garnet (Nd:YAG) laser (λ = 1064 nm) with a power of 1074 mW. The samples for Infrared spectroscopy were placed under ambient conditions onto an ATR unit using a Perkin Elmer Spectrum BX II FT-IR System spectrometer. Melting and/or decomposition points were detected with an OZM DTA 552-Ex instrument. The scanning temperature range was set from 293 K to 673 K at a scanning rate of 5 K min^{-1}. Elemental analysis was performed with a Vario EL instrument and a Metrohm 888 Titrando device.

Caution! All investigated compounds are explosives, which show partially increased sensitivities toward various stimuli (e.g., higher temperatures, impact, friction, or electrostatic discharge). Therefore, proper safety precautions (safety glasses, Kevlar gloves, and earplugs) have to be applied while synthesizing and handling the described compounds.

1-Fluoro-2,4,6-trinitrobenzene. 1-Fluoro-2,4-dinitrobenzene (13.6 g, 72.9 mmol) was slowly added to a nitration mixture consisting of 61.9 mL sulfuric acid, 50.8 mL Oleum (65%), and potassium nitrate (42.0 g, 415.4 mmol) at 0 °C. The reaction mixture was then stirred for 15 min at 0 °C and subsequently warmed to room temperature before the solution was finally heated to 125 °C for five days. The obtained suspension was allowed to cool to ambient temperature and afterward poured onto 750 mL of iced water. The solid was collected by suction filtration and washed with water (3 × 200 mL) until the filtrate ran clear. The filter cake was dried and recrystallized from boiling tetrachlorocarbon to afford the product upon cooling as pale-yellow crystals (9.7 g, yield: 57%).

^{1}H NMR (Chloroform-d$_1$, 400 MHz): δ 9.20 (d, 2H, $^4J_{FH}$ = 5.6 Hz) ppm. **^{13}C{^{1}H} NMR** (Chloroform-d$_1$, 100 MHz): δ 154.2 (d, $^1J_{FC}$ = 292.0 Hz), 142.4 (s, broad), 139.4 (s, broad), 125.9 (d, $^3J_{FC}$ = 0.8 Hz) ppm. **^{14}N NMR** (Chloroform-d$_1$, 29 MHz): δ −24 (NO_2) ppm. **^{19}F NMR** (Chloroform-d$_1$, 377 MHz): δ −113.2 (t, $^4J_{FH}$ = 5.6 Hz) ppm. **IR** (ATR, cm^{-1}): $\tilde{\nu}$ 3110 (w), 3089 (w), 3063 (m), 2887 (w), 1620 (s), 1541 (vs), 1482 (m), 1421 (m), 1342 (vs), 1319 (s), 1280 (m), 1258 (m), 1202 (m), 1089 (s), 948 (w), 938 (m), 923 (s), 827 (vw), 776 (w), 757 (w), 737 (s), 718 (s), 709 (vs), 672 (m), 649 (s), 551 (m), 519 (m), 481 (w), 462 (w), 406 (w). **Raman** (1064 nm, 1000 mW, 25 °C, cm^{-1}): $\tilde{\nu}$ 3063 (9), 2643 (2), 1621 (14), 1548 (36), 1364 (100), 1347 (51), 1279 (14), 1187 (4), 1090 (6), 940 (11), 927 (7), 826 (21), 817 (12), 741 (3), 522 (2), 377 (5), 354 (8), 333 (20), 313 (7), 205 (26), 149 (8), 105 (48), 90 (40). **Elemental Analysis** calcd (%) for $C_6H_2FN_3O_6$: C 31.18, H 0.87, F 8.22, N 18.18, O 41.54; found: C 31.42, H 1.13, N 18.23. **DTA**: 127 °C (m.p.), 351 °C (dec.). **IS**: 10 J. **FS**: > 360 N. **ESD**: 160 mJ.

2,4,6-Trinitrophenyl methanesulfonate. Potassium picrate (10.0 g, 37.4 mmol, 1.0 eq.) was suspended in 200 mL toluene. Methanesulfonic anhydride (6.5 g, 37.4 mmol, 1.0 eq.) was added to the yellow suspension in small portions. After adding perchloric acid (60% solution in acetic acid, 10 drops) the reaction mixture was stirred for 4 h at 120 °C with a $CaCl_2$ filled drying tube on top of the reflux condenser. After cooling to room temperature, the yellowish by-product, potassium mesylate, was separated by filtration and the filter residue was washed with ~150 mL toluene. The yellow filtrate phases were combined and the solvent was removed *in vacuo*. The resulting yellow-orange oil was treated with ~15 mL of ice-cold ether to precipitate the solid product. The solvents were removed *in vacuo* and a pale-yellow solid was obtained. It was recrystallized from 150 mL chloroform to afford the product as a white solid 8.6 g (75%).

^{1}H NMR (Acetone-d$_6$, 400 MHz): δ 9.24 (s, 2H), 3.69 (s, 3H) ppm. **^{13}C{^{1}H} NMR** (Acetone-d$_6$, 100 MHz): δ 146.3, 145.8, 138.8, 126.0, 40.4 ppm. **^{14}N NMR** (Acetone-d$_6$, 29 MHz): δ −22 (NO$_2$) ppm. **IR** (ATR, cm^{-1}): ṽ 3095 (w), 2163 (w), 2004 (w), 1614 (w), 1543 (m), 1373 (m), 1343 (s), 1243 (m), 1192 (m), 1169 (m), 1087 (w), 969 (w), 919 (m), 847 (s), 823 (m), 792 (m), 775 (s), 730 (s), 716 (s), 668 (s), 634 (m), 560 (m), 536 (s), 505 (s). **Raman** (1064 nm, 1000 mW, 25 °C, cm^{-1}): ṽ 3097 (18), 3035 (15), 2942 (46), 1616 (55), 1547 (42), 1363 (100), 1245 (50), 1089 (25), 823 (31), 636 (37), 565 (21), 367 (23), 330 (33), 250 (17). **Elemental Analysis** calcd (%) for $C_7H_5N_3O_9S$: C 27.37, H 1.64, S 10.44, N 13.68, O 46.87; found: C 27.34, H 1.69, N 13.60, S 10.99. **DTA**: 139 °C (m.p.), 237 °C (dec.). **IS**: 9 J. **FS**: > 360 N. **ESD**: 50 mJ.

2,4,6-Trinitrobenzaldehyde. Trinitrotoluene (10.0 g, 44.0 mmol, 1 eq.) and *N*,*N*-dimethyl-*p*-nitrosoaniline (7.0 g, 47.0 mmol, 1.1 eq.) were dissolved in 15 mL pyridine with 50 mg of iodine as a catalyst. The mixture was stirred for 7 days at 20–25 °C. The organic solid was separated by filtration and washed with cold acetone. The obtained crude product was dried in vacuo and then dissolved in 180 mL of aqueous HCl (36%) and stirred at 80 °C for two hours. The product was then separated by filtration and washed acid-free with water. This way 6.4 g (61%) of pure TNBA could be obtained as a black solid.

^{1}H NMR (DMSO-d$_6$, 400 MHz): δ 10.55 (s, 1H), 9.16 (s, 2H) ppm. **^{13}C{^{1}H} NMR** (DMSO-d$_6$,100 MHz): δ 188.1, 148.1, 147.7, 134.2, 124.7 ppm. **^{14}N NMR** (DMSO-d$_6$, 29 MHz): δ −20 (NO$_2$) ppm. **IR** (ATR, cm^{-1}): ṽ 3096 (w), 2916 (vw), 1714 (m), 1605 (m), 1554 (s), 1535 (vs), 1452 (w), 1405 (w), 1343 (vs), 1194 (m), 1185 (w), 1157 (m), 1075 (w), 979 (w), 935 (w), 919 (m), 839 (m), 826 (m), 772 (m), 742 (m), 729 (s), 701 (m), 570 (w), 538 (w), 475 (w), 435 (m). **Raman** (1064 nm, 1000 mW, 25 °C, cm^{-1}): ṽ 3104 (8), 2911 (7), 2903 (8), 1713 (16), 1623 (15), 1553 (29), 1382 (32), 1351 (81), 1274 (10), 1197 (12), 981 (8), 938 (7), 842 (13), 826 (18), 334 (22), 292 (8), 255 (7), 232 (19), 203 (34), 192 (26), 151 (36), 88 (100). **Elemental Analysis** calcd (%) for $C_7H_3N_3O_7$: C 34.87, H 1.25, N 17.43; found: C 34.87, H 1.38, N 17.12. **DTA**: 102 °C (m.p.), 185 °C (dec.). **IS**: 10 J. **FS**: 360 N. **ESD**: 120 mJ.

X-Ray Measurements. 1-Fluoro-2,4,6-trinitrobenzene and 2,4,6-trinitrobenzaldehyde were dissolved in ethyl acetate, and single crystals have been received after slow solvent evaporation. Single crystals of 2,4,6-trinitrophenyl methanesulfonate have been received after slow solvent evaporation of chloroform. Data collection was performed with an Oxford Xcalibur3 diffractometer with a CCD area detector, equipped with a multilayer monochromator, a Photon 2 detector and a rotating-anode generator were employed for data collection using Mo-Kα radiation (λ = 0.7107 Å). Data collection and reduction were carried out using the CrysAlisPRO software.[34] The structures were solved by direct methods (SIR-2014)[35] and refined (SHELXLE)[36] by full-matrix least-squares on F2 (ShelxL)[37-38] and finally checked using the platon software[39] integrated in the WinGX software suite.[40] The non-hydrogen atoms were refined anisotropically and the hydrogen atoms were located and freely refined. All Diamond 3 plots are shown with thermal ellipsoids at the 50% probability level and hydrogen atoms are shown as small spheres of arbitrary radius.

Associated Content

The Supporting Information is available free of charge on the ACS Publication website.
^{1}H, ^{13}C, ^{19}F, ^{14}N NMR spectra; Crystallographic information; Detonation parameter calculations (output files);
X-ray data for 1-Fluoro-2,4,6-trinitrobenzene (CIF); CCDC: 2016176
X-ray data for 2,4,6-Trinitrophenyl methanesulfonate (CIF); CCDC: 2016174
X-ray data for 2,4,6-Trinitrobenzaldehyde (CIF); CCDC: 2016175
This material is available free of charge via the Internet at http://pubs.acs.org

Acknowledgment

For financial support of this work by Ludwig–Maximilian University (LMU), the Office of Naval Research (ONR) under grant no. ONR.N00014-16-1-2062 and the Strategic Environmental Research and Development Program (SERDP) under contract no. WP19-1287 are gratefully acknowledged. The authors also thank Dr. Teresa Küblböck for her help with the graphics and F–Select GmbH for the generous donation of fluorochemicals.

References

[1] Hirshfeld, F.L. Bonded-atom fragments for describing molecular charge densities. *Theor. Chim. Acta* **1977**, *44*, 129-138.

[2] Spackman, M. A.; Byrom, P. G. A novel definition of a molecule in a crystal. *Chem. Phys. Lett.* **1997**, *267*, 215-220.

[3] McKinnon, J. J.; Mitchell, A. S.; Spackman, M. A. Hirshfeld Surfaces: A New Tool for Visualising and Exploring Molecular Crystals. *Chem. – Eur. J.* **1998**, *4*, 2136-2141.

[4] Spackman, M. A.; McKinnon, J. J. Fingerprinting intermolecular interactions in molecular crystals. *CrystEngComm* **2002**, *4*, 378-392.

[5] McKinnon, J. J.; Spackman, M. A.; Mitchell, A. S. Novel tools for visualizing and exploring intermolecular interactions in molecular crystals. *Acta Crystallogr, Sect. B: Struct. Sci.* **2004**, *60*, 627-668.

[6] McKinnon, J. J.; Jayatilaka, D.; Spackman, M. A. Towards quantitative analysis of intermolecular interactions with Hirshfeld surfaces. *Chem. Commun.* **2007**, 3814-3816.

[7] Ma, Y.; Zhang, A.; Xue, X.; Jiang, D.; Zhu, Y.; Zhang, C. Crystal Packing of Impact-Sensitive High-Energy Explosives. *Cryst. Growth & Des.* **2014**, *14*, 6101-6114.

[8] Li, H.; Zhang, L.; Petrutik, N.; Wang, K.; Ma, Q.; Shem-Tov, D.; Zhao F.; Gozin, M. Molecular and Crystal Features of Thermostable Energetic Materials: Guidelines for Architecture of "Bridged" Compounds. *ACS Cent. Sci.* **2020**, *6*, 54-75.

[9] Reichel, M.; Dosch, D.; Klapötke, T.; Karaghiosoff, K. Correlation between Structure and Energetic Properties of Three Nitroaromatic Compounds: Bis(2,4-dinitrophenyl) Ether, Bis(2,4,6-trinitrophenyl) Ether, and Bis(2,4,6-trinitrophenyl) Thioether. *J. Am. Chem. Soc.* **2019**, *141*, 19911-19916.

[10] Zhang, J.; Zhang, Q.; Vo, T. T.; Parrish, D. A.; Shreeve, J. Energetic Salts with π-Stacking and Hydrogen-Bonding Interactions Lead the Way to Future Energetic Materials. *J. Am. Chem. Soc.* **2015**, *137*, 1697-1704.

[11] Klapötke, T.M. *Chemie der hochenergetischen Materialien*; 1st ed.; De Gruyter: Berlin, Boston, **2009**.

[12] Gao, H.; Shreeve, J. Azole-Based Energetic Salts. *Chem. Rev. (Washington, DC, U. S.)* **2011**, *111*, 7377-7436.

[13] Zhi, C. Y.; Cheng, X. L.; Zhao, F. The Correlation between Electric Spark Sensitivity of Polynitroaromatic Compounds and Their Molecular Electronic Properties. *Propellants, Explos., Pyrotech.* **2010**, *35*, 555-560.

[14] Thottempudi, V.; Gao, H.; Shreeve, J. Trinitromethyl-substituted 5-nitro- or 3-azo-1,2,4-triazoles: synthesis, characterization, and energetic properties. *J. Am. Chem. Soc.* **2011**, *133*, 6464-6471.

[15] Tang, Y.; Zhang, J.; Mitchell, L. A.; Parrish, D. A.; Shreeve, J. Taming of 3,4-Di(nitramino)furazan. *J. Am. Chem. Soc.* **2015**, *137*, 15984–15987.

[16] Spackman, M. A.; Jayatilaka, D. Hirshfeld surface analysis. *CrystEngComm* **2009**, *11*, 19-32.

[17] Hussain, I.; Tariq, M. I.; Siddiqui, H. L. Structure Elucidation of Chromogen Resulting from Jaffes's Reaction. *J. Chem. Soc. Pak.* **2009**, *31*, 937-948.

[18] Soojhawon, I.; Lokhande, P. D.; Kodam, K. M.; Gawai, K. R. Biotransformation of nitroaromatics and their effects on mixed function oxidase system. *Enzyme Microb. Technol.* **2005**, *37*, 527-533.

[19] Lewis, I. R.; Daniel, N. W.; Griffiths, P. R. Interpretation of Raman Spectra of Nitro-Containing Explosive Materials. Part I: Group Frequency and Structural Class Membership. *Appl. Spectrosc.* **1997**, *51*, 1854-1867.

[20] Li, J. Relationships for the Impact Sensitivities of Energetic C-Nitro Compounds Based on Bond Dissociation Energy. *J. Phys. Chem. B,* **2010**, *114*, 2198-2202.

[21] Li, J. A quantitative relationship for the shock sensitivities of energetic compounds based on X–NO_2 (X = C, N, O) bond dissociation energy. *Hazard. Mater.* **2010**, *180*, 768-772.

[22] NATO STANAG 4489: *Explosives. Impact Sensitivity Tests*; NATO Standardization Office, Brussels, Belgium, **1999**.

[23] NATO STANAG 4487: *Explosives. Friction Sensitivity Tests*; NATO Standardization Office, Brussels, Belgium, **2002**.

[24] www.reichel-partner.com.

[25] Test methods according to the UN Manual of Tests and Criteria, Recommendations on the Transport of Dangerous Goods, 4th revised ed.; United Nations Publication: Geneva, **2003**. Impact: insensitive > 40 J, less sensitive ≥ 35 J, sensitive ≥ 4 J, very sensitive ≤ 3 J; friction: insensitive > 360 N, less sensitive: 360 N, sensitive < 360N and > 80 N, very sensitive ≤ 80 N, extremely sensitive ≤10 N.

[26] Köhler, J.; Meyer, R.; Homburg, A. *Explosives*; 10th ed.; Wiley-VCH: Weinheim, **2008**.

[27] Klapötke, T. M. *Chemistry of High-Energy Materials*; 5th ed.; DeGruyter: Boston, **2019**.

[28] Klapötke, T. M. *Energetic Materials Encyclopedia*; De Gruyter: Berlin, Boston, **2018**.

[29] Zhang, C.; Xue, C.; Cao, Y.; Zhou, Y.; Li, H.; Zhou, J.; Gao, T. Intermolecular friction symbol derived from crystal information. *CrystEngComm* **2013**, *15*, 6837-6844.

[30] Curtiss, L. A.; Raghavachari, K.; Redfern, P. C.; Pople, J. A. Assessment of Gaussian-2 and density functional theories for the computation of enthalpies of formation. *J. Chem. Phys.* **1997**, *106*, 1063-1079.

[31] Byrd, E.; Rice, B. M. Improved Prediction of Heats of Formation of Energetic Materials Using Quantum Mechanical Calculations. *J. Phys. Chem. A* **2006**, *110*, 1005-1013.

[32] Sućeska, M., EXPLO5, Version 6.05, Brodarski Institute, Zagreb, **2018**.

[33] Klapötke, T. M.; Krumm, B.; Steemann, F. X.; Umland, K.-D. Bis(1,3-dinitratoprop-2-yl) nitramine, a new sensitive explosivecombining a nitrate ester with a nitramine. *Z. Anorg. Allg. Chem.* **2010**, *636*, 2343-2346.

[34] CrysAlisPRO, Oxford Diffraction /Agilent Technologies UK Ltd., Yarnton, England, **2009**.

[35] Burla, M. C.; Caliandro, R.; Carrozzini, B.; Cascarano, G. L.; Cuocci, C.; Giacovazzo, C.; Mallamo, M.; Mazzone, A.; Polidori, G. Crystal structure determination and refinement via SIR2014. *J. Appl. Crystallogr.* **2015**, *48*, 306-309.

[36] Hübschle, C. B.; Sheldrick, G. M.; Dittrich, B. ShelXle: a Qt graphical user interface for SHELXL. *J. Appl. Crystallogr.* **2011**, *44*, 1281-1284.

[37] Sheldrick, G. M. SHELXL-97: Program for the Refinement of Crystal Structures, University of Göttingen, Germany, **1997**.

[38] Sheldrick, G. A short history of SHELX. *Acta Cryst. A.* **2008**, *64*, 112-122.

[39] Spek, A. L. PLATON – a Multipurpose Crystallographic Tool, Utrecht University, Netherlands, **1999**.

[40] Farrugia, L. J. WinGX and ORTEP for Windows: an update. *J. Appl. Cryst.* **2012**, 849-854.

4.5 Supporting Information

4.5.1 NMR Spectra

Compound 1

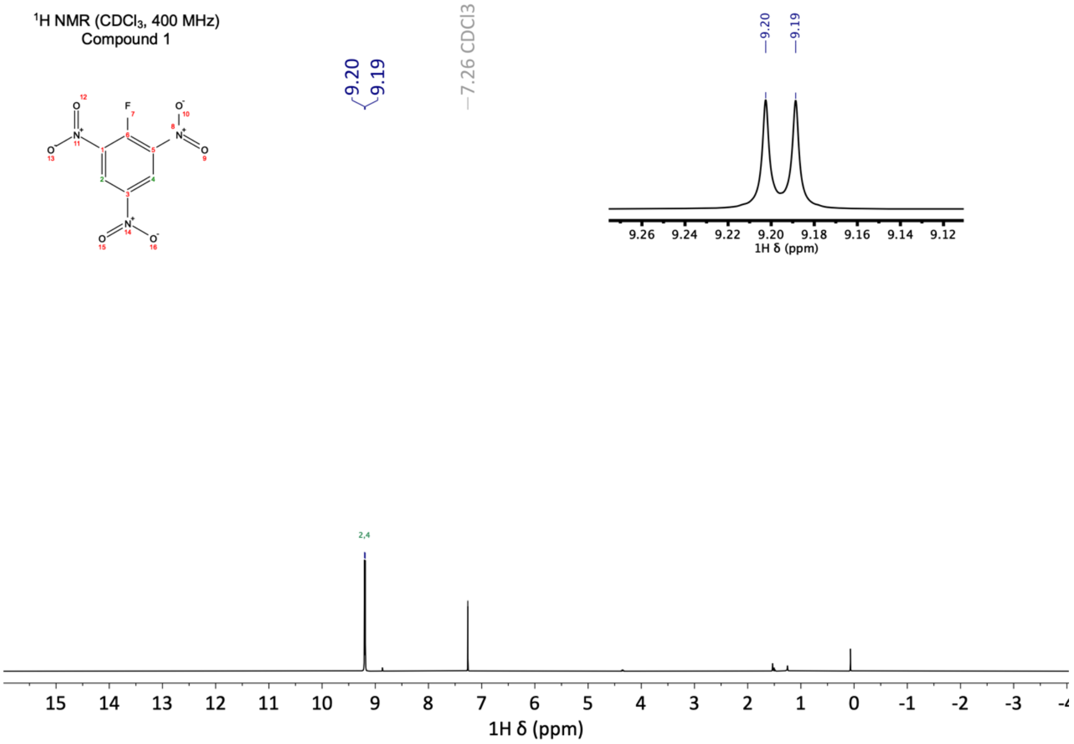

Figure S 4.1. Proton spectrum (^{1}H) of compound **1**.

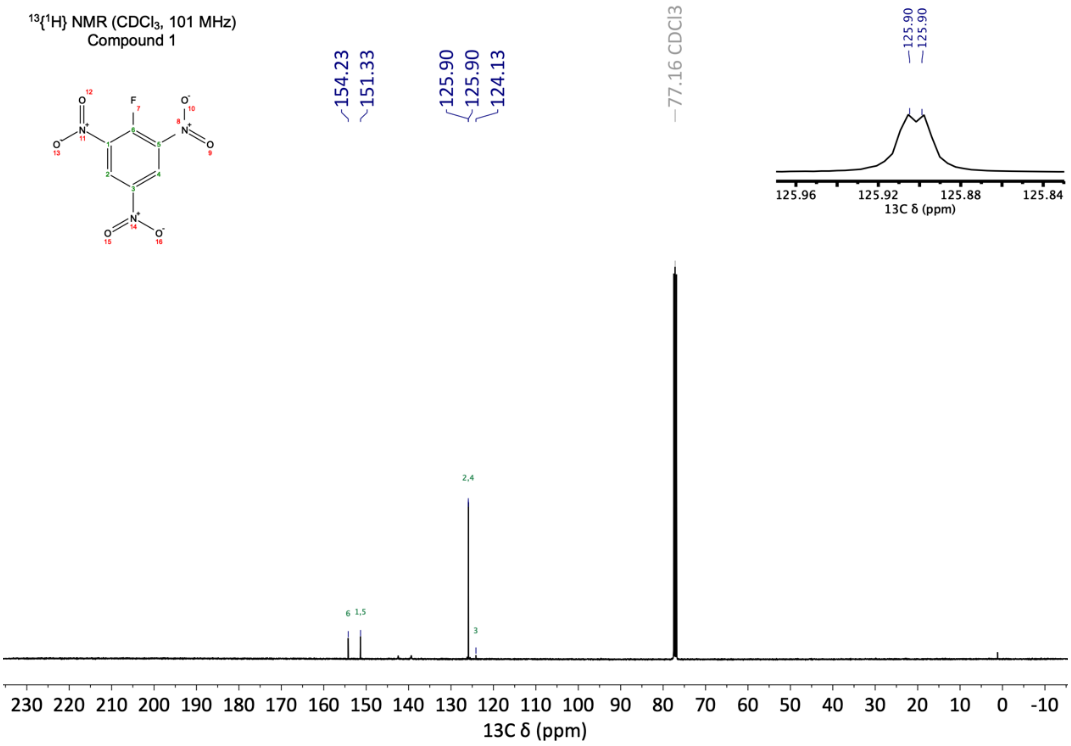

Figure S 4.2. Carbon spectrum (^{13}C) of compound **1**.

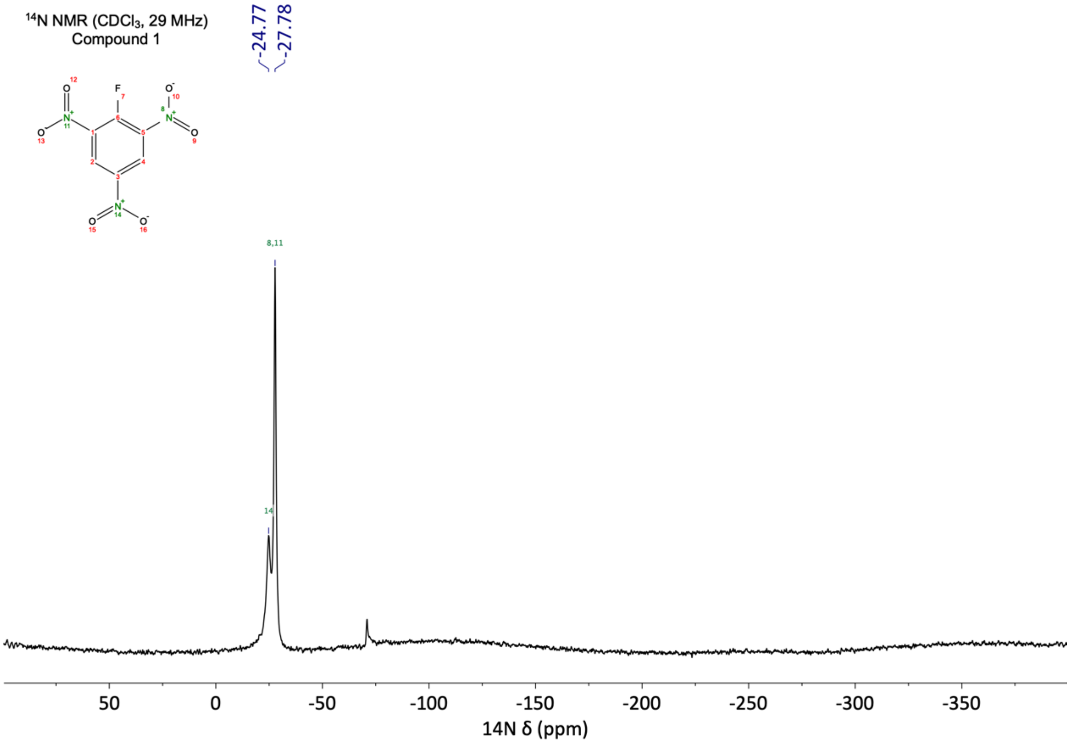

Figure S 4.3. Nitrogen spectrum (^{14}N) of compound **1**.

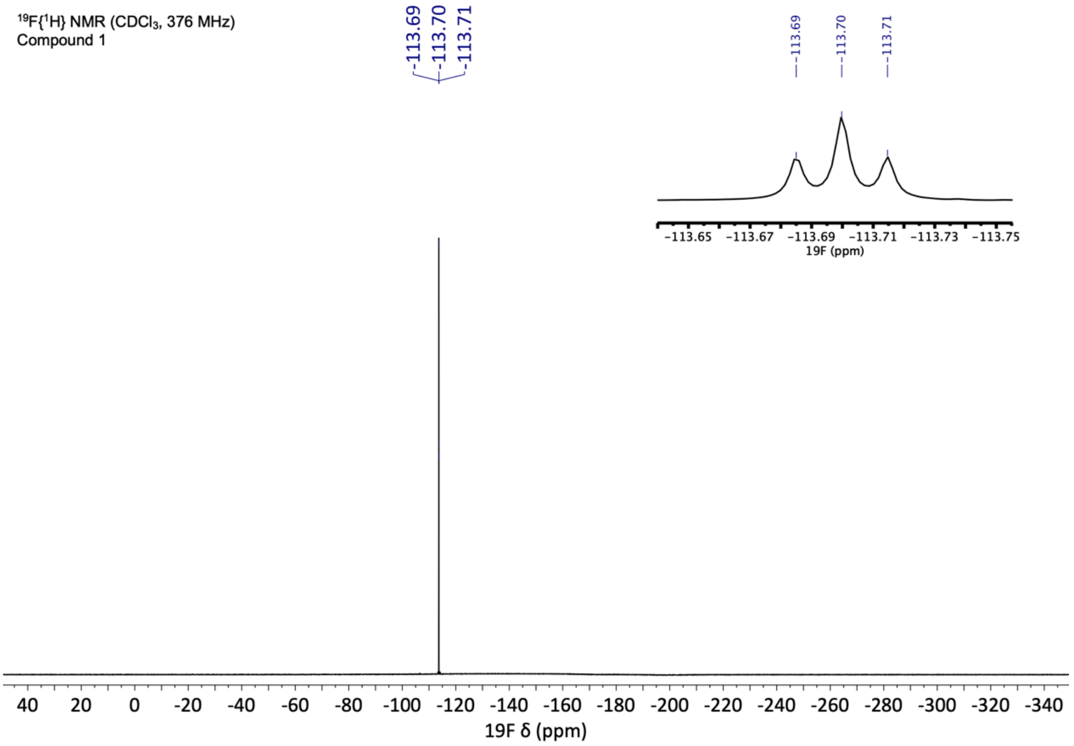

Figure S 4.4. Fluorine spectrum (^{19}F) of compound **1**.

Compound 2

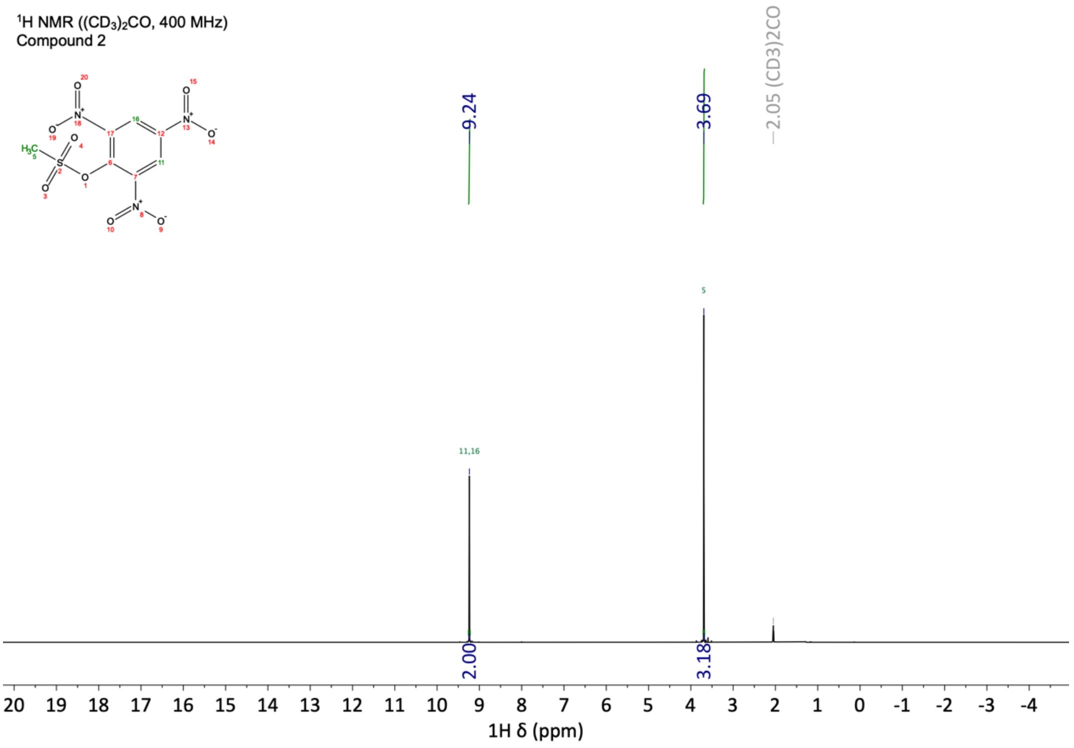

Figure S 4.5. Proton spectrum (^1H) of compound **2**.

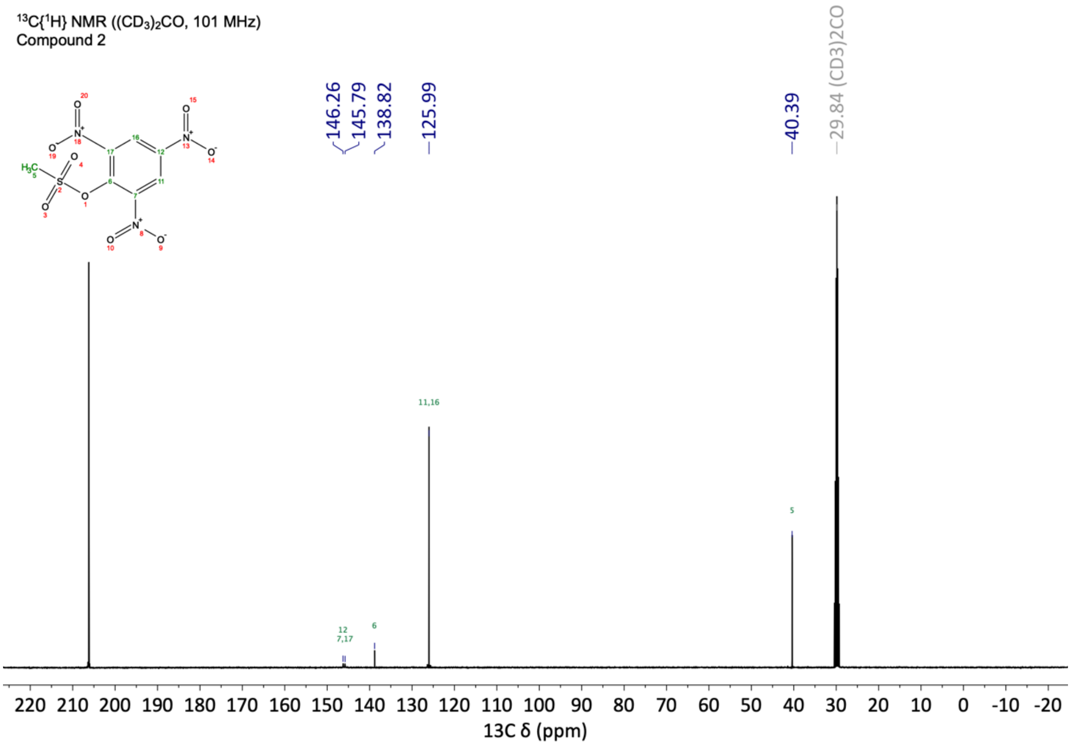

Figure S 4.6. Carbon spectrum (^{13}C) of compound **2**.

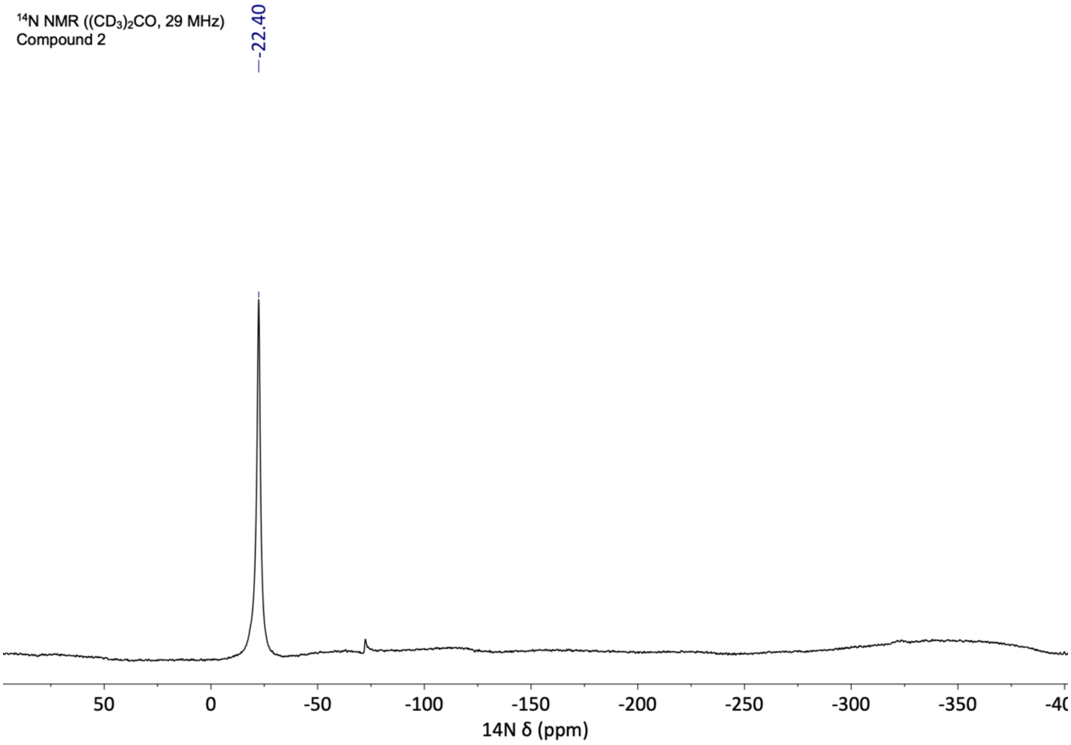

Figure S 4.7. Nitrogen spectrum (^{14}N) of compound **2**.

Compound 3

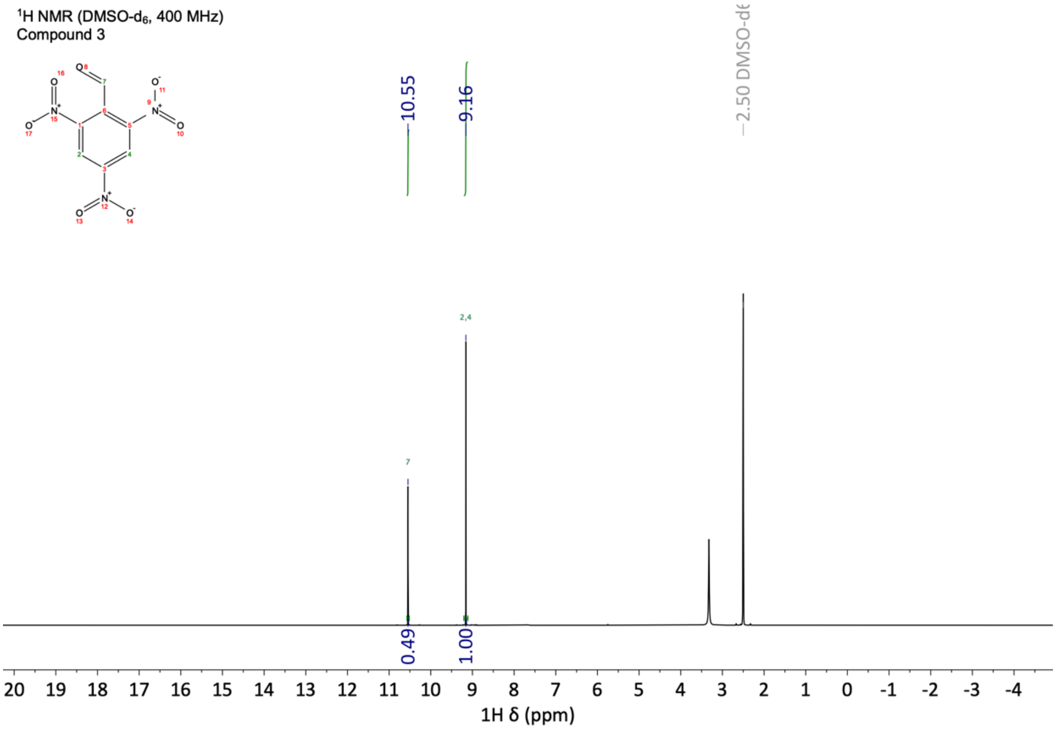

Figure S 4.8. Proton spectrum (^{1}H) of compound **3**.

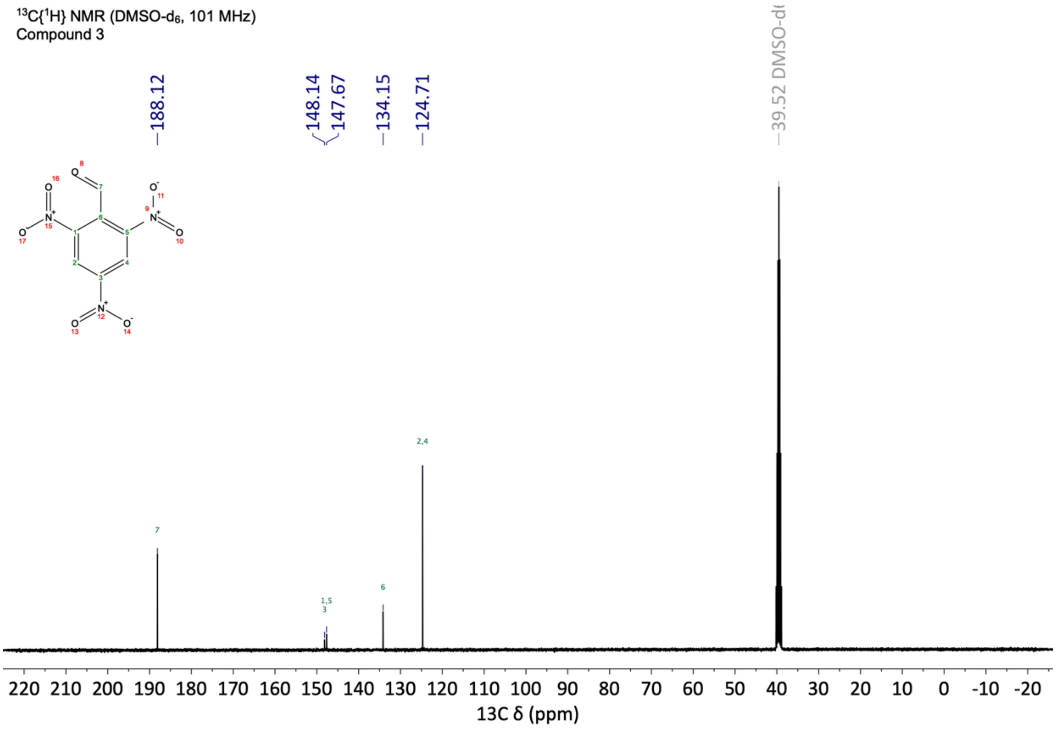

Figure S 4.9. Carbon spectrum (^{13}C) of compound **3**.

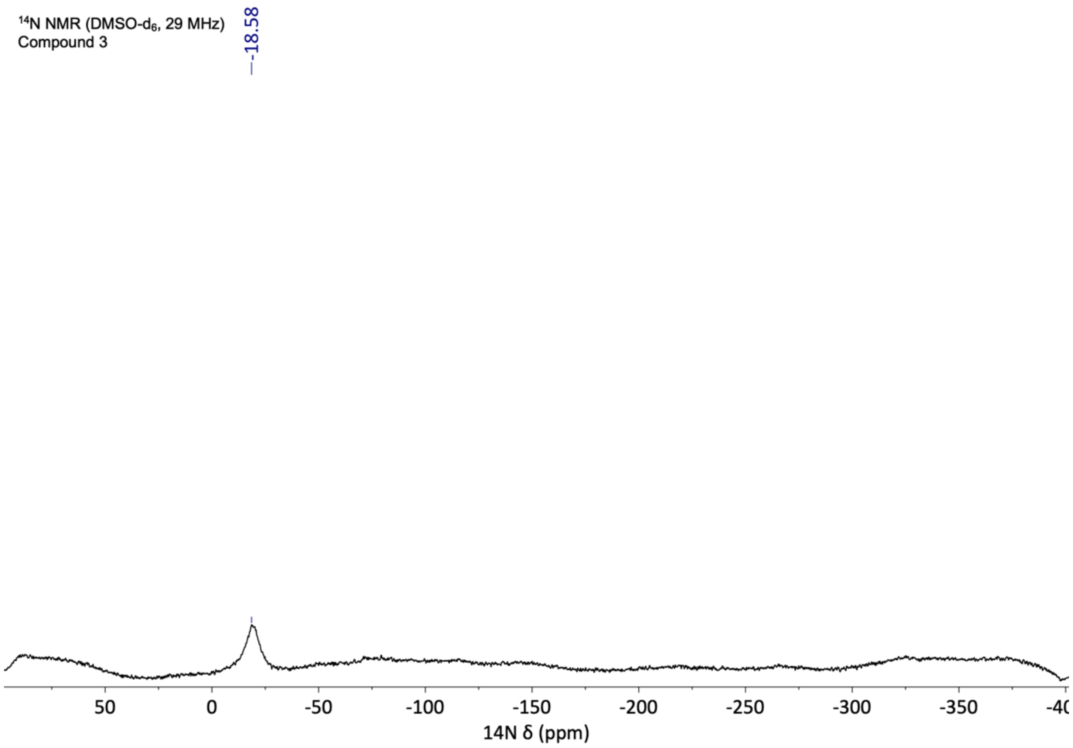

Figure S 4.10. Nitrogen spectrum (^{14}N) of compound **3**.

4.5.2 Detonation Parameter

Compound 1

C(6,000) H(2,000) N(3,000) O(6,000) F(1,000)

Molecular weight = 231,09
Density of reactant = 1,837 g/cm^3
Initial pressure = 0,1 MPa
Oxygen balance = -45,00052%
Enthalpy of formation = -1670,75 kJ/kg
Internal energy of formation = -1603,71 kJ/kg

Detonation parameters (at the C-J point):

Heat of detonation = -4070,915 kJ/kg
Detonation temperature = 3301,012 K
Detonation pressure = 23,86535 GPa
Detonation velocity = 7376,067 m/s
Particle velocity = 1761,295 m/s
Sound velocity = 5614,772 m/s

```
Density of products              = 2,413247 g/cm3
Volume of products               = 0,4143794 cm3/g
Exponent 'Gamma'                 = 3,187853
Moles of gaseous products        = 5,734581 mol/mol explosive
Moles of condensed products      = 2,679472 mol/mol explosive
Volume of gas at STP             = 606,8738 dm3/kg
Mean molecular mass of gas. prod.          = 34,6867 g/mol
Mean molecular mass of cond. prod.         =12,011 g/mol
Mean molecular mass of all prod.           = 27,46557 g/mol
Entropy of products              = 5,7983 kJ/kg K
Internal energy of products      = 5622,008 kJ/kg, i.e. 10,32763 kJ/cm3
Compression energy               = 1551,093 kJ/kg, i.e. 2,849357 kJ/cm3
Total heat energy                = -4070,915 kJ/kg, i.e. -7,478271 kJ/cm3

Composition of detonation products (47):
----------------------------------------------------------------------------------------------------
Products        mol/mol EM      mol/kg EM       Mol %       Mass %
----------------------------------------------------------------------------------------------------
C(d) =          2,679472E+00    1,159473E+01    31,8452     3,9264
CO2 =           2,142781E+00    9,272333E+00    25,4667     40,8075
N2 =            1,497698E+00    6,480902E+00    17,8000     18,1550
CO =             8,285554E-01   3,585361E+00    9,8473      10,0426
HF =            4,377052E-01    1,894057E+00    5,2021      3,7893
CH2O2 =         2,990076E-01    1,293879E+00    3,5537      5,9551
H2O =           2,876848E-01    1,244882E+00    3,4191      2,2427
H2F2 =          1,844428E-01    7,981289E-01    2,1921      3,1938
CF4 =           4,705893E-02    2,036354E-01    0,5593      1,7922
H2 =            2,905926E-03    1,257465E-02    0,0345      0,0025
HCN =           2,566023E-03    1,110381E-02    0,0305      0,0300
NH3 =           2,019898E-03    8,740591E-03    0,0240      0,0149
H3F3 =          1,490167E-03    6,448316E-03    0,0177      0,0387
CH2F2 =         2,035239E-04    8,806976E-04    0,0024      0,0046
CFO =           1,582283E-04    6,846926E-04    0,0019      0,0032
CH4 =           1,325425E-04    5,735436E-04    0,0016      0,0009
F =             1,046203E-04    4,527174E-04    0,0012      0,0009
C2H4 =          1,832081E-05    7,927862E-05    0,0002      0,0002
CNO =           1,054605E-05    4,563534E-05    0,0001      0,0002
H =             8,407203E-06    3,638002E-05    0,0001      0,0000
H4F4 =          8,134671E-06    3,520070E-05    0,0001      0,0003
```

CH3OH =	7,273919E-06	3,147602E-05	0,0001	0,0001
NH2 =	3,564576E-06	1,542479E-05	0,0000	0,0000
HCNO =	3,309321E-06	1,432024E-05	0,0000	0,0001
CH2O =	2,676408E-06	1,158147E-05	0,0000	0,0000
C2H6 =	2,567320E-06	1,110942E-05	0,0000	0,0000
H2O2 =	8,090705E-07	3,501045E-06	0,0000	0,0000
N2H4 =	6,373253E-07	2,757862E-06	0,0000	0,0000
N =	2,148729E-07	9,298074E-07	0,0000	0,0000
N2O =	1,371812E-07	5,936165E-07	0,0000	0,0000
F2 =	6,305020E-08	2,728336E-07	0,0000	0,0000
CFN =	5,508686E-08	2,383743E-07	0,0000	0,0000
H6F6 =	4,275934E-08	1,850301E-07	0,0000	0,0000
FO =	3,661208E-08	1,584294E-07	0,0000	0,0000
HFO =	3,420147E-08	1,479981E-07	0,0000	0,0000
H5F5 =	1,061634E-08	4,593947E-08	0,0000	0,0000
NF =	8,485902E-09	3,672056E-08	0,0000	0,0000
CF2 =	3,814907E-09	1,650803E-08	0,0000	0,0000
CHF =	2,935616E-09	1,270312E-08	0,0000	0,0000
NF3 =	1,007263E-09	4,358673E-09	0,0000	0,0000
CF =	2,293456E-10	9,924344E-10	0,0000	0,0000
CHF3 =	2,278122E-10	9,857989E-10	0,0000	0,0000
CF2O =	1,499837E-10	6,490161E-10	0,0000	0,0000
F2O =	1,336626E-11	5,783905E-11	0,0000	0,0000
CF3 =	2,299087E-12	9,948709E-12	0,0000	0,0000
C(gr) =	7,169055E-17	3,102225E-16	0,0000	0,0000
C2HF =	1,574275E-19	6,812273E-19	0,0000	0,0000

Compound 2

C(7,000) H(5,000) N(3,000) O(9,000) S(1,000)

Molecular weight = 307.19
Density of explosive = 1.795 g/cm^3
Oxygen balance = -49,47784%
Enthalpy of formation = -1734,44 kJ/kg
Internal energy of formation = -1655,76 kJ/kg

Detonation parameters (at the C-J point):

Heat of detonation = -3904,681 kJ/kg

Detonation temperature = 2240,498 K
Detonation pressure = 12,57338 GPa
Detonation velocity = 5862,976 m/s
Particle velocity = 1194,72 m/s
Sound velocity = 4668,256 m/s
Density of products = 2,254384 g/cm^3
Volume of products = 0,4435802 cm^3/g
Exponent 'Gamma' = 3,907376
Moles of gaseous products = 4,82162 mol/mol explosive
Moles of condensed products = 5,870428 mol/mol explosive
Volume of gas at STP = 383,86 dm3/kg
Mean molecular mass of gas. prod. = 31,24055 g/mol
Mean molecular mass of cond. prod. = 26,67034 g/mol
Mean molecular mass of all prod. = 28,73129 g/mol
Entropy of products = 5,9155 kJ/kg K
Internal energy of products = 4618,37 kJ/kg, i.e. 8,289973 kJ/cm^3
Compression energy = 713,6889 kJ/kg, i.e. 1,281072 kJ/cm^3
Total heat energy = -3904,681 kJ/kg, i.e. -7,008902 kJ/cm^3

Composition of detonation products:

Products	mol/mol EM	mol/kg EM	Mol %	Mass %
C(gr) =	4,870561E+00	1,585526E+01	45,5531	19,0437
N2 =	1,487744E+00	4,843091E+00	13,9145	13,5670
CO2 =	1,474806E+00	4,800973E+00	13,7935	21,1291
H2O =	1,162167E+00	3,783232E+00	10,8695	6,8156
H2SO4(l) =	9,998671E-01	3,254892E+00	9,3515	31,9237
CO =	3,860281E-01	1,256647E+00	3,6104	3,5199
CH2O2 =	2,512905E-01	8,180321E-01	2,3503	3,7650
NH3 =	2,342778E-02	7,626505E-02	0,2191	0,1299
H2 =	1,991075E-02	6,481597E-02	0,1862	0,0131
CH4 =	1,371934E-02	4,466091E-02	0,1283	0,0716
HCN =	1,079142E-03	3,512959E-03	0,0101	0,0095
C2H6 =	9,113819E-04	2,966844E-03	0,0085	0,0089
C2H4 =	2,912388E-04	9,480769E-04	0,0027	0,0027
H2S =	1,155614E-04	3,761900E-04	0,0011	0,0013
CH3OH =	1,012711E-04	3,296703E-04	0,0009	0,0011
SO2 =	1,607743E-05	5,233724E-05	0,0002	0,0003

CH2O =	6,274240E-06	2,042469E-05	0,0001	0,0001
HCNO	2,517524E-06	8,195359E-06	0,0000	0,0000
H =	8,063507E-07	2,624933E-06	0,0000	0,0000
NH2 =	7,235816E-07	2,355493E-06	0,0000	0,0000
N2H4 =	5,472519E-07	1,781483E-06	0,0000	0,0000
COS =	5,225123E-07	1,700947E-06	0,0000	0,0000
SO =	4,870590E-07	1,585535E-06	0,0000	0,0000
S =	8,669488E-08	2,822200E-07	0,0000	0,0000
CNO =	2,646984E-08	8,616794E-08	0,0000	0,0000
H2SO4 =	1,779389E-08	5,792489E-08	0,0000	0,0000
H2O2 =	1,261897E-08	4,107885E-08	0,0000	0,0000
SO3 =	1,161260E-08	3,780279E-08	0,0000	0,0000
S2 =	9,768153E-09	3,179851E-08	0,0000	0,0000
NS =	3,991198E-09	1,299265E-08	0,0000	0,0000
N2O =	6,494896E-10	2,114300E-09	0,0000	0,0000
N =	8,409478E-11	2,737558E-10	0,0000	0,0000
CS =	2,622255E-12	8,536292E-12	0,0000	0,0000
C(d) =	2,686988E-14	8,747018E-14	0,0000	0,0000
S(l) =	5,109685E-24	1,663368E-23	0,0000	0,0000

Compound 3

C(7,000) H(3,000) N(3,000) O(7,000)

Molecular weight = 241,11
Density of reactant = 1,721 g/cm^3
Initial pressure = 0,1 MPa
Oxygen balance = -56,40203 %
Enthalpy of formation = -676,87 kJ/kg
Internal energy of formation = -602,33 kJ/kg

Detonation parameters (at the C-J point):

Heat of detonation = -4391,028 kJ/kg
Detonation temperature = 3361,192 K
Detonation pressure = 20,43825 GPa
Detonation velocity = 7062,668 m/s
Particle velocity = 1681,48 m/s
Sound velocity = 5381,188 m/s
Density of products = 2,258767 g/cm^3

Volume of products = 0,4427193 cm^3/g
Exponent 'Gamma' = 3,200252
Moles of gaseous products = 6,073771 mol/mol explosive
Moles of condensed products = 3,279312 mol/mol explosive
Volume of gas at STP = 616,0655 dm3/kg
Mean molecular mass of gas. prod. = 33,21294 g/mol
Mean molecular mass of cond. prod. = 12,011 g/mol
Mean molecular mass of all prod. = 25,77926 g/mol
Entropy of products = 6,1434 kJ/kg K
Internal energy of products = 5804,73 kJ/kg, i.e. 9,989941 kJ/cm^3
Compression energy = 1413,702 kJ/kg, i.e. 2,432981 kJ/cm^3
Total heat energy = -4391,028 kJ/kg, i.e. -7,55696 kJ/cm^3

Composition of detonation products:

Products	mol/mol EM	mol/kg EM	Mol %	Mass %
C(d)	3,279251E+00	1,360059E+01	35,0606	16,3357
CO2 =	1,841066E+00	7,635760E+00	19,6841	33,6050
N2 =	1,488687E+00	6,174281E+00	15,9165	17,2960
CO =	1,249791E+00	5,183469E+00	13,3624	14,5189
H2O =	8,341380E-01	3,459560E+00	8,9183	6,2325
CH2O2 =	6,168757E-01	2,558472E+00	6,5954	11,7754
H2 =	1,720835E-02	7,137107E-02	0,1840	0,0144
NH3 =	1,360286E-02	5,641740E-02	0,1454	0,0961
HCN =	8,953327E-03	3,713363E-02	0,0957	0,1004
CH4 =	2,576904E-03	1,068763E-02	0,0276	0,0171
C2H4 =	4,559740E-04	1,891137E-03	0,0049	0,0053
C2H6 =	1,652431E-04	6,853405E-04	0,0018	0,0021
CH3OH =	1,227484E-04	5,090948E-04	0,0013	0,0016
C(gr) =	6,114367E-05	2,535914E-04	0,0007	0,0003
H =	3,718788E-05	1,542355E-04	0,0004	0,0000
CH2O =	2,582675E-05	1,071156E-04	0,0003	0,0003
NH2 =	2,155524E-05	8,939968E-05	0,0002	0,0001
CNO =	1,718879E-05	7,128993E-05	0,0002	0,0003
HCNO =	1,710196E-05	7,092983E-05	0,0002	0,0003
N2H4 =	6,513339E-06	2,701386E-05	0,0001	0,0001
H2O2 =	2,417571E-06	1,002680E-05	0,0000	0,0000
N =	3,764218E-07	1,561197E-06	0,0000	0,0000

N2O =	1,914663E-07	7,941001E-07	0,0000	0,0000

4.5.3 Structure Refinement Data

Compound 1

Empirical formula	$C_6H_2FN_3O_6$	
Formula weight	231.11	
Temperature	123(2) K	
Wavelength	0.71073 Å	
Crystal system	Trigonal	
Space group	R-3	
Unit cell dimensions	a = 21.7651(3) Å	α = 90°.
	b = 21.7651(3) Å	β = 90°.
	c = 8.9198(2) Å	γ = 120°.
Volume	3659.37(13) $Å^3$	
Z	18	
Density (calculated)	1.888 Mg/m^3	
Absorption coefficient	0.185 mm^{-1}	
F(000)	2088	
Crystal size	0.400 x 0.400 x 0.300 mm^3	
Theta range for data collection	2.526 to 30.502°.	
Index ranges	-31<=h<=31, -31<=k<=31, -12<=l<=12	
Reflections collected	24440	
Independent reflections	2477 [R(int) = 0.0224]	
Completeness to theta = 25.242°	99.3 %	
Absorption correction	Semi-empirical from equivalents	
Max. and min. transmission	1.00000 and 0.89869	
Refinement method	Full-matrix least-squares on F^2	
Data / restraints / parameters	2477 / 0 / 147	
Goodness-of-fit on F^2	1.035	
Final R indices [I>2sigma(I)]	R1 = 0.0316, wR2 = 0.0851	
R indices (all data)	R1 = 0.0358, wR2 = 0.0885	
Extinction coefficient	n/a	
Largest diff. peak and hole	0.456 and -0.177 $e.Å^{-3}$	

Compound 2

Empirical formula	$C_7H_5N_3O_9S$
Formula weight	307.20
Temperature	143(2) K

Wavelength	0.71073 Å	
Crystal system	Monoclinic	
Space group	$P2_1$	
Unit cell dimensions	a = 8.3195(6) Å	α = 90°.
	b = 7.9947(5) Å	β = 103.585(7)°.
	c = 8.5747(6) Å	γ = 90°.
Volume	554.36(7) Å3	
Z	2	
Density (calculated)	1.840 Mg/m3	
Absorption coefficient	0.349 mm-1	
F(000)	312	
Crystal size	0.450 x 0.400 x 0.050 mm3	
Theta range for data collection	3.531 to 28.275°.	
Index ranges	-11<=h<=11, -10<=k<=10, -11<=l<=10	
Reflections collected	4825	
Independent reflections	2522 [R(int) = 0.0170]	
Completeness to theta = 25.242°	99.7 %	
Absorption correction	Semi-empirical from equivalents	
Max. and min. transmission	1.00000 and 0.69252	
Refinement method	Full-matrix least-squares on F2	
Data / restraints / parameters	2522 / 1 / 201	
Goodness-of-fit on F2	1.056	
Final R indices [I>2sigma(I)]	R1 = 0.0267, wR2 = 0.0656	
R indices (all data)	R1 = 0.0285, wR2 = 0.0678	
Absolute structure parameter	0.32(4)	
Extinction coefficient	n/a	

Compound 3

Empirical formula	$C_7H_3N_3O_7$	
Formula weight	241.12	
Temperature	143(2) K	
Wavelength	0.71073 Å	
Crystal system	Orthorhombic	
Space group	Pbcn	
Unit cell dimensions	a = 10.5782(10) Å	α = 90°.
	b = 14.2749(16) Å	β = 90°.
	c = 12.0267(13) Å	γ = 90°.
Volume	1816.1(3) Å^3	
Z	8	

Density (calculated)	1.764 Mg/m3
Absorption coefficient	0.162 mm-1
F(000)	976
Crystal size	0.200 x 0.100 x 0.050 mm3
Theta range for data collection	4.151 to 28.281°.
Index ranges	-11<=h<=14, -19<=k<=18, -16<=l<=14
Reflections collected	15402
Independent reflections	2245 [R(int) = 0.0616]
Completeness to theta = 25.242°	99.5 %
Absorption correction	Semi-empirical from equivalents
Max. and min. transmission	1.00000 and 0.90557
Refinement method	Full-matrix least-squares on F2
Data / restraints / parameters	2245 / 0 / 166
Goodness-of-fit on F2	1.032
Final R indices [I>2sigma(I)]	R1 = 0.0432, wR2 = 0.0950
R indices (all data)	R1 = 0.0748, wR2 = 0.1110
Extinction coefficient	n/a
Largest diff. peak and hole	0.247 and -0.208 e.Å-3

4.5.4 Enlarged View of the Figures

Figure 2

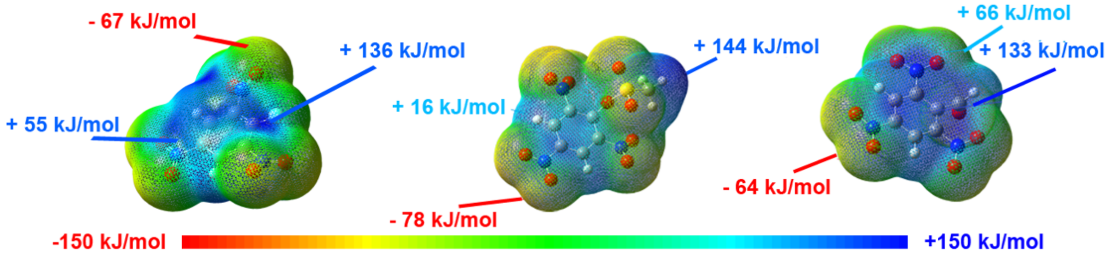

Figure S 4.11. ESP of **1** (left), **2** (center), and **3** (right), calculated on the 0.02 electron bohr^{-3} hypersurface.

Figure 3

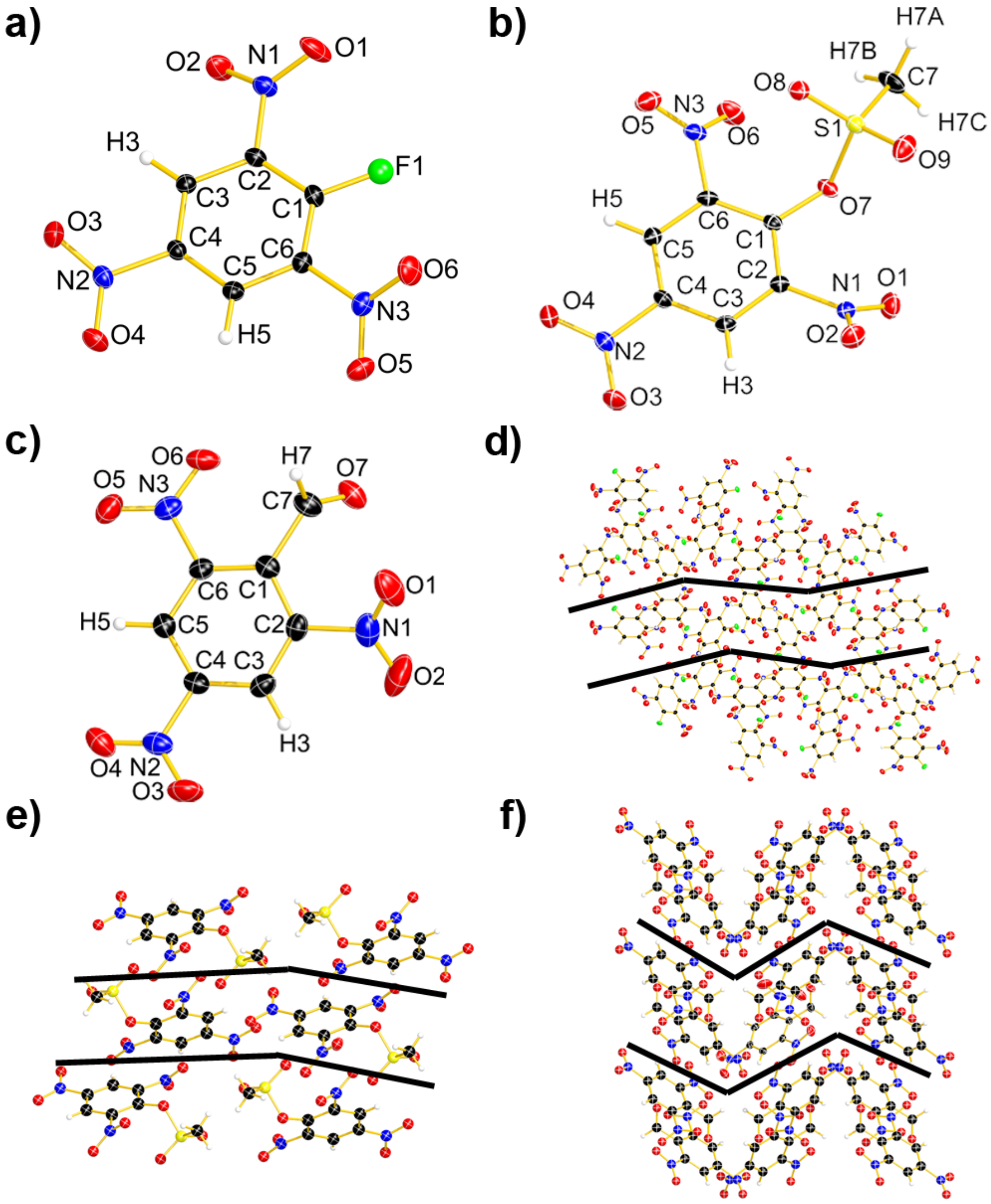

Figure S 4.12. Single-crystal X-ray structure of **1** (a), **2** (b), **3** (c) and the crystal packing of **1** (d), **2** (e), **3** (f).

Figure 4

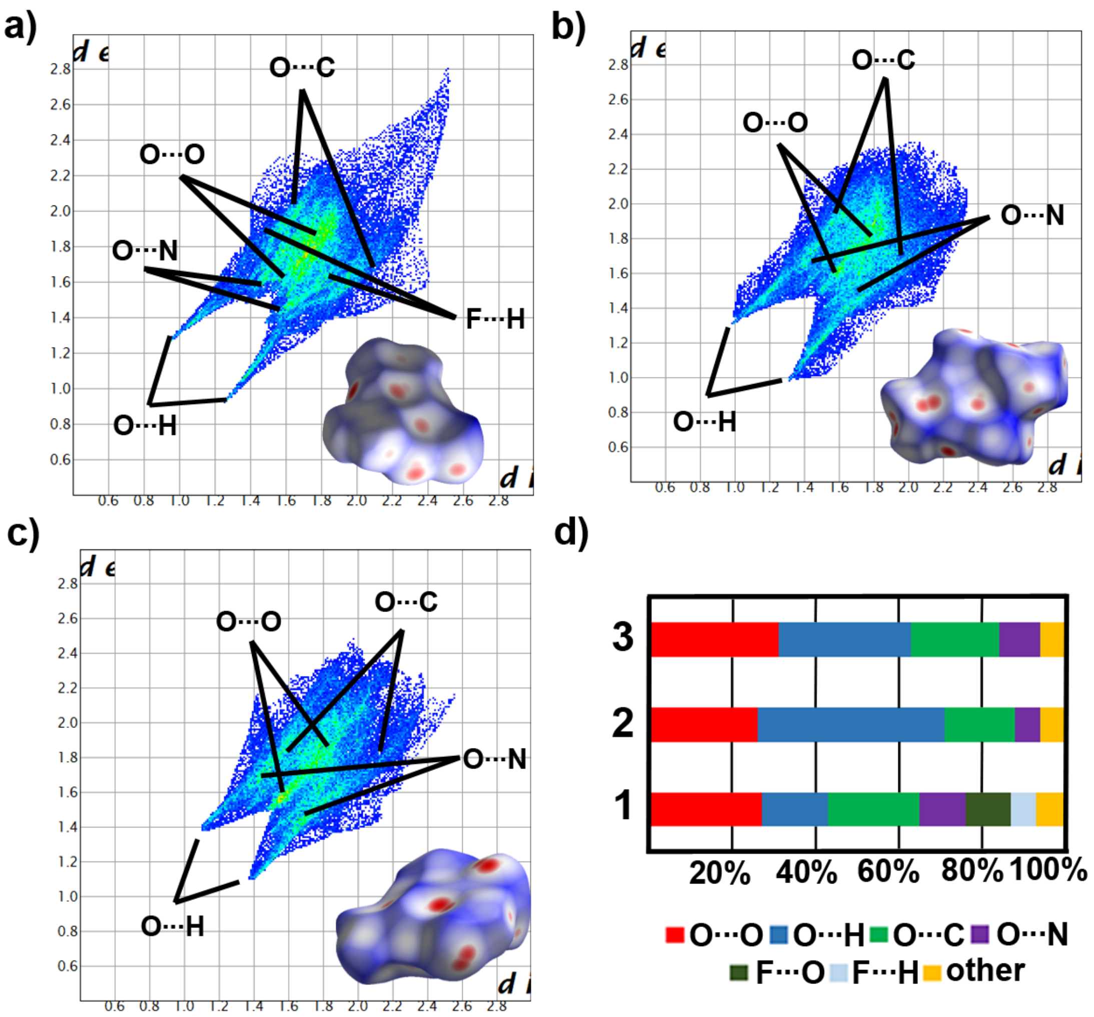

Figure S 4.13. Two-dimensional Fingerprint plot in crystal stacking as well as the corresponding Hirshfeld surface (bottom right in 2D plot) of **1** (a), **2** (b), and **3** (c) (color coding: white, distance *d* equals VDW distance; blue, *d* exceeds VDW distance; red, *d* smaller than VDW distance). Population of close contacts of **1**, **2**, and **3** in crystal stacking (d).

5 Improved Preparation of 3-Oximinooxetane – An Important Precursor to Energetic Oxetanes

by

Max Born, Konstantin Karaghiosoff and Thomas M. Klapötke

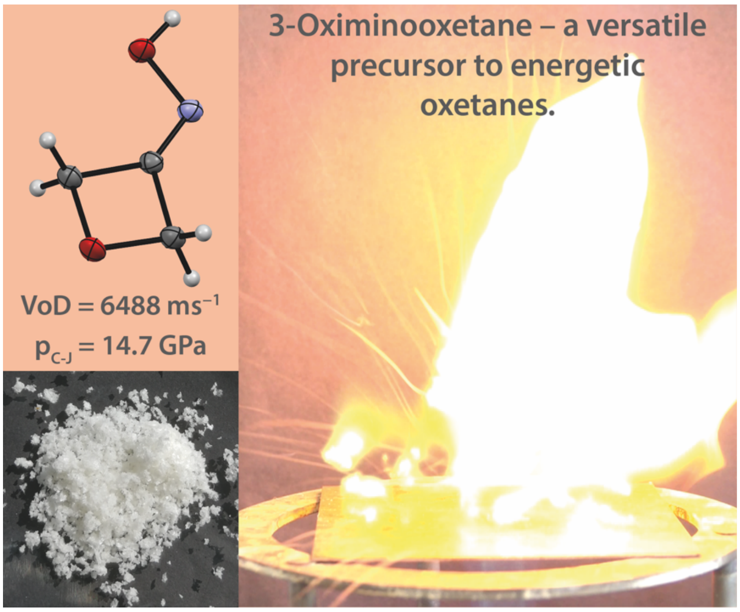

as published in
Propellants, Explosives, Pyrotechnics **2022**, *47*, e202100277
(doi:10.1002/prep.202100277)

Abstract

Oximes represent an extremely versatile building block in energetic materials chemistry. While oxidation with peroxyacids affords the corresponding mononitro compounds, tandem oxidation-nitration reactions such as the Scholl reaction lead to geminal dinitro compounds. Furthermore, the corresponding amines can be obtained by reduction of the oxime group. Accordingly, 3-oximinooxetane represents a suitable precursor for 3-nitro- and 3,3-dinitrooxetane as well as 3-aminooxetane. 3-Oximinooxetane, which is poorly described in the literature, has now been extensively characterized by vibrational-, mass- and NMR spectroscopy, as well as elemental and thermal analysis. In addition, its synthesis has been significantly improved compared to literature. The molecular structure was elucidated by single crystal X-ray diffraction. Since 3-oximinooxetane is energetic by itself, its performance was calculated using the EXPLO5 V6.04 thermochemical code and its sensitivity toward external stimuli such as impact, friction and electrostatic discharge was determined by BAM standard procedures.

Keywords: 3-Oximinooxetane, oxetan-3-one oxime, energetic monomer, energetic oxetanes.

5.1 Introduction

Oximes play an important role in the chemistry of energetic materials. They can be easily obtained from corresponding keto compounds and offer a great synthetic potential. Their reduction allows the synthesis of amines[1], which can be converted to nitramines or nitro compounds by oxidation of the amino group.[2] Direct oxidation of oximes with peroxyacids such as peroxytrifluoroacetic acid allows conversion into the corresponding mononitro compounds.[2] Tandem nitration-oxidation reactions such as the *Scholl* or *Ponzio* reaction even directly afford the respective geminal dinitro compounds (Scheme 1).[2]

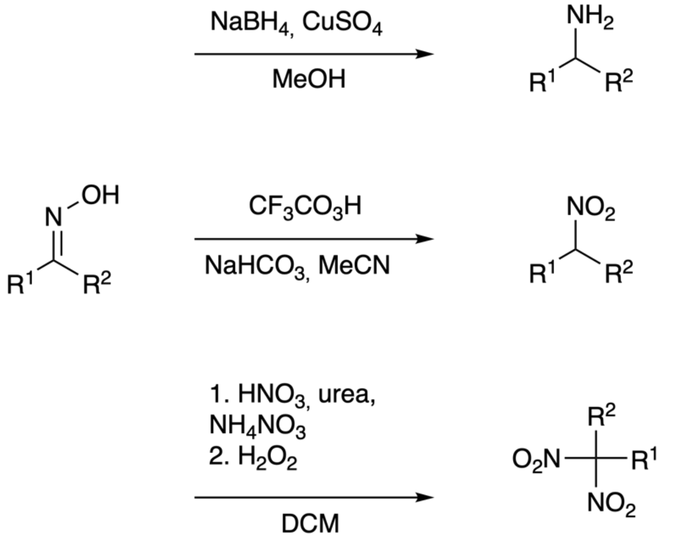

Scheme 5.1. Typical functional group transformations of oximes and exemplary reagents.[1,2]

Accordingly, 3-oximinooxetane is an important and general precursor for 3-nitrooxetane, 3,3-dinitrooxetane and 3-aminooxetane, which are currently only accessible via multiple steps starting from oxetan-3-ol (Scheme 2).[3]

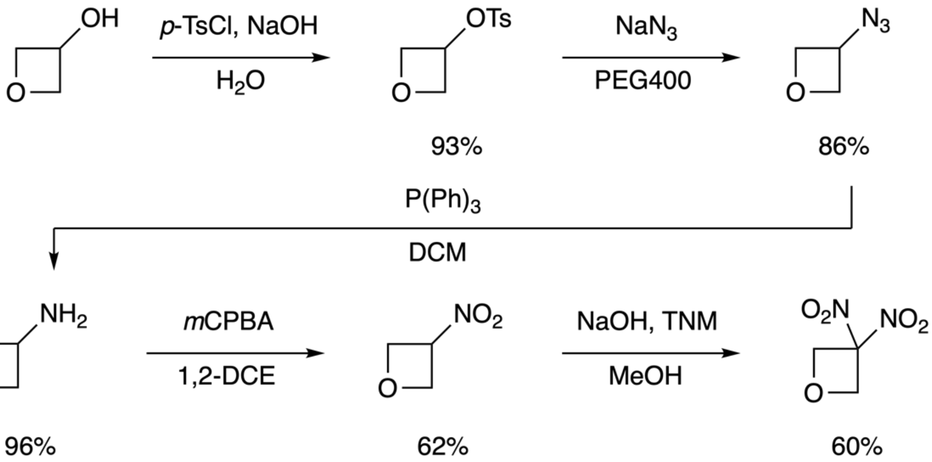

Scheme 5.2. Literature procedure for the preparation of 3-amino-, 3-nitro- and 3,3-dinitrooxetane.

The utility of 3-oximinooxetane as valuable starting material is further supported by the commercial availability of oxetan-3-one in the meantime. Despite this, the synthesis of 3-oximinooxetane is only poorly described in the literature, and its physicochemical and energetic properties are scarcely known or not known at all. A synthetic procedure for 3-oximinooxetane is disclosed in a patent by DuPont describing it as useful polymer intermediate.[4] Unfortunately, the reported yield of 82% is obtained after an overall reaction time of three days. A more recent and perhaps faster synthesis is indicated by Chen et al. in a general procedure for the preparation of cyclobutanone oxime esters.[5] However, 3-oximinooxetane is only used here as an intermediate and the required reaction time as well as the yield and further characterization of the compound are not reported. Thus, a straightforward synthesis of 3-oximinooxetane in high yield is still highly desirable.

Herein, we report an improved synthesis of 3-oximinooxetane with high yield and purity starting from the corresponding carbonyl compound oxetane-3-one. Its crystal and molecular structure was elucidated by single crystal X-ray diffraction for the first time. The compound was also studied in detail by thermal analysis and spectroscopic methods. First indications about its energetic performance were obtained applying the EXPLO5 V6.04 thermochemical code[6] and its sensitivity to external stimuli such as impact and friction was determined.

5.2 Experimental Section

5.2.1 Methods and Materials

All reagents and solvents were used as received (Sigma-Aldrich, ABCR, TCI). FT-IR spectra were measured with a Perkin Elmer Spectrum One FT-IR instrument using neat compounds. Raman spectra were recorded with a Bruker MultiRam FT Raman spectrometer using a neodymium-doped yttrium aluminum garnet (Nd:YAG) laser (λ = 1064 nm) and 1074 mW output. NMR spectra were measured with a Bruker Avance 400 instrument operating at 400.1 MHz (^{1}H), 100.6 MHz (^{13}C) and 40.5 MHz (^{15}N) using TMS (^{1}H and ^{13}C) or nitromethane (^{15}N) as reference. X-ray data were collected using an Oxford Xcalibur3 diffractometer equipped with a CCD area detector and operating with Mo Kα radiation (λ = 0.7107 Å). Thermal behavior was assessed using a Mettler Toledo DSC822e instrument at a heating rate of 5 °C min^{-1} using 40 µL aluminum crucibles with a lid hole and nitrogen purge gas at a flow rate of 30 mL min^{-1}. Elemental analysis was performed with an Elementar Vario EL device by sample pyrolysis and subsequent analysis of formed gases. The density of 3-oximinooxetane was calculated from the obtained X-ray density using a thermal correction factor ($\rho_{298\,K} = \rho_{143\,K}/1.028$). The sensitivity data was assessed using a BAM (Bundesanstalt für Materialforschung) drop hammer according to STANAG 4489 modified instruction[7] and a BAM friction tester according to STANAG 4487 modified instruction.[8]

5.2.2 Synthesis of 3-Oximinooxetane

Oxetan-3-one (2.00 g, 27.8 mmol) was dissolved in methanol (25.0 mL) and the solution added to a mixture of hydroxylammonium chloride (2.89 g, 41.6 mmol, 1.5 eq.) and sodium hydroxide (1.67 g, 41.6 mmol, 1.5 eq.) in a 50 mL round bottom flask. An instantaneous exothermic reaction was observed causing a mild boiling. The flask was quickly equipped with a reflux condenser and the obtained suspension was vigorously refluxed for two hours using an oil bath. Subsequently, the mixture was evaporated to dryness and dichloromethane (40 mL) was added. Afterward, all inorganic salts were removed by filtration through a Celite plug which was thoroughly rinsed with additional dichloromethane (2 × 30 mL). The solvent was removed by rotary evaporation to afford 2.22 g (25.5 mmol, 92%) of 3-oximinooxetane as colorless solid.

^{1}H NMR (400 MHz, $CDCl_3$, 25 °C): δ = 8.67 (s, 1H, NOH), 5.33 (A-part of AA'BB', 2H, CH_2), 5.27 (B-part of AA'BB', 2H, CH_2). **^{13}C{^{1}H} NMR** (101 MHz, $CDCl_3$, 25 °C): δ = 153.61, 79.07, 79.06. **^{15}N NMR** (41 MHz, $CDCl_3$, 25 °C): δ = −66.9. **FT-IR** (ATR, cm^{-1}): ṽ = 3298 (m), 3184 (m), 2983 (w), 2940 (m), 2884 (m), 1462 (m), 1443 (m), 1433 (m), 1304 (w), 1184 (m), 1114 (w), 1049 (w), 964 (s), 939 (vs), 920 (s), 863 (s), 737 (s), 666 (vs), 535 (s), 420 (m). **Raman** (1075 nm, 1000 mW, cm^{-1}): ṽ = 3310 (8), 2982 (37), 2946 (67), 2915 (12), 2851 (10), 1746 (12), 1731 (10), 1453 (45), 1432 (18), 1308 (12), 1279 (16), 1183 (10), 1139 (24), 1106 (8), 965 (100), 938 (47), 927 (63), 871 (10), 738 (18), 543 (80), 421 (37). **EA** calcd. for $C_3H_5NO_2$ (87.08 g mol^{-1}): C 41.38, H 5.79, N 16.09. Found: C 41.10, H 5.81, N 15.81. **HRMS** (EI) m/z: $[M]^+$ calcd. for $C_3H_5NO_2$ 87.0320. Found 88.0394 $[M+H]^+$, 70.0288 $[C_3H_4NO]^+$, 59.0366 $[C_2H_5NO]^+$, 57.0210 $[C_2H_3NO]^+$, 56.0132 $[C_2H_2NO]^+$, 43.0178 $[C_2H_3O]^+$, 41.0258 $[C_3H_5NO_2]^+$. **DSC** (5 °C min^{-1}): 88.9 °C (m.p.) 178.6 °C (dec.). **IS**: > 40 J. **FS**: > 360 N. **ESD**: 1.0 J.

5.3 Results and Discussion

5.3.1 Synthesis

First a short comparative screening was performed (0.5 g scale) to assess optimum conditions for the preparation of 3-oximinooxetane. In all cases, hydroxylammonium chloride (1.5 eq.) was employed and sodium hydroxide (1.5 eq.) was used as base to form hydroxylamine *in situ*. Water, acetonitrile and methanol were chosen as suitable, polar solvents. In addition to ambient conditions, reflux conditions and sonication were investigated. According to literature, silica gel acts as catalyst in the solvent-free synthesis of oximes.[9] Although a solvent-free synthesis was not attempted, silica was added to reference batches to study a potential influence on the reaction. However, no apparent effect could be found in this case. The results of the respective trials are summarized in Table 1.

Table 5.1. Preparation of 3-oximinooxetane using different conditions.

Condition	**rt**	**Ultrasound**		**Reflux**			
Solvent	Water	MeCN		MeCN		MeOH	
Silica gel	no	no		no	yes	no	yes
Time [h]	48	2	4	3	3	1.5	1.5
Yield [%]	38	66	44	75	82	93	78

The best result was obtained using methanol as solvent and reflux conditions without any catalyst. Upscaling by a factor of four required a slightly prolonged reaction time to afford a similar yield (Scheme 3).

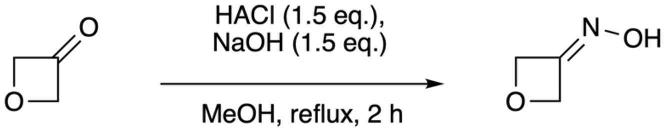

1 (92%)

Scheme 5.3. Improved preparation of 3-oximinooxetane.

5.3.2 Crystallography

Single crystals of 3-oximinooxetane were obtained by slow evaporation of a saturated solution in chloroform. The compound crystallizes in the monoclinic space group $P2_1/n$ with four formula units per unit cell and a density of 1.486 g cm^{-1} (143 K) corresponding to a room temperature density of 1.450 g cm^{-1}. As expected, all bond angles of the oxetane ring show significant deviations from the ideal tetrahedral angle of sp^3-hybridized carbon atoms. Within the oxetane ring, angles range from 88.8(8)° (O1–C2–C3) and 89.1(8)° (O1–C1–C3) up to 89.6(8)° (C2–C3–C1), while the largest angle is found at the oxygen atom (C1–O1–C2, 92.4(7)°). The shortest bond within the ring is found between O1 and C1 (1.462(1) Å) and the longest between C2 and C3 (1.501(1) Å) (Figure 1 a).

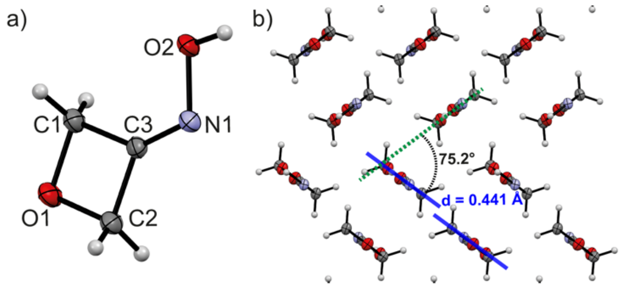

Figure 5.1. a) Molecular structure of 3-oximinooxetane in the crystal. b) Arrangement of the 3-oximinooxetane molecules in the crystal, view along the *c* axis.

The oxetane ring is essentially planar with a puckering angle of only 1.38°, which is much smaller than in the unsubstituted parent compound oxetane (8.7(2)°, 140 K).[10] The oximino group is slightly bend out of the oxetane plane (C1–C3–C3) by 0.9°. Both the C–N bond length (1.263(2) Å) and N–O bond length (1.416(1) Å) are in the expected range.[11] The view along the *c* axis (Figure 1 b) reveals an arrangement of the molecular entities in two types of parallel layers which intersect at an angle of 75.2°. Between parallel layers, an interlayer distance of 0.441 Å is found.

5.3.3 Physicochemical and Energetic Properties

The thermal behaviour of 3-oximinooxetane was analyzed by differential scanning calorimetry (DSC) at a heating rate of 5 °C min^{-1} revealing a melting point of 88.9 °C and a decomposition temperature of 178.6 °C. When heated on a copper plate by means of a Bunsen burner (hot plate test), the material deflagrates quite violently with a bright orange flame and a hissing noise (see Supporting Information). The heat of formation was calculated by *ab-initio* methods using Gaussian16 on the CBS-4M level of theory making use of the obtained crystal structure.[12] A heat of formation of −84.5 kJ mol^{-1} was calculated. Subsequently, the EXPLO5 V6.04 thermochemical code was used to assess the energetic performance of 3-oximinooxetane.[6] Although it has not previously been described in the literature as an energetic or sensitive compound, the oxime exhibits a detonation velocity of 6488 ms^{-1} and a detonation pressure of 14.7 GPa and shows sensitivity toward mechanical stimuli and electrostatic discharge (Table 2). Based on calculated values, it outperforms the well-known oxetane monomer NIMMO and even competes with the highly performant BAMO. Thus, it represents an considerably energetic, but "insensitive" compound.[13]

Table 5.2. Important physicochemical and energetic properties of 3-oximinooxetane in comparison to NIMMO and BAMO.

	1	**NIMMO**	**BAMO**
Formula	$C_3H_5NO_2$	$C_5H_9NO_4$	$C_5H_8N_6O$
FW [$g\cdot mol^{-1}$]	87.08	147.13	168.16
IS[a] [J]	40	40	40
FS[b] [N]	360	360	360
Ω[c] [%]	−64.3	−59.8	−76.12
T_m[d]/ T_{dec}[e] [°C]	88.9, 178.6	−13.8, 170.3	-, 207.3
ρ[f] [$g\cdot cm^{-3}$]	1.45	1.19	1.23
$\Delta H_f°$[g] [$kJ\cdot mol^{-1}$]	84.5	−268.9	510.5
		EXPLO5 V6.04	
$-\Delta_E U°$[h] [$kJ\cdot kg^{-1}$]	3833	3949	4479
T_{C-J}[i] [K]	2453	2507	2786
p_{C-J}[j] [GPa]	14.7	10.6	12.4
D_{C-J}[k] [$m\cdot s^{-1}$]	6488	5906	6548
V_0[l] [$dm^3\cdot kg^{-1}$]	772	827	797

[a] Impact sensitivity (BAM drop hammer, method 1 of 6). [b] Friction sensitivity (BAM friction apparatus, method 1 of 6). [c] Oxygen balance based on CO formation. [d] Melting point (DSC, $\beta = 5\ °C\cdot min^{-1}$). [e] Decomposition temperature (DSC, $\beta = 5\ °C\cdot min^{-1}$). [f] Density at 298 K – weighing of 100 µL (NIMMO, BAMO). [g] Standard molar enthalpy of formation. [h] Detonation energy. [i] Detonation temperature. [j] Detonation pressure. [k] Detonation velocity. [l] Volume of detonation gases at standard temperature and pressure.

5.4 Conclusion

Due to the significantly improved synthetic procedure in comparison to literature methods, 3-oximinooxetane can now be obtained in very high yield and purity after a short reaction time starting from commercially available materials. It has been extensively characterized for the first time, its crystal and molecular structure has been elucidated and its energetic properties investigated and demonstrated. As a result, 3-oximinooxetane is likely to be employed as precursor for the synthesis of the energetic derivatives 3-nitrooxetane and 3,3-dinitrooxetane in the future. These can be used to prepare useful energetic binders by cationic ring-opening polymerization. Furthermore, the described oxime is capable to provide 3-aminooxetane by reduction, which can also serve as a versatile precursor to various energetic oxetane derivatives.

Abbreviations

BAMO, 3,3-bis(azidomethyl)oxetane; 1,2-DCE, 1,2-dichloroethane; DCM, dichloromethane; HACl, hydroxylammonium chloride; *m*CPBA, *meta*-chloroperoxybenzoic acid; NIMMO, 3-

nitratomethyl-3-methyloxtane; *p*-TsCl, *para*-toluenesulfonyl chloride; TNM, tetranitromethane.

Acknowledgements

Financial support of this research by the Ludwig Maximilian University of Munich (LMU) and the Office of Naval Research (ONR) under grant no. ONR N00014-19-1-2078 and the Strategic Environmental Research and Development Program (SERDP) under contract no. W912HQ-19C0033 is gratefully acknowledged. We also thank Stefan Huber for sensitivity testing.

References

[1] Rao, H.; Bharathi, B. Reduction of oximes with sodium borohydride - copper(II)sulfate in methanol. *Indian J. Chem.* **2002,** *41B*, 1072-1074.

[2] Agrawal, J.; Hodgson, R. *Organic Chemistry of Explosives*, John Wiley & Sons Ltd.: Hoboken, New Jersey, **2006**, pp 1-65.

[3] Baum, K.; Berkowitz, P. T.; Grakauskas, V.; Archibald, T. G. Synthesis of electron-deficient oxetanes. 3-Azidooxetane, 3-nitrooxetane, and 3,3-dinitrooxetane. *J. Org. Chem.* **1983**, *48*, 2953-2956.

[4] Berezin, G. H. Oxetane Derivatives, US 3 449 369, **1969**.

[5] He, B.-Q.; Yu, X.-Y.; Wang, P.-Z.; Chen, J.-R.; Xiao, W.-J. A photoredox catalyzed iminyl radical-triggered C–C bond cleavage/addition/Kornblum oxidation cascade of oxime esters and styrenes: synthesis of ketonitriles. *Chem. Commun.* **2018**, *54*, 12262-12265.

[6] Sućeska, M., EXPLO5, Version 6.04, Brodarski Institute, Zagreb, **2017**.

[7] NATO STANAG 4489: *Explosives. Impact Sensitivity Tests*; NATO Standardization Office, Brussels, Belgium, **1999**.

[8] NATO STANAG 4487: *Explosives. Friction Sensitivity Tests*; NATO Standardization Office, Brussels, Belgium, **2002**.

[9] Damljanović, I.; Vukićević, M.; Vukićević, R. D. A Simple Synthesis of Oximes. Monatshefte für Chemie / Chemical Monthly **2006**, *137*, 301-305.

[10] Luger, P.; Buschmann, J. Oxetane: the first x-ray analysis of a nonsubstituted four-membered ring. *J. Am. Chem. Soc.* **1984**, *106*, 7118-7121.

[11] Orpen, A. G.; Brammer, L.; Allen, F. H.; Kennard, O.; Watson, D. G.; Taylor, R. In *Struct. Correl.* **1994**, pp 752-858.

[12] Frisch, M. J.; Trucks, G. W.; Schlegel, H. B.; Scuseria, G. E.; Robb, M. A.; Cheeseman, J. R.; Scalmani, G.; Barone, V.; Petersson, G. A.; Nakatsuji, H.; Li, X.; Caricato, M.; Marenich, A. V.; Bloino, J.; Janesko, B. G.; Gomperts, R.; Mennucci, B.; Hratchian, H. P.; Ortiz, J. V.; Izmaylov, A. F.; Sonnenberg, J. L.; Williams; Ding, F.; Lipparini, F.; Egidi, F.; Goings, J.; Peng, B.; Petrone, A.; Henderson, T.; Ranasinghe, D.; Zakrzewski, V. G.; Gao, J.; Rega, N.; Zheng, G.; Liang, W.; Hada, M.; Ehara, M.; Toyota, K.; Fukuda, R.; Hasegawa, J.; Ishida, M.; Nakajima, T.; Honda, Y.; Kitao, O.; Nakai, H.; Vreven, T.; Throssell, K.; Montgomery Jr., J. A.; Peralta, J. E.; Ogliaro, F.; Bearpark, M. J.; Heyd, J. J.; Brothers, E. N.; Kudin, K. N.; Staroverov, V. N.; Keith, T. A.; Kobayashi, R.; Normand, J.; Raghavachari, K.; Rendell, A. P.; Burant, J. C.; Iyengar, S. S.; Tomasi, J.; Cossi, M.; Millam, J. M.; Klene, M.; Adamo, C.; Cammi, R.; Ochterski, J. W.; Martin, R. L.; Morokuma, K.; Farkas, O.; Foresman, J. B.; Fox, D. J., Gaussian 16 Rev. C.01, **2016**.

[13] United Nations (UN), UN Recommendations on the Transport of Dangerous Goods, Manual of Tests and Criteria, **2009**.

5.5 Supporting Information

5.5.1 NMR Spectra

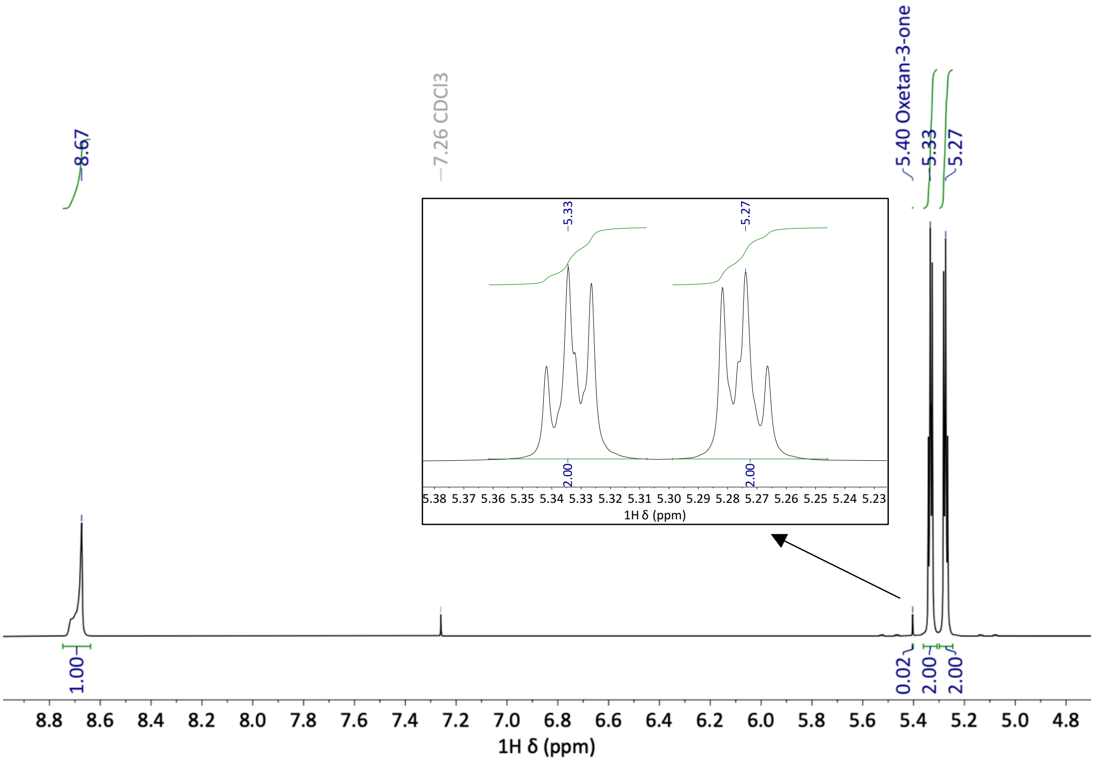

Figure S 5.1. Proton spectrum (^{1}H) of 3-oximinooxetane.

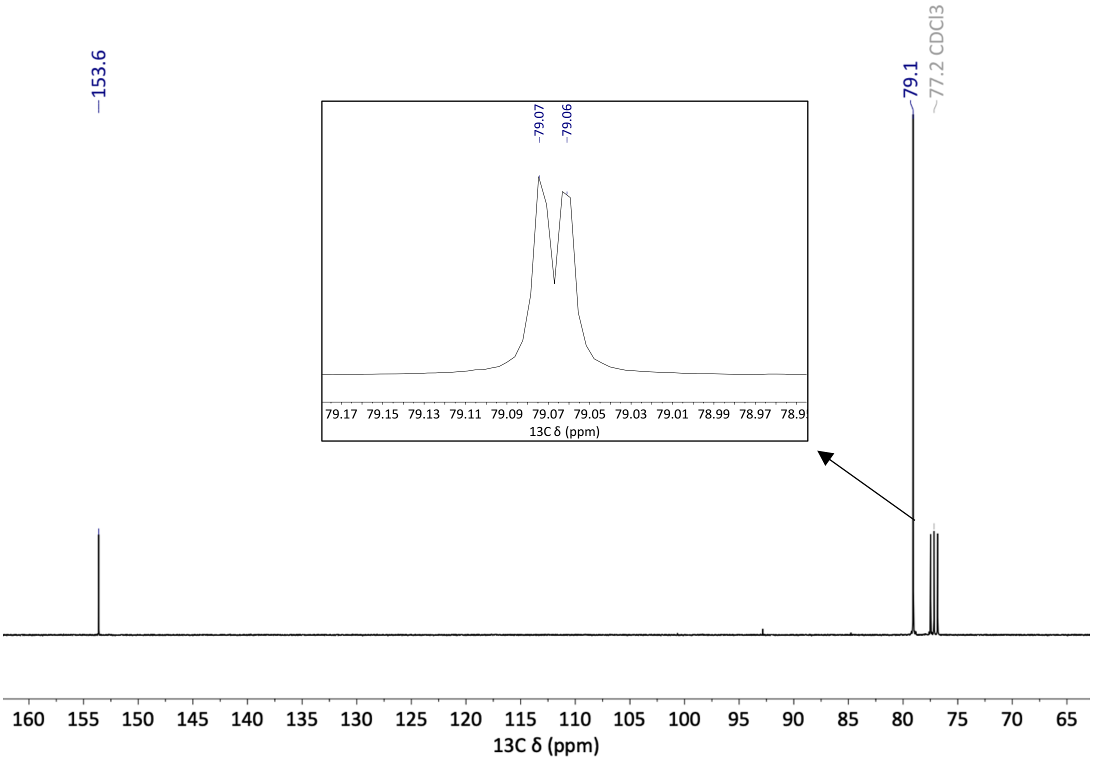

Figure S 5.2. Carbon spectrum (^{13}C) of 3-oximinooxetane.

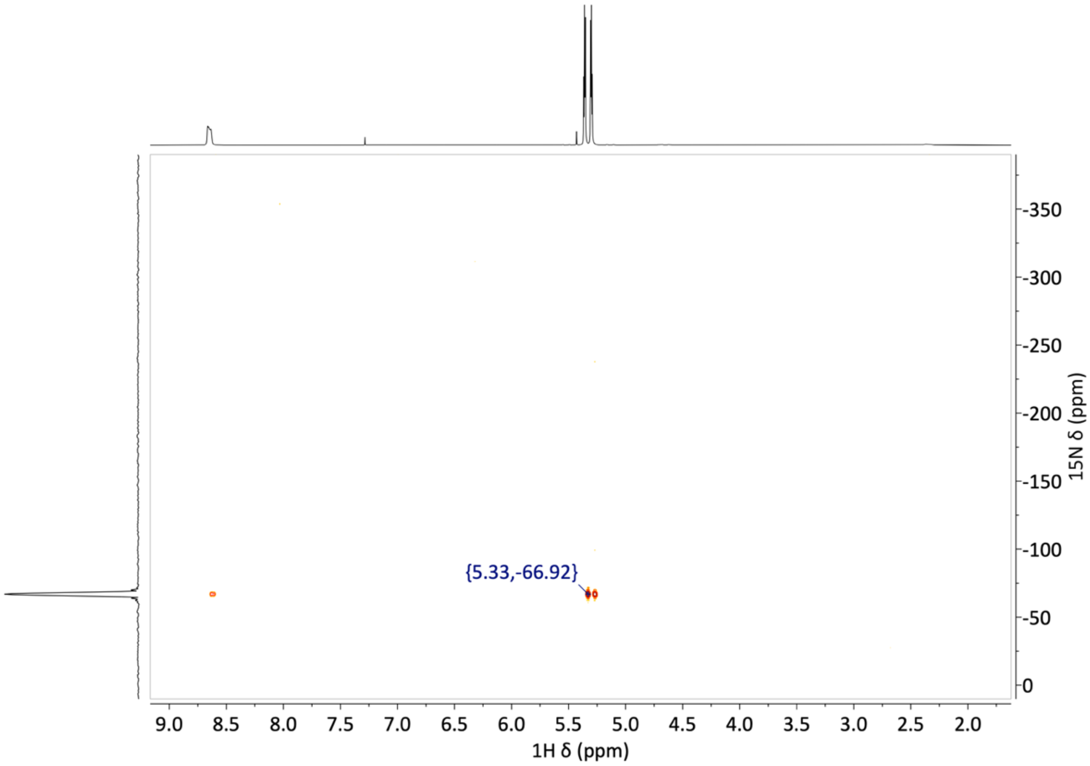

Figure S 5.3. Nitrogen spectrum (^{1}H, ^{15}N HMBC) of 3-oximinooxetane.

5.5.2 Heat of Formation Calculation and Thermal Analysis

The atomization method was used to determine the heat of formation of 3-oximinooxetane using the atom energies in Table S 1.[1,2]

$$\Delta_f H^\circ_{(g,\ M,\ 298)} = H_{(molecule,\ 298)} - \Sigma H^\circ_{(atoms,\ 298)} + \Sigma \Delta_f H^\circ_{(atoms,\ 298)}$$

Table S 5.1. CBS-4M electronic enthalpies for atoms C, H, N, and O and their literature values.

	$-H^{298}$/ a.u.	$\Delta_f H^\circ_{gas}$[2]
H	0.500991	217.998
C	37.786156	716.68
N	54.522462	472.68
O	74.991202	249.18

The Gaussian16 program package was used to calculate room temperature enthalpies on the CBS-4M level of theory.[3] To obtain the energy of formation, Trouton's Rule was applied with regard to solids ($\Delta H_{sub} = 188 \cdot T_m$) or liquids ($\Delta H_{sub} = 90 \cdot T_m$), respectively.

Table S 5.2. Heat of formation calculation results for 3-oximinooxetane (**1**), NIMMO and BAMO.

M	$-H^{298}$[a] [a.u.]	$\Delta_f H^\circ(g, M)$[b] [kJ mol^{-1}]	$\Delta_{sub} H^\circ$ (M)[c] [kJ mol^{-1}]	$\Delta_f H^\circ(s/l)$ [d] [kJ mol^{-1}]	Δn	$\Delta_f U(s/l)$ [e] [kJ kg^{-1}]
3-OXO	321.978475	−16.5	68.0654	−84.5	−4.0	−856.9
NIMMO	550.685978	−229.0	39.9105	−268,9	−7.0	−1709.7
BAMO	598.057987	553.7	43.2405	510,5	−7.5	3146.4

[a] CBS-4M electronic enthalpy. [b] Gas phase enthalpy of formation. [c] Sublimation enthalpy. [d] Standard liquid/solid state enthalpy of formation. [e] Solid state energy of formation.

The thermal behavior of 3-oximinooxetane was analyzed by DSC at a heating rate of 5 °C min^{-1} to determine melting point and decomposition temperature. The obtained thermogram is depicted.

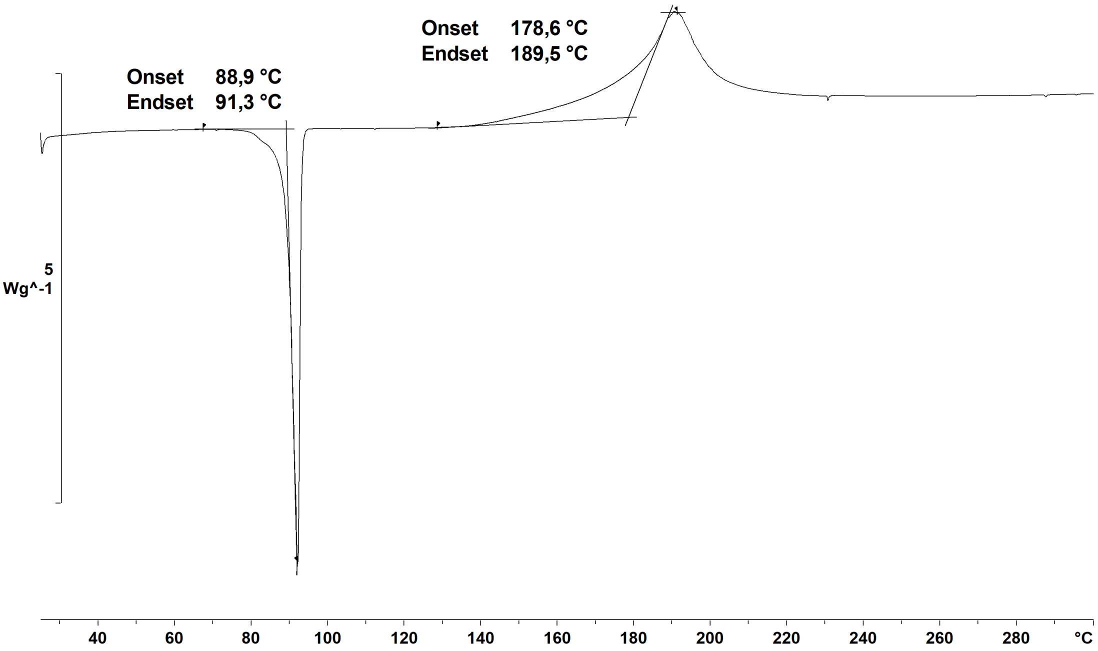

Figure S 5.4. DSC evaluation of 3-oximinooxetane.

5.5.3 Hot Plate Test

A hot plate test was performed by heating 50 mg of 3-oximinooxetane on a copper plate by means of a Bunsen burner. A violent deflagration occurs indicating the energetic character of the investigated oxime.

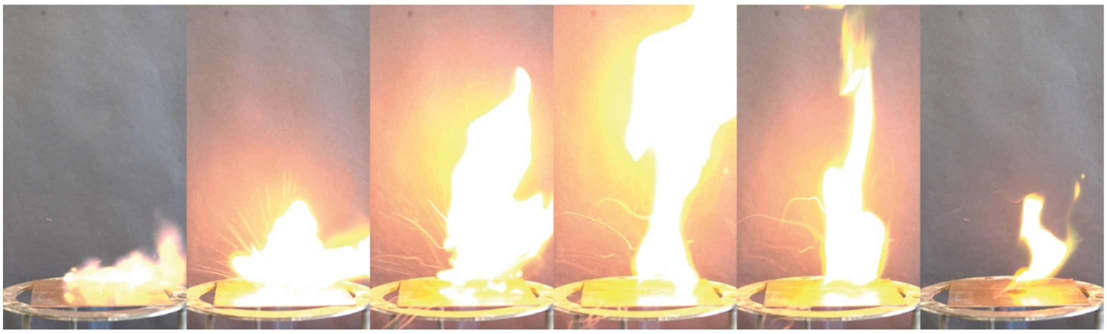

Figure S 5.5. Deflagration 3-oximinooxetane (50 mg).

References

[1] Altenburg, T.; Klapötke, Thomas M.; Penger, A.; Stierstorfer, J. Two Outstanding Explosives Based on 1,2-Dinitroguanidine: Ammonium- dinitroguanidine and 1,7-Diamino-1,7-dinitrimino-2,4,6-trinitro-2,4,6-triazaheptane. *Z. Anorg. Allg. Chem.* **2010**, *636*, 463-471.

[2] Chase, M. W. NIST-JANAF Thermochemical Tables, Fourth Edition, *J. Phys. Chem. Red. Data, Monograph 9,* **1998**, 1–1951.

[3] Frisch, M. J.; Trucks, G. W.; Schlegel, H. B.; Scuseria, G. E.; Robb, M. A.; Cheeseman, J. R.; Scalmani, G.; Barone, V.; Petersson, G. A.; Nakatsuji, H.; Li, X.; Caricato, M.; Marenich, A. V.; Bloino, J.; Janesko, B. G.; Gomperts, R.; Mennucci, B.; Hratchian, H. P.; Ortiz, J. V.; Izmaylov, A. F.; Sonnenberg, J. L.; Williams; Ding, F.; Lipparini, F.; Egidi, F.; Goings, J.; Peng, B.; Petrone, A.; Henderson, T.; Ranasinghe, D.; Zakrzewski, V. G.; Gao, J.; Rega, N.; Zheng, G.; Liang, W.; Hada, M.; Ehara, M.; Toyota, K.; Fukuda, R.; Hasegawa, J.; Ishida, M.; Nakajima, T.; Honda, Y.; Kitao, O.; Nakai, H.; Vreven, T.; Throssell, K.; Montgomery Jr., J. A.; Peralta, J. E.; Ogliaro, F.; Bearpark, M. J.; Heyd, J. J.; Brothers, E. N.; Kudin, K. N.; Staroverov, V. N.; Keith, T. A.; Kobayashi, R.; Normand, J.; Raghavachari, K.; Rendell, A. P.; Burant, J. C.; Iyengar, S. S.; Tomasi, J.; Cossi, M.; Millam, J. M.; Klene, M.; Adamo, C.; Cammi, R.; Ochterski, J. W.; Martin, R. L.; Morokuma, K.; Farkas, O.; Foresman, J. B.; Fox, D. J., Gaussian 16 Rev. C.01, **2016**.

6 3,3-Dinitratooxetane – An Important Leap Towards Energetic Oxygen-Rich Monomers and Polymers

by

Max Born, Thomas C. Fessard, Lucas Göttemann, Thomas M. Klapötke, Jörg Stierstorfer and Michael Voggenreiter

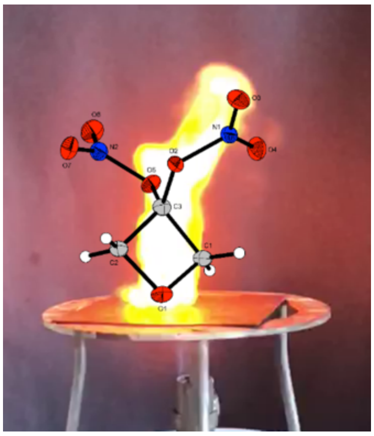

as published in
Chemical Communications **2021**, 57, 2804–2807
(doi:10.1039/D1CC00466B)

Abstract

3-Substituted oxetanes are valuable monomers for modern ring-opening polymerizations. A new solid-state oxidizer, 3,3-dinitratooxetane ($C_3H_4N_2O_7$), which has an oxygen content of 62.2% was synthesized by the addition of N_2O_5 to oxetan-3-one. Monoclinic single-crystals suitable for X-ray diffraction (ρ 1.80 g cm^3) were obtained by recrystallization from dichloromethane. In addition, 3-nitratooxetane was prepared by an improved method and 3-nitrato-3-methyloxetane was synthesized for the first time. Theoretical calculations were computed by the EXPLO5 software and additionally sensitivities toward impact and friction were determined.

6.1 Main Part

Since the synthesis of oxetane by Reboul in 1878, oxetanes have long remained a niche structural motif.[1] However, this changed drastically in the last two decades due to the use of the oxetane motif in the field of medicinal chemistry.[1,2] Here, it is employed as a bioisoster for geminal methyl groups or carbonyl groups. Due to this development, an increasing number of oxetane derivatives are becoming commercially available.[3] This concerns, for example, oxetan-3-one, which rich chemistry has become known in the literature.[4] The field of energetic polymers is largely defined by 3,3-bis-(azidomethyl)oxetane (BAMO), 3-azidomethyl-3-methyloxetane (AMMO) and 3-nitratomethyl-3-methyloxetane (NIMMO), all of which have a very poor oxygen balance in common.[5,6] Especially oxygen-rich monomers and polymers have been very limited so far. Baum et al. succeeded in a first step by preparing the oxygen-rich 3,3-dinitrooxetane and the corresponding polymer. However, its preparation is a six-step synthesis starting from oxetan-3-ol with an accordingly low overall yield.[7] The state of the art is mainly dominated by the constitutional isomers glycidyl nitrate (**A**) and 3-nitratooxetane (**2**), which lead to useful binders after cationic ring-opening polymerization.[6,8,9] Nitrate esters as energetic structural motifs are also used in common explosives. Although accidents happen every year due to its high impact sensitivity, nitroglycerine (**C**) is still widespread and used in double or triple base propellants. For today's application as booster, pentaerythritol tetranitrate (PETN) (**B**) is preferred. The compounds **A**–**C** have the nitrato moiety in common (Fig. 1).

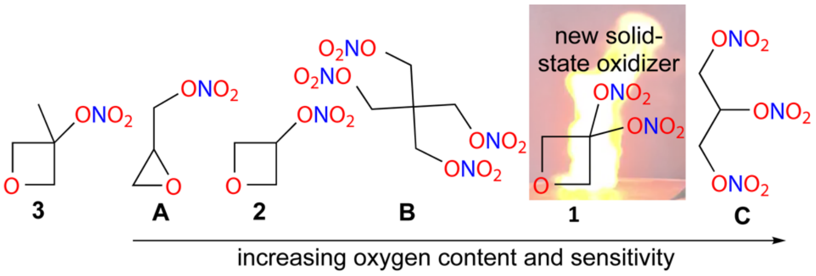

Figure 6.1. Structural formula of 3-nitrato-3-methyloxetane (**3**), glycidyl nitrate (**A**), 3-nitratooxetane (**2**), pentaerythritol tetranitrate (**B**), the new solid-state oxidizer 3,3-dinitratooxetane (**1**) and nitroglycerine (**C**) in the ascending order of oxygen content and sensitivity.

The use of this structural motif is one of the most promising ways to synthesize molecules with positive oxygen balance. This is due to the ability to form O_2 besides N_2, H_2O and CO/CO_2 during combustion. In literature, there are only a few examples of molecules having a carbon-bonded dinitrato moiety. In 1938, Travagli reported the synthesis of the simplest and first geminal C-nitrato compound, dinitratomethane, which he obtained by nitration of 1,3,5-trioxane in mixed acid.[10] The synthesis of dinitratomethane was improved by Reichel et al. in 2019 by the reaction of silver nitrate with diiodomethane in acetonitrile.[11] Dinitrogen pentoxide can be added to the double bond of aldehydes to obtain the dinitrato compound. This was done by Kacmarek et al. in 1975, when he added dinitrogen pentoxide to acetaldehyde to obtain 1,1-dinitratoethane.[12] In 2016, Fischer et al. impressively demonstrated the power of this synthetic route: he added dinitrogen pentoxide to monomeric glyoxal and obtained tetranitratoethane in quantitative yield.[13] The synthetic pathway was used for the reaction according to Scheme 1 in order to synthesize the title compound.

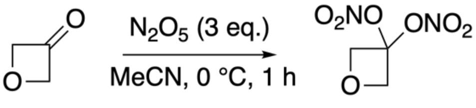

1

Scheme 6.1. Synthesis of **1** via the addition of N_2O_5 to oxetane-3-one.

Oxetan-3-one was added to a solution of dinitrogen pentoxide in acetonitrile at 0 °C. After one hour, the reaction mixture was poured into ice water and extracted with ethyl acetate. After washing with bicarbonate solution to remove residues of acid, the solvent was removed to obtain crude **1** as a colorless solid, which was purified by recrystallization from dichloromethane. The crystals obtained were suitable for X-ray diffraction and were dried under high vacuum. The purified material is stable at 20 °C under a dry atmosphere. At ambient temperature, 3,3-dinitratooxetane slowly decomposes forming NO_x radicals. In air, the product hydrolyses to form nitric acid and oxetan-3-one again as indicated by a singlet resonance of low intensity (5.37 ppm) next to the signal of the target compound, which is also a singlet (5.11 ppm) due to its A_4 spin system. However, the hydrolysis is slow enough to allow quenching of the reaction with ice water. 3-Nitratooxetane (**2**) was prepared by modified literature procedures using acetyl nitrate as mild and cost-efficient nitrating agent.[8] Since the crude product is usually contaminated with acetyl nitrate, this was quantitatively removed by selective hydrolysis with hydrogen carbonate solution without decomposing the ester. This allows subsequent purification by distillation without the risk of explosion induced by acetyl nitrate. ^1H NMR spectroscopy showed an AA'BB'X spin system of higher order. Two multiplet signals were obtained for both methylene groups (4.68, 4.93 ppm) while the coupling of the methine–proton with the AB-part caused a triplet of triplets. Similar to compound **2**, liquid 3-nitrato-3-methyloxetane (**3**) was obtained by nitration of the corresponding alcohol with N_2O_5 (Scheme 2).

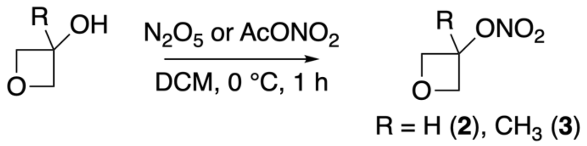

Scheme 6.2. Preparation of 3-nitratooxetane (**2**) and 3-nitrato-3-methyloxetane (**3**).

Despite the highest basicity of the oxetane oxygen in the series of reactants used, ring-opening was so avoided and the product obtained in high purity and yield as yellow liquid. The corresponding ^{1}H NMR spectrum was of high purity, showed doublet signals for the methylene groups (4.52, 4.78 ppm) and a singlet for the methyl group following the $A_2B_2X_3$ spin system. Regarding vibrational spectroscopy (IR, Raman), the characteristic asymmetric (1629–1687 cm^{-1}) and symmetric stretching vibrations (1275–1306 cm^{-1}) of the nitrato groups were found for all compounds. Beyond, the well-known ring-breathing motion of the oxetane moiety was observed as strong absorption band in all IR-spectra (977–1042 cm^{-1}). Being the only solid in the series, compound **1** crystallizes in the monoclinic space group $P2_1/c$ with four molecules in the unit cell and a density of 1.80 g cm^3 at 107 K.

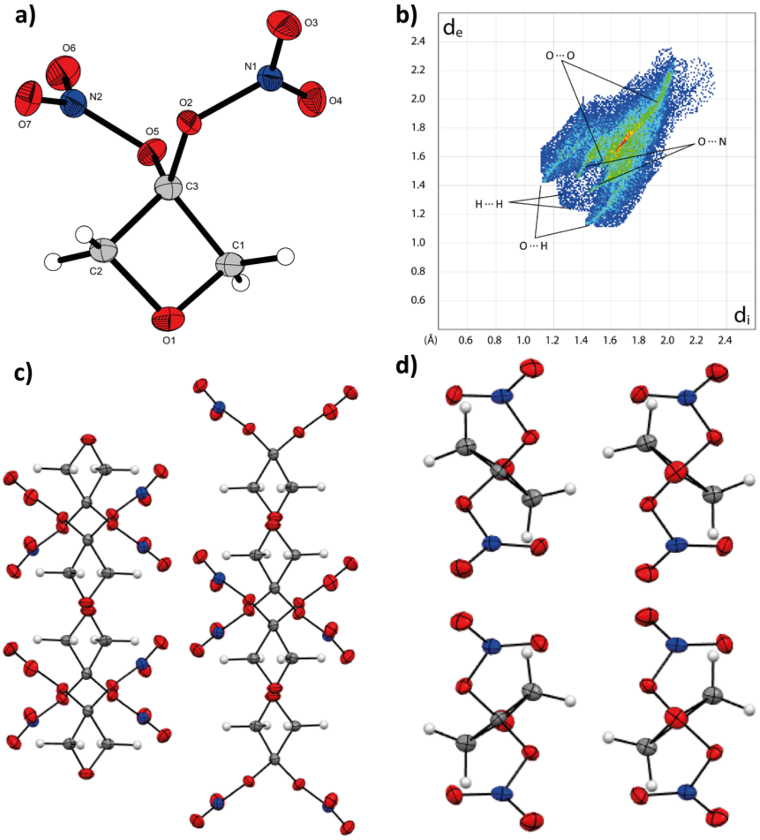

Figure 6.2. a) Molecular structure of compound **1**. Thermal ellipsoids are drawn at the 50% probability level. b) Two-dimensional Hirshfeld fingerprint plot. c) View along the *a* axis. d) View in the direction of the *c* axis.

The angles in the oxetane motif vary between 86.9(3)° at C1–C3–C2 to 92.3(3)° at C2–O1–C1 and thus provide insight into the high ring strain. The oxetane ring shows a puckering of 5.4(3)° while both nitrato groups are planar. The view along the *a* axis reveals that the oxetane moieties form corridors and nitrato groups are spaced away from each other as far as possible. Hirshfeld analysis showed a high percentage of repulsive O···O contacts (31.6%) which cause strong repulsive interactions upon lattice deformation by mechanic stimuli and therefore indicate a high sensitivity.[14–16] Accordingly, the view (*a* axis) also reveals pairwise layers of nitrato groups directed to each other causing this particular oxygen–oxygen repulsion. A large population of normally stabilizing O···H interactions (54.4%) was found, but they are weak due to their large distance (> 2.5 Å) and thus cannot contribute significantly to the stabilization of 3,3-dinitratooxetane. Another possible destabilizing effect is N···O interaction, but the extent is low (7.5%) and also weak due to the large distance.[17] In total, the O···O interaction is hardly counterbalanced by stabilizing effects and high sensitivity and low thermal stability must be assumed. This is in excellent agreement with measured values. DTA analysis of **1** shows a melting point at 69 °C, followed by another endo-peak at 88 °C, which is associated with the cleavage of a nitrato group. The exothermic decomposition is observed directly afterward at 93 °C. 3,3-Dinitratooxetane is extremely sensitive toward impact (< 1 J) which is comparable to the impact sensitivity of nitroglycerine and way more sensitive than PETN (Table 1).

Compound **1** is also very sensitive to friction with a sensitivity of 1 N. These high sensitivities are a result of the nitrato groups arranged in the crystal (Fig. 2c), which are in spatial vicinity to each other. If these layers are moved against each other by mechanical stimuli, the distance between these groups decreases and the repulsion between the groups increases, which then causes explosion. Also, the electronegative nitrato groups on one side of the molecule and the electropositive oxetane ring on the other side, which is an uneven distribution, makes the molecule more sensitive. In contrast, the liquid 3-nitratooxetane (**2**), which has only one nitrato moiety, shows a drastically higher decomposition temperature of 153 °C as assessed by DSC. Furthermore, only one nitrato group causes the compound to be completely insensitive toward impact and friction, while the sensitivity of **1** already falls in the range of primary explosives. Unexpectedly, 3-nitrato-3-methyloxetane (**3**) has an even lower decomposition temperature of 141 °C (DSC) and was found to be insensitive toward impact according to expectation. Despite, it is slightly sensitive toward friction with a value of 160 N. This might be explained by the heat generally caused by friction, which can obviously be sufficient to cause thermal initiation. 3,3-Dinitratooxetane features an outstanding oxygen content that is even higher than the content of pentaerythritol tetranitrate but slightly lower than the content of nitroglycerine. With ease, it surpasses the oxygen balance of commonly known energetic monomers such as GLYN and 3-NO (Table 1). The Gaussian16 program package was used to calculate the room temperature enthalpy of formation on the CBS-4M level of theory using the atomization method for all investigated compounds. The EXPLO5 code was used to calculate the energetic properties of compounds **1**–**3**. Here, DNO shows the highest performance with a detonation velocity of almost 8300 ms^{-1} and a specific impulse of 264 s as pure substance and 267 s as a mixture with aluminum, whereby these values considerably exceed the specific impulse for ammonium perchlorate. To the best of our knowledge, this resembles the highest performance known in the field of energetic oxetanes. Both 3,3-dinitratooxetane (**1**) and 3-nitrato-3-methyloxetane (**3**) were prepared by the versatile use of dinitrogen pentoxide and investigated by multinuclear spectroscopy. Summarizing the physicochemical properties of compound **1**, especially the low thermal stability, the decomposition at room temperature, and the high sensitivities will probably exclude it from application. Possibly **1** could be much safer and more stable when the polymer is formed, and our investigation are ongoing. Offering both the highest oxygen content and performance ever obtained in the field of oxetanes, 3,3-dinitratooxetane represents an important step toward especially oxygen-rich and high-performing oxetane compounds. Its synthesis is anticipated to trigger more intensive research with regard to oxetane-based polynitro- and polynitrato compounds and is likely to accelerate the development in this field.

Financial support of this work by the Ludwig-Maximilian University of Munich (LMU), the Office of Naval Research (ONR) under grant no. ONR N00014-19-1-2078 and the Strategic Environmental Research and Development Program (SERDP) grant WP19-1287 under contract no. W912HQ19C0033 is gratefully acknowledged.

Table 6.1. Physicochemical values of 3,3-dinitratooxetane (**DNO**, **1**), 3-nitratooxetane (**3-NO**, **2**), 3-nitrato-3-methyloxetane (**3N3MO**, **3**), ammonium perchlorate (**AP**), nitroglycerine (**NG**), pentaerythritol tetranitrate (**PETN**) and glycidyl nitrate (**GLYN**).

	DNO (1)	**3-NO (2)**	**3N3MO (3)**	**AP**[18]	**NG**[18-20]	**PETN**[18-20]	**GLYN**[9,19,20]
Formula	$C_3H_4N_2O_7$	$C_3H_5NO_4$	$C_4H_7NO_4$	NH_4ClO_4	$C_3H_5N_3O_9$	$C_5H_8N_4O_{12}$	$C_3H_5NO_4$
FW [$g \cdot mol^{-1}$]	180.07	119.08	133.10	117.49	227.09	316.14	119.08
IS[a] [J]	<1	40	>40	20	0.2	3	2–4
FS[b] [N]	1	>360	>160	> 360	> 360	60	>360
N, O[c] [%]	15.56, 62.19	11.76, 53.74	10.52, 48.08	11.92, 54.47	18.5, 63.41	17.72, 60.73	11.76, 53.74
Ω_{CO}, Ω_{CO2}[d] [%]	+17.77, −8.89	−20.15, −60.46	−42.07, −90.20	+34.04, +34.04	+24.66, +3.50	+15.18, −10.12	−20.15, −60.46
T_m[e]/ $T_{dec.}$[f] [°C]	69/93	−/153	−/141	−/240	13/185	141/202	−/195
ρ[g] [$g \cdot cm^{-3}$]	1.74	1.34	1.33	1.95	1.60	1.77	1.33
$\Delta H_f°$[h] [$kJ \cdot mol^{-1}$]	−302.6	−168.0	−245.8	−295.8	−311.3	−479.7	−199.3
				EXPLO5 V6.04[10]			
$-\Delta_E U°$[i] [$kJ \cdot kg^{-1}$]	6176	5089	4356	1419	6305	6165	4852
$D_{C\text{-}J}$[k] [$m \cdot s^{-1}$]	8275	6771	6456	6903	7823	8369	6664
$p_{C\text{-}J}$ [GPa]	29.7	16.6	13.9	18.6	23.7	30.5	15.8
I_{sp} [l] [s]	264	235	204	157	275	267	228
I_{sp} [m] [s] (15% Al)	267	265	245	236	267	270	261

[a] Impact sensitivity (BAM drop hammer, method 1 of 6). [b] Friction sensitivity (BAM friction tester, method 1 of 6). [c] Nitrogen and oxygen content. [d] Oxygen balance toward carbon monoxide (Ω_{CO} = (nO − xC − yH/2)(1600/FW) and carbon dioxide (Ω_{CO2} = (nO − 2xC − yH/2)(1600/FW)). [e] Melting point (DSC, β = 5 °C·min^{-1}). [f] Temperature of decomposition (DSC, β = 5 °C·min^{-1}). [g] Density at 298 K. [h] Standard molar enthalpy of formation. [i] Detonation energy. [j] Detonation temperature. [k] Detonation velocity. [l] Specific impulse of neat compound (70.0 bar chamber pressure, isobaric combustion conditions (1 bar), equilibrium expansion). [m] Specific impulse for compositions with 85% compound and 15% aluminum (70.0 bar chamber pressure, isobaric combustion conditions (1 bar), equilibrium expansion).

References

[1] Burkhard, J. A.; Wuitschik, G.; Rogers-Evans, M.; Müller, K.; Carreira, E. M. Oxetanes as Versatile Elements in Drug Discovery and Synthesis. *Angew. Chem. Int. Ed.* **2010**, *49*, 9052-9067.

[2] Burkhard, J. A.; Wuitschik, G.; Evans, M. R.; Müller, K.; Carreira, E. M. Oxetanes as Unique Building Blocks in Medicinal Chemistry. *MedChemNews* **2012**, *22*, 8-15.

[3] https://spirochem.com/catalog/oxetanes.html (accessed 2021-01)

[4] Ruider, S. A.; Müller, S.; Carreira, E. M. Ring Expansion of 3-Oxetanone-Derived Spirocycles: Facile Synthesis of Saturated Nitrogen Heterocycles. *Angew. Chem. Int. Ed.* **2013**, *52*, 11908-11911.

[5] Dreyfuss, M. P.; Dreyfuss, P. Oxetane Polymers. In *Encyclopedia of Polymer Science and Technology*, (Ed.), John Wiley & Sons: Hoboken, New Jersey, **2011**. DOI 10.1002/0471440264.pst520

[6] Ang, H. G.; Pisharath, S. *Energetic Polymers: Binders and Plasticizers for Enhancing Performance*; Wiley-VCH: Weinheim, **2012**.

[7] Baum, K.; Berkowitz, P. T.; Grakauskas, V.; Archibald, T. G. Synthesis of electron-deficient oxetanes. 3-Azidooxetane, 3-nitrooxetane, and 3,3-dinitrooxetane. *J. Org. Chem.* **1983**, *48*, 2953-2956.

[8] Baum, K.; Lin, W. H.; Willer, R. L. Synthesis of poly-(3-nitratooxetane). US 8 030 440 B1, **2011**.

[9] Urbanski, T. *Chemie und Technologie der Explosivstoffe*; Vol. 2; VEB Dt. Verl. f. Grundstoffindustrie: Leipzig, **1963**.

[10] G. Travagli, Methylene Glycol dinitrate, *Gazz. Chim. Ital.*, **1938**, *68*, 718.

[11] Reichel, M.; Krumm, B.; Vishnevskiy, Y. V.; Blomeyer, S.; Schwabedissen, J.; Stammler, H.-G.; Karaghiosoff, K.; Mitzel, N. W. Solid-State and Gas-Phase Structures and Energetic Properties of the Dangerous Methyl and Fluoromethyl Nitrates. *Angew. Chem. Int. Ed.* **2019**, *58*, 18557-18561.

[12] Kacmarek, A. J.; Jarke, F. H.; Shamir, J.; Solomon, I. J.; Lustig, M. Formation of gem-dinitrates from acetaldehyde and trifluoroacetaldehyde. *J. Org. Chem.* **1975**, *40*, 1851-1854.

[13] Fischer, D.; Klapötke, T. M.; Stierstorfer, J. Tetranitratoethane. *Chem. Commun.* **2016**, *52*, 916-918.

[14] Dosch, D. E.; Reichel, M.; Born, M.; Klapötke, T. M.; Karaghiosoff, K. Investigation of Structure–Property Relationships of Three Nitroaromatic Compounds: 1-Fluoro-2,4,6-trinitrobenzene, 2,4,6-Trinitrophenyl Methanesulfonate, and 2,4,6-Trinitrobenzaldehyde. *Cryst. Growth Des.* **2021**, *21*, 243-248.

[15] Ma, Y.; Zhang, A.; Xue, X.; Jiang, D.; Zhu, Y.; Zhang, C. Crystal Packing of Impact-Sensitive High-Energy Explosives. *Cryst. Growth Des.* **2014**, *14*, 6101-6114.

[16] Spackman, M. A.; Jayatilaka, D. Hirshfeld surface analysis. *CrystEngComm* **2009**, *11*, 19-32.

[17] Reichel, M.; Dosch, D.; Klapötke, T.; Karaghiosoff, K. Correlation between Structure and Energetic Properties of Three Nitroaromatic Compounds: Bis(2,4-dinitrophenyl) Ether, Bis(2,4,6-trinitrophenyl) Ether, and Bis(2,4,6-trinitrophenyl) Thioether. *J. Am. Chem. Soc.* **2019**, *141*, 19911-19916.

[18] Klapötke, T. M. *Chemistry of High-Energy Materials*; 5th ed.; DeGruyter: Boston, **2019**.

[19] Klapötke, T. M. *Energetic Materials Encyclopedia*; Vol. 1–3; De Gruyter: Berlin, Boston, **2021**.

[20] Liu, J. *Nitrate Esters Chemistry and Technology*; 1st ed.; Springer: Singapore, **2019**.

6.2 Supporting Information

6.2.1 Experimental Part and General Methods

Caution! 3,3-Dinitratooxetane is a powerful energetic material with high sensitivities toward shock and friction. Therefore, proper security precautions (safety glass, face shield, earthed equipment and shoes, Kevlar gloves and ear plugs) have to be applied while synthesizing and handling the described compounds.

Chemicals and solvents were employed as received (Sigma-Aldrich, Acros, TCI, Spirochem AG). ^{1}H, ^{13}C and ^{14}N spectra were recorded using a Bruker AMX 400 instrument. The chemical shifts quoted in ppm refer to tetramethylsilane (^{1}H, ^{13}C) and nitromethane (^{14}N). Decompositions temperatures were determined on a Mettler Toledo DSC822e at a heating rate of 5 °C min^{-1} using 40 μL aluminum crucibles and nitrogen purge gas at a flow rate of 30 mL min^{-1}. Evaluations of thermal behavior were performed using the STAR^{e} Software Version 16.20. Infrared (IR) spectra were recorded using a Perkin-Elmer Spektrum One FT-IR instrument. Raman spectra were obtained using a Bruker MultiRam FT Raman spectrometer and a neodymium-doped yttrium aluminum garnet (Nd:YAG) laser (λ = 1064 nm, P = 1074 mW). Elemental analyses were performed with an Elementar Vario el by pyrolysis of the sample and subsequent analysis of formed gases (standard deviation liquids: +/- 0.5%). The sensitivity data were collected using a BAM (Bundesanstalt für Materialforschung) drop hammer[1] according to STANAG 4489[2] modified instruction[3] and a BAM friction tester[1] according to STANAG 4487[4] modified instruction.[5] The classification of the tested compounds results from the 'UN Recommendations on the Transport of Dangerous Goods'.[6]

3,3-Dinitratooxetane

Oxetan-3-one (0.50 g, 6.94 mmol, 1.0 eq.) was dissolved in acetonitrile (5 mL) and added to a solution of dinitrogen pentoxide (2.25 g, 20.8 mmol, 3.0 eq.) in acetonitrile (10 mL) which was cooled to 0 °C. The mixture was stirred for 1 hour at 0 °C and then let come to ambient temperature over 30 minutes. The solution was poured into ice water (70 mL) and was extracted with ethyl acetate (3 × 25 mL). The organic layer was washed with saturated bicarbonate solution (2 × 30 mL) prior to drying over sodium sulfate. The solvent was removed, and the product was dried under high vacuum to give 0.51 g of 3,3-dinitratooxetane (2.83 mmol, 41%) as colorless solid. The product has to be stored at −20 °C under dry atmosphere to prevent decomposition.

DSC (T_{onset}, 5 °C min^{-1}): 69.4 °C (m.p.) , 93.3 °C (dec.); **FT-IR** (ATR, cm^{-1}): $\tilde{\nu}$ = 2962 (w), 1687 (m), 1655 (s), 1445 (w), 1305 (s), 1286 (m), 1180 (m), 1158 (s), 1113 (m), 982 (s), 961 (m), 935 (w), 884 (m), 842 (m), 791 (s), 739 (s), 669 (s), 591 (m), 438 (m); **^{1}H NMR** (400 MHz, Acetone-d$_6$, 25 °C): δ

= 5.11 (s, 4H) ppm; **^{13}C NMR{^{1}H}** (101 MHz, Acetone-d$_6$, 25 °C): δ = 77.5, 103.8 ppm; **^{14}N NMR** (29 MHz, Acetone-d$_6$, 25 °C): δ = −56.3 ppm; **EA** ($C_3H_4N_2O_7$) calcd.: C 20.01, H 2.24, N 15.56; found: C 20.25, H 2.52, N 15.29; **BAM drop hammer** < 1 J (> 500 µm); **Friction test** 1 N (> 500 µm).

3-Nitratooxetane

3-Nitratooxetane was prepared according to modified literature procedures.[7]

Acetic anhydride (6.00 g, 58.8 mmol) was dissolved in dry dichloromethane (5.00 mL) and white fuming nitric acid (100%, 3.90 g, 61.9 mmol) was added at −10 °C using an ice bath with sodium chloride. The mixture was stirred for one hour prior to the addition of oxetan-3-ol (3.00 g, 40.5 mmol) in dry dichloromethane (5.00 mL). The solution was stirred for one hour and then poured onto ice (15.0 g). Dichloromethane (10.0 mL) was added and the layers were separated. The organic layer was washed with saturated sodium bicarbonate solution (3 × 20 mL) and separated. The solvent was then removed by rotary evaporation to give a slightly yellowish liquid and sodium bicarbonate solution (10%, 20.0 mL) was added. The resulting emulsion was heavily stirred for 30 minutes (to remove any traces of acetyl nitrate) and the target compound subsequently extracted with dichloromethane (3 × 30 mL). After drying over sodium sulfate, the solvent was removed to give 2.78 g (23.3 mmol, 58%) of 3-nitratooxetane as slightly yellowish liquid. The product may be further purified by distillation (27 mbar, 65 °C) to give colorless 3-nitratooxetane suitable for polymerization reactions.

DSC (T_{onset}, 5 °C min^{-1}): 152.8 °C (dec.); **FT-IR** (ATR, cm^{-1}): $\tilde{\nu}$ = 3112 (w), 2961 (m), 2887 (w), 2803 (w), 1629 (vs), 1373 (m), 1327 (m), 1275 (vs), 1175 (m), 1069 (m), 975 (s), 928 (w), 881 (s), 846 (s), 754 (m), 690 (m), 556 (w), 404 (w); **Raman** (1064 nm, 1074 mW, cm^{-1}): $\tilde{\nu}$ = 2975 (100), 2932 (78), 2892 (88), 1642 (14), 1480 (36), 1374 (32), 1328 (22), 1279 (63), 1177 (36), 1116 (20), 1071 (47), 1042 (27), 977 (15), 932 (32), 853 (75), 693 (25), 558 (41), 406 (19); **^{1}H NMR** (400 MHz, Acetone-d$_6$, 25 °C): δ = 4.68 (ddd, 2H, CH$_2$, J = 8.2, 4.9, 1.1 Hz), 4.93 (ddd, 2H, CH$_2$, J = 8.3, 6.2, 1.2 Hz), 5.68 (tt, 1H, CH, J = 6.2, 4.9 Hz) ppm; **^{13}C NMR{^{1}H}** (101 MHz, Acetone-d$_6$, 25 °C): δ = 74.8, 75.3 ppm; **^{14}N NMR** (29 MHz, Acetone-d$_6$, 25 °C): δ = −45.6 ppm; **EA** ($C_3H_4N_2O_7$) calcd.: C 30.26, H 4.23, N 11.76; found: C 29.76, H 3.73, N 11.49; **BAM drop hammer** > 40 J; **Friction test** > 160 N.

3-Nitrato-3-methyloxetane

3-Hydroxy-3-methyloxetane (0.50 g, 5.67 mmol) was added to a solution of dinitrogen pentoxide (674 mg, 6.24 mmol, 1.1 eq.) in dry dichloromethane (15 mL) at 0 °C using an ice bath. The resulting solution was stirred for 1 h at the initial temperature and subsequently poured into ice-water (50 mL). Additional dichloromethane (20 mL) was added and the phases were separated. The organic phase was washed again with water (30 mL) and finally with saturated sodium bicarbonate solution (25 mL) prior to drying over sodium sulfate. The solvent was removed by rotary evaporation to give 0.74 g (3.92 mmol, 69%) as yellow liquid.

DSC (5 °C min^{-1}): 141.0 °C (dec.); **FT-IR** (ATR, cm^{-1}): $\tilde{\nu}$ = 3113 (m), 2962 (m), 2887 (m), 2803 (m), 1754 (w), 1628 (s), 1447 (m), 1385 (s), 1304 (vs), 1254 (m), 1178 (s), 1138 (m), 977 (s), 925 (m), 850 (s), 755 (m), 691 (m); **Raman** (1064 nm, 1074 mW, cm^{-1}): $\tilde{\nu}$ = 2977 (69), 2942 (100), 2888 (70), 2751 (7), 1636 (11), 1480 (24), 1461 (19), 1349 (8), 1306 (47), 1254 (11), 1191 (12), 1139 (13), 992 (31), 982 (35), 855 (37), 736 (12), 693 (13), 506 (35), 433 (19); **^{1}H NMR** (400 MHz, CDCl$_3$, 25 °C): δ = 1.81 (s, 3H, CH$_3$), 4.52 (d, 2H, CH$_2$, J = 8.6 Hz), 4.78 (d, 2H, CH$_2$, J = 8.6 Hz) ppm; **^{13}C NMR{^{1}H}** (101 MHz, CDCl$_3$, 25 °C): δ = 20.6, 79.8, 83.4 ppm; **^{14}N NMR** (29 MHz CDCl$_3$, 25 °C): δ = −46.2 ppm; **EA** ($C_3H_4N_2O_7$) calcd.: C 36.10, H 5.30, N 10.52; found: C 36.37, H 5.17, N 10.26; **BAM drop hammer** > 40 J; **Friction test** >160 N.

6.2.2 NMR Spectra of Prepared Compounds

3,3-Dinitratooxetane

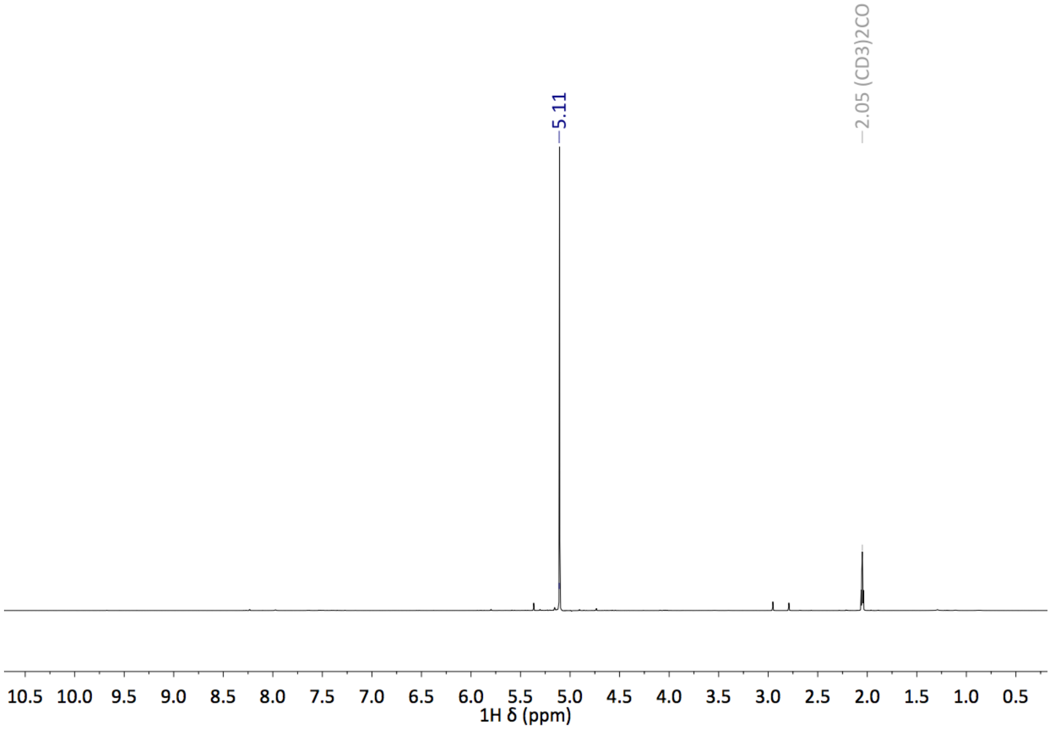

Figure S 6.1. Proton spectrum (^{1}H) of 3,3-dinitratooxetane.

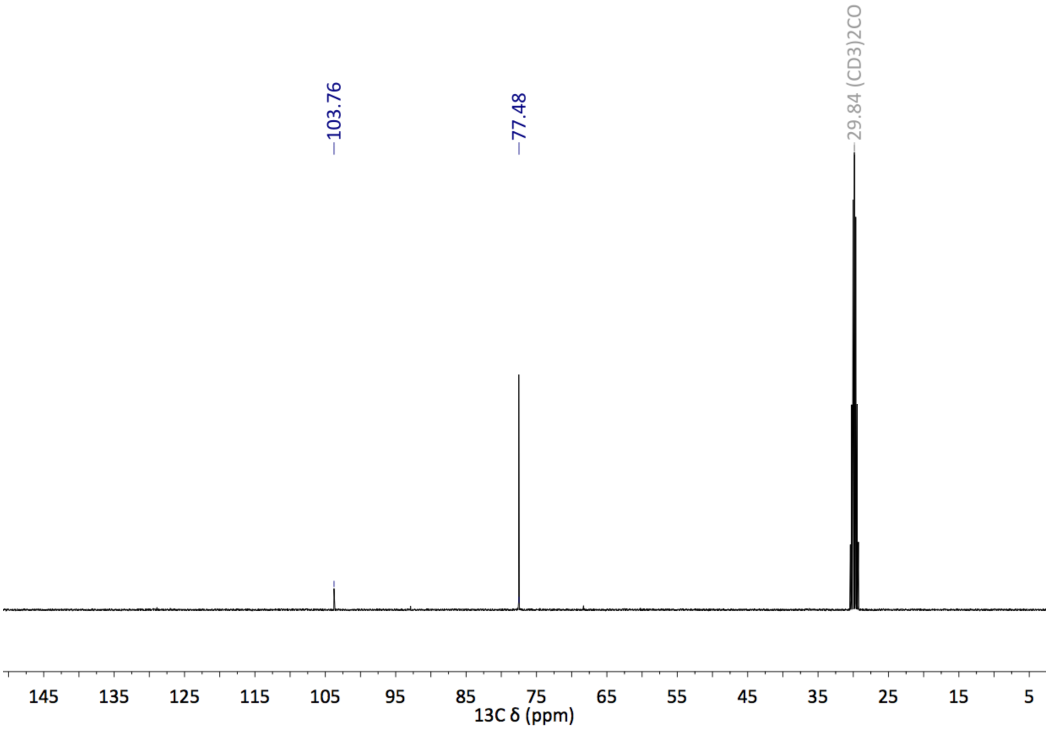

Figure S 6.2. Carbon spectrum (^{13}C) of 3,3-dinitratooxetane.

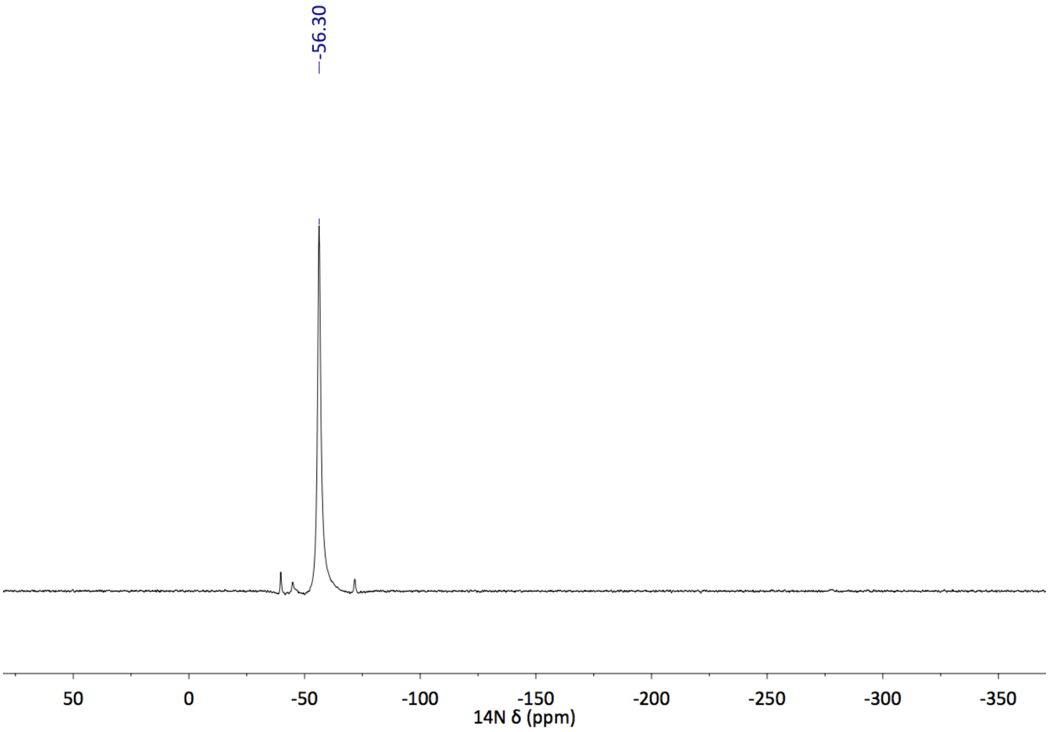

Figure S 6.3. Nitrogen spectrum (^{14}N) of 3,3-dinitratooxetane.

3-Nitratooxetane

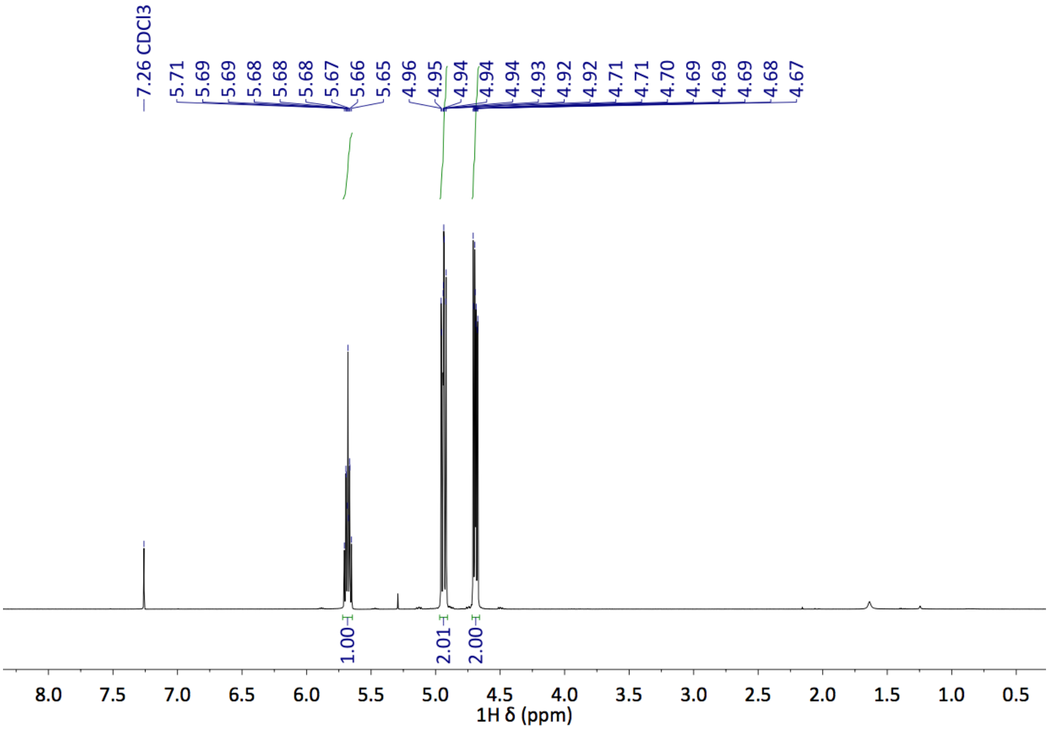

Figure S 6.4. Proton spectrum (^{1}H) of 3-nitratooxetan.

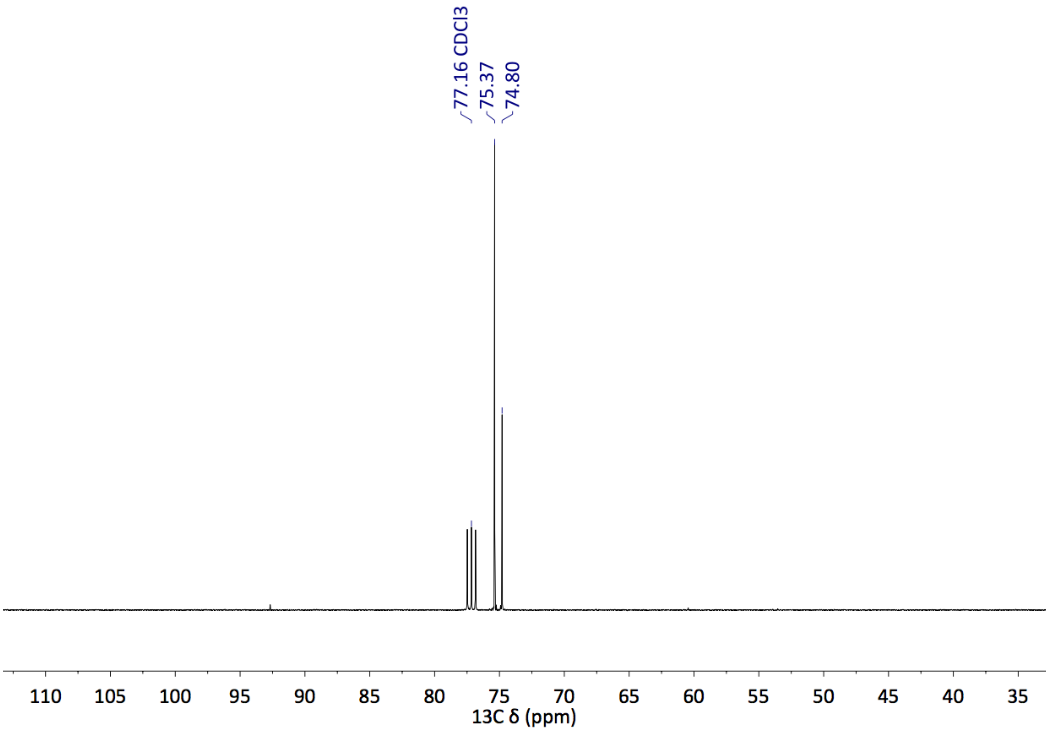

Figure S 6.5. Carbon spectrum (^{13}C) of 3-nitratooxetane.

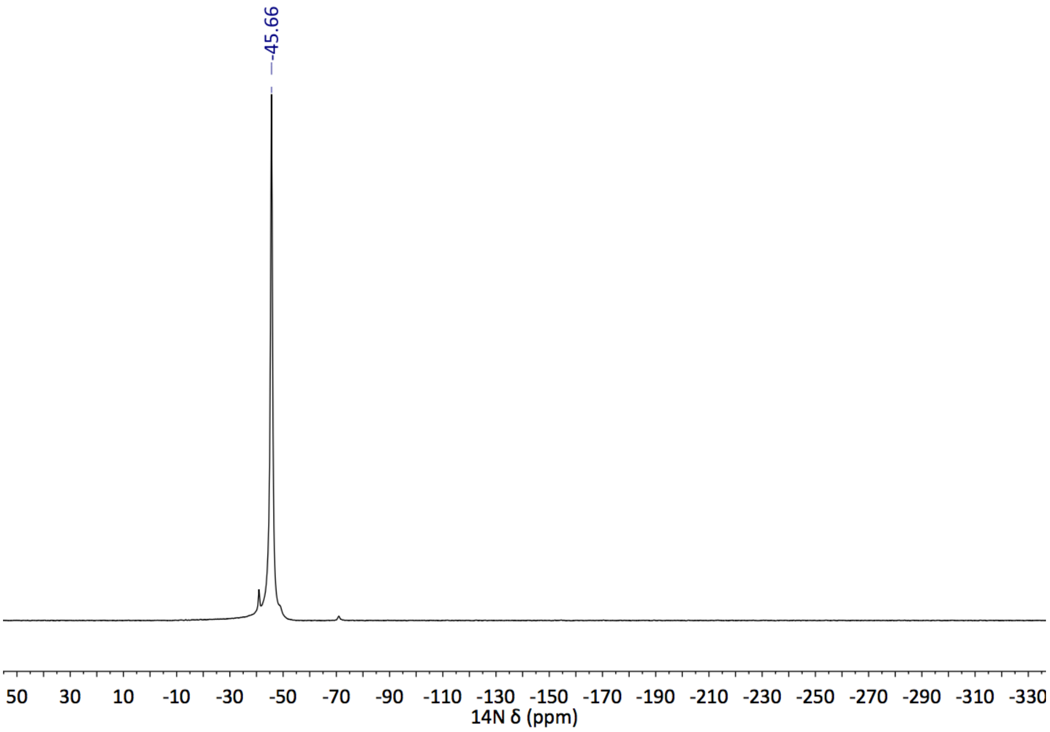

Figure S 6.6. Nitrogen spectrum (^{14}N) of 3-nitratooxetane.

3-Nitrato-3-methyloxetane

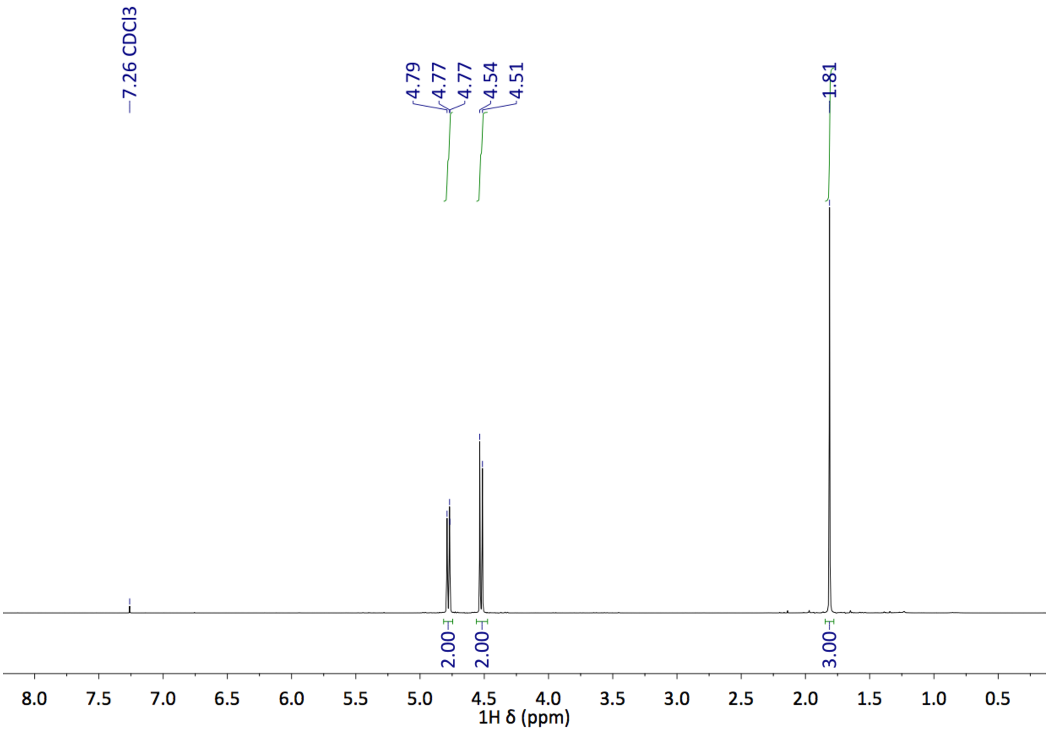

Figure S 6.7. Proton spectrum (^{1}H) of 3-nitrato-3-methyloxetane.

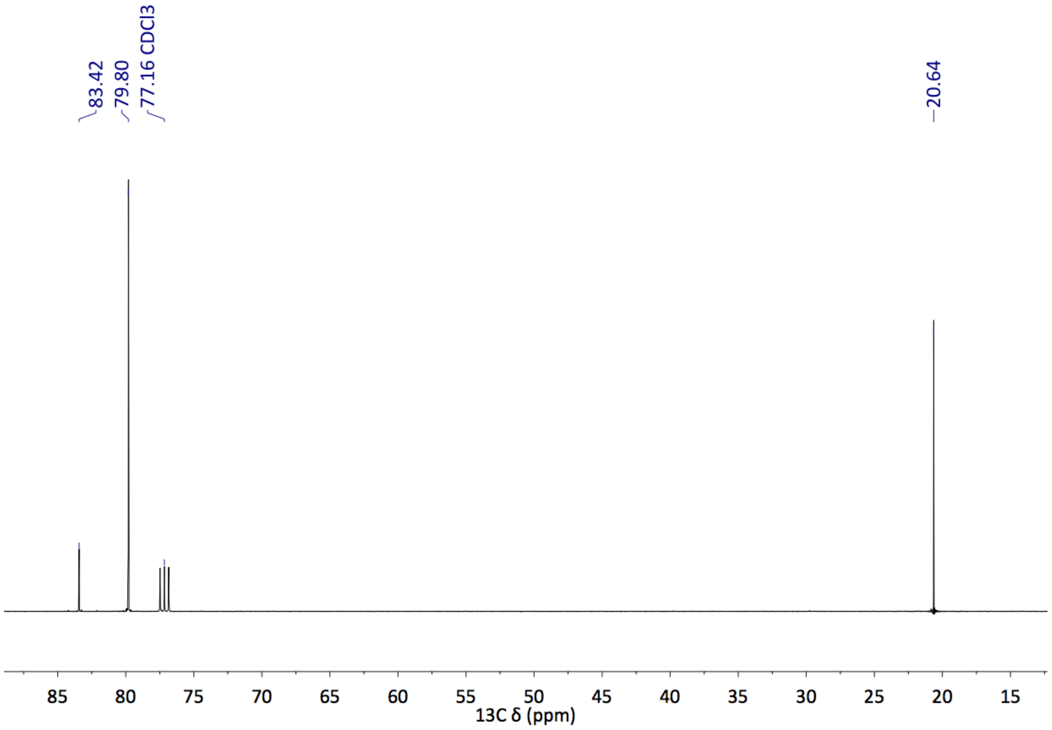

Figure S 6.8. Carbon spectrum (^{13}C) of 3-nitrato-3-methyloxetane.

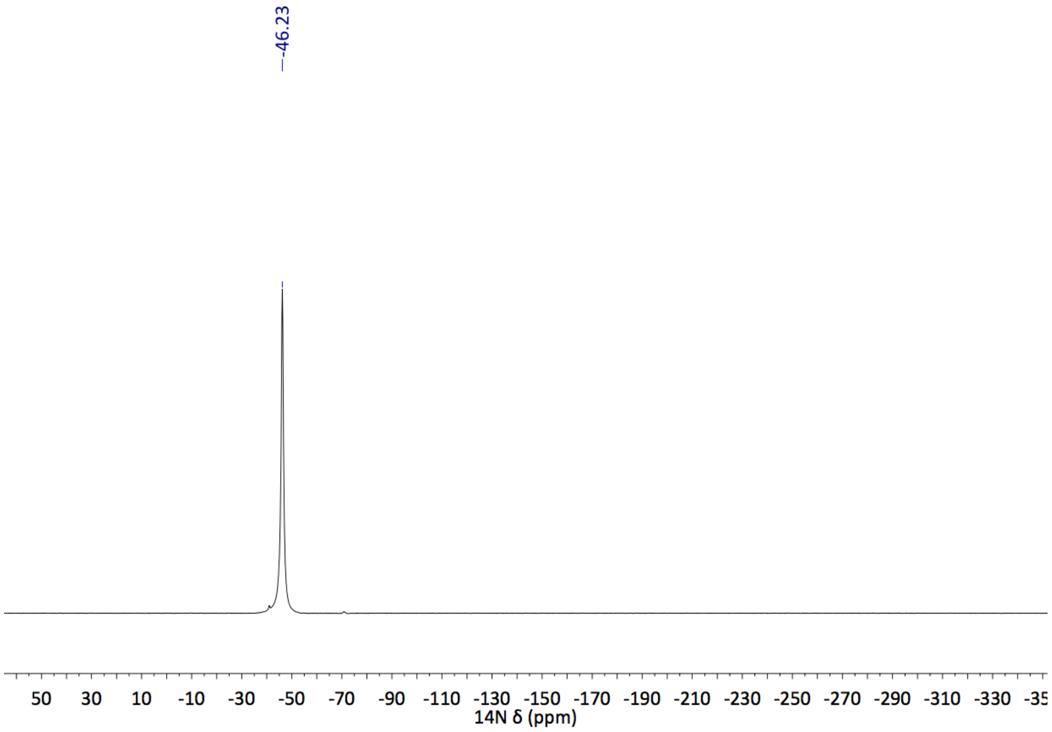

Figure S 6.9. Nitrogen spectrum (^{14}N) of 3-nitrato-3-methyloxetane.

6.2.3 X-ray Diffraction and Hirshfeld Analysis

The crystals unfortunately had a twinning problem. Data collection was performed with an Oxford Xcalibur3 diffractometer with a CCD area detector, equipped with a multilayer monochromator; a Photon 2 detector and a rotating-anode generator were employed for data collection using Mo Kα radiation (λ = 0.7107 Å). Data collection and reduction were carried out using the CrysAlisPRO software.[8] The structures were solved by direct methods (SIR-2014)[9] and refined (SHELXLE)[10] by full-matrix least-squares on F2 (ShelxL)[11,12] and finally checked using the Platon software[13] integrated in the WinGX software suite.[14] The non-hydrogen atoms were refined anisotropically, and the hydrogen atoms were located and freely refined. All Diamond 3 plots are shown with thermal ellipsoids at the 50% probability level, and hydrogen atoms are shown as small spheres of arbitrary radius. The twin reflexes were cut out.

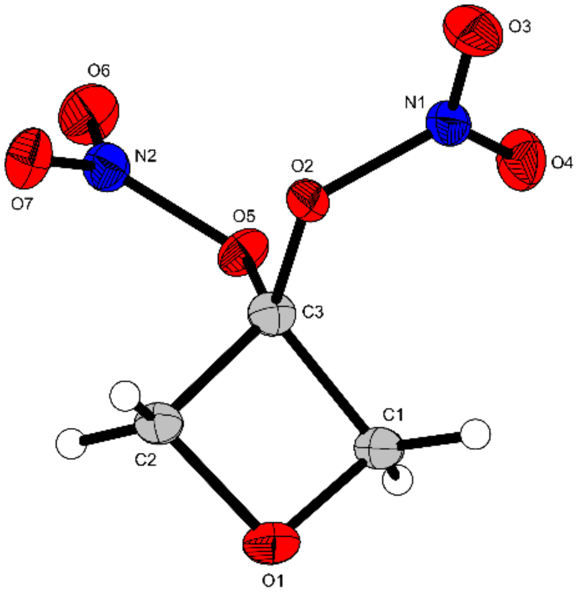

Figure S 6.10. Molecular structure of 3,3-dinitratooxetane. Thermal ellipsoids are drawn at 50% probability level.

Table S 6.1. Detailed crystallographic information of 3,3-dinitratooxetane (**1**).

	1
Formula	$C_3H_4N_2O_7$
FW [g mol^{-1}]	180.08
Crystal System	monoclinic
Space Group	$P2_1/c$
Color / Habit	colorless block
Size [mm]	0.20 x 0.12 x 0.05
a [Å]	9.259(2)
b [Å]	12.501(3)
c [Å]	5.7467(11)
α [°]	90
β [°]	92.46(2)
γ [°]	90
V [Å^3]	664.6(3)
Z	4
$\rho_{calc.}$ [g cm^{-3}]	1.800
μ [mm^{-1}]	0.183
F (000)	368
$\lambda_{MoK\alpha}$ [Å]	0.71073
T [K]	107
ϑ min-max [°]	2.739, 26.370
Dataset h; k; l	−11:11; −8:15; −7:7
Reflect. coll.	1313
Independ. Refl.	1313
$R_{int.}$	0.057
Reflection obs.	822
No. parameters	109
R1 (obs.)	0.0749
wR2 (all data)	0.1672
S	1.049
Resd. Dens. [e Å^{-3}]	−0.395, 0.365
Device Type	Oxford XCalibur3 CCD
Solution	Sir2014
Refinement	SHELXLE
Absorpt. corr.	Multi-scan
CCDC	2013564

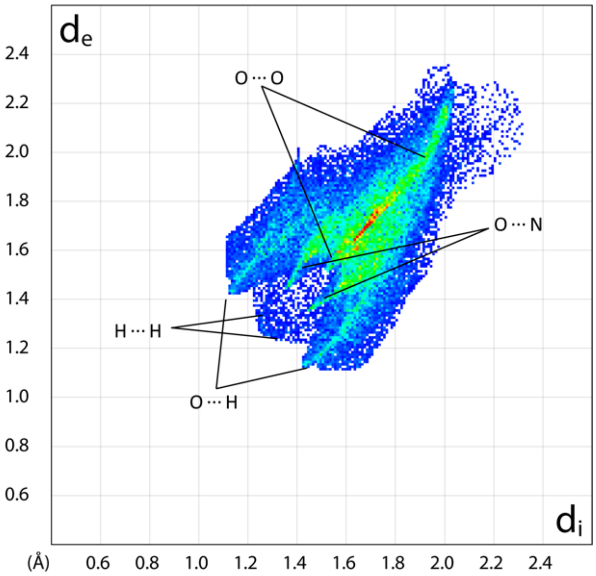

Figure S 6.11. Two-dimensional fingerprint plot in crystal stacking of 3,3-dinitratooxetane.

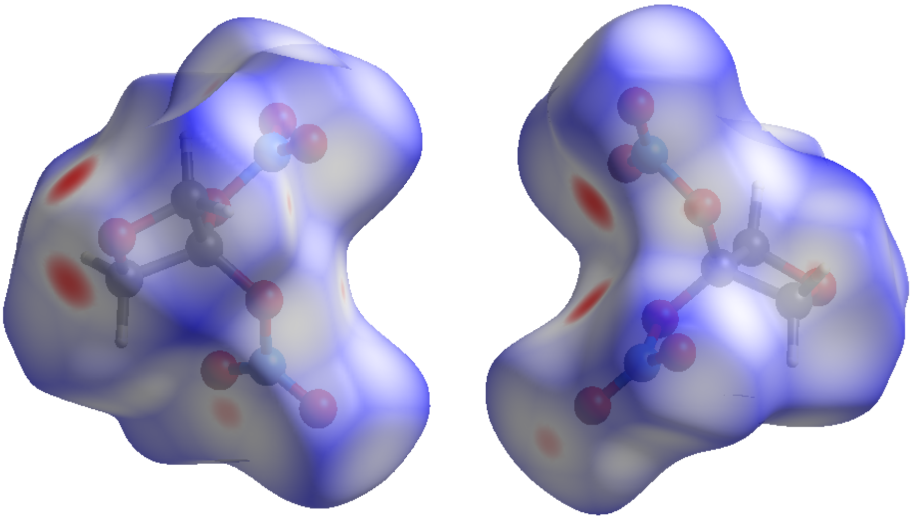

Figure S 6.12. Calculated Hirshfeld surface of compound **1**.

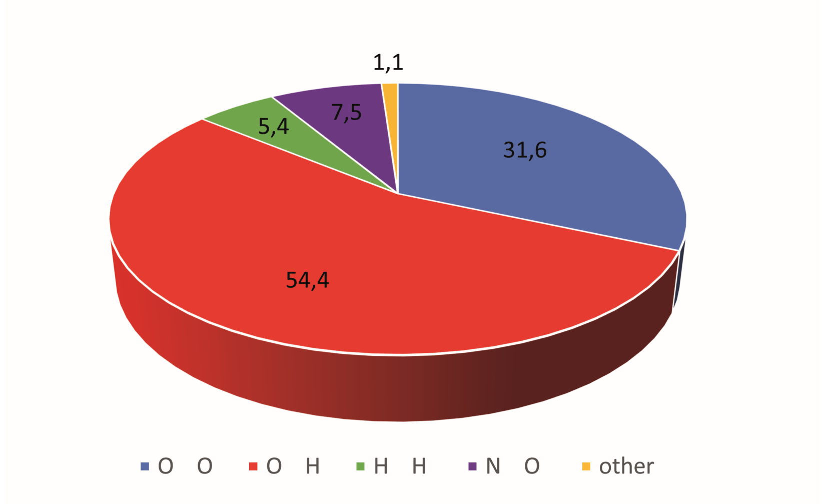

Figure S 6.13. Population of close contacts in compound **1**.

6.2.4 Heat of Formation Calculation and Thermal Analysis

The atomization was used to determine the heat of formation of **1**–**3** using the atom energies in Table S 2.

$$\Delta_f H^\circ_{(g,\ M,\ 298)} = H_{(molecule,\ 298)} - \Sigma H^\circ_{(atoms,\ 298)} + \Sigma\Delta_f H^\circ_{(atoms,\ 298)}$$

Table S 6.2. CBS-4M electronic enthalpies for atoms C, H, N, and O and their literature values.

	$-H^{298}$ / a.u.	$\Delta_f H^\circ{}_{gas}$[15]
H	0.500991	217.998
C	37.786156	716.68
N	54.522462	472.68
O	74.991202	249.18

The Gaussian16 program package was used to calculate room temperature enthalpies on the CBS-4M level of theory.[16] In order to obtain the energy of formation for the solid phase of **1**, Trouton's Rule has to be applied ($\Delta H_{sub} = 188 \cdot T_m$). As compounds **2** and **3** are liquid, a different factor is applied ($\Delta H_{sub} = 90 \cdot T_m$).

Table S 6.3. Heat of formation calculation results for compounds **1**–**3**.

M	$-H^{298}$ [a] [a.u.]	$\Delta_f H^\circ(g, M)$ [b] [kJ mol^{-1}]	$\Delta_{sub}H^\circ$ (M) [c] [kJ mol^{-1}]	$\Delta_f H^\circ(s)$ [d] [kJ mol^{-1}]	Δn	$\Delta_f U(s)$ [e] [kJ kg^{-1}]
1	751.610116	−233.4	69.2122	−302.6	−6.5	−1590.9
2	472.193794	−129.6	38.3355	−168.0	−5.0	−1306.5
3	511.451024	−208.6	37.2735	−245.8	−6.0	−1735.1

[a] CBS-4M electronic enthalpy. [b] Gas phase enthalpy of formation. [c] Sublimation enthalpy. [d] Standard solid state enthalpy of formation. [e] Solid state energy of formation.

The thermal behavior of compounds **1**–**3** was analyzed by DSC at a heating rate of 5 °C min^{-1}. The obtained thermogram and its evaluation is depicted in Figure S14.

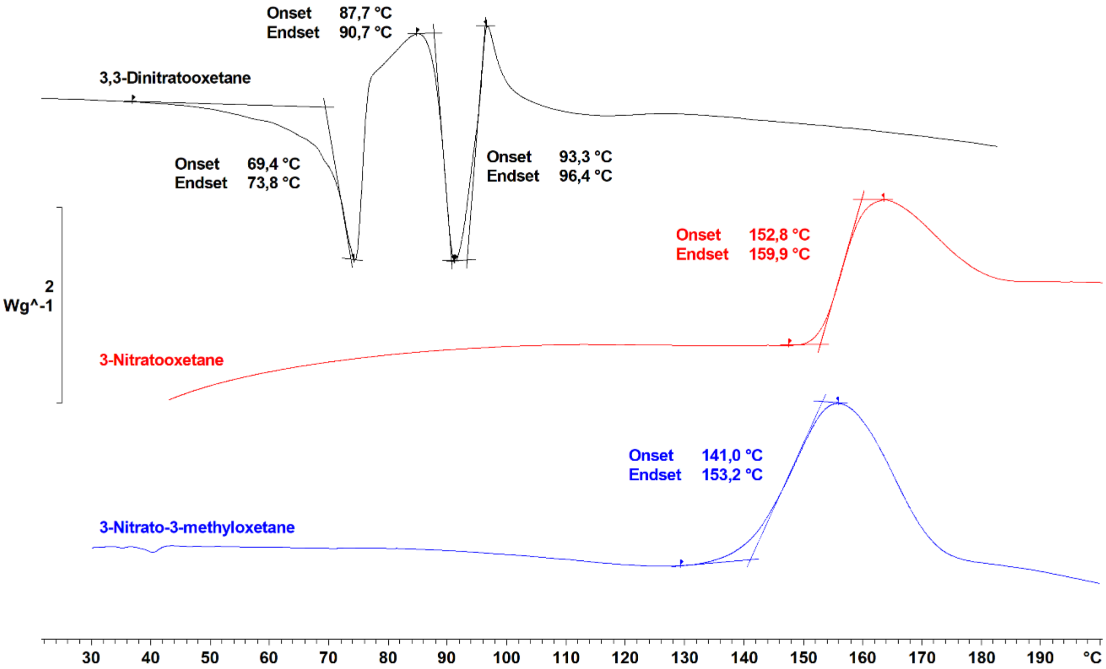

Figure S 6.14. DSC evaluation result for compounds **1**–**3** (exo-up).

References

[1] http://www.bam.de

[2] NATO STANAG 4489: *Explosives. Impact Sensitivity Tests*; NATO Standardization Office, Brussels, Belgium, **1999**.

[3] WIWEB-Standardarbeitsanweisung 4-5.1.02, Ermittlung der Explosionsgefährlichkeit, hier der Schlagempfindlichkeit mit dem Fallhammer, November 8, **2002**.

[4] NATO STANAG 4487: *Explosives. Friction Sensitivity Tests*; NATO Standardization Office, Brussels, Belgium, **2002**.

[5] WIWEB-Standardarbeitsanweisung 4-5.1.03, Ermittlung der Explosionsgefährlichkeit oder der Reibeempfindlichkeit mit dem Reibeapparat, November 8, **2002**.

[6] Impact: Insensitive > 40 J, less sensitive ≤ 35 J, sensitive ≤ 4 J, very sensitive ≤ 3 J; Friction: Insensitive > 360 N, less sensitive = 360 N, sensitive 80 N, very sensitive ≤ 80 N, extreme sensitive ≤10 N; According to the UN Recommendations on the Transport of Dangerous Goods (+) indicates: not safe for transport.

[7] Baum, K.; Lin, W. H.; Willer, R. L. Synthesis of poly-(3-nitratooxetane). US 8 030 440 B1, **2011**.

[8] CrysAlisPRO, Oxford Diffraction /Agilent Technologies UK Ltd., Yarnton, England, **2009**.

[9] Burla, M. C.; Caliandro, R.; Carrozzini, B.; Cascarano, G. L.; Cuocci, C.; Giacovazzo, C.; Mallamo, M.; Mazzone, A.; Polidori, G. Crystal structure determination and refinement via SIR2014. *J. Appl. Crystallogr.* **2015**, *48*, 306-309.

[10] Hübschle, C. B.; Sheldrick, G. M.; Dittrich, B. ShelXle: a Qt graphical user interface for SHELXL. *J. Appl. Crystallogr.* **2011**, *44*, 1281-1284.

[11] Sheldrick, G. M. SHELXL-97: Program for the Refinement of Crystal Structures, University of Göttingen, Germany, **1997**.

[12] Sheldrick, G. A short history of SHELX. *Acta Cryst. A.* **2008**, *64*, 112-122.

[13] Spek, A. L. PLATON – a Multipurpose Crystallographic Tool, Utrecht University, Netherlands, **1991**.

[14] Farrugia, L. J., WinGX and ORTEP for Windows: an update. *J. Appl. Crystallogr.* **2012**, *45*, 849-854.

[15] Chase, M. W. NIST-JANAF Thermochemical Tables, Fourth Edition, *J. Phys. Chem. Red. Data, Monograph 9,* **1998**, 1–1951.

[16] Frisch, M. J.; Trucks, G. W.; Schlegel, H. B.; Scuseria, G. E.; Robb, M. A.; Cheeseman, J. R.; Scalmani, G.; Barone, V.; Petersson, G. A.; Nakatsuji, H.; Li, X.; Caricato, M.; Marenich, A. V.; Bloino, J.; Janesko, B. G.; Gomperts, R.; Mennucci, B.; Hratchian, H. P.; Ortiz, J. V.; Izmaylov, A. F.; Sonnenberg, J. L.; Williams; Ding, F.; Lipparini, F.; Egidi, F.; Goings, J.; Peng, B.; Petrone, A.; Henderson, T.; Ranasinghe, D.; Zakrzewski, V. G.; Gao, J.; Rega, N.; Zheng, G.; Liang, W.; Hada, M.; Ehara, M.; Toyota, K.; Fukuda, R.; Hasegawa, J.; Ishida, M.; Nakajima, T.; Honda, Y.; Kitao, O.; Nakai, H.; Vreven, T.; Throssell, K.; Montgomery Jr., J. A.; Peralta, J. E.; Ogliaro, F.; Bearpark, M. J.; Heyd, J. J.; Brothers, E. N.; Kudin, K. N.; Staroverov, V. N.; Keith, T. A.; Kobayashi, R.; Normand, J.; Raghavachari, K.; Rendell, A. P.; Burant, J. C.; Iyengar, S. S.; Tomasi, J.; Cossi, M.; Millam, J. M.; Klene, M.; Adamo, C.; Cammi, R.; Ochterski, J. W.; Martin, R. L.; Morokuma, K.; Farkas, O.; Foresman, J. B.; Fox, D. J., Gaussian 16 Rev. C.01, **2016**.

7 Oxetane Monomers Based On the Powerful Explosive LLM-116: Improved Performance, Insensitivity, and Thermostability

by
Max Born, Konstantin Karaghiosoff, Thomas M. Klapötke, and Michael Voggenreiter

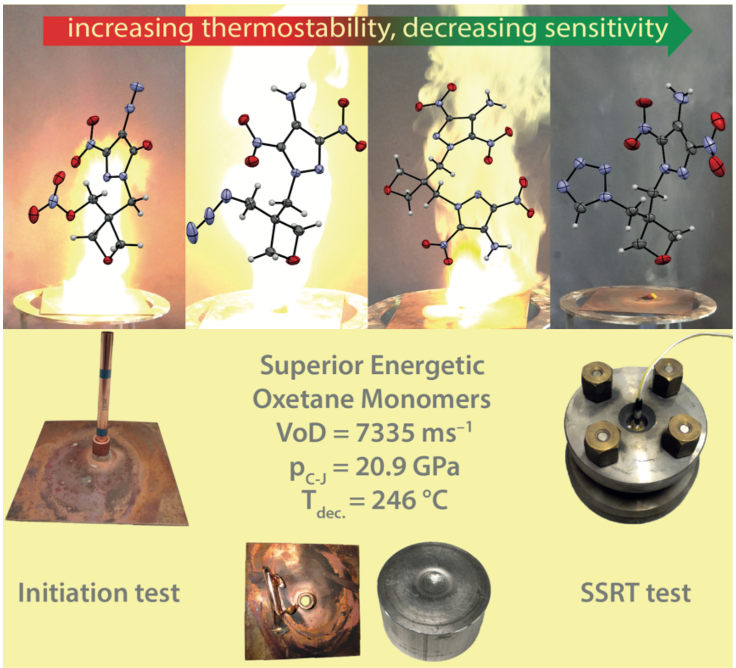

Beating the prior art: Several oxetane monomers based on the explosive LLM-116 were synthesized, characterized and practically evaluated regarding performance and insensitivity. By applying an inexpensive and straightforward chemistry, energetic performances and thermostabilities were obtained which vastly exceed those of known energetic oxetanes.

as published in
ChemPlusChem **2022**, *87*, e202200049
(doi:10.1002/cplu202200049)

Abstract

3-Bromomethyl-3-hydroxymethyloxetane represents an inexpensive and versatile precursor for the synthesis of 3,3-disubstituted oxetane derivatives. In the present work, its synthesis was improved and energetic oxetanes based on the explosive LLM-116 (4-amino-3,5-dinitro-1*H*-pyrazole) prepared. Reaching detonation velocities and pressures of up to 7335 $\mathrm{ms^{-1}}$ and 20.9 GPa in combination with a high thermostability and insensitivity, these surpass the prior art by far. Next to a symmetric LLM-116 derivative, three asymmetric compounds were prepared using azido-, nitrato- and tetrazolyl-moieties. All compounds were intensively characterized by vibrational-, mass- and multinuclear (^{1}H, ^{13}C, ^{14}N) NMR spectroscopy, differential scanning calorimetry and elemental analysis. The molecular structures were elucidated by single crystal X-ray diffraction. Hirshfeld analysis allowed to estimate their sensitivity next to a practical evaluation using BAM standard procedures. Their performance was calculated using the EXPLO5 V6.04 code and a small-scale shock reactivity test and initiation test demonstrated their insensitivity and performance.

Keywords: Energetic materials, heterocycles, LLM-116, nitration, oxetane monomers.

7.1 Introduction

The state of the art in the field of energetic polymers is mainly represented by well-known polyethers such as GAP (glycidyl azide polymer), poly(3,3-bis(azidomethyl)oxetane) (polyBAMO), poly(3-azidomethyl-3-methyloxetane) (polyAMMO), poly(3-nitratomethyl-3-methyloxetane) (polyNIMMO) and poly(glycidyl nitrate) (polyGLYN).[1] Unfortunately, the respective monomers show performances way inferior to TNT or more recent developments in the field of secondary explosives. They can be subdivided into two groups – azides, which feature a relatively high thermostability at the price of poor oxygen balance and organic nitrates with improved oxygen balance at the cost of thermostability below modern requirements.[2] Their polymers are preferred over non-energetic binders, but their energetic contribution in formulations is low. Therefore, new monomers combining higher performance and thermostability with less sensitivity are highly desirable. For example, binders prepared thereof could find application in especially safe low-vulnerability ammunitions (LOVA) and propellants.[3] In this context, a patent describes 3-bromomethyl-3-hydroxymethyloxetane (BMHMO) as very suitable starting material for the preparation of asymmetric oxetane monomers. For instance, the preparation of the powerful compound 3-azidomethyl-3-nitratomethyloxetane is disclosed.[4] Indeed, BMHMO shows advantageous properties. It can be prepared inexpensively by Williamson ether synthesis and is chemically very versatile. For example, the excellent leaving group enables functionalization with nucleophiles and follow-up reactions with electrophiles making use of the hydroxy group may afford asymmetric species. Conversion of this group into a leaving group enables access to either symmetric or asymmetric derivatives by further substitution reactions. Beyond, the present methylene spacers diminish the adverse effect of mostly electron-withdrawing explosophoric groups on the oxetane oxygen atom. This is of advantage as the success of a cationic ring-opening polymerization strongly depends on the basicity of the oxygen atom.[5] However, the scaffold of BMHMO imposes a detrimental carbon-hydrogen ballast, rendering it beneficial to use larger energetic motifs as substituents to mitigate or compensate this particular influence. For this purpose, powerful secondary explosives with functional groups like 4-amino-3,5-dinitro-1*H*-pyrazole (LLM-116 or ADNP) are very promising. ADNP was first described as protected compound in 1993 by Vinogradov and later as unprotected compound by Shevelev in 1998.[6] Since then, it has been made accessible by several synthetic routes, whereas 4-chloro-1*H*-pyrazole provides the highest yield when used as starting material.[7] ADNP impresses with a high density (1.90 g cm^{-3}) and a correspondingly high detonation velocity and pressure (8680 ms^{-1}, 32.8 kbar).[8] Already in 2014, it was employed in a pilot scale study by Ek and Latypov and prepared in 200 g batches.[7] Due to its favorable properties, ADNP has been increasingly used for the synthesis of new energetic materials since 2011.[9-11] Herein, we report a significantly improved synthesis of BMHMO, rendering it an even more attractive starting material for the synthesis of energetic oxetane monomers. Ultimately, it was used to prepare symmetric and asymmetric derivatives based on LLM-116. Here, high yields and the preferential use of commercially available materials contribute to low costs. The molecular structures of all products were elucidated by X-ray diffraction, also allowing Hirshfeld analysis, which made the high insensitivity of some target compounds and the results of the SSRT and initiation test comprehensible. In terms of performance and thermostability, the target compounds are largely superior to prior art energetic oxetane monomers. Based on the fine balance of these new monomers between performance, thermostability, and insensitivity, they are promising candidates for the preparation of energetic polymers with improved properties in these key aspects.

7.2 Results and Discussion

7.2.1 Synthetic Procedures

The Williamson reaction to give 3-bromomethyl-3-hydroxymethyloxetane (BMHMO, **1**) was significantly improved by changing base and solvent from NaOEt/EtOH to NaOH/MeOH to give a crude yield of 93%. Subsequent vacuum distillation removed by-products (e.g., spiro-compound) and unreacted starting material to afford pure BMHMO as colorless oil in 85% (+33%) yield, while the literature reports only 52% after purification.[4] Reaction of **1** with the potassium salt of 4-amino-3,5-dinitro-1*H*-pyrazole (K-ADNP, **2**) in DMF led to alcohol **3**, which was isolated by the precipitation of inorganic salts using ethyl acetate, filtration through a Celite plug, and rotary evaporation to remove all volatiles. Residual traces of DMF were co-evaporated (cold ether) to afford **3** as bright-yellow solid in quantitative yield (Scheme 1). It was tried to obtain the corresponding nitrate **4** using acetyl nitrate as mild and cost-efficient nitrating agent, but several attempts failed (recovery of starting material). However, aprotic nitration using dinitrogen pentoxide was successful while minimizing the risk of undesired ring-opening of the

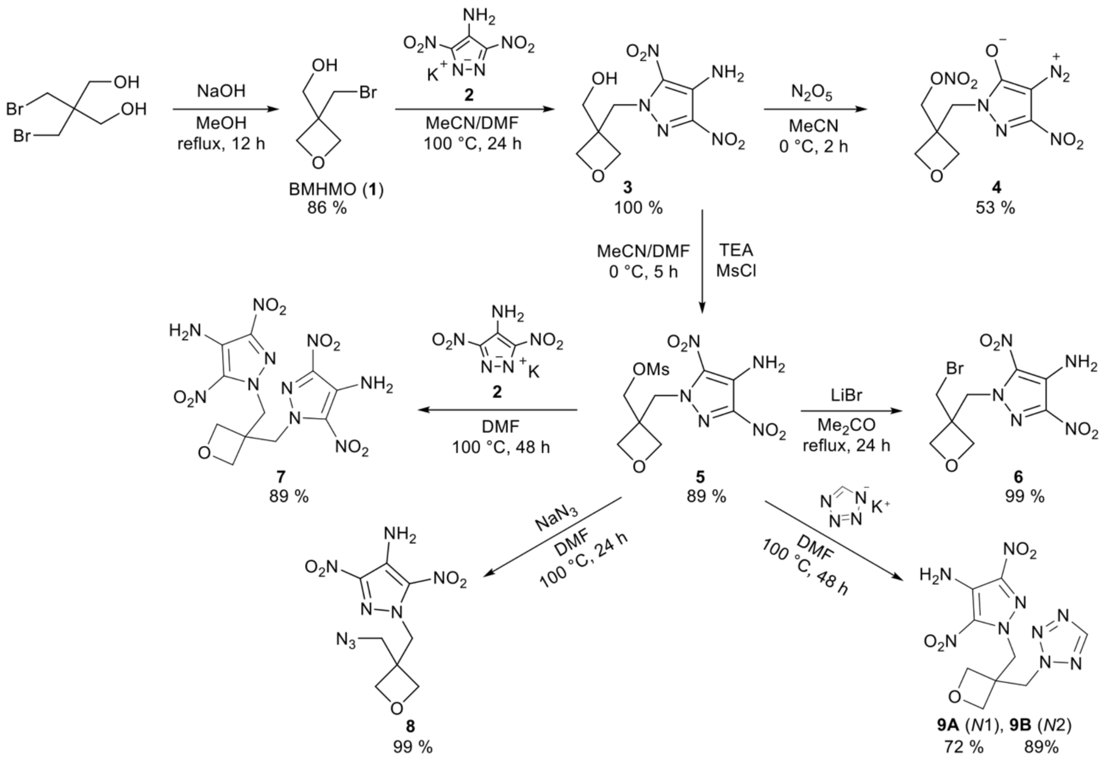

Scheme 7.1. Synthetic pathway starting with the ring-closure of 2,2-bis(bromomethyl)propane-1,3-diol toward BMHMO (**1**). Subsequent substitution using the potassium salt of LLM-116 affords compound **3**. Nitration results in target compound **4** while mesylation gives compound **5** providing access to target compounds **6**–**9** in high overall yield.

oxetane ring by hydrolysis. Unfortunately, the pyrazole motif suffered from severe chemical changes and the zwitterionic diazonium olate **4** was obtained. Similar zwitterionic pyrazole compounds are known to literature, but usually obtained by targeted diazotation reactions.[12] Fischer reported a very similar diazonium olate by nitrating the structurally related bis(4-amino-3,5-dinitropyrazolyl)methane with mixed acid followed by quenching on water.[10] However, no mechanism for the formation of this particular structure was proposed. As nitro groups are prone to act as leaving groups in aromatic nucleophilic substitution reactions, we assume a nucleophilic attack of water upon quenching. This leads to the formation of nitrous acid as source of nitrosyl cations. These cause a quick, subsequent diazotation reaction toward compound **4** (Scheme 2).

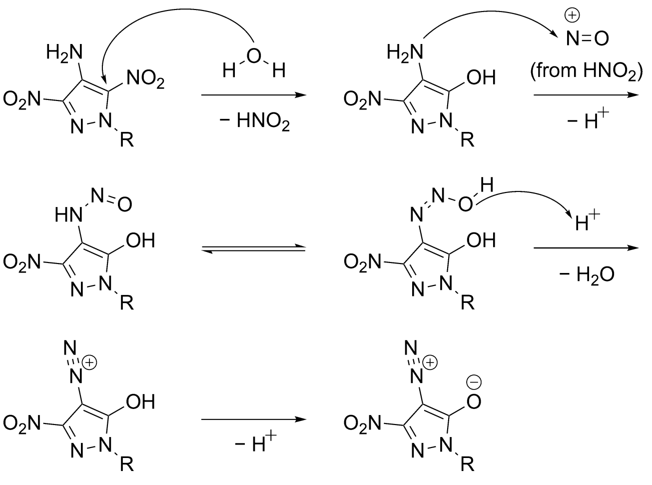

Scheme 7.2. Proposed mechanism for the formation of diazonium olate **4**.

Despite various solvent/anti-solvent precipitation attempts, the crude compound remained an extremely viscous oil. Ultimately, column chromatography (SiO_2, EtOAc) afforded **4** in 53% yield as orange solid. To enable further substitution reactions, compound **3** was mesylated to provide a good leaving group. Due to the tailored solvent system, methanesulfonic ester **5** precipitated as lemon-yellow solid after a short reaction time and was obtained by suction filtration in high purity and yield (85%). Since particularly weak or sterically demanding nucleophiles are not always able to readily substitute the mesyl group, compound **5** was converted to the bromo-species **6** in a Finkelstein-type reaction using lithium bromide in acetone to provide an alternative leaving group. Filtration through silica (EtOAc) to separate inorganic salts gave compound **6** in high purity and quantitative yield (Scheme 1). However, all follow-up substitution reactions were successfully performed using mesylate **5** thus avoiding this additional step. DMF was employed as solvent as it allows high reaction temperatures and removal by rotary evaporation, while it dissolves sodium azide, K-ADNP and potassium tetrazol-1-ide rather well. The reaction of **5** with K-ANDP (**2**) was complete after 48 h according to TLC. The high reaction time can be explained by the steric demand of the nucleophile. All inorganic salts were separated as previously described and DMF was evaporated. The crude material was suspended in diethyl ether and collected by suction filtration to give **7** in high yield and purity (89%) as yellow solid. Compound **8** was prepared analogously from **5** using sodium azide. The same work-up routine was applied and traces of DMF removed by co-evaporation to give **8** in 99% yield. Dissolution of **8** in a small amount of acetone followed by precipitation (*n*-hexane) gave pure **8** as bright yellow solid without yield loss. As in case of compound **7**, the reaction of **5** with potassium tetrazol-1-ide required a prolonged reaction time of 48 h according to TLC. The work-up was performed as described before and the crude isomeric mixture (**9A**, **9B**) was suspended in a small amount of acetone prior to the addition of an excess of diethyl ether. After suction filtration, a yield of 98% was obtained and ^{1}H NMR spectroscopy revealed a *N*1/*N*2 ratio of 1:2. The regioisomers were separated by refluxing the mixture in toluene and filtration of the hot suspension. The filtrate was evaporated to give pure *N*2-isomer (**9B**) with a yield of 89%. The filter residue contained 10% *N*2-isomer (^{1}H NMR) and was recrystallized from acetone to give 72% of *N*1-isomer (**9A**) also as yellow solid. Thereby, an overall yield of 84% (*N*1, *N*2) was achieved without column chromatography.

7.2.2 Crystallography

Single crystals of the following compounds were obtained by slow evaporation of their solutions using ethyl acetate (**4**, **8**), DMF (**7**), toluene (**9B**) and acetone (**9A**). Detailed crystallographic data can be found in the Supporting Information. Compound **4** crystallizes in the monoclinic space group $P2_1/n$ with four molecules in the unit cell and a calculated density of 1.667 g cm^{-3} at 123 K (Figure 1a).

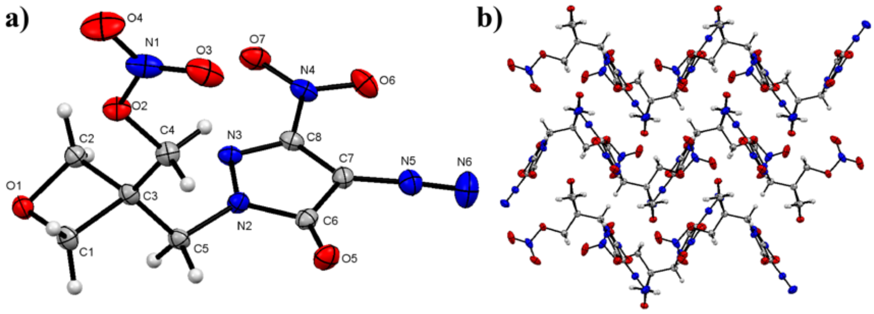

Figure 7.1. a) Molecular structure of **4** in the crystal. Thermal ellipsoids are drawn at the 50% probability level. b) View along the *a* axis – the molecules form a wave-like pattern.

The bond lengths of C6–O5 (1.218(2) Å) corresponds to a C=O double bond.[13] Further, C7–N5 has a length of 1.327(2) Å which is approximately the length of a C=N double bond.[14] The diazo group is nearly linear with an angle of 176.2° (C7–N5–N6) and shows a very short interatomic distance of 1.110(2) Å (N5–N6) which can be attributed to a N≡N triple bond. The angles within the oxetane ring range between 91.14(9)° at O1–C2–C3 and 91.52(9)° at O1–C1–C3. The smallest angle is observed at C1–C3–C2 (84.72(9)°). The oxetane ring shows a puckering angle of 12.5° which is slightly larger than the puckering angle found in unsubstituted oxetane (8.7°, 140 K).[15] The nitro group of the pyrazole motif essentially matches the pyrazole plane. In the crystal, the molecules are arranged to form a wave-like pattern along the *a* axis (Figure 1b).

Compound **7** crystallizes in the monoclinic space group $P2_1/n$ with four formula units in the unit cell. The crystal contains one dimethylformamide molecule per formula unit and displays a density of 1.639 g cm^{-3} at 123 K (Figure 2).

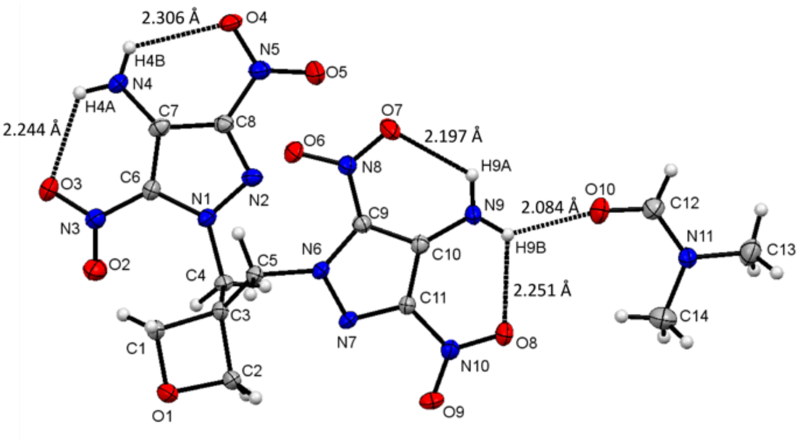

Figure 7.2. Molecular structure of **7** in the crystal and interactions with the crystallized dimethylformamide molecule. Thermal ellipsoids are drawn at the 50% probability level.

The angles within the oxetane ring vary from 83.82(2)° at C1–C3–C2 to 91.72(2)° at O1–C2–C3. The oxetane ring is strongly folded with a puckering angle of 15.9° which is considerably larger than the corresponding angle in unsubstituted oxetane (8.7° at 140 K).[15] One of the pyrazole rings has both nitro groups in the ring plane, the other pyrazole ring has the nitro group at C6 twisted by 16.81° and the nitro group at C8 twisted by 3.28°. The amino group at C7 features intramolecular interactions with the neighboring nitro groups with distances of 2.306(2) Å and 2.244(2) Å. The other amino group at C10 shows the same interaction with distances of 2.197(2) Å and 2.251(2) Å. In addition, an intermolecular hydrogen bridge is found between this amino group and the oxygen atom of the dimethyl formamide molecule with a distance of 2.084(2) Å.

Compound **8** crystallizes in the monoclinic space group $P2_1/c$ with four formula units in the unit cell and a density of 1.608 g cm^{-3} at 123 K (Figure 3a).

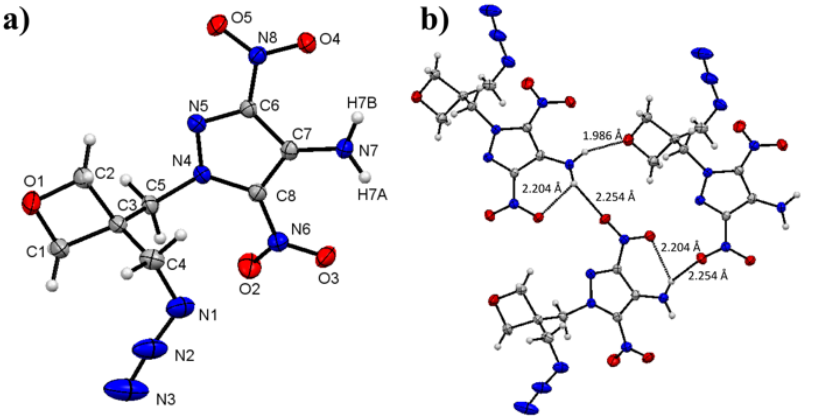

Figure 7.3. a) Molecular structure of **8** in the crystal. Thermal ellipsoids are drawn at the 50% probability level. b) Intra- and intermolecular hydrogen bonding in the crystal structure of **8**.

The angles within the oxetane motif vary from 84.72(2)° at C1–C3–C2 to 92.72(2)° at C1–O1–C3. The oxetane ring is found to be essentially planar and the azido group is almost linear (N1–N2–N3, 174.0(3)°). The nitro groups at C8 and C6 are twisted out of the pyrazole plane by 19.58° and 5.62°, respectively. The molecule displays an intramolecular hydrogen bond from H7B to O4 with a distance of 2.204(2) Å (Figure 3b). Further, there are intermolecular hydrogen bonds of the amino group to two adjacent molecules. One between H7B and O5 (nitro group) with a distance of 2.254(2) Å and another between H7A and O1 (oxetane ring) with a length of 1.986(2) Å. These hydrogen bonds contribute to a stabilization the molecule in the solid state. Compound **9A** crystallizes in the monoclinic space group $P2_1/c$ with four formula units in the unit cell and **9B** crystallizes in the triclinic space group *P*–1 with two formula units in the unit cell (Figure 4).

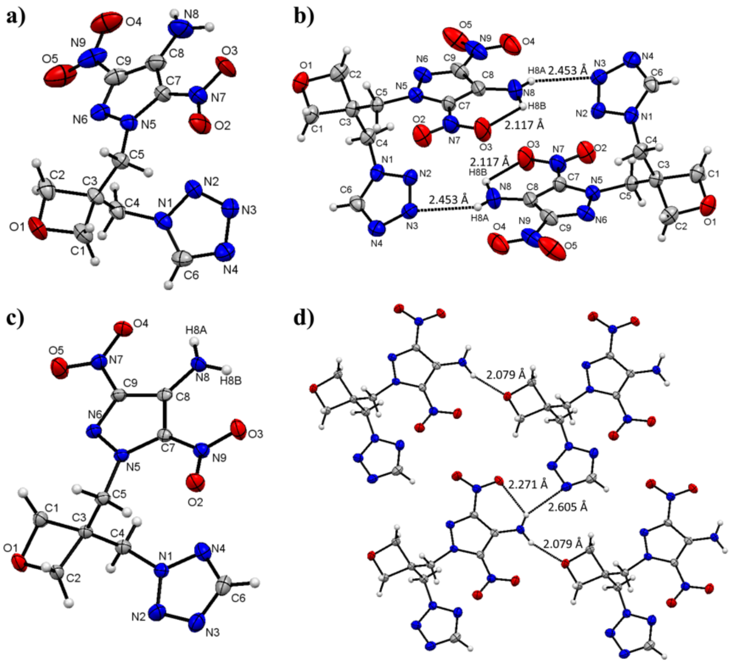

Figure 7.4. Molecular structure of **9A** (a) and the corresponding pairs formed in the solid state (b). Crystal structure of **9B** (c) and the network which is formed in the crystal (d). Thermal ellipsoids are drawn at the 50% probability level.

Compound **9B** has a density of 1.691 g cm^{-3} at 123 K which is marginally higher than the density of **9A** (1.630 g cm^{-3}) at 123 K. The puckering angle in the oxetane ring of **9B** is 14.5° while **9A** exhibits a way smaller puckering angle of 10.2°. For compound **9A**, two molecules arrange in pairs due to strong hydrogen bonding between the amino group and the tetrazole ring (N3) of a neighboring molecule with a distance of 2.453(5) Å. Intramolecular hydrogen bonding is found between the amino group (H8B) and an adjacent nitro group (O3) with a distance of 2.117(4) Å. An analogous intramolecular hydrogen bond is observed in case of compound **9B** involving H8A of the amino group and the neighboring oxygen atom O4 of the nitro group with a distance of 2.271(3) Å. In addition, H8A shows an intermolecular short contact bond to the tetrazole moiety (N3) of an adjacent molecule with a distance of 2.605(3) Å, which is quite long for a hydrogen bond. Moreover, an intermolecular short contact bond with a distance of 2.079(3) Å is found between H8B of the amino group and the oxetane oxygen atom O1 of a neighboring molecule.

7.2.3 Hirshfeld Analysis

When a mechanical force acts upon a solid energetic material, it causes vertical compression and horizontal sliding of layers in the crystal leading to internal strains.[16] If the related strain energy is higher than the lowest bond dissociation energy in the molecule, decomposition will occur.[17] In this context, intermolecular interactions can have a stabilizing or destabilizing effect establishing a direct correlation with an energetic materials' sensitivity.[17,18] A valuable tool to explore these interactions is Hirshfeld analysis.[19,20] Hence, we calculated the Hirshfeld surface (HFS) of all target compounds using CrystalExplorer V17.5 to find correlations.[21] On the HFS, close contact interactions are shown as red dots. In addition, we visualized all interactions and their distances $d_i + d_e$ (d_i = distance from HFS to the closest atom interior, d_e = distance from HFS to closest atom exterior) in a 2D fingerprint plot (Figure 5).[22]

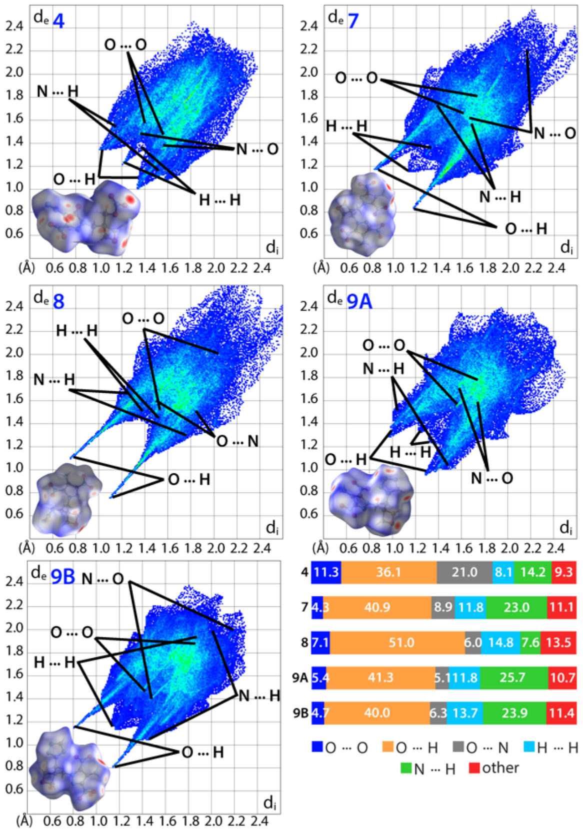

Figure 7.5. Calculated Hirshfeld surfaces and 2D fingerprint plots for compounds **4** and **7**–**9**. The bar chart summarizes the respective populations of close contacts in the crystal.

Interactions with distances below 2.4 Å are considered strong, while interactions with distances larger than roughly 3 Å are considered weak. Especially characteristic for sensitive compounds are high populations of repulsive O···O interactions next to destabilizing, repulsive O···N or H···H contacts. High sensitivity is particularly encountered when these are poorly balanced by stabilizing interactions like N···H or O···H close contacts.[17,18] Further, a comparison of the respective percentages (bar diagram, Fig. 5) and the interaction distances ($d_i + d_e$) enables a weighting. This allows a reasonable estimation of the sensitivity and a ranking of the compounds relative to each other. For example, compound **4** shows stabilizing, strong ($d_i + d_e < 2.4$ Å) O···H interactions (36.1%) and moderately strong N···H (14.2%) interactions. These are counterbalanced by strong, repulsive H···H interactions and weak ($d_i + d_e > 3$ Å) destabilizing O···N (21.0%) and O···O interactions (11.3%). Even if these are weak, their high proportion significantly counteracts the stabilizing interactions. Therefore, a significant sensitivity toward mechanical stimuli can be anticipated. In comparison, compound **7** shows a significantly higher proportion of strong O···H interactions (40.9%). The stabilizing N···H interactions are weak, but their high proportion (23.0%) contributes significantly to the overall stabilization. With a total of 63.9%, they easily compensate found destabilizing interactions – these are made up by a low population of strong, repulsive H···H interactions (11.8%) next to weak O···N (8.9%) and O···O (4.2%) interactions with almost negligible proportions. As a consequence, low sensitivity can be expected. The highest population of strong O···H interactions (51.0%) is found in case of compound **8**. Additional stabilization arises from weak N···H interactions (7.6%). These are only attenuated by few and weak destabilizing interactions. Hereby, repulsive H···H interactions (14.8%) represent the largest fraction along with O···O and O···N interactions, with a cumulative share of only 13.1%. As stabilizing interactions (58.6%) clearly dominate, a low sensitivity is indicated. Since compounds **9A** and **9B** are regioisomers, very similar sensitivity might be expected. This is indeed reflected by very similar interaction proportions. Both compounds are equally dominated by strong O···H interactions with populations of 41.3% and 40%, respectively, and N···H interactions with high percentages of 25.7% and 23.9%. In compound **9A**, this interaction has a higher significance as the proportion is higher and the relative share of strong interactions ($d_i + d_e < 2.4$ Å) is more pronounced. The total population of stabilizing interactions is the highest of all investigated compounds with 67.0% (**9A**) and 63.9% (**9B**). Rather weak, repulsive H···H interactions impose a destabilizing effect on both **9A** (11.8%) and **9B** (13.7%). The same applies to O···N interactions with populations of 5.1% (**9A**) and 6.3% (**9B**) next to O···O interactions with proportions of 5.4% and 4.7%, respectively. Due to their low population and weak nature, they cause negligible destabilization. Based on found interactions, their population and respective strength, **9A** and **9B** should not only be very insensitive, but the least sensitive of all investigated compounds – closely followed by compounds **7** and **8** with compound **4** showing the highest sensitivity. This agrees well with the experimental values for impact and friction sensitivity (Table 2). However, an absolute difference in case of **7**–**9** cannot be quantified due to their generally high insensitivity.

7.2.4 Thermal Analysis

Thermal analysis of all compounds was performed by differential scanning calorimetry (DSC) at a heating rate of 5 °C min^{-1}. Here, compound **4** shows the lowest melting point (95 °C) and, due to the presence of the diazonium and the nitrate ester moiety, which impose thermal instability, also the lowest decomposition temperature (184 °C) of all investigated compounds. Considerably higher decomposition temperatures were found for compounds **7**–**9**. Compound **8** shows a melting point at 101 °C and a decomposition temperature of 238 °C, which is very high as most organic azides already decompose at roughly 180 °C according to literature.[23] This can be attributed to stabilizing effects in the crystal (see Hirshfeld discussion). While isomer **9B** shows a phase transition at 161 °C, features a high melting point of 173 °C and decomposes at 241 °C, compounds **7** and **9A** do not show a melting point and directly decompose exothermically at 246 °C and 241 °C (Figure 6). The different and thus interesting thermal behavior of regioisomers **9A** (*N*1) and **9B** (*N*2) can be attributed to interactions in the crystal. In direct comparison, the *N*1-isomer shows a higher proportion of stabilizing interactions (O···H, N···H) and a lower proportion of repulsive H···H interactions (Figure 5). Specifically, the intermolecular hydrogen bond (H8A–N3, d = 2.453 Å) is shorter and thus stronger than the analogous interaction in the *N*2 isomer with a distance of 2.605 Å. Further and contrary to the *N*2-isomer, parallel-displaced π-stacking interactions occur between spatially opposing pyrazole rings as well as tetrazole rings. In sum, the higher interactions prevent melting of **9A** prior to decomposition. Overall, **7** is the most thermostable compound of all, followed by **9B**, **9A**, **8**, and organic nitrate **4**. As a result, the decomposition temperatures essentially correlate with the ratio of stabilizing and destabilizing effects in the crystal as indicated by Hirshfeld analysis. The effect of substitution is particularly interesting in case of compounds **7**–**9**, since the parent compound (ADNP) decomposes already at 183.6 °C when a heating rate of 10 °C min^{-1} is applied.[24]

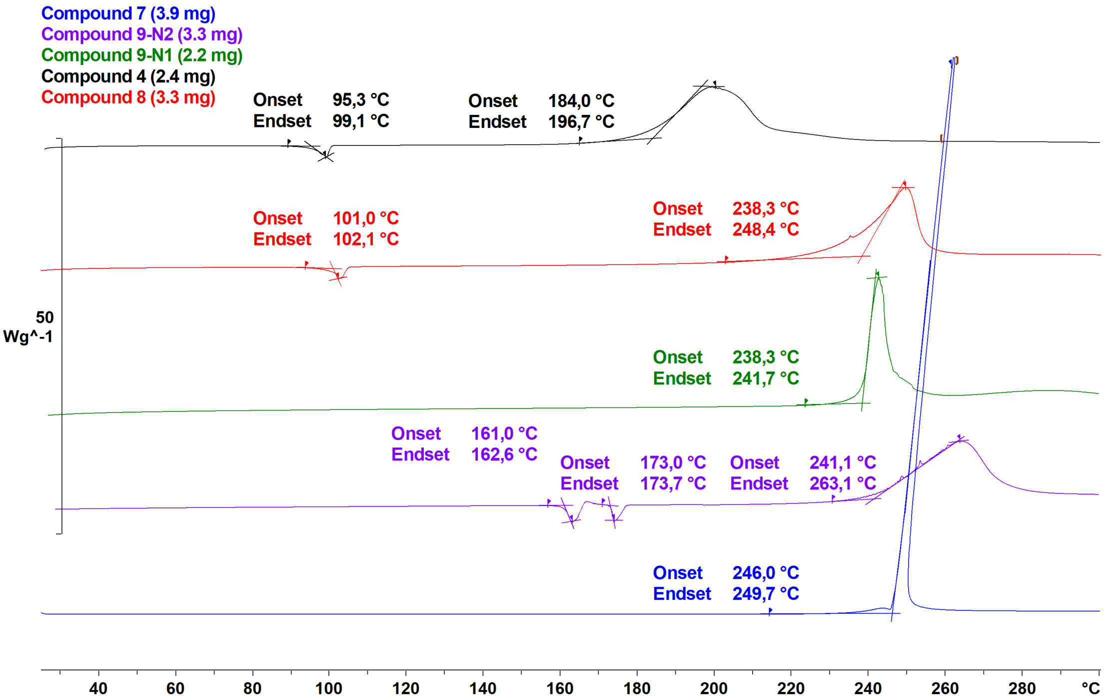

Figure 7.6. DSC thermogram of compounds **4** and **7**–**9**.

7.2.5 Small-Scale Shock Reactivity and Initiation Test

In order to evaluate the explosive performance of compounds **4** and **7**–**9**, a small-scale shock reactivity test (SSRT) was performed (Figure 7).

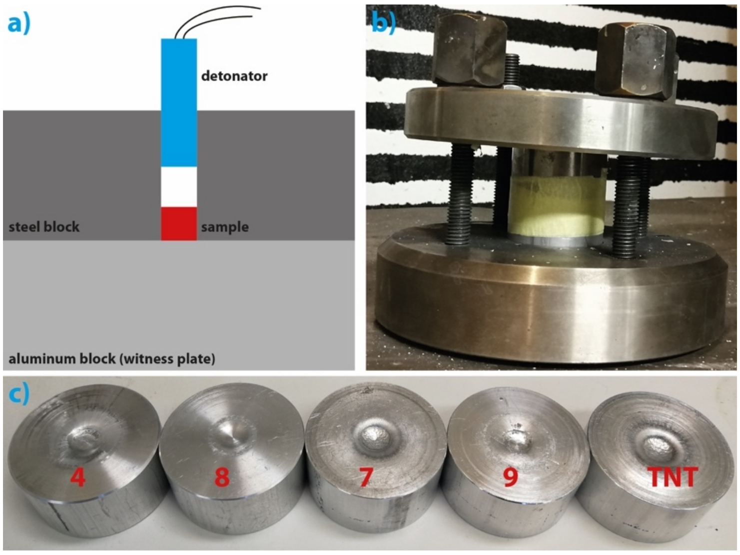

Figure 7.7. a) Schematic setup of a SSRT. b) Steel block and witness plate confined between heavy steel plates prior to the test. c) Aluminum witness plates with dents caused by the respective sample.

This test is suitable to assess the shock reactivity (explosiveness) of an energetic material – often below its critical diameter and without requiring transition to detonation.[25] It combines the advantages of both lead block test and gap test while it requires small quantities of roughly 500 mg.[26] In each test, the same sample volume V_S is used (284 mm^3) and the required amount of explosive (m_E) is calculated by the formula $m_E = V_S \cdot \rho_{XR} \cdot 0.95$ where ρ is the density determined via X-ray diffraction or helium pycnometry. Regarding the setup, each sample was pressed into a perforated steel block on top of an aluminum witness block with a pressure of three tons and five seconds duration. Subsequently, the arrangement is confined between two steel plates (Figure 7b). The pressed charge is then initiated by a commercial detonator (Orica Dynadet C2) using an air gap of 1.5 cm. The obtained dent sizes of the witness blocks can be compared to each other by filling them with finely powdered SiO_2 and measuring the respective weight. Alternatively, the actual dent volumes can be measured using a 3D profilometer. Hereby, the performance of the energetic materials can be compared relative to each other. As all investigated compounds show calculated performances comparable to 2,4,6-trinitrotoluene (TNT), it was used as reference. Interestingly, almost no indentation was obtained in case of compound **8** and plenty of unaffected material was found (see ESI). In case of compounds **4**, **7** and **9**, significant dents were obtained, but much smaller than in case of TNT (Table 1) and thus far behind expectation. Since the critical diameter has little relevance in this test and its determination would require the detonation of numerous charges on a multigram scale at different charge diameters, the insensitivity of the investigated compounds was considered to be the main cause. In this case, the applied shock impulse would be insufficient for a complete initiation rendering the results plausible. To prove this assumption, all compounds were subjected to a systematic initiation test in closed copper tubes with an inner diameter of 7 mm which is comparable to the SSRT diameter of 7.5 mm (Figure 8). Each tube was filled with 200 mg of the respective compound prior to pressing the charge (3 tons, 5 seconds). Afterward, each tube was charged with 50 mg of loosely packed military-grade lead azide (LA) and placed on top of a copper witness plate. Then, the primary explosive was initiated by the spark of an electrical ignitor. In case of compound **4**, the main charge (200 mg) was initiated by LA causing the destruction of the copper tube and an indentation of the witness plate. In case of compounds **7**–**9**, the copper tubes were left completely intact as only the LA top charge detonated proving the extreme insensitivity of these compounds (Figure 8c). Therefore, the test was repeated for compounds **7**–**9** using an additional booster charge of 50 mg pentaerythritol tetranitrate (PETN) which was pressed onto the sample charge and 50 mg of unpressed lead azide was again added

Table 7.1. Mass of explosive *versus* dent size in the SSRT.

Compound	**4**	**7**	**8**	**9**	**TNT**
m_e (mg)	426	459	424	428	445
Vdent (mm^3)	160	298	34	162	343

prior to firing the charges with an electrical igniter. In all cases, the copper tube was destroyed and the witness plate perforated (**8**, **9**) or heavily dented (**7**) (Figure 8d). It can be concluded that all compounds except **4** are too insensitive to be initiated by the detonation of a lead azide primary charge. Instead, a booster explosive such as PETN is required for initiation. Therefore, compounds **7**–**9** have proved to combine notable performance and thermostability with low sensitivity.

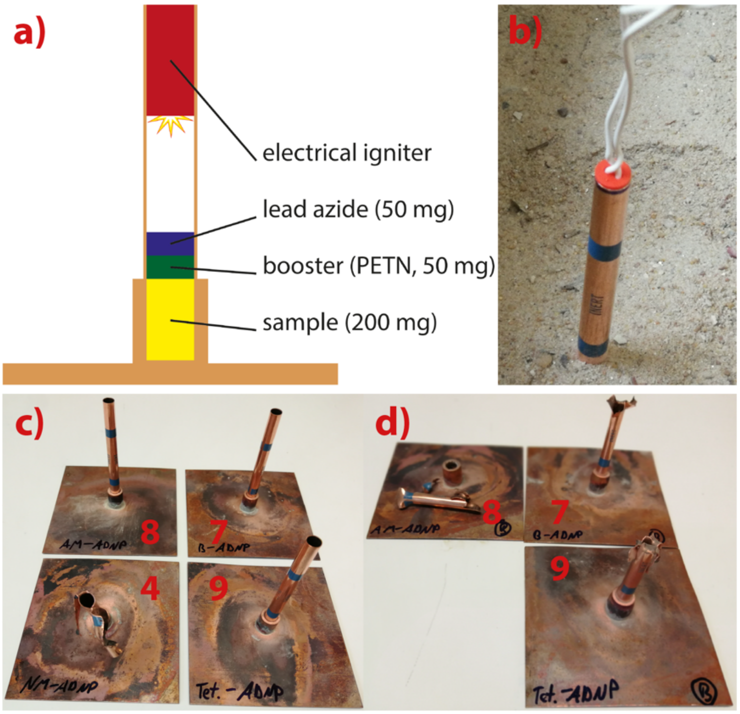

Figure 7.8. a) Schematic test setup. b) Prepared charge in a sandbox. c) Negative (**7**, **8**, **9**) and positive result (**4**) using lead azide. d) Positive result using PETN as booster (**7**, **8**, **9**).

7.2.6 Energetic Properties

All compounds were determined to be very insensitive toward impact and friction except **4**, which is sensitive toward impact (3 J) but rather insensitive toward friction (288 N). All target compounds possess a combined nitrogen and oxygen content (N+O) between 63.4% (**9**) and 66.3% (**4**). The Gaussian16 program package was used to calculate the room temperature enthalpy of formation for all energetic target compounds at the CBS-4M level of theory using the atomization method.[27,28] All compounds exhibit a positive heat of formation in a range of 105.2 to 263.0 kJ mol^{-1}. The EXPLO5 V6.04 code was used to calculate the energetic performance of compounds **4** and **7**–**9**. Isomers **9B** and **9A** show a calculated detonation velocity of 6820 ms^{-1} and 7088 ms^{-1} linked to detonation pressures of 16.7 and 18.3 GPa, respectively, which are therefore in the range of TNT (6809 ms^{-1}, 18.7 GPa). The same applies to azide **8**, which features comparable performance. In contrast, compounds **4** and **7** outperform TNT with detonation velocities of 7124 $\mathrm{ms^{-1}}$ and 7335 $\mathrm{ms^{-1}}$ and detonation pressures of 20.1 GPa and 20.9 GPa, respectively (Table 2). As compound **7** combines the highest performance and thermal stability of all presented compounds with great insensitivity, it is probably the most promising compound for the preparation of future energetic binders with superior characteristics in these aspects. With respect to performance, all compounds are superior to state-of-the-art energetic oxetane monomers (Table S5 (ESI) and Table 2). With exception of compound **4**, this also applies to the thermal stability.

Table 7.2. Physiochemical properties of compounds **4**, **7**, **8**, **9A** and **9B** in comparison to **NIMMO** and **TNT.**

	4	**7**	**8**	**9A (*N*1)**	**9B (*N*2)**	**NIMMO**	**TNT**
Formula	$C_8H_8N_6O_7$	$C_{11}H_{12}N_{10}O_9$	$C_8H_{10}N_8O_5$	$C_9H_{11}N_9O_5$	$C_9H_{11}N_9O_5$	$C_5H_9NO_4$	$C_7H_5N_3O_6$
FW [g·mol^{-1}]	300.19	428.28	298.22	325.27	325.27	147.13	227.12
IS[a] [J]	3	>40	>40	>40	>40	> 40	15
FS[b] [N]	288	>360	>360	>360	>360	360	> 353
N / N+O[c] [%]	28.0/65.3	32.7/66.3	37.6/64.4	38.8/63.4	38.8/63.4	9.5/52.2	18.5/60.5
Ω_{CO}, Ω_{CO2}[d] [%]	−26.6, −69.3	−29.9, −71.0	−42.9, −85.8	−46.7, −91.0	−46.7, −91.0	−59.8, −114	−24.7, −74.0
T_m[e]/ $T_{dec.}$[f] [°C]	95/184	−/246	101/238	−/238	161/241	−14/170	81/290
ρ[g] [g·cm^{-3}]	1.62	1.70	1.56	1.64	1.59	1.19	1.64
$\Delta H_f°$[h] [kJ·mol^{-1}]	115.2	105.2	315.3	238.0	263.0	−268.9	−219.0
				EXPLO5 V6.04			
$-\Delta E_U°$[i] [kJ·kg^{-1}]	4634	4206	4244	3769	3682	3949	4380
$T_{C\text{-}J}$[j] [K]	3276	2981	2948	2669	2649	2507	3190
$D_{C\text{-}J}$[k] [m·s^{-1}]	7124	7335	6962	7088	6820	5906	6809
$p_{C\text{-}J}$ [l] [GPa]	20.1	20.9	17.8	18.3	16.7	10.6	18.7
V_0 [m] [dm^3·kg^{-1}]	707	710	746	730	734	827	640

[a] Impact sensitivity (BAM drop hammer, method 1 of 6). [b] Friction sensitivity (BAM friction apparatus, method 1 of 6). [c] Nitrogen and oxygen content. [d] Oxygen balance with regard to carbon monoxide (ΩCO = (nO − xC − yH/2)(1600/FW) and carbon dioxide (ΩCO_2 = (nO − 2xC − yH/2)(1600/FW)). [e] Melting point (DSC, β = 5 °C·min^{-1}). [f] Temperature of decomposition (DSC, β = 5 °C·min^{-1}). [g] Density at 298 K (ρX-ray/1.028) or helium pycnometry (**7**). [h] Standard molar enthalpy of formation. [i] Detonation energy. [j] Detonation temperature. [k] Detonation velocity. [l] Detonation pressure. [m] Volume of detonation products (assuming only gaseous products).

7.3 Conclusion

The synthesis of BMHMO (**1**) was significantly improved compared to literature methods to provide a yield of 85% (+33%), rendering it an inexpensive and versatile precursor for the synthesis of both energetic and non-energetic oxetanes. Substitution using K-ADNP (**2**) afforded alcohol **3** in quantitative yield, which can directly provide various energetic monomers using suitable electrophiles (**4**). Beyond, mesylation gave sulfonic ester **5** which was used to obtain symmetric compound **7** and asymmetric derivatives **8** and **9** in high yield. With exception of compound **4**, all compounds show an interplay of performance, thermostability, and insensitivity unparalleled in the field of energetic oxetanes and exhibit an advantageous, positive heat of formation. Their calculated performance is in range of the standard military explosive TNT (**8**, **9**) or even higher (**4**, **7**). Thus, they are clearly superior to typical energetic oxetane monomers which constitute the current state of the art (e.g., NIMMO, AMMO, BAMO). The molecular structures of all compounds were elucidated by single crystal X-ray crystallography, allowing a sensitivity estimation via Hirshfeld analysis next to the practical evaluation. Compound **4** was found to be rather sensitive, while compounds **7**–**9** are highly insensitive, which was also reflected by the SSRT and initiation test. Like other energetic oxetanes we are studying, **4** and **8** show melting points around 100 °C. Hence, higher performances may even allow oxetanes to enter the field of melt-cast explosives. For now, compounds **7**–**9** compounds are most well-suited to prepare low-sensitivity energetic binders with enhanced performance to be applied in low-vulnerability ammunitions (LOVA). Unfortunately, the steric demand of compound **7** is very likely to complicate its homopolymerization. However, copolymerization with sterically less demanding compounds (e.g., THF) may even benefit from the bulky substituents as back-biting reactions become effectively suppressed. Based on the current results, we conclude that BMHMO and ADNP are promising structural motifs for the synthesis of energetic monomers surpassing the prior art in key aspects like performance, sensitivity, and thermostability. We anticipate that these motifs and the investigated compounds are helpful to develop the next generation of energetic binders and to lessen the lack of available monomers for their preparation.

Experimental Section

A Supporting Information is available comprising the following: Synthetic procedures, ^{1}H, ^{13}C, ^{14}N NMR spectra, Crystallographic information, DSC graphs, Hot plate test of compounds **4**, **7**–**9** (video, hot plate test.mp4).

Deposition Numbers CCDC 2097524 (**3**), CCDC 2097531 (**4**), CCDC 2097526 (**5**), CCDC 2097528 (**6**), CCDC 2097525 (**7**), CCDC 2097527 (**8**), CCDC 2097530 (**9A**), CCDC 2097529 (**9B**) contain the supplementary crystallographic data for this paper. These data are provided free of charge by the joint Cambridge Crystallographic Data Centre and Fachinformationszentrum Karlsruhe Access Structures service www.ccdc.cam.ac.uk/structures.

Acknowledgements

Financial support of this work by the Ludwig-Maximilians University of Munich (LMU), the Office of Naval Research (ONR) under grant no. ONR N00014-19-1-2078 and the Strategic Environmental Research and Development Program (SERDP) grant WP19-1287 under contract no. W912HQ19C0033 is gratefully acknowledged. The authors also thank Stefan Huber for his help regarding sensitivity evaluations and Jakob Plank for his extensive help with all preparative tasks as well as Maximilian Benz for the dent volume measurements (SSRT). The authors declare no conflict of interest.

References

[1] Ang, H. G.; Pisharath, S. *Energetic Polymers: Binders and Plasticizers for Enhancing Performance*; Wiley-VCH: Weinheim, **2012**.

[2] Klapötke, T. M. *Chemistry of High-Energy Materials*; 5th ed.; DeGruyter: Boston, **2019**.

[3] Kirshenbaum, M.S.; Avrami L.; Strauss, B. *Sensitivity Characterization of low vulnerability (LOVA) propellants*; ADA126130; US Army Armament Research and Development Command, Large Caliber Weapon Systems Laboratory: Dover, NJ, **1983**.

[4] Manser, G. E.; Malik, A. A.; Archibald, T. G. 3-Azidomethyl-3-Nitratomethyloxetane. US 5 489 700, **1996**.

[5] Dreyfuss, M. P.; Dreyfuss, P. Oxetane Polymers. In *Encyclopedia of Polymer Science and Technology*, (Ed.), John Wiley & Sons: Hoboken, New Jersey, **2011**. DOI 10.1002/0471440264.pst520

[6] Vinogradov, V. M.; Cherkasova, T. I.; Dalinger, I. L.; Shevelev, S. A. Nitropyrazoles. *Russ. Chem. Bull.* **1993,** *42*, 1552-1554.

[7] Ek, S.; Latypov, N. V. Four Syntheses of 4-Amino-3,5-dinitropyrazole. *J. Heterocycl. Chem.* **2014,** *51*, 1621-1627.

[8] Klapötke, T. M. *Energetic Materials Encyclopedia*; Vol. 1–3; De Gruyter: Berlin, Boston, **2021**.

[9] Zhang, Y.; Huang, Y.; Parrish, D. A.; Shreeve, J. M. 4-Amino-3,5-dinitropyrazolate salts—highly insensitive energetic materials. *J. Mater. Chem.* **2011,** *21*, 6891-6897.

[10] Fischer, D.; Gottfried, J. L.; Klapötke, T. M.; Karaghiosoff, K.; Stierstorfer, J.; Witkowski, T. G. Synthesis and Investigation of Advanced Energetic Materials Based on Bispyrazolylmethanes. *Angew. Chem. Int. Ed.* **2016,** *55*, 16132-16135.

[11] Zhang, M.-X.; Pagoria, P. F.; Imler, G. H.; Parrish, D. Trimerization of 4-Amino-3,5-dinitropyrazole: Formation, Preparation, and Characterization of 4-Diazo-3,5-bis(4-amino-3,5-dinitropyrazol-1-yl) pyrazole (LLM-226). *J. Heterocycl. Chem.* **2019,** *56*, 781-787.

[12] Dalinger, I. L.; I. Cherkasova, T. I.; Shevelev, S. A. Synthesis of 4-diazo-3,5-dinitropyrazole and characteristic features of its behaviour towards nucleophiles. *Mendeleev Commun.* **1997,** *7*, 58-59.

[13] Orpen, A. G.; Brammer, L.; Allen, F. H.; Kennard, O.; Watson, D. G.; Taylor, R. In *Struct. Correl.* **1994**, pp 752-858.

[14] de Athayde-Filho, P. F.; Miller, J.; Simas, A. M.; Lira, B. F.; de Souza Luis, J. A.; Zuckerman-Schpector, J. Synthesis, Characterization and Crystallographic Studies of Three 2-Aryl-3-methyl-4-aryl-1,3-thiazolium-5-thiolates. *Synthesis* **2003**, *2003*, 0685-0690.

[15] Luger, P.; Buschmann, J. Oxetane: the first x-ray analysis of a nonsubstituted four-membered ring. *J. Am. Chem. Soc.* **1984,** *106*, 7118-7121.

[16] Zhang, J.; Zhang, Q.; Vo, T. T.; Parrish, D. A.; Shreeve, J. Energetic Salts with π-Stacking and Hydrogen-Bonding Interactions Lead the Way to Future Energetic Materials. *J. Am. Chem. Soc.* **2015**, *137*, 1697-1704.

[17] Reichel, M.; Dosch, D.; Klapötke, T.; Karaghiosoff, K. Correlation between Structure and Energetic Properties of Three Nitroaromatic Compounds: Bis(2,4-dinitrophenyl) Ether, Bis(2,4,6-trinitrophenyl) Ether, and Bis(2,4,6-trinitrophenyl) Thioether. *J. Am. Chem. Soc.* **2019**, *141*, 19911-19916.

[18] Dosch, D. E.; Reichel, M.; Born, M.; Klapötke, T. M.; Karaghiosoff, K. Investigation of Structure–Property Relationships of Three Nitroaromatic Compounds: 1-Fluoro-2,4,6-trinitrobenzene, 2,4,6-Trinitrophenyl Methanesulfonate, and 2,4,6-Trinitrobenzaldehyde. *Cryst. Growth Des.* **2021**, *21*, 243-248.

[19] Spackman, M. A.; Jayatilaka, D. Hirshfeld surface analysis. *CrystEngComm* **2009,** *11*, 19-32.

[20] McKinnon, J. J.; Spackman, M. A.; Mitchell, A. S. Novel tools for visualizing and exploring intermolecular interactions in molecular crystals. *Acta Cryst. B.* **2004**, *60*, 627-668.

[21] Turner, M. J.; McKinnon, J. J.; Wolff, S. K.; Grimwood, D. J.; Spackman, P. R.; Jayatilaka, D; Spackman, M. A. CrystalExplorer17 (**2017**). University of Western Australia. https://hirshfeldsurface.net.

[22] Spackman, M. A.; McKinnon, J. J. Fingerprinting intermolecular interactions in molecular crystals. CrystEngComm **2002,** *4*, 378-392.

[23] Keicher, T.; Löbbecke S. Lab-scale Synthesis of Azido Compounds: Safety Measures and Analysis. In *Organic Azides: Syntheses and Applications*; Bräse, S., Banert, K., Eds.; John Wiley & Sons Ltd: Chichester (UK), **2010**. DOI 10.1002/9780470682517

[24] Schmidt, R. D.; Lee, G. S.; Pagoria, P. F.; Mitchell, A. R.; Gilardi, R. Synthesis of 4-amino-3,5-dinitro-1H-pyrazole using vicarious nucleophilic substitution of hydrogen. J. Heterocycl. Chem. **2001**, *38*, 1227-1230.

[25] Felts, J. E.; Sandusky, H. W.; Granholm, R.H. Development of the small-scale shock sensitivity test. In: *AIP Conference Proceedings*, American Institute of Physics, College Park, MD, **2009**, *1195*, 233-236.

[26] Köhler, J.; Meyer, R.; Homburg, A. *Explosives*; 6th ed.; Wiley-VCH: Weinheim, **2007**.

[27] Frisch, M. J.; Trucks, G. W.; Schlegel, H. B.; Scuseria, G. E.; Robb, M. A.; Cheeseman, J. R.; Scalmani, G.; Barone, V.; Petersson, G. A.; Nakatsuji, H.; Li, X.; Caricato, M.; Marenich, A. V.; Bloino, J.; Janesko, B. G.; Gomperts, R.; Mennucci, B.; Hratchian, H. P.; Ortiz, J. V.; Izmaylov, A. F.; Sonnenberg, J. L.; Williams; Ding, F.; Lipparini, F.; Egidi, F.; Goings, J.; Peng, B.; Petrone, A.; Henderson, T.; Ranasinghe, D.; Zakrzewski, V. G.; Gao, J.; Rega, N.; Zheng, G.; Liang, W.; Hada, M.; Ehara, M.; Toyota, K.; Fukuda, R.; Hasegawa, J.; Ishida, M.; Nakajima, T.; Honda, Y.; Kitao, O.; Nakai, H.; Vreven, T.; Throssell, K.; Montgomery Jr., J. A.; Peralta, J. E.; Ogliaro, F.; Bearpark, M. J.; Heyd, J. J.; Brothers, E. N.; Kudin, K. N.; Staroverov, V. N.; Keith, T. A.; Kobayashi, R.; Normand, J.; Raghavachari, K.; Rendell, A. P.; Burant, J. C.; Iyengar, S. S.; Tomasi, J.; Cossi, M.; Millam, J. M.; Klene, M.; Adamo, C.; Cammi, R.; Ochterski, J. W.; Martin, R. L.; Morokuma, K.; Farkas, O.; Foresman, J. B.; Fox, D. J. Gaussian 16 Rev. C.01, Wallingford, CT, **2016**.

[28] Altenburg, T.; Klapötke, Thomas M.; Penger, A.; Stierstorfer, J. Two Outstanding Explosives Based on 1,2-Dinitroguanidine: Ammonium-dinitroguanidine and 1,7-Diamino-1,7-dinitrimino-2,4,6-trinitro-2,4,6-triazaheptane. *Z. Anorg. Allg. Chem.* **2010**, *636*, 463-471.

7.4 Supporting Information

7.4.1 Experimental Part

Caution! All disclosed compounds are powerful energetic materials with sensitivities toward stimuli like shock, friction, and electrostatic discharge. Therefore, proper security precautions (safety glasses, face shield, earthed equipment and shoes, Kevlar gloves and ear protection) have to be applied while preparing and handling the described compounds.

General information:
All reagents and solvents were used as received (Sigma-Aldrich, Acros Organics, ABCR, TCI). Potassium tetrazol-1-ide was used from a workgroup internal stockpile. FTIR spectra were recorded on a Perkin Elmer Spectrum One FT-IR instrument using neat compounds. Raman spectra were obtained on a Bruker MultiRam FT Raman spectrometer and a neodymium-doped yttrium aluminum garnet (Nd:YAG) laser (λ = 1064 nm, P = 1074 mW). ^{1}H, ^{13}C and ^{14}N spectra were recorded using a Bruker AV400 or JEOL ECX400 using TMS (^{1}H and ^{13}C) or nitromethane (^{14}N) as internal reference. Thermal characteristics were determined using an OZM 552-Ex Differential Thermal Analyzer with Meavy 2.1.2 software or a Mettler Toledo DSC822e and a heating rate of 5 °C min^{-1} and Mettler Toledo STAR^{e} Version 16.20 evaluation software. Mass spectra were obtained using a ThermoFinnigan MAT 90 or MAT 95. Elemental analyses were conducted on an Elementar Vario EL or Elementar Vario Micro using pyrolysis and subsequent gas analysis. Crystallographic measurements were performed on a Xcalibur Sapphire3. Helium pycnometry was performed using a Quantachrome Ultrapyc 1200e device. The sensitivity data were collected using a BAM (Bundesanstalt für Materialforschung) drop hammer according to STANAG 4489 modified instruction and a BAM friction tester according to STANAG 4487 modified instruction.[1,2] The classification of the tested compounds results from the 'UN Recommendations on the Transport of Dangerous Goods'.[3] The dents of the SSRT were measured using a Keyence VR 5100 3D profilometer.

3-Bromomethyl-3-hydroxymethyloxtane (BMHMO, 1)
2,2-bis(bromomethyl)propane-1,3-diol (20.0 g, 76.4 mmol) was dissolved in methanol (200 mL) and sodium hydroxide (3.67 g, 91.8 mmol, 1.2 eq.) was added under vigorous stirring. The solution was refluxed for 12 hours prior to rotary evaporation. Dichloromethane (300 mL) was added to the suspension and all inorganics were removed by filtering through Celite. The solvent was removed to give a yellowish oil, which was subject to vacuum distillation (10^{-3} mbar). By-products (e.g., spiro-compound) distilled over at 100 °C, followed by the target compound which distilled over at 120–130 °C to give 11.9 g (86%) of BMHMO (**1**) as colorless oil.

^{1}H NMR (400 MHz, $CDCl_3$): δ = 4.44 (m, 4H, CH_2, ring), 3.90 (d, 2H, *J* = 5.1 Hz, CH_2), 3.74 (s, 2H, CH_2), 2.86 ppm (t, 1H, *J* = 5.1 Hz, OH); **IR** (ATR, cm^{-1}): $\tilde{\nu}$ = 3376 (m), 2952 (m), 2877 (m), 1434 (m), 1269 (m), 1228 (m), 1108 (m), 1036 (vs), 968 (vs), 913 (s), 851 (m), 832 (s), 700 (s), 642 (s), 502 (s), 459 (s), 430 (s), 405 (s); **Raman** (1075 nm, 1000 mW, 25 °C, cm^{-1}): $\tilde{\nu}$ = 3015 (14), 2963 (58), 2884 (68), 1490 (38), 1347 (12), 1272 (24), 1229 (14), 1143 (18), 1112 (18), 1069 (14), 971 (34), 923 (16), 832 (20), 703 (14), 647 (100), 504 (14). **HRMS (EI)** m/z: $[M]^+$ Calcd for $C_5H_9BrO_2$ 179.9786; Found 180.9856 $[C_5H_{10}O_2Br]^+$, 162.9750 $[C_5H_8OBr]^+$, 148.9594 $[C_4H_6OBr]^+$, 132.9646 $[C_4H_6Br]^+$, 92.9334 $[CH_2Br]^+$, 71.0491 $[C_4H_7O]^+$. **Anal. Calcd** for $C_5H_9BrO_2$: H, 5.01; C, 33.17. Found: H, 5.56; C, 33.98%.

Potassium 4-amino-3,5-dinitropyrazol-1-ide (2)

4-Amino-3,5-dinitro-1*H*-pyrazole (5.00 g, 28.9 mmol) was dissolved in boiling water (100 mL) and the pH-value was set to 9 by the dropwise addition of a saturated aqueous potassium hydroxide solution. The solution was then cooled to 5 °C my means of an ice bath and ethanol (200 mL) was added. The precipitated yellow solid was collected by suction filtration and washed with ethanol (50 mL) and diethyl ether (50 mL) to give 5.77 g (27.3 mmol, 94%) of potassium 4-amino-3,5-dinitropyrazol-1-ide (**2**) as yellow solid.

IR (ATR, cm^{-1}): $\tilde{\nu}$ 3507 (w), 3391 (m), 3272 (w), 3226 (w), 3167 (w), 1628 (s), 1455 (s), 1425 (s), 1393 (s), 1288 (vs), 1201 (s), 1133 (s), 914 (s), 835 (s), 758 (s), 671 (m), 503 (s), 430 (s). **Raman** (1075 nm, 1000 mW, 25 °C, cm^{-1}): $\tilde{\nu}$ 1627 (14), 1569 (8), 1443 (24), 1422 (24), 1389 (70), 1308 (17), 1303 (17), 1272 (30), 1251 (51), 830 (100), 722 (49), 647 (9). **Anal. Calcd** for $C_3H_2KN_5O_4$: N, 33.16; H, 0.95; C, 17.06. Found: N, 33.33; H, 0.96; C, 17.01 %. **DSC** (5 °C min^{-1}): 74.8 °C (m.p.), 312.3 °C (dec.). **IS**: > 40 J. **FS** > 360 N.

(3-((4-Amino-3,5-dinitro-1*H*-pyrazol-1-yl)methyl)oxetan-3-yl)methanol (3)

Compound **2** (2.00 g, 9.47 mmol) and BMHMO (2.23 g, 12.3 mmol, 1.3 eq.) were added to a mixture of MeCN (20 mL) and DMF (8 mL). The suspension was heated to 100 °C resulting in a solution. The temperature was maintained for 24 h, and the reaction mixture was subsequently allowed to cool to ambient temperature and poured into ethyl acetate (250 mL). The suspension was filtered through Celite and the solvents removed using a rotary evaporator (100 °C, 20 mbar) to give a yellow, oily residue. Cold diethyl ether (30 mL) was added two times and evaporated to remove any traces of DMF and 2.59 g (9.49 mmol, 100 %) of compound **3** were obtained as yellow solid.

^{1}H NMR (400 MHz, DMSO-d_6): δ = 7.28 (s, 2H, NH_2), 5.04 (bs, 1H, *J* = 5.3 Hz, OH), 4.90 (s, 2H, CH_2), 4.46 (d, 2H, *J* = 6.5 Hz, CH_2 (Ox.)), 4.30 (d, 2H, J = 6.4 Hz, CH_2 (Ox.)), 3.65 (d, 2H, *J* = 5.2 Hz, CH_2). **^{13}C{^{1}H} NMR** (101 MHz, DMSO-d_6): δ = 140.3, 132.5, 130.5, 75.0, 63.5, 55.0, 44.8. **^{14}N NMR** (29 MHz, DMSO-d_6) δ = −26.7. **IR** (ATR, cm^{-1}): $\tilde{\nu}$ 3448 (m), 3317 (m), 1633 (s), 1516 (m), 1471 (vs), 1443 (s), 1372 (m), 1349 (m), 1302 (vs), 1259 (s), 1225 (m), 1207 (m), 1055 (s), 988 (m), 948 (s), 910 (s), 891 (m), 827 (s), 788 (s), 761 (m), 747 (m), 736 (m), 661 (m), 487 (s), 467 (s). **Raman** (1075 nm, 1000 mW, 25 °C, cm^{-1}): $\tilde{\nu}$ 2980 (4), 1632 (15), 1584 (7), 1470 (8), 1401 (21), 1372 (100), 1353 (17), 1310 (20), 1229 (4), 990 (4), 913 (3), 832 (20), 792 (11), 664 (4). **Anal. Calcd** for $C_8H_{10}N_8O_5$: C, 35.17; H, 4.06; N, 25.63 %. Found: C, 34.81; H, 4.02; N, 25.67%. **HRMS (EI)** m/z: $[M]^+$ Calcd for $C_8H_{10}N_8O_5$ 273.0709; Found 273.0705 $[C_8H_{11}N_5O_6]^+$, 179.0548 $[C_6H_{11}O_6]^+$, 112.0132 $[C_3H_2O_2N_3]^+$. **DSC** (5 °C min^{-1}): 180.2 °C (m.p.), 210.5 °C (dec.). **IS**: > 40 J. **FS** > 360 N. **R$_f$**: 0.65 (SiO_2, EtOAc).

(3-((4-Diazo-3-nitro-5-oxo-4,5-dihydro-1*H*-pyrazol-1-yl)methyl)oxetan-3-yl)methyl nitrate (4)

Compound **3** (1.50 g, 5.49 mmol) was added to a solution dinitrogen pentoxide (2.36 g, 12.9 mmol, 2.36 eq.) in acetonitrile (20 mL) at 0 °C using an ice bath. The yellow solution was stirred for two hours at the initial temperature and was then poured into ice water (200 mL). The aqueous phase was extracted with ethyl acetate (3 × 30 mL) and the organic phase was washed with water (2 × 50 mL) and saturated sodium bicarbonate solution (2 × 30 mL). The organic phase was dried over sodium sulfate and the solvent removed by rotary evaporation to give a yellow semi-solid. The crude material was purified by column chromatography (SiO_2, EtOAc) to give 0.87 g (2.90 mmol, 53%) of compound **4** as a bright yellow solid.

^{1}H NMR (400 MHz, DMSO-d$_6$): δ = 4.76 (s, 2H, CH_2), 4.53 (d, 2H, *J* = 6.5 Hz, CH_2 (Ox.)), 4.45 (d, 2H, *J* = 6.6 Hz, CH_2 (Ox.)), 4.26 (s, 2H, CH_2). **^{13}C{^{1}H} NMR** (101 MHz, DMSO-d$_6$): δ = 162.0, 143.7, 74.5, 73.3, 46.8, 42.3. **^{14}N NMR** (29 MHz, DMSO-d$_6$): δ = −28.8, −41.9, −141.3. **IR** (ATR, cm^{-1}): $\tilde{\nu}$ 2984 (w), 2896 (w), 2164 (s), 1700 (s), 1643 (m), 1622 (s), 1559 (m), 1521 (s), 1512 (s), 1487 (m), 1457 (s), 1437 (m), 1369 (s), 1338 (m), 1318 (m), 1281 (s), 1246 (m), 1213 (m), 1154 (m), 1141 (w), 1084 (m), 1072 (m), 1013 (m), 975 (s), 946 (m), 907 (m), 876 (s), 834 (s), 797 (s), 753 (s), 717 (m), 704 (s), 601 (m), 574 (m), 507 (w). **Anal. Calcd** for $C_8H_8N_6O_7$: N, 27.90; H, 3.01; C, 31.90. Found: N, 27.86; H, 2.93; C, 31.99 %. **HRMS (ESI)** m/z: $[M]^+$ Calcd for $C_8H_8N_6O_7$ 300.0454; Found 300.0460 $[C_8H_8N_6O_7]^+$, 254.0555 $[C_8H_8N_5O_5]^+$, 156.0004 $[C_1H_4O_7N_2]^+$. **DSC** (5 °C min^{-1}): 95.3 °C (m.p.), 184.0 °C (dec.). **R$_f$**: 0.65 (SiO_2, EtOAc).

(3-((4-Amino-3,5-dinitro-1*H*-pyrazol-1-yl)methyl)oxetan-3-yl)methyl methanesulfonate (5)

Compound **3** (0.50 g, 1.83 mmol) was dissolved in a mixture of acetonitrile (20 mL) and DMF (2 mL) and triethylamine (370 mg, 3.66 mmol, 2 eq.) was added. The orange solution was cooled to 0 °C using an ice bath and a solution of methane sulfonyl chloride (252 mg, 2.19 mmol, 1.2 eq.) in acetonitrile (2 mL) was added dropwise. The instantaneous precipitation of a bright yellow solid was observed, and the reaction mixture was stirred for 5 hours at the initial temperature and subsequently poured onto ice (50 g). The ice was allowed to melt and the solid was collected by suction filtration and washed with cold ethanol (20 mL) and diethyl ether (20 mL) to give 575 mg (89%) of compound **5** as yellow powder.

^{1}H NMR (400 MHz, DMSO-d$_6$): δ = 7.34 (s, 2H, NH$_2$), 5.02 (s, 2H, CH$_2$), 4.57 (d, 2H, *J* = 6.8 Hz, CH$_2$ (Ox.)), 4.40 (d, 2H, *J* = 6.8 Hz, CH$_2$), 3.21 (s, 3H, CH$_3$). **^{13}C{^{1}H} NMR** (101 MHz, DMSO-d$_6$): δ = 140.5, 132.4, 130.6, 74.3, 70.7, 54.4, 42.9, 36.5. **^{14}N NMR** (29 MHz, DMSO-d$_6$): δ = −27.1. **IR** (ATR, cm^{-1}): ṽ 3460 (m), 3307 (w), 1633 (s), 1519 (m), 1473 (s), 1456 (m), 1448 (m), 1344 (s), 1307 (vs), 1291 (s), 1178 (s), 1142 (w), 1058 (m), 1007 (m), 989 (s), 973 (s), 955 (m), 929 (m), 884 (w), 859 (s), 840 (s), 830 (s), 788 (s), 760 (m), 746 (w), 718 (w), 666 (m), 535 (s), 503 (s), 488 (s), 461 (s). **Raman** (1075 nm, 1000 mW, 25 °C, cm^{-1}): ṽ 2977 (6), 2946 (6), 1636 (19), 1586 (9), 1470 (11), 1403 (24), 1376 (100), 1351 (19), 1326 (30), 1310 (24), 1293 (9), 1279 (6), 1170 (7), 954 (6), 832 (22), 790 (13), 763 (6), 535 (6). **Anal. Calcd** for $C_9H_{13}N_5O_8S$: N, 19.94; H, 3.73; C, 30.77. Found: N, 19.92; H, 3.69; C, 30.85%. **HRMS (EI)** m/z: [M]$^+$ Calcd for $C_9H_{13}N_5O_8S$ 351.0485; Found 351.0473 $[C_9H_{13}N_5O_8{}^{32}S_1]^+$, 334.0433 $[C_9H_{12}N_5O_7{}^{32}S_1]^+$, 179.0549 $[C_6H_{11}O_6]^+$. **DSC** (5 °C min^{-1}): 188.4 °C (dec.). **R$_f$**: 0.59 (SiO$_2$, EtOAc/petrol ether/toluene 3:1:1).

1-((3-(Bromomethyl)oxetan-3-yl)methyl)-3,5-dinitro-1*H*-pyrazol-4-amine (6)

Compound **5** (0.50 g, 1.42 mmol) was suspended in acetone (10 mL) and lithium bromide (247 mg, 2.85 mmol, 2 eq.) was added. The reaction mixture was set to reflux for 24 h, and the solvent was removed by rotary evaporation. Ethyl acetate was added to dissolve the crude compound and all inorganics were removed by filtration through a silica-plug, which was thoroughly rinsed with ethyl acetate. The solvent was again removed by rotary evaporation to give 476 mg (99 %, 1.42 mmol) of compound **6** as an intense yellow solid.

^{1}H NMR (400 MHz, Acetone-d$_6$): δ = 7.01 (s, 2H, NH$_2$), 5.19 (s, 2H, CH$_2$), 4.65 (d, 2H, *J* = 6.8 Hz, CH$_2$ (Ox.)), 4.46 (d, 2H, *J* = 6.8 Hz, CH$_2$), 4.01 (s, 2H, CH$_2$). **^{13}C{^{1}H} NMR** (101 MHz, Acetone-d$_6$): δ = 131.4, 77.2, 56.3, 45.6, 38.1. **^{14}N NMR** (29 MHz, Acetone-d$_6$): δ = −23.6, −28.4. **IR** (ATR, cm^{-1}): ṽ 3443 (w), 3315 (w), 1644 (s), 1515 (m), 1473 (s), 1431 (s), 1409 (m), 1377 (w), 1309 (vs), 1269 (s), 1256 (m), 1244 (s), 1197 (m), 1155 (m), 1084 (m), 1044 (m), 954 (s), 906 (s), 864 (m), 850 (m), 825 (s), 788 (s), 760 (m), 747 (m), 663 (m), 642 (s), 611 (m), 521 (vs), 449 (s). **Raman** (1075 nm, 1000 mW, 25 °C, cm^{-1}): ṽ 2965 (6), 1636 (19), 1575 (7), 1472 (13), 1436 (11), 1411 (13), 1386 (45), 1372 (100), 1339 (25), 1326 (22), 1310 (18), 1258 (13), 1227 (10), 830 (23), 792 (10), 699 (6), 670 (7), 643 (7). **Anal. Calcd** for $C_9H_{13}N_5O_8S$: N, 20.84; H, 3.00; C, 28.59. Found: N, 21.02; H, 3.00; C, 28.79%. **HRMS (EI)** m/z: [M]$^+$ Calcd for $C_9H_{13}N_5O_8S$ 334.9865; Found 335.9924 $[C_8H_{11}N_5O_5{}^{79}Br]^+$, 334.9863 $[C_8H_{10}N_5O_5{}^{79}Br]^+$, 226.0706 $[C_8H_{10}O_4N_4]^+$, 179.0570 $[C_7H_7O_2N_4]^+$. **DSC** (5 °C min^{-1}): 157.3 °C (m.p.), 197.5 °C (dec.). **R$_f$**: 0.83 (SiO$_2$, EtOAc/petrol ether/toluene 3:1:1).

1,1'-(Oxetane-3,3-diylbis(methylene))bis(3,5-dinitro-1*H*-pyrazol-4-amine) (7)

Compound **5** (500 mg, 1.42 mmol) and potassium 4-amino-3,5-dinitropyrazol-1-ide (300 mg, 1.42 mmol) were dissolved in DMF (10.0 mL) and the reaction mixture heated to 100 °C for 48 h, which was accompanied by the formation of a colorless precipitate. The mixture was then poured into ethyl acetate (100 mL) to precipitate all inorganics and filtered through Celite to give a bright yellow solution. The solvent was evaporated and the obtained solid recrystallized from ethyl acetate to give 541 mg (89%) of compound **7** as a yellow solid.

^{1}H NMR (400 MHz, DMSO-d$_6$): δ = 7.31 (s, 4H, NH$_2$), 5.09 (s, 4H, CH$_2$), 4.57 (s, 4H, CH$_2$). **^{13}C{^{1}H} NMR** (101 MHz, DMSO-d$_6$): δ = 140.1, 132.2, 130.5, 75.7, 55.4, 43.6. **^{14}N NMR** (29 MHz, DMSO-d$_6$) δ = −19.8. **IR** (ATR, cm^{-1}): ṽ 3487 (w), 3422 (w), 3370 (m), 3282 (w), 3199 (w), 1634 (s), 1523 (m), 1505 (m), 1490 (m), 1466 (s), 1452 (s), 1430 (s), 1396 (m), 1371 (m), 1353 (m), 1297 (vs), 1276 (vs), 1217 (m), 1142 (m), 1050 (m), 978 (m), 964 (s), 946 (s), 889 (m), 829 (s), 796 (s), 787 (s), 758 (m), 747 (m), 667 (s), 643 (m), 482 (vs), 457 (s). **Raman** (1075 nm, 1000 mW, 25 °C, cm^{-1}): ṽ 2969 (4), 1640 (15), 1584 (8), 1565 (8), 1528 (5), 1474 (14), 1432 (10), 1372 (100), 1355 (66), 1320 (32), 1301 (22), 1241 (11), 1187 (5), 979 (5), 946 (5), 832 (29), 797 (13), 792 (14), 739 (6), 670 (5), 645 (4), 622 (6), 518 (5). **Anal. Calcd** for $C_{11}H_{12}N_{10}O_9$: N, 32.71; H, 2.28; C, 30.85. Found: N, 32.00; H, 2.88; C, 30.84%. **HRMS (EI)** m/z: [M]$^+$ Calcd for $C_{11}H_{12}N_{10}O_9$ 428.0789; Found 428.0800 $[C_{11}H_{12}N_{10}O_9]^+$, 411.0831 $[C_{11}H_{11}N_{10}O_8]^+$, 179.0569 $[C_7H_7N_4O_2]^+$. **DSC** (5 °C min^{-1}): 246.0 °C (dec.). **R$_f$**: 0.25 (SiO$_2$, EtOAc).

1-((3-(Azidomethyl)oxetan-3-yl)methyl)-3,5-dinitro-1*H*-pyrazol-4-amine (8)

Compound **5** (500 mg, 1.42 mmol) was dissolved in dimethylformamide (20 mL) together with sodium azide (185 mg, 2.85 mmol, 2 eq.) and the reaction mixture was heated to 100 °C for 24 h to give a deep orange solution. The reaction mixture was poured into ethyl acetate (150 mL) and the resulting suspension was filtered through Celite to remove all salts. The solvent was removed by rotary evaporation (40 °C, 240 mbar; 100 °C, 20 mbar) to give a slightly orange solid. Residues of dimethylformamide were removed by co-evaporation with cold diethyl ether (20 mL) and cold ethyl acetate (20 mL) to give 421.3 mg (1.41 mmol, 99%) of compound **8** as a yellow to orange solid. If necessary, the compound can be dissolved in the minimum amount of acetone and precipitated with n-Hexane to give a bright yellow solid with no yield loss.

^{1}H NMR (400 MHz, Acetone-d$_6$): δ = 7.00 (bs, 2H, NH$_2$), 5.09 (s, 2H, CH$_2$), 4.63 (d, 2H, *J* = 6.8 Hz, CH$_2$ (Ox.)), 4.44 (d, 2H, *J* = 6.8 Hz, CH$_2$), 3.94 (s, 2H, CH$_2$). **^{13}C{^{1}H} NMR** (101 MHz, Acetone-d$_6$): δ = 141.7, 133.6, 131.4, 76.5, 56.2, 55.3, 44.9. **^{14}N NMR** (29 MHz, Acetone-d$_6$): δ = −23.0, −27.8, −133.8, −172.5. **IR** (ATR, cm^{-1}): ṽ 3447 (m), 3294 (m), 3207 (w), 2886 (w), 2096 (s), 1636 (s), 1582 (w), 1516 (m), 1470 (vs), 1442 (s), 1373 (m), 1302 (vs), 1274 (vs), 1240 (s), 1206 (s), 1141 (m), 1102 (m), 1052 (m), 979 (s), 958 (m), 915 (s), 889 (m), 865 (m), 828 (s), 789 (s), 761 (m). **Raman** (1075 nm, 1000 mW, 25 °C, cm^{-1}): ṽ 2977 (4), 2892 (2), 2105 (1), 1638 (13), 1590 (7), 1488 (2), 1470 (7), 1445

(3), 1403 (15), 1374 (100), 1353 (15), 1306 (19), 1245 (3), 1150 (2), 994 (3), 925 (2), 830 (24), 792 (11), 674 (3), 618 (2). **Anal. Calcd** for $C_8H_{10}N_8O_5$: N, 37.58; H, 3.38; C, 32.22. Found: N, 37.45; H, 3.32; C, 32.41%. **HRMS (EI)** m/z: $[M]^+$ Calcd for $C_8H_{10}N_8O_5$ 298.0774; Found 298.0769 $[C_8H_{10}N_8O_5]^+$, 194.0675 $[C_7H_8N_5O_2]^+$. **DSC** (5 °C min^{-1}): 101.0 °C (m.p.), 238.3 °C (dec.).

1-((3-((1*H*-tetrazol-1-yl)methyl)oxetan-3-yl)methyl)-3,5-dinitro-1*H*-pyrazol-4-amine (9A) and 1-((3-((2H-tetrazol-2-yl)methyl)oxetan-3-yl)methyl)-3,5-dinitro-1*H*-pyrazol-4-amine (9B)

Compound **5** (2.00 g, 5.69 mmol) and potassium tetrazol-1-ide (924 mg, 8.54 mmol, 1.5 eq.) were dissolved in DMF (50.0 mL) and the reaction mixture heated to 100 °C for 48 h, which was accompanied by the formation of a gelatinous precipitate. The mixture was then poured into ethyl acetate (200 mL) to precipitate all inorganics and filtered through Celite to give an orange solution. All volatiles were evaporated and a small quantity of acetone (10 mL) added to the obtained slurry. Diethyl ether was added (100 mL) to precipitate the target compound as a bright orange solid which was collected by suction filtration to give 1.81 g (98%) of the isomeric mixture (**9A**, **9B**), which was afterward refluxed in toluene. The suspension was filtered hot to give 1.07 g (89%) of compound **9A** as yellow solid. The filter residue was recrystallized from hot acetone to give 439 mg (72%) of compound **9B** as yellow solid, corresponding to an overall yield of 84%.

*Note: The respective yield stated for the N1-isomer **9A** (89%) and the N2-isomer **9B** (72%) refer to the calculated amount of these isomers in the crude mixture which comprises the monomers in a 2:1 ratio according to ^{1}H NMR spectroscopy.*

Compound 9A (*N*1):

^{1}H NMR (400 MHz, Acetone-d$_6$): δ = 9.26 (s, 1H, CH), 7.01 (s, 2H, NH$_2$), 5.12 (s, 2H, CH$_2$), 5.08 (s, 2H, CH$_2$), 4.73 (d, *J* = 7.2 Hz, 2H, CH$_2$), 4.69 (d, *J* = 7.1 Hz, 2H, CH$_2$). **^{13}C{^{1}H} NMR** (101 MHz, Acetone-d$_6$): δ = 145.4, 124.7, 77.6, 55.7, 51.3, 45.0. **^{14}N NMR** (29 MHz, DMSO-d$_6$): δ = −29.0. **IR** (ATR, cm^{-1}): ṽ 3484 (w), 3366 (m), 3130 (w), 3044 (w), 2963 (w), 2896 (w), 1634 (s), 1509 (m), 1487 (m), 1469 (vs), 1437 (m), 1389 (m), 1360 (m), 1344 (m), 1319 (vs), 1299 (vs), 1258 (m), 1245 (m), 1215 (m), 1162 (m), 1135 (m), 1107 (s), 1060 (m), 973 (s), 952 (s), 911 (s), 890 (m), 839 (m), 830 (s), 791 (s), 759 (m), 749 (m), 721 (m), 680 (m), 667 (m), 619 (w), 450 (s). **Raman** (1075 nm, 1000 mW, 25 °C, cm^{-1}): ṽ 2975 (14), 2897 (5), 1627 (22), 1563 (14), 1524 (5), 1478 (17), 1468 (18), 1440 (6), 1428 (5), 1399 (53), 1368 (100), 1357 (99), 1314 (19), 1297 (11), 1283 (12), 1249 (5), 1218 (6), 1033 (6), 988 (6), 832 (31), 792 (14), 736 (6). **Anal. Calcd** for $C_9H_{11}N_9O_5$: N, 38.76; H, 3.41; C, 33.24. Found: N, 37.76; H, 3.34; C, 32.97%. **HRMS (EI)** m/z: $[M]^+$ Calcd for $C_9H_{11}N_9O_5$ 325.0883; Found 325.0890 $[C_9H_{11}N_9O_5]^+$, 324.0812 $[C_9H_{10}N_9O_5]^+$, 295.0910 $[C_9H_{11}N_8O_4]^+$, 172.0111 $[C_3H_2N_5O_4]^+$. **DSC** (5 °C min^{-1}): 238.3 °C (dec.).

Compound 9B (*N*2):

^{1}H NMR (400 MHz, Acetone-d$_6$): δ = 8.75 (s, 1H, CH), 6.99 (s, 2H, NH$_2$), 5.29 (s, 2H, CH$_2$), 5.08 (s, 2H, CH$_2$), 4.75 (d, *J* = 7.1 Hz, 2H, CH$_2$), 4.71 (d, *J* = 7.1 Hz, 2H, CH$_2$). **^{13}C{^{1}H} NMR** (101 MHz, Acetone-d$_6$): δ = 154.0, 141.6, 131.3, 76.5, 56.1, 55.7, 44.9. **^{14}N NMR** (29 MHz, Acetone-d$_6$) δ = −23.6, −28.4, −101.8. **IR** (ATR, cm^{-1}): $\tilde{\nu}$ 3444 (w), 3322 (m), 3138 (w), 2966 (w), 2890 (w), 1635 (s), 1582 (w), 1515 (m), 1466 (s), 1434 (s), 1412 (m), 1393 (w), 1380 (w), 1370 (w), 1356 (m), 1306 (vs), 1278 (vs), 1246 (m), 1186 (m), 1148 (m), 1132 (m), 1066 (m), 1024 (s), 1006 (m), 985 (m), 970 (s), 925 (m), 906 (m), 827 (s), 798 (s), 763 (s), 749 (m), 709 (m), 689 (m), 671 (m), 663 (m), 615 (m), 526 (s), 470 (s). **Raman** (1075 nm, 1000 mW, 25 °C, cm^{-1}): $\tilde{\nu}$ 2969 (7), 2955 (6), 1640 (23), 1582 (9), 1567 (6), 1522 (6), 1476 (12), 1438 (16), 1413 (30), 1393 (69), 1380 (100), 1339 (66), 1279 (11), 1254 (19), 1247 (16), 1189 (6), 1025 (7), 1008 (5), 973 (6), 828 (36), 797 (13), 765 (7), 695 (9), 672 (9), 502 (5), 471 (5).**Anal. Calcd** for $C_9H_{11}N_9O_5$: N, 38.76; H, 3.41; C, 33.24. Found: N, 39.03; H, 3.50; C, 33.48%. **HRMS (EI)** m/z: [M]$^+$ Calcd for $C_9H_{11}N_9O_5$ 325.0883; Found 325.0889 [$C_9H_{11}N_9O_5$]$^+$, 324.0812 [$C_9H_{10}N_9O_5$]$^+$, 298.0895 [$C_9H_{12}N_7O_5$]$^+$, 172.0112 [$C_3H_2N_5O_4$]$^+$. **DSC** (5 °C min^{-1}): 161.0 °C (phase transition), 173.0 °C (m.p.), 241.1 °C (dec.).

7.4.2 NMR Spectra

3-Bromomethyl-3-hydroxymethyloxtane (1)

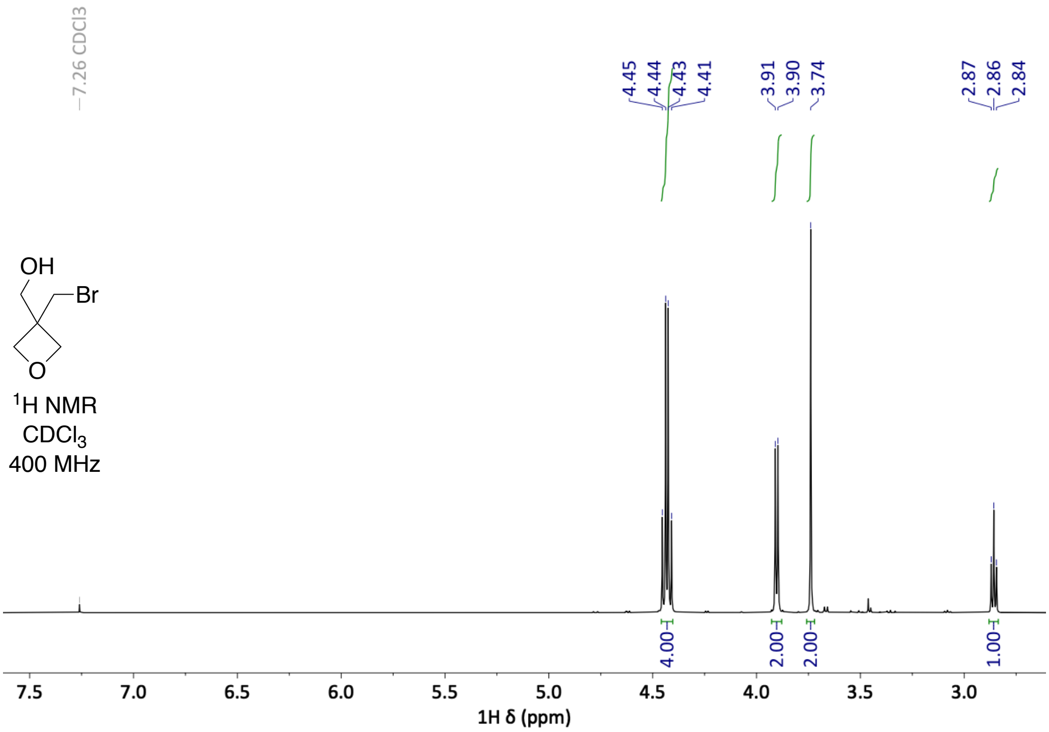

Figure S 7.1. Proton spectrum (^{1}H) of 3-bromomethyl-3-hydroxymethyloxetane (BMHMO, **1**).

(3-((4-Amino-3,5-dinitro-1*H*-pyrazol-1-yl)methyl)oxetan-3-yl)methanol (3)

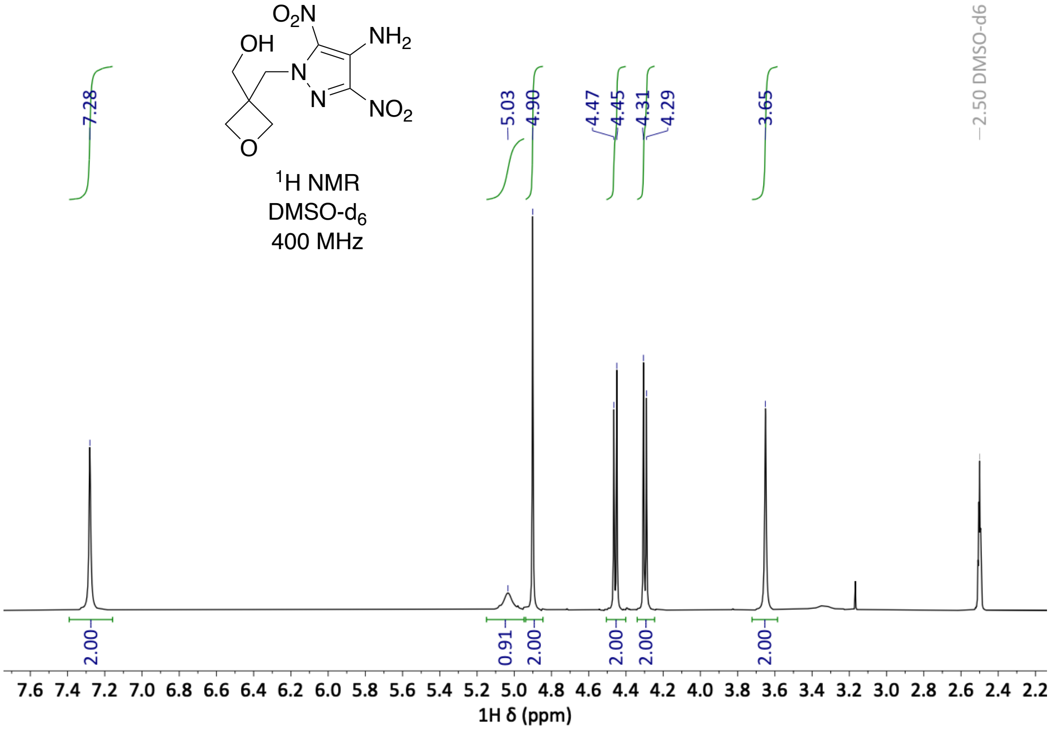

Figure S 7.2. Proton spectrum (^{1}H) of compound **3**.

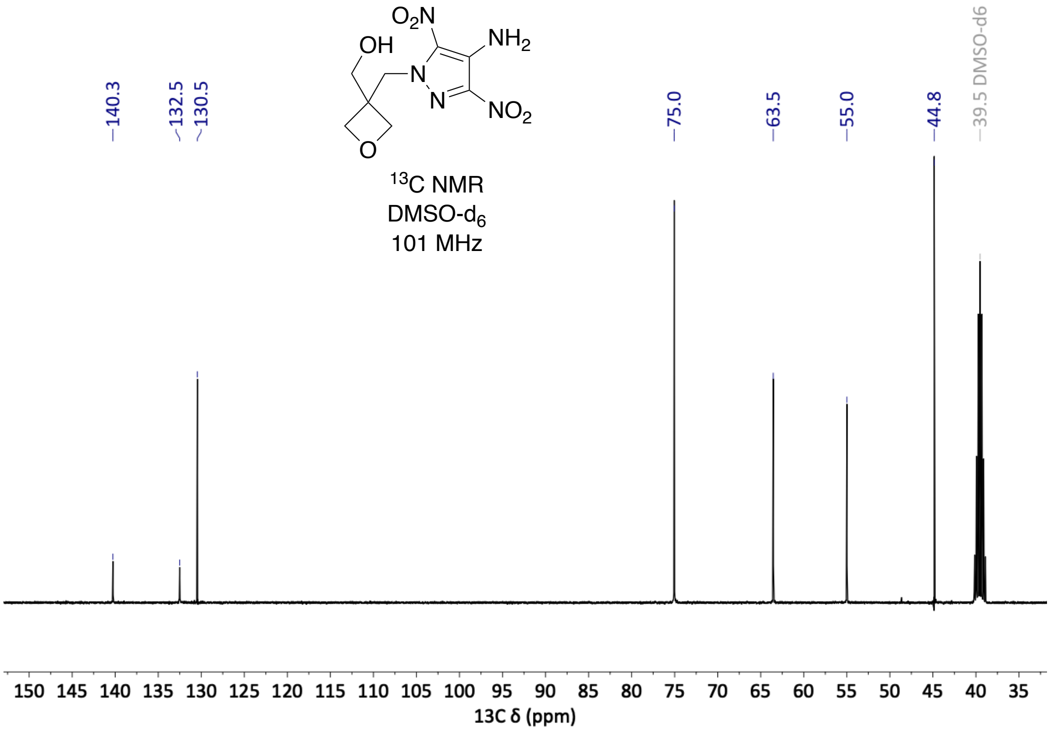

Figure S 7.3. Carbon spectrum (^{13}C) of compound **3**.

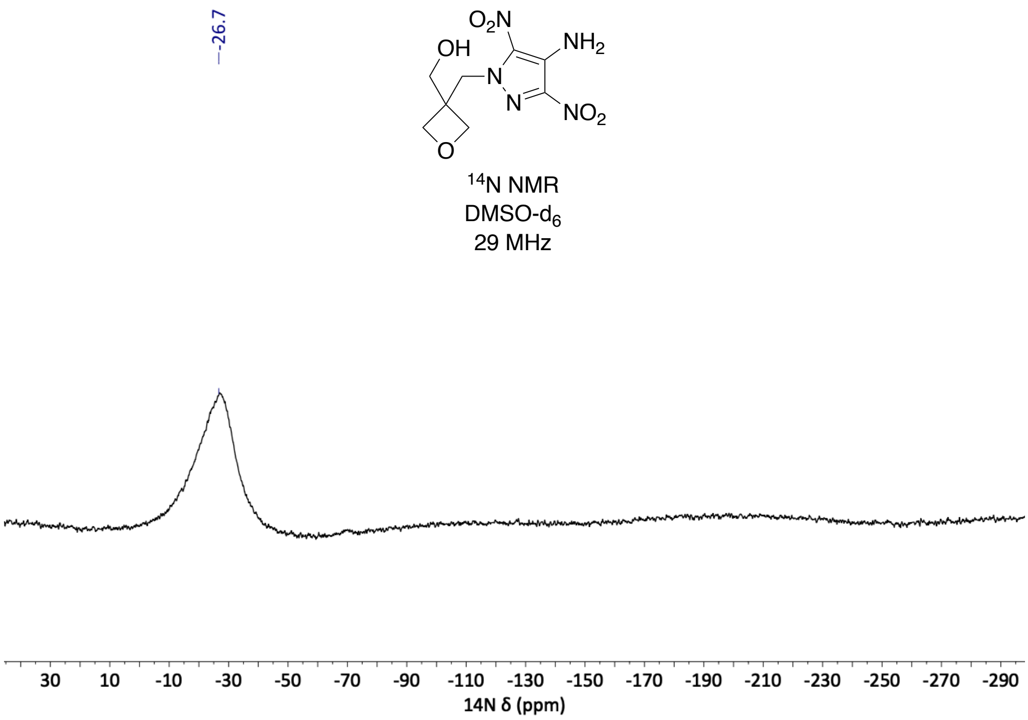

Figure S 7.4. Nitrogen spectrum (^{14}N) of compound **3**.

(3-((4-Diazo-3-nitro-5-oxo-4,5-dihydro-1*H*-pyrazol-1-yl)methyl)oxetan-3-yl)methyl nitrate (4)

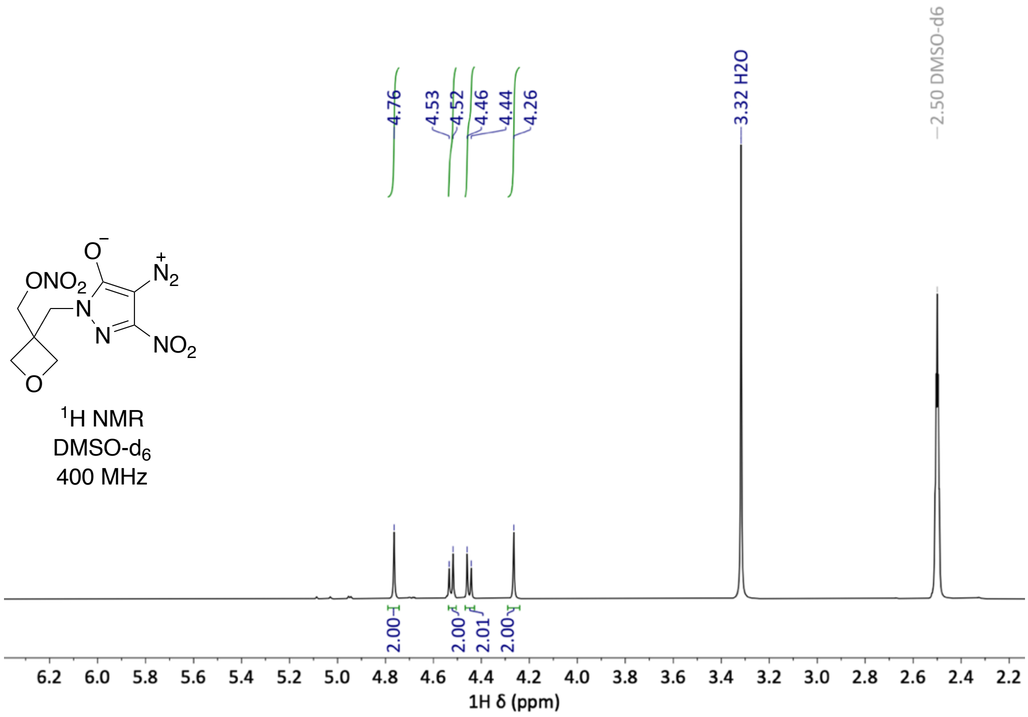

Figure S 7.5. Proton spectrum (^{1}H) of compound **4**.

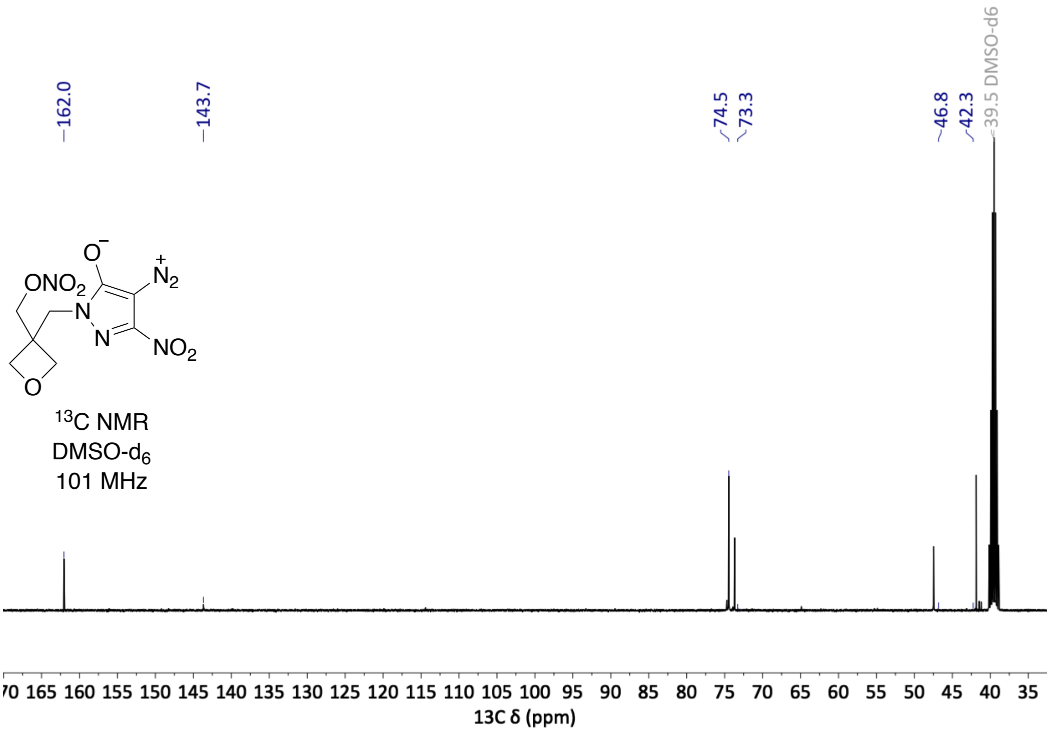

Figure S 7.6. Carbon spectrum (^{13}C) of compound **4**.

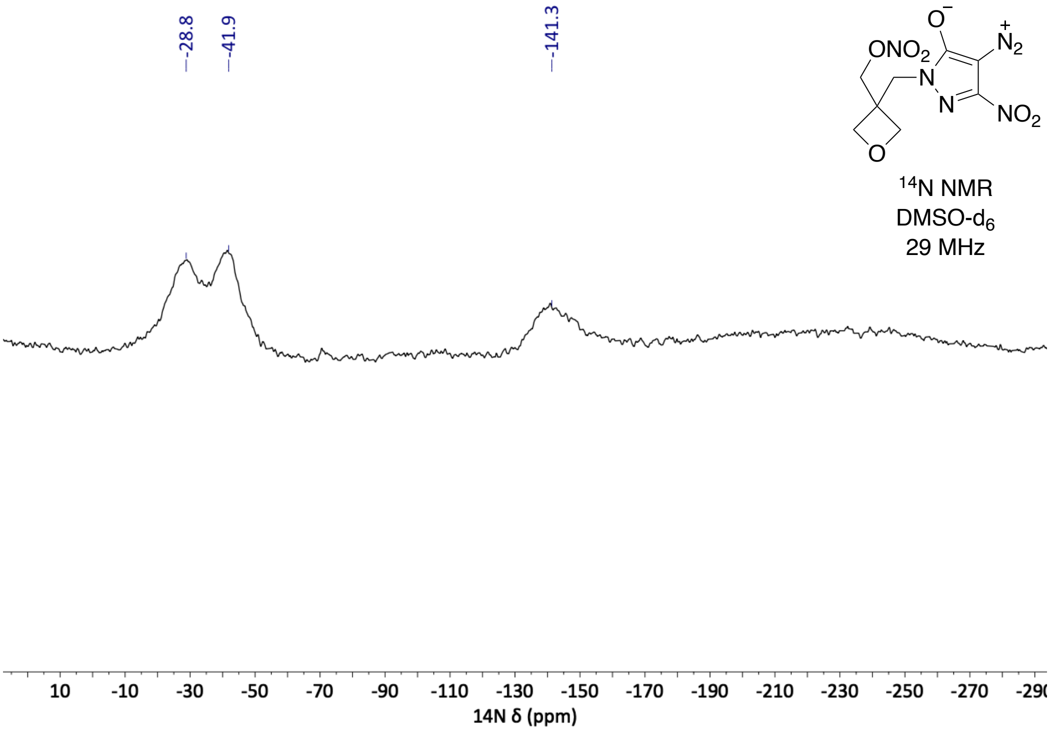

Figure S 7.7. Nitrogen spectrum (^{14}N) of compound **4**.

(3-((4-Amino-3,5-dinitro-1*H*-pyrazol-1-yl)methyl)oxetan-3-yl)methylmethanesulfonate (5)

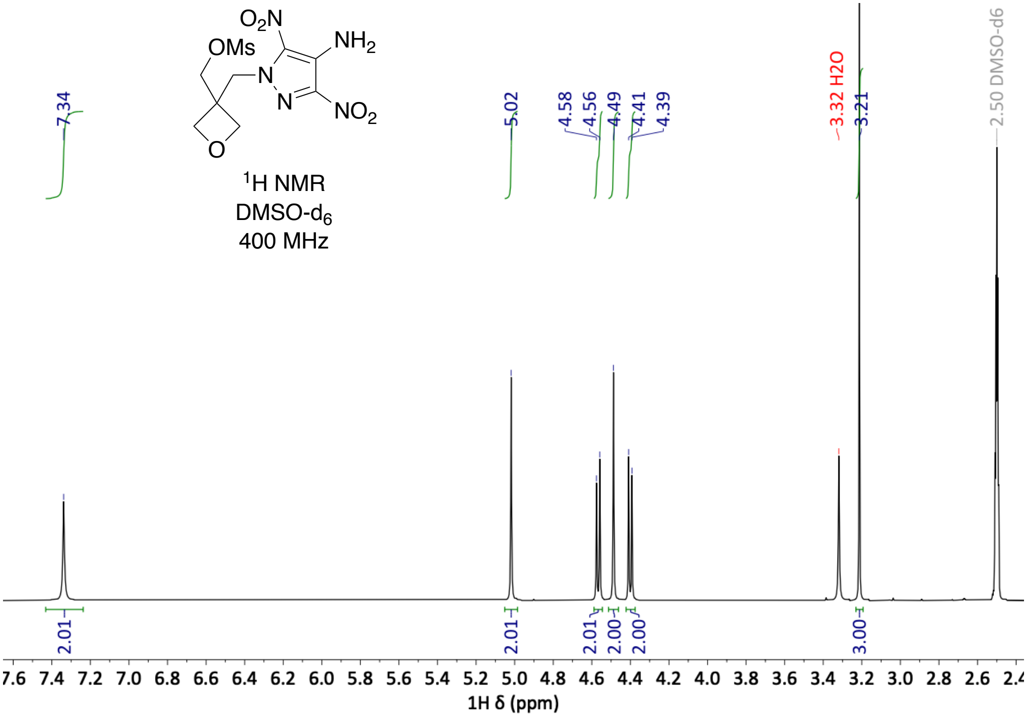

Figure S 7.8. Proton spectrum (^{1}H) of compound **5**.

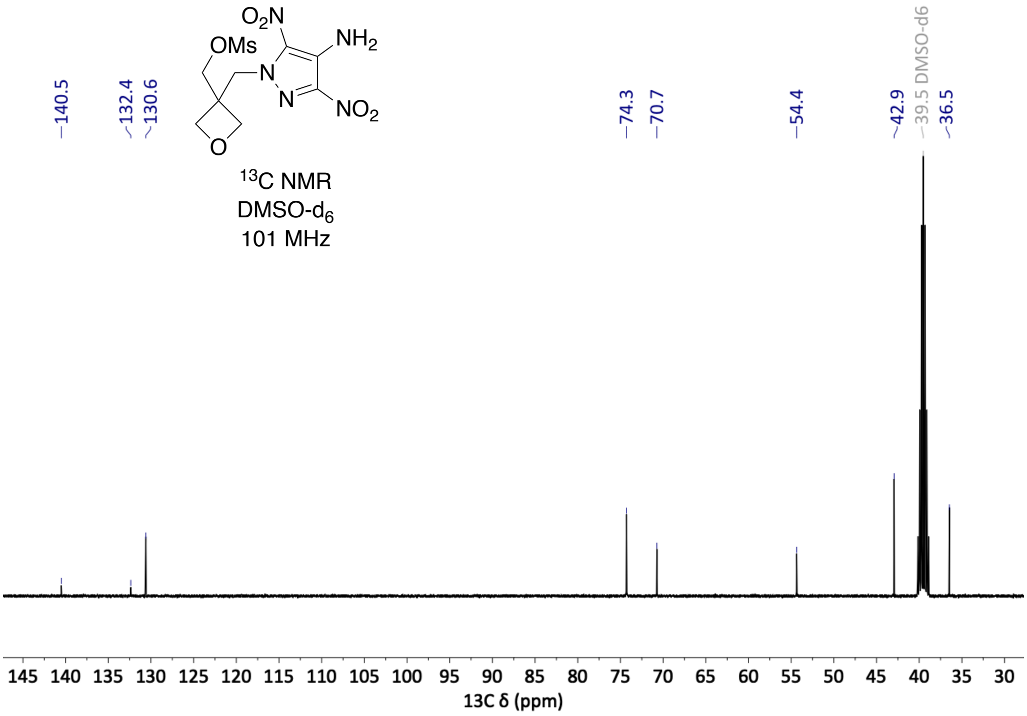

Figure S 7.9. Carbon spectrum (^{13}C) of compound **5**.

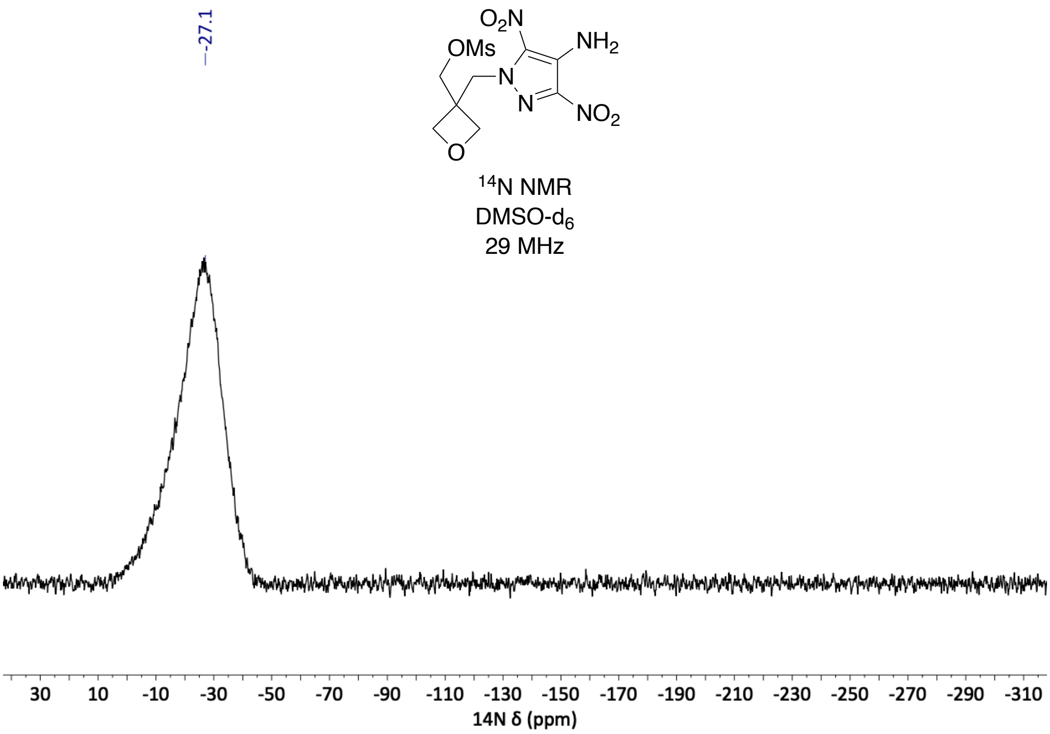

Figure S 7.10. Nitrogen spectrum (^{14}N) of compound **5**.

1-((3-(Bromomethyl)oxetan-3-yl)methyl)-3,5-dinitro-1*H*-pyrazol-4-amine (6)

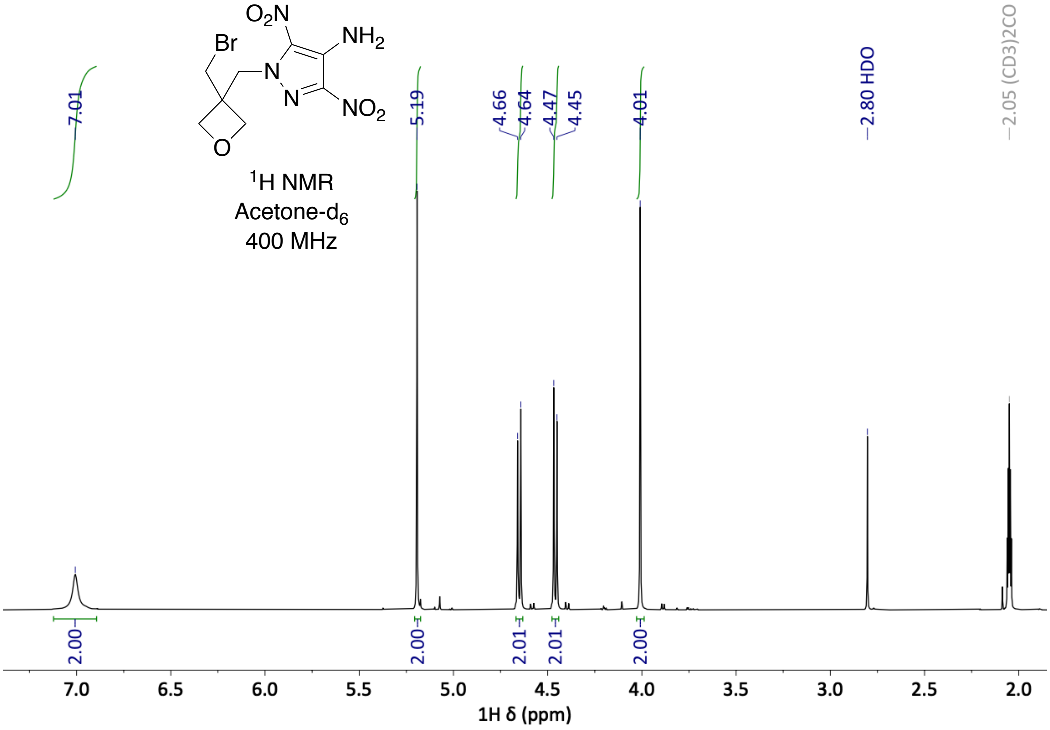

Figure S 7.11. Proton spectrum (^{1}H) of compound **6**.

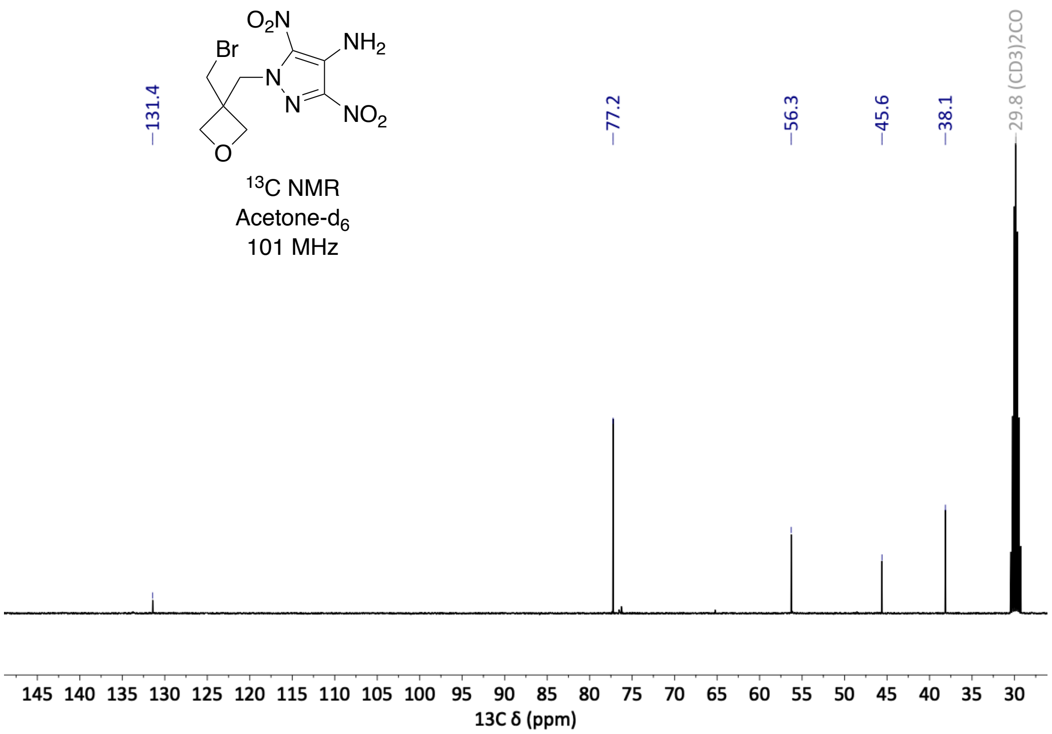

Figure S 7.12. Carbon spectrum (^{13}C) of compound **6**.

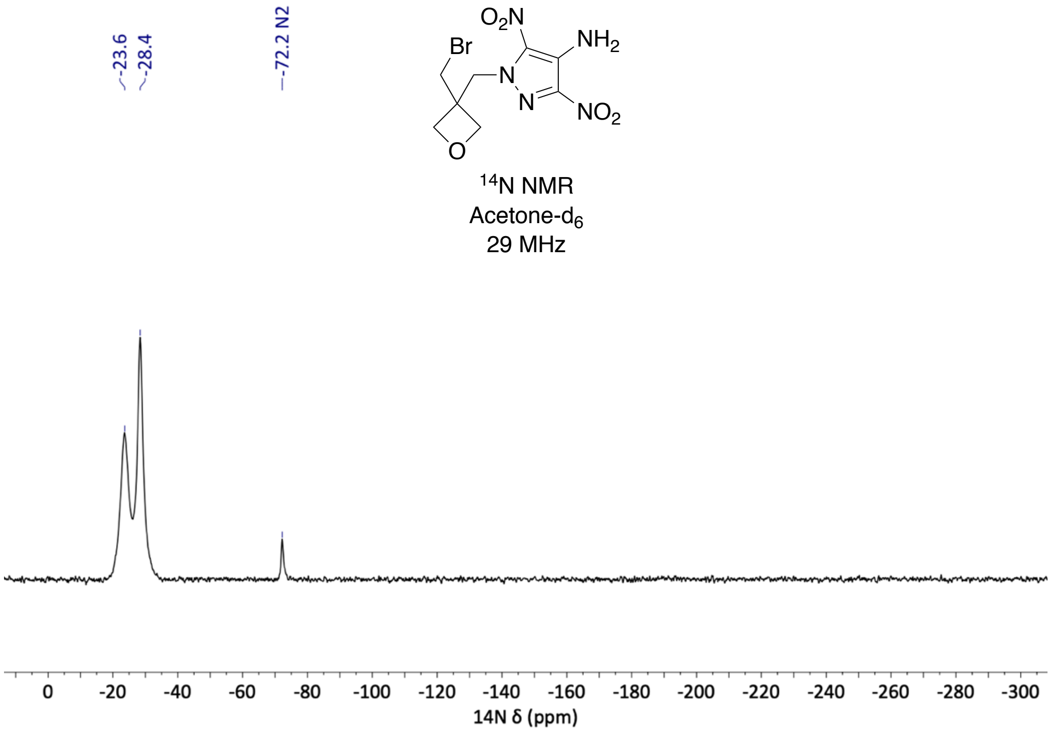

Figure S 7.13. Nitrogen spectrum (^{14}N) of compound **6**.

1,1'-(Oxetane-3,3-diylbis(methylene))bis(3,5-dinitro-1*H*-pyrazol-4-amine) (7)

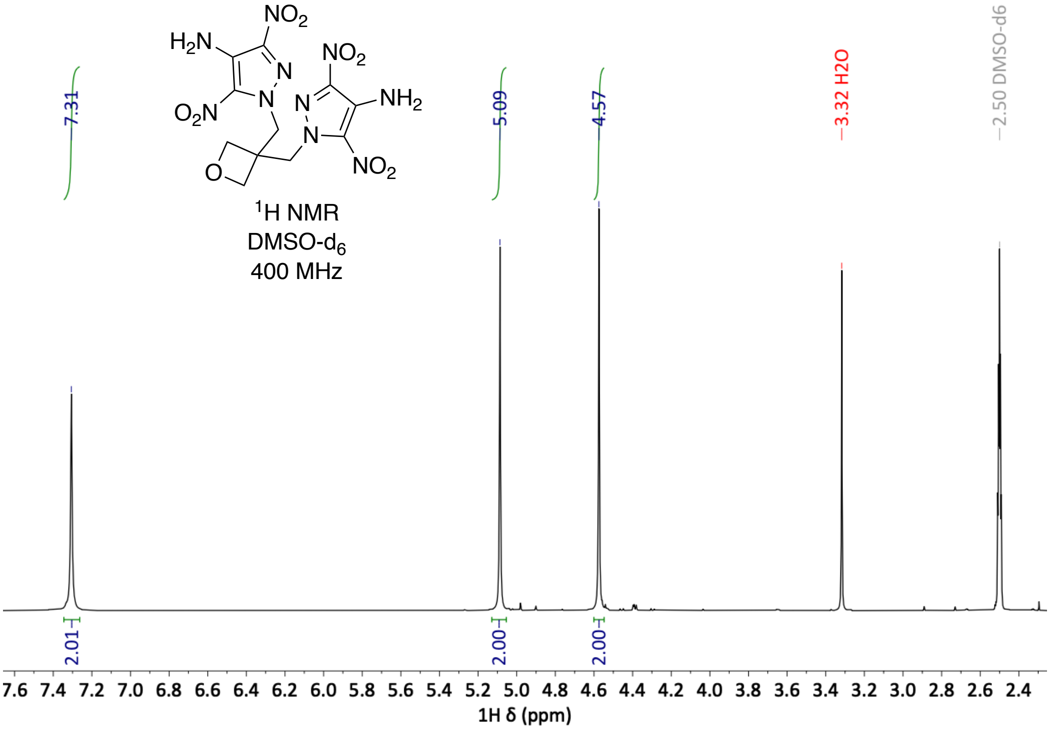

Figure S 7.14. Proton spectrum (^{1}H) of compound **7**.

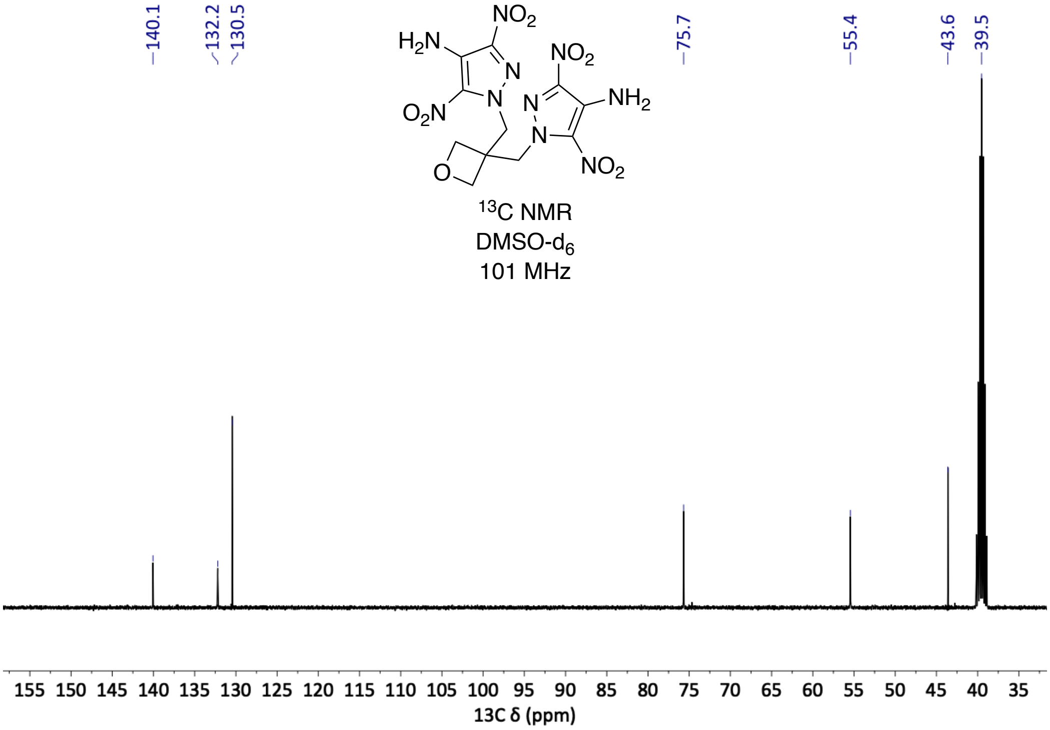

Figure S 7.15. Carbon spectrum (^{13}C) of compound **7**.

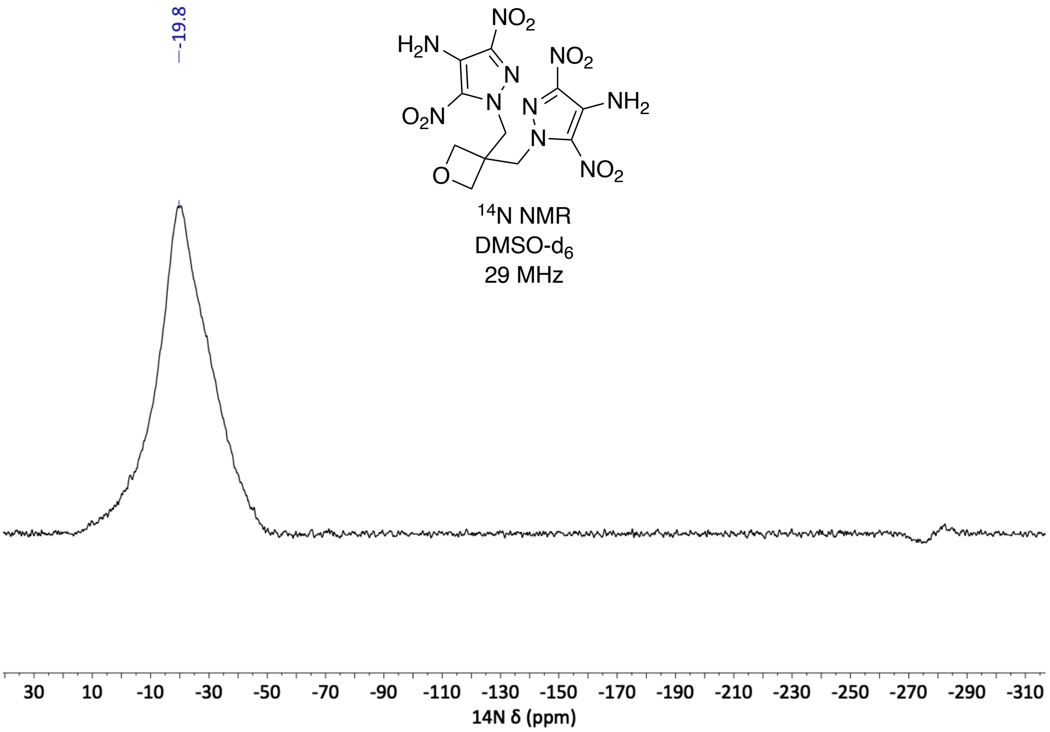

Figure S 7.16. Nitrogen spectrum (^{14}N) of compound **7**.

1-((3-(Azidomethyl)oxetan-3-yl)methyl)-3,5-dinitro-1*H*-pyrazol-4-amine (8)

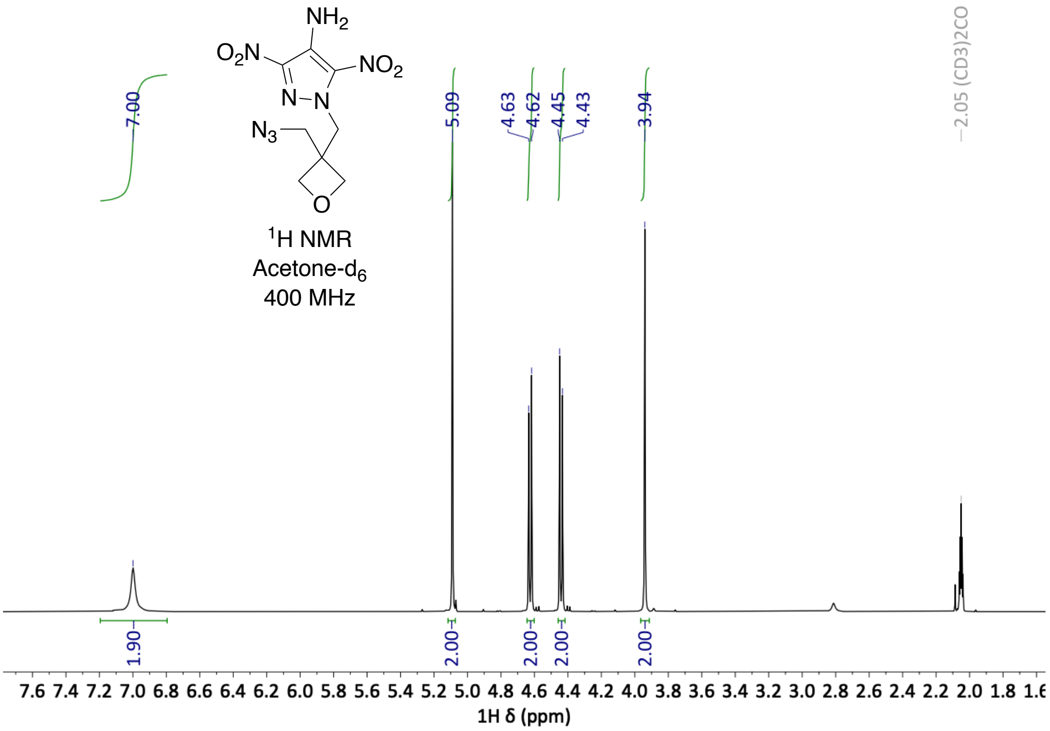

Figure S 7.17. Proton spectrum (^{1}H) of compound **8**.

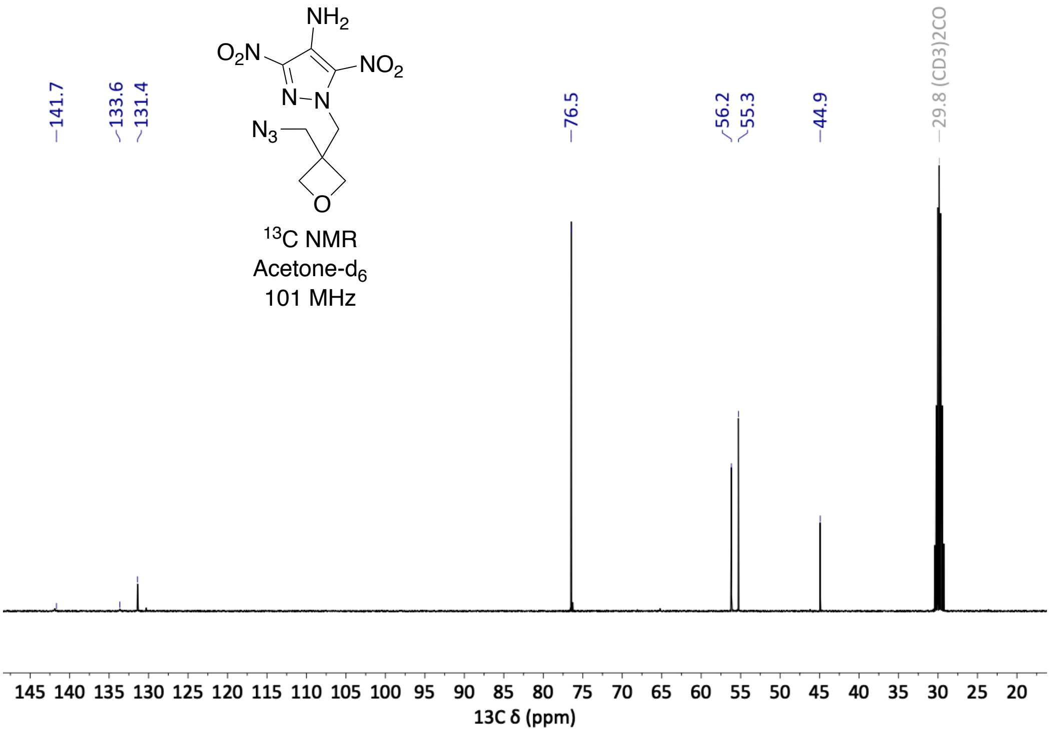

Figure S 7.18. Carbon spectrum (^{13}C) of compound **8**.

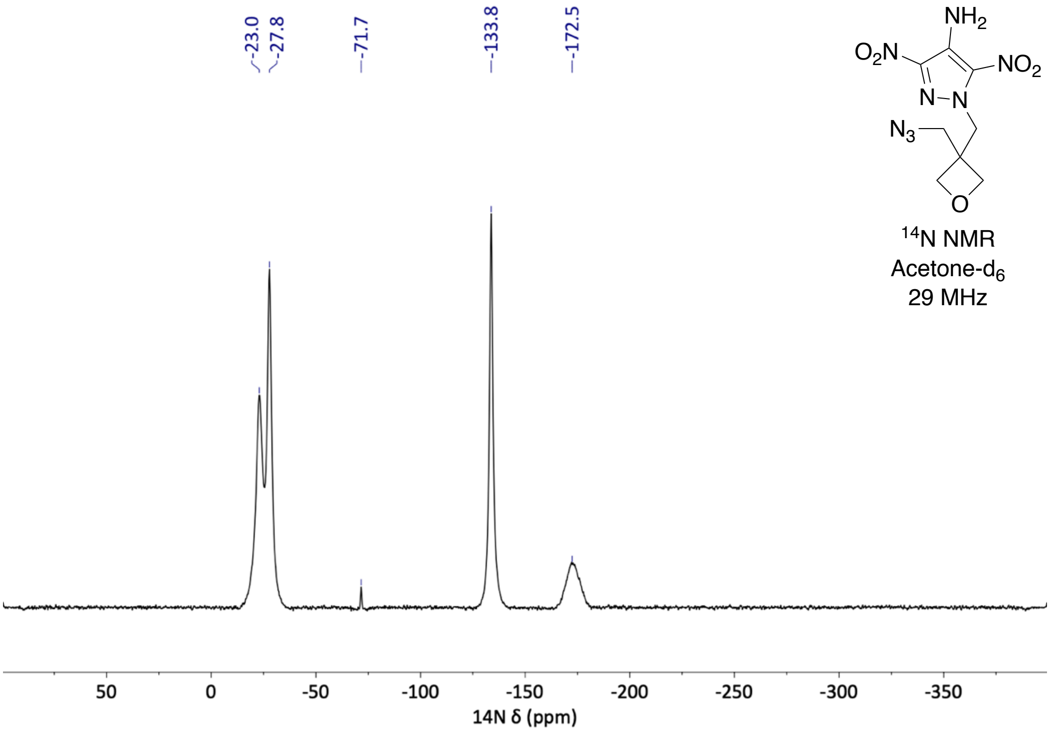

Figure S 7.19. Nitrogen spectrum (^{14}N) of compound **8**.

1-((3-((1*H*-tetrazol-1-yl)methyl)oxetan-3-yl)methyl)-3,5-dinitro-1*H*-pyrazol-4-amine (9A)

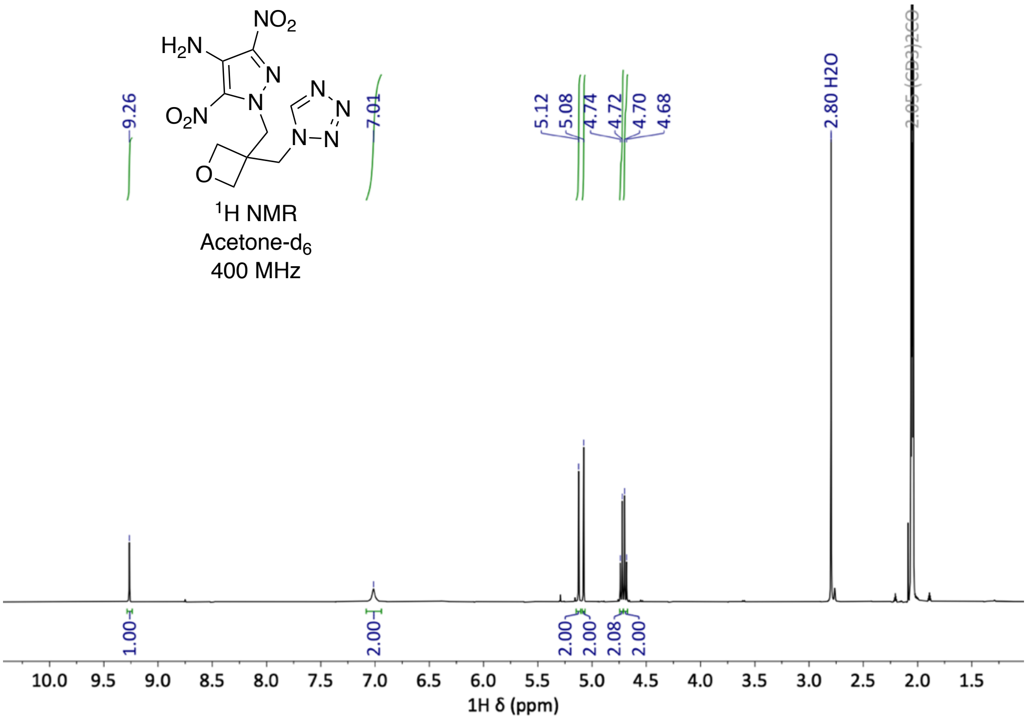

Figure S 7.20. Proton spectrum (^{1}H) of compound **9A**.

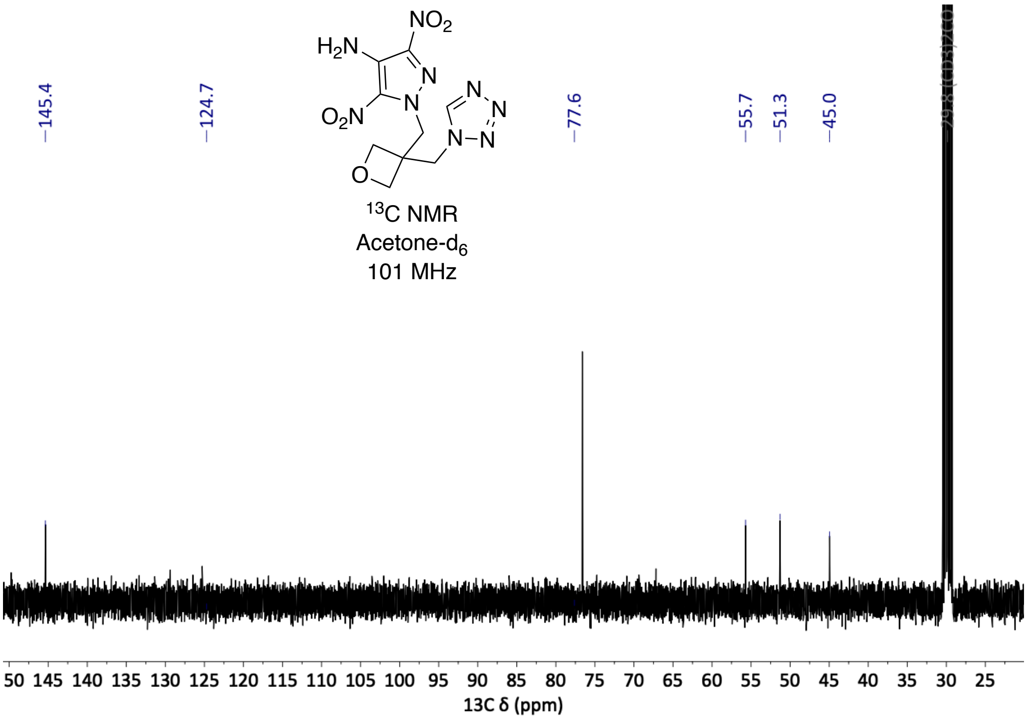

Figure S 7.21. Carbon spectrum (^{13}C) of compound **9A**.

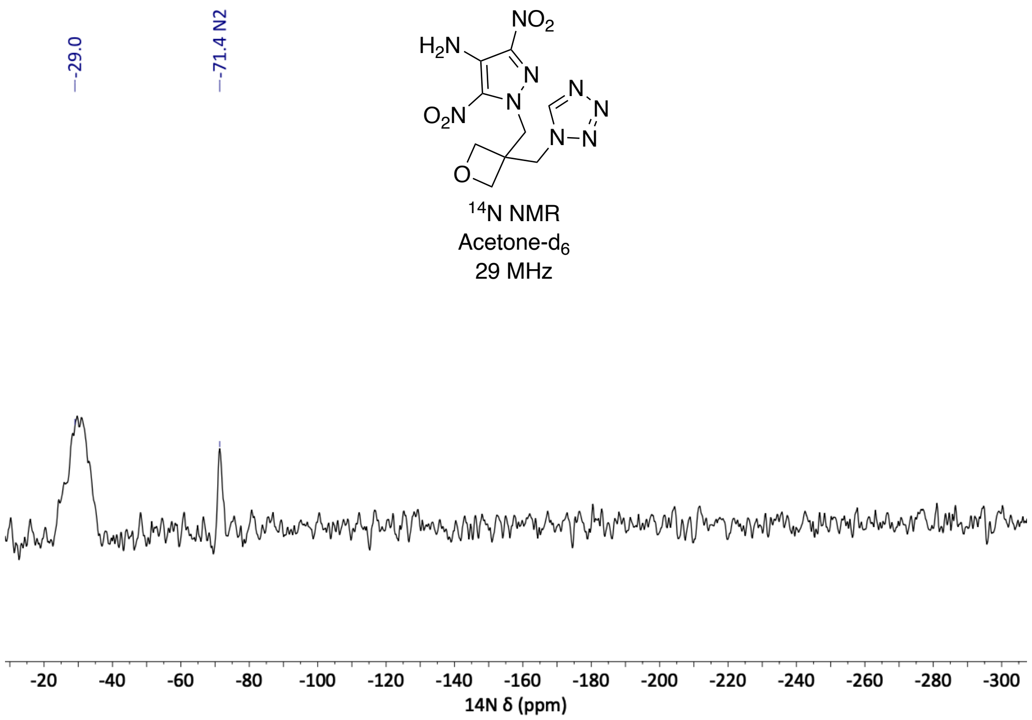

Figure S 7.22. Nitrogen spectrum (^{14}N) of compound **9A**.

1-((3-((2*H*-tetrazol-2-yl)methyl)oxetan-3-yl)methyl)-3,5-dinitro-1*H*-pyrazol-4-amine (9B)

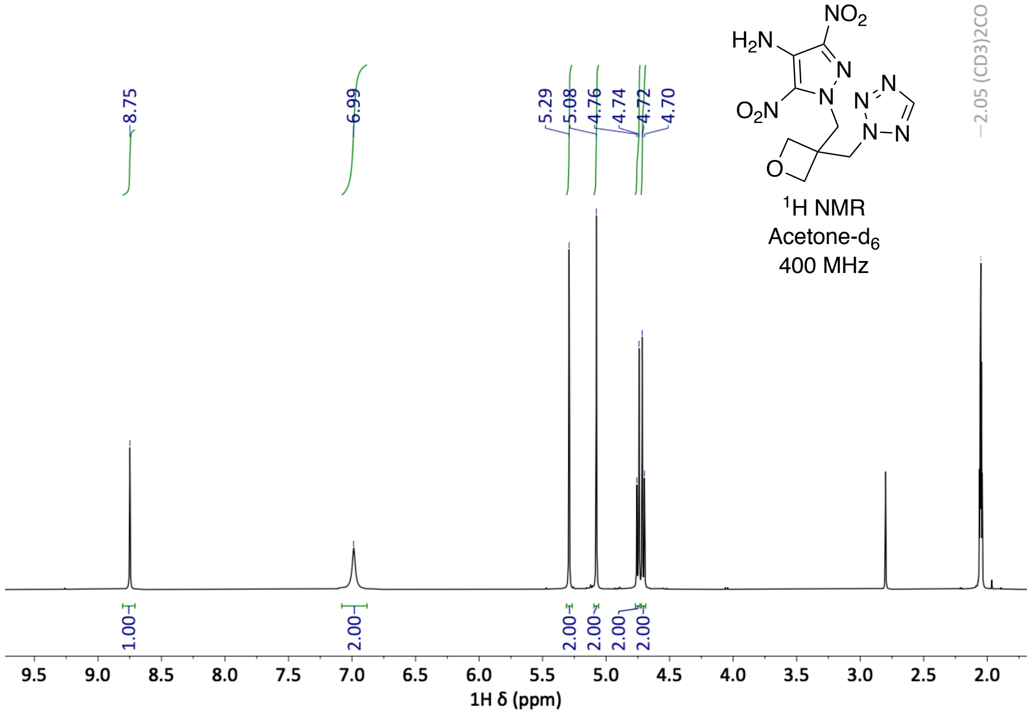

Figure S 7.23. Proton spectrum (^{1}H) of compound **9B**.

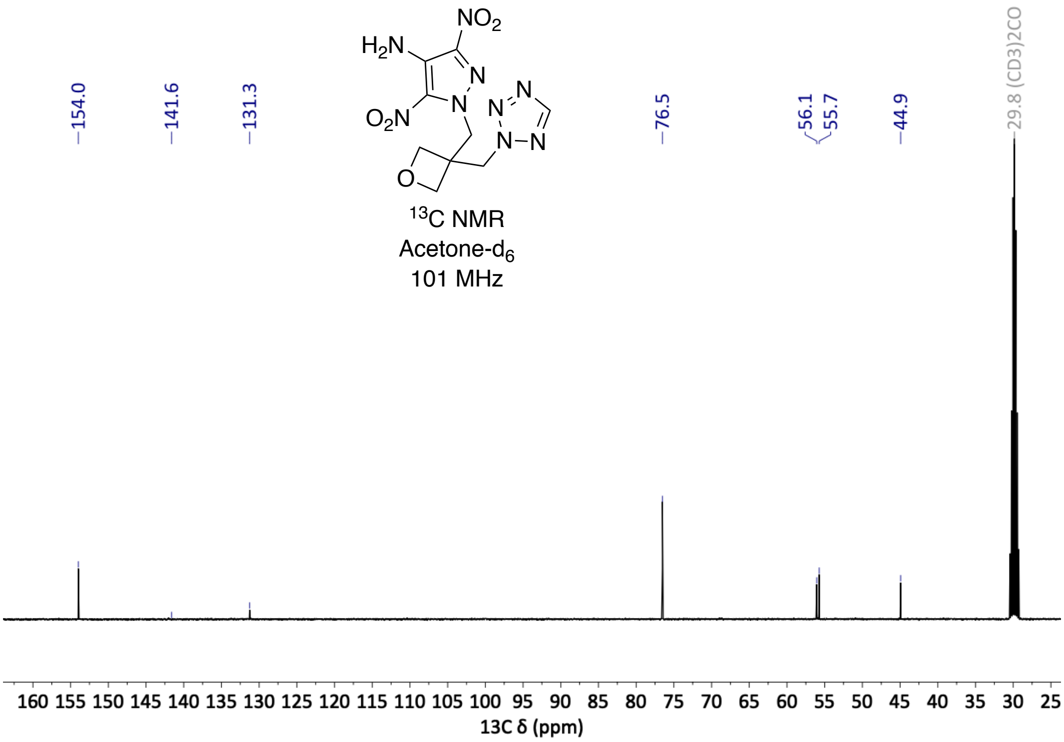

Figure S 7.24. Carbon spectrum (^{13}C) of compound **9B**.

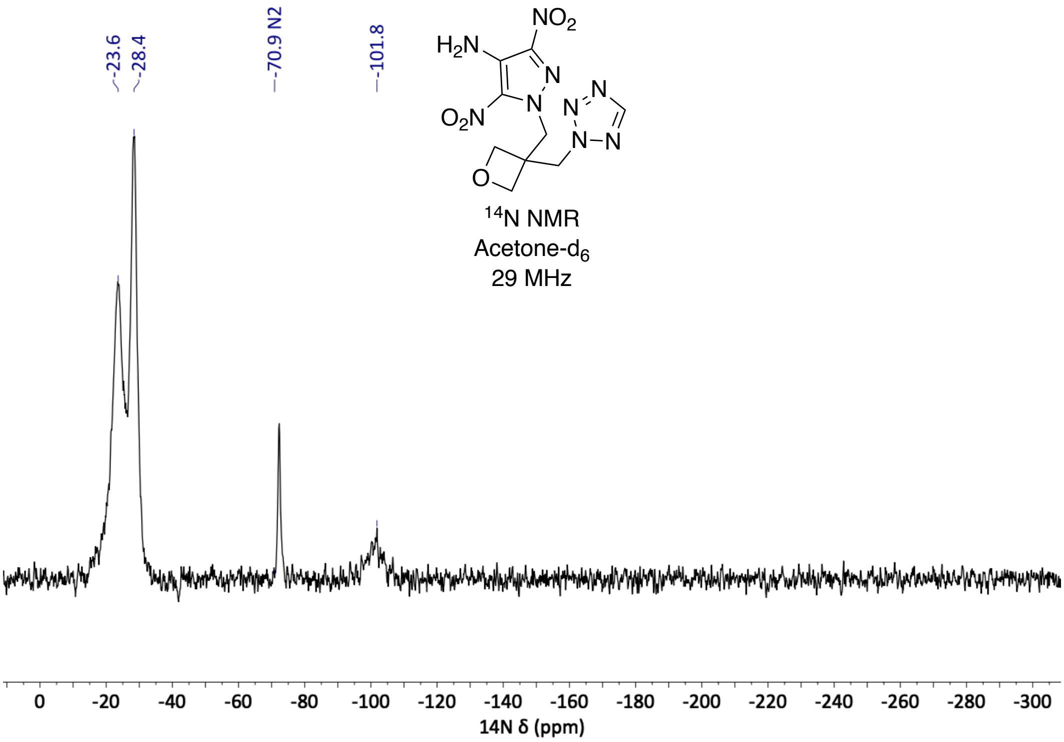

Figure S 7.25. Nitrogen spectrum (^{14}N) of compound **9B**.

7.4.3 Crystallography and Hirshfeld Analysis

Crystal structure data were obtained from an Oxford Xcalibur3 diffractometer with a Spellman generator (voltage 50 kV, current 40 mA) and a Kappa CCD area for data collection using Mo-Kα radiation (λ = 0.71073 Å) or a Bruker D8 Venture TXS diffractometer equipped with a multilayer monochromator, a Photon 2 detector and a rotation-anode generator (Mo-Kα radiation). The data collection was performed using the CRYSTALIS RED software.[4] The solution of the structure was performed by direct methods and refined by full-matrix least-squares on F2 (SHELXT)[5] implemented in the OLEX2[6] software suite. The non-hydrogen atoms were refined anisotropically, and the hydrogen atoms were located and freely refined. The absorption correction was carried out by a SCALE3 ABSPACK multiscan method.[7] The MERCURY 2020.3.0 plots show thermal ellipsoids at the 50% probability level, and hydrogen atoms are shown as small spheres of arbitrary radius. The SADABS program embedded in the Bruker APEX3 software was used for multi-scan absorption corrections in all structures.[8] Hirshfeld analysis was performed using the CrystalExplorer17 software.[9]

7.4.3.1 Molecular Structures of Precursor Compounds (3, 5, 6)

Single crystals suitable for X-ray diffraction of compound **3** and **5** have been obtained by slow evaporation of a saturated ethyl acetate solution. The same method was applied in case of **6** using acetone as solvent.

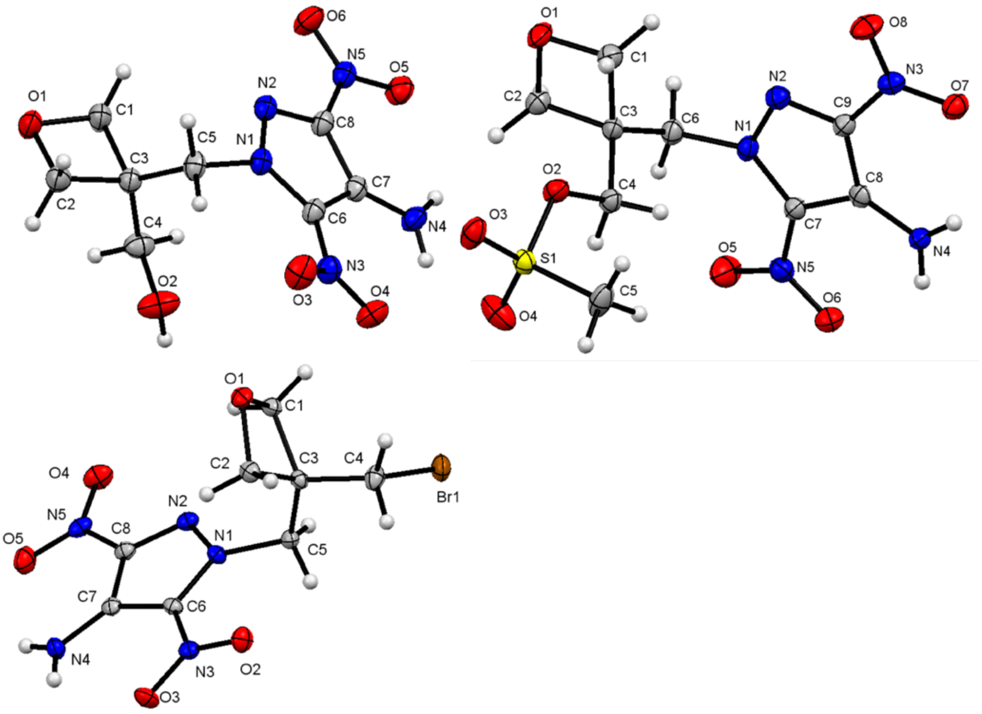

Figure S 7.26. Molecular structures of compounds **3** (top left), **5** (top right), **6** (bottom left) in the crystal. Ellipsoids drawn at the 50% probability level.

(3-((4-Amino-3,5-dinitro-1*H*-pyrazol-1-yl)methyl)oxetan-3-yl)methanol (3)

Compound **3** crystallizes in the monoclinic space group $P2_1/c$ with four formula units in the unit cell and a density of 1.614 g cm^{-3} at 123 K. All bond lengths are in the range of the standard bond lengths. The angles in the oxetane motif range from 91.3(1)° (C3–C1–O1) over 91.2(1)° (O1–C2–C3) down to 91.0(1)° (C1–O1–C2) while the smallest angle is found at C1–C3–C2 (85.4(1))°. The angles between the sp^3-hybridized C3 atom and the substituents are slightly larger than ideal tetrahedral angles with 116.6(2)° at C1–C3–C5 and 114.1(1)° at C2–C3–C4. The oxetane ring has a puckering angle of 10.6°, which is significantly higher than in the parent compound oxetane (8.7(2)°, 140 K).[10] The increased puckering angle is caused by the substituents in 3-position. The pyrazole motif is found to be almost planar with a torsion of only 1.8°. The nitro-groups are twisted out of the pyrazole plane with a torsion of 2.9° for the nitro group connected to C8. The other nitro group reveals a much higher torsion of 18.9° against the pyrazole plane.

(3-((4-Amino-3,5-dinitro-1*H*-pyrazol-1-yl)methyl)oxetan-3-yl)methyl methanesulfonate (5)

Compound **5** crystallizes in the monoclinic space group $P2_1/c$ with four formula units in the unit cell and a density of 1.716 g cm^{-3} at 123 K. All bond lengths are in the range of the standard bond lengths. The angles in the oxetane ring range from 91.8(2)° over 91.5(2)° to 91.4(2)°. The smallest angle is found at C1–C3–C2 (85.3(2)°). As expected, deviance from the ideal tetrahedral angle is found at the sp^3-hybridized C3 atom with 115.8(2)° at C1–C3–C6 and 116.1(2)° at C2–C3–C4. The oxetane ring as well as the pyrazole ring are both planar. The nitro groups are only slightly twisted out of the pyrazole plane with 8.8° at C9 and 6.3° at C7, respectively. The planarity of the oxetane motif is caused by the introduction of the mesyl leaving group as the direct precursor (**3**) shows a higher puckering angle than the unsubstituted parent compound oxetane.

1-((3-(Bromomethyl)oxetan-3-yl)methyl)-3,5-dinitro-1*H*-pyrazol-4-amine (6)

Compound **6** crystallizes in the monoclinic space group $P2_1/c$ with four molecules in the unit cell and a density of 1.890 g cm^{-3} at 123 K. All bond lengths are in the range of the standard bond lengths. Within the oxetane motif, a bond angle of 91.0(2)° is found at both O1–C2–C3 and C3–C1–O1, while a slightly smaller angle is found at C1–O1–C2 (90.2(2)°). The smallest angle is again found at C2–C3–C1 (84.3(2)°). Surprisingly, an almost ideal tetrahedral angle of 109.0(2)° is found at C2–C3–C4, causing the angle at C1–C3–C5 to be even larger (121.0(2)°) than in aforementioned compounds. The oxetane motif shows an extremely strong puckering with an angle of 19.9° caused by the exchange of the mesyl group for a bromine atom. The pyrazole moiety is almost planar. Both nitro groups are rotated out of the pyrazole plane with torsion angles of 3.5° at C8 and 7.1° at C6, respectively.

7.4.3.2 Crystallographic Data Collection

Table S 7.1. Detailed crystallographic information of compounds **3**–**6**.

	3	**4**	**5**	**6**
Formula	$C_8H_{11}N_5O_6$	$C_8H_8N_6O_7$	$C_9H_{13}N_5O_8S$	$C_8H_{10}BrN_5O_5$
FW [g mol^{-1}]	273.22	300.19	351.30	336.12
Crystal System	monoclinic	monoclinic	monoclinic	monoclinic
Space Group	$P2_1/c$	$P2_1/n$	$P2_1/c$	$P2_1/c$
Color / Habit	yellow block	brown block	yellow block	yellow block
Size [mm]	0.40 x 0.40 x 0.10	0.25 x 0.25 x 0.25	0.50 x 0.25 x 0.20	0.35 x 0.30 x 0.20
a [Å]	10.8018(6)	11.3896(4)	12.6134(6)	5.6775(3)
b [Å]	9.7487(4)	9.4491(3)	10.1342(4)	17.9225(8)
c [Å]	11.8318(7)	11.5447(4)	10.9720(5)	11.8409(6)
α [°]	90	90	90	90
β [°]	115.498(7)	105.683(3)	104.236(5)	101.295(5)
γ [°]	90	90	90	90
V [Å^3]	1124.58(12)	1196.20(7)	1359.44(11)	1181.53(10)
Z	4	4	4	4
$\rho_{calc.}$ [g cm^{-3}]	1.614	1.667	1.716	1.890
μ [mm^{-1}]	0.139	0.148	0.295	3.507
F (000)	568	616	728	672
$\lambda_{MoK\alpha}$ [Å]	0.71073	0.71073	0.71073	0.71073
T [K]	123	123	123	123
ϑ min-max [°]	3.473, 26.368	2.229, 30.502	2.776, 26.371	2.273, 30.505
Dataset h; k; l	−13:13; −12:11; −14:14	−16:16; −12:13; −16:13	−15:15; −12:12; −13:13	−8:8; −25:25; −16:16
Reflect. coll.	8061	12680	19746	23528
Independ. Refl.	2305	3646	2769	3586
$R_{int.}$	0.033	0.023	0.049	0.029
Reflection obs.	1834	3030	2301	2848
No. parameters	184	190	260	184
R1 (obs.)	0.0380	0.0296	0.0399	0.0380
wR2 (all data)	0.0975	0.0942	0.0976	0.0918
S	1.041	1.017	1.020	1.045
Resd. Dens. [e Å^{-3}]	−0.189, 0.289	−0.195, 0.419	−0.290, 0.481	−0.489, 0.933
Device Type	Oxford XCalibur3 CCD	Oxford XCalibur3 CCD	Oxford XCalibur3 CCD	Oxford XCalibur3 CCD
Solution	SHELXS-97	SHELXS-97	SHELXS-97	SHELXS-97
Refinement	SHELXLE 2014-3	SHELXLE 2014-3	SHELXLE 2014-3	SHELXLE 2014-3
Absorpt. corr.	Multi-scan	Multi-scan	Multi-scan	Multi-scan
CCDC	2097524	2097531	2097526	2097528

Table S 7.2. Detailed crystallographic information of compounds **7**–**9**.

	7	**8**	**9A**	**9B**
Formula	$C_{14}H_{19}N_{11}O_{10}$	$C_8H_{10}N_8O_5$	$C_9H_{11}N_9O_5$	$C_9H_{11}N_9O_5$
FW [g mol^{-1}]	501.37	298.24	325.27	325.27
Crystal System	monoclinic	monoclinic	triclinic	monoclinic
Space Group	$P2_1/n$	$P2_1/c$	$P{-}1$	$P2_1/c$
Color / Habit	yellow block	yellow plate	yellow plate	yellow block
Size [mm]	0.25 x 0.10 x 0.05	0.20 x 0.10 x 0.02	0.30 x 0.30 x 0.02	0.20 x 0.10 x 0.02
a [Å]	13.7945(8)	12.2346(9)	8.5694(8)	11.4135(10)
b [Å]	10.0128(4)	9.7192(4)	9.0576(9)	7.3682(7)
c [Å]	15.9803(11)	11.4141(8)	9.8868(10)	15.9533(13)
α [°]	90	90	111.396(9)	90
β [°]	113.001(7)	114.824(9)	106.502(9)	98.914(2)
γ [°]	90	90	102.627(8)	90
V [Å^3]	2031.7(2)	1231.85(16)	638.89(12)	1325.4(2)
Z	4	4	2	4
$\rho_{calc.}$ [g cm^{-3}]	1.639	1.608	1.691	1.630
μ [mm^{-1}]	0.140	0.136	0.141	0.136
F (000)	1040	616	336	672
$\lambda_{MoK\alpha}$ [Å]	0.71073	0.71073	0.71073	0.71073
T [K]	123	123	123	123
ϑ min-max [°]	2.461, 26.371	3.575, 26.368	2.415, 26.355	3.052, 26.022
Dataset h; k; l	−17:17; −12:12; −19:19	−15:15; −12:12; −7:14	−10:10; −10:11; −12:12	−14:14; −9:9; −19:19
Reflect. coll.	25112	9467	4961	18850
Independ. Refl.	4131	2509	2600	2592
$R_{int.}$	0.078	0.058	0.025	0.090
Reflection obs.	2873	1780	1941	1649
No. parameters	341	198	221	220
R1 (obs.)	0.0534	0.0475	0.0418	0.0682
wR2 (all data)	0.1269	0.1105	0.0956	0.1301
S	1.053	1.012	1.013	1.061
Resd. Dens. [e Å^{-3}]	−0.280, 0.515	−0.266, 0.263	−0.206, 0.284	−0.257, 0.275
Device Type	Oxford XCalibur3 CCD	Oxford XCalibur3 CCD	Oxford XCalibur3 CCD	Oxford XCalibur3 CCD
Solution	SHELXS-97	SHELXS-97	SHELXS-97	SHELXS-97
Refinement	SHELXLE 2014-3	SHELXLE 2014-3	SHELXLE 2014-3	SHELXLE 2014-3
Absorpt. corr.	Multi-scan	Multi-scan	Multi-scan	Multi-scan
CCDC	2097525	2097527	2097530	2097529

7.4.3.3 Hydrogen Bonding Analysis of Compound 4

As compound **4** apparently shows no hydrogen bonds which are, however, among the most important intermolecular interactions, all hydrogen bonds have been mapped separately in Table S3.

Table S 7.3. Mapping of all hydrogen bonds in compound **4**.

D···A	Distance (Å)	H···A	Distance (Å)	D–H···A	Angle (deg.)
C1···O5	3.275(1)	H1B···O5	2.457(1)	C1–H1B···O5	139.70
C1···C7	3.452(1)	H1B···C7	2.724(1)	C1–H1B···C7	130.65
C1···O7	3.220(1)	H1A···O7	2.558(1)	C1–H1A···O5	124.13
C2···O6	3.097(1)	H2A···O6	2.498(3)	C2–H2A···O6	118.57
C2···N3	3.424(1)	H2B···N3	2.716(4)	C2–H2B···N3	128.70
C4···O5	3.269(1)	H4A···O5	2.716(9)	C4–H4A···O5	115.64
C5···O3	3.403(2)	H5A···O3	2.452(1)	C5–H5B···O3	160.77
C5···N3	3.594(1)	H5B···N3	2.686(6)	C5–H5B···N3	152.45

7.4.3.4 Hirshfeld Analysis

The following figure shows an enlarged depiction of all calculated Hirshfeld surfaces. Close contacts appear as red dots on the respective surface.

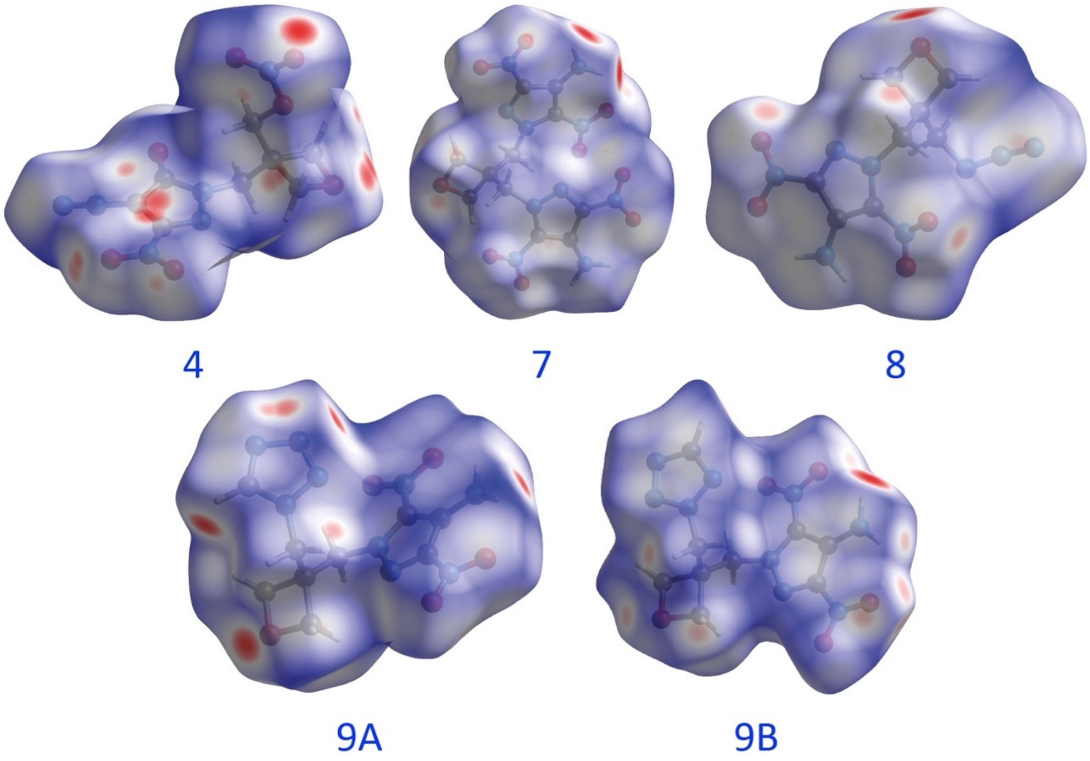
4
7
8
9A
9B

Figure S 7.27. Enlarged depiction of the calculated Hirshfeld surfaces for compounds **4** and **7**–**9**.

7.4.4 Heat of Formation Calculation and Thermal Analysis

The atomization method was used to determine the heat of formation of energetic target compounds (**4**, **7**–**9**) using the atom energies in Table S 4.[11]

$$\Delta_f H°_{(g,\ M,\ 298)} = H_{(molecule,\ 298)} - \Sigma H°_{(atoms,\ 298)} + \Sigma \Delta_f H°_{(atoms,\ 298)}$$

Table S 7.4. CBS-4M electronic enthalpies for atoms C, H, N, and O and their literature values.

	$-H^{298}$ / a.u.	$\Delta_f H°_{gas}$[12]
H	0.500991	217.998
C	37.786156	716.68
N	54.522462	472.68
O	74.991202	249.18

The Gaussian16 program package was used to calculate room temperature enthalpies on the CBS-4M level of theory.[13] In order to obtain the energy of formation for compounds **4** and **7**–**9**, Trouton's Rule has to be applied ($\Delta H_{sub} = 188 \cdot T_m$).

Table S 7.5. Heat of formation calculation results for all target compounds (**4**, **7**, **8**, **9A/B**).

M	$-H^{298}$ [a] [a.u.]	$\Delta_f H°(g, M)$ [b] [kJ mol^{-1}]	$\Delta_{sub} H°(M)$ [c] [kJ mol^{-1}]	$\Delta_f H°(s)$ [d] [kJ mol^{-1}]	Δn	$\Delta_f U(s)$ [e] [kJ kg^{-1}]
4	1162.892687	184.4	69.2498	115.2	−10.5	470.3
7	1648.381352	202.8	97.6002	105.2	−15.5	335.4
8	1123.216883	385.6	70.3402	315.3	−11.5	1152.7
9A (N2)	1216.578143	344.6	81.6202	263.0	−12.5	903.8
9B (N1)	1216.564679	379.9	96.1526	283.8	−12.5	967.8

[a] CBS-4M electronic enthalpy. [b] Gas phase enthalpy of formation. [c] Sublimation enthalpy. [d] Standard solid state enthalpy of formation. [e] Solid state energy of formation.

The thermal behavior of the target compounds (**4**, **7**, **8**, **9A**/**B**) and all precursors was analyzed by differential scanning calorimetry (DSC) at a heating rate of 5 °C min^{-1}. The obtained thermograms and respective evaluations are depicted.

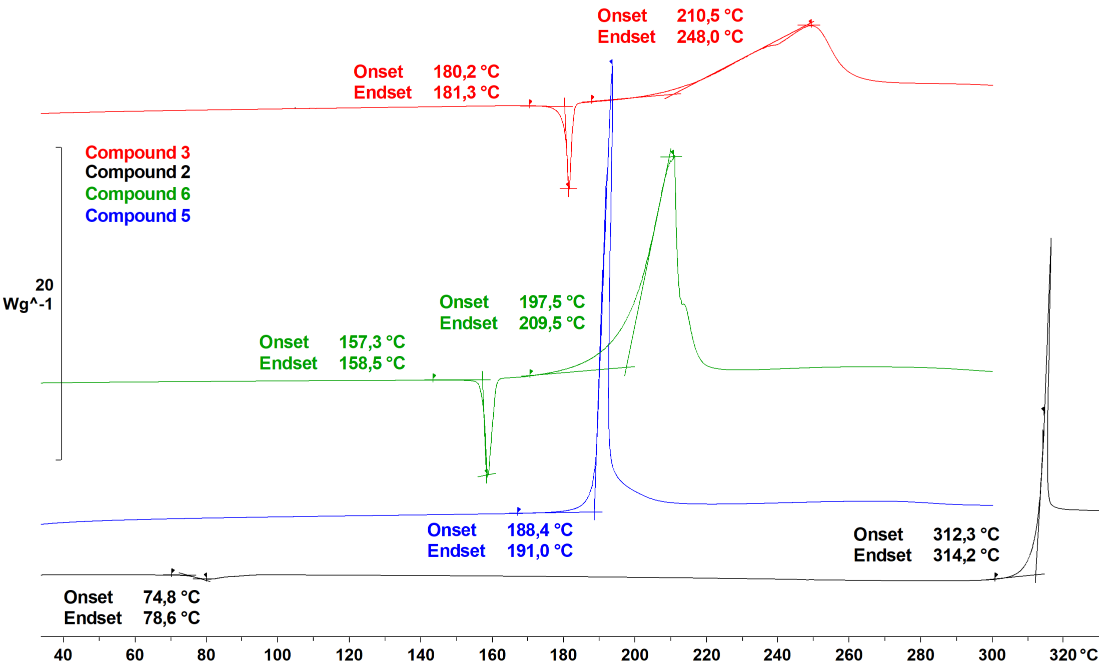

Figure S 7.28. DSC evaluation of energetic precursor compounds (**2**, **3**, **5**, **6**).

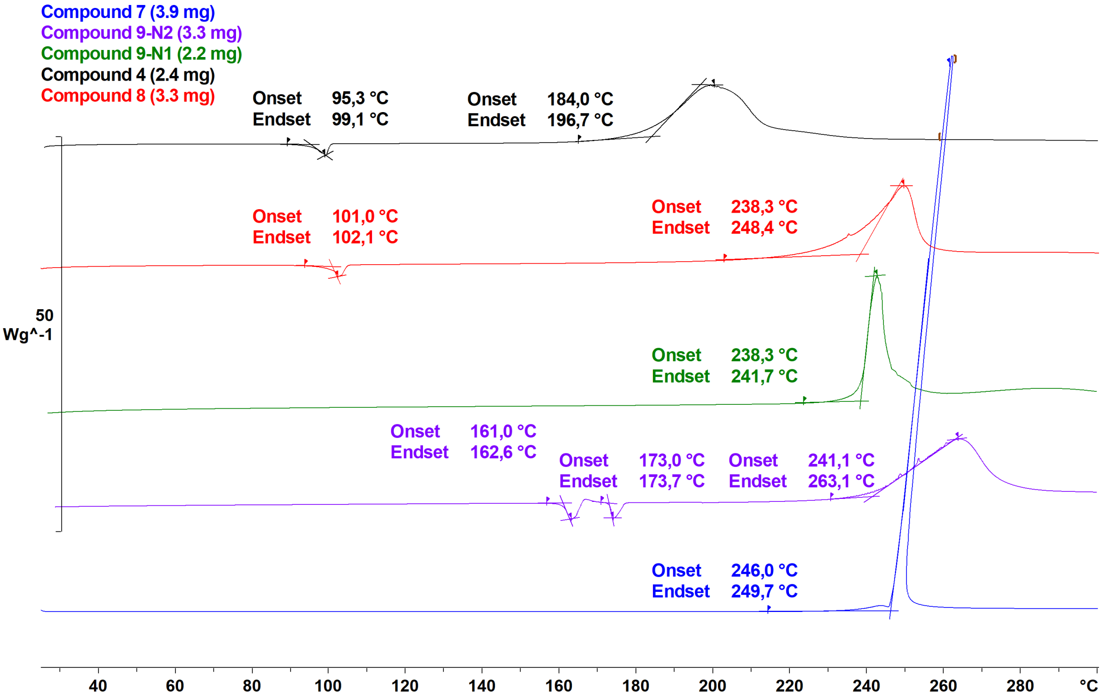

Figure S 7.29. DSC evaluation of target compounds.

7.4.5 Performance Calculation for State-of-the-Art Monomers (Comparison)

To facilitate a performance comparison of obtained compounds with the prior art in the field of energetic oxetanes, the performance of the most prevalent oxetane monomers was calculated using the EXPLO5 V6.04 thermochemical code. For this purpose, the heats of formation were calculated as described in the previous section. Aforementioned prior art is mainly made up by the organic azides 3-azidomethyl-3-methyloxetane (AMMO), 3,3-bis(azidomethyl)oxetane (BAMO) and the less known 3-azidooxetane (3AO). The most well-known organic nitrate is 3-nitratomethyl-3-methyloxetane (NIMMO) among the less prevalent direct comparison nitrates 3-nitratooxetane (3NO) and 3-azidomethyl-3-nitratomethyloxetane (AMNMO). In direct comparison to compound **7**, it becomes evident that the latter is superior in all relevant parameters such as detonation velocity, detonation pressure, thermostability and sensitivity (Table 6).

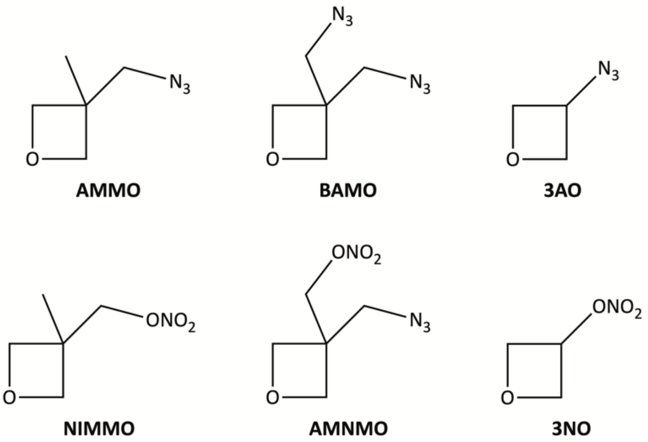

Figure S 7.30. Molecular structures of the most prevalent energetic oxetane monomers (state of the art).

Table S 7.6. Physicochemical and energetic properties of **AMMO**, **BAMO**, **3AO**, **NIMMO** and **AMNMO** as state-of-the-art monomers in comparison to compound **7**.

	AMMO	**BAMO**	**3AO**	**NIMMO**	**3NO**[14]	**AMNMO**	**7**
Formula	$C_5H_9N_3O$	$C_5H_8N_6O$	$C_3H_5N_3O$	$C_5H_9NO_4$	$C_3H_5NO_4$	$C_5H_8N_4O_4$	$C_{11}H_{12}N_{10}O_9$
FW [g·mol^{-1}]	127.15	168.16	99.09	147.13	119.08	188.14	428.28
IS[a] [J]	> 40	40	3	> 40	40	7	>40
FS[b] [N]	360	360	>192	360	>360	288	>360
Ω[c] [%]	−106.96	−76.12	−72.7	−59.81	−20.15	−42.52	−29.9
T_m[d]/ T_b[e]/ T_{dec}[f] [° C]	-/178/210	-/-/207.3	-/140/190	−13.8/-/170.3	-/-/153	−12.4/-/178.2	-/-/246
ρ[g] [g·cm^{-3}]	1.05	1.23	1.18	1.19	1.34	1.33	1.70
ΔH_f°[h] [kJ·mol^{-1}]	148.3	510.5	225.6	−268.9	−168.0	93.8	105.2
				EXPLO5 V6.04			
$-\Delta_E U^\circ$[i] [kJ·kg^{-1}]	3411	4479	4520	3949	5089	4768	4206
$T_{C\text{-}J}$[j] [K]	2086	2786	2813	2507	3394	3129	2981
$p_{C\text{-}J}$[k] [GPa]	7.69	12.4	11.5	10.6	16.6	15.2	20.9
$D_{C\text{-}J}$[l] [m·s^{-1}]	5544	6548	6307	5906	6771	6729	7335
V_0[m] [dm^3·kg^{-1}]	803	797	820	827	829	817	710

[a] Impact sensitivity (BAM drop hammer, method 1 of 6). [b] Friction sensitivity (BAM friction apparatus, method 1 of 6). [c] Oxygen balance regarding carbon monoxide (Ω_{CO} = (nO − xC − yH/2)(1600/FW). [d] Melting point (DSC, β = 5 °C·min^{-1}). [e] Boiling point (DSC, β = 5 °C min^{-1}). [f] Decomposition temperature (DSC, β = 5 °C min^{-1}). [g] Density at 298 K. [h] Standard molar enthalpy of formation. [i] Detonation energy. [j] Detonation temperature. [k] Detonation pressure. [l] Detonation velocity. [m] Volume of detonation gases at standard temperature and pressure conditions.

7.4.6 Practical Tests

7.4.6.1 Hot Plate Test

A hot plate test was performed by placing 50 mg of each target compound on a copper plate prior to heating with a Bunsen burner. Compounds **4** and **8** show a violent deflagration, while compound **7** partially sublimates before it ignites. Compound **9** thermally decomposes without visible flame.

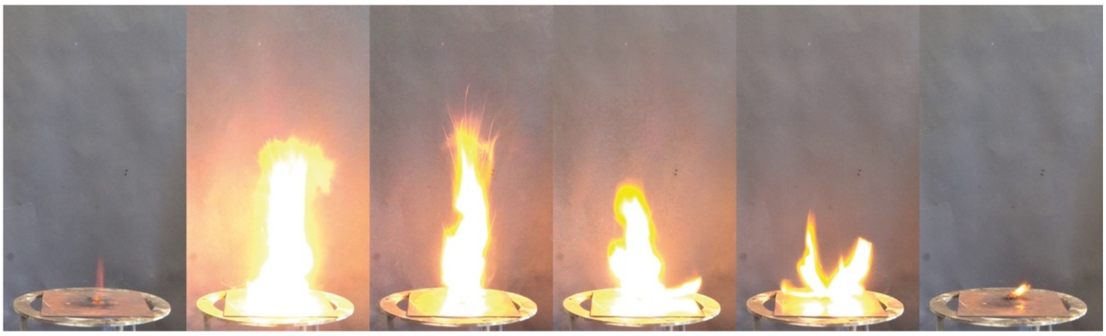

Figure S 7.31. Deflagration of compound **4**.

Figure S 7.32. Violent deflagration of compound **8**.

Figure S 7.33. Partial sublimation of compound **7** prior to ignition.

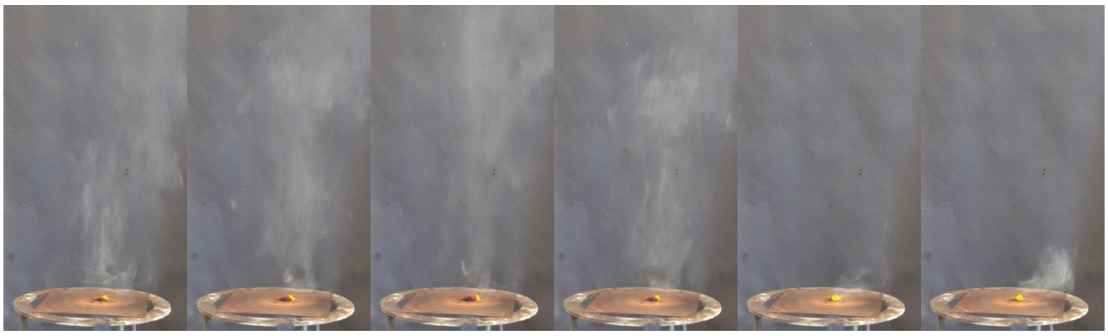

Figure S 7.34. Decomposition of compound **9** (isomeric mixture) without visible flame.

7.4.6.2 SSRT (Small-Scale Reactivity Test)

The small-scale reactivity tests were performed as described and the dents volume of each aluminum witness plate was measured using a 3D profilometer.

Figure S 7.35. Aluminum witness blocks and indentation caused by the respective compound (**4**, **7**, **8**, **9**).

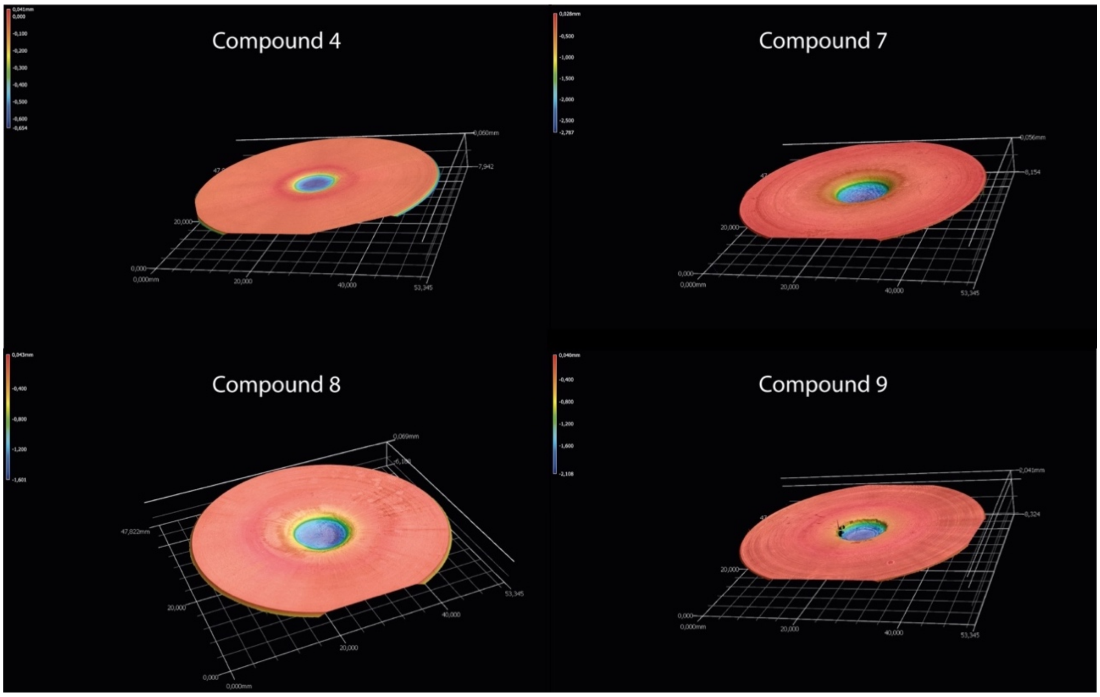

Figure S 7.36. Dent volume determination using a 3D profilometer.

7.4.6.3 Initiation Test

The initiation tests were performed as described in the main document.

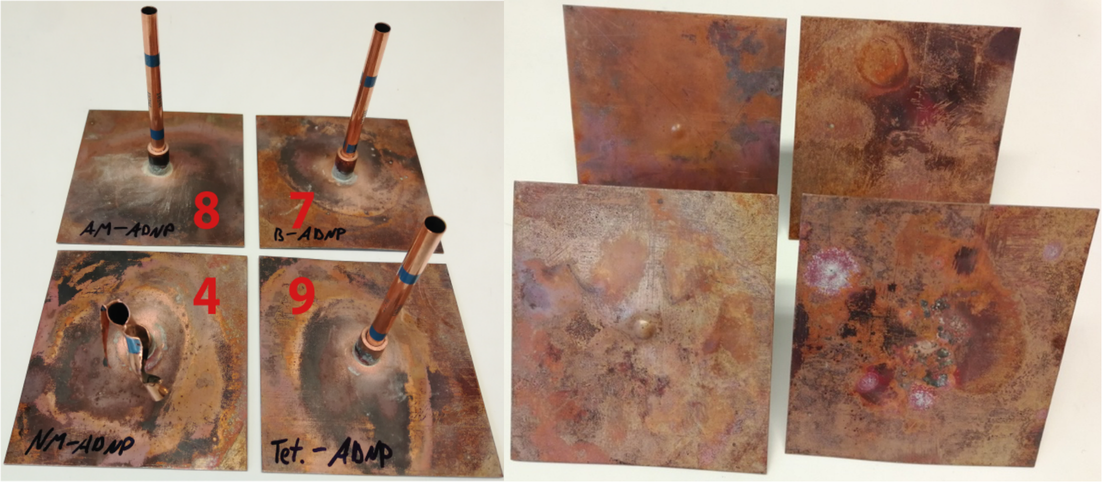

Figure S 7.37. Negative test results using neat lead azide (left) and bottom of the respective witness plates (right).

Figure S 7.38. Unaffected material (compound **8**) after detonation of 50 mg lead azide (left) and witness plates after successful initiation using PETN as booster charge.

References

[1] NATO STANAG 4489: *Explosives. Impact Sensitivity Tests*; NATO Standardization Office, Brussels, Belgium, **1999**.

[2] NATO STANAG 4487: *Explosives. Friction Sensitivity Tests*; NATO Standardization Office, Brussels, Belgium, **2002**.

[3] United Nations (UN), UN Recommendations on the Transport of Dangerous Goods, Manual of Tests and Criteria, **2009**.

[4] CrysAlisPRO (Version 171.33.41), Oxford Diffraction /Agilent Technologies UK Ltd., Yarnton, England, **2009**.

[5] Sheldrick, G., SHELXT - Integrated space-group and crystal-structure determination. *Acta Crystallogr., Sect. A: Found. Adv.* **2015,** *71*, 3-8.

[6] Dolomanov, O. V.; Bourhis, L. J.; Gildea, R. J.; Howard, J. A. K.; Puschmann, H., OLEX2: a complete structure solution, refinement and analysis program. *J. Appl. Crystallogr.* **2009,** *42* (2), 339-341.

[7] SCALE3 ABSPACK –An Oxford Diffraction program (1.0.4, gui: 1.0.3), Oxford Diffraction Ltd., Yarnton, England, **2005**.

[8] APEX3, Bruker AXS Inc., Madison, Wisconsin, USA, **2016**.

[9] Turner, M. J.; McKinnon, J. J.; Wolff, S. K.; Grimwood, D. J.; Spackman, P. R.; Jayatilaka, D; Spackman, M. A. CrystalExplorer17 (**2017**). University of Western Australia. https://hirshfeldsurface.net.

[10] Luger, P.; Buschmann, J., Oxetane: the first x-ray analysis of a nonsubstituted four-membered ring. *J. Am. Chem. Soc.* **1984,** *106* (23), 7118-7121.

[11] Altenburg, T.; Klapötke, Thomas M.; Penger, A.; Stierstorfer, J., Two Outstanding Explosives Based on 1,2-Dinitroguanidine: Ammonium- dinitroguanidine and 1,7-Diamino-1,7-dinitrimino-2,4,6-trinitro-2,4,6-triazaheptane. *Z. Anorg. Allg. Chem.* **2010,** *636* (3-4), 463-471.

[12] Chase, M. W. NIST-JANAF Thermochemical Tables, Fourth Edition, *J. Phys. Chem. Red. Data, Monograph 9,* **1998**, 1–1951.

[13] Frisch, M. J.; Trucks, G. W.; Schlegel, H. B.; Scuseria, G. E.; Robb, M. A.; Cheeseman, J. R.; Scalmani, G.; Barone, V.; Petersson, G. A.; Nakatsuji, H.; Li, X.; Caricato, M.; Marenich, A. V.; Bloino, J.; Janesko, B. G.; Gomperts, R.; Mennucci, B.; Hratchian, H. P.; Ortiz, J. V.; Izmaylov, A. F.; Sonnenberg,

J. L.; Williams; Ding, F.; Lipparini, F.; Egidi, F.; Goings, J.; Peng, B.; Petrone, A.; Henderson, T.; Ranasinghe, D.; Zakrzewski, V. G.; Gao, J.; Rega, N.; Zheng, G.; Liang, W.; Hada, M.; Ehara, M.; Toyota, K.; Fukuda, R.; Hasegawa, J.; Ishida, M.; Nakajima, T.; Honda, Y.; Kitao, O.; Nakai, H.; Vreven, T.; Throssell, K.; Montgomery Jr., J. A.; Peralta, J. E.; Ogliaro, F.; Bearpark, M. J.; Heyd, J. J.; Brothers, E. N.; Kudin, K. N.; Staroverov, V. N.; Keith, T. A.; Kobayashi, R.; Normand, J.; Raghavachari, K.; Rendell, A. P.; Burant, J. C.; Iyengar, S. S.; Tomasi, J.; Cossi, M.; Millam, J. M.; Klene, M.; Adamo, C.; Cammi, R.; Ochterski, J. W.; Martin, R. L.; Morokuma, K.; Farkas, O.; Foresman, J. B.; Fox, D. J. *Gaussian 16 Rev. C.01*, Wallingford, CT, **2016**.

[14] Klapötke, T. M.; Born, M.; Fessard, T.; Göttermann, L.; Stierstorfer, J.; Voggenreiter, M., 3,3-Dinitratooxetane - An Important Leap Towards Energetic Oxygen-Rich Monomers and Polymers. *Chem. Commun.* **2021**, *57*, 2804–2807.

8 3-(Nitromethylene)oxetane: A Very Versatile and Promising Building Block for Energetic Oxetane Based Monomers

by

Max Born, Thomas C. Fessard, Lucas Göttemann, Konstantin Karaghiosoff, Jakob Plank and Thomas M. Klapötke

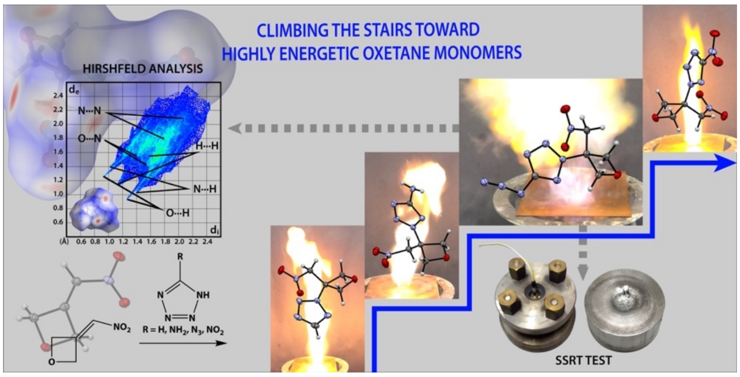

as published in
Materials Advances **2022**, *3*, 3479–3489
(doi:10.1039/D2MA00088A)

Abstract

In the field of energetic materials, older developments (e.g., RDX, ONC, CL20) are increasingly replaced by more environmentally benign, less expensive, and likewise or more powerful compounds. This is mainly achieved through nitrogen-rich motifs like tetrazoles. However, such materials are mostly used as formulations containing polymeric energetic binders. Unfortunately, prior art binders show very poor performances and therefore reduce the overall performance. To address this problem, new monomers with enhanced performance are a prerequisite. Since the majority of energetic binders is oxetane-based, we chose 3-(nitromethylene)oxetane as a promising building block. It exhibits an explosophoric group, has recently become commercially available, and provides suitable monomers by elegant and cost-efficient one-pot syntheses via conjugate addition. Herein, we report derivatives based on 1*H*-tetrazole, 1*H*-tetrazole-5-amine and the rather exotic but extremely powerful primary explosives 5-azido-1*H*-tetrazole (5AzT) and 5-nitro-2*H*-tetrazole (5NT). The sensitivities toward external stimuli like impact, friction, and electrostatic discharge were assessed by BAM standard procedures. As all molecular structures were elucidated by X-ray diffraction, Hirshfeld analysis was applied to explain the surprisingly low sensitivities found for the 5AzT- and 5NT-derivatives. Further, the compounds were studied by vibrational- and multinuclear NMR spectroscopy (^{1}H, ^{13}C, ^{14}N), differential scanning calorimetry, and elemental analysis. Their performance was calculated using the EXPLO5 V6.04 thermochemical code. Based on obtained values, the 5AzT- and 5NT-derivatives outperform prior art energetic oxetanes and TNT. Therefore, their performance was additionally demonstrated and evaluated by a small-scale shock reactivity test (SSRT).

8.1 Introduction

Since the first synthesis of 5-cyano-2-phenyltetrazole by Emil Fischer in 1878[1], tetrazoles have been an important structural unit widely used in chemistry. Their applications cover a broad spectrum from dyes and agrochemicals[2,3] to pharmaceuticals due to their fungicidal, antibacterial, antiallergic[4] and as later discovered, cytostatic effects.[5] In addition, they play a key role in the field of energetic materials due to their high nitrogen content and the associated, positive enthalpy of formation.[6] The aromatic system also often provides a high thermostability.[3,6] Particularly interesting are 5-substituted derivatives featuring nitrogen- and oxygen-rich groups. Due to the high nitrogen content, they mainly form molecular nitrogen upon decomposition and serve as motifs for more environmentally benign, "greener" energetic materials.[7] Next to their application in propellant systems, they are suitable for the synthesis of powerful, heavy metal-free primary explosives such as K_2DNABT[8] or high-performance secondary explosives such as TKX-50, which competes with benchmark compounds such as CL20 or octanitrocubane (ONC) regarding performance while being less expensive.[9] However, the performance of such energetic materials seems to have reached a maximum for now. As these materials are often used as a formulation containing high proportions of binders, improved energetic polymers offer additional room for enhanced performance. Unfortunately, all prior art energetic monomers and their corresponding polymers show performances inferior to TNT, which was already prepared in 1863 by Wilbrand. Hence, new monomers with higher performances are very desirable. Since energetic binder research is mainly focused on polyoxetanes (e.g., poly(AMMO), poly(BAMO), poly(NIMMO))[10] while tetrazoles represent a key motif in the development of new energetic materials, tetrazole-based oxetanes appear as a promising approach. In this context, we identified 3-(nitromethylene)oxetane as suitable starting material. It was first prepared in 2008 by Wuitschik via condensation of nitromethane and oxetan-3-one.[11] Since then, it has proven to be an excellent Michael acceptor and reacts readily with a wide variety of heteroatom- and carbon nucleophiles under 1,4-selectivity and has been used in drug discovery to obtain 3,3-disubstituted oxetanes.[12] For instance, it was employed by Carreira et al. to prepare oxetane peptidomimetics.[13] It is of interest to the field of energetic materials as it already features an explosophoric nitro group while offering the possibility to prepare monomers in one-pot syntheses via conjugate addition. To provide monomers based on inexpensive and commercially available materials, we selected 1*H*-tetrazole and 1*H*-tetrazol-5-amine, while 5-azido-1*H*-tetrazole (5AzT) and 5-nitro-2*H*-tetrazole (5NT) were selected to gain especially high performance. The latter represent primary explosives[2,14,15] with a performance comparable to high-explosives such as RDX.[15,16] Among monocyclic tetrazoles, 5AzT features the highest nitrogen content (88.3%), a detonation velocity ($V_{det.}$) of 8986 ms^{-1} and a detonation pressure ($p_{C\text{-}J}$) of 32.7 GPa.[14] 5NT ($V_{det.}$ 9457 ms^{-1}; $p_{C\text{-}J}$ 39.0 GPa) outperforms both 5AzT and RDX ($V_{det.}$ 8750 ms^{-1}; $p_{C\text{-}J}$ 34.6 GPa).[15] Accordingly, the addition products show calculated performances (EXPLO5 V6.04) superior to prior art energetic oxetanes and TNT as secondary explosive. For verification, a small-scale shock reactivity test (SSRT) was performed.[16] As the molecular structure of all target compounds was elucidated by single-crystal X-ray diffraction, Hirshfeld analysis was applied which made the surprisingly low sensitivity of the 5AzT- and 5NT-derivative comprehensible based on interactions in the crystal. Overall, we obtained satisfying to high yields in each case – even if poor nucleophiles have been used, indicating the excellent acceptor properties of the nitroalkene. In general, various known energetic compounds can be directly added to 3-(nitromethylene)oxetane to provide new oxetane monomers in an almost assembly line manner. Therefore, we expect the nitroalkene to contribute to a faster progress in the field of energetic oxetane-based monomers and polymers.

8.2 Results and Discussion

8.2.1 Synthesis

The precursor to all target compounds, 3-(nitromethylene)oxetane, was used as provided by Spirochem AG. 1*H*-tetrazole and 1*H*-tetrazol-5-amine were used as provided by ABCR. 5-Azido-1*H*-tetrazole was prepared according to the literature by 1,3-dipolar cycloaddition using cyanogen bromide and two equivalents of sodium azide in aqueous methanol solution.[14] Protonation of the intermediate (sodium salt) using 2M hydrochloric acid gave the neutral compound, which was extracted with diethyl ether. The organic phase was split into several plastic vials for evaporation to ensure quantities no larger than 100 mg for safety reasons. 5-Nitro-2*H*-tetrazole was prepared accordingly by acidifying an aqueous solution of sodium 5-nitrotetrazolate dihydrate followed by extraction of the neutral compound with ether and splitting into batches as described. The salt was prepared according to literature methods.[17] All aza-Michael additions were first carried out analogously to literature by equimolar conversion of the respective tetrazole derivatives with nitroalkene **1** in anhydrous DMSO.[18] Unfortunately, subsequent liquid-liquid extraction (brine, EA/Et_2O 1:2) caused a significant loss of material leading to yields in a range of 30–40% and impurities caused by the addition of water to unreacted nitroalkene during work-up. Therefore, the solvent was changed to dry acetonitrile (argon atmosphere), which allowed direct monitoring by thin-layer chromatography (TLC). In addition, the need for liquid-liquid extraction was hereby eliminated, as the solvent can be removed by rotary evaporation. For all reactions, a quantitative conversion was observed (TLC) using a reaction temperature of 65 °C and reaction times between 17 and 36 h (Scheme 1).

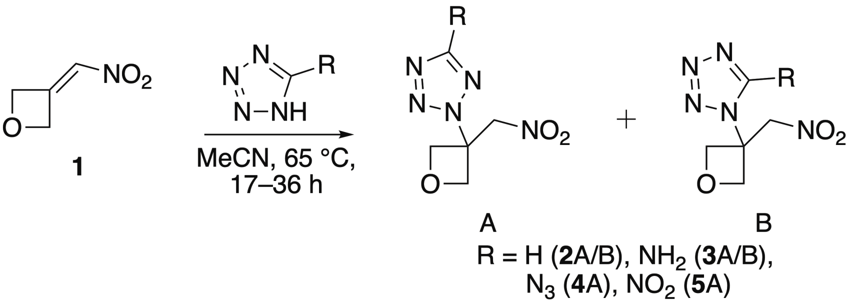

Scheme 8.1. General method for the preparation of compounds **2**–**5** via an aza-Michael reaction.

This was confirmed by ^{1}H NMR spectroscopy after solvent removal by rotary evaporation. In the case of 1*H*-tetrazole derivative **2** (A/B), an isomeric ratio (*N*2/*N*1) of 2:1 was determined by ^{1}H NMR spectroscopy after 17 h and separation was achieved by column chromatography (SiO_2, EA/petroleum ether/toluene 3:1:1) to give 86% yield of compound **2**A (with regard to the theoretical amount of *N*2-isomer) and 71% yield of **2**B, respectively. Despite that 1*H*-tetrazol-5-amine is only sparingly soluble in acetonitrile, full conversion was obtained in case of compound **3** (A/B) after 24 h. Hereby, the initial suspension turned into a solution upon first product formation and became a suspension again as the less polar *N*2-isomer precipitated. An isomeric ratio of roughly 9:1 (*N*2/*N*1) was assessed by ^{1}H NMR spectroscopy. The solubility behavior was utilized to isolate **3**A in high purity and yield (77%) by evaporating two thirds of the solvent volume, cooling (fridge, 5 °C), and removal of the liquid phase. The remaining solid was washed with a small volume of cold acetonitrile and the supernatant was again removed to give **3**A as colorless solid. As impurities concentrate in the collected liquid phase, the *N*1-isomer (**3**B) was isolated by filtration through a silica plug using aforementioned solvent mixture to remove residual *N*2-isomer. After rotary evaporation, ethyl acetate was added to dissolve crude **3**B. The solvent was then allowed to evaporate slowly at ambient conditions. Upon formation of colorless crystals, the supernatant was removed by means of a syringe to afford pure material with a yield of 35% due to work-up and purification losses. Furthermore, negligible trace amounts of compound **3**C were obtained. In this case, the conjugated addition took place at both the *endo*- and *exo*-cyclic NH-position of 1*H*-tetrazol-5-amine. Unfortunately, the amount was insufficient for analytic purposes, but a few single-crystals formed and the structure was elucidated by X-ray diffraction. As 5-azido-1*H*-tetrazole is a weaker nucleophile by comparison, quantitative conversion toward compound **4** required a slightly prolonged reaction time (36 h) and raised equivalents with respect to the employed tetrazole (1.3 equiv.). According to ^{1}H NMR spectroscopy, the formation of the *N*2-isomer was found to be strongly favored, resulting in an isomer ratio (*N*2/*N*1) of roughly 10:1. Due to this excess, we renounced the isolation of the *N*1-isomer in favor of avoiding column chromatography, as its necessity often excludes compounds from application in the field of energetic materials due to increased costs and a lack of scalability. After rotary evaporation, the obtained colorless oil was dissolved in dichloromethane (DCM) and filtration through a silica plug removed surplus 5-azido-1*H*-tetrazole. After rotary evaporation, overlaying of the obtained oil with a small amount of toluene and deep-freezing (−30 °C) resulted in crystals of the *N*2-isomer in the form of large, colorless rods. The toluene layer was removed to afford **4**A in high yield (78%). In case of the addition of 5-nitro-2*H*-tetrazole to nitroalkene **1**, an almost quantitative conversion was observed after 17 h. Unfortunately, higher reaction times led to a dark brown color of the reaction solution indicating partial decomposition. Correspondingly, a significant impurity of the crude product was encountered. This can be attributed to undesired side reactions due to the high acidity of 5-nitro-2*H*-tetrazole. An isomeric ratio (*N*2/*N*1) of 12:1 was obtained according to ^{1}H NMR spectroscopy indicating a strong favoring of the *N*2-isomer. As in case of **4**, the isomeric mixture was dissolved in DCM after rotary evaporation and filtered through a silica plug to remove excess tetrazole and impurities to give **5** as off-white solid slightly contaminated with *N*1-isomer according to ^{1}H NMR spectroscopy. Due to the extremely similar polarity, separation of the isomers by column chromatography failed using various solvent mixtures. Recrystallization was largely complicated by the extremely high solubility of compound **5** in nearly all laboratory solvents. However, recrystallization from hot toluene helped to reduce the fraction of *N*1-isomer (4.8%) in the target product and compound **5** was isolated with a still satisfying yield of 51%.

8.2.2 Crystallography

Single crystals of compound **1** were obtained by slow evaporation of a saturated chloroform solution. The same method was applied to compounds **2** (A, B), **3** (A, B, C), **4** and **5** using ethyl acetate as solvent. Detailed crystallographic data and the discussion of the *N*1-isomers (**2**B, **3**B) as well as compound **3**C can be found in the Supporting Information.

3-(Nitromethylene)oxetane (**1**) crystallizes in the monoclinic space group *C*2/c with eight formula units per cell and a density of 1.589 g cm^{-3} (143 K) corresponding to a room temperature density of 1.550 g cm^{-3} (Figure 1).

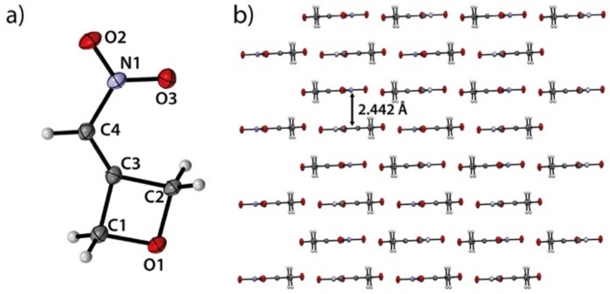

Figure 8.1. a) Molecular structure of compound **1** in the crystal. Thermal ellipsoids drawn at 50% probability level. b) View along *b* axis.

Bond angles of the oxetane moiety range from 90.16(9)° (O1–C1–C3) over 90.37(9)° (O1–C2–C3) to considerably small angles of only 88.32(9)° (C1–C3–C2). The largest angle is found at the oxetane oxygen atom (C1–O1–C2) with an angle of 91.13(9)°. The large deviations from the ideal tetrahedral angle of sp^3-hybridized carbon atoms (109.5°) give insight to the increased p-character of the endocyclic bonds and the prevailing ring tension. The shortest endocyclic bond is observed between C1 and O1 (1.460(2) Å), while the longest is found between C3 and C1 with a length of 1.503(2) Å. The ring itself is essentially planar with a puckering angle of only 1.23°, which is considerably smaller than the puckering angle of unsubstituted oxetane with 8.7(2)° at 140 K.[19] The double bond between C3 and C4 shows a typical value of 1.327(2) Å as well as the C4–N1 bond with a length of 1.442(2) Å.[20] The nitro group itself is twisted by only 0.4° against the oxetane ring plane (C1–C2–C3). Therefore, the entire molecule is essentially planar. The view along the *b* axis (Figure 1b) shows compound **2** forming closely adjacent, step-like and pairwise parallel layers with step heights of only 0.226 Å and 0.285 Å. These parallel segments in turn form layers with a minimum spacing of 2.442 Å and are rotated 180° relative to each other.

2-(3-(Nitromethyl)oxetan-3-yl)-2*H*-tetrazole (**2**A) crystallizes in the monoclinic space group *P*2$_1$/c with four formula units per unit cell and a density of 1.609 g cm^{-3} (102 K) which correlates to a room temperature density of 1.560 g cm^{-3} (Figure 2).

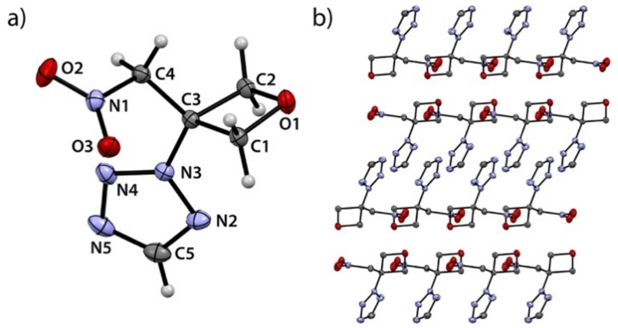

Figure 8.2. a) Molecular structure of compound 2A in the crystal. Thermal ellipsoids drawn at 50% probability level. b) View along *b* axis.

As expected, all oxetane bond angles show large deviations from the ideal tetrahedral angle ranging from 91.5(1)° (O1–C1–C3) over 91.1(1)° (O1–C2–C3) to only 85.1(1)° (C1–C3–C2). An angle of 91.9(1)° is found at the oxetane oxygen atom (C1–O1–C2). The shortest bond is observed between O1 and C2 (1.449(2) Å) and the longest between C2 and C3 (1.548(2) Å). A rather small puckering angle of 6.95° (102 K) is found in comparison to the unsubstituted parent compound (10.7(1)°, 90 K).[19] The single bond between C3 and the tetrazole moiety features a length of 1.464(2) Å, which is shorter than in similar tetrazole-derivatives.[21-23] The bond between C3 and C4 is shorter (1.506(2) Å) than the average bond length between sp^3-hybridized carbons atoms.[20] A deviation from typical values is also found for the bond between C4 and N1 (1.500(2) Å), which is longer compared to similar nitroaliphatic compounds (1.490(3) Å) and therefore expected to be weaker.[24] Furthermore, the view along the *b* axis (Figure 2b) shows alternating layers with one layer being made up of two bands, each containing the oxetane rings and the nitromethylene groups. The other layer comprises the tetrazole moieties which interlock emanating from aforementioned bands. Within this layer, the tetrazolyl-substituents themselves align in parallel layers.

2-(3-(Nitromethyl)oxetan-3-yl)-2*H*-tetrazol-5-amine (**3**B) crystallizes in the triclinic space group *P*–1 with four entities per unit cell and a density of 1.584 g cm^{-3} (100 K) corresponding to 1.535 g cm^{-3} at room temperature (Figure 3).

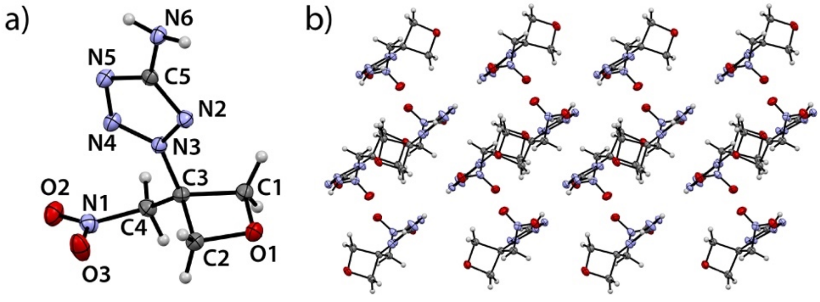

Figure 8.3. a) Molecular structure of compound **3**A in the crystal. Thermal ellipsoids drawn at the 50% probability level. b) View along *b* axis.

In addition, the unit cell is made up of two pairs of crystallographically independent entities. The oxetane ring shows bond angles between 91.5(1)° (O1–C1–C3), 91.3(1)° (O1–C2–C3) down to 85.1(1)° (C1–C3–C2) and 91.5(1)° at the oxetane oxygen atom (C1–O1–C2). The longest bond within the oxetane ring is observed between C1–C3 (1.544(3) Å) and the shortest between O1 and C1 (1.452(2) Å). The oxetane ring is folded with a puckering angle of only 8.82° (100 K) which is surprisingly close to unsubstituted oxetane (10.7(1)°, 90 K).[19] The bond between C3 and N3 is found to be considerably shorter (1.463(2) Å) than a typical bond between a tetrazole nitrogen atom and a sp^3-hybridized carbon atom.[21-23] The bond between the amino group (N6) and carbon atom C5 features a length of 1.363(3) Å and is therefore slightly longer than in the parent compound 1*H*-tetrazol-5-amine (1.333(1) Å).[25] Both amino group and tetrazole ring lie in the same plane. The C3–C4 bond is longer (1.514(3) Å) than typical bonds between sp^3-hybridized carbons,[20] while the C4–N1 bond is longer (1.499(2) Å) than in similar nitroalkanes (1.485 Å).[24] The view along the *b* axis (Figure 3b) shows oxetane rings forming tunnel-like corridors in which the rings are twisted against each other in a pairwise manner so that the endocyclic oxygen atoms point away from each other. The tetrazole substituents are arranged in two different types of adjacent, pairwise parallel layers which intersect at an angle of 11.8°. These types of layers alternate within the crystallographic framework. Similar geometries and bond length were found for the entity not depicted in Figure 3.

5-Azido-2-(3-(Nitromethyl)oxetan-3-yl)-2*H*-tetrazole (**4**) crystallizes in the monoclinic space group P2$_1$/n with four formula units per cell and a density of 1.646 g cm^{-3} (123 K) corresponding to a room temperature density of 1.601 g cm^{-3} (Figure 4).

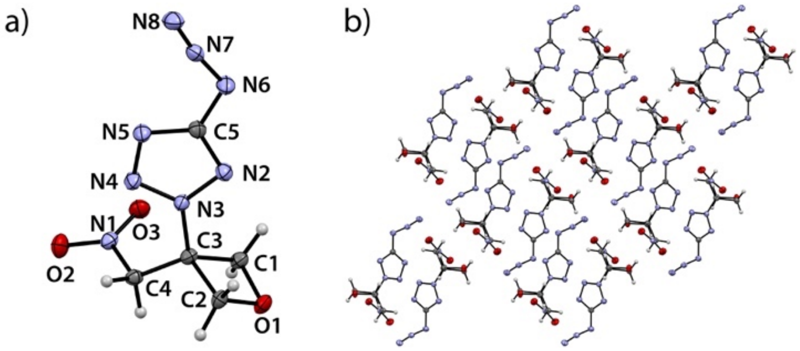

Figure 8.4. a) Molecular structure of compound **4** in the crystal. Thermal ellipsoids drawn at the 50% probability level. b) View along *b* axis.

As in aforementioned compounds, extreme bond angles are found within the ring ranging from 91.49(8)° (O1–C1–C3) over 91.42(7)° (O1–C2–C3) to values of only 84.94(7)° (C1–C3–C2). The largest angle is found at the oxetane oxygen atom (C1–O1–C2, 91.73(7)°). The shortest bond is observed between O1 and C1 (1.451(1) Å), while the longest is again found between C2 and C3 (1.543(1) Å). A puckering angle of 6.85° (123 K) is found, which is rather small for a substituted oxetane species taking the corresponding angle in the parent compound oxetane into account (8.7(2)° at 140 K).[19] The bond between oxetane and tetrazole ring (C3–N3) shows a length of 1.463(1) Å and is thereby shorter than in comparable *N*2-alkylsubstituted tetrazoles.[21-23] The azido group is twisted against the tetrazole ring plane by an angle of 12.41° and angulated (N8–N7–N6, 172.0(1)°) which can be explained by hyperconjugation effects.[26] The single bond between C4 and N1 is significantly longer (1.498(1) Å) than a typical bond between a sp^3-hybridized carbon atom and a nitro group (1.485 Å).[24] Therefore, it is assumed to be rather weak. The view along *b* axis (Figure 4b) shows an arrangement of the formula units in alternating layers – one layer consisting of two parallelly arranged bands containing both the oxetane- and nitromethylene moiety, while the other is made up by interlocking tetrazole moieties originating from the aforementioned bands. In this arrangement, two formula units oppose each other rotated by 180°, causing the opposing oxetane rings to point in opposite directions. Correspondingly, the tetrazole moieties originate from these bands in opposite spatial directions and are rotated by 180° with respect to each other. They thus form pairwise parallel layers with a spacing of 0.483 Å. In the crystal, these paired layers occur in two spatial orientations and intersect at an angle of 70.9°.

5-Nitro-2-(3-(Nitromethyl)oxetan-3-yl)-2*H*-tetrazole (5) crystallizes in the orthorhombic space group *P*bca with eight formula units per cell at a density of 1.729 g cm^{-3} (123 K) corresponding to 1.682 g cm^{-3} at ambient conditions (Figure 5).

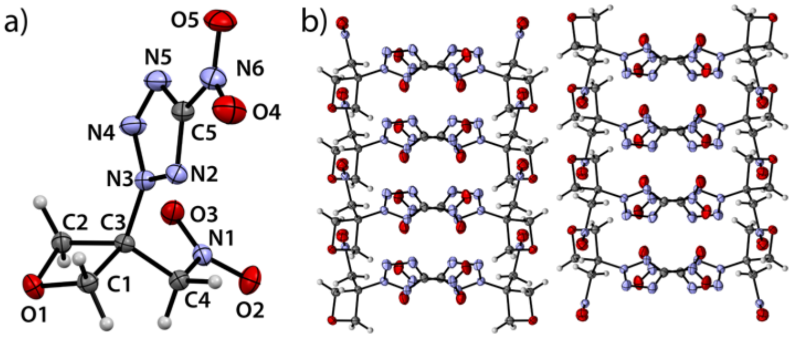

Figure 8.5. a) Molecular structure of compound **5** in the crystal. Thermal ellipsoids drawn at the 50% probability level. b) View along *a* axis.

The largest bond angle (91.9(1)°) of the oxetane motif is found at the oxygen atom (C1–O1–C2), while all other endocyclic angles range from 91.1(1)° (C3–C2–O1) over 91.0(1)° (O1–C1–C3) down to 85.2(1)° (C2–C3–C1). The shortest bond is observed between O1 and C1 with a length of 1.446(2) Å, while the longest (1.544(2) Å) is found between C1 and C3. The ring puckering angle was determined to be 10.1° (123 K) and is thus again close to the puckering angle of the unsubstituted parent compound at a comparable temperature, as in the compounds described above.[19] Since the substitution of the ring often leads to an increase of disadvantageous eclipsing interactions and correspondingly larger puckering angles, the influences of the substituents in compounds **2**–**5** seem to compensate each other to a certain extent. The nitro group is slightly rotated with respect to the tetrazole plane by an angle of 6.38°. The C3–N3 bond shows a slightly increased length of 1.469(2) Å, which is longer and thereby weaker than in compounds **2**, **3** and **4** and may correlate with the lower thermal stability of compound **5**. The C5–N6 bond features a length according to expectation (1.450(2) Å).[20] The C3–C4 shows a typical bond length of (1.509(2) Å).[20] The C4–N1 bond is slightly longer (1.496(2) Å) than in comparable compounds.[24] The view along *a* axis (Figure 5b) shows the same layered structure as described for compound **4**. One layer contains interlocked tetrazole moieties, the other two parallel bands contain the oxetane scaffold. Also, two formula units oppose each other being rotated by 180°. Thereby, the tetrazole moieties form two types of pairwise parallel layers (distance: 1.227 Å) which intersect at an angle of 76.9°.

8.2.3 Hirshfeld Analysis

When an energetic material is exposed to a mechanical stimulus, a vertical compression and/or a horizontal sliding of layers in the crystal leads to internal strains.[27] If the associated strain energy is high enough, bonds may break and trigger the material's decomposition.[28] Here, intermolecular interactions can impose a destabilizing or stabilizing effect depending on their nature and strength. For this reason, the sensitivity of an energetic material is linked to close contact interactions in the crystal.[28,29] A powerful tool to analyze these interactions is Hirshfeld analysis. The method's fundamentals were already developed in 1977.[30] Since then, the method was continuously improved – especially by Spackman and McKinnon.[31,32] Ultimately, the development of the CrystalExplorer software in 2004 allowed a user-friendly application.[33] However, the method was not applied to energetic materials until 2014.[34] Since then, Hirshfeld analysis is used to estimate the sensitivity of energetic materials and to render experimentally assessed values plausible based on the crystal structure. As suitable crystallographic data were obtained for compounds **2**A, **3**A, **3**B, **4** and **5**, we calculated their Hirshfeld surfaces (HFS) using CrystalExplorer V17.5.[35] On this surface, close contacts are indicated by red dots. To summarize all interactions and their distances $d_i + d_e$ (d_i, distance from HFS to the closest atom interior; d_e, distance from HFS to the closest atom exterior), we used a 2D fingerprint plot (Figure 6).[32,35]

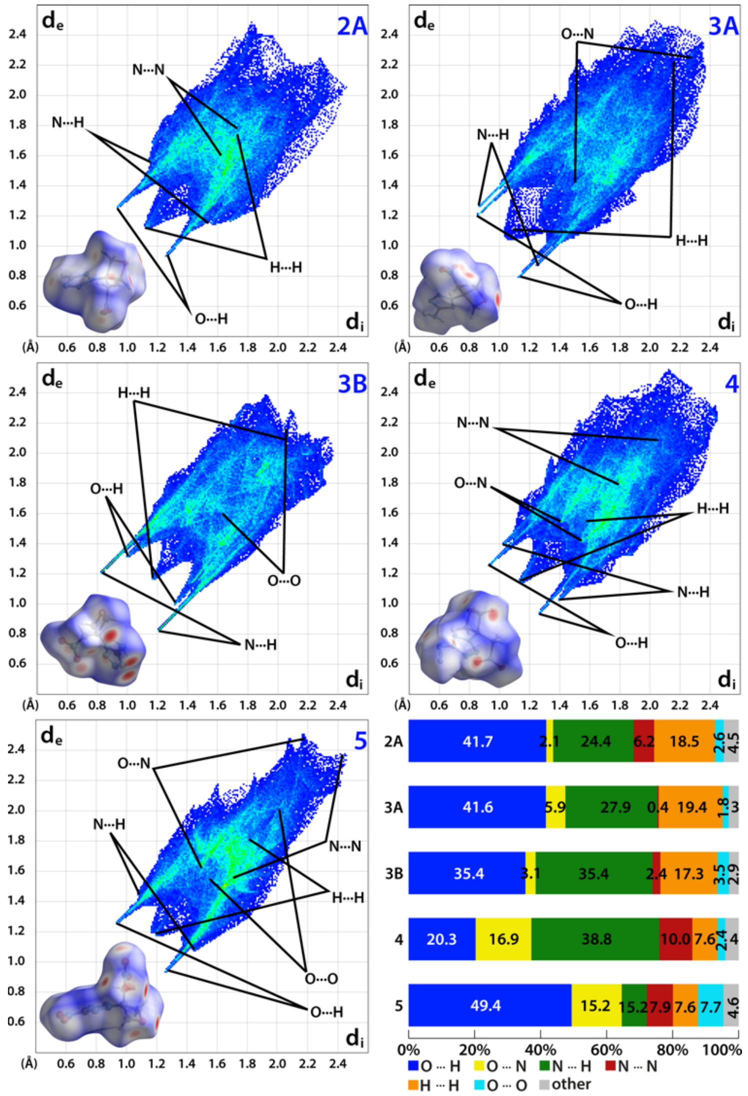

Figure 8.6. Calculated Hirshfeld surfaces and 2D fingerprint plots of compounds **2**A, **3** (A, B), **4** and **5** showing important close contacts in the crystal. The bar chart summarizes the interaction percentages.

Distances larger than 3 Å correspond to weak interactions, distances below 2.4 Å are linked to strong interactions.[28] The analysis of the interaction populations and their distance allows a weighting of their influence. In general, insensitive compounds are often designated by high populations of strong, stabilizing O···H and N···H interactions which form a rather rigid intermolecular 3D network which counteracts a detrimental sliding of layers to a certain extent.[28] In addition, correspondingly low percentages of destabilizing H···H, O···N and O···O interactions are found among insensitive compounds. For example, compound **2**A exhibits a very high fraction of strong ($d_i + d_e < 2.4$ Å), stabilizing O···H (41.7%) and N···H interactions (24.4%). These are contrasted by repulsive, destabilizing H···H interactions (18.5%) and N···N interactions (6.2%). However, the 2D Fingerprint plot shows that only a small proportion of the H···H interactions are strong ($d_i + d_e < 2.4$ Å). Therefore, they only cause minor destabilization.

The same is true for the N···N interactions, which are also weak according to their distance ($d_i + d_e > 3.2$ Å). All remaining interactions have a negligible contribution below 5%. Hence, a very insensitive material can be expected which correlates well to obtained values for its impact (IS) and friction sensitivity (FS) with values of 40 J and 360 N, respectively. Very similar proportions for strong, stabilizing O···H (41.6%) and N···H interactions (27.9%) were found for compound **3**A. These are counterbalanced by weak O···N interactions (5.9%) and H···H interactions (19.4%), which are also mostly weak. Compared to **2**A, a similar sensitivity can be assumed which was confirmed in practice (IS: 35 J, FS: 360 N). The difference of 5 J is likely to be linked to the higher melting temperature of **3**A, which allows less energy to be dissipated by partial melting upon impact. As the ratio of stabilizing to destabilizing interactions barely changes for **3**B, a similar sensitivity was expected and found (IS: 40 J, FS: 360 N). Since 5-azido-1*H*-tetrazole is very sensitive (IS: < 1 J, FS: < 5 N)[14], compound **4** was expected to show a slightly lower but still comparable sensitivity. However, the high proportion of strong and stabilizing O···H (20.3%) and N···H (38.8%) interactions is only counteracted by O···N (16.9%), N···N (10%), and H···H interactions (7.6%) which are mostly weak giving the impression of a rather low sensitivity. Indeed, surprisingly low values were assessed (IS: 2–3 J, FS: 120 N). Accordingly, the estimation based on Hirshfeld analysis turned out to be correct. Compound **5**, which is a derivative of the also very sensitive 5-nitro-2*H*-tetrazole (IS: < 1 J, FS: < 5 N)[15], was found to be dominated by strong, stabilizing O···H (49.4%) and N···H (7.6%) interactions. These are contrasted by a small fraction of destabilizing N···N (7.9%), H···H (7.6%), O···N (15.2%), and O···O (7.7%) interactions. As these are largely very weak, a sensitivity comparable to compound **4** was assumed. Against expectation, practical tests revealed an impressively insensitive material (IS: 40 J, FS: 360 N). Although similar sensitivities have been expected for compounds **4** and **5**, Hirshfeld analysis estimated correctly that both compounds are significantly less sensitive than the parent tetrazoles and can be handled more safely (Table 1).

8.2.4 Physicochemical and Energetic Properties

The thermal behavior of compound **4** was assessed by differential thermal analysis (DTA) at a heating rate of 5 °C min^{-1}. The thermal stability of all other compounds was assessed by differential scanning calorimetry (DSC) at the same heating rate. The precursor to all compounds, 3-(nitromethylene)oxetane (**1**) melts at 52 °C and decomposes rather early at 165 °C. Regarding compounds **2**–**5**, the lowest thermal stability is observed for compound **5**, which decomposes at 160 °C, while all other compounds (**2**–**4**) decompose in a narrow interval of 182–185 °C. All compounds melt before they decompose. Here, compound **2**A is especially interesting as it melts at 94 °C potentially allowing melt-cast applications. The highest melting point is found for compound **3**A (161 °C). The heats of formation of compounds **2**–**5** were calculated using the Gaussian16 program package on the CBS-4M level of theory using the atomization method.[37,38] All compounds were found to be endothermic with high positive heats of formation between 106.4 and 154.3 kJ mol^{-1}, exceeding common secondary explosives like TNT (–75.3 kJ mol^{-1})[36] and RDX (79.1 kJ mol^{-1})[39], while compound **4** shows an outstanding heat of formation of 487.9 kJ mol^{-1}. The sensitivities toward external stimuli like shock and friction were assessed using a BAM (Bundesanstalt für Materialforschung) drop hammer apparatus and a BAM friction tester according to STANAG 4489 and STANAG 4487 modified instruction, respectively.[40,41] Here, compounds **2** (A, B), **3**B and **5** were found to be insensitive according to the UN classification for the transport of dangerous goods with an impact sensitivity of 40 J and a friction sensitivity of 360 N.[42] The low sensitivity of **5** can be partially explained by stabilizing intermolecular interactions (see Hirshfeld discussion). A marginally lower sensitivity was found for compound **3**A (IS: 35 J, FS: 360 N), which can be classified as "less sensitive".[42] Generally speaking, the impact sensitivity of compound **4** is high (2–3 J), but at the same time surprisingly low taking the very sensitive parent compound 5AzT into account. Furthermore, the IS (3 J) is only marginally below the value of PETN (pentaerythritol tetranitrate) as widely used booster explosive.[16,36] The friction sensitivity is even the same as for RDX (120 N) and half of PETN (60 N).[36] However, compound **4** needs to be classified as "sensitive" to "very sensitive".[42] The energetic performance of compounds **2**–**5** was calculated using the EXPLO5 V6.04 thermochemical code.[43] Compounds **2**A and **3**A show detonation pressures of 17.2 GPa and 16.9 GPa and detonation velocities of 6924 ms^{-1} and 6950 ms^{-1}, respectively. A slightly higher performance was calculated for their corresponding *N*1-isomers (**2**B, **3**B) as they show a higher density and heat of formation (Table 1). The performance of compound **2** (A, B) and **3** (A, B) is therefore notably higher than in case of prior art oxetane monomers like NIMMO (10.6 GPa, 5906 ms^{-1}) and comparable to TNT. Especially high performance was found in case of **4** (20.8 GPa, 7452 ms^{-1}) and **5** (23.5 GPa, 7686 ms^{-1}). Therefore, both compounds are not only superior to prior art energetic oxetanes, but even outperform TNT.[36] To the best of our knowledge, they are currently the most powerful energetic oxetanes known next to 3,3-dinitratooxetane (DNO) that we described recently.[44] However, since DNO decomposes at 93 °C, they offer a better balance between performance, sensitivity, and thermal stability, rendering them the more promising candidates for the preparation of performant energetic polymers.

Table 8.1. Physicochemical and energetic properties of compounds **2**–**5** together with TNT and the prior art monomer NIMMO for comparative purposes.

	2A	**2B**	**3A**	**3B**	**4**	**5**	**TNT**[16,36]	**NIMMO**
Formula	$C_5H_7N_5O_3$		$C_5H_8N_6O_3$		$C_5H_6N_8O_3$	$C_5H_6N_6O_5$	$C_7H_5N_3O_6$	$C_5H_9NO_4$
FW [g·mol^{-1}]	185.14		200.16		226.16	230.14	227.12	147.13
IS[a] [J]	40	40	35	40	2(3)	40	15	> 40
FS[b] [N]	360	360	360	360	120	360	> 353	360
N+O [%]	63.75		65.97		70.77	71.28	60.76	53.02
Ω_{CO}[c] [%]	−47.53		−47.96		−35.37	−20.86	−25.3	−59.81
T_m[d]/ $T_{dec.}$[e] [°C]	94/182	145/169	161/183	129/177	56/185	138/160	81/290	−14/170
ρ[f] [g·cm^{-3}]	1.56	1.59	1.54	1.56	1.60	1.69	1.64	1.19
$\Delta H_f°$[g] [kJ·mol^{-1}]	125.9	154.3	106.4	151.0	487.9	148.1	−219.0	−268.9
				EXPLO5 V 6.04				
$-\Delta_E U°$[h] [kJ·kg^{-1}]	3888	4041	3627	3842	4629	4761	4380	3949
$T_{C\text{-}J}$[i] [K]	2707	2770	2564	2657	3271	3336	3190	2507
$D_{C\text{-}J}$[j] [m·s^{-1}]	6924	7078	6950	7121	7452	7686	6809	5906
$p_{C\text{-}J}$[k] [GPa]	17.2	18.2	16.9	17.9	20.8	23.5	18.7	10.6
V_0[l] [dm^3·kg^{-1}]	760	758	789	789	766	742	639	827

[a] Impact sensitivity (BAM drop hammer, method 1 of 6). [b] Friction sensitivity (BAM friction apparatus, method 1 of 6). [c] Oxygen balance regarding carbon monoxide (Ω_{CO} = (nO − xC − yH/2)(1600/FW). [d] Melting point (DSC, β = 5 °C·min^{-1}). [e] Temperature of decomposition (DSC, β = 5 °C·min^{-1}). [f] Density at 298 K (ρX-ray/1.028). [g] Standard molar enthalpy of formation. [h] Detonation energy. [i] Detonation temperature. [j] Detonation velocity. [k] Detonation pressure at C-J-point. [l] Volume of detonation products.

8.2.5 Bond Dissociation Energy Calculation

Since all compounds, with exception of **5**, decompose in a narrow temperature interval (182–185 °C), a trigger bond inherent to all compounds was anticipated. When this bond breaks under thermal stress, it initiates the exothermic decomposition.[28] As both the oxetane and the 1*H*-tetrazole motif are usually quite thermostable, three bonds were under particular suspicion – the C–N bond between both ring structures, the C–N bond between the exocyclic methylene group and the nitro group as well as the C–C bond between oxetane ring and the nitromethylene group. Therefore, the respective bond dissociation energy (BDE) was calculated on the CBS-QB3 level of theory using **2**A as model compound and its crystal structure as input file for the calculation using Gaussian 16.[38] For this purpose, the molecule was formally split into the radical fragments of interest (Figure 7) and their gas phase enthalpies of formation were calculated.

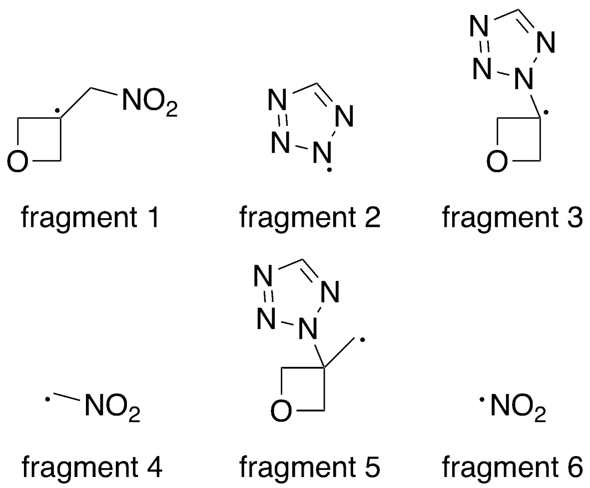

Figure 8.7. Radical fragments used for the BDE calculation.

The obtained values for compound **2**A and each fragment are summarized in Table 2.

Table 8.2. CBS-QB3 enthalpies (Hartree) and gas-phase enthalpies of formation (kJ mol⁻¹).

Fragment	Formula	–H(CBS-QB3) [H]	$\Delta_f H°(g)$ [kJ mol^{-1}]
2A	$C_5H_7N_5O_3$	692.997417	+209.0
1	$C_4H_6NO_3$	435.621358	+67.3
2	CHN_4	257.208636	+581.0
3	$C_4H_5N_4O$	448.828069	+453.7
4	CH_2NO_2	244.028508	+149.8
5	$C_5H_7N_4O$	488.049907	+441.7
6	NO_2	204.848641	+26.7

The BDE is obtained as the enthalpy difference between the molecule and the combined enthalpy of the respective fragments. Hereby, a BDE of 439.3 kJmol^{-1} was assessed for the C–N bond between tetrazole and oxetane ring while the C–C bond shows a similar BDE of 394.5 kJmol^{-1}. As a considerably lower value of 259.4 kJmol^{-1} was found for the C–NO_2 bond, we identified it as trigger bond. Since compound **5** decomposes even earlier, the C–NO_2 bond of the tetrazole motif can be assumed as trigger bond in this case. To increase the thermal stability of the investigated compounds, the nitro group should be reduced to provide an amino group. This would also allow further functionalization of the compounds.

8.2.6 Hot Plate Test

The *N*2-isomers of compounds **2**–**5** were subjected to a hot plate test. In each case, 50 mg were placed on a copper witness plate which was subsequently heated by means of a Bunsen burner (see SI). Compounds **2**A, **3**A, and **5** showed a violent deflagration with flame heights of up to 70 cm. Contrary to this, azidotetrazole-derivative **4** detonated violently upon heating leaving a dent on the witness plate. Instantaneous detonation of compound **4** was also observed when small crumbs were exposed to a flame on a steel syringe needle, further proving its very fast deflagration-to-detonation transition (DDT) even in small, unconfined amounts. To the best of our knowledge, **4** is the first oxetane-based compound to exhibit this behavior otherwise characteristic of primary explosives. Therefore, the compound may represent an important leap toward yet unknown oxetane-based and potentially polymerizable primary explosives.

8.2.7 Hot Needle Test

The hot plate test of compound **4** did not only show its astonishing explosive power, but also its capability to undergo DDT like an primary explosives.[16] However, to be classified as such, additional criteria need to be fulfilled. One is a positive response (detonation) upon contact of a needle heated to red heat with a Bunsen burner (Figure 8).

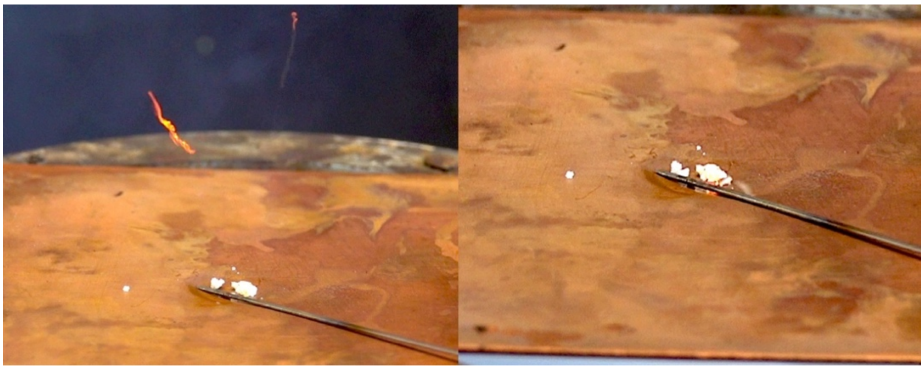

Figure 8.8. Partial deflagration of unconfined compound **4** upon contact to a hot needle.

In case of compound **4**, crackling noises indicated partial DDT, but the material mainly deflagrates while spreading on the copper plate due to gas generation. This behavior can be explained by the low melting point of compound **4** (55.8 °C), which allows the material to dissipate external thermal energy. As a consequence, only material with direct contact to the needle is initiated, while surrounding material melts, deflagrates, or spreads. A more positive result is obtained when the material is prevented from spreading by confining it under a Tesafilm® strip (Figure 9).

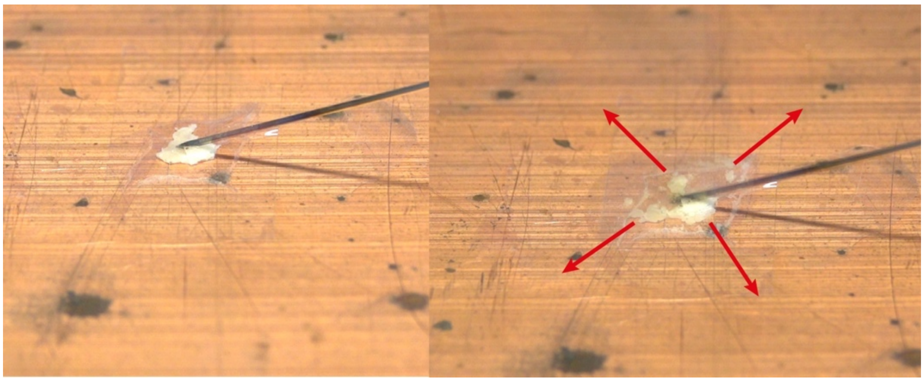

Figure 8.9. Compound **4** confined under Tesafilm (left) and scattered material after partial detonation upon contact to a hot needle.

In this case, partial detonation is observed. As neither complete detonation nor full deflagration occurred, the test is negative. However, compound **4** is very close to the typical behavior of a primary explosive.

8.2.8 Initiation Test

Another criterion for the classification as primary explosive is a positive initiation test. In this test, a small sample (50–100 mg) is placed on top of a booster explosive of rather high sensitivity (PETN) within a copper shell. The shell itself is placed on top of a copper witness plate. Then, the sample is exposed to a spark provided by an electrical igniter. In the case of a positive result, the sample will detonate and thereby trigger detonation of the adjacent booster charge. This causes the copper shell to burst and the witness plate to be perforated (Figure 10).

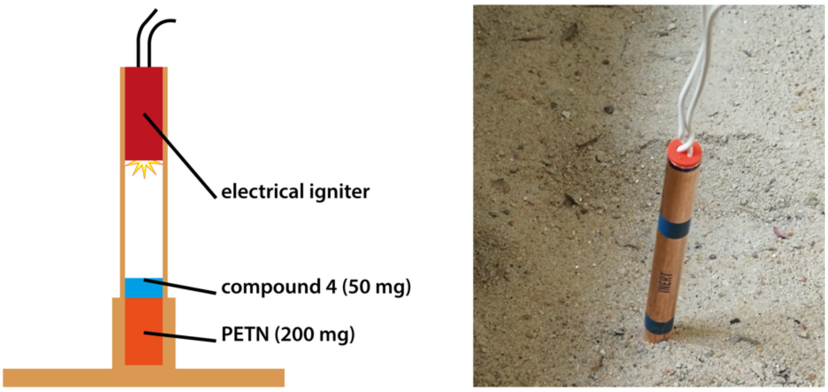

Figure 8.10. Schematic setup of the initiation test (left) and actual test in a sandbox (right).

The test was performed using 50 mg of loosely packed compound **4** and 200 mg of PETN as booster charge. However, the test was negative three times in a row. Analysis of the charge showed that compound **4** had only partially melted upon exposure to sparks provided by the electrical ignitor. However, different results may be obtained using additives that improve its spark-response.

8.2.9 Small-Scale Shock Reactivity Test (SSRT)

As their calculated performance is superior to TNT, a SSRT was performed with compounds **4** and **5**. In this test, the shock reactivity (explosiveness) can be determined even below a material's critical diameter and without requiring transition to detonation.[45] Therefore, it combines the advantages of both lead block and gap test[46] requiring amounts of roughly 500 mg. In each test, the same sample Volume V_S is used (284 mm^3). Therefore, the required mass of explosive m_e was calculated by the formula $m_e = V_s \cdot \rho_e \cdot 0.95$ where ρ_e is the density of the explosive. The sample is filled into a perforated steel block with an aluminum witness block underneath and pressed (3 tons, 5 seconds). Subsequently, the charge is fired using a commercial Orica Dynadet C2 detonator (Figure 11).

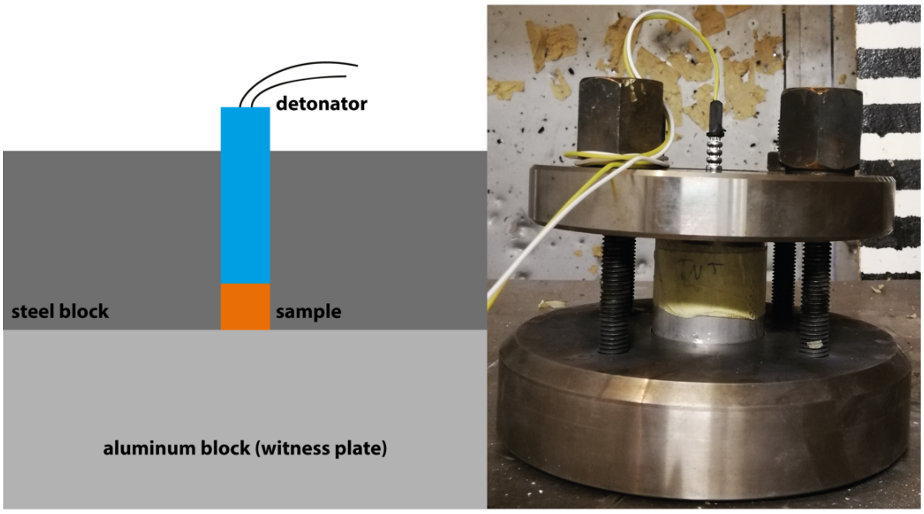

Figure 8.11. Schematic (left) and actual SSRT setup (right).

The obtained witness plate dents were measured using a profilometer to compare the relative performance. As compounds **4** and **5** are superior to TNT according to EXPLO5 calculations, it was used as reference. Table 3 summarizes the employed amounts and the corresponding dent volumes.

Table 8.3. Results of the SSRT. Mass of explosive *versus* dent volume.

	4	**5**	**TNT**
m_e(mg)	411	454	464
D_V (mm^3)	917	715	971
D_V/m_e (mm^3/mg)	2.23	1.57	2.09

As volume-based method (284 mm^3 per sample), the SSRT shows the largest indentation for TNT, followed by compound **4** and **5**. Here, the result for compound **5** seems to contradict the calculated performance. However, the low dent volume may be attributed in part to the fact that **5** partially liquefied during pressing causing a reduced density. This in turn negatively affects the performance.[16] We assume the impurification with the *N*1-isomer as cause of this behavior. Compound **4** actually shows a performance comparable to TNT as expected. Further, when the dent volume is correlated with the employed mass (mm^3/mg), compound **4** indeed outperforms TNT. This agrees well with the EXPLO5 calculation and a higher performance can be anticipated for the pure (solid) *N*2-isomer of compound **5**.

8.3 Conclusions

By aza-Michael addition between the commercially available 3-(nitromethylene)oxetane and selected tetrazoles, four new energetic oxetane derivatives were prepared by simple but elegant one-step syntheses. Each product (isomeric mixture) was obtained in moderate to high yield proving the excellent acceptor properties of nitroalkene **1**, especially with respect to the low nucleophilicity of 5-azido-1*H*-tetrazole and 5-nitro-2*H*-tetrazole. The products form two groups – compounds **2** and **3** are fully based on commercially available materials and inexpensive tetrazoles while compounds **4** and **5** have been prepared from tetrazoles that belong to the most nitrogen-rich and powerful of their kind. These have been rarely used as building blocks for energetic materials due to their high sensitivity and low thermostability. However, compounds **4** and **5** successfully demonstrate that 5-azido-1*H*-tetrazole and 5-nitro-2*H*-tetrazole are tamable and can provide derivatives with moderate (**4**) or even surprisingly low sensitivity (**5**). Despite their non-elaborate synthesis and simple structure, the former group (**2**, **3**) exhibits a performance notably higher than state-of-the-art energetic oxetanes. Binders prepared thereof may find application as insensitive, high-performing and rather nitrogen-rich fuels. The other group (**4**, **5**) shows calculated performances higher than in the case of TNT as common secondary explosive. Hence, they are not only superior to prior art monomers (e.g., AMMO, BAMO, NIMMO), but are probably among the most powerful known oxetane derivatives, along with DNO. They are therefore suitable to prepare binders for energetic formulations where performance is of utmost importance. In addition, compound **4** is a first leap toward oxetane-based and potentially polymerizable primary explosives, which are yet unknown. As the C–NO_2 bond of the target compounds acts as trigger bond, a reduction of the nitro group is likely to provide higher thermostabilities next to the possibility of further functionalization. Since 3-

(nitromethylene)oxetane readily reacts with a broad variety of carbon- and heteroatom nucleophiles, a wide variety of known energetic compounds can be directly employed as Michael donors (e.g., azoles). We therefore conclude that it represents a very potent scaffold for the rapid synthesis of a large number of chemically diverse energetic oxetane monomers. We further anticipate that it will thereby facilitate the preparation of energetic binders with enhanced performance to mitigate the existing performance gap between binders and highly performant fillers in energetic formulations.

Associated Content

Electronic Supplementary Information (ESI) available: Synthetic procedures; NMR spectra (^{1}H, ^{13}C, ^{14}N); Crystallographic information; DTA and DSC graphs; Hot plate test of compounds **2**–**5** (video, hot plate test.mp4); Hot needle test of compound **4** (video, hot needle test.mp4); Flame test of compound **4** (video, flame test.mp4);
X-ray data for compounds **1** CCDC: 2119618), **2**A (CCDC: 2119623), **2**B (CCDC: 2119795), **3**A (CCDC: 2119619), **3**B (CCDC: 2119620), **3**C (CCDC: 2119621), **4** (CCDC: 2119622), **5** (CCDC: 2119624).
See DOI: 10.1039/D2MA00088A

Abbreviations

AMMO, 3-azidomethyl-3-methyloxetane; BAMO, 3,3-bis(azidomethyl)oxetane; CL20, 2,4,6,8,10,12-hexanitro-2,4,6,8,10,12-hexaazaisowurtzitane; EA, ethyl acetate; K_2DNABT, potassium 1,1'-dinitramino-5,5'-bistetrazolate; NIMMO, 3-nitratomethyl-3-methyloxetane; RDX, hexahydro-1,3,5-trinitro-1,3,5-triazin; TNT, 2,4,6-trinitrotoluene.

Acknowledgements

Financial support by the Ludwig-Maximilian-University (LMU), the Office of Naval Research (ONR) under grant no. ONR.N00014-16-1-2062 and the Strategic Environmental Research and Development Program (SERDP) under contract no. WP19-1287 is gratefully acknowledged. The authors also thank Stefan Huber for his help regarding the determination of sensitivities. Furthermore, we thank Marcus Lommel for providing generous amounts of sodium 5-nitrotetrazolate.

References

[1] Fischer, E. Ueber die Hydrazinverbindungen; Erste Abhandlung. *Liebigs Ann. Chem.* **1878**, *190*, 67-183.

[2] Stierstorfer, J. Advanced Energetic Materials Based on 5-Aminotetrazole. Ph. D. Dissertation, Ludwig-Maximilian University (LMU) Munich, Munich, Germany, **2009**.

[3] Koldobskii, G. I.; Ostrovskii, V. A.; Popavskii, V. S. Advances in the chemistry of tetrazoles (review). *Chem. Heterocycl. Compd.* **1981**, *17*, 965-988.

[4] Benson, F. R. *The Tetrazoles*; Vol. 8; Wiley: New York, **1967**.

[5] Uchida, M.; Komatsu, M.; Morita, S.; Kanbe, T.; Nakagawa, K. Studies on Gastric Antiulcer Active Agents. II.: Synthesis of Tetrazole Alkanamides and Related Compounds. *Chem. Pharm. Bull.* **1989**, *37*, 322-326.

[6] Fischer, N.; Klapötke, T. M.; Stierstorfer, J.; Wiedemann, C. 1-Nitratoethyl-5-nitriminotetrazole derivatives – Shaping future high explosives. *Polyhedron* **2011**, *30*, 2374-2386.

[7] Klapötke, T. M.; Stein, M.; Stierstorfer, J. Salts of 1H-Tetrazole – Synthesis, Characterization and Properties. *Z. Anorg. Allg. Chem.* **2008**, *634*, 1711-1723.

[8] Fischer, D.; Klapötke, T. M.; Stierstorfer, J. Potassium 1,1′-Dinitramino-5,5′-bistetrazolate: A Primary Explosive with Fast Detonation and High Initiation Power. *Angew. Chem. Int. Ed.* **2014**, *53*, 8172-8175.

[9] Fischer, N.; Fischer, D.; Klapötke, T. M.; Piercey, D. G.; Stierstorfer, J. Pushing the limits of energetic materials – the synthesis and characterization of dihydroxylammonium 5,5′-bistetrazole-1,1′-diolate. *J. Mater. Chem.* **2012**, *22*, 20418-20422.

[10] Ang, H. G.; Pisharath, S. *Energetic Polymers: Binders and Plasticizers for Enhancing Performance*; Wiley-VCH: Weinheim, **2012**.

[11] Wuitschik, G. Oxetanes in Drug Discovery. Ph. D. Dissertation, Swiss Federal Institute of Technology (ETH) Zürich, Zürich, Switzerland, **2008**.

[12] Burkhard, J. A.; Wuitschik, G.; Rogers-Evans, M.; Müller, K.; Carreira, E. M. Oxetanes as Versatile Elements in Drug Discovery and Synthesis. *Angew. Chem. Int. Ed.* **2010**, *49*, 9052-9067.

[13] Bull, J. A.; Croft, R. A.; Davis, O. A.; Doran, R.; Morgan, K. F. Oxetanes: Recent Advances in Synthesis, Reactivity, and Medicinal Chemistry. *Chem. Rev.* **2016**, *116*, 12150-12233.

[14] Stierstorfer, J.; Klapötke, T. M.; Hammerl, A.; Chapman, R. D. 5-Azido-1H-tetrazole – Improved Synthesis, Crystal Structure and Sensitivity Data. *Z. Anorg. Allg. Chem.* **2008**, *634*, 1051-1057.

[15] Miró Sabaté, C. H. Azole-based energetic materials. Ph. D. Dissertation, Ludwig-Maximilian University (LMU) Munich, Munich, Germany, **2008**.

[16] Klapötke, T. M. *Chemistry of High-Energy Materials*; 5th ed.; DeGruyter: Boston, **2019**.

[17] Klapötke, T. M.; Piercey, D. G.; Mehta, N.; Oyler, K. D.; Jorgensen, M.; Lenahan, S.; Salan, J. S.; Fronabarger, J. W.; Williams, M. D. Preparation of High Purity Sodium 5-Nitrotetrazolate (NaNT): An Essential Precursor to the Environmentally Acceptable Primary Explosive, DBX-1. *Z. Anorg. Allg. Chem.* **2013**, *639*, 681-688.

[18] McLaughlin, M.; Yazaki, R.; Fessard, T. C.; Carreira, E. M. Oxetanyl Peptides: Novel Peptidomimetic Modules for Medicinal Chemistry. *Org. Lett.* **2014**, *16*, 4070-4073.

[19] Luger, P.; Buschmann, J. Oxetane: the first x-ray analysis of a nonsubstituted four-membered ring. *J. Am. Chem. Soc.* **1984**, *106*, 7118-7121.

[20] Orpen, A. G.; Brammer, L.; Allen, F. H.; Kennard, O.; Watson, D. G.; Taylor, R. In *Struct. Correl.* **1994**, p 752-858.

[21] Martirosyan, A. O.; Aleksanyan, M. V.; Terzyan, S. S.; Ter-Zakharyan, Y. Z.; Agababyan, R. V.; Karapetyan, A. A.; Mndzhoyan, S. L.; Tamazyan, R. A. Synthesis and Molecular and Crystal Structure of 1-(5-Benzyl-2-tetrazolyl)-1-cyclopentanecarboxylic Acid. Penicillin and Cephalosporins Based on This Acid. *Pharm. Chem. J.* **2001**, *35*, 169-171.

[22] Polyakova, I. N.; Saraev, V. V.; Gavrilov, A. S.; Golod, E. L. Crystal and molecular structure of four adamantyl-substituted tetrazoles. *Crystallogr. Rep.* **2009**, *54*, 441-448.

[23] Han, F.; Yang, L.; Li, Z.; Xia, C. Acidic-functionalized ionic liquid as an efficient, green and reusable catalyst for hetero-Michael addition of nitrogen, sulfur and oxygen nucleophiles to α,β-unsaturated ketones. *Org. Biomol. Chem.* **2012**, *10*, 346-354.

[24] Lam, Y.-L.; Koh, L. L.; Huang, H. H. IR spectra, crystal structure, dipole moment, ab initio and AM1 study of 1,2-dinitroethane. *J. Chem. Soc., Perkin Trans. 2* **1993**, 175-180.

[25] Fujihisa, H.; Honda, K.; Obata, S.; Yamawaki, H.; Takeya, S.; Gotoh, Y.; Matsunaga, T. Crystal structure of anhydrous 5-aminotetrazole and its high-pressure behavior. *CrystEngComm* **2011**, *13*, 99-102.

[26] Alsfasser, R.; Janiak, C.; Klapötke, T. M.; Meyer, H.-J. Nichtmetallchemie. In *Moderne Anorganische Chemie*, 3rd ed.; Riedel. E. (Ed.); De Gruyter: Berlin, New York, **2008**; pp 1-168.

[27] Zhang, J.; Zhang, Q.; Vo, T. T.; Parrish, D. A.; Shreeve, J. n. M. Energetic Salts with π-Stacking and Hydrogen-Bonding Interactions Lead the Way to Future Energetic Materials. *J. Am. Chem. Soc.* **2015**, *137*, 1697-1704.

[28] Dosch, D. E.; Reichel, M.; Born, M.; Klapötke, T. M.; Karaghiosoff, K. Investigation of Structure–Property Relationships of Three Nitroaromatic Compounds: 1-Fluoro-2,4,6-trinitrobenzene, 2,4,6-Trinitrophenyl Methanesulfonate, and 2,4,6-Trinitrobenzaldehyde. *Cryst. Growth Des.* **2021**, *21*, 243-248.

[29] Reichel, M.; Dosch, D.; Klapötke, T.; Karaghiosoff, K. Correlation between Structure and Energetic Properties of Three Nitroaromatic Compounds: Bis(2,4-dinitrophenyl) Ether, Bis(2,4,6-trinitrophenyl) Ether, and Bis(2,4,6-trinitrophenyl) Thioether. *J. Am. Chem. Soc.* **2019**, *141*, 19911-19916.

[30] Hirshfeld, F. L. Bonded-atom fragments for describing molecular charge densities. *Theor. Chim. Acta* **1977**, *44*, 129-138.

[31] McKinnon, J. J.; Mitchell, A. S.; Spackman, M. A. Hirshfeld Surfaces: A New Tool for Visualising and Exploring Molecular Crystals. *Chem. - Eur. J.* **1998**, *4*, 2136-2141.

[32] Spackman, M. A.; McKinnon, J. J. Fingerprinting intermolecular interactions in molecular crystals. *CrystEngComm* **2002**, *4*, 378-392.

[33] McKinnon, J. J.; Spackman, M. A.; Mitchell, A. S. Novel tools for visualizing and exploring intermolecular interactions in molecular crystals. *Acta Cryst. B.* **2004**, *60*, 627-668.

[34] Ma, Y.; Zhang, A.; Xue, X.; Jiang, D.; Zhu, Y.; Zhang, C. Crystal Packing of Impact-Sensitive High-Energy Explosives. *Cryst. Growth Des.* **2014**, *14*, 6101-6114.

[35] Turner, M. J.; McKinnon, J. J.; Wolff, S. K.; Grimwood, D. J.; Spackman, P. R.; Jayatilaka, D; Spackman, M. A. CrystalExplorer17 (**2017**). University of Western Australia. https://hirshfeldsurface.net.

[36] Klapötke, T. M. *Energetic Materials Encyclopedia*; Vol. 1–3; De Gruyter: Berlin, Boston, **2021**.

[37] Altenburg, T.; Klapötke, Thomas M.; Penger, A.; Stierstorfer, J. Two Outstanding Explosives Based on 1,2-Dinitroguanidine: Ammonium- dinitroguanidine and 1,7-Diamino-1,7-dinitrimino-2,4,6-trinitro-2,4,6-triazaheptane. *Z. Anorg. Allg. Chem.* **2010**, *636*, 463-471.

[38] Frisch, M. J.; Trucks, G. W.; Schlegel, H. B.; Scuseria, G. E.; Robb, M. A.; Cheeseman, J. R.; Scalmani, G.; Barone, V.; Petersson, G. A.; Nakatsuji, H.; Li, X.; Caricato, M.; Marenich, A. V.; Bloino, J.; Janesko, B. G.; Gomperts, R.; Mennucci, B.; Hratchian, H. P.; Ortiz, J. V.; Izmaylov, A. F.; Sonnenberg, J. L.; Williams; Ding, F.; Lipparini, F.; Egidi, F.; Goings, J.; Peng, B.; Petrone, A.; Henderson, T.; Ranasinghe, D.; Zakrzewski, V. G.; Gao, J.; Rega, N.; Zheng, G.; Liang, W.; Hada, M.; Ehara, M.; Toyota, K.; Fukuda, R.; Hasegawa, J.; Ishida, M.; Nakajima, T.; Honda, Y.; Kitao, O.; Nakai, H.; Vreven, T.; Throssell, K.; Montgomery Jr., J. A.; Peralta, J. E.; Ogliaro, F.; Bearpark, M. J.; Heyd, J. J.; Brothers, E. N.; Kudin, K. N.; Staroverov, V. N.; Keith, T. A.; Kobayashi, R.; Normand, J.; Raghavachari, K.; Rendell, A. P.; Burant, J. C.; Iyengar, S. S.; Tomasi, J.; Cossi, M.; Millam, J. M.;

Klene, M.; Adamo, C.; Cammi, R.; Ochterski, J. W.; Martin, R. L.; Morokuma, K.; Farkas, O.; Foresman, J. B.; Fox, D. J., Gaussian 16 Rev. C.01, **2016**.

[39] Krien, G.; Licht, H. H.; Zierath, J. Thermochemische untersuchungen an nitraminen. *Thermochim. Acta* **1973**, *6*, 465-472.

[40] NATO STANAG 4489: *Explosives. Impact Sensitivity Tests*; NATO Standardization Office, Brussels, Belgium, **1999**.

[41] NATO STANAG 4487: *Explosives. Friction Sensitivity Tests*; NATO Standardization Office, Brussels, Belgium, **2002**.

[42] United Nations (UN), UN Recommendations on the Transport of Dangerous Goods, Manual of Tests and Criteria, **2009**.

[43] Sućeska, M., EXPLO5, Version 6.04, Brodarski Institute, Zagreb, **2017**.

[44] Klapötke, T. M.; Born, M.; Fessard, T.; Göttermann, L.; Stierstorfer, J.; Voggenreiter, M. 3,3-Dinitratooxetane - An Important Leap Towards Energetic Oxygen-Rich Monomers and Polymers. *Chem. Commun.* **2021**, *57*, 2804-2807.

[45] Felts, J. E.; Sandusky, H. W.; Granholm, R.H. Development of the small-scale shock sensitivity test. In: *AIP Conference Proceedings*, American Institute of Physics, College Park, MD, **2009**, *1195*, 233-236.

[46] Köhler, J.; Meyer, R.; Homburg, A. *Explosives*; 10th ed.; Wiley-VCH: Weinheim, **2008**.

8.4 Supporting Information

8.4.1 Experimental Part

General information

Caution! Even though we have not experienced any difficulties with the handling of described materials, all compounds are energetic materials with certain sensitivities toward shock, friction and electrostatic discharge. Particular caution is required in case of the 5-azido-1*H*-tetrazole and 5-nitro-2*H*-tetrazole as well as compound **4**. Therefore, proper safety precautions (safety goggles, face shield, earthed equipment and shoes, Kevlar gloves and ear plugs) have to be applied while synthesizing and handling the described compounds.

Chemicals and solvents were employed as received (Sigma-Aldrich, Acros, TCI, Spirochem AG). ^{1}H, ^{13}C and ^{14}N spectra were recorded on a Bruker AMX 400 instrument. The chemical shifts refer to tetramethylsilane (^{1}H, ^{13}C) and nitromethane (^{14}N). Decompositions temperatures were either determined on a Mettler Toledo DSC822e device at a heating rate of 5 °C min^{-1} using 40 µL aluminum crucibles and nitrogen purge gas at a flow rate of 30 mL min^{-1} or using a OZM Research DTA 552-Ex instrument. DSC evaluations of thermal behavior were performed using the STAR^{e} Software Version 16.20 while DTA measurements were evaluated using Meavy 2.1.2 software. Infrared (IR) spectra were recorded using a Perkin-Elmer Spektrum One FT-IR instrument. Raman spectra were obtained using a Bruker MultiRam FT Raman spectrometer and a neodymium-doped yttrium aluminum garnet (Nd:YAG) laser (λ = 1064 nm, P = 1074 mW). Elemental analyses were performed with an Elementar Vario el by pyrolysis and subsequent gas analysis. Retention factors refer to a 3:1:1 mixture of ethyl acetate, toluene and petrol ether using silica (SiO_2) TLC plates. The sensitivity data were collected using a BAM (Bundesanstalt für Materialforschung) drop hammer according to STANAG 4489[1] modified instruction as well as a BAM friction tester according to STANAG 4487[2] modified instruction. The classification of the tested compounds was based on the 'UN Recommendations on the Transport of Dangerous Goods'.[3] The dent sizes of the SSRT were measured using a Keyence VR 5100 3D profilometer.

2-(3-(Nitromethyl)oxetan-3-yl)-2*H*-tetrazole (2A) and 1-(3-(nitromethyl)oxetan-3-yl)-1*H*-tetrazole (2B)

3-(Nitromethylene)oxetane (1.00 g, 8.69 mmol) was added to a round bottom flask which was flooded with protective atmosphere (argon) and closed with a silicone rubber septum. Subsequently, a solution of 1*H*-tetrazole (609 mg, 8.69 mmol) in dry acetonitrile (20.0 mL) was added. The septum was pinched with a syringe needle and the reaction mixture heated to 65 °C for 24 h to give a yellow solution. Subsequently, the solvent was removed by rotary evaporation to give the isomeric mixture in quantitative yield (^{1}H NMR, *N*2/*N*1 = 2:1). The isomers were separated by column chromatography (SiO_2, 3:1:1 EA/toluene/petrol ether) to give 925 mg (86%) of compound **2A** and 382 mg (71%) of compound **2B** as colorless solid.

2-(3-(Nitromethyl)oxetan-3-yl)-2*H*-tetrazole (2A).

^{1}H NMR (400 MHz, Acetone-d_6): δ 8.91 (s, 1H, CH), 5.93 (s, 2H, CH_2NO_2), 5.28 (d, 2H, CH_2, *J* = 7.7 Hz), 5.20 (d, 2H, CH_2, *J* = 7.7 Hz). **^{13}C{^{1}H} NMR** (101 MHz, Acetone-d_6): δ 154.3, 78.8, 76.7, 65.8. **^{14}N NMR** (29 MHz, Acetone-d_6): δ −5.7, −92.8. **IR** (ATR, cm^{-1}): $\tilde{\nu}$ 2952 (m), 1557 (s), 1456 (w), 1414 (s), 1380 (s), 1373 (s), 1362 (s), 1346 (m), 1291 (s), 1280 (m), 1261 (m), 1207 (m), 1173 (m), 1129 (m), 1063 (m), 1023 (s), 1003 (m), 986 (vs), 967 (m), 950 (m), 940 (m), 903 (s), 884 (s), 869 (m), 811 (m), 721 (m), 707 (m), 696 (s), 626 (s), 573 (m), 455 (s), 413 (m). **Raman** (1064 nm, 1074 mW, cm^{-1}): $\tilde{\nu}$ 3146 (54), 3025 (54), 2998 (33), 2977 (79), 2951 (79), 2934 (33), 2911 (17), 2892 (25), 1563 (21), 1476 (33), 1420 (21), 1382 (100), 1291 (29), 1279 (25), 1262 (42), 1173 (25), 1144 (17), 1065 (25), 1025 (25), 1004 (38), 986 (21), 967 (29), 907 (29), 869 (17), 628 (17), 452 (21), 414 (58). **Anal. Calcd** for $C_5H_7N_5O_3$: C, 32.44; H, 3.81; N, 37.83. Found: C, 32.36; H, 3.63; N, 36.95. **HRMS** (EI) m/z: $[M]^+$ Calcd. for $C_5H_7N_5O_3$ 185.0549; Found 70.0286 $[C_4H_6O]^+$, 69.0340 $[CHN_4]^+$. **DSC** (T_{onset}, 5 °C min^{-1}): 94.2 °C (m.p.), 182.2 °C (dec.). **R_f** = 0.58. **BAM drop hammer** 40 J. **Friction test** 360 N.

1-(3-(Nitromethyl)oxetan-3-yl)-1*H*-tetrazole (2B).

^{1}H NMR (400 MHz, Acetone-d_6): δ 9.66 (s, 1H, CH), 5.81 (s, 2H, CH_2NO_2), 5.21 (s, 4H, CH_2). **^{13}C{^{1}H} NMR** (101 MHz, Acetone-d_6): δ 143.4, 78.6, 77.9, 62.2. **^{14}N NMR** (29 MHz, Acetone-d_6): δ −5.1, −137.1. **IR** (ATR ,cm^{-1}): $\tilde{\nu}$ 3140 (w), 1560 (vs), 1556 (vs), 1536 (m), 1467 (m), 1460 (m), 1418 (m), 1409 (m), 1382 (s), 1339 (m), 1312 (m), 1257 (w), 1178 (s), 1101 (s), 1067 (w), 1024 (m), 990 (s), 970 (m), 959 (m), 942 (m), 908 (m), 869 (m), 711 (m), 672 (vs), 622 (m), 610 (m), 566 (m), 478 (w). **Raman** (1064 nm, 1074 mW, cm^{-1}): $\tilde{\nu}$ 3142 (36), 2998 (91), 2961 (100), 2905 (64), 2897 (64), 1492 (55), 1467 (27), 1413 (55), 1384 (91), 1351 (27), 1312 (36), 1260 (45), 1181 (27), 1104 (27), 1071 (36), 1025 (64), 973 (36), 911 (45), 871 (27), 487 (27), 408 (64). **Anal. Calcd** for $C_5H_7N_5O_3$: C, 32.44; H, 3.81; N, 37.83. Found: C, 32.42; H, 3.63; N, 37.82. **HRMS** (EI) m/z: $[M]^+$ Calcd. for $C_5H_7N_5O_3$ 185.0549; Found 70.0291 $[C_4H_6O]^+$, 69.0347 $[CHN_4]^+$. **DSC** (T_{onset}, 5 °C min^{-1}): 104.8 °C (phase transition), 144.6 °C (m.p.), 168.5 °C (dec.). **R_f** = 0.34. **BAM drop hammer** 40 J. **Friction test** 360 N.

2-(3-(Nitromethyl)oxetan-3-yl)-2*H*-tetrazol-5-amine (3A) and 1-(3-(nitromethyl)oxetan-3-yl)-1*H*-tetrazol-5-amine (3B)

3-(Nitromethylene)oxetane (1.15 g, 9.99 mmol) and 1*H*-tetrazol-5-amine (0.85 g, 9.99 mmol) were added to a round bottom flask which was flooded with protective atmosphere (argon) and closed with a silicone rubber septum prior to the addition of dry acetonitrile (20.0 mL). The septum was pinched with a syringe needle and the suspension heated to 65 °C for 24 h. Hereby, the initial suspension turned into a solution and back into a suspension as product started to precipitate (*N*2-isomer). Afterward, two-thirds of the total volume were removed by rotary evaporation (~13 mL) and the flask cooled to 5 °C in a refrigerator. The liquid phase was then removed using a syringe and cold (0° C) acetonitrile added (2 mL) and also subsequently collected using same syringe. The remaining wet solid was evaporated to dryness to give 1.47 g (74%) of pure 2-(3-(nitromethyl)oxetan-3-yl)-2*H*-tetrazol-5-amine (**3A**) (*N*2-isomer) as colorless crystals. The collected liquid phase was evaporated and the obtained yellow solid suspended in a solvent mixture (3:1:1 EA/Toluene/petrol ether). The suspension was filtered through a silica plug to remove any traces of compound **3A** and the plug was thoroughly rinsed with aforementioned solvent mixture (3 × 15 mL). The filtrate was evaporated to give crude **3B** as yellow solid which was recrystallized from ethyl acetate by slow evaporation of same at ambient conditions until colorless crystals had formed layered with little ethyl acetate. The supernatant was removed using a syringe to give 71 mg (35%) of 1-(3-(nitromethyl)oxetan-3-yl)-1*H*-tetrazol-5-amine (**3B**). Overall yield (*N*2, *N*1-isomer): 1.54 g (77%).

2-(3-(Nitromethyl)oxetan-3-yl)-2*H*-tetrazol-5-amine (3A).
^{1}H NMR (400 MHz, Acetone-d$_6$): δ 6.34 (s, 2H, NH$_2$), 5.63 (s, 2H, CH$_2$NO$_2$), 5.23 (d, 2H, CH$_2$, *J* = 7.9 Hz), 5.19 (d, 2H, CH$_2$, *J* = 8.0 Hz). **^{13}C{^{1}H} NMR** (101 MHz, Acetone-d$_6$): δ 61.1, 76.8, 77.3, 155.5. **^{14}N NMR** (29 MHz, Acetone-d$_6$): δ −4.1. **IR** (ATR, cm^{-1}): $\tilde{\nu}$ 3300 (m), 3292 (m), 3154 (m), 1660 (m), 1587 (s), 1551 (vs), 1471 (m), 1459 (m), 1419 (m), 1382 (s), 1352 (m), 1319 (m), 1139 (m), 1119 (m), 1104 (s), 992 (s), 874 (m), 785 (s), 753 (m), 708 (s), 686 (m), 649 (m), 625 (m), 568 (m), 554 (m), 525 (m), 511 (m), 426 (m). **Raman** (1064 nm, 1074 mW, cm^{-1}): $\tilde{\nu}$ 3152 (27), 3032 (27), 3007 (36), 2971 (100), 2942 (36), 2897 (64), 1576 (36), 1561 (27), 1482 (64), 1422 (36), 1384 (82), 1353 (36), 1333 (82), 1148 (55), 1104 (36), 1062 (27), 1008 (45), 977 (45), 907 (45), 793 (36), 772 (55), 653 (27), 423 (73), 400 (27). **Anal. Calcd** for $C_5H_8N_6O_3$: C, 30.00; H, 4.03; N 41.99. Found: C, 30.08; H, 4.05; N, 42.24. **HRMS** (EI) m/z: [M]$^+$ Calcd. for $C_5H_8N_6O_3$ 200.0658; Found 200.0654 [M]$^+$, 154.0729 [$C_5H_8N_5O$]$^+$, 116.0348 [$C_4H_6N_5O_3$]$^+$, 70.0291 [$C_4H_6O_3$]$^+$. **DSC** (T_{onset}, 5 °C min^{-1}): 161.0 °C (m.p.), 183.0 °C (dec.). **R_f** = 0.40. **BAM drop hammer** 35 J. **Friction test** 360 N.

1-(3-(Nitromethyl)oxetan-3-yl)-1*H*-tetrazol-5-amine (3B).
^{1}H NMR (400 MHz, Acetone-d$_6$) δ 5.76 (s, 2H, CH$_2$), 5.69 (s, 2H, NH$_2$), 5.20 (d, 2H, CH$_2$, *J* = 7.4 Hz), 5.09 (d, 2H, CH$_2$, *J* = 7.4 Hz). **^{13}C{^{1}H} NMR** (101 MHz, Acetone-d$_6$) δ 168.4, 78.5, 76.6, 64.8. **^{14}N NMR** (29 MHz, Acetone-d$_6$): δ −3.7, −104.4. **IR** (ATR, cm^{-1}): $\tilde{\nu}$ 3410 (w), 3324 (m),3232 (w), 3176 (w), 1634 (m),1589 (m),1550 (vs), 1479 (w), 1460 (m), 1451 (w), 1421 (m), 1382 (s), 1347 (m), 1285 (w), 1256 (m), 1223 (m), 1200 (m), 1159 (w), 1144 (w), 1126 (w), 1076 (m), 998 (m), 968 (s), 908 (m), 868 (m), 809 (m), 756 (m), 717 (m),678 (m), 668 (m), 625 (m), 556 (s), 506 (m), 481 (s), 463 (s), 433 (m), 426 (m), 403 (s). **Raman** (1064 nm, 1074 mW, cm^{-1}): $\tilde{\nu}$ 3050 (25), 3004 (25), 2994 (33), 2977 (67), 2938 (17), 2924 (25), 2897 (25), 2888 (17), 1630 (25), 1565 (33), 1480 (42), 1422 (25), 1384 (92), 1127 (25), 1079 (42), 998 (100), 971 (33), 909 (50), 867 (33), 475(25), 414 (50). **Anal. Calcd** for $C_5H_8N_6O_3$: C, 30.00; H, 4.03; N 41.99. Found: C, 29.99; H, 3.88; N, 41.99. **HRMS** (EI)

m/z: $[M]^+$ Calcd. for $C_5H_8N_6O_3$: 200.0658; Found 200.0654 $[M]^+$, 85.0380 $[CH_3N_5]^+$, 69.0335 $[C_4H_5O_3]^+$. **DSC** (T_{onset}, 5 °C min^{-1}): 129.0 °C (m.p.), 177.0 °C (dec.). $\mathbf{R_f}$ = 0.10. **BAM drop hammer** 40 J. **Friction test** 360 N.

5-Azido-2-(3-(nitromethyl)oxetan-3-yl)-2*H*-tetrazole (4)

3-(Nitromethylene)oxetane (319 mg, 2.77 mmol) was added to a round bottom flask which was flooded with protective atmosphere (argon) and closed with a silicone rubber septum. Subsequently, a solution of 5-azido-1*H*-tetrazole (400 mg, 3.60 mmol, 1.3 eq.) in dry acetonitrile (7.00 mL) was added. The septum was pinched with a syringe needle and the reaction mixture heated to 65 °C for 36 h to give a slightly yellowish solution. The solvent was removed by rotary evaporation to give a yellow oil which was dissolved in DCM (30 mL). The solution was then filtered through a silica plug to remove any traces of surplus 5-azido-1*H*-tetrazole and the silica plug was thoroughly rinsed with DCM (4 × 20 mL). The filtrate was evaporated (rotary evaporation) and the obtained almost colorless oil was layered with a small amount of toluene (3–5 mL). Subsequently, the flask was placed in a refrigerator (−30 °C) overnight causing the formation of large, colorless crystals. Toluene was removed using a syringe and subsequent rotary evaporation afforded 491 mg (78%) of 5-azido-2-(3-(nitromethyl)oxetan-3-yl)-2*H*-tetrazole (**4**) as colorless solid.

$\mathbf{^1H}$ **NMR** (400 MHz, Acetone-d_6): δ 5.89 (s, 2H, CH_2NO_2), 5.25 (d, 2H, CH_2, *J* = 7.7 Hz), 5.17 (d, 2H, CH_2, *J* = 8.4 Hz). $\mathbf{^{13}C\{^1H\}}$ **NMR** (101 MHz, Acetone-d_6): δ 163.5, 78.4, 76.3, 66.5. $\mathbf{^{14}N}$ **NMR** (29 MHz, Acetone-d_6): δ −5.4 (NO_2), −94.8 (N_β), −144.3 (N_γ). **IR** (ATR, cm^{-1}): $\tilde{\nu}$ 2940 (w), 2146 (s), 1555 (s), 1513 (vs), 1467 (m), 1428 (s), 1399 (s), 1381 (s), 1368 (m), 1355 (m), 1346 (m), 1220 (m), 1196 (s), 1070 (w), 1010 (m), 989 (vs), 970 (m), 952 (m), 940 (m), 905 (s), 869 (w), 818 (m), 788 (w), 736 (m), 723 (m), 650 (m), 593 (w), 533 (m), 474 (m), 458 (m). **Raman** (1064 nm, 1074 mW, cm^{-1}): $\tilde{\nu}$ 3011 (40), 2977 (33), 2940 (38), 2153 (30), 1509 (100), 1474 (28), 1430 (16), 1401 (44), 1384 (28), 1370 (26), 1262 (16), 1206 (19), 1197 (31), 1071 (25), 1011 (69), 990 (16), 973 (26), 909 (19), 869 (20), 477 (20), 456 (21), 402 (31). **Anal. Calcd** for $C_5H_6N_8O_3$: C, 26.55; H, 2.67; N, 49.55. Found: C, 26.90; H, 2.82; N, 47.62. **HRMS** (EI) m/z: $[M]^+$ Calcd. for $C_5H_6N_8O_3$ 226.0563; Found 110.0219 $[CN_7]^+$. **DTA** (T_{onset}, 5 °C min^{-1}): 55.8 °C (m.p.), 185.7 °C (dec.). **BAM drop hammer** 2 J. **Friction test** 120 N.

5-Nitro-2-(3-(nitromethyl)oxetan-3-yl)-2*H*-tetrazole (5)

3-(Nitromethylene)oxetane (107 mg, 0.93 mmol) was added to a round bottom flask which was flooded with protective atmosphere (argon) and closed with a silicone rubber septum. Subsequently, a solution of 5-nitro-2*H*-tetrazole (139 mg, 1.21 mmol, 1.3 eq.) in dry acetonitrile (3.00 mL) was added. The septum was pinched with a syringe needle and the reaction mixture heated to 65 °C for 17 h to result in a dark orange solution which was evaporated to give a brownish slurry which was suspended in DCM (20 mL). The suspension was filtered through a silica plug to remove traces of surplus 5-nitro-2*H*-tetrazole and decomposed material. After repeatedly rinsing the silica plug with dichloromethane (3 × 15 mL), the filtrate was evaporated to give crude compound **5** as off-white solid which was recrystallized from hot toluene to give 109 mg (51%) of 5-nitro-2-(3-(nitromethyl)oxetan-3-yl)-2*H*-tetrazole (**5**) as colorless solid.

Note: The material exhibits slight impurities of the respective *N*1-isomer.
^{1}H NMR (400 MHz, Acetone-d_6): δ 6.03 (s, 2H, CH_2NO_2), 5.34 (d, 2H, CH_2, *J* = 8.5 Hz), 5.29 (d, 2H, CH_2, *J* = 7.8 Hz). **^{13}C{^{1}H} NMR** (101 MHz, Acetone-d_6): δ 78.3, 76.2, 68.3. **^{14}N NMR** (29 MHz, Acetone-d_6): δ −6.1 (NO_2), −34.4 (NO_2). **IR** (ATR, cm^{-1}): $\tilde{\nu}$ 2940 (w), 2146 (s), 1555 (s), 1513 (vs), 1467 (m), 1428 (s), 1399 (s), 1381 (s), 1368 (m), 1355 (m), 1346 (m), 1220 (m), 1196 (s), 1070 (w), 1010 (m), 989 (vs), 970 (m), 952 (m), 940 (m), 905 (s), 869 (w), 818 (m), 788 (w), 736 (m), 723 (m), 650 (m), 593 (w), 533 (m), 474 (m), 458 (m). **Raman** (1064 nm, 1074 mW, cm^{-1}): $\tilde{\nu}$ 3011 (40), 2977 (33), 2940 (38), 2153 (30), 1509 (100), 1474 (28), 1430 (16), 1401 (44), 1384 (28), 1370 (26), 1262 (16), 1206 (19), 1197 (31), 1071 (25), 1011 (69), 990 (16), 973 (26), 909 (19), 869 (20), 477 (20), 456 (21), 402 (31). **Anal. Calcd** for $C_5H_6N_6O_5$: C, 26.09; H, 2.63; N, 36.52. Found: C, 26.04; H, 2.77; N, 37.17. **HRMS** (EI) m/z: $[M]^+$ Calcd. for $C_5H_6N_6O_5$ 230.0400; Found 70.07 $[C_4H_6O]^+$. **DSC** (T_{onset}, 5 °C min^{-1}): 138.3 °C (m.p.), 160.1 °C (dec.). **BAM drop hammer** 40 J. **Friction test** 360 N.

8.4.2 NMR Spectra

2-(3-(Nitromethyl)oxetan-3-yl)-2*H*-tetrazole (2A)

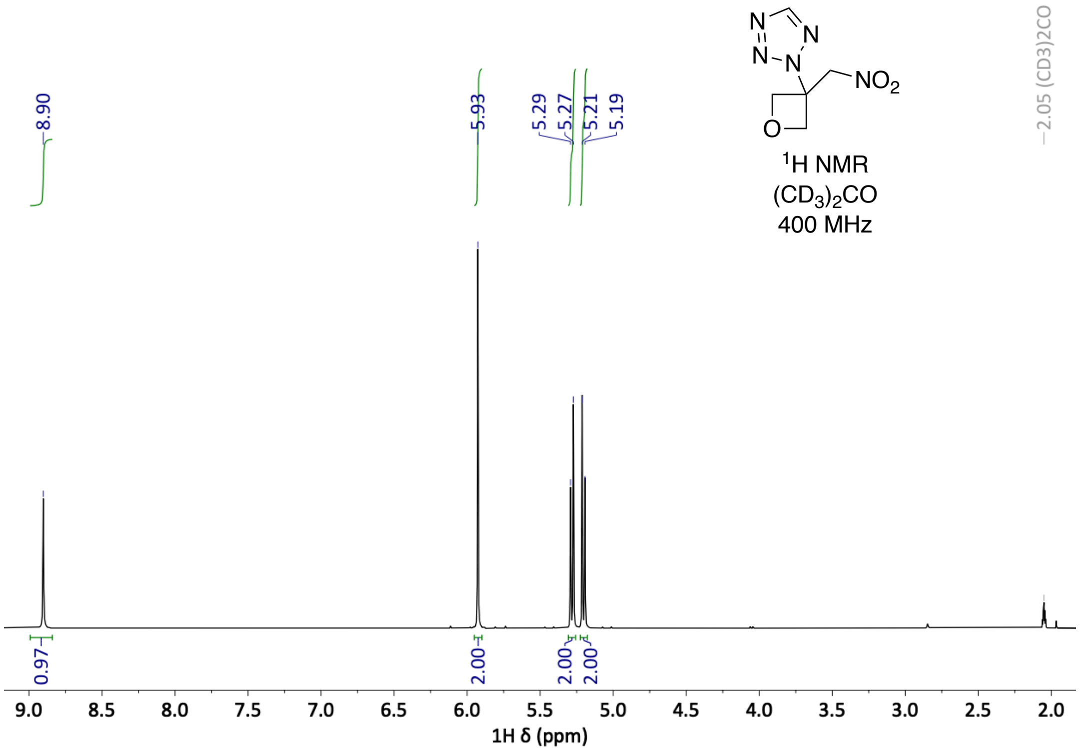

Figure S 8.1. Proton spectrum (^{1}H) of 2-(3-(nitromethyl)oxetan-3-yl)-2*H*-tetrazole.

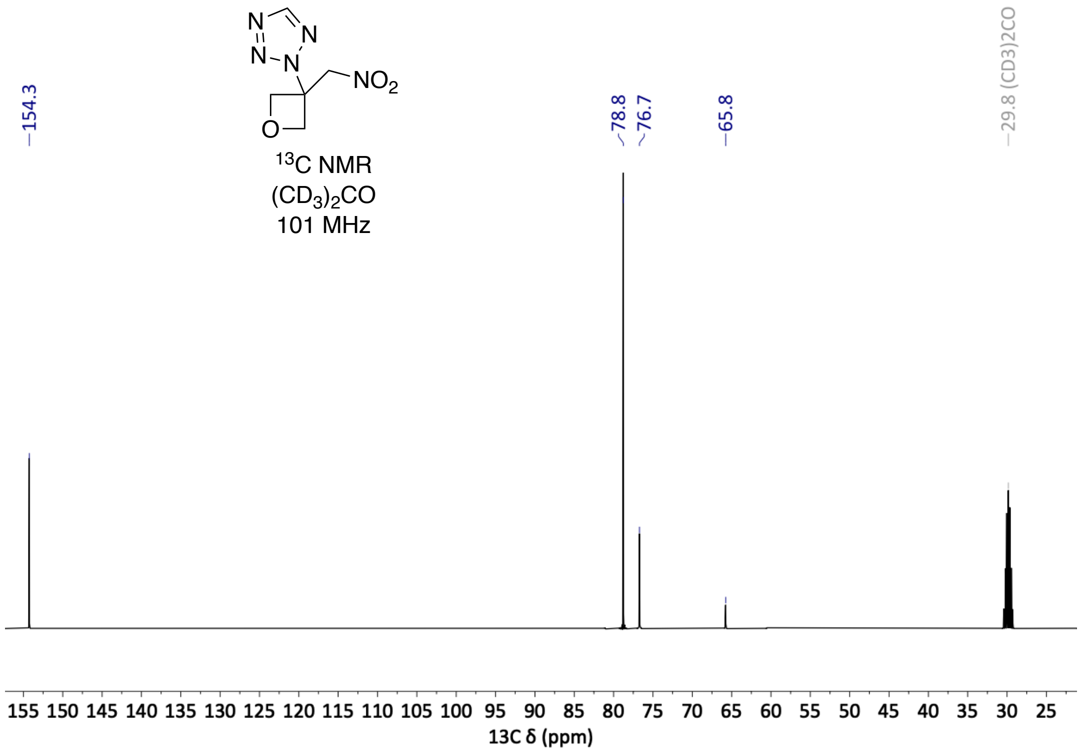

Figure S 8.2. Carbon spectrum (^{13}C) of 2-(3-(nitromethyl)oxetan-3-yl)-2*H*-tetrazole.

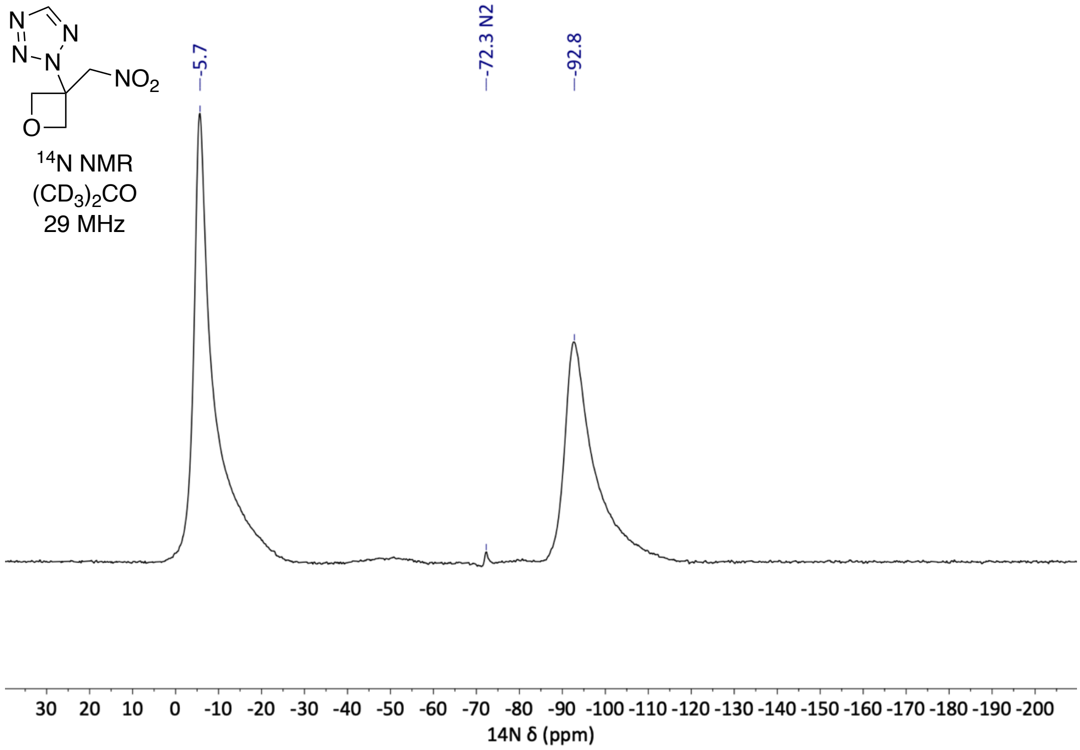

Figure S 8.3. Nitrogen spectrum (^{14}N) of 2-(3-(nitromethyl)oxetan-3-yl)-2*H*-tetrazole.

1-(3-(Nitromethyl)oxetan-3-yl)-1*H*-tetrazole (2B)

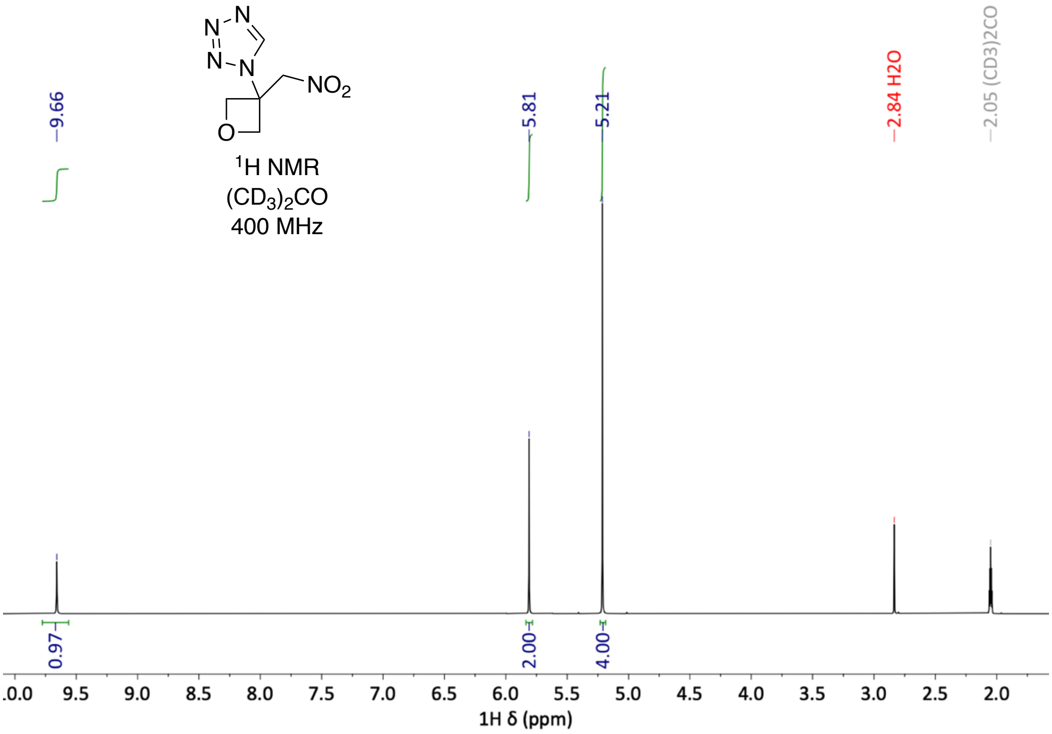

Figure S 8.4. Proton spectrum (^{1}H) of 1-(3-(nitromethyl)oxetan-3-yl)-1*H*-tetrazole.

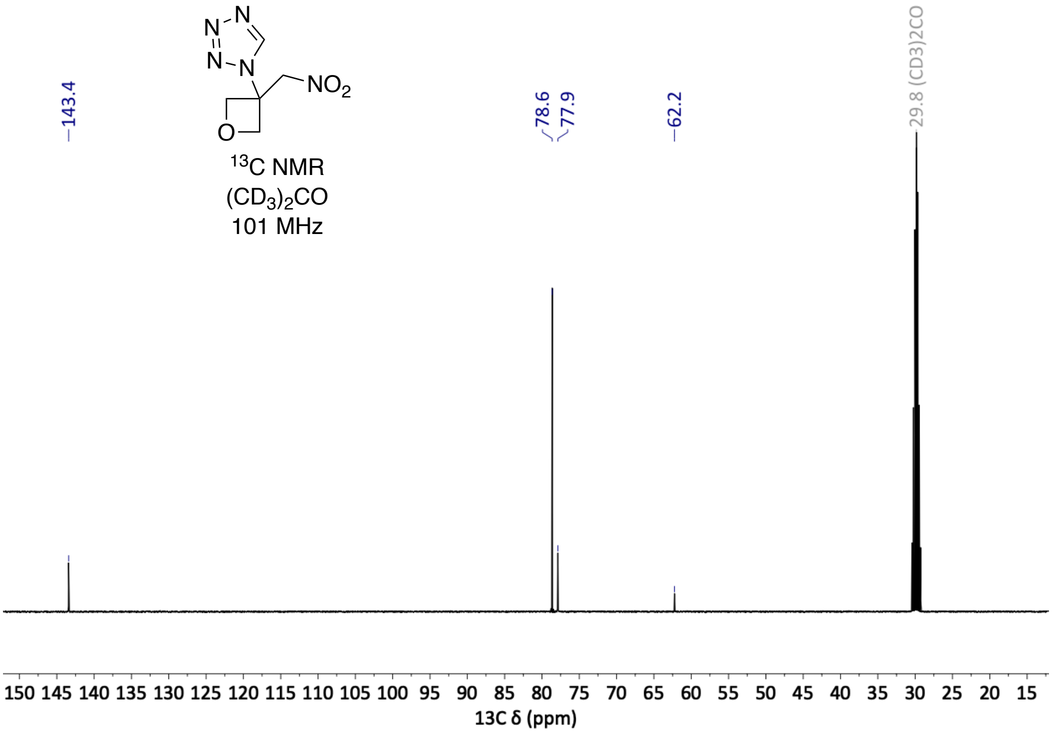

Figure S 8.5. Carbon spectrum (^{13}C) of 1-(3-(nitromethyl)oxetan-3-yl)-1*H*-tetrazole.

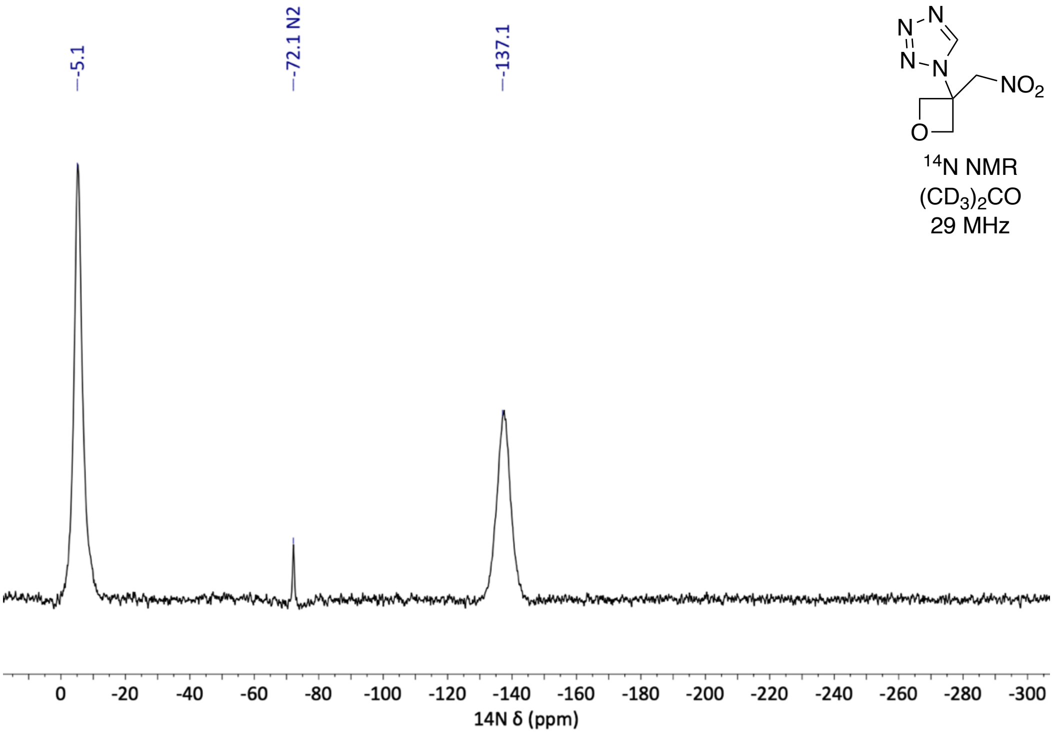

Figure S 8.6. Nitrogen spectrum (^{14}N) of 1-(3-(nitromethyl)oxetan-3-yl)-1*H*-tetrazole.

2-(3-(Nitromethyl)oxetan-3-yl)-2*H*-tetrazol-5-amine (3A)

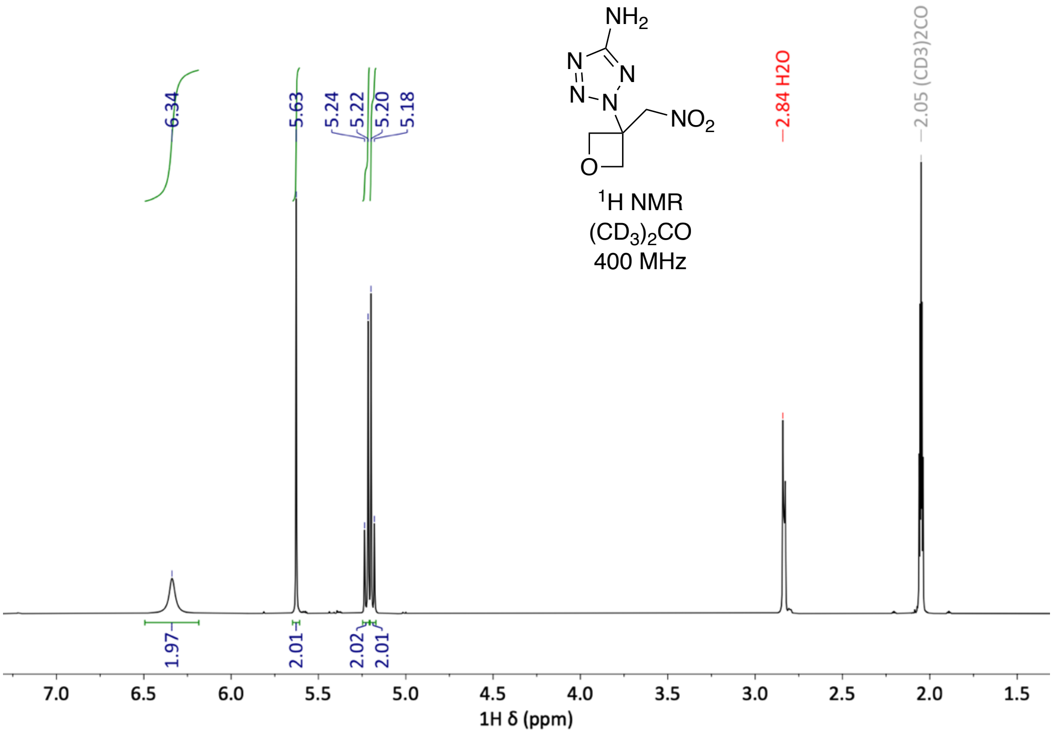

Figure S 8.7. Proton spectrum (^{1}H) of 2-(3-(nitromethyl)oxetan-3-yl)-2*H*-tetrazol-5-amine.

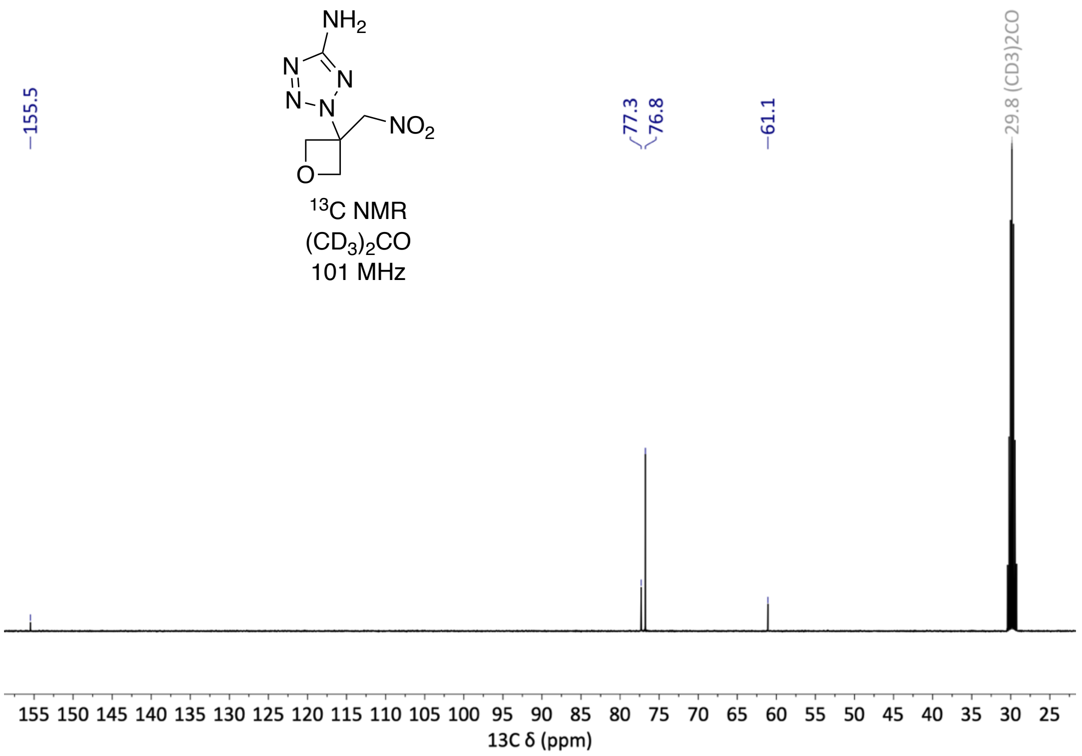

Figure S 8.8. Carbon spectrum (^{13}C) of 2-(3-(nitromethyl)oxetan-3-yl)-2*H*-tetrazol-5-amine.

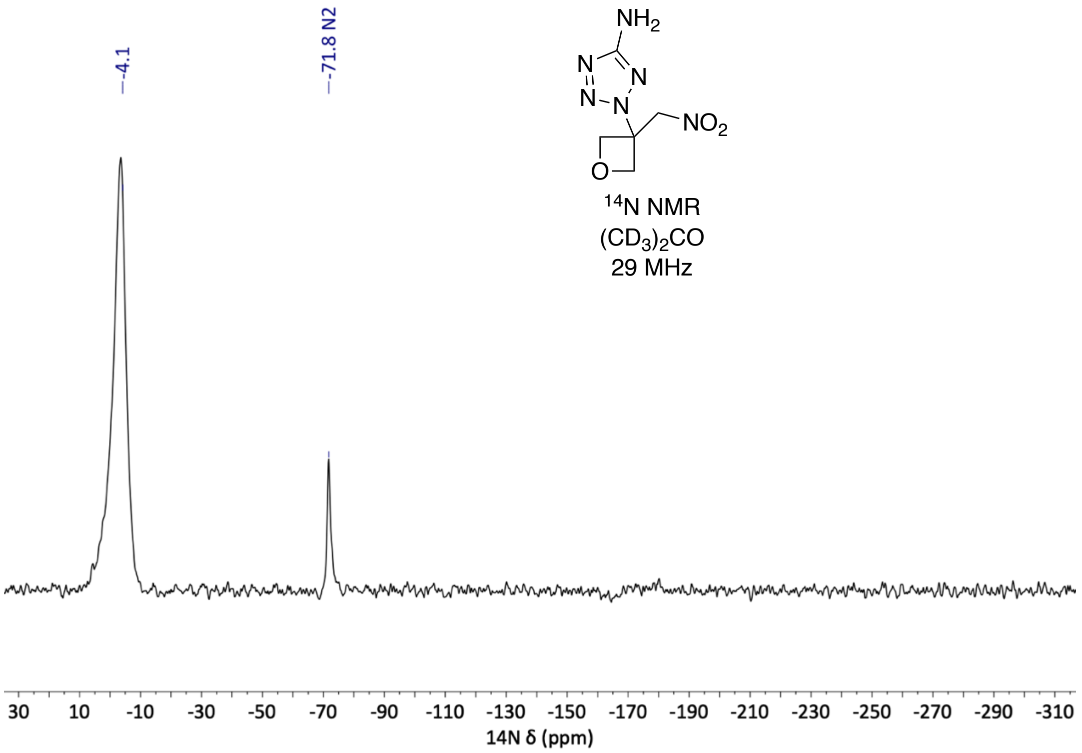

Figure S 8.9. Nitrogen spectrum (^{14}N) of 2-(3-(nitromethyl)oxetan-3-yl)-2*H*-tetrazol-5-amine.

1-(3-(Nitromethyl)oxetan-3-yl)-1*H*-tetrazol-5-amine (3B)

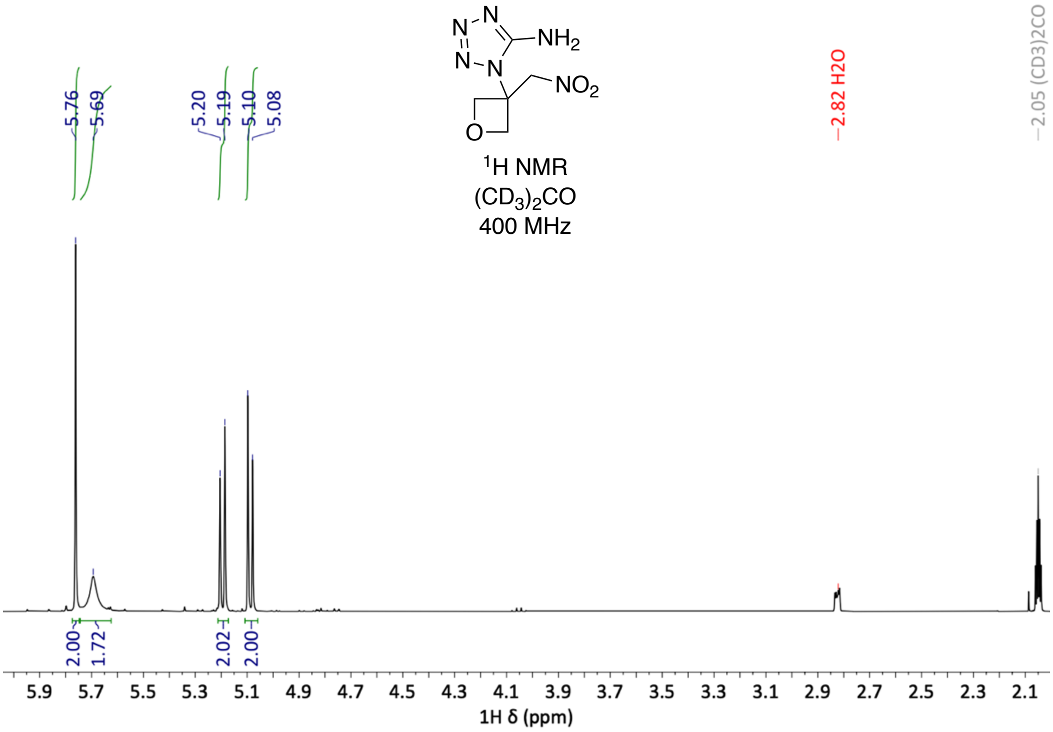

Figure S 8.10. Proton spectrum (^{1}H) of 1-(3-(nitromethyl)oxetan-3-yl)-1*H*-tetrazol-5-amine.

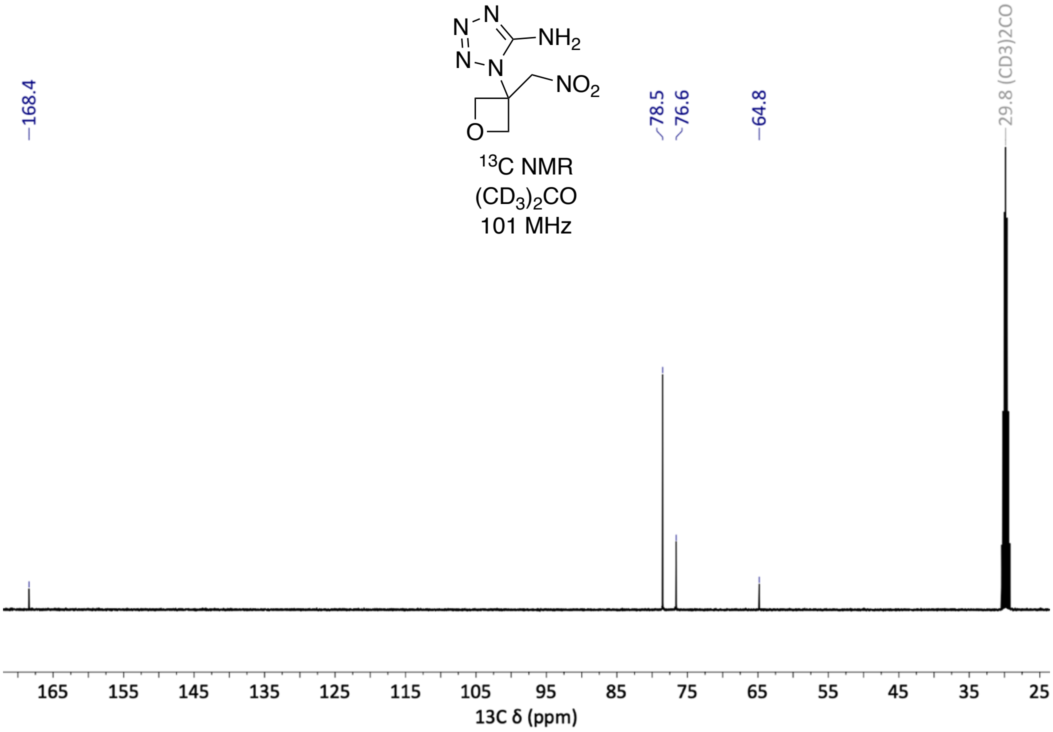

Figure S 8.11. Carbon spectrum (^{13}C) of 1-(3-(nitromethyl)oxetan-3-yl)-1*H*-tetrazol-5-amine.

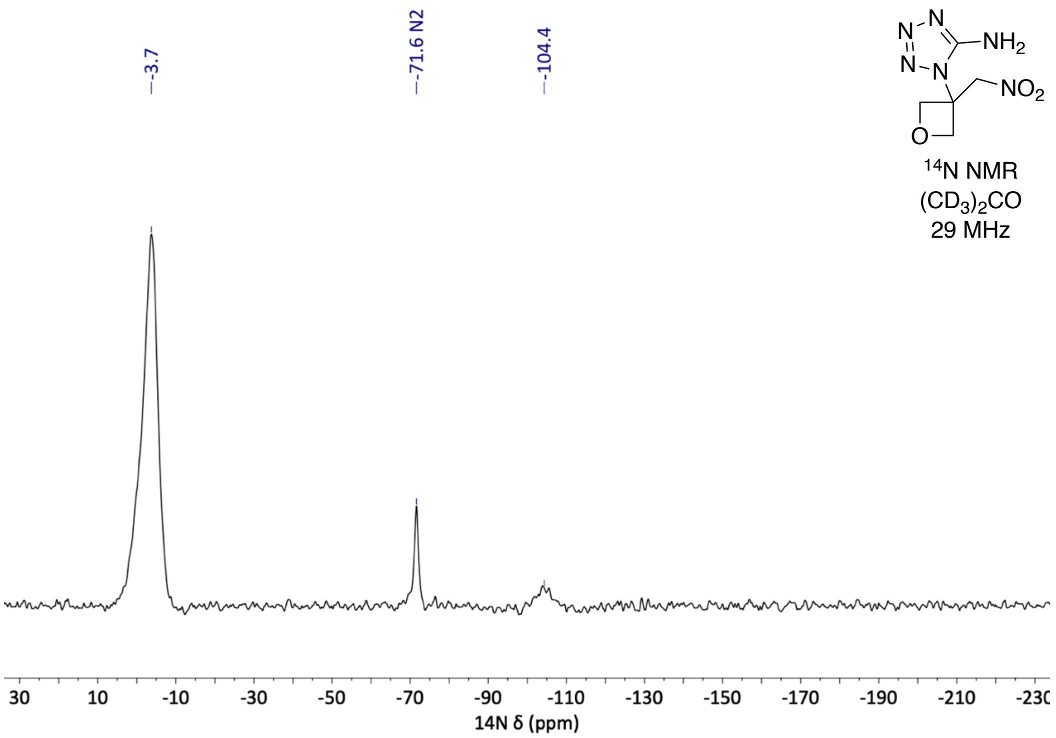

Figure S 8.12. Nitrogen spectrum (^{14}N) of 1-(3-(nitromethyl)oxetan-3-yl)-1*H*-tetrazol-5-amine.

5-Azido-2-(3-(nitromethyl)oxetan-3-yl)-2*H*-tetrazole (4)

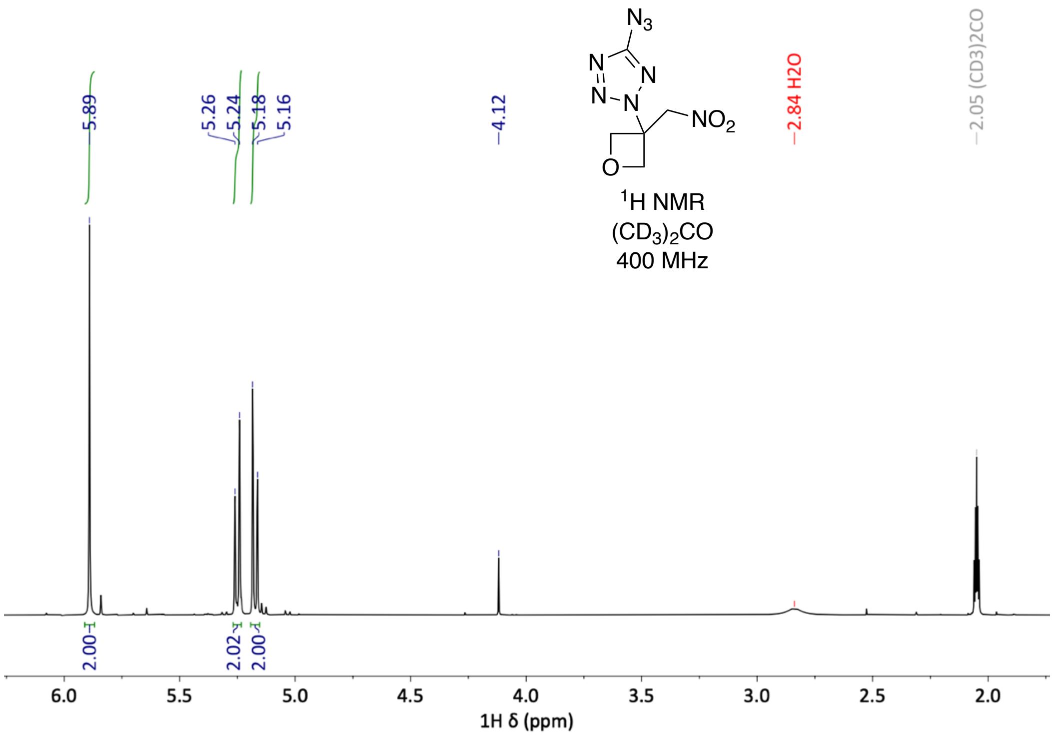

Figure S 8.13. Proton spectrum (^{1}H) of 5-azido-2-(3-(nitromethyl)oxetan-3-yl)-2*H*-tetrazole.

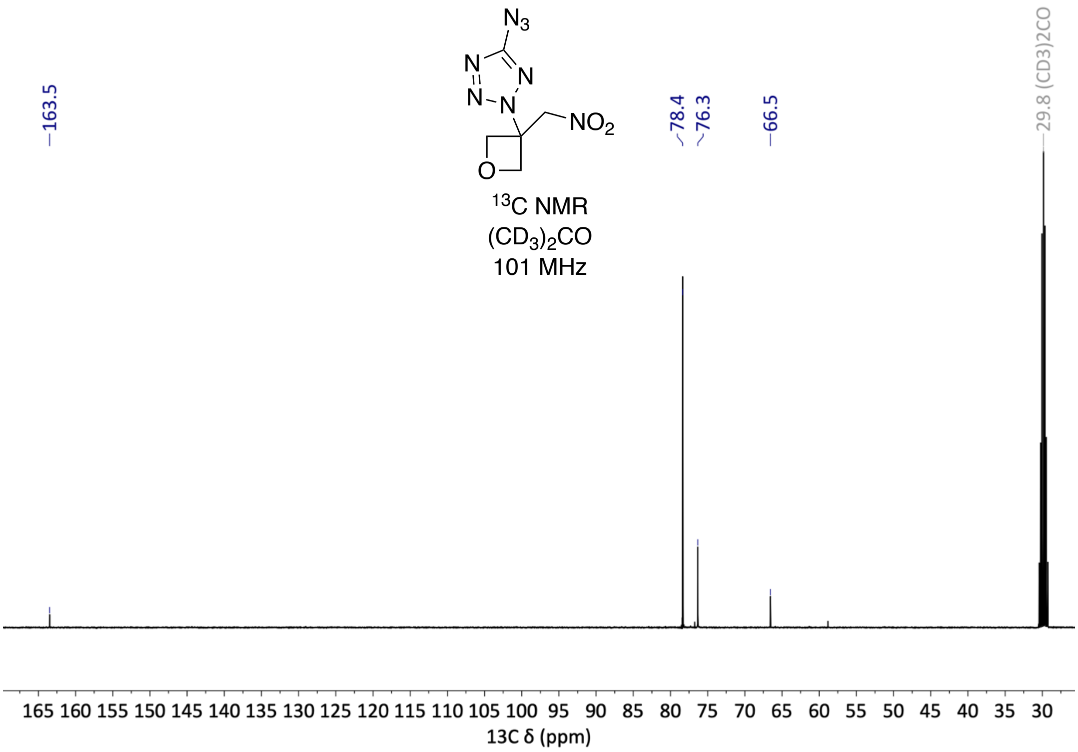

Figure S 8.14. Carbon spectrum (^{13}C) of 5-azido-2-(3-(nitromethyl)oxetan-3-yl)-2*H*-tetrazole.

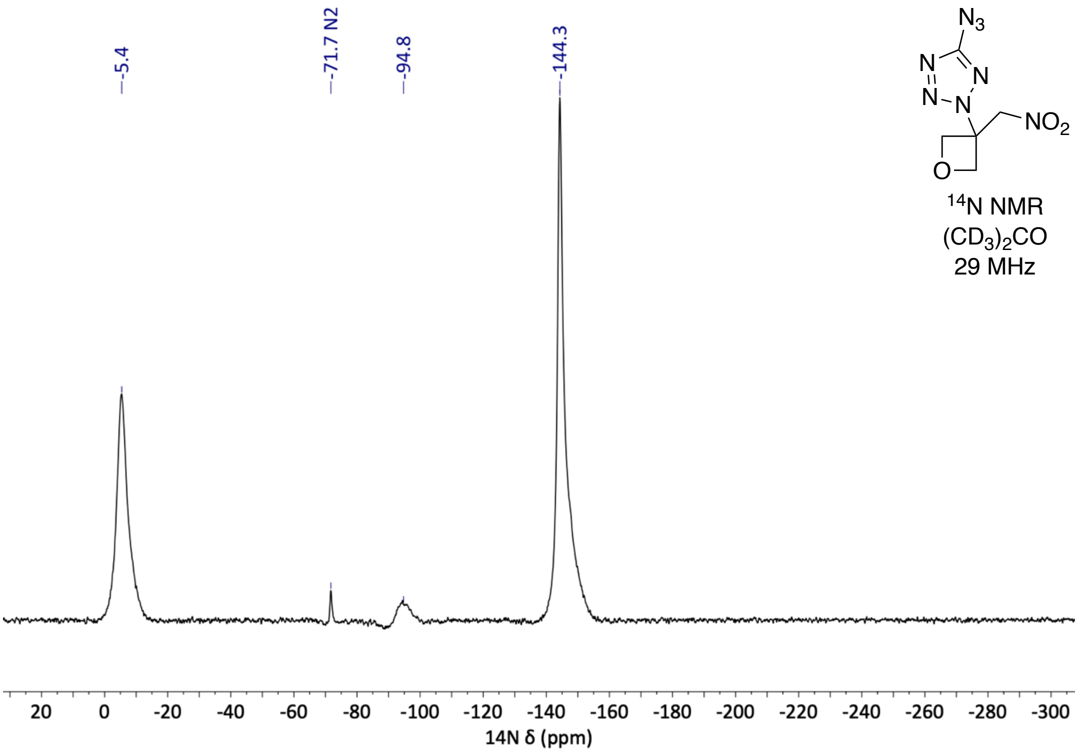

Figure S 8.15. Nitrogen spectrum (^{14}N) of 5-azido-2-(3-(nitromethyl)oxetan-3-yl)-2*H*-tetrazole.

5-Nitro-2-(3-(nitromethyl)oxetan-3-yl)-2*H*-tetrazole (5)

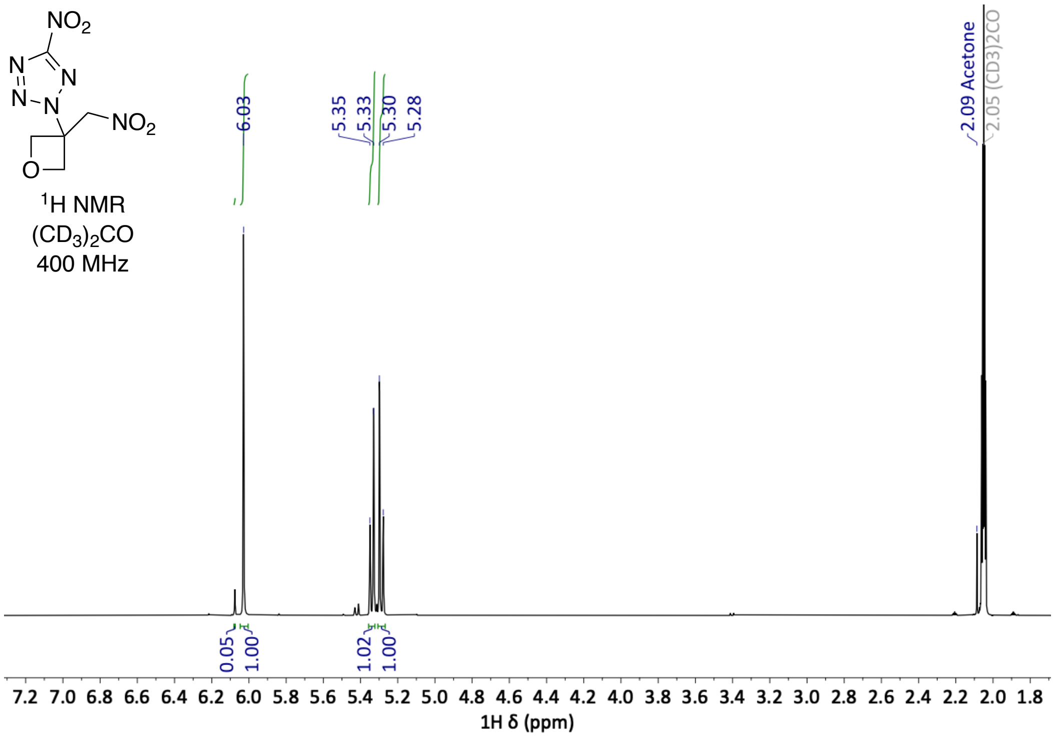

Figure S 8.16. Proton spectrum (^{1}H) of 5-nitro-2-(3-(nitromethyl)oxetan-3-yl)-2*H*-tetrazole.

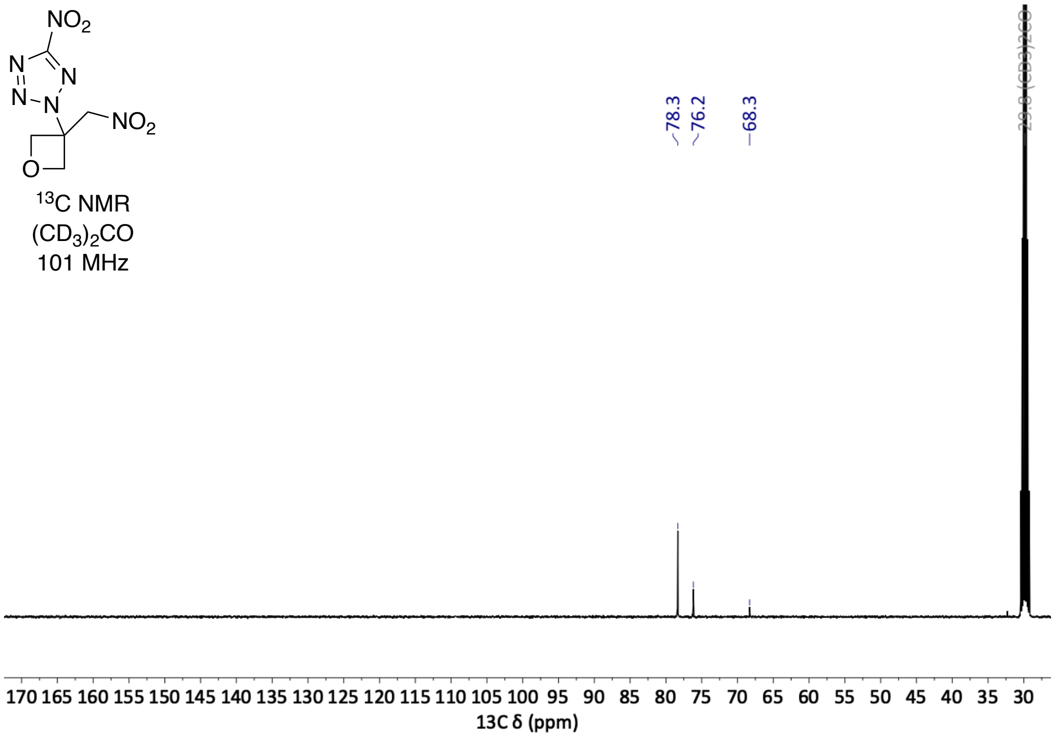

Figure S 8.17. Carbon spectrum (^{13}C) of 5-nitro-2-(3-(nitromethyl)oxetan-3-yl)-2*H*-tetrazole.

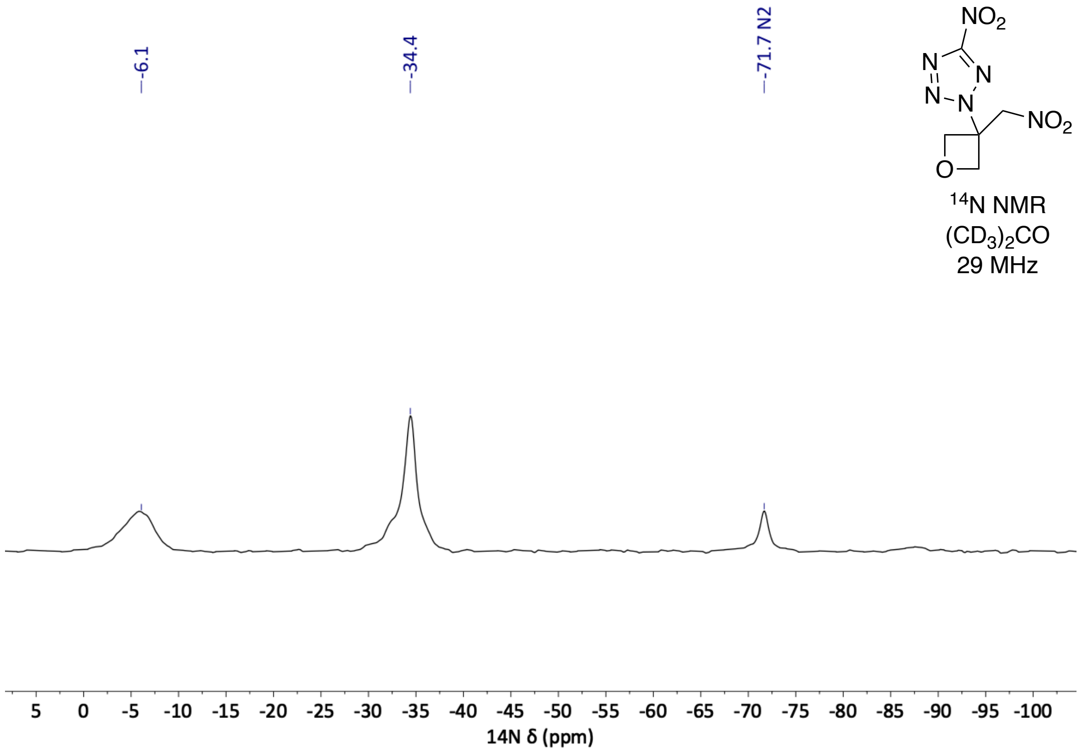

Figure S 8.18. Nitrogen spectrum (^{14}N) of 5-nitro-2-(3-(nitromethyl)oxetan-3-yl)-2*H*-tetrazole.

8.4.3 Crystallography

Crystal Structures of Compounds **2**B, **3**B and **3**C

1-(3-(Nitromethyl)oxetan-3-yl)-1*H*-tetrazole 2B

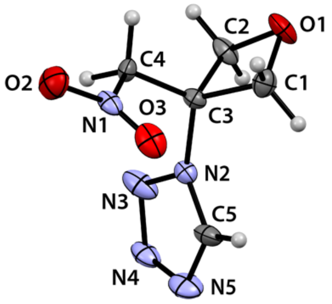

Figure S 8.19. Molecular structure compound 2B in the crystal as obtained after splitting of atoms.

In the crystal, compound 2B is disordered over two positions. The structure was solved by splitting all atoms of the compound over these positions. The split positions of the heavy atoms (C, N, O) could be refined anisotropically giving an acceptable result. As a result of the disorder, standard deviations of the structural parameters are very large. Therefore, we refrained from a discussion of these parameters.

3.1.2 1-(3-(Nitromethyl)oxetan-3-yl)-1*H*-tetrazol-5-amine 3B

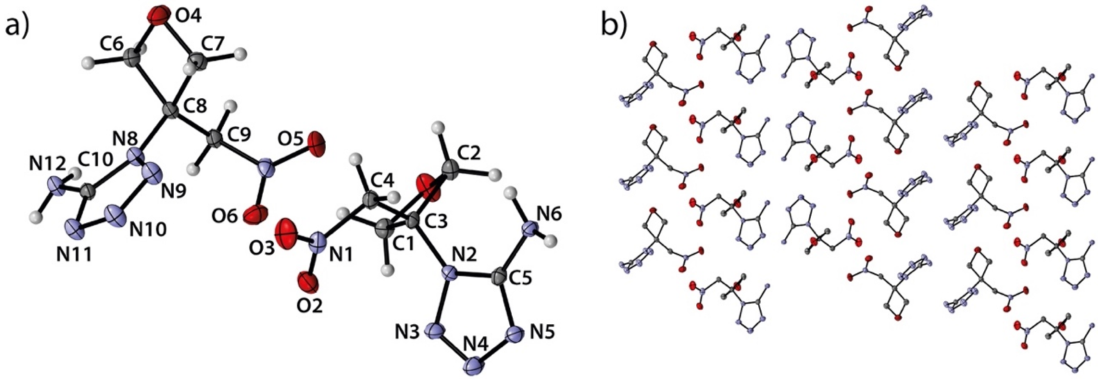

Figure S 8.20. a) Molecular structure compound **3**B in the crystal (crystallographically independent entities). Thermal ellipsoids drawn at the 50% probability level. b) View along *a* axis.

Compound **3**B crystallizes in the triclinic space group *P*–1 with four entities per unit cell and a density of 1.601 g cm^{-3} (123 K) corresponding to a room temperature density of 1.557 g cm^{-3}. Further, the unit cell is made up by two pairs of crystallographically independent entities. As similar parameters are found for both entities, only one (Figure S 20a) is discussed. The oxetane ring shows bond angles ranging from 91.6(2)° (O1–C1–C3) over 91.1(2)° (C3–C2–O1) down to only 84.7(2)° at C1–C3–C2 and 92.6(2)° at the oxetane oxygen atom (C1–O1–C2). The longest bond within the oxetane motif is found between C2–C3 (1.541(4) Å) and the shortest between O1 and C1 (1.431(4) Å). The oxetane ring is almost planar with a puckering angle of only 0.87° (123 K), which is way smaller than in the unsubstituted parent compound oxetane (10.7°, 100 K).[4] In accordance to expectation, the tetrazole motif is planar, and only the amino group's nitrogen atom is slightly shifted out of the tetrazole plane. The C3–N2 bond features a length of 1.462(3) Å which is slightly shorter than the distance between a sp^3-hybridized carbon atom and the tetrazole nitrogen atom in similar compounds.[5-7] The observed bond length between C3 and C4 is rather long with a distance of 1.527(4) Å.[8] The C4–N1 bond is marginally longer (1.493(4) Å) than found in similar nitroalkanes.[9] A bond length of 1.349(4) Å is found between C5 and N6 which is longer than in unsubstituted 1*H*-tetrazol-5-amine.[10] The view along *a* axis reveals alternating layers. One layer is made by a double layer comprising the tetrazole motifs, while the other layer comprises a double layer of the residual structural motif. Within the former layer, all tetrazole motifs arrange in a pairwise parallel manner.

N,2-bis(3-(nitromethyl)oxetan-3-yl)-2H-tetrazol-5-amine 3C

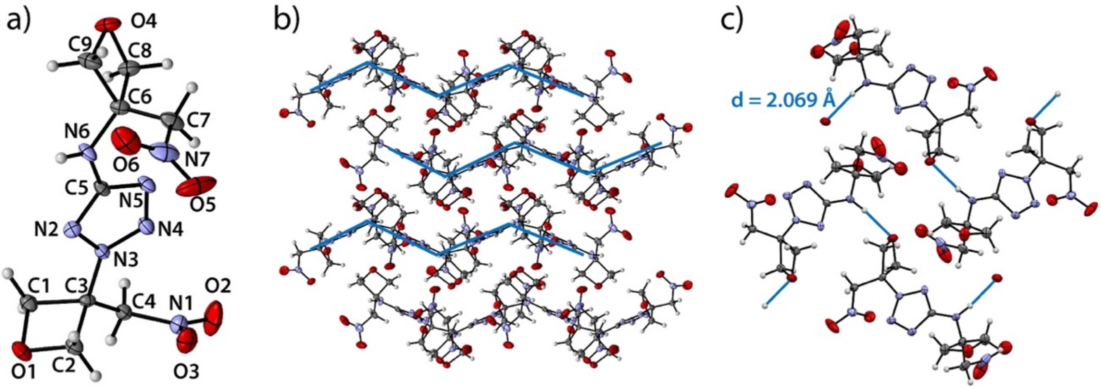

Figure S 8.21. a) Molecular structure of compound **3**C (side-product) in the crystal. Thermal ellipsoids drawn at the 50% probability level. b) View along *c* axis and wave-like pattern. c) Hydrogen bridges between the molecular entities.

Compound **3**C crystallizes in the monoclinic space group $P2_1$/n with four entities per unit cell and a density of 1.587 g cm^{-3} (143 K) corresponding to a calculated density of 1.548 g cm^{-3} at room temperature. The oxetane ring connected to N3 displays angles ranging from 91.3(2)° (O1–C2–C3) over 91.2(2)° (C3–C1–O1) to only 85.2(2)° at C2–C3–C1. An angle of 91.1(2)° is found at the oxetane oxygen atom. Very similar values with a deviation no larger than 1° are found for the oxetane ring connected to N6. The N3-connected oxetane ring shows a puckering angle of 11.37° while the N6-connected shows a slightly higher angle of 13.29°, which is in both cases higher than in the unsubstituted parent compound oxetane (8.7°, 140 K).[4] The tetrazole motif is planar. The largest distance in the N3-connected oxetane moiety is found between C1 and C3 (1.535(3) Å) and the shortest between C2 and O1 (1.454(3) Å). Very similar values are observed in the second oxetane motif. The C3–C4 bond is rather long with a distance of 1.505(3) Å as well as the C6–C7 bond (1.509(3) Å).[8] The C4–N1 bond shows a length of 1.492(3) Å while C7–N7 displays a length of 1.485(4) Å which is in range of similar nitroalkanes.[9] The C6–N6 bond is notably shorter (1.440(3) Å) compared to the bond between C3 and the endocyclic N3-position (1.460(3) Å). The C5–N6 bond (1.354(3) Å) is longer than in the parent compound 1*H*-tetrazol-5-amine.[10] The view along *c* axis shows the arrangement of the molecular entities in a wavelike pattern. Hereby, the molecules are connected by hydrogen bridges which occur between the oxetane oxygen atom of one motif and the secondary amino group of another entity.

Table S 8.1. Detailed crystallographic information of compounds **1**, **2** (A, B) and **3**A.

	1	**2A**	**2B**	**3A**
Formula	$C_4H_5NO_3$	$C_5H_7N_5O_3$	$C_5H_7N_5O_3$	$C_5H_8N_6O_3$
FW [g mol^{-1}]	115.09	185.14	185.14	200.17
Crystal System	Monoclinic	Monoclinic	Monoclinic	Triclinic
Space Group	*C*2/c	*P*2$_1$/c	*C*c	*P*–1
Color / Habit	Colorless block	Colorless block	Colorless block	Colorless block
Size [mm]	0.30 x 0.25 x 0.10	0.50 x 0.50 x 0.30	0.4 x 0.40 x 0.25	0.50 x 0.50 x 0.50
a [Å]	12.5374(10)	10.3115(6)	13.2428(16)	6.6779(6)
b [Å]	5.7930(3)	10.3339(7)	5.8688(4)	9.9578(8)
c [Å]	13.2478(8)	7.3393(5)	10.8791(10)	13.9118(13)
α [°]	90	90	90	103.269(8)
β [°]	90.740(6)	102.240(7)	116.862(10)	101.444(8)
γ [°]	90	90	90	104.382(7)
V [Å^{-3}]	962.10(11)	764.28(9)	754.28(14)	839.56(14)
Z	8	4	4	4
$\rho_{calc.}$ [g cm^{-3}]	1.589	1.609	1.630	1.584
μ [mm^{-1}]	0.138	0.135	0.136	0.132
F (000)	480	384	384	416
λ MoKα [Å]	0.71073	0.71073	0.71073	0.71073
T [K]	143	102	123	100
ϑ min-max [°]	4.162, 26.368	2.823, 26.362	3.449, 30.501	2.301, 26.371
Dataset h; k; l	−15:15; −7:6; −13:16	−12:12; −12:11; -9:9	−18:18; −8:8; −15:15	−7:8; −11:12; −13:17
Reflect. coll.	984	1552	2001	3391
Independ. Refl.	896	1309	1729	2650
Rint.	0.023	0.023	0.040	0.020
Reflection obs.	896	1309	1729	2650
No. parameters	73	146	222	313
R1 (obs.)	0.0348	0.0340	0.0377	0.0398
wR2 (all data)	0.0979	0.0820	0.0867	0.0966
S	1.065	1.059	1.053	1.039
Resd. Dens. [e Å^{-3}]	−0.204, 0.301	−0.209, 0.282	−0.134, 0.161	−0.230, 0.249
Device Type	Oxford XCalibur3 CCD	Oxford XCalibur3 CCD	Oxford XCalibur3 CCD	Oxford XCalibur3 CCD
Solution	SHELXS-97	SHELXS-97	SHELXS-97	SHELXS-97
Refinement	SHELXL-2018/1	SHELXL-2018/1	SHELXL-2018/1	SHELXL-2018/1
Absorpt. Corr.	Multi-scan	Multi-scan	Multi-scan	Multi-scan
CCDC	2119618	2119623	2119795	2119619

Table S 8.2. Detailed crystallographic information of compounds **3** (B/C), **4** and **5**.

	3B	**3C**	**4**	**5**
Formula	$C_5H_8N_6O_3$	$C_9H_{13}N_7O_6$	$C_5H_6N_8O_3$	$C_5H_6N_6O_5$
FW [g mol^{-1}]	200.16	315.26	226.18	230.16
Crystal System	Triclinic	Monoclinic	Monoclinic	Orthorhombic
Space Group	*P*–1	*P*2$_1$/n	*P*2$_1$/n	*P*bca
Color / Habit	Colorless block	Colorless needle	Colorless rod	Colorless platelet
Size [mm]	0.20 x 0.10 x 0.05	0.30 x 0.12 x 0.02	0.40 x 0.10 x 0.10	0.40 x 0.30 x 0.02
a [Å]	5.9708(2)	11.3155(17)	11.0695(5)	10.4514(5)
b [Å]	5.9762(4)	10.2060(10)	7.1343(2)	7.0564(3)
c [Å]	23.6021(13)	11.8112(14)	12.2573(5)	23.9816(11)
α [°]	96.514(5)	90	90	90
β [°]	94.962(4)	104.753(14)	109.469(5)	90
γ [°]	94.389(4)	90	90	90
V [Å^{-3}]	830.44(8)	1319.1(3)	912.65(7)	1768.63(14)
Z	4	4	4	8
ρcalc. [g cm^{-3}]	1.601	1.588	1.646	1.729
μ [mm^{-1}]	0.134	0.135	0.138	0.154
F (000)	416	656	464	944
λMoKα [Å]	0.71073	0.71073	0.71073	0.71073
T [K]	123	143	123	123
ϑ min-max [°]	2.618, 26.372	2.226, 26.370	3.035, 30.507	1.698, 28.281
Dataset h; k; l	−7:7; −7:7; −29:29	−13:14; −12:12; −14:12	−15:15; −10:10; −17:17	−13:13; −9:9; −31:31
Reflect. coll.	3350	2682	2778	2186
Independ. Refl.	2856	1653	2308	1751
Rint.	0.044	0.064	0.033	0.062
Reflection obs.	2856	1653	2308	1751
No. parameters	275	249	169	169
R1 (obs.)	0.0622	0.0593	0.0340	0.0393
wR2 (all data)	0.1408	0.0822	0.0882	0.0973
S	1.150	1.007	1.059	1.033
Resd. Dens. [e Å^{-3}]	−0.328, 0.404	−0.206, 0.256	−0.209, 0.412	−0.164, 0.367
Device Type	Oxford XCalibur3 CCD	Oxford XCalibur3 CCD	Oxford XCalibur3 CCD	Oxford XCalibur3 CCD
Solution	SHELXS-97	SHELXS-97	SHELXS-97	SHELXT 2018/2
Refinement	SHELXL-2014	SHELXL-2018/1	SHELXL-2018/1	SHELXL-2018/1
Absorpt. Corr.	Multi-scan	Multi-scan	Multi-scan	Multi-scan
CCDC	2119620	2119621	2119622	2119624

8.4.4 Heat of Formation Calculation and Thermal Analysis

The atomization method was used to determine the heat of formation of **2**–**5** using the atom energies in Table S 3.[12]

$$\Delta_f H°_{(g,\ M,\ 298)} = H_{(molecule,\ 298)} - \Sigma H°_{(atoms,\ 298)} + \Sigma \Delta_f H°_{(atoms,\ 298)}$$

Table S 8.3. CBS-4M electronic enthalpies for atoms C, H, N, and O and their literature values.

	$-H^{298}$ / a.u.	$\Delta_f H°_{gas}$
H	0.500991	217.998
C	37.786156	716.68
N	54.522462	472.68
O	74.991202	249.18

The Gaussian16 program package was used to calculate room temperature enthalpies on the CBS-4M level of theory.[13] In order to obtain the energy of formation for compounds **2**–**5**, Trouton's Rule has to be applied ($\Delta H_{sub} = 188 \cdot T_m$).

Table S 8.4. Heat of formation calculation results for compounds **2**–**5**.

M	$-H^{298}$ [a] [a.u.]	$\Delta_f H°(g, M)$ [b] [kJ mol^{-1}]	$\Delta_{sub}H°(M)$ [c] [kJ mol^{-1}]	$\Delta_f H°(s)$ [d] [kJ mol^{-1}]	Δn	$\Delta_f U(s)$ [e] [kJ kg^{-1}]
2A	693.080339	195.0	69.0430	125.9	−7.5	780.5
2B	693.065898	232.9	78.5370	154.3	−7.5	934.0
3A	748.369497	188.0	81.6014	106.4	−8.5	637.0
3B	748.354787	226.6	75.6042	151.0	−8.5	859.9
4	856.468681	549.7	61.8426	487.9	−8.5	2250.5
5	897.359449	225.4	77.2962	148.1	−8.5	734.9

[a] CBS-4M electronic enthalpy. [b] Gas phase enthalpy of formation. [c] Sublimation enthalpy. [d] Standard solid state enthalpy of formation. [e] Solid state energy of formation.

The thermal behavior of compounds **2** (A, B), **3** (A, B), and **5** was analyzed by DSC at a heating rate of 5 °C min^{-1}. As compound **4** detonates violently upon heating, the thermal behavior was assessed on a robust OZM DTA machine at a heating rate of 5 °C min^{-1}. The obtained thermograms and evaluations are depicted.

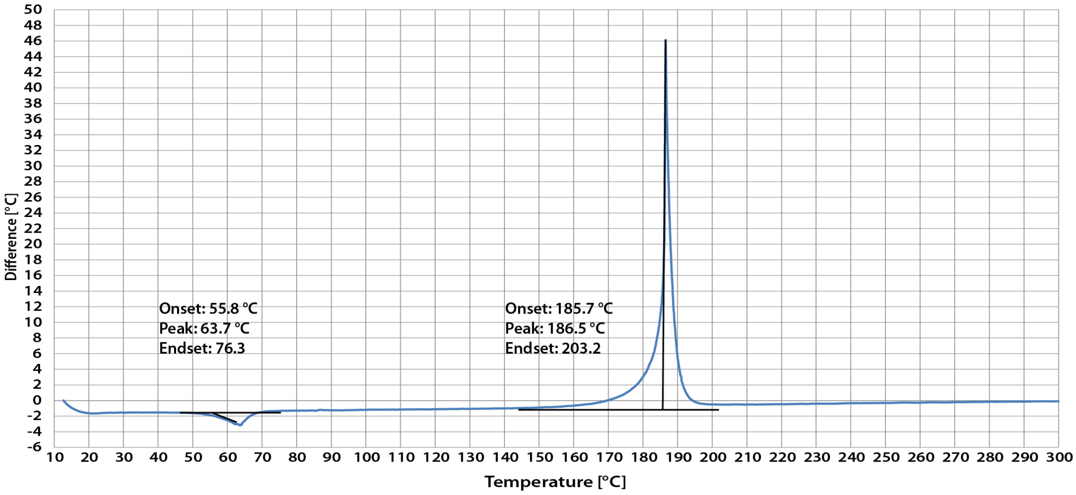

Figure S 8.22. DTA evaluation of compound **4**.

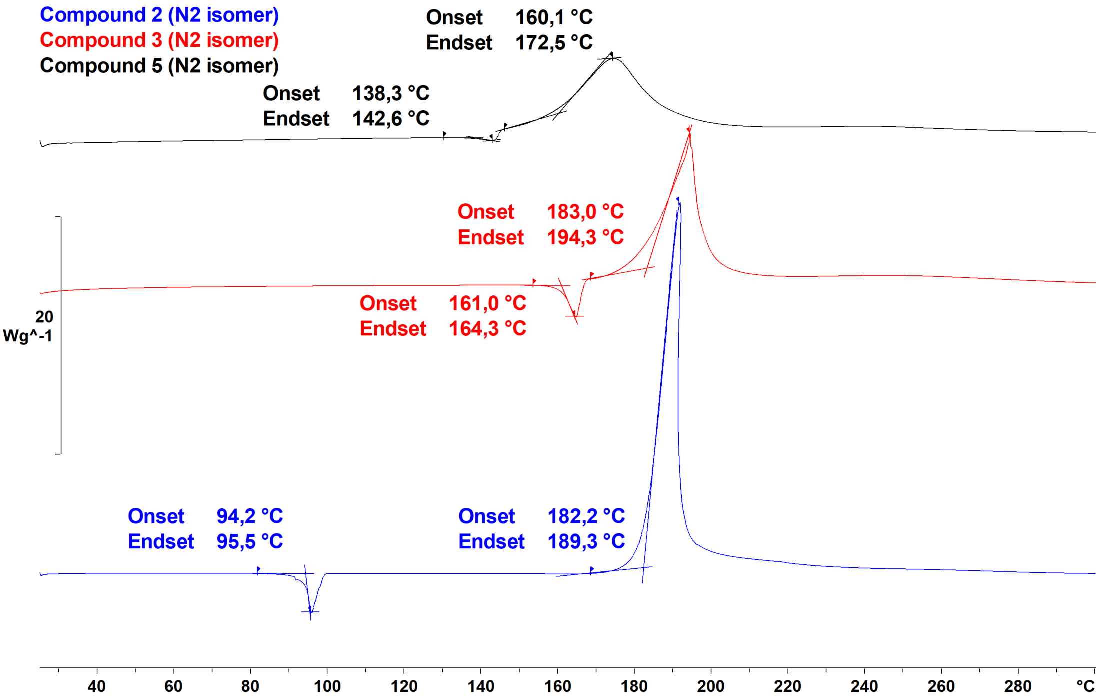

Figure S 8.23. DSC evaluation of compounds **2**A, **3**A and **5** (*N*2 isomers).

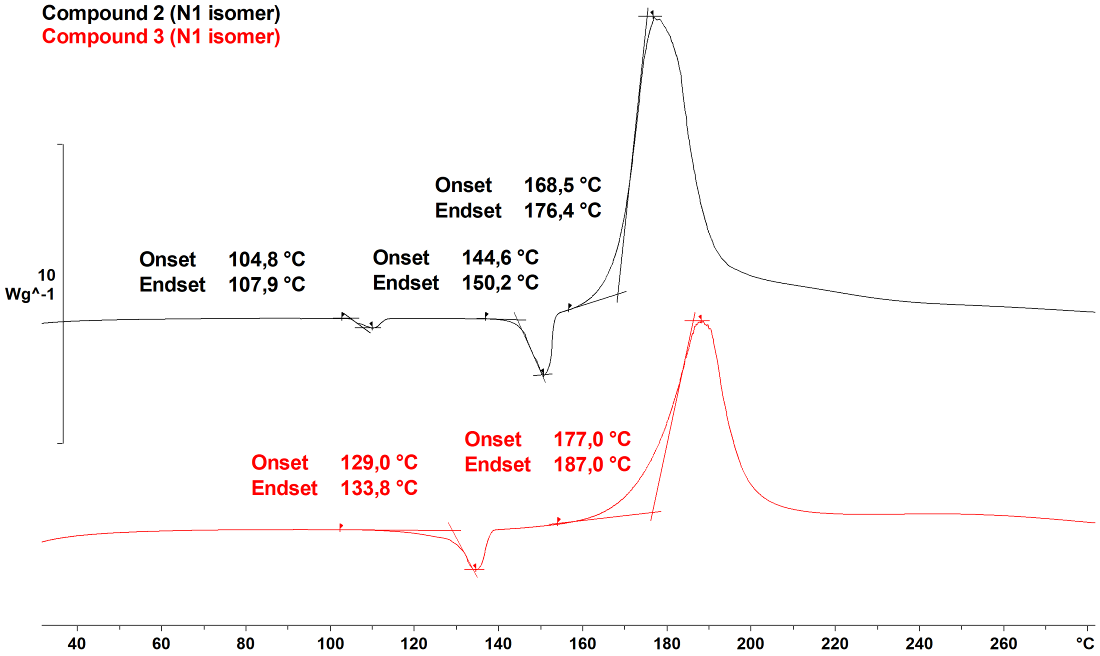

Figure S 8.24. DSC evaluation of compounds 2B and 3B (*N*1 isomers).

8.4.5 Thermal Stress Tests and SSRT

Hot Plate Test

Each compound (2A, 3A, **4**, **5**) is placed on a copper witness plate (50 mg) and heated with a Bunsen burner as thermal stress test.

Figure S 8.25. Hot plate test of compound 2A (50 mg).

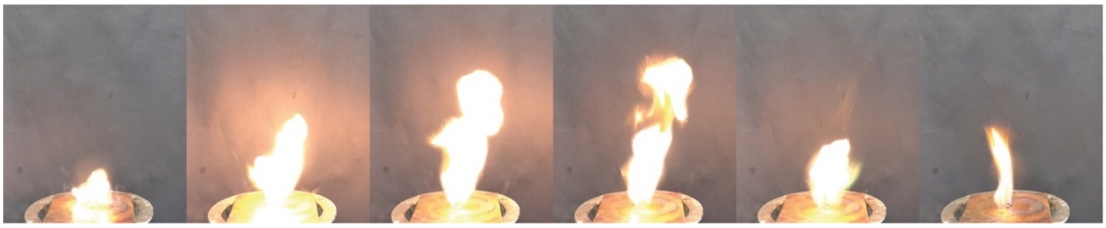

Figure S 8.26. Hot plate test of compound **3**A (50 mg).

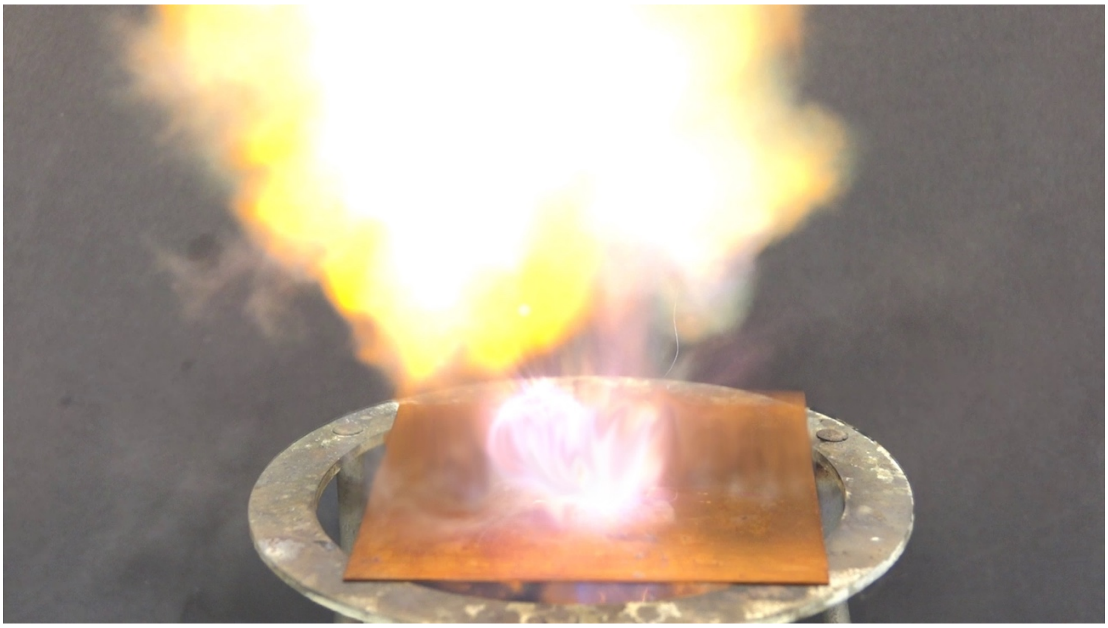

Figure S 8.27. Hot plate test of compound **4** (50 mg) showing a violent detonation. Overlap of two video frames (50 fps).

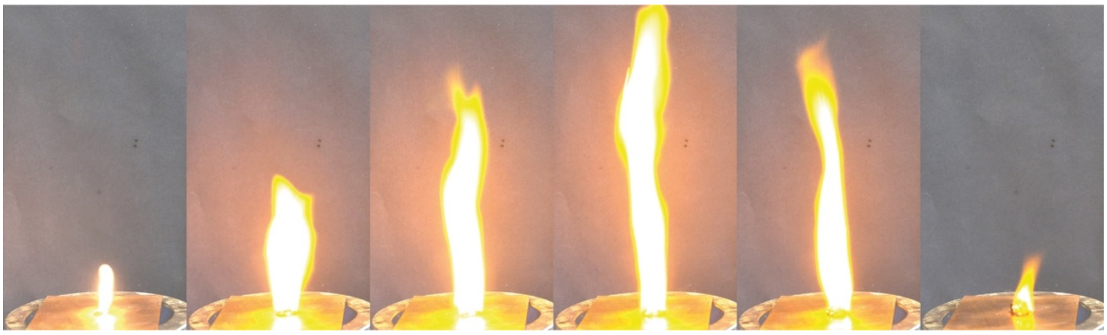

Figure S 8.28. Hot plate test of compound **5** (50 mg).

Flame Test

Crumbs of compound **4** are exposed to the flame of a Bunsen burner. The material initially deflagrates and then violently detonates (deflagration to detonation transition, DDT).

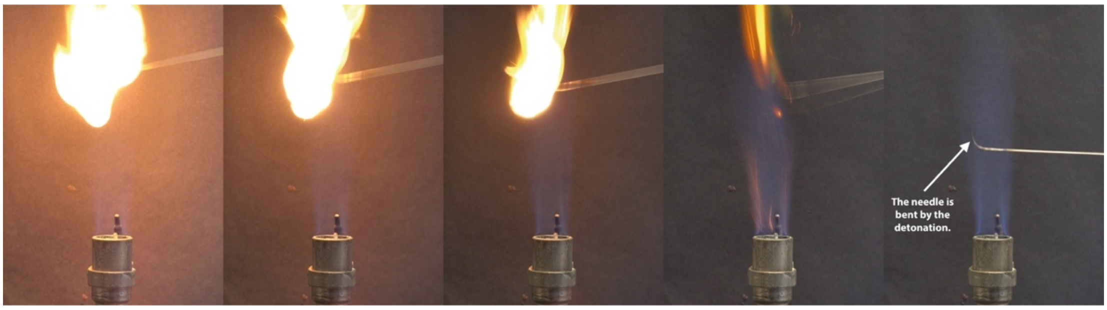

Figure S 8.29. Flame test of compound **4** and deflagration to detonation transition (DDT).

SSRT Test

The small-scale reactivity test (SSRT) was performed as described in the main document.

Figure S 8.30. Aluminum witness plates after the small-scale-reactivity test (SSRT) with indentation caused by TNT (left), compound **4** (middle), and compound **5** (right).

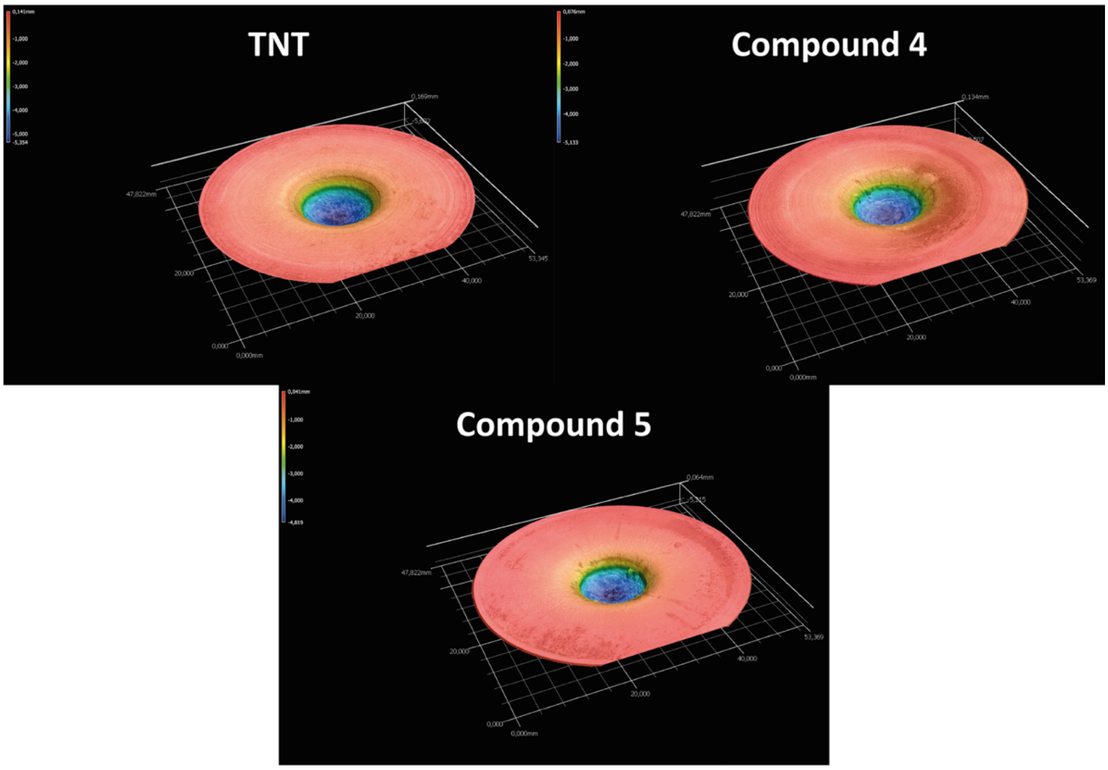

Figure S 8.31. Dent volume determination using a 3D profilometer.

References

[1] NATO STANAG 4489: *Explosives. Impact Sensitivity Tests*; NATO Standardization Office, Brussels, Belgium, **1999**.

[2] NATO STANAG 4487: *Explosives. Friction Sensitivity Tests*; NATO Standardization Office, Brussels, Belgium, **2002**

[3] United Nations (UN), UN Recommendations on the Transport of Dangerous Goods, Manual of Tests and Criteria, **2009**.

[4] Luger, P.; Buschmann, J. Oxetane: the first x-ray analysis of a nonsubstituted four-membered ring. *J. Am. Chem. Soc.* **1984**, *106*, 7118-7121.

[5] Han, F.; Yang, L.; Li, Z.; Xia, C. Acidic-functionalized ionic liquid as an efficient, green and reusable catalyst for hetero-Michael addition of nitrogen, sulfur and oxygen nucleophiles to α,β-unsaturated ketones. *Org. Biomol. Chem.* **2012**, *10*, 346-354.

[6] Polyakova, I. N.; Saraev, V. V.; Gavrilov, A. S.; Golod, E. L. Crystal and molecular structure of four adamantyl-substituted tetrazoles. *Crystallogr. Rep.* **2009**, *54*, 441-448.

[7] Martirosyan, A. O.; Aleksanyan, M. V.; Terzyan, S. S.; Ter-Zakharyan, Y. Z.; Agababyan, R. V.; Karapetyan, A. A.; Mndzhoyan, S. L.; Tamazyan, R. A. Synthesis and Molecular and Crystal Structure of 1-(5-Benzyl-2-tetrazolyl)-1-cyclopentanecarboxylic Acid. Penicillin and Cephalosporins Based on This Acid. *Pharm. Chem. J.* **2001**, *35*, 169-171.

[8] Orpen, A. G.; Brammer, L.; Allen, F. H.; Kennard, O.; Watson, D. G.; Taylor, R. In *Struct. Correl.* **1994**, p 752-858.

[9] Lam, Y.-L.; Koh, L. L.; Huang, H. H. IR spectra, crystal structure, dipole moment, ab initio and AM1 study of 1,2-dinitroethane. *J. Chem. Soc., Perkin Trans. 2* **1993**, 175-180.

[10] Fujihisa, H.; Honda, K.; Obata, S.; Yamawaki, H.; Takeya, S.; Gotoh, Y.; Matsunaga, T. Crystal structure of anhydrous 5-aminotetrazole and its high-pressure behavior. *CrystEngComm* **2011**, *13*, 99-102.

[11] Turner, M. J.; McKinnon, J. J.; Wolff, S. K.; Grimwood, D. J.; Spackman, P. R.; Jayatilaka, D; Spackman, M. A. CrystalExplorer17 (**2017**). University of Western Australia. https://hirshfeldsurface.net.

[12] Altenburg, T.; Klapötke, Thomas M.; Penger, A.; Stierstorfer, J. Two Outstanding Explosives Based on 1,2-Dinitroguanidine: Ammonium- dinitroguanidine and 1,7-Diamino-1,7-dinitrimino-2,4,6-trinitro-2,4,6-triazaheptane. *Z. Anorg. Allg. Chem.* **2010**, *636*, 463-471.

[13] Frisch, M. J.; Trucks, G. W.; Schlegel, H. B.; Scuseria, G. E.; Robb, M. A.; Cheeseman, J. R.; Scalmani, G.; Barone, V.; Petersson, G. A.; Nakatsuji, H.; Li, X.; Caricato, M.; Marenich, A. V.; Bloino, J.; Janesko, B. G.; Gomperts, R.; Mennucci, B.; Hratchian, H. P.; Ortiz, J. V.; Izmaylov, A. F.; Sonnenberg, J. L.; Williams; Ding, F.; Lipparini, F.; Egidi, F.; Goings, J.; Peng, B.; Petrone, A.; Henderson, T.; Ranasinghe, D.; Zakrzewski, V. G.; Gao, J.; Rega, N.; Zheng, G.; Liang, W.; Hada, M.; Ehara, M.; Toyota, K.; Fukuda, R.; Hasegawa, J.; Ishida, M.; Nakajima, T.; Honda, Y.; Kitao, O.; Nakai, H.; Vreven, T.; Throssell, K.; Montgomery Jr., J. A.; Peralta, J. E.; Ogliaro, F.; Bearpark, M. J.; Heyd, J. J.; Brothers, E. N.; Kudin, K. N.; Staroverov, V. N.; Keith, T. A.; Kobayashi, R.; Normand, J.; Raghavachari, K.; Rendell, A. P.; Burant, J. C.; Iyengar, S. S.; Tomasi, J.; Cossi, M.; Millam, J. M.; Klene, M.; Adamo, C.; Cammi, R.; Ochterski, J. W.; Martin, R. L.; Morokuma, K.; Farkas, O.; Foresman, J. B.; Fox, D. J., Gaussian 16 Rev. C.01, **2016**.

9 A GAP Replacement: Improved Synthesis of 3-Azidooxetane and Its Homopolymer Based on Sulfonic Acid Esters of Oxetan-3-ol

by

Max Born, Konstantin Karaghiosoff, and Thomas M. Klapötke

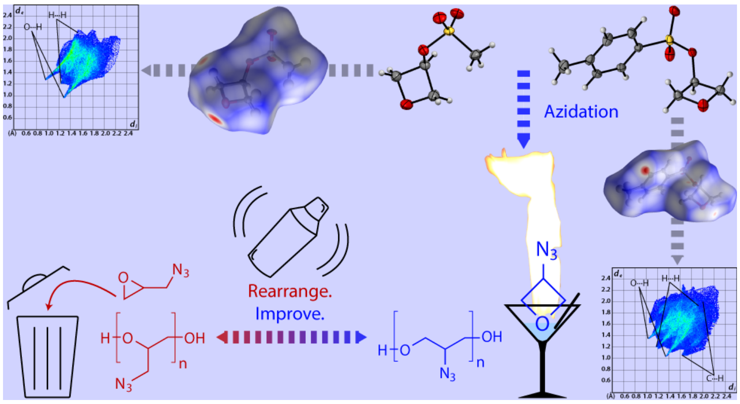

as published in
Journal of Organic Chemistry **2021**, *86*, 12607–12614
(doi:10.1021/acs.joc.1c01060)

Abstract

In the field of energetic binders, only hydroxy-terminated glycidyl azide polymer (GAP) has found widespread application and prevailed in the market. However, oxiranes such as glycidyl azide (GA) allow two ring-opening modes during polymerization and thus lead to polymers of different termination causing inhomogeneous curing results. An elegant solution is the polymerization of 3-azidooxetane as only terminating primary hydroxy groups are formed. Beyond this, poly(3-azidooxetane) and GAP are equal in other aspects due to the similar repetition unit. Since literature methods for the preparation of 3-azidooxetane either employed toxic solvents, gave low yields or impurified product, or could not be reproduced, a new synthesis method was developed to afford pure material and satisfying yields. The syntheses of toluene and methanesulfonic acid esters of oxetan-3-ol as precursors were also significantly improved in comparison to the literature and their molecular structures elucidated by single-crystal X-ray diffraction. The aforementioned compounds and poly(3-azidooxetane) were intensively studied by vibrational and multinuclear NMR spectroscopy (^{1}H, ^{13}C, ^{14}N), differential scanning calorimetry, and elemental analysis. The key compound, 3-azidooxetane, was compared to glycidyl azide regarding performance using the EXPLO5 V6.04 thermochemical code and their sensitivity toward external stimuli like shock and friction assessed according to BAM standard procedures.

Keywords: Oxetane monomers, energetic oxetanes, 3-azidooxetane, glycidyl azide, poly(3-azidooxetane), glycidyl azide polymer.

9.1 Introduction

Since the development of the first energetic polyoxetanes such as poly(3-azidomethyl-3-methyloxetane) (PAMMO) and poly(3,3-bis(azidomethyl)oxetane) (PBAMO) by Manser in 1984 and poly(3-nitratomethyl-3-methyloxetane) (PNIMMO) in 1993, the corresponding literature has been significantly influenced by these polymers.[1–3] Obtained by cationic ring-opening polymerization (CROP), they represented promising candidates for an application in energetic formulations (e.g., polymer-bonded explosives) due to their low viscosity and good mechanical properties after curing.[1] Despite this, only GAP prepared in 1972 by Vandenberg gained larger significance and is nowadays widely used in energetic formulations.[1,4] This might be attributed to the broad availability, low price, and excellent polymerizability of epichlorohydrin, which yields poly(epichlorohydrin) (PECH).[1,5] This prepolymer can then be converted to GAP by polymer-analogous transformation (PAT), which is mainly terminated by secondary hydroxy groups. These are less reactive than primary hydroxy groups and show the same reactivity toward isocyanates as water. This allows the isocyanate to be decomposed by traces of water under the release of carbon dioxide, causing cracks and bubbles in cured propellants and explosives.[1] Ampleman developed a method to control the termination by regiospecific epoxidation and subsequent ring-opening of these epoxides.[1,6] In contrast, a significantly more elegant, time- and cost-saving solution is the polymerization of 3-azidooxetane – the constitution isomer of glycidyl azide. The corresponding polymer, poly(3-azidooxetane), only forms the desired and more reactive primary hydroxy groups and therefore bypasses described curing issues. As the repetition unit is extremely similar to GAP, no drawbacks arise from its alternative use as factors like crystallinity, elasticity, thermal stability, and compatibility stay basically the same. Unfortunately, literature methods for preparing 3-azidooxetane as developed by Baum et al. gave low yields, required long reaction times, made use of toxic solvents (HMPA), or could not be reproduced.[7,8] In the present work, required precursors like 3-tosyloxyoxetane (**1**) and 3-mesyloxyoxetane (**2**) were obtained in both high yield and purity with the help of now commercially available oxetan-3-ol using strongly improved methods. Both compounds can be used to prepare 3-azidooxetane in high yield, making poly(3-azidooxetane) a promising alternative to GAP. In addition, both sulfonic acid esters represent valuable building blocks for the general synthesis of 3-substituted oxetanes by nucleophilic substitution reactions. Their molecular structure was elucidated by single-crystal X-ray diffraction for the first time. As constitution isomers, 3-azidooxtetane and glycidyl azide were compared with regard to their energetic properties using the EXPLO5 V6.04 thermochemical code.[9] To our knowledge, this also filled gaps in the literature regarding physicochemical as well as energetic properties since otherwise only the corresponding polymers were found to be sufficiently characterized. It should also be mentioned that 3-azidooxetane obtained in high yield allows the synthesis of 3-aminooxetane (Staudinger reaction), which finds increasing application in the field of pharmaceutical chemistry.[10] In addition, it can be used to prepare 3-nitro- and 3,3-dinitrooxetane, which provide valuable energetic binders and are thus now more readily available. Ultimately, 3-azidooxetane was successfully polymerized in high yield using CROP, while the polymerization of glycidyl azide fails due to lack of monomer reactivity.[1] Hence, it is suitable for the direct synthesis of copolymers without PAT, demonstrating its overall superiority.

9.2 Results and Discussion

9.2.1 Precursor Synthesis

The synthesis of 3-azidooxetane starting from oxetan-3-ol was first described by Wojtowicz and Polak in 1973.[11] Hereby, oxetan-3-ol was allowed to react with *p*-toluenesulfonyl chloride (*p*-TsCl) in the presence of aqueous base to obtain the precursor 3-tosyloxyoxetane (**1**). Residual tosyl chloride was removed by ammonia solution during workup. The method was largely adopted by Baum, who claimed an outstanding yield of 93% obtained by only washing the crude product with warm water as purification.[7] Despite all efforts, these results could not be reproduced. Instead, in both cases a product heavily contaminated with tosyl chloride (40–50%) was obtained, which could not be purified by recrystallization and required column chromatography. More recent patent literature disclosed a synthesis using both organic base and solvent (DCM/TEA), which gave higher yield and purity (68%, traces of *p*-TsCl). However, the claimed yield of 94% could also not be reproduced following the patent procedure.[12] As it is known that the choice of base can be crucial for a tosylation reaction, a screening was conducted to find the optimum conditions. Here, aqueous bases did not allow yields higher than 70% and resulted in contaminated product. The low solubility of *p*-TsCl in water and the parallel hydrolysis are assumed as reason for failure. Disperse potassium carbonate in DCM insufficiently trapped hydrogen chloride formed, causing ring-opening and likewise low yields. Pyridine as an organic base reacted with the target compound. All in all, the best results were obtained using triethylamine in either dichloromethane or chloroform. However, a high yield loss occurred at longer reaction times under reflux conditions. This can be explained by the acidic character of triethylamine hydrochloride, which decomposes oxetan-3-ol on prolonged contact. However, it was possible to find optimum conditions for the aforementioned reaction system (Scheme 1) which gave 3-tosyloxyoxetane in 83% yield after only 4 h.

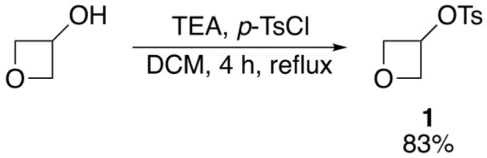

Scheme 9.1. Improved preparation of 3-tosyloxyoxetane.

Significant impurities with starting materials could be successfully avoided, and re-crystallization from hot chloroform gave **1** as extremely pure material in 75% yield. Since compound **1** offers poor atom economy in subsequent substitution reactions due to the large leaving group, 3-mesyloxyoxetane was considered as alternative since it also offers less steric hindrance for nucleophiles. It was initially prepared according to recent patent literature, which claims quantitative yield using a reaction system similar to the patent disclosing compound **1**.[13] In fact, a high yield (82%) was achieved, but ethyl methanesulfonate formed as byproduct due to ring fragmentation and showed very similar physicochemical properties as the target compound. Therefore, separation of the oily mixture by distillation or column chromatography ($CHCl_3$/MeOH; 21:1) appeared promising but failed. Several other common bases like DBU, DABCO, and sodium bis(trimethylsilyl)amide caused not only the same byproduct but also highly varying yields. Hence, a new method was developed (Scheme 2) by deprotonating oxetan-3-ol with lithium hydride in ice-cold THF prior to the addition of mesyl chloride (MsCl).

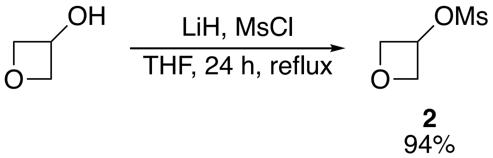

Scheme 9.2. Improved preparation of 3-mesyloxyoxetane.

Precipitation of lithium chloride can be observed during the reaction. Due to its way higher purity in the crude state, compound **2** could be obtained as off-white solid for the first time, whereas literature methods gave oil. Thus, the method is not only superior to literature methods, but provides a precursor for 3-azidooxetane in higher yield and purity than in case of compound **1**. The target compound, 3-azidooxetane (**3**), was first prepared by Baum using 3-tosyloxyoxetane with sodium azide in poly(ethylene oxide) and distilling the product from the reaction mixture. Despite all efforts, this method only gave trace amounts (2%) instead of the claimed 86%.[7] Synthesis in acetonitrile under phase-transfer catalysis disclosed in patent literature gave 24% in good accordance to claimed 28%. The disclosed synthesis in HMPA (claimed: 50%) was discarded from the beginning due to its toxic properties.[8] Being less prone to substitution, a short screening was performed using 3-tosyloxyoxetane as a model compound. It was found that only DMF and DMSO gave quantitative conversion according to TLC after a suitable reaction time of 36 h. Being more environmentally benign, DMSO was finally chosen. To facilitate its removal during workup, the solvent volume was reduced to a minimum making use of molten compound **1** or **2** as co-solvent.

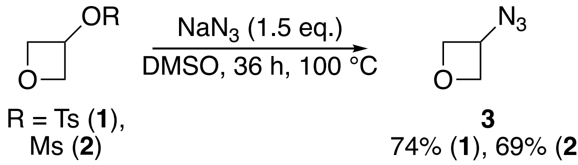

Scheme 9.3. Improved preparation of 3-azidooxetane starting from sulfonic acid esters of oxetan-3-ol.

A tailored solvent mixture (Et_2O/EA, 2:1) was employed for extracting the rather polar, water-soluble azide to give high and satisfactory yields using either compound **1** (74%) or compound **2** (69%) (Scheme 3). In order to achieve a purity suitable for CROP, compound **3** was subject to vacuum distillation to give colorless **3** in 60% yield.

9.2.2 Polymerization

Baum and Berkowitz polymerized 3-azidooxetane in dichloromethane using neat boron trifluoride etherate as catalyst and employed highly varying reactions conditions as summarized in Table 1.[7,8]

Table 9.1. Literature conditions for the polymerization of 3-azidooxetane and respective outcome.

Attempt	**1**	**2**	**3**	**4**	**A**
Scale[a] [g]	8.40	9.90	0.21	150	1.0
c_M[b] [mol·L^{-1}]	9.7	0.65	2.0	1.5	2.0
c_I[c] [mol %]	6	7	10	5	10
t[d] [°C]	−30	−30	0	0−5	rt
t[e] [h]	0.083	48	4.5	4.5	48
Yield [%]	88	49	43	55	67
M_n[f]	2200	2350	2100	3110	540
EW[g] [g·eq^{-1}]	1200	-	-	-	1319

[a] Scale of reaction. [b] Monomer concentration. [c] Initiator concentration. [d] Reaction temperature. [e] Reaction time. [f] Average molecular weight by vapor pressure osmometry. [g] Equivalent weight by silylation (NMR spectroscopy).

Surprisingly, the average molecular weight as determined by vapor pressure osmometry falls in a rather narrow range of 2100–3110 g mol^{-1}. Unfortunately, the equivalent weight is only stated in one case, and no information is provided about the monomer- or catalyst feeding course. Beyond that, obtained polymers remained uncharacterized with regard to their molecular weight distribution. It was decided to polymerize compound **3** under similar conditions (Table 1, attempt A) using the boron trifluoride etherate/1,4-butandiol (1,4-BDO) initiating system, which favors the activated monomer mechanism (AMM) over the active chain-end mechanism (ACE) and thereby reduces or avoids backbiting resulting in less cyclic oligomers, improved molecular weight control, and end-group functionality as well as more narrow polydispersity (PDI) (Scheme 4).[14,15] Hereby, homopolymer **4A** was obtained with a satisfying yield (67%) as dark orange honey-like oil.

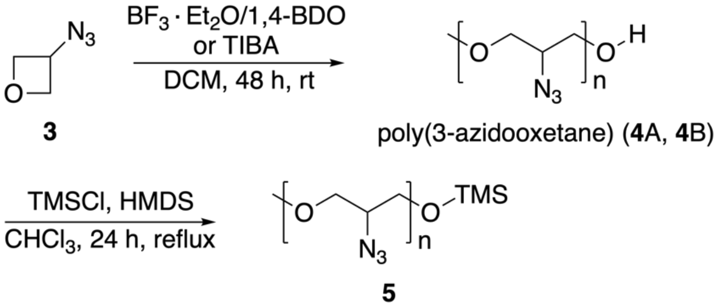

Scheme 9.4. Cationic ring-opening polymerization of 3-azidooxetane and end-group protection (silylation).

The obtained polymer was subjected to gel permeation chromatography (GPC) to analyze the molecular weight distribution (Figure 1). The number average molecular weight M_n was found to be rather low (540 ± 7.4 g mol^{-1}), and the weight average M_W was found to be

1186 ± 6.6 g mol^{-1}, corresponding to a narrow polydispersity of 2.19. However, the results were obtained under non-optimized polymerization conditions. It is anticipated that higher molecular weights and an even more narrow polydispersity can be achieved by a longer monomer feeding course and lower initiator concentrations.

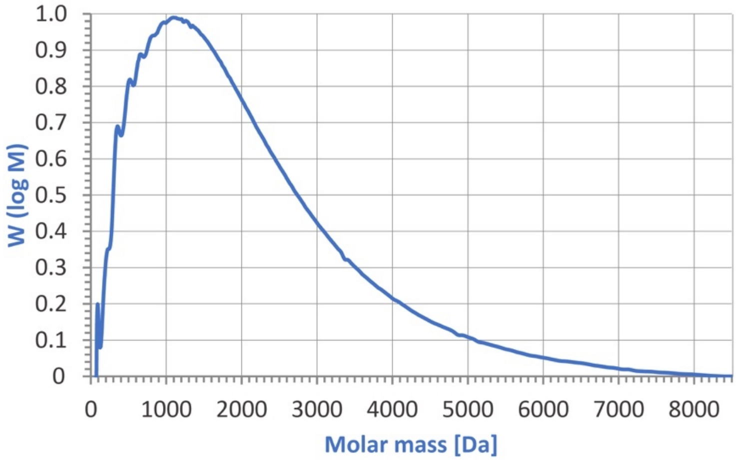

Figure 9.1. Molecular weight distribution of poly(3-azidooxtane) determined by gel permeation chromatography (GPC).

Silylation of end groups using trimethylsilyl chloride (TMSCl) (Scheme 4) was performed analogous to the literature in the case of **4A** to determine the equivalent weight by ^{1}H NMR spectroscopy. The protecting groups integral (TMS) was compared to the integral of the repetition unit (see the SI), and an equivalent weight of 1319 g equiv^{-1} calculated. We also attempted to polymerize 3-azidooxetane using the triisobutylaluminum–water catalyst (TIBA), which is known to give polyoxetanes of especially high molecular mass.[16] The use of TIBA resulted in **4B** as brittle material hardly soluble even in hot DMF or DMSO. Nevertheless, NMR spectroscopy confirmed the presence of a repetition unit. The IR spectrum revealed very weak absorptions, but both an azido group (2095 cm^{-1}) and C–O–C polyether linkage (1100 cm^{-1}) were observed. Elemental analysis showed a drastically reduced nitrogen content consistent with DSC, which showed an exothermic signal in the region of **4A** but a too small integral. It can be concluded that the highly reactive trialkylaluminum species led to side reactions causing degradation of the azido groups.[16]

9.2.3 Crystallography and Hirshfeld Analysis

Single crystals of compounds **1** and **2** were obtained by slow evaporation of saturated chloroform solutions. Detailed crystallographic data can be found in the Supporting Information. 3-Tosyloxyoxetane (Figure 2a) crystallizes in the monoclinic space group $P2_1/n$ with four formula units in the unit cell and a density of 1.463 g cm^{-1} (143 K) corresponding to a room temperature density of 1.428 g cm^{-1}.

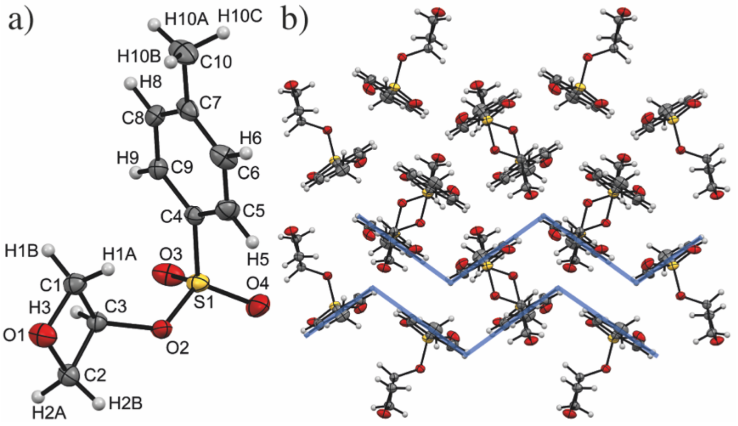

Figure 9.2. a) Molecular structure of compound **1** in the crystal. Thermal ellipsoids drawn at 50% probability level. b) View along *c* axis and wavelike pattern.

As expected, all oxetane bond angles show large deviations from the ideal tetrahedral angle of sp^3-hybridized carbon atoms and range from 90.9(1)° (O1–C2–C3, O1–C1–C3) to extreme values of only 85.9(1)° (C1–C3–C2). In accordance with this, an angle of 91.4(1)° is observed at the oxetane–oxygen (C1–O1–C2). The shortest bond within the oxetane ring is observed between O1 and C1 (1.448(3) Å) and the longest between C1 and C3 (1.526(3) Å). A puckered conformation is found (9.37°, 143 K) in good accordance to the parent compound oxetane (8.7(2)°, 140 K).[17] The bond between the oxetane moiety and the leaving group (C3–O2) shows a typical value of 1.448(2) Å as well as the oxygen–sulfur single bond (O2–S1) with a length of 1.579(1) Å.[18] Furthermore, the view along the *c* axis (Figure 2b) beautifully reveals the parallel arrangement of the aromatic rings to form a wavelike pattern with a gearing of 64.3°. In adjacent layers, the aromatic rings are displaced to one another. Overlapping, sandwich-like parallel layers are separated by a rather long distance of 6.25 Å. On the basis of the molecular structure, steric hindrance may occur between sterically demanding nucleophiles and the tosyl group. Compound **2** (Figure 3a) crystallizes in the triclinic space group *P*–1 with a density of 1.580 g cm^{-1} (180 K) corresponding to a room temperature density of 1.551 g cm^{-1}.

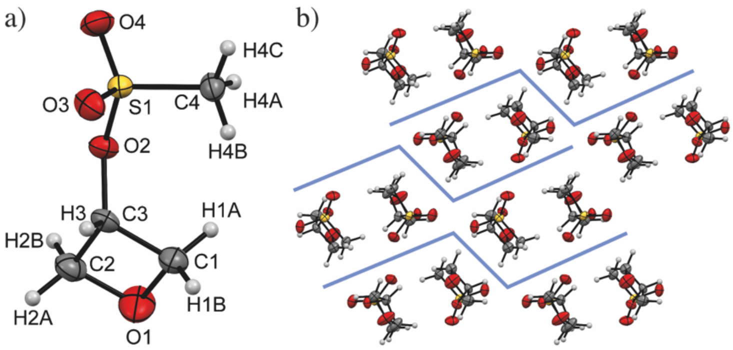

Figure 9.3. a) Selected, crystallographically independent molecular entity of compound **2** in the crystal. Thermal ellipsoids drawn at 50% probability level. b) View along *a* axis and wave-pattern.

The unit cell comprises two pairs of crystallographically independent molecular entities. As in compound **1**, the bond angles within the oxetane moiety largely differ from the ideal tetrahedral angle and range from 91.1(1)° (O1–C1–C3) over 91.0(1)° (O1–C2–C3) down to 86.1(1)° (C1–C3–C3). A high angle strain is also observed at the oxetane oxygen atom (91.8(2)°, C1–O1–C2). The endocyclic C1–O1 bond is the shortest (1.441(2) Å) within the oxetane ring, while the longest is C1–C3 (1.519(2) Å). As in the case of **1**, the ring is not planar and shows a puckering of 5.82° (180 K), which is lower than in compound **1** and the parent compound oxetane.[17] The bond between ring and leaving group (C3–O2) shows a typical length of 1.454(2) Å as well as the oxygen–sulfur bond (O2–S1) with a length of 1.581(1) Å.[18] The view along the *a* axis (Figure 3b) shows wavelike layering and the pairwise parallel arrangement of oxetane rings which are twisted by 180° against each other. Similar bond lengths and geometries were found for the entity not depicted in Figure 3a. Compared to **1**, less steric hindrance at C3 for nucleophiles can be assumed.

Both sulfonic acid esters were subjected to Hirshfeld analysis. Next to the calculated Hirshfeld surface, near contacts of the crystal framework are displayed in a 2D Fingerprint plot (Figure 4).[19,20]

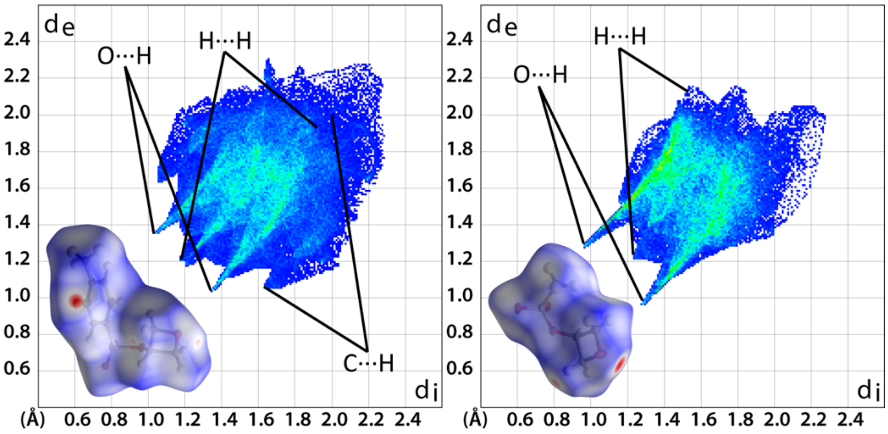

Figure 9.4. Hirshfeld surface and 2D fingerprint plot of compound **1** (left) and compound **2** (right).

3-Mesyloxyoxetane (**2**) was found to be dominated (65.2%) by weak O···H interactions ($d_i + d_e > 2.4$ Å), with the shortest contact being 2.34(6) Å between the oxetane oxygen atom and a neighboring methyl group. The remaining population of close contacts is mainly limited to repulsive H···H interactions (32.7%) as depicted in Figure 5.

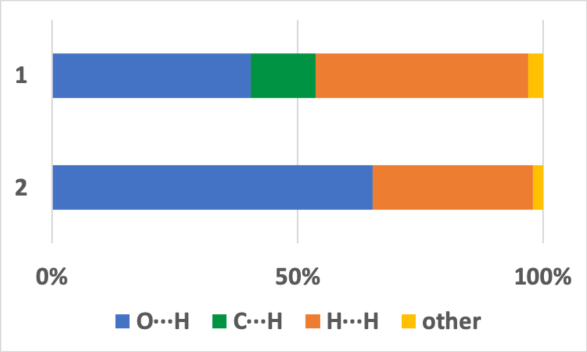

Figure 9.5. Population analysis of crystal interactions of compounds **1** and **2**.

In addition, the crystal structure of 3-tosyloxyoxetane (**1**) was found to be also dominated by weak O···H interactions (40.4%) with a minimum distance of 2.50(9) Å between an ester group oxygen atom and a neighboring aromatic proton. These are counterbalanced by a similar fraction of destabilizing H···H interactions (43.4%). The major difference between compounds **1** and **2** arises from stabilizing C···H interactions (13.2%) and π-stacking of the aromatic rings (Figure 5). This difference is consistent with the higher melting temperature (88 °C) and the better crystallization behavior of compound **1**, while compound **2** crystallizes very slowly at room temperature and can already be liquefied by hand heat due to its low melting point of 37 °C. Thus, Hirshfeld analysis has proven to be a valuable tool to correlate macroscopic effects with the crystal structure and to make these effects plausible.

9.2.4 Spectroscopic Analysis

The presented compounds were analyzed by both ^{1}H and ^{13}C NMR spectroscopy ($CDCl_3$) as well as ^{14}N NMR spectroscopy in case of both organic azides. For all compounds, the five protons of the oxetane ring form an AA′BB′M spin system with all resonances occurring within 0.70 ppm. While the AB part (CH_2) is of high order, the M nucleus (CH) displays due to its symmetrical location with respect to the A and B nuclei a triplet of triplets (**1**: 5.28 ppm; **2**: 5.48 ppm), which can be evaluated according to first order to give the $^{3}J_{HH}$ coupling constants to the A and B hydrogen atoms. These were determined to be 6.3 Hz/5.3 Hz for compound **1** and 6.4 Hz/5.4 Hz for compound **2**. In the case of **3**, the difference between J_{AM} and J_{BM} is too small to be resolved and a quintet-like pattern is observed (see the Supporting Information). The ^{13}C NMR spectra of **1**–**3** show shifts characteristic for oxetane species between about 40 and 80 ppm (**1**: 71.6, 77.2 ppm; **2**: 71.2, 77.4 ppm; **3**: 54.6, 77.2 ppm). The ^{14}N NMR spectrum of 3-azidooxetane shows the expected, concise resonances for N_β (−135 ppm) and N_γ (−164 ppm) as well as a weaker resonance for N_α (−305 ppm). The infrared spectra of **1**–**3** show an intense and characteristic absorption for the asymmetric and symmetric C–O–C stretching vibration of the oxetane ring (ring breathing) between 947 and 974 cm^{-1}.[11,21] The intense absorptions of the sulfonic ester group between 816–884 and 1162–1181 cm^{-1} are characteristic for esters **1** and **2**.[11,22] The characteristic band for the azido group in compound **3** and in poly(3-azidooxetane) appears at

2097 and 2088 cm^{-1}, respectively. The Raman spectra of **1**–**3** complement the IR data of the compounds.

9.2.5 Physicochemical and Energetic Properties

The thermal behavior of the constitutional isomers glycidyl azide and 3-azidooxetane was investigated by differential scanning calorimetry at a heating rate of 5 °C min^{-1}. Boiling temperatures were obtained using 40 µL Mettler-Toledo aluminum crucibles featuring a lid hole. Subsequently, the decomposition temperatures were determined employing same 40 µL crucibles with a 50 µm lid-hole to allow further heating of the sample under pressure equilibrium until decomposition occurred. The room temperature enthalpies for both compounds were calculated using the Gaussian16 program package at the CBS-4M level of theory, and the atomization method was used to assess the heat of formation.[23,24] The EXPLO5 V6.04 code was subsequently used to calculate the energetic performance of 3-azidooxetane in comparison to glycidyl azide.[9] The results are summarized in Table 2.

Table 9.2. Physicochemical and energetic properties of glycidyl azide (GA) and 3-azidooxetane (3-AO) in comparison.

	GA	**3-AO**
Formula	$C_3H_5N_3O$	$C_3H_5N_3O$
FW [g·mol^{-1}]	99.09	99.09
IS[a] [J]	5	3
FS[b] [N]	>240	>192
Ω[c] [%]	−72.7	−72.7
T_b[d]/ T_{dec}[e] [°C]	145/213	140/190
ρ[f] [g·cm^{-3}]	1.14	1.18
ΔH_f°[g] [kJ·mol^{-1}]	220.9	225.6
	EXPLO5 V6.04	
$-\Delta_E U^\circ$[h] [kJ·kg^{-1}]	4445	4520
$T_{C\text{-}J}$[i] [K]	2794	2813
$p_{C\text{-}J}$[j] [GPa]	10.6	11.5
$D_{C\text{-}J}$[k] [m·s^{-1}]	6129	6307
V_0[l] [dm^3·kg^{-1}]	828	820

[a] Impact sensitivity (BAM drop hammer, method 1 of 6). [b] Friction sensitivity (BAM friction apparatus, method 1 of 6). [c] Oxygen balance based on CO formation. [d] Boiling point (DSC, β = 5 °C min^{-1}). [e] Decomposition temperature (DSC, β = 5 °C min^{-1}). [f] Density at 298 K (weighing of 100 µL). [g] Standard molar enthalpy of formation. [h] Detonation energy. [i] Detonation temperature. [j] Detonation pressure. [k] Detonation velocity. [l] Volume of detonation gases at standard temperature and pressure.

To the best of our knowledge, this is the first time that the sensitivity and thermostability of the monomers have been described reliably or at all. Here, it is noteworthy that 3-azidooxetane marginally outperforms glycidyl azide due to its higher enthalpy of formation and density. This is reflected by the higher detonation velocity, higher detonation pressure, and the slightly higher detonation energy. However, this is at the expense of lower thermostability and higher sensitivity to impact and friction. Overall, however, the isomers are very similar regarding their performance. In addition, poly(3-azidooxetane) was found to be comparable to commonly used GAP in terms of thermostability and sensitivity.[25]

9.3 Conclusion

The sulfonic acid esters of the now commercially available oxetan-3-ol represent synthetically extremely valuable compounds since they can be easily substituted due to the excellent leaving group quality. Hereby, they can not only provide oxetanes for pharmaceutical applications but also polymerizable, energetic derivatives to gain new energetic binders. In the present work, strongly improved synthetic protocols have been developed which provide the target oxetanes in high yield and purity, making follow-up compounds more available and cost-efficient. In addition, their molecular structures have been elucidated for the first time. It was successfully demonstrated that both sulfonic acid esters are suitable for the synthesis of 3-azidooxetane to achieve higher yields than ever before. This in turn favors their use as precursors for 3-aminooxetane in the pharmaceutical sector and the subsequent synthesis of highly energetic monomers such as 3-nitro- and 3,3-dinitrooxetane using the aforementioned amine. The in-depth investigation of 3-azidooxetane's physicochemical and energetic properties in comparison to its constitution isomer glycidyl azide did not only complete its information in literature but also revealed its slightly higher performance. As its homopolymer was obtained in high yield, poly(3-azidooxetane) resembles a first-rate alternative to GAP as it exhibits similar properties while solving long-term curing issues due to the absence of terminating secondary hydroxy groups. For full competitivity, the polymerization conditions need to be optimized toward higher molecular weights. Ultimately, 3-azidooxetane is a valuable building block for future energetic copolymers due to its good polymerizability, high enthalpy of formation, and performance.

9.4 Experimental Section

General Information.

All reagents and solvents were used as received (Sigma-Aldrich, ABCR, TCI, Spirochem AG). FT-IR spectra were recorded on a PerkinElmer Spectrum One FT-IR instrument using neat compounds. Raman spectra were obtained on a Bruker MultiRam FT Raman spectrometer using a neodymium-doped yttrium aluminum garnet (Nd:YAG) laser (λ = 1064 nm) and 1074 mW output. NMR spectra were measured on a Bruker AV400 or JEOL ECX400 using TMS (^{1}H and ^{13}C) or nitromethane (^{14}N) as internal reference operating at 400.1 MHz (^{1}H), 100.6 MHz (^{13}C), and 28.9 MHz (^{14}N). X-ray data collection was performed using an Oxford Xcalibur3 diffractometer equipped with a CCD area detector operating with Mo Kα radiation (λ = 0.7107 Å). Thermal behavior was analyzed on a Mettler Toledo DSC822e instrument at a heating rate of 5 °C min^{-1} using 40 µL aluminum crucibles and nitrogen purge gas at a flow rate of 30 mL min^{-1}. Elemental analyses were performed with an Elementar Vario EL device by pyrolysis of the sample and subsequent analysis of formed gases (standard deviation liquids: 0.5%). Molecular weight distribution was measured by GPC on a HITACHI L-2350 device equipped with a RI and UV detector and a “PSS SDV combination low” column (100–60.000 Da). THF was employed as solvent at a flow rate of 1.0 mL min^{-1}. Polystyrene standards were used for calibration and analysis was performed using PSS WinGPC software. The polymer density was determined by helium pycnometry and a Quantachrome Ultrapyc 1200e device. The sensitivity data was assessed using a BAM (Bundesanstalt für Materialforschung) drop hammer according to STANAG 4489 modified instructions and a BAM friction tester according to STANAG 4487 modified instructions.[26,27]

Caution! The described organic azides are energetic materials with sensitivity toward external stimuli like friction, shock, and electrostatic discharge. We encountered no special hazards during their preparation and handling, but adequate safety measures (e.g., safety googles, face shield, ear protection, Kevlar gloves, body armor, earthed equipment) should be taken at all times.

Oxetan-3-yl 4-Methylbenzenesulfonate (1). Oxetan-3-ol (4.00 g, 54.0 mmol) and triethylamine (6.01 g, 59.4 mmol, 1.1 equiv.) were dissolved in DCM (100 mL) and the solution cooled to 0 °C by means of an ice bath. *p*-Toluenesulfonyl chloride (11.3 g, 59.4 mmol, 1.1 equiv.) was added portionwise and the reaction mixture stirred for 30 min at this temperature. Subsequently, the solution was refluxed for 4 h using an oil bath. The reaction mixture was then washed with concentrated ammonia solution (2 × 70 mL) and brine solution (2 × 70 mL). The organic layer was dried over sodium sulfate and evaporated to give 10.3 g (83%) of crude oxetan-3-yl 4-methylbenzenesulfonate as a pale beige solid which was recrystallized from hot chloroform to give 9.19 g (75%) of compound **1** as colorless solid.

^{1}H NMR ($CDCl_3$, 400 MHz): δ 7.77 (d, *J* = 8.3 Hz, 2H, CH), 7.35 (d, *J* = 8.0 Hz, 2H, CH), 5.28 (tt, ^{1}H, *J* = 6.3, 5.5 Hz, $CH_{Ox.}$), 4.70 (ddd, 2H, CH_2), 4.65 (ddd, 2H, CH_2), 2.45 (s, 3H, CH_3). **^{13}C{^{1}H} NMR (**$CDCl_3$, 101 MHz)**:** δ 145.6, 133.0, 130.2, 127.9, 77.2, 71.6, 21.8. **IR** (ATR, cm^{-1}): $\tilde{\nu}$ = 3002 (w), 2986 (vw), 2955 (w), 2885 (w), 1596 (w), 1496 (vw), 1458 (w), 1401 (w), 1375 (m), 1356 (s), 1312 (w), 1297 (w), 1212 (vw), 1192 (m), 1181 (s), 1162 (m), 1124 (w), 1111 (w), 1096 (w), 1073 (s), 1027 (m), 1022 (m), 972 (s), 947 (s), 884 (s), 863 (m), 848 (m), 816 (s), 795 (m), 720 (s), 706 (m), 657 (s), 635 (w), 568 (s), 552 (vs), 496 (m), 482 (m), 431 (m). **Raman** (1075 nm, 1000 mW, 25 °C, cm^{-1}): $\tilde{\nu}$ = 3069 (68), 3001 (41), 2986 (51), 2926 (70), 2897 (38), 1597 (73), 1480 (30), 1385 (19), 1373 (19), 1356 (16), 1192 (22), 1177 (100), 1163 (46), 1115 (19), 1075 (24), 820 (22), 797 (70), 635 (32). **Anal. Calcd** for $C_{10}H_{12}O_4S$: C, 56.62; H, 5.30; S, 14.05. Found: C, 52.41; H, 5.30; S, 14.32. **DSC** (5 °C min^{-1}): 88.6 °C (m.p.), 271.6 °C (dec.).

Oxetan-3-yl Methanesulfonate (2). Lithium hydride (120 mg, 15.1 mmol, 1.1 equiv.) was suspended in dry THF (18 mL), and a solution of oxetan-3-ol (1.12 g, 15.1 mmol, 1.1 equiv.) in dry THF (2 mL) was added. The suspension was stirred for 10 min and cooled to 0 °C by means of an ice bath, and a solution of methanesulfonyl chloride (1.57 g, 13.7 mmol) in dry THF (2 mL) was added dropwise over a period of 5 min. The reaction mixture was then refluxed for 24 h using an oil bath and allowed to cool to room temperature. In order to precipitate inorganic salts quantitatively, DCM was added (20 mL). The suspension was filtered through a Celite plug and the solvent evaporated to give 1.97 g (94%) of crude oxetan-3-yl methanesulfonate as a yellowish oil. The crude material was distilled under vacuum conditions (100 °C, 10^{-3} mbar) to give 1.77 g (85%) of compound **2** as colorless liquid which slowly crystallizes at room temperature.

^{1}H NMR ($CDCl_3$, 400 MHz): δ 5.48 (tt, *J* = 6.3, 5.3 Hz, 1H, CH), 4.87 (ddd, 2H, CH_2), 4.78 (ddd, 2H, CH_2), 3.04 (s, 3H, CH_3).**^{13}C{^{1}H}** NMR ($CDCl_3$, 101 MHz)**:** δ 77.4, 71.2, 38.1. **IR** (ATR, cm^{-1}): ṽ = 3029 (w), 3012 (w), 2968 (vw), 2933 (w), 2890 (w), 1372 (w), 1344 (s), 1333 (s), 1316 (m), 1286 (w), 1240 (w), 1180 (s), 1165 (s), 1138 (w), 1113 (w), 1067 (s), 1030 (m), 972 (s), 939 (s), 883 (s), 826 (s), 770 (m), 711 (m), 524 (vs), 460 (m), 433 (w), 408 (w). **Raman** (1075 nm, 1000 mW, 25 °C, cm^{-1}): ṽ = 3061 (10), 3028 (29), 3007 (39), 2984 (42), 2934 (100), 2897 (35), 1485 (32), 1416 (16), 1385 (10), 1373 (13), 1352 (19), 1181 (19), 1161 (52), 1111 (23), 1071 (19), 1032 (16), 982 (13), 940 (13), 770 (16), 714 (13), 529 (39), 461 (13). **Anal. Calcd** for $C_4H_8O_4S$: C, 31.57; H, 5.30; S, 21.07. Found: C, 31.47; H, 5.27; S, 21.20. **DSC** (5 °C min^{-1}): 37.0 °C (m.p.), 254.0 °C (dec.).

3-Azidooxetane (3) – Method A. Oxetan-3-yl 4-methylbenzenesulfonate (4.56 g, 20.0 mmol) and sodium azide (1.95 g, 30.0 mmol, 1.5 equiv) were suspended in dry DMSO (6 mL) and heated to 100 °C for 36 h in a closed (silicone rubber septum) round-bottom flask by means of an oil bath. Afterward, the reaction mixture was poured into saturated sodium chloride solution (75 mL) and the aqueous phase extracted with a 2:1 mixture of diethyl ether and ethyl acetate (5 × 25 mL) until the organic phase became colorless. The combined organic phases were then washed with saturated sodium chloride solution (3 × 30 mL) and dried over sodium sulfate. The solvent was removed by rotary evaporation to give 1.47 g (74%) of 3-azidooxetane as a yellowish liquid. The crude product was subject to vacuum distillation (75 °C, 10 mbar) to give 1.19 g (60%) of 3-azidooxetane (**3**) as colorless liquid with purity suitable for polymerization.

^{1}H NMR ($CDCl_3$, 400 MHz): δ 4.84 (ddd, 2H, CH_2), 4.62 (ddd, 2H, CH_2), 4.55 (m, 1H, CH). **^{13}C{^{1}H} NMR** ($CDCl_3$, 101 MHz): δ 77.2, 54.6. **^{14}N NMR** ($CDCl_3$, 29 MHz): δ −135.8 (N_β), −164.1 (N_γ),

−305.0 (N_α). **IR** (ATR, cm^{-1}): $\tilde{\nu}$ = 2961 (w), 2880 (w), 2097 (vs), 1359 (m), 1310 (m), 1260 (s), 1062 (w), 1044 (w), 974 (s), 924 (m), 852 (m), 751 (w), 553 (m), 405 (w). **Raman** (1075 nm, 1000 mW, 25 °C, cm^{-1}): $\tilde{\nu}$ = 2973 (12), 2932 (9), 2886 (15), 2253 (48), 2107 (4), 1482 (4), 1264 (4), 1164 (3), 930 (7), 911 (6), 736 (15), 649 (100). **Anal. Calcd** for $C_3H_5N_3O$: C, 36.36; H, 5.09; N, 42.21. Found: C, 36.48; H, 4.99; N, 43.02. **LRMS** (EI) m/z: [M]$^+$ Calcd for $C_3H_5N_3O$ 99.0433; Found 57.13 [C_3H_5O]$^+$. **IS**: 3 J. **FS**: > 192 N.

3-Azidooxetane (3) – Method B (Preferred). Oxetan-3-yl methanesulfonate (3.04 g, 20.0 mmol) and sodium azide (1.95 g, 30.0 mmol, 1.5 equiv.) were suspended in dry DMSO (6 mL), and the reaction mixture was heated to 100 °C for 36 h (oil bath) in a closed (silicone rubber septum) round bottom flask. The work-up was performed as described above to give 1.37 g (69%) of 3-azidooxetane as yellowish liquid.

Glycidyl Azide.[28,29] Glycidyl azide was prepared according to combined and modified literature procedures. Magnesium perchlorate (content: 83 wt%) (4.82 g, 17.9 mmol) was dissolved in water (16 mL) and the solution was cooled to 0–5 °C by means of an ice bath. Sodium azide (2.62 g, 40.3 mmol) was added keeping the initial temperature prior to the addition of epichlorohydrin (2.69 g, 29.1 mmol) over a period of 5 min. The reaction mixture was stirred for 20 min and subsequently allowed to stand in a refrigerator overnight. The precipitated magnesium hydroxide was then removed by suction filtration and washed with dichloromethane (2 × 30 mL). The organic layer was separated and the aqueous layer extracted with additional dichloromethane (3 × 20 mL). The combined organic phases were dried over sodium sulfate and the solvent evaporated to give 3.00 g (99%) of crude 1-azido-3-chloropropan-2-ol as yellowish liquid which was then added to water (2.7 mL). A 10 M sodium hydroxide solution (2.2 mL) was added over a period of 1.5 h under vigorous stirring. Stirring was continued for 20 min and the aqueous phase extracted with diethyl ether (3 × 30 mL). The organic phase was dried over sodium sulfate. Ether was removed by rotary evaporation and the yellowish liquid subject to vacuum distillation (15 mbar, 65 °C, oil bath) to give 1.45 g (66%) of glycidyl azide as colorless liquid.

^{1}H NMR ($CDCl_3$, 400 MHz): δ 3.52 (dd, 1H, CH_2), 3.26 (dd, 1H, CH_2), 3.16 (m, 1H, CH), 2.80 (dd, 1H, CH_2), 2.67 (dd, 1H, CH_2). **^{13}C{^{1}H}** NMR ($CDCl_3$, 101 MHz): δ 52.3, 50.3, 44.8. **^{14}N NMR** ($CDCl_3$, 29 MHz): δ −133.4 (N_β), −168.9 (N_γ), −316.4 (N_α). **IR** (ATR, cm^{-1}): $\tilde{\nu}$ = 2090 (vs), 1441 (w), 1417 (w), 1317 (w), 1284 (m), 1256 (s), 1232 (m), 1135 (w), 987 (w), 925 (w), 882 (m), 845 (m), 836 (m), 763 (m), 744 (w), 670 (w), 560 (m), 472 (m), 422 (w), 409 (w). **Raman** (1075 nm, 1000 mW, 25 °C, cm^{-1}): $\tilde{\nu}$ = 3067 (25), 3009 (86), 2930 (100), 2869 (20), 2861 (18), 2097 (25), 1482 (12), 1443 (14), 1416 (16), 1260 (57), 1231 (24), 1154 (12), 1137 (16), 1119 (12), 923 (12), 884 (41), 849 (20), 765 (14), 473 (10). **Anal. Calcd** for $C_3H_5N_3O$: C, 36.36; H, 5.09; N, 42.21. Found: C, 36.52; H, 4.88; N, 42.63. **HRMS** (EI) m/z: $[M]^+$ Calcd for $C_3H_5N_3O$ 99.0433; Found 99.0427, 58.0434 $[C_3H_6O]^+$. **IS**: 5 J. **FS**: > 240 N.

Poly(3-azidooxetane) (Preferred Method). A Schlenk round bottom flask was closed with a silicone rubber septum and thoroughly dried under a protective atmosphere (argon). Butane-1,4-diol (44.6 µL, 505 µmol, 0.05 equiv.) and boron trifluoride etherate (124 µL, 1.01 mmol, 0.1 equiv.) were added using a 100 µL Hamilton syringe. The initiating mixture was stirred for 15 min prior to the addition of dry dichloromethane. Subsequently, a solution of 3-azidooxetane (1.00 g, 10.1 mmol) in dry dichloromethane (3.54 mL) was added over a period of 2 h using a syringe pump. The reaction mixture was stirred at 250 rpm for 48 h causing a color change to orange. The polymerization was quenched by the addition of water (15 mL) and vigorously stirred for 5 min. The yellowish, honey-like polymer was allowed to settle, and the aqueous phase was decanted. Water (10 mL) was added and the sticky emulsion stirred for 5 min prior to decanting of the aqueous phase. The polymer was transferred to another round-bottom flask using acetone and all volatiles were removed by rotary evaporation. The yellowish polymer was dried under vacuum conditions (10^{-3} mbar, 5 h) to give 0.67 g (67%) of poly(3-azidooxetane) as dark orange oil of high viscosity.

^{1}**H NMR** (400 MHz, $CDCl_3$): δ 3.94–3.37. **FT-IR** (ATR, cm^{-1}): $\tilde{\nu}$ = 2914 (w), 2871 (w), 2088 (vs), 1477 (w), 1267 (s), 1111 (s), 921 (m), 840 (m), 659 (m), 626 (m), 556 (m). **Anal. Calcd** for $(C_3H_5N_3O)_n$: C 36.36, H 5.09, N 42.41. Found: C 37.43, H 5.40, N 37.67. **DSC** (5 °C min^{-1}): −54.6 °C (glass transition), 211.7 °C (dec). **EW** (g eq^{-1}) = 1319 g mol^{-1}**.** **GPC**: M_w = 1186 g mol^{-1}, M_n = 540 g mol^{-1}, M_p = 941 g mol^{-1}, M_z = 2079 g mol^{-1}, PDI = 2.19. **Density**: ρ = 1.30 g cm^{-3}. **IS**: > 10 J. **FS** > 360 N.

Poly(3-azidooxetane) (TIBA Method). ***Catalyst Preparation.*** A 1.1 M triisobutylaluminum solution (20.0 mL, 22.0 mmol) was cooled to 0 °C under protective atmosphere (argon) using an ice bath. Water (277 µL, 15.4 mmol) was added under vigorous stirring, which was continued for 24 h. A Schlenk round bottom flask was closed with a silicone rubber septum, thoroughly dried under protective atmosphere (argon), and charged with 3-azidooxetane (0.60 g, 6.05 mmol) and dry DCM (2.48 mL). Subsequently, 1.1 M TIBA solution (550 µL) was added over a period of 1 h using a syringe pump at 0 °C. Subsequently, the reaction mixture was allowed to warm to ambient temperature, stirred for 48 h and quenched with water (5 mL) under vigorous stirring. All volatiles were evaporated to give colorless, brittle flakes which were dried under high vacuum conditions (10^{-3} mbar, 5 h) to obtain 126 mg (21%) of polymeric material.

^{1}**H NMR** (400 MHz, DMSO-d_6): δ 3.86–3.12. **FT-IR** (ATR, cm^{-1}): $\tilde{\nu}$ = 2925 (w), 2871 (w), 2095 (m), 1467 (vw), 1266 (w), 1100 (w), 611 (s), 453 (vs). **Anal. Calcd** for $(C_3H_5N_3O)_n$: C 36.36, H 5.09, N 42.41. Found: C 10.21, H 3.75, N 5.66. **DSC** (5 °C min^{-1}): 194.6 °C (dec.).

Associated Content

The Supporting Information is available free of charge at https://pubs.acs.org/doi/10.1021/acs.joc.1c01060.
^{1}H, ^{13}C, and ^{14}N NMR spectra; Crystallographic information; Detonation parameter calculations (output files); DSC graphs (PDF); Deflagration video (hot plate test) of glycidyl azide (MP4); Deflagration video (hot-plate test) of 3-azidooxetane (MP4); Deflagration video (hot plate test) of poly(3-azidooxetane) (MP4).

Accession Codes

CCDC 1916317–1916318 contain the supplementary crystallographic data for this paper. These data can be obtained free of charge via www.ccdc.cam.ac.uk/data_request/cif, or by emailing data_request@ccdc.cam.ac.uk, or by contacting The Cambridge Crystallographic Data Centre, 12 UnionRoad, Cambridge CB2 1EZ, UK; fax: +44 1223 336033.

Acknowledgements

Financial support of this research by the Ludwig Maximilian University of Munich (LMU) and the Office of Naval Research (ONR) under grant no. ONR N00014-19-1-2078 is gratefully acknowledged. We also thank Stefan Huber for his sensitivity testing support and Tessa Kustermann as well as Jakob Plank for their relentless and dedicated help with all preparative tasks.

References

[1] Ang, H. G.; Pisharath, S. *Energetic Polymers: Binders and Plasticizers for Enhancing Performance*; Wiley-VCH: Weinheim, **2012**.

[2] Manser, G. E. Energetic Copolymers and method of making same. US 4 483 978, **1984**.

[3] Manser, G. E.; Hajik R. M. Method of synthesizing nitrato alkyl oxetanes. US 5 214 166, **1993**.

[4] Vandenberg, E. J. Polyethers containing azidomethyl side chains. US 3 645 917, **1972**.

[5] Murali Mohan, Y.; Mohana Raju, K.; Sreedhar, B. Synthesis and Characterization of Glycidyl Azide Polymer with Enhanced Azide Content. *Int. J. Polym. Mater.* **2006**, *55*, 441.

[6] Ampleman, G. Glycidyl azide polymer. US 5 256 804, **1993**.

[7] Baum, K.; Berkowitz, P. T.; Grakauskas, V.; Archibald, T. G. Synthesis of electron-deficient oxetanes. 3-Azidooxetane, 3-nitrooxetane, and 3,3-dinitrooxetane. *J. Org. Chem.* **1983**, 48, 2953-2956.

[8] Grakauskas, V.; Berkowitz, P. T.; Baum, K. Synthesis and polymerization of 3-azidooxetane. US 4 414 384, **1983**.

[9] Sućeska, M. EXPLO5, Version 6.04, Brodarski Institute, Zagreb, **2017**.

[10] Bull, J. A.; Croft, R. A.; Davis, O. A.; Doran, R.; Morgan, K. F. Oxetanes: Recent Advances in Synthesis, Reactivity, and Medicinal Chemistry. *Chem. Rev.* **2016**, *116*, 12150-12233.

[11] Wojtowicz, J. A.; Polak, R. J. 3-Substituted oxetanes. *J. Org. Chem.* **1973**, *38*, 2061-2066.

[12] Wu, W.-L.; Burnett, D. A.; Greenlee, W. J. Gamma Secretase Inhibitors. WO 2012/138 678 A1, **2012**.

[13] Jones, R. M; Buzard, D. J.; Han, S.; Kim, S. H.; Lehrmann, J.; Zhu, X. Modulators of the GPR119 Receptor and the treatment of disorders related thereto. WO 2013/055 910 A1, **2013**.

[14] Hafner, S. Internal plasticized glycidyl azide copolymers for energetic solid propellant binders. Ph. D. Dissertation, Ludwig-Maximilian University (LMU) Munich, Munich, Germany, **2019**.

[15] Penczek, S. Cationic ring-opening polymerization [CROP] major mechanistic phenomena. *J. Polym. Sci., Part A: Polym. Chem.* **2000**, *38*, 1919-1933.

[16] Mukhametshin, T. I.; Petrov, A. I.; Kuznetsova, N. V.; Petrov, V. A.; Averianova, N. V.; Garaev, I. K.; Kostochko, A. V.; Gubaidullin, A. T.; Vinogradov, D. B.; Bulatov, P. V. Synthesis and copolymerization of azidomethyl-substituted oxetanes: the morphology of statistical block copolymers. *Chem. Heterocycl. Compd.* **2017**, *53*, 811-821.

[17] Luger, P.; Buschmann, J. Oxetane: the first x-ray analysis of a nonsubstituted four-membered ring. *J. Am. Chem. Soc.* **1984**, *106*, 7118-7121.

[18] Orpen, A. G.; Brammer, L.; Allen, F. H.; Kennard, O.; Watson, D. G.; Taylor, R. In *Struct. Correl.* **1994**, p 752-858.

[19] Spackman, M. A.; Jayatilaka, D. Hirshfeld surface analysis. *CrystEngComm* **2009**, *11*, 19-32.

[20] Spackman, M. A.; McKinnon, J. J. Fingerprinting intermolecular interactions in molecular crystals. *CrystEngComm* **2002**, *4*, 378-392.

[21] Klapoetke, T. M.; Born, M.; Fessard, T.; Göttermann, L.; Stierstorfer, J.; Voggenreiter, M. 3,3-Dinitratooxetane - An Important Leap Towards Energetic Oxygen-Rich Monomers and Polymers. *Chem. Commun.* **2021**, *57*, 2804–2807.

[22] Nersasian, A.; Johnson, P. R. Infrared spectra of alkanesulfonic acids, chlorosulfonated polyethylene, and their derivatives. *J. Appl. Polym. Sci.* **1965**, *9*, 1653-1668.

[23] Frisch, M. J.; Trucks, G. W.; Schlegel, H. B.; Scuseria, G. E.; Robb, M. A.; Cheeseman, J. R.; Scalmani, G.; Barone, V.; Petersson, G. A.; Nakatsuji, H.; Li, X.; Caricato, M.; Marenich, A. V.; Bloino, J.; Janesko, B. G.; Gomperts, R.; Mennucci, B.; Hratchian, H. P.; Ortiz, J. V.; Izmaylov, A. F.; Sonnenberg, J. L.; Williams Ding, F.; Lipparini, F.; Egidi, F.; Goings, J.; Peng, B.; Petrone, A.; Henderson, T.; Ranasinghe, D.; Zakrzewski, V. G.; Gao, J.; Rega, N.; Zheng, G.; Liang, W.; Hada, M.; Ehara, M.; Toyota, K.; Fukuda, R.; Hasegawa, J.; Ishida, M.; Nakajima, T.; Honda, Y.; Kitao, O.; Nakai, H.; Vreven, T.; Throssell, K.; Montgomery, J. A., Jr.; Peralta, J. E.; Ogliaro, F.; Bearpark, M. J.; Heyd, J. J.; Brothers, E. N.; Kudin, K. N.; Staroverov, V. N.; Keith, T. A.; Kobayashi, R.; Normand, J.; Raghavachari, K.; Rendell, A. P.; Burant, J. C.; Iyengar, S. S.; Tomasi, J.; Cossi, M.; Millam, J. M.; Klene, M.; Adamo, C.; Cammi, R.; Ochterski, J. W.; Martin, R. L.; Morokuma, K.; Farkas, O.; Foresman, J. B.; Fox, D. J. Gaussian 16, Rev. C.01; Gaussian, Inc., **2016**.

[24] Altenburg, T.; Klapötke Thomas, M.; Penger, A.; Stierstorfer, J. Two Outstanding Explosives Based on 1,2-Dinitroguanidine: Ammonium- dinitroguanidine and 1,7-Diamino-1,7-dinitrimino-2,4,6-trinitro-2,4,6-triazaheptane. *Z. Anorg. Allg. Chem.* **2010**, *636*, 463-471.

[25] Klapötke, T. M. *Energetic Materials Encyclopedia*; Vol. 1–3; De Gruyter: Berlin, Boston, **2021**.

[26] NATO STANAG 4489: Explosives. Impact Sensitivity Tests; NATO Standardization Office, Brussels, Belgium, **1999**.

[27] NATO STANAG 4487: *Explosives. Friction Sensitivity Tests*; NATO Standardization Office, Brussels, Belgium, **2002**.

[28] Petty, W. L.; Nichols, P. L. Rate of Addition of the Nitrate Ion to the Ethylene Oxide Ring 1. *J. Am. Chem. Soc.* **1954**, *76*, 4385-4289.

[29] Ingham, J. D.; Petty, W. L.; Nichols, J. P. L. Notes- The Addition of Azide Ion to Epoxides. *J. Org. Chem.* **1956**, *21*, 373-375.

9.5 Supporting Information

9.5.1 Screening Attempts

Table S 9.1. Reaction condition screening for 3-tosyloxyoxetane (**1**).

Batch	**Oxetan-3-ol (g, mmol)**	**Base (mmol, eq.)**	***p*-TsCl (mmol, eq.)**	**t (h), T (°C)**	**Crude yield (%)**	**Solvent, volume [mL]**
	2.00, 27.0	NaOH (29.7, 1.1)	28.4, 1.05	1, 50	13	Water, 5.30
B	1.00, 13.5	NaOH (14.9, 1.1)	14.2, 1.05	2, 50	70	Water, 2.65
C	0.50, 6.75	Pyridine (8.10, 1.2)	7.42, 1.1	5, reflux	0	$CHCl_3$, 20.0
D	0.25, 3.37	K_2CO_3 (6.75, 2.0)	3.71, 1.1	5, reflux	36	DCM, 50.0
E	2.00, 27.0	TEA (29.7, 1.1)	27.0, 1.0	4, reflux	53	$CHCl_3$, 50.0
F	2.00, 27.0	TEA (29.7, 1.1)	27.0, 1.0	6, reflux	42	$CHCl_3$, 50.0
G	1.00, 13.5	TEA (14.9, 1.1)	13.5, 1.0	24, rt.	68/57*	DCM, 25.0
H	2.00, 27.0	TEA (29.7, 1.1)	29.7, 1.1	24, reflux	32	DCM, 50.0
I	4.00, 54.0	TEA (59.4, 1.1)	59.4, 1.1	4, reflux	83/75*	DCM, 100

* Yield of pure material after recrystallization.

Table S 9.2. Base screening for the preparation of 3-mesyloxyoxetane (**2**).

Batch	**Oxetan-3-ol (g, mmol)**	**Base (mmol, eq.)**	**MsCl (mmol, eq.)**	**t (h), T (°C)**	**Crude yield (%)**	**Solvent, volume [mL]**
I	0.50, 6.75	DBU (13.5, 2.0)	7.42, 1.1	3, rt.	30	DCM, 15.0
II	0.50, 6.75	DABCO (6.75, 2.0)	7.42, 1.1	3, rt.	87	DCM, 15.0
III	0.30, 4.05	NaHMDS (8.19, 2.0)	4.46, 1.1	3, rt.	23	MeCN, 15.0

The azidation step was roughly screened using 3-tosyloxyoxetane (**1**) as model compound because it was found to be less prone to substitution than 3-mesyloxyoxetane (**2**). The reactions were monitored by TLC and ^1H NMR spectroscopy was used to qualitatively determine whether the turnover was low (<30%), medium (30–60%), high (> 60%) or even quantitative. Overall, DMSO gave the best result and was the most environmentally friendly compared to other solvents.

Table S 9.3. Use of different azidation agents and solvents to prepare 3-azidooxetane.

Solvent	Azidation agent	t (h), T (°C)	Conversion
Chloroform	TBAA*	24, reflux	very low
THF	TBAA	24, reflux	very low
MeCN	NaN_3, 18-crown-6	96, reflux	low
1,4-Dioxane/water 9:1	NaN_3	24, reflux	low
Acetone/water 1:1	NaN_3	36, reflux (80 °C)	medium
Sulfolane	NaN_3	36, 100 °C	high
DMF	NaN_3	36, 100 °C	quantitative
DMSO	NaN_3	36, 100 °C	quantitative

* TBAA = tetrabutylammonium azide

9.5.2 NMR Spectra

Oxetan-3-yl 4-methylbenzenesulfonate (compound 1)

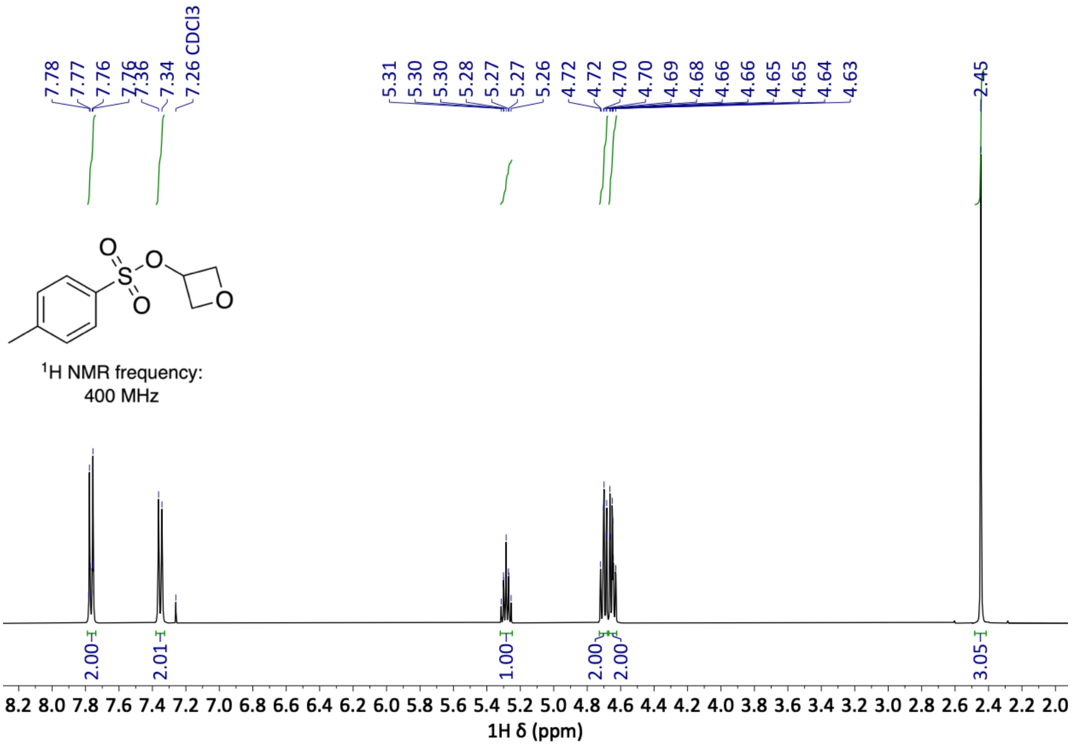

Figure S 9.1. Proton spectrum (^1H) of oxetan-3-yl 4-methylbenzenesulfonate.

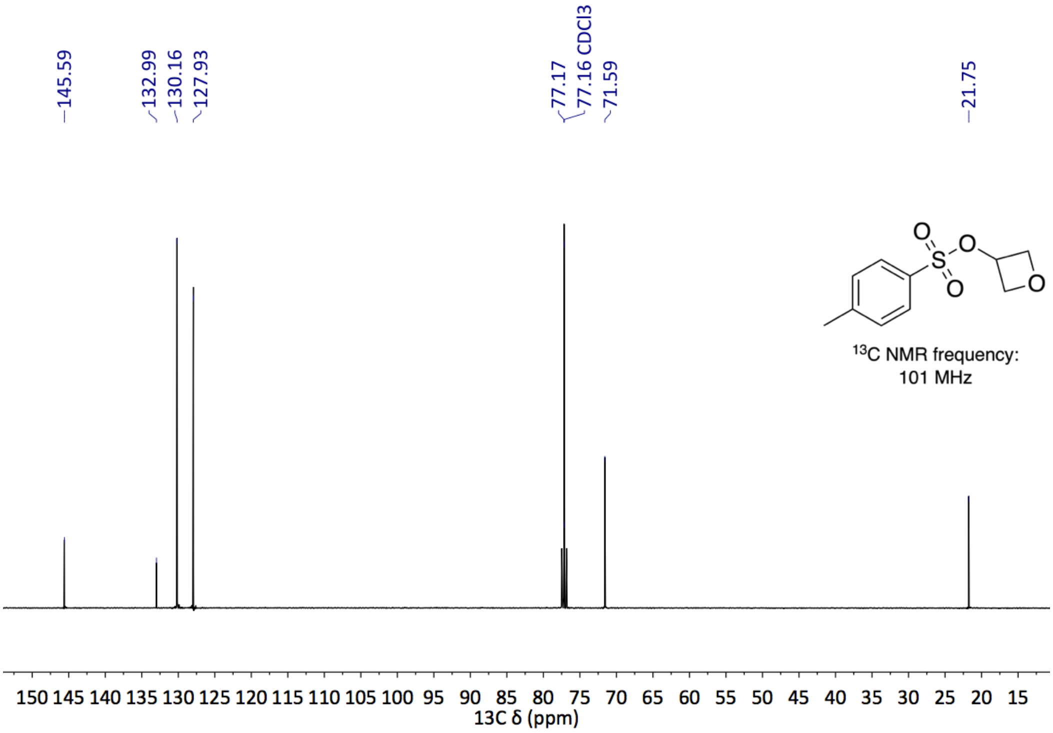

Figure S 9.2. Carbon spectrum (^{13}C) of oxetan-3-yl 4-methylbenzenesulfonate.

Oxetan-3-yl methanesulfonate (compound 2)

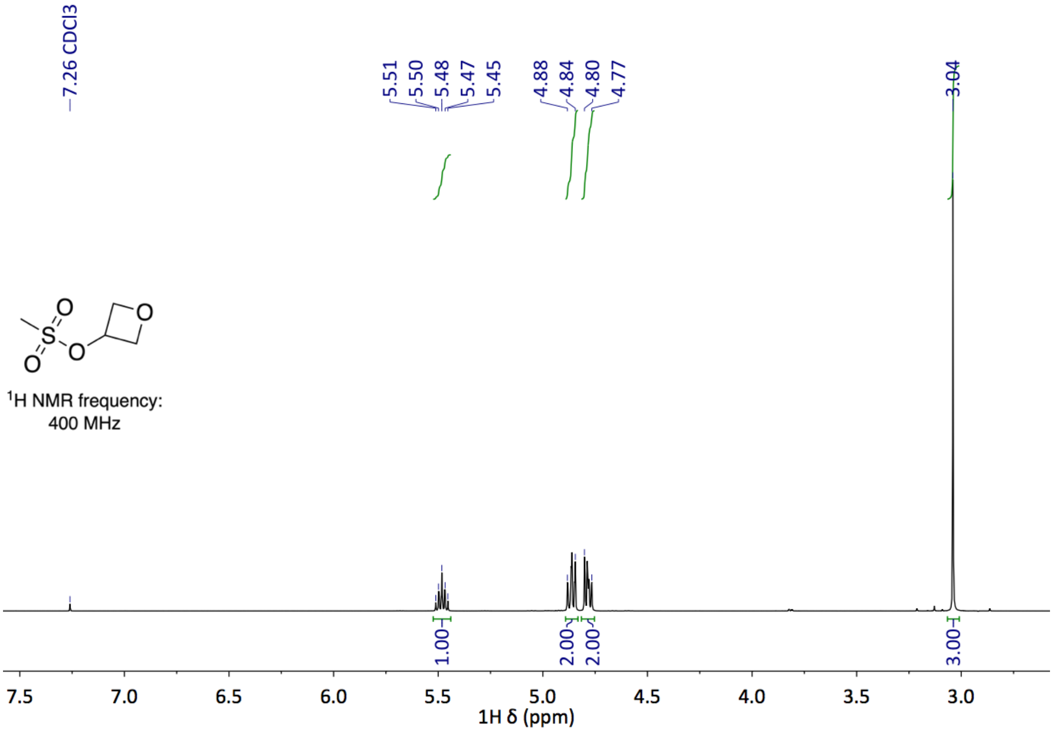

Figure S 9.3. Proton spectrum (^{1}H) of oxetan-3-yl methanesulfonate.

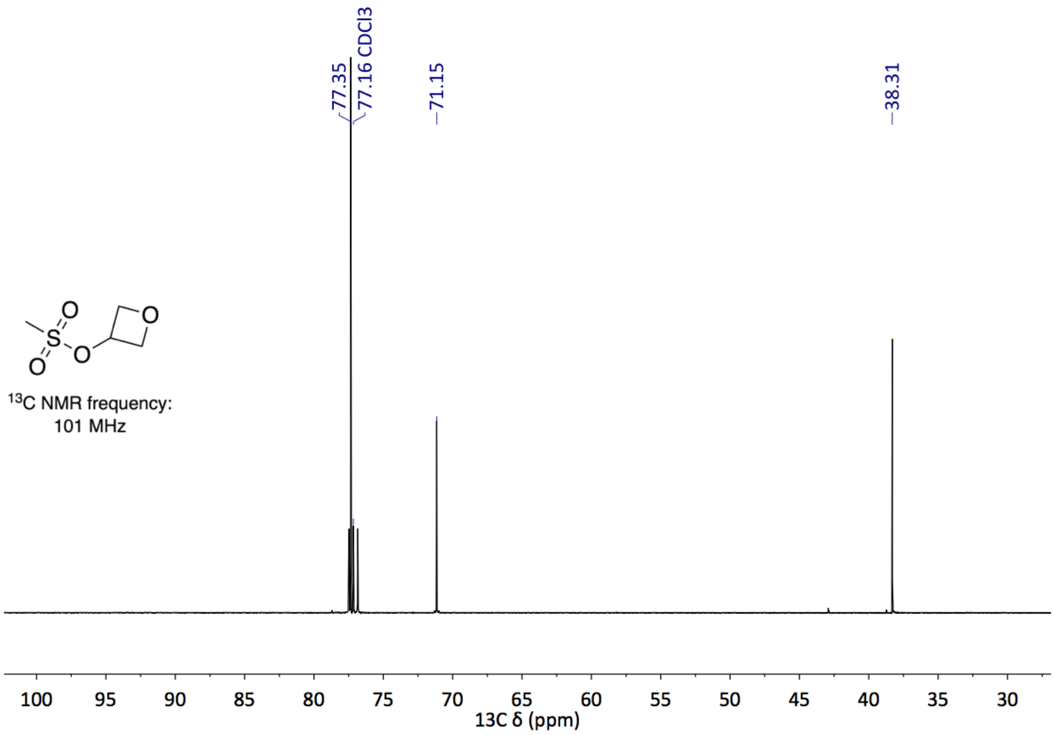

Figure S 9.4. Carbon spectrum (^{13}C) of oxetan-3-yl methanesulfonate.

3-Azidooxetan (compound 3)

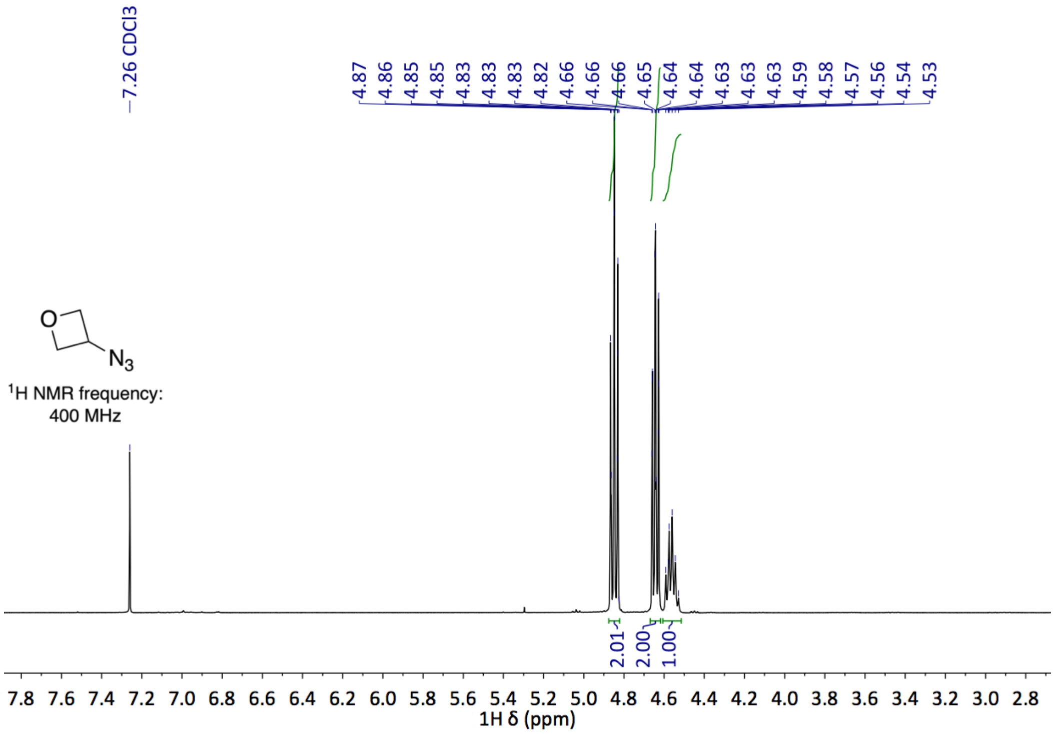

Figure S 9.5. Proton spectrum (^{1}H) of 3-azidooxetane.

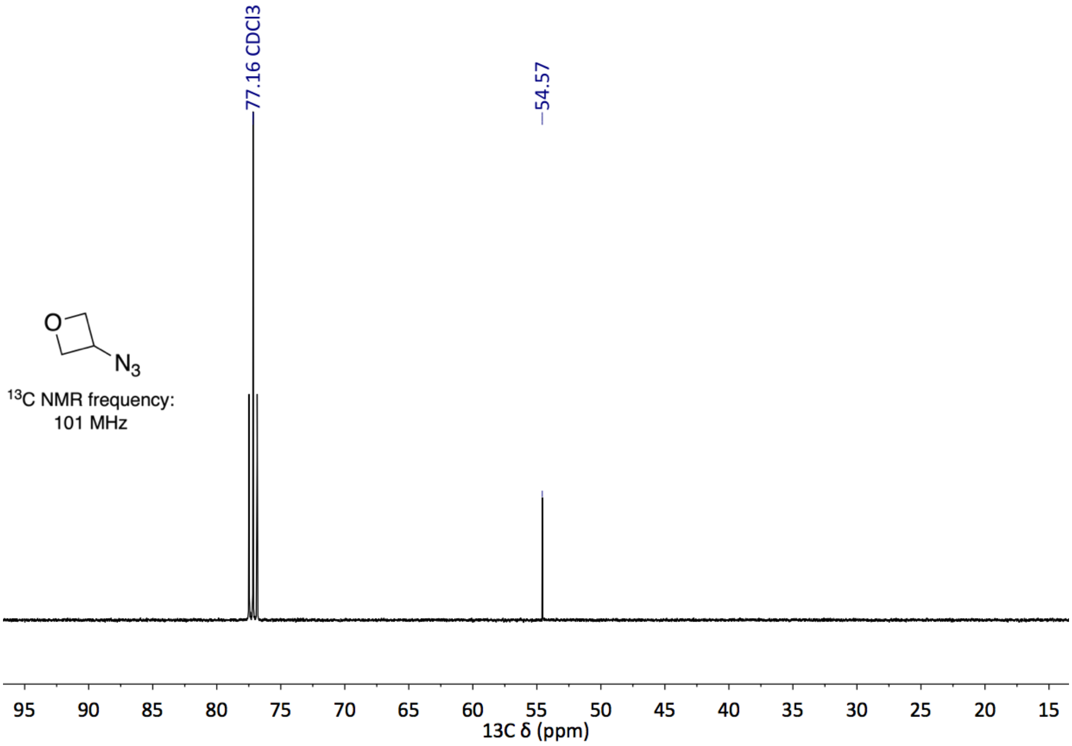

Figure S 9.6. Carbon spectrum (^{13}C) of 3-azidooxetane.

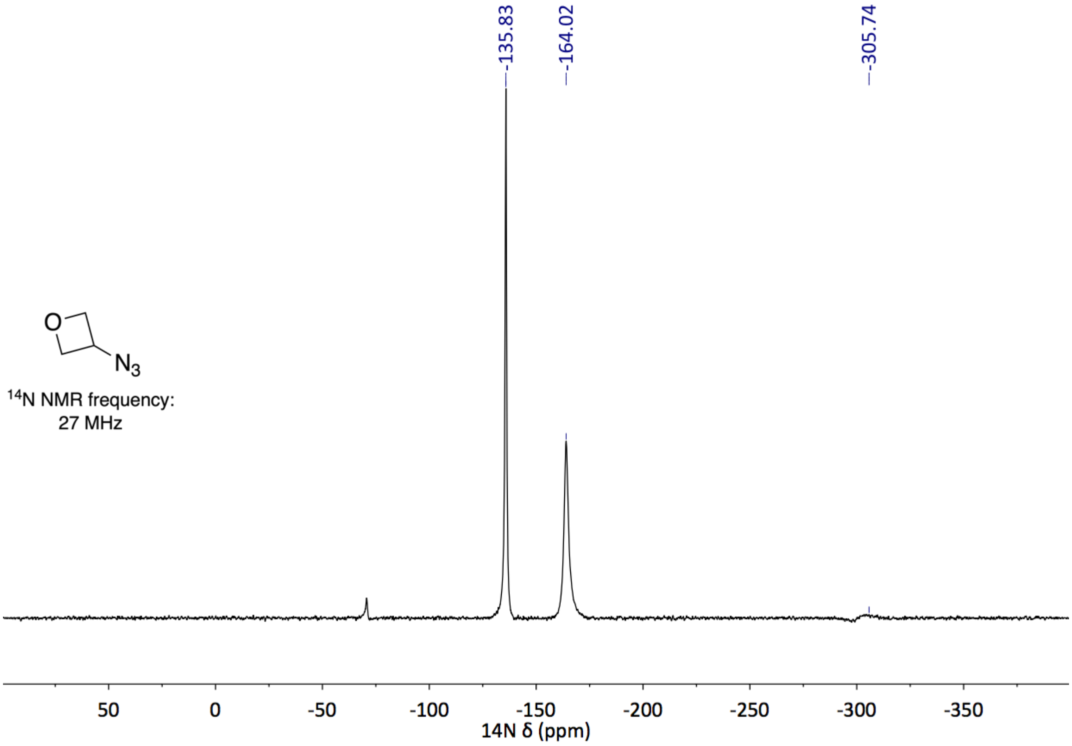

Figure S 9.7. Nitrogen spectrum (^{14}N) of 3-azidooxetane.

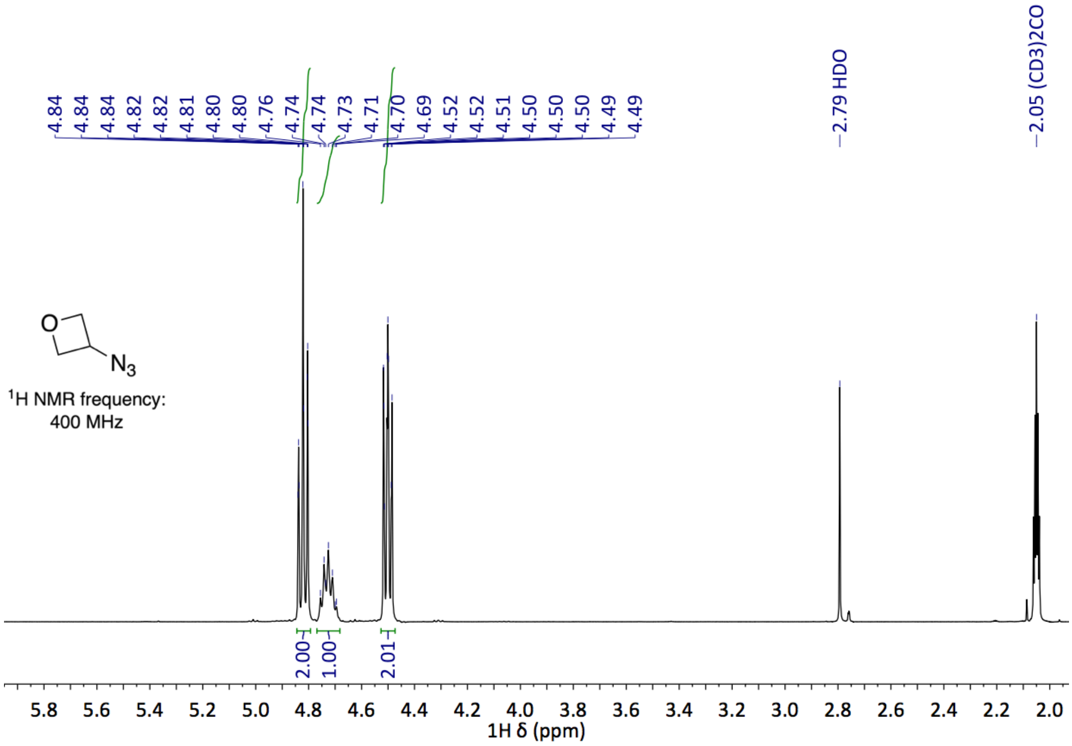

Figure S 9.8. Proton spectrum (^{1}H) of 3-azidooxetane using acetone-d$_6$.

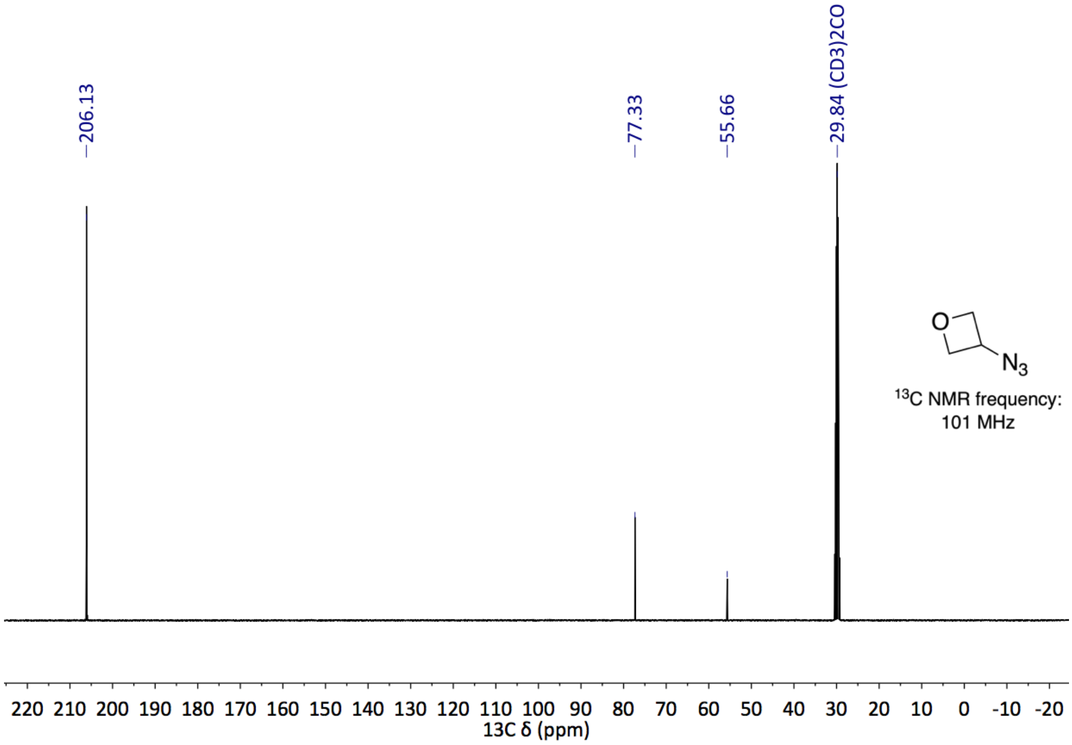

Figure S 9.9. Carbon spectrum (^{13}C) of 3-azidooxetane using acetone-d$_6$.

Glycidyl azide

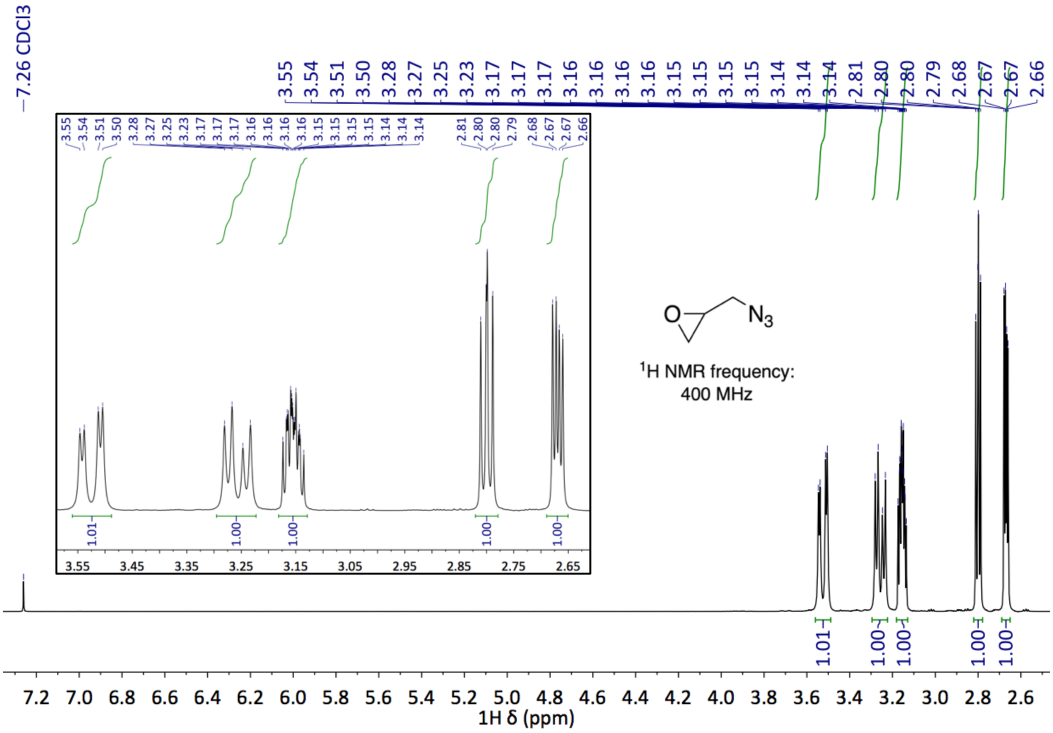

Figure S 9.10. Proton spectrum (^{1}H) of glycidyl azide.

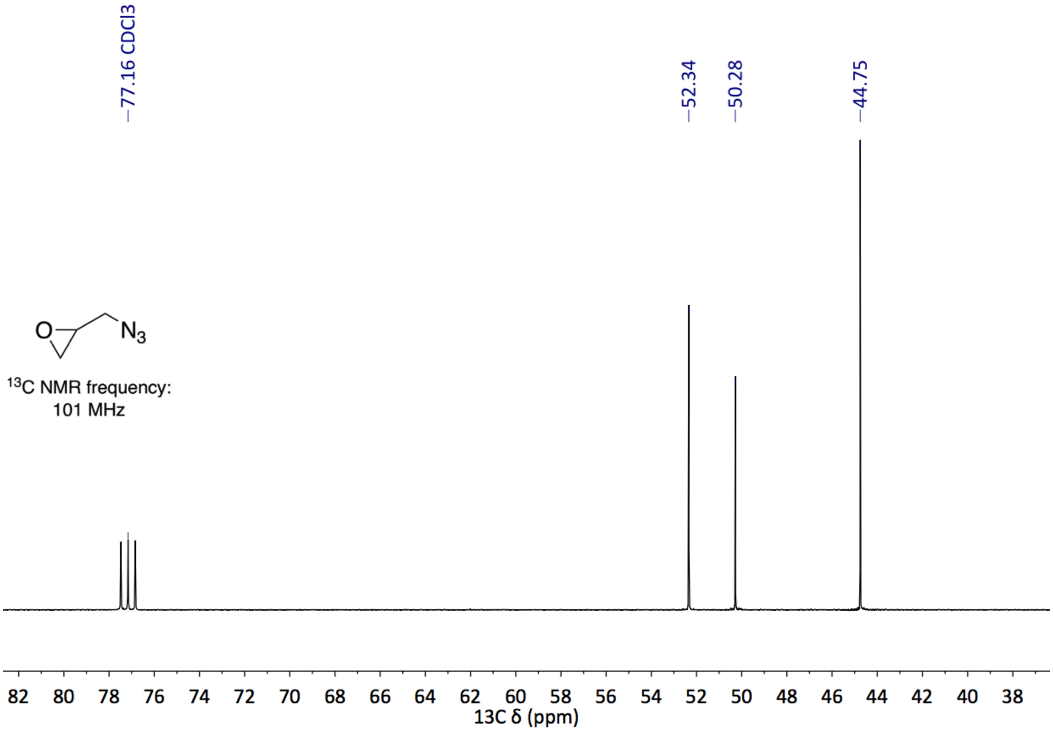

Figure S 9.11. Carbon spectrum (^{13}C) of glycidyl azide.

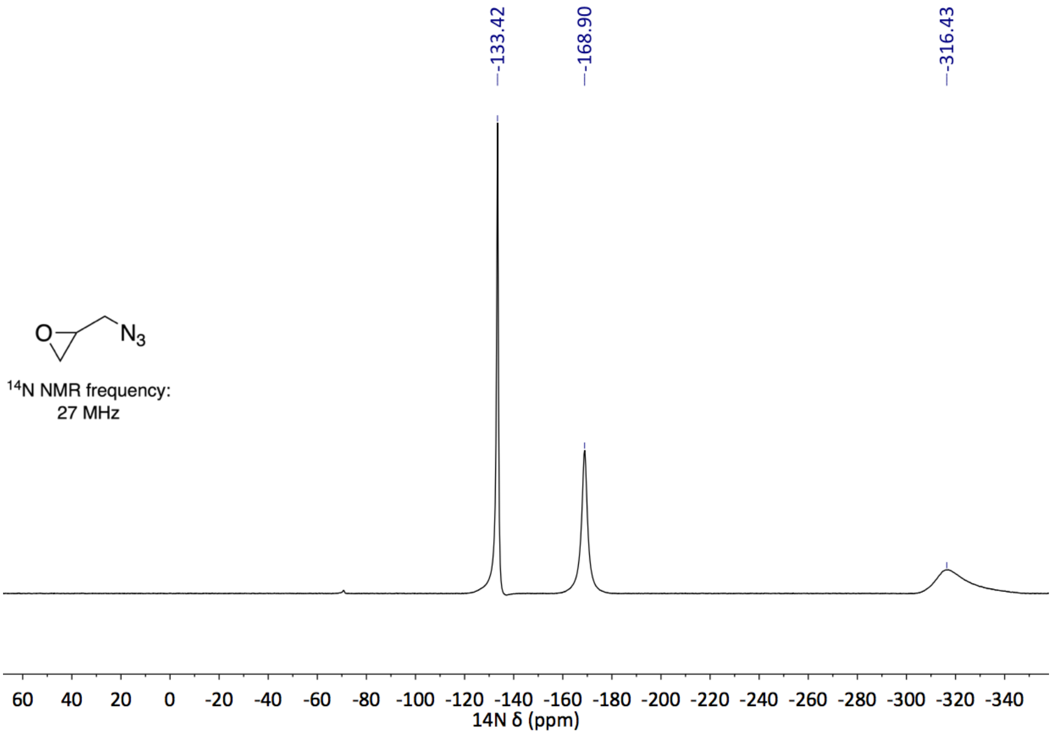

Figure S 9.12. Nitrogen spectrum (^{14}N) of glycidyl azide.

Poly(3-azidooxetane) (compound 4)

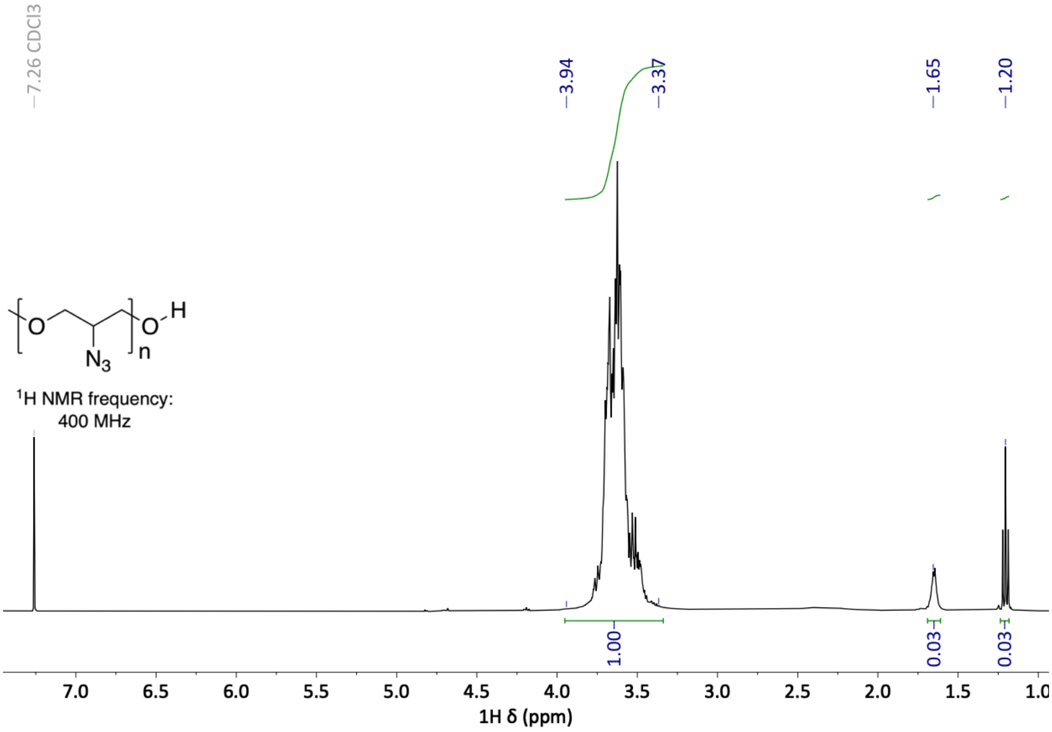

Figure S 9.13. Proton spectrum (^{1}H) of poly(3-azidooxetane).

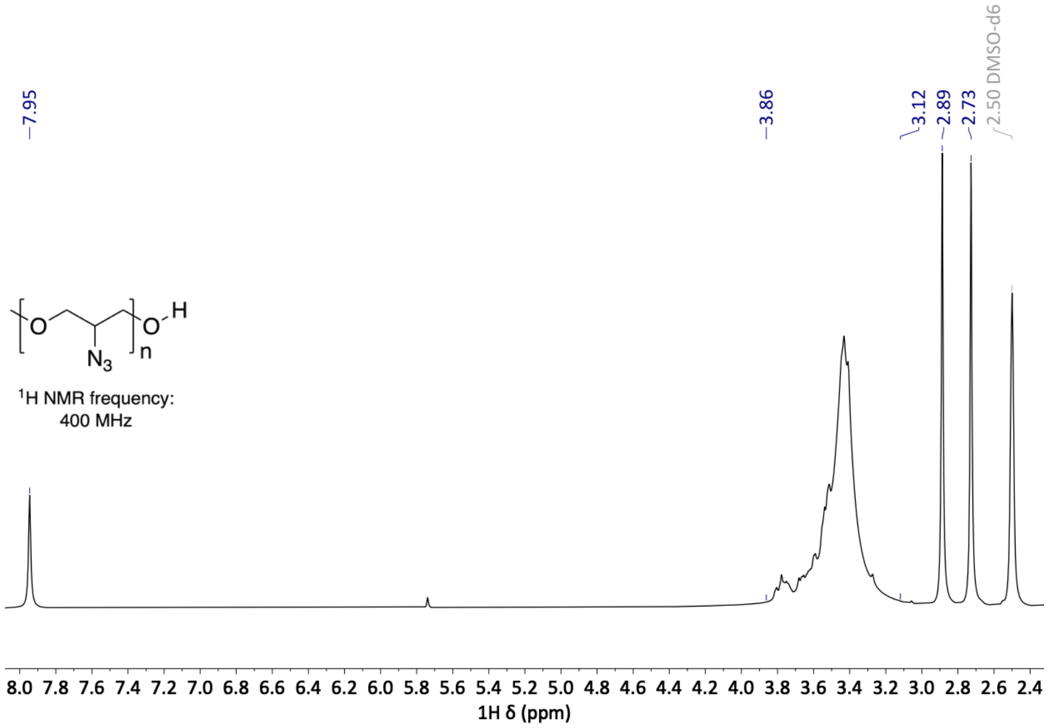

Figure S 9.14. Proton spectrum (^1H) of the attempted preparation of poly(3-azidooxetane) using triisobutylaluminum–water as catalyst. DMF as co-solvent.

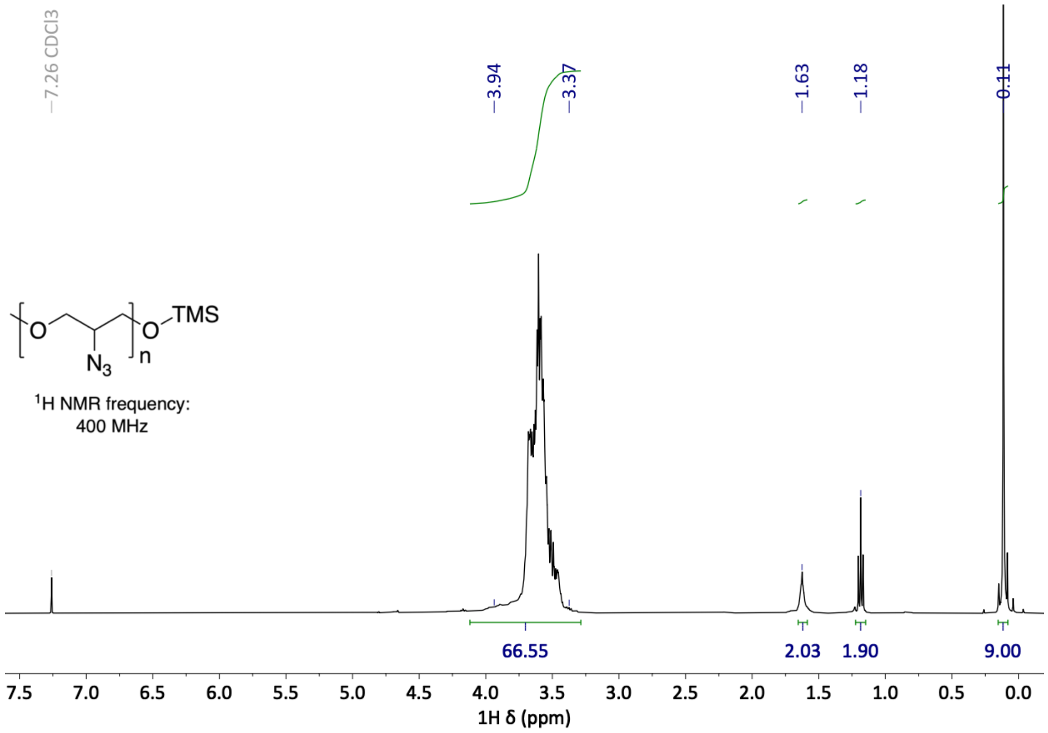

Figure S 9.15. Proton spectrum (^1H) of poly(3-azidooxetane) with end-group protection (TMS) to calculate the equivalent weight.

9.5.3 Crystallography and Hirshfeld Analysis

9.5.3.1 Crystallography

Oxetan-3-yl 4-methylbenzenesulfonate (**1**) and oxetan-3-yl methanesulfonate (**2**) were dissolved in chloroform and single crystals have been obtained after slow evaporation of the solvent. The data collection was performed using an Oxford Xcalibur3 diffractometer featuring a CCD area detector equipped with a multilayer monochromator, Photon 2 detector and a rotating-anode generator operating with Mo-Kα radiation (λ = 0.7107 Å). Both data collection and reduction were performed using the CrysalisPRO software.[1] The structures were solved by direct methods (SIR-92, SIR-97)[2,3] and refined by full-matrix least-squares on F2 (ShelXL).[4–6] and finally checked using the Platon software integrated in the WinGX suite.[7,8] Non-hydrogen atoms were refined anisotropically and the hydrogen atoms were located and freely refined. All structure plots depict thermal ellipsoids at the 50% probability level and hydrogen atoms are shown as small spheres of arbitrary radius.

Table S 9.4. Detailed crystallographic information of oxetan-3-yl 4-methylbenzenesulfonate (**1**) and oxetan-3-yl methanesulfonate (**2**).

	1	**2**
Formula	$C_{10}H_{12}O_4S$	$C_4H_8O_4S$
FW [g mol^{-1}]	228.26	152.15
Crystal System	Monoclinic	Triclinic
Space Group	$P2_1/n$	$P{-}1$
Color / Habit	Colorless block	Colorless block
Size [mm]	0.43 x 0.39 x 0.22	0.50 x 0.50 x 0.40
a [Å]	9.638(6)	7.8381(7)
b [Å]	7.381(3)	9.4125(9)
c [Å]	14.929(3)	9.6897(9)
α [°]	90	109.546(9)
β [°]	102.65(3)	103.557(8)
γ [°]	90	96.702(7)
V [Å ^{3}]	1036.36(7)	639.87(11)
Z	4	4
$\rho_{calc.}$ [g cm^{-3}]	1.463	1.580
μ [mm^{-1}]	0.303	0.446
F (000)	480	320
$\lambda_{MoK\alpha}$ [Å]	0.71073	0.71073
T [K]	143	180
ϑ min-max [°]	4.7450, 28.5980	4.3860, 28.4470
Dataset h; k; l	−9:12; −9:8; −9:8	−9:9; −4:11; −12:11
Reflect. coll.	2084	2558
Independ. Refl.	1724	2207
$R_{int.}$	0.027	0.017
Reflection obs.	1724	2207
No. parameters	137	165
R1 (obs.)	0.0367	0.0322
wR2 (all data)	0.0941	0.0784
S	1.051	1.058
Resd. Dens. [e Å^{-3}]	−0.352, 0.266	−0.338, 0.229
Device Type	Oxford XCalibur3 CCD	Oxford XCalibur3 CCD
Solution	Sir92	Sir97
Refinement	SHELXLE	SHELXLE
Absorpt. Corr.	Multi-scan	Multi-scan
CCDC	1916318	1916317

Oxetan-3-yl 4-methylbenzenesulfonate (1)

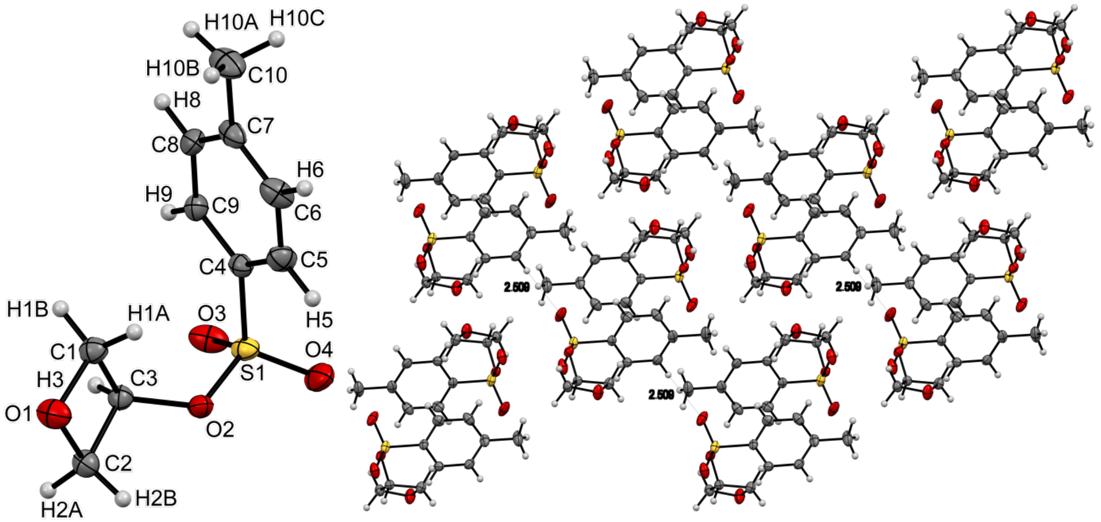

Figure S 9.16. a) Molecular structure of compound **1**. Thermal ellipsoids drawn at the 50% probability level. b) View along *b* axis showing the closest contact in the crystal framework.

Oxetan-3-yl 4-methanesulfonate (2)

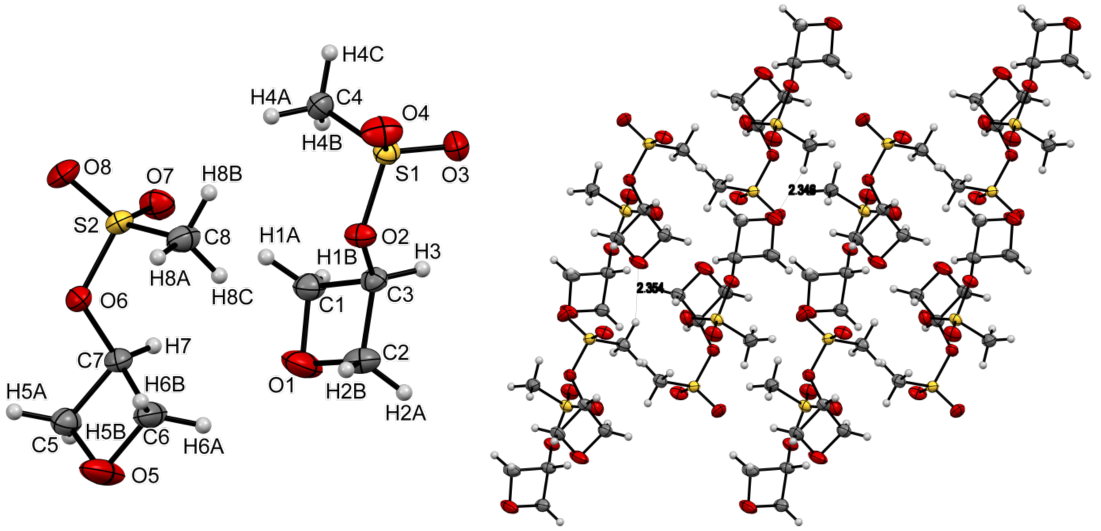

Figure S 9.17. a) Molecular structure and crystallographic twins of compound **2**. b) View along *b* axis showing the closest contact within the crystal.

9.5.3.2 Hirshfeld Analysis

The following data was collected with CrystalExplorer V17.5.[9]

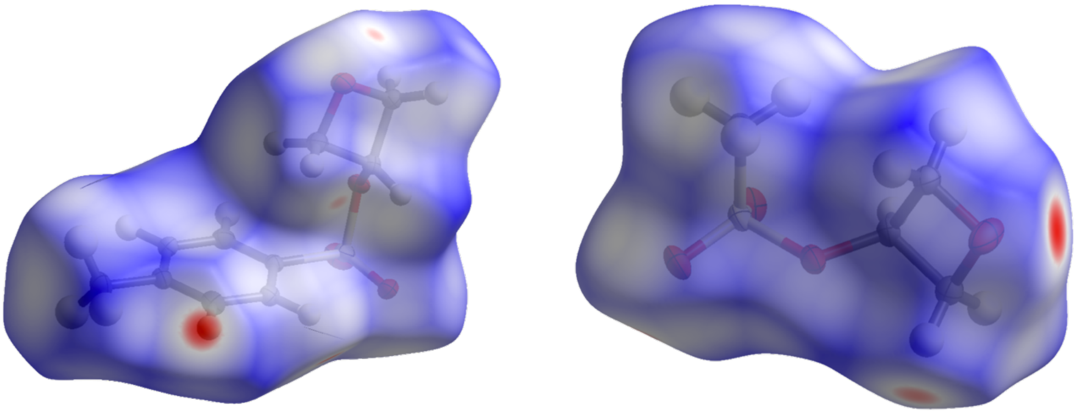

Figure S 9.18. Calculated Hirshfeld surfaces for compound **1** (left) and compound **2** (right) indicating close contacts.

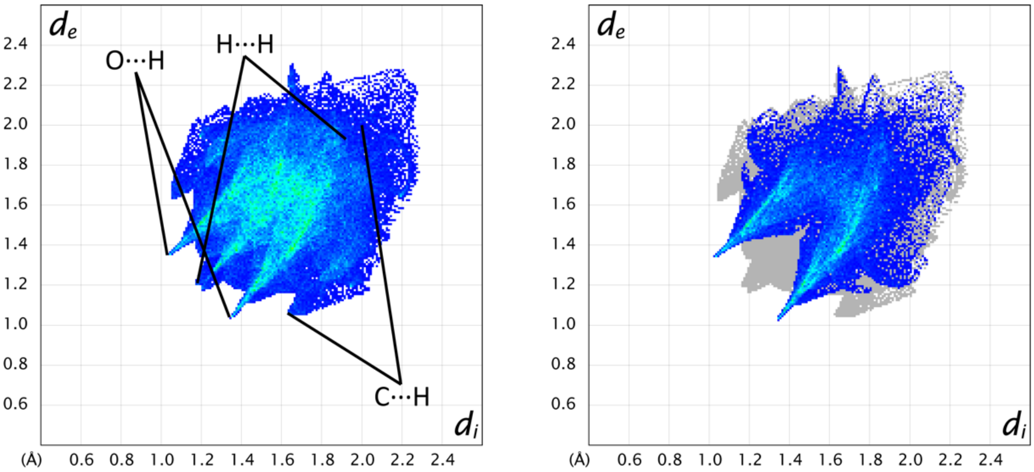

Figure S 9.19. 2D fingerprint plot of 3-oxetanyl methylbenzenesulfonate (**1**) showing all interactions (left) and the high population of stabilizing O-H-interactions (right).

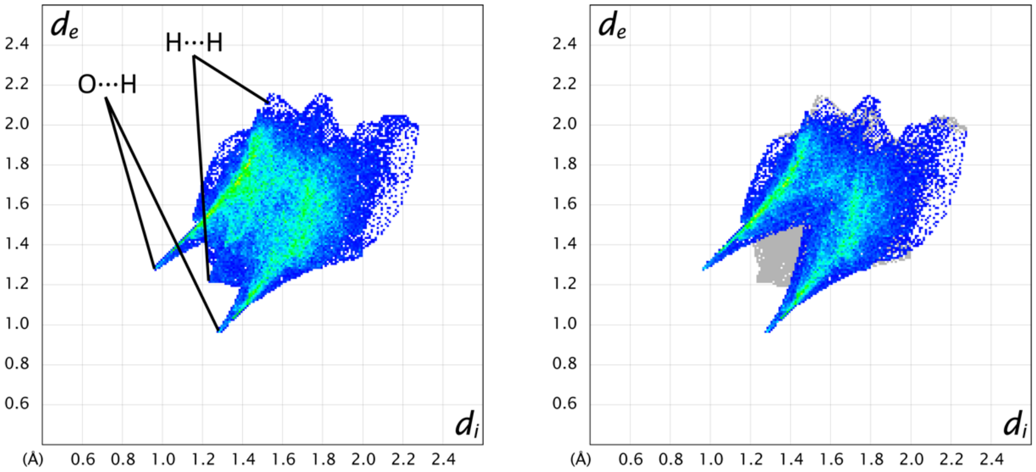

Figure S 9.20. 2D fingerprint plot of 3-oxetanyl methanesulfonate (**2**) showing all interactions (left) and the high percentage of stabilizing O-H-interactions (right).

9.5.4 Heat of Formation Calculation and Thermal Analysis

The atomization method was used to determine the heat of formation of 3-azidooxetane and glycidyl azide using the atom energies in Table S 5.[10]

$$\Delta_f H°_{(g,\ M,\ 298)} = H_{(molecule,\ 298)} - \Sigma H°_{(atoms,\ 298)} + \Sigma\Delta_f H°_{(atoms,\ 298)}$$

Table S 9.5. CBS-4M electronic enthalpies for atoms C, H, N, and O and their literature values.

	$-H^{298}$ / a.u.	$\Delta_f H°_{gas}$[11]
H	0.500991	217.998
C	37.786156	716.68
N	54.522462	472.68
O	74.991202	249.18

The Gaussian16 program package was used to calculate room temperature enthalpies on the CBS-4M level of theory.[12] To obtain the energy of formation for the liquid phase of **1** and **2**, Trouton's Rule was applied ($\Delta H_{sub} = 90 \cdot T_m$).

Table S 9.6. Heat of formation calculation results for compound **3** and glycidyl azide.

M	$-H^{298}$ [a] [a.u.]	$\Delta_f H°(g, M)$ [b] [kJ mol^{-1}]	$\Delta_{sub}H°(M)$ [c] [kJ mol^{-1}]	$\Delta_f H°(s/l)$ [d] [kJ mol^{-1}]	Δn	$\Delta_f U(s/l)$ [e] [kJ kg^{-1}]
3AO	356.191018	262.7	41.8	221.0	−4.5	2342.4
GA	356.192618	258.5	42.0	216.5	−4.5	2297.2

[a] CBS-4M electronic enthalpy. [b] Gas phase enthalpy of formation. [c] Sublimation enthalpy. [d] Standard liquid state enthalpy of formation. [e] Solid state energy of formation.

The thermal behavior of compounds **1** and **2** was analyzed by DSC at a heating rate of 5 °C min^{-1} to determine their decomposition temperatures (Figure S 21). In addition, the boiling points and decomposition temperatures for compound **3** and glycidyl azide were assed. Last but not least, the thermal behavior of poly(3-azidooxetane) (**4**) was assessed to determine both glass transition and decomposition temperature. The obtained thermograms are depicted.

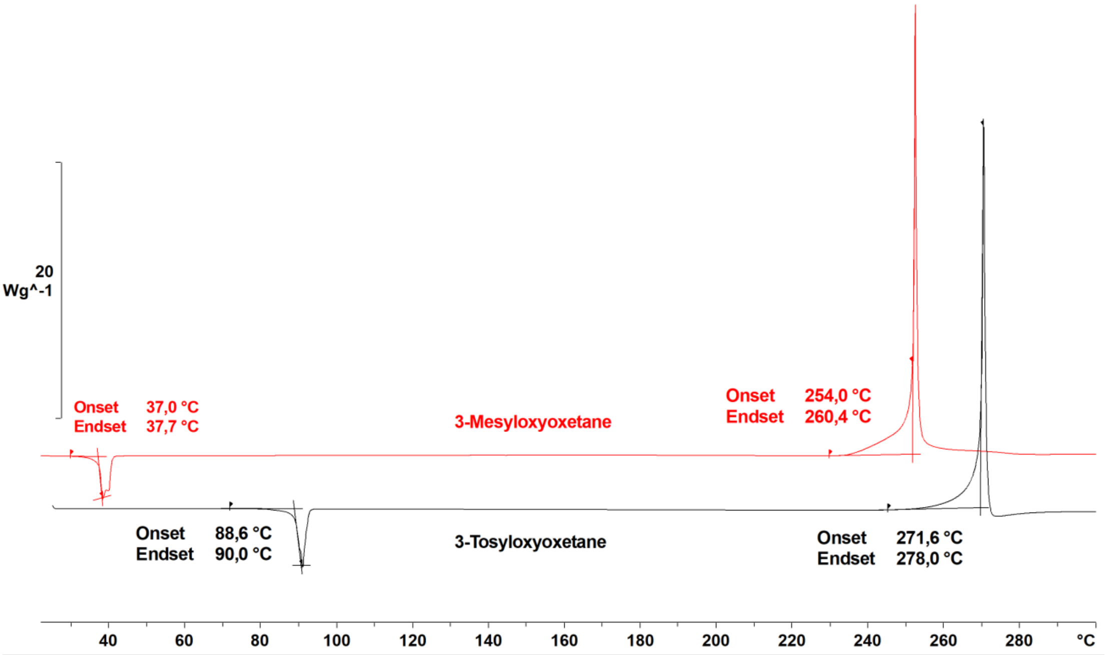

Figure S 9.21. DSC evaluation of compounds **1** and **2**.

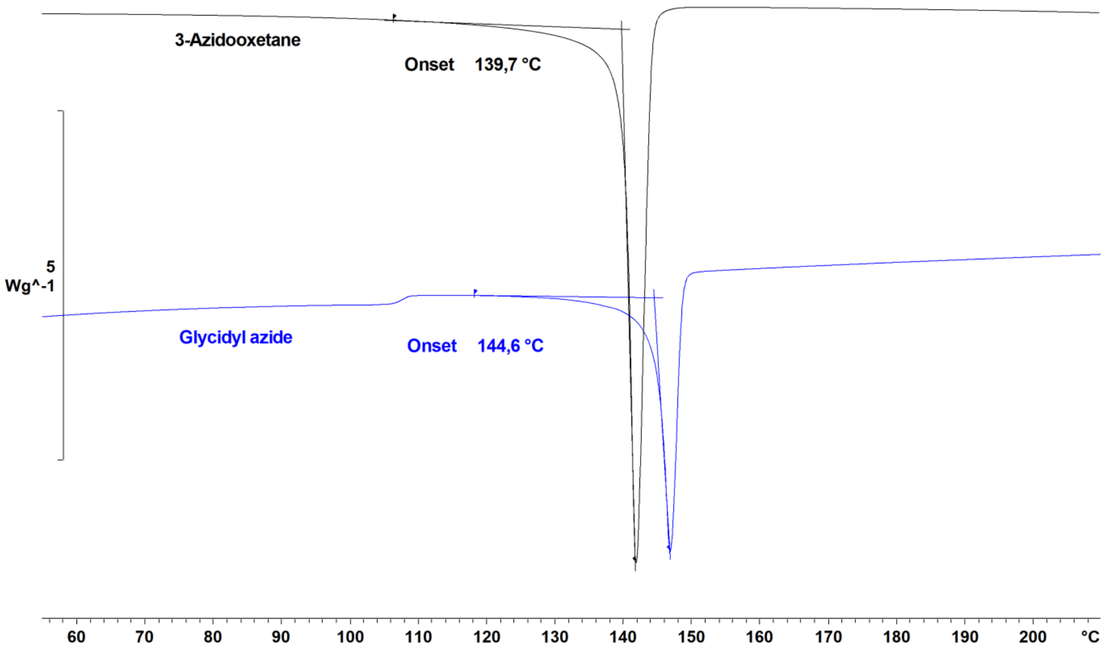

Figure S 9.22. DSC evaluation for the boiling points of 3-azidooxetane (**3**) and glycidyl azide.

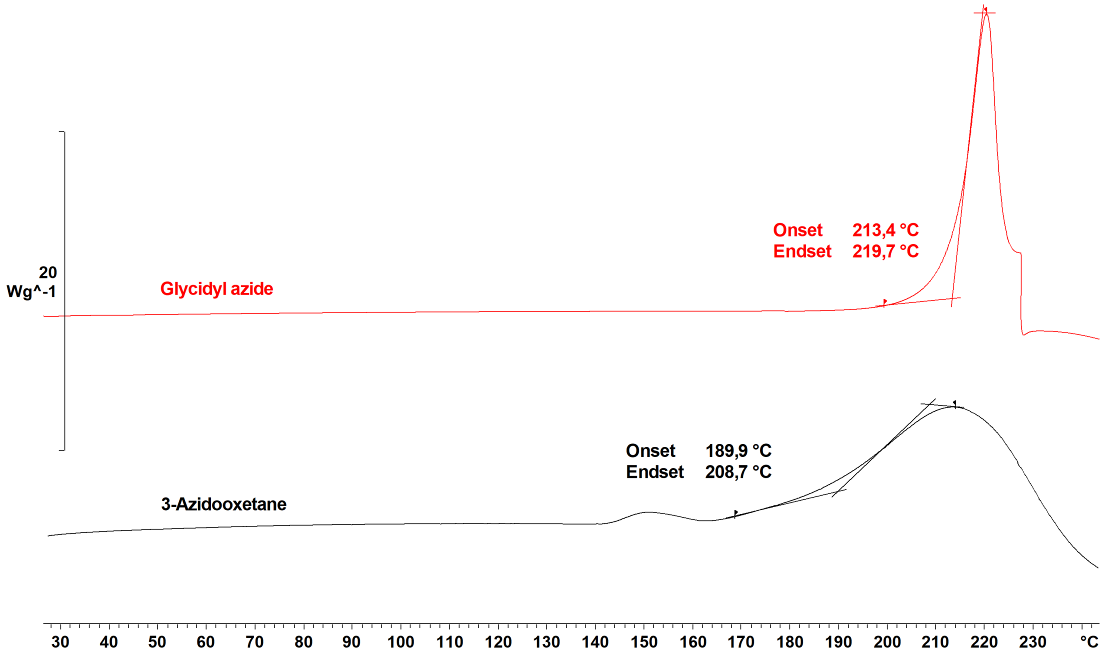

Figure S 9.23. DSC evaluation of the decomposition temperatures of 3-azidooxetane (**3**) and glycidyl azide in closed 40µL aluminum crucibles.

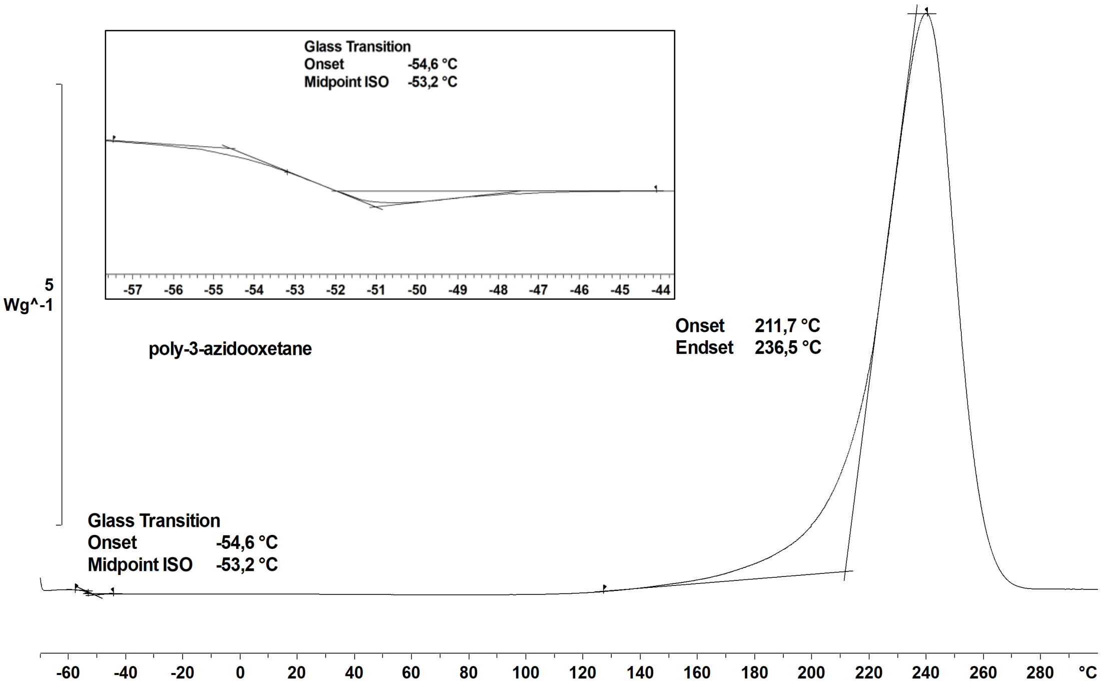

Figure S 9.24. Thermal analysis of poly(3-azidooxtane) with regard to glass transition and decomposition temperature.

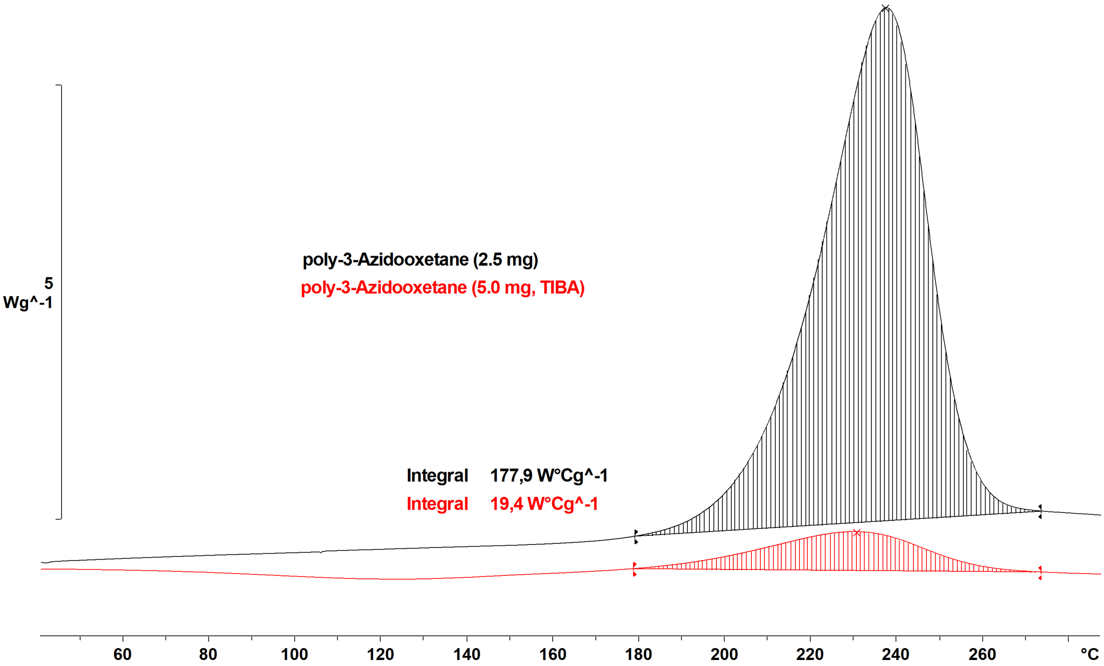

Figure S 9.25. Thermal decomposition analysis of low-molecular-weight poly(3-azidooxtane) (black) in comparison to polymeric material (red) obtained with triisobutylaluminum–water as catalyst (TIBA). The integrals indicate the reduced nitrogen content in the second case.

9.5.5 Detonation Parameters and Hot Plate Test

The following output data was obtained using the EXPLO5 V6.04 thermochemical code.[13]

9.5.5.1 Glycidyl azide

C(3,000) H(5,000) N(3,000) O(1,000)

Molecular weight = 99,09
Density of explosive = 1,14 g/cm^3
Oxygen balance = -121,0908 %
Enthalpy of formation = 2229,22 kJ/kg
Internal energy of formation = 2341,78 kJ/kg

Detonation parameters (at the C-J point):

Heat of detonation = -4444,648 kJ/kg
Detonation temperature = 2793,657 K
Detonation pressure = 10,55701 GPa
Detonation velocity = 6121,845 m/s
Particle velocity = 1512,704 m/s
Sound velocity = 4609,141 m/s
Density of products = 1,514144 g/cm^3
Volume of products = 0,6604391 cm^3/g
Exponent 'Gamma' = 3,046954
Moles of gaseous products = 3,356081 mol/mol explosive
Moles of condensed products = 2,012745 mol/mol explosive
Volume of gas at STP = 828,2757 dm^3/kg
Mean molecular mass of gas. prod. = 22,3226 g/mol
Mean molecular mass of cond. prod. = 12,011 g/mol
Mean molecular mass of all prod. = 18,45683 g/mol
Entropy of products = 7,745953 kJ/kg K
Internal energy of products = 5588,796 kJ/kg, i.e. 6,371227 kJ/cm^3
Compression energy = 1144,148 kJ/kg, i.e. 1,304328 kJ/cm^3
Total heat energy = -4444,648 kJ/kg, i.e. -5,066899 kJ/cm^3

Composition of detonation products:

Products	mol/mol	mol/kg	Mol %
C(gr) =	2,012745	20,31168	37,48948
N2 =	1,368801	13,8133	25,49535
H2O =	0,6685275	6,746466	12,45202
CH4 =	0,3758942	3,793347	7,001421
H2 =	0,2469643	2,492248	4,599967
NH3 =	0,2413439	2,435529	4,495281
CO =	0,2204848	2,225029	4,10676
C2H6 =	0,1211049	1,222134	2,255705
C2H4 =	0,03587345	0,362018	0,6681803
CO2 =	0,03200336	0,3229629	0,5960959
CH2O2 =	0,02294971	0,2315977	0,4274623
HCN =	0,02088441	0,2107556	0,3889939
CH3OH =	0,0009939731	0,01003071	0,01851379
CH2O =	7,140602E-05	0,0007205959	0,001330012
NH2 =	6,182649E-05	0,0006239238	0,001151583
H =	6,069322E-05	0,0006124875	0,001130475
N2H4 =	4,556461E-05	0,0004598166	0,0008486884
CHNO =	1,578617E-05	0,0001593066	0,0002940338
CNO =	2,897577E-07	2,924098E-06	5,397038E-06
N =	1,326933E-08	1,339079E-07	2,471552E-07
N2O =	3,814201E-09	3,849112E-08	7,104347E-08
C(d) =	3,889382E-10	3,924982E-09	7,24438E-09
NO2 =	7,40085E-11	7,46859E-10	1,378486E-09

9.5.5.2 3-Azidooxetane

C(3,000) H(5,000) N(3,000) O(1,000)

Molecular weight = 99,09
Density of explosive = 1,18 g/cm^3
Oxygen balance = -121,0908 %
Enthalpy of formation = 2276,65 kJ/kg
Internal energy of formation = 2389,21 kJ/kg

Detonation parameters (at the C-J point):

Heat of detonation = -4520,494 kJ/kg
Detonation temperature = 2813,306 K
Detonation pressure = 11,50812 GPa
Detonation velocity = 6307,581 m/s
Particle velocity = 1546,179 m/s
Sound velocity = 4761,402 m/s
Density of products = 1,563183 g/cm^3
Volume of products = 0,6397202 cm^3/g
Exponent 'Gamma' = 3,079464
Moles of gaseous products = 3,323059 mol/mol explosive
Moles of condensed products = 2,069524 mol/mol explosive
Volume of gas at STP = 820,1259 dm^3/kg
Mean molecular mass of gas. prod. = 22,33921 g/mol
Mean molecular mass of cond.prod. = 12,011 g/mol
Mean molecular mass of all prod. = 18,37553 g/mol
Entropy of products = 7,699582 kJ/kg K
Internal energy of products = 5715,838 kJ/kg, i.e. 6,744689 kJ/cm^3
Compression energy = 1195,345 kJ/kg, i.e. 1,410507 kJ/cm^3
Total heat energy = -4520,494 kJ/kg, i.e. -5,334182 kJ/cm^3

Composition of detonation products:

Products	mol/mol	mol/kg	Mol %
C(gr) =	2,069524	20,88466	38,37723
N2 =	1,361183	13,73642	25,24176
H2O =	0,7013227	7,077419	13,00532
CH4 =	0,355711	3,589668	6,596301
NH3 =	0,2586558	2,610233	4,796511
H2 =	0,2272663	2,293464	4,214423
CO =	0,188192	1,899146	3,489831
C2H6 =	0,1228524	1,239769	2,278174
C2H4 =	0,03316479	0,3346834	0,6150075
CO2 =	0,02916582	0,2943277	0,5408506
CH2O2 =	0,02557261	0,2580667	0,4742181
HCN =	0,01879159	0,1896359	0,348471
CH3OH =	0,0009443772	0,00953021	0,01751252

NH2 =	6,08983E-05	0,0006145571	0,001129297
N2H4 =	5,743006E-05	0,0005795571	0,001064982
H =	5,457085E-05	0,0005507034	0,001011961
CH2O =	5,260582E-05	0,0005308732	0,0009755217
CHNO =	1,117029E-05	0,0001127253	0,0002071418
CNO =	2,735643E-07	2,760682E-06	5,072974E-06
N =	1,431497E-08	1,444599E-07	2,654567E-07
N2O =	3,611852E-09	3,644911E-08	6,697814E-08
C(d) =	4,788678E-10	4,832509E-09	8,88012E-09
NO2 =	8,629467E-11	8,708453E-10	1,600247E-09

9.5.5.3 Hot Plate Test

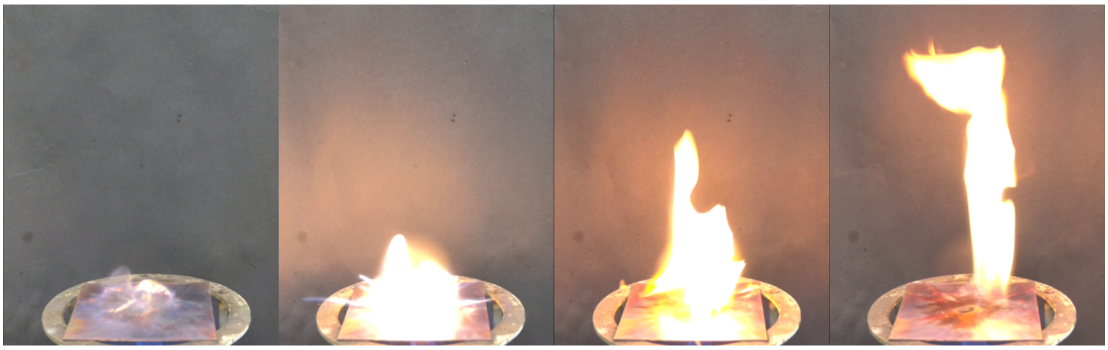

Figure S 9.26. A drop of 3-azidooxetane falls on a hot copper plate resulting in a violent deflagration.

Figure S 9.27. A drop of glycidyl azide causing a violent deflagration upon impact on a hot copper plate.

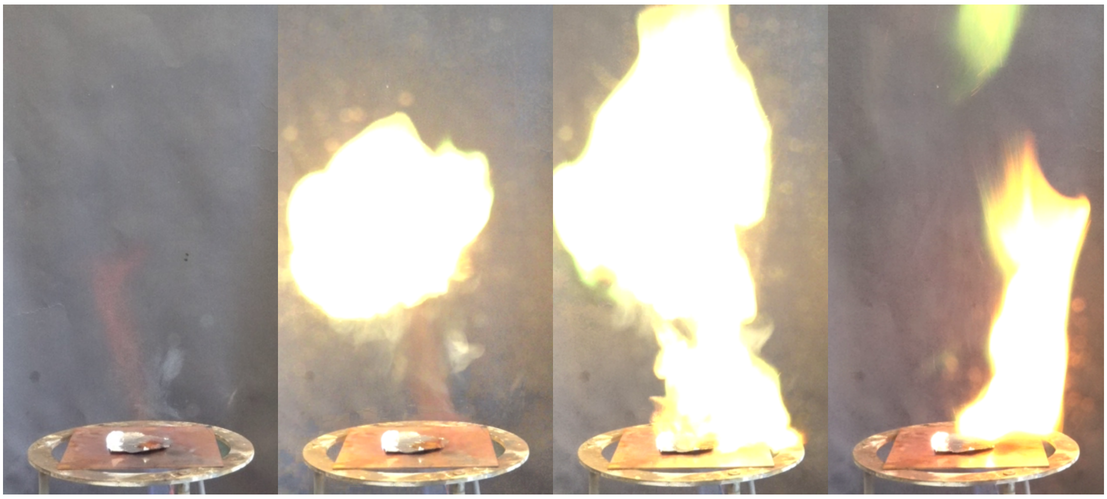

Figure S 9.28. Deflagration of poly(3-azidooxetane) (50 mg).

9.5.6 References

[1] CrysAlisPRO, Oxford Diffraction /Agilent Technologies UK Ltd, Yarnton, England, **2009**,

[2] Altomare, A.; Cascarano, G.; Giacovazzo, C.; Guagliardi, A.; Burla, M. C.; Polidori, G.; Camalli, M. SIR92 - a program for automatic solution of crystal structures by direct methods. *J. Appl. Crystallogr.* **1994**, *27*, 435.

[3] Altomare, A.; Burla, M. C.; Camalli, M.; Cascarano, G. L.; Giacovazzo, C.; Guagliardi, A.; Moliterni, A. G. G.; Polidori, G.; Spagna, R. SIR97: a new tool for crystal structure determination and refinement. *J. Appl. Crystallogr.* **1999**, *32*, 115.

[4] Sheldrick, G. M. SHELXL-97: Program for the Refinement of Crystal Structures, University of Göttingen, Germany, **1997**.

[5] Sheldrick, G. A short history of SHELX. *Acta Cryst. A.* **2008**, *64*, 112-122.

[6] Hübschle, C. B.; Sheldrick, G. M.; Dittrich, B. ShelXle: a Qt graphical user interface for SHELXL. *J. Appl. Crystallogr.* **2011**, *44*, 1281-1284.

[7] Spek, A. Single-crystal structure validation with the program PLATON. *J. Appl. Crystallogr.* **2003**, *36*, 7-13.

[8] Farrugia, L. J. WinGX and ORTEP for Windows: an update. *J. Appl. Crystallogr.* **2012**, *45*, 849-854.

[9] Turner, M. J.; McKinnon, J. J.; Wolff, S. K.; Grimwood, D. J.; Spackman, P. R.; Jayatilaka, D; Spackman, M. A. CrystalExplorer17 (**2017**). University of Western Australia. https://hirshfeldsurface.net.

[10] Altenburg, T.; Klapötke, Thomas M.; Penger, A.; Stierstorfer, J. Two Outstanding Explosives Based on 1,2-Dinitroguanidine: Ammonium- dinitroguanidine and 1,7-Diamino-1,7-dinitrimino-2,4,6-trinitro-2,4,6-triazaheptane. *Z. Anorg. Allg. Chem.* **2010**, *636*, 463-471.

[11] Chase, M. W. NIST-JANAF Thermochemical Tables, Fourth Edition, *J. Phys. Chem. Red. Data, Monograph 9,* **1998**, 1–1951.

[12] Frisch, M. J.; Trucks, G. W.; Schlegel, H. B.; Scuseria, G. E.; Robb, M. A.; Cheeseman, J. R.; Scalmani, G.; Barone, V.; Petersson, G. A.; Nakatsuji, H.; Li, X.; Caricato, M.; Marenich, A. V.; Bloino, J.; Janesko, B. G.; Gomperts, R.; Mennucci, B.; Hratchian, H. P.; Ortiz, J. V.; Izmaylov, A. F.; Sonnenberg, J. L.; Williams; Ding, F.; Lipparini, F.; Egidi, F.; Goings, J.; Peng, B.; Petrone, A.; Henderson, T.; Ranasinghe, D.; Zakrzewski, V. G.; Gao, J.; Rega, N.; Zheng, G.; Liang, W.; Hada, M.; Ehara, M.; Toyota, K.; Fukuda, R.; Hasegawa, J.; Ishida, M.; Nakajima, T.; Honda, Y.; Kitao, O.; Nakai, H.;

Vreven, T.; Throssell, K.; Montgomery Jr., J. A.; Peralta, J. E.; Ogliaro, F.; Bearpark, M. J.; Heyd, J. J.; Brothers, E. N.; Kudin, K. N.; Staroverov, V. N.; Keith, T. A.; Kobayashi, R.; Normand, J.; Raghavachari, K.; Rendell, A. P.; Burant, J. C.; Iyengar, S. S.; Tomasi, J.; Cossi, M.; Millam, J. M.; Klene, M.; Adamo, C.; Cammi, R.; Ochterski, J. W.; Martin, R. L.; Morokuma, K.; Farkas, O.; Foresman, J. B.; Fox, D. J., Gaussian 16 Rev. C.01, **2016**.

[13] Sućeska, M., EXPLO5, Version 6.04, Brodarski Institute, Zagreb, **2017**.

10 A GAP Replacement, Part 2: Preparation of Poly(3-azidooxetane) via Azidation of Poly(3-tosyloxyoxetane) and Poly(3-mesyloxyoxetane)

by

Max Born, Thomas C. Fessard, Lucas Göttemann, Jakob Plank, and Thomas M. Klapötke

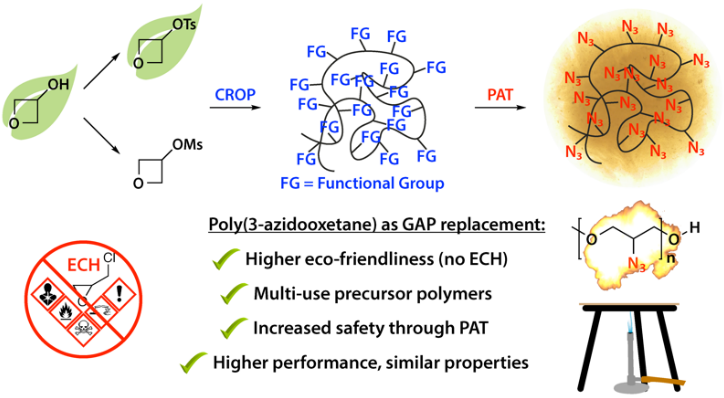

as published in
Journal of Organic Chemistry **2022**, *87*, 4097-4106
(doi:10.1021/acs.joc.1c02907)

Abstract

Despite the variety of energetic polyoxetane binders, the oxirane-based glycidyl azide polymer (GAP) has largely succeeded in the market due to its advantageous properties. Nevertheless, it suffers from various drawbacks such as nonuniform chain termination, possible chlorine content (flame retardant), and toxic epichlorohydrin required for its synthesis. These problems can be bypassed using the structurally related poly(3-azidooxetane). Unfortunately, it is only accessible in moderate yield by polymerization of 3-azidooxetane. Herein, we describe its synthesis by polymer-analogous transformation using the new polymers poly(3-tosyloxy-oxetane) and poly(3-mesyloxyoxetane) as precursors. This results in a significantly increased yield and improved safety as handling of the very sensitive 3-azidooxetane is avoided. The aforementioned prepolymers were prepared using boron trifluoride etherate as well as triisobutylaluminum as catalysts. The latter provides polymers of particularly high molecular weight, and the corresponding poly(3-azidooxetane) species was obtained and studied for the first time. In order to shed light on the applicability of poly(3-azidooxetane) as a GAP substitute, it was thoroughly studied with regard to thermal behavior, energetic performance (EXPLO5), plasticizer compatibility, and curing. Moreover, the aquatic toxicity of all involved monomers was analyzed and compared to epichlorohydrin. Here, poly(3-azidooxetane) turned out as a fully adequate, if not more environmentally benign, substitute.

Keywords: Oxetanes, energetic oxetanes, energetic polymers, ring-opening polymerization, prepolymers, poly(3-azidooxetane), GAP replacement.

10.1 Introduction

The vast majority of energetic formulations (e.g., composite propellants or explosives) contain polymeric binders that fulfill technical tasks such as prevention of segregation, detrimental crack formation by cyclic thermal stresses, and reduction of sensitivity.[1-3] For this purpose, low-viscosity polymers are used, cross-linkable by curing agents after the addition of fillers to form an elastic binder matrix. Due to its mechanical properties and low glass transition temperature, hydroxy-terminated polybutadiene (HTPB) is widely used and can be cured with di- or polyfunctional isocyanates.[4] However, as non-energetic binders reduce the overall performance, they are increasingly replaced by energetic polymers such as poly(3-nitratomethyl-3-methyloxetane) (poly(NIMMO)), poly(3-azidomethyl-3-methyloxetane) (poly(AMMO)), poly(3,3-bis(azidomethyl)oxetane) (poly(BAMO)), or GAP. Prepared by cationic ring-opening polymerization (CROP) from their corresponding monomers, they build the state of the art.[1–3] GAP is the most studied one and was already prepared by Vandenberg in 1970.[4,5] Due to its advantageous properties and low cost, it established itself on the market and became commercially available.[3,6] Nevertheless, GAP also suffers from various disadvantages. It is obtained by azidation of poly(epichlorohydrin) (PECH) and incomplete substitution may lead to remaining chlorine in the polymer. Unfortunately, halogens show a flame-retardant effect and thus impose a negative impact on combustion.[4] Since the monomer epichlorohydrin has two ring-opening modes, both PECH and GAP are terminated with primary and secondary hydroxy groups.[3] The latter are less reactive and allow side reactions of the curing agent with water present under carbon dioxide formation, leading to inhomogeneous formulations.[3,7] After all, epichlorohydrin itself is problematic as it is toxic, corrosive, carcinogenic, and skin resorptive.[8,9] An elegant alternative to GAP is poly(3-azidooxetane) (p3AO), which forms only primary hydroxy groups, and can be synthesized by CROP using 3-azidooxetane, the constitutional isomer of glycidyl azide.[7] Only recently, significantly improved methods for the synthesis of 3-azidooxetane have been reported, allowing the polymer to be obtained in 39% overall yield starting from commercially available oxetan-3-ol.[7] However, in order to render it competitive to GAP, higher yields are necessary. As a solution, we report its preparation by polymer-analogous transformation using the new polymers poly(3-tosyloxyoxetane) (pTsOx) and poly(3-mesyloxyoxetane) (pMsOx). This follows the upcoming trend to prepare energetic binders increasingly from tosylate and mesylate precursors.[4,10] Surprisingly, the latter are less common, although the mesyl group offers less steric hindrance for nucleophiles and improved atom economy at low cost.[4,7] The advantage is avoiding halogens, while safety is significantly increased as handling and storage of energetic monomers, which are often more unstable and sensitive than their polymers, are bypassed.[4,10,11] In addition, various energetic binders can be obtained from one precursor by selecting the nucleophile. Since azido compounds, which are popular in the field of energetic binders, are unstable toward radicals and strong acids and bases, the choice of the polymerization catalyst is limited using azido monomers.[12,13] For example, polymerization of 3-azidooxetane using triisobutylaluminum-water (TIBA) as a catalyst results in decomposition.[7] In contrast, 3-tosyloxyoxetane and 3-mesyloxyoxetane provided the corresponding high-molecular-weight polymers using this catalyst.[13,14] Accordingly, it was possible for the first time to obtain a high-molecular-weight species of poly(3-azidooxetane) by subsequent azidation. The molecular weight and polydispersity of all parent polymers (pTsOx and pMsOx) were assessed by gel permeation chromatography to gain insight into the polymerization behavior and their suitability for the preparation of curable binders. Ultimately, both the low- (LMW) and high-molecular-weight (HMW) parent polymers were fully azidated in almost quantitative yields within reasonable reaction times. As a result, poly(3-azidooxetane) can now be obtained in a significantly higher yield than by CROP of 3-azidooxetane.[7] In addition, the thermal behavior of GAP and poly(3-azidooxetane) was compared and their respective performance was calculated using EXPLO5 V.604 after assessing their heat of formation by bomb calorimetry.[15] Furthermore, poly(3-azidooxetane) was cured, its plasticizer compatibility was investigated, and the aquatic toxicity[16] of its monomeric precursors was compared to that of epichlorohydrin. Thus, light was shed on different application aspects, and poly(3-azidooxetane) did not only provide proof to be a first-rate GAP alternative but also offers a synthetic route that is likely to impose less risks to health and the environment.

10.2 Results and Discussion

10.2.1 Precursor Synthesis

Epichlorohydrin was used as received from Sigma Aldrich. Oxetan-3-ol and 3-tosyloxyoxetane (**1**) were provided by Spirochem AG Basel. To provide purity suitable for polymerization, 3-tosyloxyoxetane was recrystallized once from hot chloroform. 3-Mesyloxyoxetane (**2**) was prepared according to our recently published procedure (Scheme 1).[7]

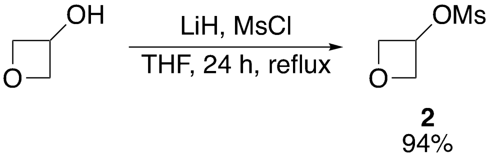

Scheme 10.1. Literature synthesis of 3-mesyloxyoxetane (**2**).

Hereby, oxetan-3-ol was deprotonated in dry THF using lithium hydride. Subsequent addition of mesyl chloride afforded compound **2** in a high yield. Further purification by high-vacuum distillation provided suitable monomer purity. Nitroglycerin as a potential oxygen-rich plasticizer for poly(3-azidooxetane) was prepared according to the literature by nitration of glycerin with mixed acid comprising 100% nitric acid and 96% sulfuric acid (Scheme 2).[17]

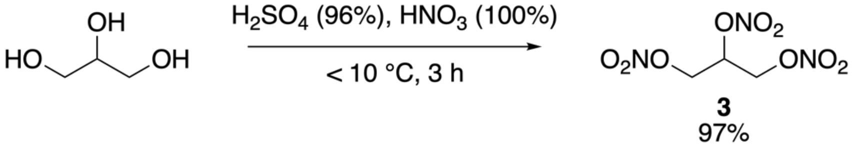

Scheme 10.2. Nitration of glycerin to give nitroglycerin (**3**).

The crude product was extracted (DCM), neutralized (sodium bicarbonate solution), and washed with water to give pure nitroglycerin in 97% yield. The azido plasticizer ethane-1,2-diyl bis(2-azidoacetate) (EDBAA) was prepared via azidation of ethane-1,2-diyl bis(2-chloroacetate), which was prepared according to the patent literature (Scheme 3).[18]

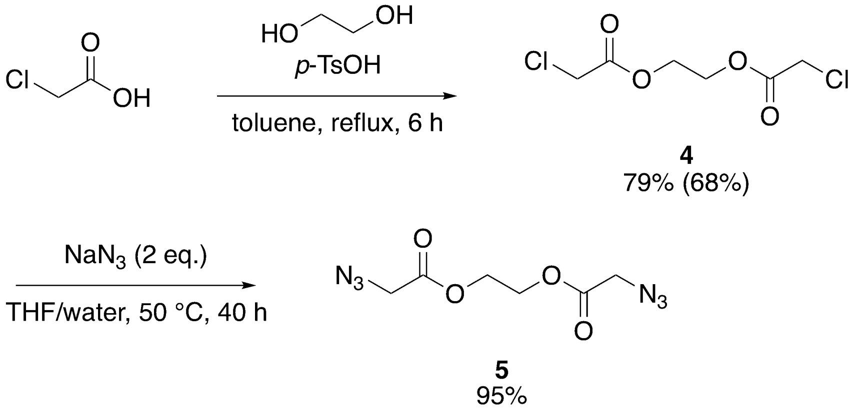

Scheme 10.3. Preparation of ethane-1,2-diyl bis(2-chloroacetate) **4** and subsequent azidation to give the azido-plasticizer EDBAA (**5**).

Here, chloroacetic acid and ethylene glycol were dissolved in toluene and *p*-toluenesulfonic acid was added as the catalyst. Upon reflux, a Dean–Stark apparatus removed formed water by distillation. After 6 h, the surplus starting material was removed by washing the toluene layer with water and sodium bicarbonate solution. A crude yield of 79% was obtained after rotary evaporation. The material was further purified by vacuum distillation (4.5×10^{-2} mbar, 110 °C) to give 68% overall yield. Subsequent azidation in aqueous THF solution followed by extraction with ethyl acetate[19] gave ethane-1,2-diyl bis(2-azidoacetate) as yellowish liquid in 95% yield and high purity according to ^{1}H NMR spectroscopy. Further purification by high vacuum distillation failed due to thermal decomposition (~110 °C) of EDBAA. If necessary, the compound may be purified by column chromatography.

10.2.2 Polymerization

The cationic ring-opening polymerization of compounds **1** and **2** using boron trifluoride etherate (BTFE) and TIBA as catalysts was investigated (Scheme 4).

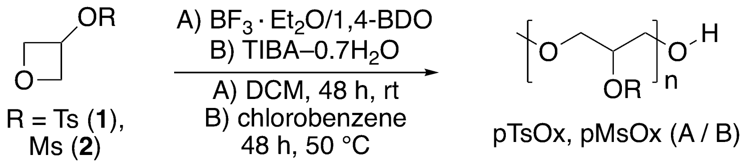

Scheme 10.4. CROP toward poly(3-tosyloxyoxetane) and poly(3-mesyloxyoxetane) using different catalysts and conditions.

In the former case, butane-1,4-diol (1,4-BDO) was used as a polyol initiator to promote propagation by the activated monomer mechanism (AMM) while limiting the contribution of the undesired active chain end (ACE) mechanism. With the AMM, the propagating chain is uncharged and hydroxy-terminated, leading to less backbiting and other chain terminating reactions. This results in less cyclic oligomers, improved molecular weight, and end-group functionality as well as a narrower polydispersity.[10,20,21] While this system usually provides rather low molecular weights ($M_W < 5000$ g mol^{-1}), TIBA is capable of providing linear polymers of especially high molecular weight.[13,14] Mechanistically, it is commonly assumed that an acidic complex forms between water and triisobutylaluminum to protonate a first monomer and thus forms an ion pair. The carbocation reacts with another monomer, causing chain growth. Hereby, the growing chain is always terminated by the carbocationic end and the counterion arising from the complex.[14] In the case of the boron trifluoride etherate/diol system, both components were added in a molar ratio of 2:1 to a thoroughly dried Schlenk round bottom flask under a protective atmosphere (argon). After 15 min, a color change from colorless to yellow was observed and dry DCM was added. Subsequently, the monomer feeding course was performed by means of a syringe pump using solutions of compound **1** or **2** in dry DCM. While all polymerizations were performed at a monomer concentration of 2 mol L^{-1} and a duration of 48 h, different initiator concentrations and feeding course durations were employed to study the influence on the average molecular weight, polydispersity, and yield. The individual polymerization conditions and corresponding yields are briefly summarized in Table 1.

Table 10.1. Polymerization conditions for poly(3-tosyloxyoxetane) and poly(3-mesyloxyoxetane) using boron trifluoride etherate.

	pTsOx I5-2	**pTsOx I5-3**	**pTsOx I10-2**	**pMsOx I5-2**	**pMsOx I10-2**
Scale[a]	2.00	10.0	2.00	2.00	2.00
[M][b]	2.00	2.00	2.00	2.00	2.00
[I][c]	5	5	10	5	10
[OH]/[BTFE][d]	1	1	1	1	1
[M]/[I][e]	20	20	10	20	10
Feed Rate [µmol/min]	73.0	48.7	73.0	109	109
t[f]	rt	rt	rt	rt	rt
Yield [%]	81	87	79	82	77

[a] Scale of reaction. [b] Monomer concentration. [c] Initiator concentration (mol%). [d] Initial hydroxy group (BDO)–catalyst (BTFE) ratio. [e] Monomer to initiator ratio. [f] Reaction temperature. Batch acronym: I5-2 = initiator concentration 5 mol%, feeding duration 2 hours.

In all cases, the polymer remained in solution and a color change from yellowish to brown was observed. The polymerization was quenched with water prior to the addition of excess methanol to precipitate the crude polymer (emulsion), which was then collected by centrifugation. Additional purification was performed by removal of the supernatant, dissolution of the respective polymer in the minimum amount of acetone, and precipitation with an excess of methanol. After centrifugation, the polymers were thoroughly dried under high vacuum conditions (10^{-2} mbar, 24 h, 70 °C). Here, poly(3-tosyloxyoxetane) was obtained as an off-white, brittle solid with yields of 79–87%. On the other hand, poly(3-mesyloxyoxetane) was obtained as a brownish, extremely viscous, sticky material with likewise satisfying yields in the range of 77–82%. In order to gain the respective high-molecular-weight species, both 3-tosyloxyoxetane and 3-mesyloxyoxetane were polymerized using triisobutylaluminum–0.7H_2O as a catalyst, which was freshly prepared according to the literature.[7] As TIBA shows increased catalytic activity at elevated temperatures, the solvent was changed from volatile DCM to chlorobenzene to allow heating of the polymerization reaction. To quantitatively remove traces of water beforehand, chlorobenzene was dried over calcium hydride followed by distillation under reduced pressure (380 mbar, 100 °C) and protective atmosphere (argon) onto a molecular sieve (3 Å) in a thoroughly dried Schlenk round-bottom flask. In order to establish comparability with the boron trifluoride etherate/diol system, both monomers were also employed at a concentration of 2 mol L^{-1} and the overall reaction time of 48 h was kept. However, in the case of TIBA, which was used at a concentration of 10 mol%, the direction of addition needs to be changed. Therefore, predried monomers were added to a thoroughly dried Schlenk round-bottom flask (argon atmosphere) followed by the addition of dry chlorobenzene. Afterward, the freshly prepared triisobutylaluminum–0.7H_2O solution ($c = 1.1$ mol L^{-1}) was added over a period of 2 h using a syringe pump. The polymerization conditions are summarized in Table 2.

Table 10.2. Polymerization conditions for poly(3-tosyloxyoxetane) and poly(3-mesyloxyoxetane) using triisobutylaluminum–0.7H_2O.

	pTsOx C10-2	**pMsOx C10-2**
Scale[a]	4.00	4.00
[M][b]	2.00	2.00
[I][c]	10	10
[M]/[I][d]	10	10
Feed Rate [µmol/min]	14.6	21.9
t[°C][e]	50	50
Yield [%]	79%	81%

[a] Scale of reaction. [b] Monomer concentration. [c] Catalyst concentration (mol%). [d] Monomer to catalyst ratio. [e] Reaction temperature. Batch acronym: C10-2 = catalyst concentration 10 mol%, feeding duration 2 hours.

In the case of poly(3-tosyloxyoxetane), a strong turbidity of the colorless reaction solution was observed, while in the case of poly(3-mesyloxyoxetane), precipitation polymerization occurred and the swollen polymer precipitated as a rubbery, colorless semi-solid, indicating a high molecular weight as the polymer became largely insoluble. Again, all polymerizations were quenched by addition of water. In the case of poly(3-tosyloxyoxetane), the crude polymer was obtained as a highly viscous and sticky semi-solid. Poly(3-mesyloxyoxetane) afforded a colorless rubber-like block. In both cases, the supernatant was decanted and the crude polymers were refluxed in THF (12 h) to remove the trapped monomer and chlorobenzene. Water was added, and the aqueous phase was decanted. This purification process was repeated once prior to drying the crude polymers under high vacuum conditions (10^{-2} mbar, 24 h, 70 °C), which were obtained as off-white, brittle solids with similar yields to the case of the boron trifluoride etherate/diol system (79–81%). The achieved high molecular weights using TIBA-water as a catalyst allowed the subsequent preparation of high-molecular-weight poly(3-azidooxetane), which has not been described in the literature so far.

10.2.3 Gel Permeation Chromatography

The molecular weight distributions of all non-energetic prepolymers prepared using either the boron trifluoride etherate/butanediol-system or TIBA-water were assessed by gel permeation chromatography (GPC) using THF at a flow rate of 1.0 mL min^{-1} on a HITACHI L-2350 device equipped with both RI and UV detectors. Calibration was performed using polystyrene (PS) standards as these are the most widespread in the literature and allow good comparability. A "PSS SDV combination low" column set with a mass range of 100–60.000 Da was used for polymers prepared using boron trifluoride etherate, and a "PSS SDV combination high" column set was used for polymers prepared using TIBA with a mass range of 100–3.000.000 Da. Data analysis was performed using the PSS WinGPC software. The number (M_n) and weight (M_W) average molecular weight of prepolymers and their dispersity ($Đ = M_W/M_n$) are summarized in Table 3.

Table 10.3. GPC analysis of poly(3-tosyloxyoxetane) and poly(3-mesyloxyoxetane) prepared with different catalysts; values rounded to hundreds.

Polymer	M_n (theo.) [g mol^{-1}]	M_n [g mol^{-1}]	M_w [g mol^{-1}]	Đ
pMsOx I5-2	3100	2200	2900	1.31
pMsOx I10-2	1600	2200	2800	1.27
pTsOx I5-2	4700	2900	5000	1.71
pTsOx I10-2	2400	2200	3300	1.49
pTsOx I5-3	4700	3300	4600	1.41
pMsOx C10*		600	800	1.44
*reflux		700	3000	4.59
*sonicated		800	6400	7.88
pTsOx C10		21200	57800	2.72

In the case of the prepolymers prepared with boron trifluoride etherate as a catalyst, the initiator concentrations (1,4-BDO) were 5 and 10 mol%, corresponding to monomer–initiator ratios ([M]/[I]) of 20 and 10, respectively. On this basis, the theoretical molecular weights were calculated and compared with the values obtained in practice (Table 3). Here, it was assumed that the initiator is incorporated into the polymer (M_n (theo.) = $[M]/[I] \cdot MW_{monomer}$ +

90.12 g mol^{-1}). For the higher initiator concentration (10 mol%), a considerably higher number average molecular weight is obtained in the case of pMsOx I10-2 than expected by calculation. For pTsOx I10-2, the GPC result agrees rather well with the calculation. In contrast, lowering the initiator concentration to 5 mol% causes stronger deviations and the actual molecular weight falls significantly below the calculation (pTsOx I5-2 and pMsOx I5-2). However, increasing the addition time by 1/3 (pTsOx I5-3) reduces this deviation. These correlations are also reflected by the found polydispersities. Under otherwise identical conditions, lower polydispersities are achieved in the case of the higher initiator concentration than in the case of the lower initiator concentration. Again, the comparison of pTsOx I5-2 to pTsOx I5-3 shows that an increased addition time provides a lower polydispersity (1.41 instead of 1.71). Thus, the results predominantly indicate a slow initiation. As a result, the monomers are ultimately added faster than consumed. This results in a larger number of growing chains, which are ultimately shorter and provide a broader chain length distribution. The very low proportion of "THF protons" in the respective polymers (^{1}H NMR) together with the found molecular weights and polydispersities contradicts a "living" character of the polymerization, and participation of the ACE mechanism is assumed. Nevertheless, all polydispersities are rather low and significantly increased feeding course durations are likely to provide even narrower chain length distributions and higher molecular weights that match the calculation. Thus, a valuable basis for the preparation of ideal prepolymers for energetic binder synthesis was established. The combined GPC plot is depicted in Figure 1.

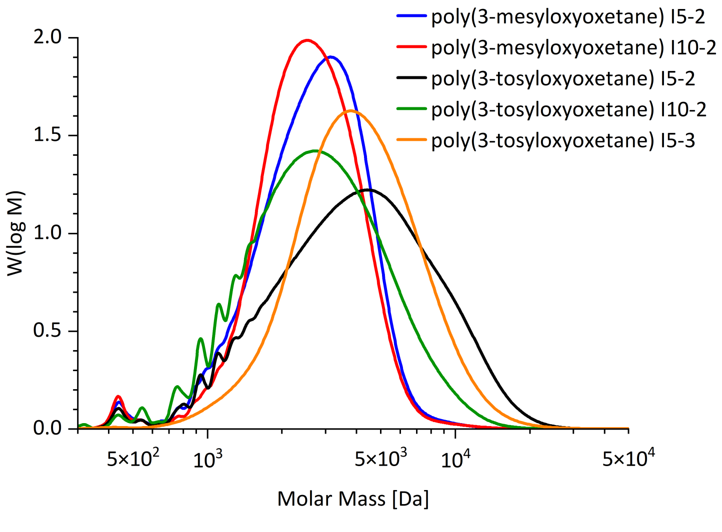

Figure 10.1. GPC curves of low-molecular-weight poly(3-tosyloxyoxetane) and poly(3-mesyloxyoxetane) using different polymerization conditions.

In the case of poly(3-tosyloxyoxetane) and poly(3-mesyloxyoxetane) prepared using the trialkylaluminum catalyst TIBA, an initiator concentration of 10 mol% was used. Here, a weight average M_W of 57.813 g mol^{-1} and number average M_n of 21.224 g mol^{-1} was obtained for pTsOx

C10, which is tremendously higher than in the case of the boron trifluoride etherate/diol-system. As expected, this is linked to a higher polydispersity (Đ = 2.72), which is still in an acceptable range taking the high molecular weight into account. The analysis of poly(3-mesyloxyoxetane) prepared under the same conditions was unfortunately impeded by its extreme insolubility in all GPC-suitable solvents. However, the highest solubility was found for THF as a typical GPC solvent. The GPC was first performed with a neat, untreated polymer, but only an oligomeric material was eluted from the column. Therefore, the polymer was, on the one hand, sonicated in THF and, on the other hand, refluxed in THF to increase the soluble fraction. Even though these procedures did not lead to any significant improvement, the best result was achieved by sonication (M_n = 814 g mol^{-1}, M_W = 6407 g mol^{-1}, Đ = 7.88). The high insolubility of the polymer pMsOx C10 can be attributed, on the one hand, to a particularly high molecular weight and, on the other hand, to stronger interpolymer interactions arising from the different side chain structure. A closer elucidation by GPC appeared unfeasible, since the corresponding azido species is also sparingly soluble. The corresponding GPC plots are summarized in Figure 2.

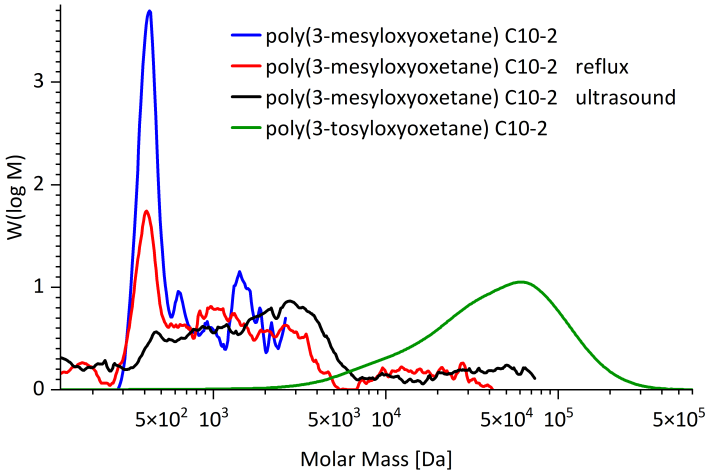

Figure 10.2. GPC curves of high-molecular-weight poly(3-tosyloxyoxetane) and poly(3-mesyloxyoxetane).

10.2.4 Azidation

The choice of solvent can be crucial for the successful azidation of tosylate or mesylate polymers. Since the entangled polymer structure further complicates the S_N2 reaction, high reaction temperatures are beneficial to achieve reasonable reaction times and both the polymer and azide source (sodium azide) must be at least partially soluble. Therefore, the choice is mainly limited to DMSO and DMF. DMSO is more environmentally benign but extremely difficult to remove from swollen polymers even under high vacuum conditions. In contrast, DMF was found to be fully removable under appropriate conditions (10^{-2} mbar, 24 h, 70 °C). Hence, DMF was chosen despite its classification as a substance of very high concern by the REACH regulation due to its reproductive toxicity.[22] The azidation of both low- and high-molecular-weight poly(3-tosyloxyoxetane) and poly(3-mesyloxyoxetane) was performed with 2 equivalents sodium azide at 100 °C using as little DMF as possible to reduce its total amount (Scheme 5).

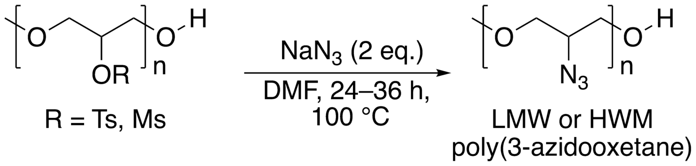

Scheme 10.5. Azidation of low- and high-molecular-weight polymeric precursors to give poly(3-azidooxetane).

The LMW polymers prepared with the BF_3·Et2O/1,4-BDO system fully dissolved, whereas the HMW polymers prepared with the trialkylaluminum catalytic system resulted in suspensions. A color change from colorless to orange or light brown was observed during all azidation reactions, as well as the precipitation of colorless sodium tosylate or mesylate. The azidated polymers were precipitated by the addition of excess water after 24 h in the case of all LMW polymers and after 36 h in the case of the HMW species to ensure quantitative azidation. The obtained low-molecular-weight p3AO was then collected by centrifugation, dissolved in a small quantity of acetone, and precipitated again with water to remove any salts prior to the final centrifugation step. The same procedure was applied to high-molecular-weight p3AO, but DMF had to be used due to the low solubility of these polymers in acetone. After drying under high vacuum, honey-like (LMW) to rubberlike (HMW) poly(3-azidooxetane) was obtained in quantitative yield with orange color in the former case and off-white color in the latter case. Complete substitution was verified by FT-IR spectroscopy. Here, the disappearance of the sulfonic acid ester bands (ν_s = 1168–1173 cm^{-1}, ν_{as} = 1329–1356 cm^{-1}) and the appearance of azido group bands (ν_s = 1266–1277 cm^{-1}, ν_{as} = 2086–2090 cm^{-1}) indicated quantitative azidation in all cases (Figures 3 and 4).

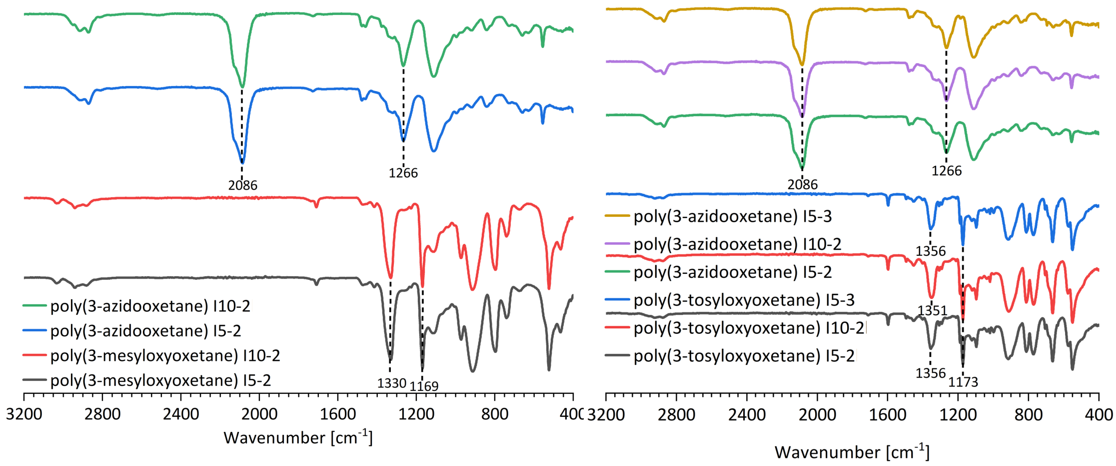

Figure 10.3. FT-IR spectra of low-molecular-weight poly(3-azidooxetane) obtained from poly(3-mesyloxyoxetane) (left) and poly(3-tosyloxyoxetane) (right).

Subsequently, all azidated polymers were subjected to elemental analysis. Here, the high nitrogen content and the absence of sulfur (0%) proved both quantitative substitution and the absence of salts. Finally, this was also confirmed by NMR spectroscopy (^{1}H) by the absence of aromatic signals in the case of tosylate parent polymers and the absence of a methyl group signal in the case of mesylate parent polymers.

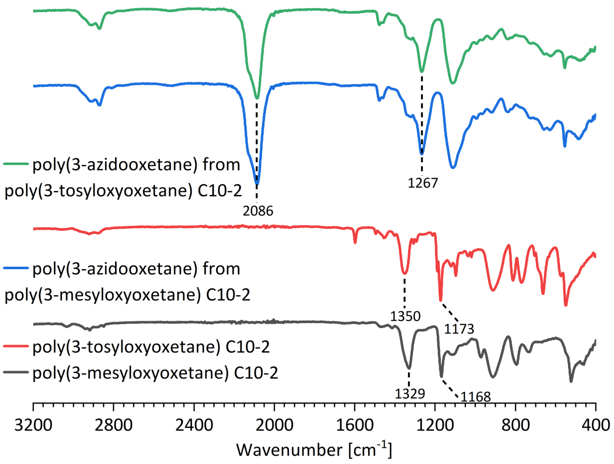

Figure 10.4. FT-IR spectra of high-molecular-weight poly(3-azidooxetane) obtained from poly(3-tosyloxyoxetane) and poly(3-mesyloxyoxetane).

10.2.5 Thermal Analysis

All non-energetic prepolymers as well as the respective azidated species were investigated by differential scanning calorimetry at a heating rate of 5 °C min^{-1} in a temperature range of −70 to +300 °C. The prepared low-molecular-weight species of poly(3-tosyloxyoxetane) show a glass transition temperature slightly below room temperature in the range of 13–15 °C. A sharp exothermic decomposition is observed rather early at roughly 196 °C. This can be attributed to the leaving group as polyether backbones are thermally extremely stable. In direct comparison, poly(3-mesyloxyoxetane) shows a lower glass transition temperature of roughly −4 °C. A sharp exothermic decomposition occurs even earlier in a range of 188–189 °C. Due to the significantly higher molecular weight, the glass transition temperature of the prepolymers prepared using TIBA−0.7H_2O is higher. In the case of HMW poly(3-tosyloxyoxetane), a T_G of 38 °C is found and 19 °C in the case of HMW poly(3-mesyloxyoxetane). A similar shift toward higher temperatures is observed with regard to decomposition. The aforementioned species decompose at 207 °C (pTsOx) and 197 °C (pMsOx), respectively. These trends also apply to the corresponding azidated polymers. Low-molecular-weight poly(3-azidooxetane) shows a T_G of −56.4 °C and decomposes at 211 °C. In contrast, the HMW species shows a 9.4 °C higher glass transition temperature (−47.0 °C). Regarding decomposition, on the other hand, the temperature difference is smaller. Depending on the parent polymer, decomposition occurs within an interval of 214–219 °C. Thus, poly(3-azidooxetane) is absolutely comparable to GAP in terms of the glass transition and decomposition temperature. None of the aforementioned polymers exhibits an exothermic crystallization peak. Therefore, all polymers are completely amorphous.

10.2.6 Bomb Calorimetry

In order to assess and compare the energetic performance of GAP and poly(3-azidooxetane) using EXPLO5 V6.04, the heats of formation of both polymers were determined by bomb calorimetry according to literature procedures.[20,23,24] For this purpose, a Parr 6200 Isoperibol bomb calorimeter was used. The device was calibrated by the combustion of benzoic acid (combustion enthalpy: 26.432 ± 32.7 J g^{-1}).[25] Nitric acid that formed in the case of CHNO compounds was directly factored by the device. For the practical measurements, the polymers were dissolved in ethyl acetate together with benzoic acid, and the solvent was rotated off to give a homogeneous solid, which was dried for 3 days at 50 °C in a drying oven. Subsequently, tablets were pressed (5 s, 3 tons), which were additionally dried for 48 h (50 °C, drying oven) to remove any traces of solvent. The tablets were subsequently burned in a pure oxygen atmosphere at a pressure of 35 bar on a platinum crucible, whereby the enthalpy of combustion H_C of the respective polymer was obtained. Based on the repetition unit, GAP and poly(3-azidooxetane) burn according to the following equation to form water, carbon dioxide, and nitrogen:

$$2\,C_3H_5N_3O + 7.5\,O_2 \rightarrow 6\,CO_2 + 5\,H_2O + 3\,N_2$$

According to Hess' law, the enthalpy of formation of the respective polymer is obtained as follows:

$$\Delta H_f^0(polymer) = \Delta H_f^0(comb.products) - \Delta H_C(polymer)$$

Since nitrogen forms in the elemental form, the enthalpy of formation is 0. For water and carbon dioxide, the literature values of −241.83 and −393.52 kJ mol^{-1} were used.[26] Tables 4 and 5 summarize the quantities used and values obtained in the case of GAP and poly(3-azidooxetane), respectively.

Table 10.4. Heat of combustion determination for poly(3-azidooxetane).

Sample	Tablet [mg]	p3AO [mg]	ΔH_c [kJ mol^{-1}]
1	631.4	145.7	−2018.3081
2	601.0	138.7	−2095.3236
3	616.2	142.2	−2048.7349
4	639.7	147.6	−2025.3076
5	599.1	138.2	−2060.8931
			Average: −2049.7135

Table 10.5. Heat of combustion determination for the glycidyl azide polymer (GAP).

Sample	Tablet [mg]	GAP [mg]	ΔH_c [kJ mol^{-1}]
1	650.8	150.2	−1841.1435
2	721.4	166.5	−1927.9377
3	667.8	154.1	−2095.9554
4	687.1	158.6	−1833.6621
5	684.2	157.9	−1853.2958
			Average: −1910.3989

For GAP, a positive heat of formation of 125 kJ mol^{-1} was calculated, while poly(3-azidooxetane) surprisingly shows roughly twice the value found for GAP (264 kJ mol^{-1}). Further details can be found in the Supporting Information.

10.2.7 Heat of Formation and Detonation Parameters

Since plasticizers are usually added to energetic formulations in rather high proportions, their energetic contribution to the overall performance of a formulation is substantial. Therefore, the performance of the selected plasticizers, nitroglycerin and ethane-1,2-diyl bis(2-azidoacetate) (EDBAA), was calculated (Table 6).

Table 10.6. Physicochemical and energetic properties of GAP, poly(3-azidooxetane) and plasticizers (NG, EGBAA).

	GAP	**p3AO**	**NG**[27,28]	**EDBAA**
Formula	$C_3H_5N_3O$	$C_3H_5N_3O$	$C_3H_5N_3O_9$	$C_6H_8N_6O_4$
FW [g·mol^{-1}]	99.09	99.09	227.09	228.17
IS[a] [J]	8	10	0.2	> 40
FS[b] [N]	360	360	> 353	360
Ω[c] [%]	−72.7	−72.7	−42.1	+3.5
T_{dec}[d] [°C]	213	190	175	−207
ρ[e] [g·cm^{-3}]	1.30	1.30	1.59	1.35
ΔH_f°[f] [kJ·mol^{-1}]	125.3	264.6	−320.6	−61.6
		EXPLO5 V6.04		
$-\Delta_E U^{\circ}$[g] [kJ·kg^{-1}]	3667.6	4957.0	6269.2	3293.6
$T_{C\text{-}J}$[h] [K]	2398.9	3043.3	4431.7	2495.3
$p_{C\text{-}J}$[i] [GPa]	12.6	17.1	23.4	12.0
$D_{C\text{-}J}$[j] [m·s^{-1}]	6536	6986	7793	6159
V_0[k] [dm^3·kg^{-1}]	791	793	782	771

[a] Impact sensitivity (BAM drop hammer, method 1 of 6). [b] Friction sensitivity (BAM friction apparatus, method 1 of 6). [c] Oxygen balance based on CO formation. [d] Decomposition temperature (DSC, β = 5 °C·min^{-1}). [e] Density at 298 K (weighing of 100 µL). [f] Standard molar enthalpy of formation. [g] Detonation energy. [h] Detonation temperature. [i] Detonation pressure. [j] Detonation velocity. [k] Volume of detonation gases at standard temperature and pressure.

For this purpose, the heat of formation (HOF) of their respective gas phase species was calculated by *ab initio* methods using the CBS-4M level of theory and Gaussian16 software package.[29] According to Trouton's rule, the HOF in the liquid state is then obtained as the difference between the gas phase enthalpy and the sublimation enthalpy.[2] The gas phase heat of formation is obtained by subtracting the atomization energies from the calculated total enthalpy of the molecule.[30] The EXPLO5 V6.04 thermochemical code[15] was then used to calculate the detonation parameters (Table 6) based on the HOF of both plasticizers and their density. In the case of nitroglycerin, the literature density was used,[27,28] while the density of both polymers was assessed by helium pycnometry. The density of EDBAA was determined by weighing a volume of 100 µL (Hamilton syringe). A detonation velocity ($V_{det.}$) of 7793 ms^{-1} at a detonation pressure ($p_{C\text{-}J}$) of 23.4 GPa was calculated for nitroglycerin, while a detonation velocity of 6159 ms^{-1} and a pressure 12.0 GPa was calculated for EDBAA. Comparable values were calculated for GAP ($V_{det.}$ = 6536 ms^{-1}, $p_{C\text{-}J}$ = 12.6 GPa), which is outperformed by poly(3-azidooxetane) ($V_{det.}$ = 6986 ms^{-1}, $p_{C\text{-}J}$ = 17.1 GPa) due to its higher heat of formation.

10.2.8 Compatibility Testing

Plasticizers are often used in energetic formulations to regulate and tailor mechanical properties. Thereby, compatibility with the polymer is of the highest importance as insufficient compatibility can lead to migration of the plasticizer out of the binder matrix, thereby changing the properties of the formulation up to an increase in sensitivity. As the compatibility of GAP with azido ester plasticizers is known, the suitability of EDBAA for the structurally related poly(3-azidooxetane) was investigated. In addition, the compatibility with nitroglycerin was evaluated as the latter becomes phlegmatized when incorporated into the polymer and shows correspondingly reduced and acceptable sensitivity. Therefore, the use of this particularly powerful and extremely oxygen-rich plasticizer was considered. Since the formation of a homogeneous mixture is an important indication for the compatibility between the polymer and plasticizer, poly(3-azidooxetane) was mixed with 50 wt% of plasticizer, whereby swelling of the polymer was observed. In both cases, no separation of the components occurred after 3 weeks of shelf life under ambient conditions. Therefore, the mixtures were further investigated by DSC (heating rate: 5 °C min^{-1}). First, a low-temperature measurement was carried out to study the influence of both plasticizers on the glass transition temperature (T_G). While the pure polymer (p3AO, LMW) shows a glass transition at −56.4 °C, admixture of nitroglycerine caused a glass transition lowered by 7.2 °C (−63.3 °C), while EDBAA (**5**) caused a superior lowering of T_G by 9.8 °C (−66.2 °C). In the subsequent high-temperature measurement, the mixture with nitroglycerine decomposed already at 163.3 °C, while pure nitroglycerine was found to decompose at 174.6 °C, revealing a detrimental effect. In the case of plasticizer **5**, the decomposition temperature remains essentially unaffected (212.8 °C). Thus, the azido ester EDBAA exhibits the expected and desired compatibility, while nitroglycerine even leads to a lower thermostability of the mixture. Thus, it only shows partial compatibility in the deep-temperature region.

10.2.9 Curing

Based on the GPC results of all prepolymers, poly(3-azidooxetane) prepared from pTsOx-I5-3 was chosen to perform curing. First, GPC of the azido polymer was performed (Figure 5).

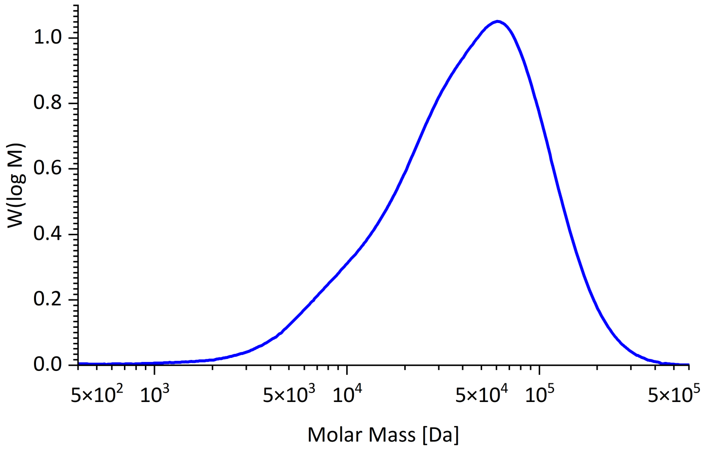

Figure 10.5. GPC curve of poly(3-azidooxetane) prepared from poly(3-tosyloxyoxetane) I5-3.

Although azidation should neither affect the chain length nor the distribution, both the molecular weight and polydispersity are higher than expected from the parent polymer (Table 7).

Table 10.7. Comparison of calculated values and GPC values for p3AO prepared from pTsOx I5-3.

Polymer	**M_n [g mol^{-1}]**	**M_W [g mol^{-1}]**	**Đ**
pTsOx I5-3 (GPC)	3288	4626	1.41
p3AO, calculated	1428	2010	~1.41
p3AO, GPC	1550	5206	3.36

This effect may be attributed to undesired chain extension due to the harsh azidation conditions. It is conceivable that highly mobile, linear oligomers perform a nucleophilic attack via their terminating hydroxy groups at unsubstituted, terminal positions of the parent polymer. This particular effect is known to the literature and matches our observation.[10] However, since polymers of different structures are compared by GPC using polystyrene standards, the different hydrodynamic volume of these polymers must also be considered as a cause. The hydroxy-equivalent weight was determined via NMR spectroscopy (^{1}H) by protecting the terminal hydroxy groups with a trimethyl-silyl group using a mixture of trimethylsilyl chloride and hexamethyldisilazane in chloroform according to the literature.[31] Comparison of the repetition unit integral (5 protons per unit) to the integral of the siloxy group (9 protons per group) gave a calculated value of 2289 g equiv^{-1}. After the polymer was thoroughly dried in a Schlenk flask under high vacuum (3 days, 70 °C, 10^{-3} mbar), TDI (2,4-toluene diisocyanate) was added as a linker under an argon atmosphere (NCO/OH ratio = 1.1) as well as a catalytic amount of DBTDL (dibutyltin dilaurate). The mixture was stirred under an argon atmosphere for 48 h at 50 °C, and the cured rubber (Figure 6) was subsequently removed from the flask.

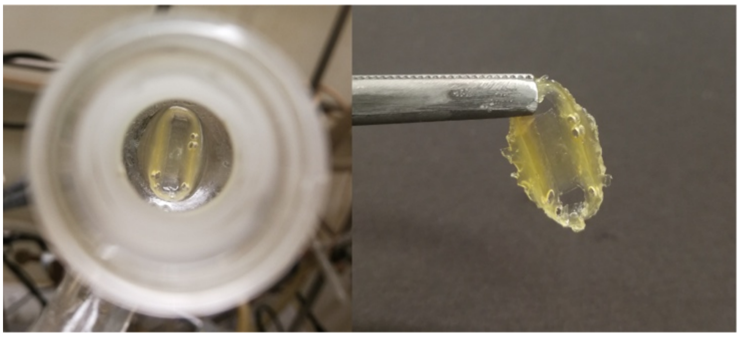

Figure 10.6. Cured poly(3-azidooxetane) before (left) and after extraction (right) from the round-bottom-flask.

10.2.10 Aquatic Toxicity

As research in the field of energetic materials increasingly focuses on environmentally friendly materials and substitutes, rapid test methods are needed to assess their toxicity. One established method is the quantification of the bioluminescence quenching of *Aliivibrio fischeri* bacteria by pollutants dissolved in water. Here, the effective bacterial concentration (EC_{50}) is determined after 15 and 30 min via the quenching effect on the bacteria's bioluminescence.[16] The extent of light extinction by a particular substance compared to other substances then allows an assessment of the relative aquatic toxicity. Accordingly, the toxicity of epichlorohydrin (ECH) required for the synthesis of PECH and ultimately GAP was investigated and compared with the toxicity of the monomers 3-tosyloxyoxetane (**1**) and 3-mesyloxyoxetane (**2**) required for the synthesis of poly-3-azidoxetane's parent polymers. For completeness, the overall precursor, oxetan-3-ol, was also investigated. To classify the toxicity, it is categorized according to the obtained EC_{50} value. Compounds causing values below 0.10 g L^{-1} are categorized as very toxic (++), values between 0.10 and 1.00 g L^{-1} are considered as toxic (+), and compounds exhibiting values higher than 1.00 g L^{-1} are categorized as "less toxic" (–) to *A. fischeri* bacteria.[32] The results are summarized in Table 8.

Table 10.8. Aquatic toxicity data of epichlorohydrin, oxetan-3-ol and monomers **1** and **2** in comparison.

Compound	**EC_{50} (15 min) [g L^{-1}]**	**EC_{50} (30 min) [g L^{-1}]**	**Toxicity level**
ECH	1.11	0.88	+
1	-	-	–
2	0.90	0.85	+
Oxetan-3-ol	1.50	1.36	–

Due to its high solubility in water, the aquatic toxicity of oxetan-3-ol is particularly relevant as it represents the precursor to all follow-up compounds. The found EC_{50} value allows oxetan-3-ol to be classified as "less toxic" to the mentioned marine bacteria. Thereby, its hazard potential is generally low and lower than in the case of ECH. Unfortunately, both epichlorohydrin and 3-

mesyloxyxetane (**2**) need to be categorized as “toxic”. In contrast, 3-tosyloxyoxetane (**1**) can be classified as non-toxic since it was found to be insoluble in water even after the addition of the maximum amount of acetone allowed in this test. Accordingly, compound **2** does not pose relevant hazards to aquatic life. Thus, poly(3-azidooxetane), prepared via oxetan-3-ol, 3-tosyloxyoxetane, and the corresponding polymer, is more environmentally benign than GAP. Even though the aquatic toxicity of 3-mesyloxyoxetane and ECH is essentially the same, the use of the sulfonic acid ester monomers **1** and **2** offers further advantages in practice. Epichlorohydrin is a liquid, and inhalation of its vapor is linked to lung irritation and an increased risk of lung cancer.[33] Since monomers **1** and **2** are solids, the risk of unintentional respiratory uptake would be significantly lower. Overall, it can be assumed that the use of poly(3-azidooxetane) as a GAP alternative would be associated with lower health and environmental hazards in the manufacturing process and should therefore be preferred.

10.3 Conclusions

The non-energetic precursor polymers poly(3-tosyloxyoxetane) and poly(3-mesyloxyoxetane) were obtained as both low- and high-molecular-weight species using boron trifluoride etherate and triisobutylaluminum-water as catalysts, respectively. Both methods afforded the polymers in high, satisfying yields. In the former case, molecular weights suitable for the synthesis of curable energetic binders were achieved and the low polydispersity of all prepolymers as well as partial initiator incorporation indicates a high contribution of the favorable AMM. Beyond that, the evaluation of the GPC results revealed possibilities to achieve higher molecular weights and narrower molecular weight distributions in the future and to enhance the “living” character of the polymerization. In this context, a lower initiator concentration in combination with a significantly increased monomer feeding time will contribute to improved results. In contrast, the polymerization with the trialkylaluminum species TIBA–H_2O gave extremely high molecular weights in comparison, resulting in a broader polydispersity as expected. In both cases, further optimization of the polymerization conditions is likely to afford both low- and high-molecular-weight prepolymers, allowing the preparation of energetic binders with tailored properties by polymer-analogous transformation using suitable energetic nucleophiles. Regardless of the molecular weight, all prepolymers allowed both quantitative azidation and recovery to afford poly(3-azidooxetane) in excellent yield. This renders a far safer preparation of poly(3-azidooxetane) possible than by polymerization of the rather sensitive monomer 3-azidooxetane. Due to the use of TIBA as a catalyst, p3AO was obtained and characterized for the first time as a high-molecular-weight species, while the low-molecular-weight species was found to be comparable to commercial GAP with regard to important properties such as molecular weight, thermal behavior, plasticizer compatibility, and curability. Furthermore, the overall yield was more than doubled compared to the old literature pathway. The formation of only primary, terminating hydroxy groups and the slightly higher performance and lower sensitivity in addition to the avoidance of flame-retardant halogens represent further advantages of poly(3-azidooxetane). In addition, according to the aquatic toxicity test, the synthetic pathway using oxetan-3-ol, 3-tosyloxyoxetane, and the homopolymer pTsOx poses a lower environmental threat than the use of epichlorohydrin to prepare GAP. Furthermore, both sulfonic acid ester monomers are solids and the risk of respiratory uptake is also lower than in the case of epichlorohydrin. However, on account of the high molecular weight of the tosyl group, this pathway provides a way poorer atom economy compared to the presented mesylate precursors. Unproblematic on the laboratory scale, this can be disadvantageous for industrial production. Therefore, environmental friendliness must be weighed against other factors. Nevertheless, our results suggest that poly(3-azidooxetane) is a flawless substitute for GAP and should be considered for application due to its advantages.

Associated Content

The Supporting Information is available free of charge at charge at
https://pubs.acs.org/doi/10.1021/acs.joc.1c02907.
Experimental procedures; ^{1}H, ^{13}C, ^{14}N NMR spectra; Graphic documentation of obtained polymers; Bomb calorimetry; Heat of formation calculation; DSC graphs; Hot plate test of glycidyl azide polymer and poly(3-azidooxetane); Hot plate test video (hot plate test.mp4).

Acknowledgements

Financial support by the Ludwig-Maximilian-University (LMU), the Office of Naval Research (ONR) under grant no. ONR.N00014-16-1-2062, and the Strategic Environmental Research and Development Program (SERDP) under contract no. WP19-1287 is gratefully acknowledged. The authors thank Stefan Huber for his dedicated help in the determination of sensitivities toward mechanical stimuli. Last but not the least, we thank Christian Riedelsheimer (M.Sc.) for the assessment of the aquatic toxicity of selected compounds.

References

[1] Provatas, A. *Energetic Polymers and Plasticizers for Explosive Formulations – A Review of Recent Advances*; DSTO-TR-0966; Defence Science & Technology Organisation (Department of Defence), Aeronautical and Maritime Research Laboratory: Melbourne, Victoria, **2000**.

[2] Klapötke, T. M. *Chemistry of High-Energy Materials*; 5th ed.; DeGruyter: Boston, **2019**.

[3] Ang, H. G.; Pisharath, S. *Energetic Polymers: Binders and Plasticizers for Enhancing Performance*; Wiley-VCH: Weinheim, **2012**.

[4] Fruci, S.; Lamia, P.; Cappello, M.; Filippi, S.; Polacco, G. Synthesis of GAP and PAMMO Homopolymers from Mesylate Polymeric Precursors AU - Mura. Claudio. *J. Energy Mater.* **2016**, *34*, 216-233.

[5] Vandenberg, E. J. Polyethers containing azidomethyl side chains. US 3 645 917, **1972**.

[6] 3M^{TM} Glycidyl Azide Polymer GAP-5527 Polyol; 3M Specialty Materials: St. Paul, MN, **2000**. https://www.machichemicals.com/pdf/3M_GAP-5527.pdf (accessed 2021-09-01).

[7] Born, M.; Karaghiosoff, K.; Klapötke, T. M. A GAP Replacement: Improved Synthesis of 3-Azidooxetane and Its Homopolymer Based on Sulfonic Acid Esters of Oxetan-3-ol. *J. Org. Chem.* **2021**, *86*, 12607-12614.

[8] National Center for Biotechnology Information. PubChem Compound Summary for CID 7835, Epichlorohydrin;. https://pubchem.ncbi.nlm.nih.gov/compound/Epichlorohydrin. (accessed 2021-08-21)

[9] 1-Chlor-2,3-epoxypropan (Epichlorohydrin) [MAK Value Documentation in German language, **2003**]. In *The MAK-Collection for Occupational Health and Safety*; Wiley-VCH: Weinheim, **2002**. DOI: 10.1002/3527600418.mb10689d0036

[10] Barbieri, U.; Keicher, T.; Polacco, G. Homo- and copolymers of 3-tosyloxymethyl-3-methyl oxetane (TMMO) as precursors to energetic azido polymers. *e-Polymers* **2009**, *9*, 565.

[11] Guo, K.; Luo, Y.; Chen, J.; Li, X.; Huang, L. Synthesis of Poly(3,3-Bis-Azidomethyl Oxetane) via Direct Azidation of Poly(3,3-Bis-Bromo Oxetane). *Propellants, Explos., Pyrotech.* **2010**, *35*, 423-424.

[12] Cheradame, H.; Andreolety, J. P.; Rousset, E. Synthesis of polymers containing pseudohalide groups by cationic polymerization, 1. Homopolymerization of 3,3-bis(azidomethyl)oxetane and its copolymerization with 3-chloromethyl-3-(2,5,8-trioxadecyl)oxetane. *Makromol. Chem.* **1991**, *192*, 901-918.

[13] Mukhametshin, T. I.; Petrov, A. I.; Kuznetsova, N. V.; Petrov, V. A.; Averianova, N. V.; Garaev, I. K.; Kostochko, A. V.; Gubaidullin, A. T.; Vinogradov, D. B.; Bulatov, P. V. Synthesis and copolymerization of azidomethyl-substituted oxetanes: the morphology of statistical block copolymers. *Chem. Heterocycl. Compd.* **2017**, *53*, 811-821.

[14] Garaev, I. K.; Kostochko, A. V.; Petrov, A. I.; Ibragimov, E. N.; Golubev, A. E. Synthesis of azidooxetane statistical polymers and copolymers. *Russ. J. Gen. Chem.* **2016**, *86*, 1459-1468.

[15] Sućeska, M. EXPLO 5, Version 6.04, Brodarski Institute, Zagreb, **2017**.

[16] Klapötke, T. M.; Scharf, R.; Stierstorfer, J.; Unger, C. C. Toxicity Assessment of Energetic Materials by Using the Luminescent Bacteria Inhibition Test. *Propellants, Explos., Pyrotech.* **2021**, *46*, 114-123.

[17] Härtel, M. Studies towards the gas-phase detection of hazardous materials by vapor pressure measurements with the transpiration method in combination with vacuum outlet GC/MS. Ph. D. Dissertation, Ludwig-Maximilian University (LMU) Munich, Munich, Germany **2017**.

[18] Bezwada, R. S. Hydrolysable Linkers and Cross-Linkers for Absorbable Polymers. US 8 048 980, **2009**.

[19] Maeno, Z.; Midogochi, K.; Mitsudome, T.; Mizugaki, T.; Jitsukawa, K. Synthesis of glycol diesters through the depolymerization of polyethylene glycols with carboxylic acids using a protonexchanged montmorillonite catalyst. *Tetrahedron Lett.* **2018**, *59*, 832-835.

[20] Hafner, S. Internal plasticized glycidyl azide copolymers for energetic solid propellant binders. Ph. D. Dissertation, Ludwig-Maximilian University (LMU) Munich, Munich, Germany, **2019**.

[21] Penczek, S. Cationic ring-opening polymerization (CROP) major mechanistic phenomena. *J. Polym. Sci.* **2000**, *38*, 1919-1933.

[22] *N,N*-dimethylformamide; European Chemicals Agency; Helsinki, Finland, **2012**. https://echa.europa.eu/documents/10162/64875a92-e9c1-3d65-6722-0fab6c7283b3 (accessed 2021-08-16).

[23] Axthammer, Q. J.; Evangelisti, C.; Klapötke, T. M. Characterization, bomb calorimetric measurements and quantum chemical calculations of high energetic dense oxidizers (HEDO). In *44th International Annual Conference of the Fraunhofer ICT, Energetic Materials – Past, Present and Future*, Karlsruhe, Germany, June 25–28, **2013**.

[24] Schmidt, R. D.; Manser, G. E. *Heats of Formation of Energetic Oxetane Monomers and Polymers*; UCRL-JC-141600; U.S. Department of Energy, Lawrence Livermore National Laboratory: Livermore, CA, **2001**.

[25] Linstrom, P. J.; Mallard, W. G., Eds., *NIST Chemistry WebBook*, *NIST Standard Reference Database Number 69*; National Institute of Standards and Technology: Gaithersburg MD; https://webbook.nist.gov (accessed 2021-10-01).

[26] Chase, M. W. NIST-JANAF Thermochemical Tables, Fourth Edition. *J. Phys. Chem. Red. Data, Monograph 9* **1998**, 1–1951.

[27] Klapötke, T. M. *Energetic Materials Encyclopedia*; Vol. 1–3; De Gruyter: Berlin, Boston, **2021**.

[28] Köhler, J.; Meyer, R.; Homburg, A. *Explosives*; 10th ed.; Wiley-VCH: Weinheim, **2008**.

[29] Frisch, M. J.; Trucks, G. W.; Schlegel, H. B.; Scuseria, G. E.; Robb, M. A.; Cheeseman, J. R.; Scalmani, G.; Barone, V.; Petersson, G. A.; Nakatsuji, H.; Li, X.; Caricato, M.; Marenich, A. V.; Bloino, J.; Janesko, B. G.; Gomperts, R.; Mennucci, B.; Hratchian, H. P.; Ortiz, J. V.; Izmaylov, A. F.; Sonnenberg, J. L.; Williams; Ding, F.; Lipparini, F.; Egidi, F.; Goings, J.; Peng, B.; Petrone, A.; Henderson, T. Ranasinghe, D.; Zakrzewski, V. G.; Gao, J.; Rega, N.; Zheng, G.; Liang, W.; Hada, M.; Ehara, M.; Toyota, K.; Fukuda, R.; Hasegawa, J.; Ishida, M.; Nakajima, T.; Honda, Y.; Kitao, O.; Nakai, H.; Vreven, T.; Throssell, K.; Montgomery, J. A., Jr.; Peralta, J. E.; Ogliaro, F.; Bearpark, M. J.; Heyd, J. J.; Brothers, E. N.; Kudin, K. N.; Staroverov, V. N.; Keith, T. A.; Kobayashi, R.; Normand, J.; Raghavachari, K.; Rendell, A. P.; Burant, J. C.; Iyengar, S. S.; Tomasi, J.; Cossi, M.; Millam, J. M.; Klene, M.; Adamo, C.; Cammi, R.; Ochterski, J. W.; Martin, R. L.; Morokuma, K.; Farkas, O.; Foresman, J. B.; Fox, D. J., Gaussian 16 Rev. C.01, Gaussian, Inc., Wallingford CT, **2016**.

[30] Curtiss, L. A.; Raghavachari, K.; Redfern, P. C.; Pople, J. A. Assessment of Gaussian-2 and density functional theories for the computation of enthalpies of formation. J. *Chem. Phys.* **1997**, *106*, 1063-1079.

[31] Baum, K.; Berkowitz, P. T.; Grakauskas, V.; Archibald, T. G. Synthesis of electron-deficient oxetanes. 3-Azidooxetane, 3-nitrooxetane, and 3,3-dinitrooxetane. *J. Org. Chem.* **1983**, *48*, 2953-2956.

[32] Cao, C. J.; Hurley, M. M.; Johnson, M. S.; Klapötke, T. M. In Vitro Approach to Rapid Toxicity Assessment of Novel High-Nitrogen Energetics. JANNAF *J. Propul. Energ.* **2012**, *5*, 39–49.

[33] Screening Assessment for the Challenge Oxirane, (chloromethyl)-(epichlorohydrin); CAS RN: 106-89-8; Environment Canada, Health Canada, **2008**. https://www.ec.gc.ca/ese-ees/BA416AA1-1073-4ECC-9D5E-C3764A7A0E7E/batch2_106-89-8_en.pdf (accessed 2021-10-01).

10.4 Supporting Information

10.4.1 Experimental Part

General information

Caution! Nitroglycerin, ethane-1,2-diyl bis(2-azidoacetate), poly(3-azidooxetane) and GAP are energetic materials with sensitivity toward stimuli like friction, shock, and electric discharge. Therefore, proper security precautions (safety glasses, face shield, earthed equipment and shoes, Kevlar gloves and ear plugs) have to be applied while preparing and handling aforementioned compounds.

Chemicals and solvents were employed as received (Sigma-Aldrich, Acros, TCI, Fischer Scientific, Spirochem AG). ^{1}H, ^{13}C and ^{14}N spectra were recorded on a Bruker AMX 400 instrument. The chemical shifts refer to tetramethylsilane (^{1}H, ^{13}C) and nitromethane (^{14}N). Decomposition temperatures were determined on a Mettler Toledo DSC822e device at a heating rate of 5 °C min^{-1} using 40 µL aluminum crucibles (with lid hole) and nitrogen purge gas at a flow rate of 30 mL min^{-1}. DSC Evaluations of thermal behavior were performed using the STARe Software Version 16.20. Infrared (IR) spectra were measured on a Perkin-Elmer Spektrum One FT-IR decive. Raman spectra were obtained using a Bruker MultiRam FT Raman spectrometer and a neodymium-doped yttrium aluminum garnet (Nd:YAG) laser (λ = 1075 nm, P = 1000 mW). Elemental analyses were performed with an Elementar Vario El by pyrolysis and subsequent gas analysis. The density of polymers was assessed by helium pycnometry using a Micromeritics AccuPyc II 1345 device. The sensitivity data was collected by means of a BAM (Bundesanstalt für Materialforschung) drop hammer according to STANAG 4489 modified instruction[1] as well as a BAM friction tester according to STANAG 4487 modified instruction.[2] The classification of the tested compounds was based on the 'UN Recommendations on the Transport of Dangerous Goods'.[3]

10.4.1.1 Monomer and Precursor Synthesis

3-Mesyloxyoxetane (2)

3-Mesyloxyoxetane was prepared according to our recently published procedure.[4]

^{1}H NMR (CDCl$_3$, 400 MHz): δ 5.48 (tt, *J* = 6.3, 5.3 Hz, 1H, CH), 4.87 (ddd, 2H, CH$_2$), 4.78 (ddd, 2H, CH$_2$), 3.04 (s, 3H, CH$_3$).**^{13}C{^{1}H} NMR** (CDCl$_3$, 101 MHz): δ 77.4, 71.2, 38.1. **IR** (ATR, cm^{-1}): $\tilde{\nu}$ 1333 (s, ν_{as} SO$_2$), 1165 (s, ν_s SO$_2$), 1067 (s, ν_{as} COC), 972 (s, ν_s COC), 883 (s, S–O), 826 (s, C–S). **Raman** (1075 nm, 1000 mW, cm^{-1}): $\tilde{\nu}$ 3061 (10), 3028 (29), 3007 (39), 2984 (42), 2934 (100), 2897 (35), 1485 (32), 1416 (16), 1385 (10), 1373 (13), 1352 (19), 1181 (19), 1161 (52), 1111 (23), 1071 (19), 1032 (16), 982 (13), 940 (13), 770 (16), 714 (13), 529 (39), 461 (13). **Anal. Calcd** for $C_4H_8O_4S$: C, 31.57; H, 5.30; S, 21.07. Found: C, 31.47; H, 5.27; S, 21.20. **HRMS** (EI) m/z: [M]$^+$ Calcd for $C_4H_8O_4S$

152.0143; Found 149.0227 $[C_4H_5O_4S]^+$, 122.0029 $[C_3H_6O_3S]^+$, 78.9827 $[CH_3O_2S]^+$. **DSC** (5 °C min^{-1}): 37.0 °C (m.p.), 254.0 °C (dec.).

Propane-1,2,3-triyl trinitrate (Nitroglycerin, 3)

*Compound **3** was prepared according to a slightly modified literature procedure.*[5]

Concentrated sulfuric acid (6.0 mL, 108 mmol, 96%) and white fuming nitric acid (4 mL, 96.0 mmol, 6.4 equiv.) were added to a 25 mL round bottom flask while cooling with an ice-salt bath. After 10 minutes, glycerin (1.38 g, 14.99 mmol) was added dropwise to the thoroughly stirred mixed acid keeping the temperature below 10 °C. A temperature between 0–10 °C was maintained for 3 h prior to quenching of the reaction mixture with iced water (100 mL). Afterward, the product was extracted with dichloromethane (4 × 20 mL) and the organic phase washed with water (20 mL), saturated sodium bicarbonate solution (2 × 20 mL) and finally with water (10 mL). The organic phase was dried over sodium sulphate and carefully evaporated (rotary evaporation) until the mass remained constant. Hereby, 3.31 g (97%) nitroglycerine was obtained as colorless, oily liquid.

^{1}H NMR (Acetone-d_6, 400 MHz): δ 5.92 (tt, *J* = 6.1, 3.4 Hz, 1H, CH), 5.15 (dd, *J* = 13.0, 3.4 Hz, 2H, CH_2), 4.97 (dd, *J* = 13.0, 6.1 Hz, 2H, CH_2). **^{13}C{^{1}H} NMR** (Acetone-d_6, 101 MHz): δ 76.8, 70.1. **^{14}N NMR** (Acetone-d_6, 29 MHz): δ −45.3, −47.7. **IR** (ATR, cm^{-1}): ṽ 1631 (vs, ν_{as} NO_2), 1266 (vs, ν_s NO_2), 1007 (m, C–N), 824 (vs, δ NO_2). **LRMS** (ESI) m/z: $[M]^+$ Calcd for $C_3H_5N_3O_9$ 227.00; Found 227.01 $[C_3H_5N_3O_9]^+$, 165.9 $[C_3H_5N_2O_6]^+$. **DSC** (5 °C min^{-1}): 174.6 °C (dec.). **BAM drop hammer**: 1 J.[5] **Friction test**: > 360 N.[5]

Ethane-1,2-diyl bis(2-chloroacetate) (EDBCA, 4)

*Compound **4** was prepared according to a slightly modified literature procedure.*[6]

Ethane-1,2-diol (5.12 g, 82.5 mmol) and chloroacetic acid (19.5 g, 206 mmol, 2.5 equiv.) were dissolved in toluene (40.0 mL) in a 100 mL round bottom flask. P-toluenesulfonic acid (50 mg) was added and the flask connected to a Dean-Stark apparatus. Subsequently, the reaction mixture was set to heavy reflux using an oil bath for 6 h until water formation subsided. The toluene phase was then washed with water (3 × 30 mL) and saturated sodium bicarbonate solution (3 × 30 mL) to remove surplus ethane-1,2-diol and acid. The organic phase was dried over sodium sulphate and evaporated to give 14.1 g (79%) of crude product as colorless liquid. The material was further purified by vacuum distillation (5×10^{-2} mbar, 110 °C) to give 12.1 g of pure EDBCA (overall yield: 68%).

^{1}H NMR ($CDCl_3$, 400 MHz): δ 4.41 (s, 2H, CH_2), 4.08 (s, 2H, CH_2). **^{13}C{^{1}H} NMR** ($CDCl_3$, 101 MHz): δ 167.2, 63.4, 40.7. **IR** (ATR, cm^{-1}): ṽ 1739 (s, C=O), 1287 (s, ν_{as} COC), 1158 (vs, ν_s COC), 781 (s, C–Cl). **Raman** (1075 nm, 1000 mW, cm^{-1}): ṽ 3004 (26), 2961 (100), 2896 (11), 1752 (16), 1455 (11), 1411 (13), 1289 (11), 1050 (8), 1035 (8), 930 (8), 882 (16), 849 (11), 784 (24), 593 (11), 419 (8). **Anal. Calcd** for $C_6H_8Cl_2O_4$: C, 33.52; H, 3.75; Cl 32.97. Found: C, 33.32; H, 3.59; Cl, 32.57. **LRMS** (ESI) m/z: $[M]^+$ Calcd for $C_6H_8Cl_2O_4$ 213.98; Found 213.44 $[C_6H_8Cl_2O_4]^+$. **DSC** (5 °C min^{-1}): 39.1 °C (m.p.), 262.0 °C (b.p.).

Ethane-1,2-diyl bis(2-azidoacetate) (EDBAA, 5)

Compound 5 was prepared according to a slightly modified literature procedure.[7]

Ethane-1,2-diyl bis(2-chloroacetate) (3.00 g, 13.9 mmol) and sodium azide (3.63 g, 55.8 mmol, 4 equiv.) were dissolved in a mixture of water (40.0 mL) and THF (20.0 mL). The solution was heated to 50 °C for 36 h by means of an oil bath. Afterward, the solution was extracted using ethyl acetate (3 × 30 mL) and the organic phase dried over sodium sulphate. The solvent was removed by rotary evaporation to afford 3.01 g (95%) of ethane-1,2-diyl bis(2-azidoacetate) as slightly yellowish liquid. Crystallization can be achieved by deep-freezing (see DSC graph).

^{1}H NMR (Acetone-d$_6$, 400 MHz): δ 4.45 (s, 2H, CH_2), 4.05 (s, 2H, CH_2). **^{13}C{^{1}H} NMR** (Acetone-d$_6$, 101 MHz): δ 169.3, 63.8, 50.5. **^{14}N NMR** (Acetone-d$_6$, 29 MHz): δ −133.8 (N_β), −169.6 (N_γ), −319.2 (N_α). **IR** (ATR, cm^{-1}): $\tilde{\nu}$ 2103 (vs, ν_{as} N_3), 1740 (s, C=O), 1281 (m, ν_s N_3), 1184 (vs, ν_{as} COC). **Raman** (1075 nm, 1000 mW, cm^{-1}): $\tilde{\nu}$ 3004 (26), 2961 (100), 2896 (11), 1752 (16), 1455 (11), 1411 (13), 1289 (11), 1050 (8), 1035 (8), 930 (8), 882 (16), 849 (11), 784 (24), 593 (11), 419 (8). **Anal. Calcd** for $C_6H_8N_6O_4$: C, 31.58; H, 3.53; N, 36.83. Found: C, 31.47; H, 3.47; N, 36.45. **LRMS** (ESI) m/z: $[M]^+$ Calcd for $C_6H_8N_6O_4$ 228.06; Found 128.04 $[C_4H_6N_3O_2]^+$. **DSC** (5 °C min^{-1}): 207.3 °C (dec.). **Density**: $\rho = 1.35$ g cm^{-3}. **BAM drop hammer**: 40 J. **Friction test**: > 360 N.

10.4.1.2 Polymer Synthesis

The following general procedure was applied for the preparation of polymers using boron trifluoride etherate as catalyst.

A Schlenk round bottom flask was closed with a silicone rubber septum and thoroughly dried (3 ×) using protective atmosphere (argon). Boron trifluoride etherate (10 or 20 mol%) and butane-1,4-diol (5 or 10 mol%) were added using a 100 µL Hamilton syringe. The initiating mixture was stirred for 15 minutes prior to the addition of dry dichloromethane (30% of the overall solvent volume). A solution of 3-tosyloxyoxetane or 3-mesyloxyoxetane (each 2.00 g) in dry dichloromethane was prepared under protective atmosphere (argon) using 70% of the required overall solvent volume. Subsequently, the monomer solution was added over a period of 2–3 hours by means of a syringe pump and the reaction mixture was stirred at 250 rpm for 48 hours. Afterward, the polymerization was quenched by the addition of water (1 mL) and vigorously stirred for five minutes. Methanol (25 mL) was added to cause precipitation of the target polymer and to dissolve residual monomer. The resulting emulsion was stirred for five minutes and the polymer collected by centrifugation (6000 rpm, 20 minutes). After decanting of the supernatant, the polymer was dissolved in the minimum amount of acetone and precipitated again with an excess of methanol. After centrifugation, the supernatant was decanted and the polymer transferred to a round bottom flask using acetone. All volatiles were removed by rotary evaporation and drying under high vacuum conditions (10^{-3} mbar, 24 h, 70 °C, oil bath). While poly(3-mesyloxyoxetane) (pMsOx) was obtained as yellow to brownish resin-like material, poly(3-tosyloxyoxetane) (pTsOx) turned into a brittle solid after cooling to room temperature.

The employed amount of all compounds and the respective yields are summarized in Table S 1. The individual batches are labeled according to the initiator concentration used and the duration of monomer addition. Thus, poly(3-tosyloxyoxetane) with an initiator concentration of 5 mol% and an addition time of 2 h corresponds to the acronym pTsOx I5-2.

Table S 10.1. Employed amounts for the polymerization of 3-tosyloxyoxetane and 3-mesyloxyoxetane using the boron trifluoride etherate/diol initiating system.

	amounts	**pTsOx I5-2**	**pTsOx I5-3**	**pTsOx I10-2**	**pMsOx I5-2**	**pMsOx I10-2**
Monomer	m [g]	2.00	10.0	2.00	2.00	2.00
	n [mmol]	8.76	43.8	8.76	13.4	13.4
	c [mol/L]	2.00	2.00	2.00	2.00	2.00
$BF_3 \cdot Et_2O$	m [mg]	124	633	249	187	373
	n [mmol]	0.876	4.38	1.75	1.31	2.63
	V [µL]	108	541	216	162	324
	c [mol%]	10	10	20	5	20
1,4-BDO	m [mg]	39.5	197	78.9	59.2	118
	n [mmol]	0.438	2.19	0.876	0.657	1.31
	V [µL]	38.7	194	77.4	58.1	116
	c [mol%]	5	5	10	5	10
Solvent	V [mL]	4.38	21.9	4.38	6.57	6.57
	Yield [g, %]	1.63, 81	8.70, 87	1.59, 79	1.64, 82	1.55, 77

Poly(3-tosyloxyoxetane) I5-2

^{1}H NMR (400 MHz, Acetone-d$_6$): δ 7.80 (d, 2H, CH$_{arom}$), 7.46 (d, 2H, CH$_{arom}$), 4.54–4.40 (m, 1H, CH), 3.58–3.32 (m, 4H, CH$_2$). **^{13}C{^{1}H} NMR** (101 MHz, Acetone-d$_6$): 145.9, 135.2, 130.9, 128.7, 80.4, 70.6, 21.7. **IR** (ATR, cm^{-1}): $\tilde{\nu}$ 2925 (w), 2878 (vw), 1598 (w), 1453 (w), 1356 (s), 1308 (w), 1293 (w), 1189 (m), 1173 (vs), 1121 (m), 1097 (s), 1036 (m), 1019 (m), 999 (m), 915 (s), 897 (s), 813 (s), 773 (s), 705 (w), 663 (s), 570 (m), 551 (vs), 463 (m), 463 (m). **Raman** (1075 nm, 1000 mW, cm^{-1}): $\tilde{\nu}$ 3069 (67), 2959 (50), 2928 (100), 2882 (50), 2863 (50), 2818 (17), 1600 (67), 1474 (17), 1386 (17), 1362 (17), 1173 (67), 1100 (33), 815 (33), 786 (50), 635 (17), 560 (17). **Anal. Calcd** for $(C_{10}H_{12}O_4S)_n$: C, 52.62; H, 5.30; S, 14.05. Found: C, 52.71; H, 5.42; S, 14.19. **DSC** (T_{onset}, 5 °C min^{-1}): 14.5 °C (glass transition), 56.1 °C (m.p.), 196.4 °C (dec.). **GPC**: M_w = 4969 g mol^{-1}, M_n = 2907 g mol^{-1}, M_p = 4905 g mol^{-1}, Đ = 1.71. **Density**: ρ = 1.33 g cm^{-3}.

Poly(3-tosyloxyoxetane) I5-3

^{1}H NMR (400 MHz, Acetone-d$_6$): δ 7.79 (d, 2H, CH$_{arom}$), 7.45 (d, 2H, CH$_{arom}$), 4.54–4.44 (m, 1H, CH), 3.57–3.40 (m, 4H, CH$_2$). **^{13}C{^{1}H} NMR** (101 MHz, Acetone-d$_6$): 155.6, 144.8, 140.5, 138.4, 90.0, 80.3, 70.6, 31.4. **IR** (ATR, cm^{-1}): ṽ 2921 (w), 2877 (w), 1598 (w), 1496 (w), 1453 (w), 1402 (w), 1351 (s), 1308 (w), 1294 (w), 1212 (w) 1189 (m), 1173 (vs), 1120 (m), 1097 (s), 1038 (m), 1019 (m), 912 (s), 813 (s), 771 (s), 705 (m), 663 (s), 635 (w), 576 (m), 550 (vs), 445 (w). **Raman** (1075 nm, 1000 mW, cm^{-1}): ṽ 3069 (55), 3036 (14), 2959 (27), 2926 (68), 2892 (23), 2880 (27), 1600 (73), 1463 (14), 1384 (18), 1191 (36), 1173 (100), 1100 (32), 819 (27), 786 (41), 635 (32), 390 (14). **Anal. Calcd** for $(C_{10}H_{12}O_4S)_n$: C, 52.62; H, 5.30; S, 14.05. Found: C, 52.64; H, 5.35; S, 13.63. **DSC** (T$_{onset}$, 5 °C min^{-1}): 19.2 °C (glass transition), 76.6 °C (m.p.), 196.6 °C (dec.). **GPC**: M_w = 4626 g mol^{-1}, M_n = 3288 g mol^{-1}, M_p = 3797 g mol^{-1}, Đ = 1.41. **Density**: ρ = 1.33 g cm^{-3}.

Poly(3-tosyoxyloxetane) I10-2

^{1}H NMR (400 MHz, Acetone-d$_6$): δ 7.80 (d, 2H, CH$_{arom}$), 7.46 (d, 2H, CH$_{arom}$), 4.54–4.40 (m, 1H, CH), 3.66–3.24 (m, 4H, CH$_2$). **^{13}C{^{1}H} NMR** (101 MHz, Acetone-d$_6$): 145.9, 135.1, 131.4, 128.7, 80.3, 70.5, 21.7. **IR** (ATR, cm^{-1}): ṽ 2925 (w), 2879 (w), 1598 (w), 1453 (w), 1351 (s), 1308 (w), 1294 (w), 1189 (m), 1173 (vs), 1120 (m), 1097 (s), 1019 (m), 913 (s), 813 (s), 771 (s), 705 (m), 663 (s), 635 (w), 576 (m), 551 (vs), 441 (w), 418 (w), 407 (w), 407 (w). **Raman** (1075 nm, 1000 mW, cm^{-1}): ṽ 3069 (67), 2926 (100), 2882 (56), 2865 (44), 2826 (11), 1600 (67), 1453 (22), 1380 (22), 1175 (89), 1098 (33), 815 (33), 786 (44), 635 (33), 487 (11). **Anal. Calcd** for $(C_{10}H_{12}O_4S)_n$: C, 52.62; H, 5.30; S, 14.05. Found: C, 52.89; H, 5.73; S, 13.78. **DSC** (T$_{onset}$, 5 °C min^{-1}): 13.1 °C (glass transition), 54.0 °C (m.p.), 196.7 °C (dec.). **GPC**: M_w = 3311 g mol^{-1}, M_n = 2227 g mol^{-1}, M_p = 3035 g mol^{-1}, Đ = 1.49. **Density**: ρ = 1.33 g cm^{-3}.

Poly(3-mesyloxyoxetane) I5-2

^{1}H NMR (400 MHz, Acetone-d$_6$): δ 4.92–4.85 (m, 1H, CH), 3.88–3.72 (m, 4H, CH$_2$), 3.21–3.12 (m, 3H, CH$_3$). **^{13}C{^{1}H} NMR** (101 MHz, Acetone-d$_6$): 80.7, 71.2, 38.8. **IR** (ATR, cm^{-1}): ṽ 3034 (vw), 2941 (w), 2881 (vw), 1709 (vw), 1472 (vw), 1414 (w), 1330 (s), 1168 (vs), 1114 (m), 972 (s), 913 (vs), 797 (s), 740 (m), 675 (w), 524 (vs), 464 (m), 413 (w), 407 (w). **Raman** (1075 nm, 1000 mW, cm^{-1}): ṽ 3027 (29), 2940 (100), 2888 (35), 2861 (29), 2826 (18), 1472 (12), 1418 (18), 1347 (12), 1258 (12), 1170 (35), 1073 (12), 975 (12), 801 (6), 741 (24), 649 (6), 531 (24), 471 (12). **Anal. Calcd** for $(C_4H_8O_4S)_n$: C, 31.57; H, 5.30; S, 21.07. Found: C, 32.44; H, 5.37; S, 20.87. **DSC** (T$_{onset}$, 5 °C min^{-1}): −4.9 °C (glass transition), 188.5 °C (dec.). **GPC**: M_w = 2925 g mol^{-1}, M_n = 2240 g mol^{-1}, M_p = 3307 g mol^{-1}, Đ = 1.31. **Density**: ρ = 1.47 g cm^{-3}.

Poly(3-mesyloxyoxetane) I10-2

^{1}H NMR (400 MHz, Acetone-d$_6$): δ 4.94–4.85 (m, 1H, CH), 3.91–3.72 (m, 4H, CH$_2$), 3.22–3.10 (m, 3H, CH$_3$). **^{13}C{^{1}H} NMR** (101 MHz, Acetone-d$_6$): 80.6, 71.1, 38.8. **IR** (ATR, cm^{-1}): ṽ 3033 (vw), 2942 (w), 2881 (vw), 1709 (w), 1472 (vw), 1415 (w), 1330 (s), 1226 (w), 1169 (vs), 1112 (m), 972 (s), 913 (vs), 796 (s), 740 (m), 675 (w), 524 (vs), 464 (m), 417 (w), 409 (w). **Raman** (1075 nm, 1000 mW, cm^{-1}): ṽ 3025 (36), 2942 (100), 2888 (36), 2861 (27), 2834 (18), 1470 (18), 1418 (18), 1362 (18), 1260 (9), 1170 (36), 741 (27), 529 (27), 495 (9), 464 (9). **Anal. Calcd** for $(C_4H_8O_4S)_n$: C, 31.57; H, 5.30; S, 21.07. Found: C, 33.13; H, 5.53; S, 20.16. **DSC** (T_{onset}, 5 °C min^{-1}): −4.1 °C (glass transition), 189.4 °C (dec.). **GPC**: M_w = 2805 g mol^{-1}, M_n = 2207 g mol^{-1}, M_p = 2721 g mol^{-1}, Đ = 1.27. **Density**: ρ = 1.47 g cm^{-3}.

The following general procedure was applied for the preparation of polymers using triisobutylaluminum–0.7H$_2$O as catalyst.

Preparation of TIBA–0.7H$_2$O solution. A Schlenk round bottom flask was closed with a silicone rubber septum and thoroughly dried under protective atmosphere (argon). A 1.1 M solution of triisobutylaluminum in toluene (20.0 mL, 22.0 mmol) was added and the solution cooled to 0 °C using an ice bath. Under vigorous stirring, water (277 µL, 15.3 mmol, 0.7 equiv.) was added dropwise and a violent reaction was observed. Stirring was then continued for 24 h. The prepared solution is storable for a couple of weeks at 0 °C (argon atmosphere).

A Schlenk round bottom flask was closed with a silicone rubber septum and thoroughly dried under protective atmosphere (argon) and dry 3-tosyloxyoxetane or 3-mesyloxyoxetane (each 4.00 g) was added under protective atmosphere (argon) prior to the addition of dry chlorobenzene. The solution was heated to 50 °C using an oil bath and the prepared TIBA solution was added over a period of two hours using a syringe pump and the reaction mixture was stirred at 250 rpm for 48 hours at the initial temperature. The polymerization was quenched by the addition of water (1 mL) and vigorously stirred for 5 minutes. Methanol (30 mL) was added to fully precipitate the polymer and to dissolve residual monomer. The supernatant was decanted and THF (50 mL) added. The polymer was refluxed in THF for 12 hours using an oil bath and the solvent decanted. This process was repeated and after decantation of THF, all volatiles were removed by rotary evaporation followed by thorough drying under high vacuum conditions (10^{-3} mbar, 24 h, 70 °C, oil bath), after which both polymers were obtained as colorless solids.

The employed amount of all compounds and the respective yields are summarized in Table S 2. The batches are labeled according to the catalyst concentration used and the duration of monomer addition as described above.

Table S 10.2. Employed amounts for the polymerization of 3-tosyloxyoxetane and 3-mesyloxyoxetane using TIBA–0.7H_2O as catalyst.

	amounts	**pTsOx C10**	**pMsOx C10**
Monomer	m [g]	4.00	4.00
	n [mmol]	17.5	26.3
	solvent [mL]	7.16	10.8
	c [mol/L]	2.00	2.00
TIBA–0.7H_2O	V [mL]	1.59	2.39
	n [mmol]	1.75	2.63
	C (mol%)	10	10
Yield [g]		3.14 (79%)	3.24 (81%)

Poly(3-tosyloxyoxetane) C10-2

^{1}H NMR (400 MHz, Acetone-d_6): δ 7.80 (d, 2H, CH$_{arom}$), 7.46 (d, 2H, CH$_{arom}$), 4.53–4.46 (m, 1H, CH), 3.55–3.36 (m, 4H, CH_2), 2.47–2.39 (s, 3H, CH_3). **^{13}C{^{1}H} NMR** (101 MHz, Acetone-d_6): 145.9, 135.1, 130.8, 128.7, 80.3, 70.6, 21.7. **IR** (ATR, cm^{-1}): $\tilde{\nu}$ 2923 (w), 2878 (w), 1598 (w), 1454 (w), 1351 (s), 1189 (m), 1173 (vs), 1121 (m), 1097 (s), 1036 (m), 1019 (m), 912 (s), 813 (s), 770 (s), 705 (m), 663 (s), 635 (m), 573 (s), 550 (vs), 495 (s), 462 (m), 442 (m), 421 (m), 421 (m), 404 (m). **Raman** (1075 nm, 1000 mW, cm^{-1}): $\tilde{\nu}$ 3067 (69), 2926 (100), 2880 (62), 2786 (23), 1715 (23), 1600 (85), 1472 (31), 1455 (31), 1378 (38), 1308 (23), 1220 (23), 1175 (100), 1148 (23), 1100 (46), 809 (46), 782 (54), 635 (38), 552 (23), 471 (23), 404 (31). **Anal. Calcd** for $(C_{10}H_{12}O_4S)_n$: C, 52.62; H, 5.30; S, 14.05. Found: C, 50.04; H, 5.24; S, 13.64. **DSC** (T_{onset}, 5 °C min^{-1}): 37.9 °C (glass transition), 205.9 °C (dec.). **GPC**: M_w = 57813 g mol^{-1}, M_n = 21224 g mol^{-1}, M_p = 61371 g mol^{-1}, Đ =2.72. **Density**: ρ = 1.37 g cm^{-3}.

Poly(3-mesyloxyoxetane) C10-2

^{1}H NMR (400 MHz, DMSO-d_6): δ 4.87–4.75 (m, 1H, CH), 3.82–3.53 (m, 4H, CH_2), 3.25–3.12 (m, 3H, CH_3). **^{13}C{^{1}H} NMR** (101 MHz, DMSO-d_6): 79.6, 69.8, 38.0. **IR** (ATR, cm^{-1}): $\tilde{\nu}$ 3034 (w), 2919 (w), 2850 (w), 1472 (w), 1415 (w), 1330 (s), 1169 (vs), 1116 (m), 972 (s), 912 (vs), 795 (s), 732 (m), 667 (m), 647 (m), 611 (m), 594 (m), 523 (vs), 497 (s), 468 (s), 460 (s), 441 (m), 419 (m), 409 (m), 409 (m), 404 (m). **Raman** (1075 nm, 1000 mW, cm^{-1}): $\tilde{\nu}$ 3225 (7), 3025 (27), 2942 (100), 2909 (27), 2882 (20), 1472 (13), 1418 (20), 1360 (7), 1349 (7), 1249 (13), 1171 (40), 973 (13), 923 (13), 743 (33), 556 (13), 529 (27), 466 (13). **Anal. Calcd** for $(C_4H_8O_4S)_n$: C, 31.57; H, 5.30; S, 21.07. Found: C, 30.21; H, 5.35; S, 19.88. **DSC** (T_{onset}, 5 °C min^{-1}): 19.4 °C (glass transition), 196.6 °C (dec.). **GPC***: M_w > 6407 g mol^{-1}, M_n > 814 g mol^{-1}, M_p > 2723 g mol^{-1}. **Density**: ρ = 1.56 g cm^{-3}.

**The GPC data relates to the soluble fraction after sonication. GPC data for the overall polymer could not be assessed due to its insolubility.*

Poly(epichlorohydrin) (PECH)

A Schlenk round bottom flask was closed with a silicone rubber septum and thoroughly dried under protective atmosphere (argon). Subsequently, a solution of epichlorohydrin (3.00 g, 32.4 mmol) in dry dichloromethane (13.3 mL) was added and a 1.1 M triisobutylaluminum–0.7H_2O solution (2.95 mL, 3.24 mmol, 0.10 equiv.) was fed over a period of one hour by means of a syringe pump. The reaction mixture was stirred at 250 rpm for 24 hours at room temperature and the reaction was then quenched by the addition of water (7 mL). Methanol (12 mL) was added and the resulting emulsion vigorously stirred for 5 minutes prior to collecting the polymer by centrifugation (20 min, 6000 rpm). The supernatant was decanted and the crude polymer washed with 1 M hydrochloric acid (30 mL) and water (30 mL). The polymer was transferred to a round bottom flask and dried under high vacuum conditions (10^{-3} mbar, 24 h, 70 °C, oil bath) to give 2.12 g (71%) of poly(epichlorohydrin) as colorless solid.

^{1}H NMR (400 MHz, Acetone-d_6): δ 4.01–3.56 (m, 5H, CH and CH_2).**^{13}C{^{1}H} NMR** (101 MHz, Acetone-d_6): 80.0, 70.3, 44.9. **IR** (ATR, cm^{-1}): $\tilde{\nu}$ 2956 (w), 2933 (w), 2883 (w), 2874 (w), 1727 (w), 1629 (w), 1472 (w), 1436 (m), 1345 (m), 1300 (m), 1286 (m), 1257 (m), 1235 (m), 1176 (s), 1107 (vs), 1041 (s), 977 (m), 904 (m), 836 (m), 745 (s), 716 (s), 611 (s), 567 (m), 567 (m), 527 (s), 441 (m). **Raman** (1064 nm, 1074 mW, cm^{-1}): $\tilde{\nu}$ 3408 (11), 3260 (11), 3112 (11), 3075 (11), 3013 (33), 2967 (100), 2882 (44), 2720 (11), 2496 (11), 2145 (11), 1821 (11), 1532 (11), 1470 (22), 1436 (22), 1359 (22), 1112 (11), 751 (22), 711 (44), 564 (11), 525 (11). **Anal. Calcd** for $(C_3H_5ClO)_n$: C, 38.95; H, 5.45; Cl, 38.32. Found: C, 38.86; H, 5.35; Cl, 38.15. **DSC** (T_{onset}, 5 °C min^{-1}): −31.0 °C (glass transition), 306.6 °C (dec.). **GPC***: M_w = 9090 g mol^{-1}, M_n = 1258 g mol^{-1}, M_p = 2910 g mol^{-1}, Đ = 7.22.

**The GPC data relates to the soluble fraction (THF). GPC data for the overall polymer could not be assessed due to its low solubility.*

10.4.1.3 Azidation of Non-Energetic Polymers

The azidation of all non-energetic prepolymers was performed according to the following general procedures.

A. Azidation of polymers obtained using the boron trifluoride etherate/butane-1,4-diol initiating system.

Poly(3-tosyloxyoxetane) or poly(3-mesyloxyoxetane) were dissolved in a small amount of dimethylformamide and sodium azide (2 equiv.) was added. The resulting suspension was heated to 100 °C for 24 h using an oil bath and subsequently poured onto water (50 mL) to dissolve all inorganic salts. The obtained emulsions were subject to centrifugation (6000 rpm, 20 minutes) to collect crude poly(3-azidooxetane) as yellow to orange oil. The supernatant was decanted and the crude polymer dissolved in a small amount of acetone. The polymer was precipitated a second time by the addition of water and collected by centrifugation (6000 rpm, 20 minutes). The supernatant was decanted and the respective polymer transferred into a round bottom flask using acetone. All volatiles were afterward removed by rotary evaporation and drying under high vacuum conditions (10^{-2} mbar, 24 h, 70 °C, oil bath) to give poly(3-azidooxetane) as yellow to orange, honey-like liquid in almost quantitative yield.

The employed amounts of polymer, sodium azide, solvent and the respective yields are summarized in Table S 3.

Table S 10.3. Employed amounts for the azidation of low-molecular-weight poly(3-tosyloxyoxetane) and poly(3-mesyloxyoxetane).

	pTsOx I5-2	**pTsOx I10-2**	**pTsOx I5-3**	**pMsOx I5-2**	**pMsOx I10-2**
Polymer [g]	1.00	1.00	2.00	1.00	1.00
Sodium azide [g, mmol, equiv.]	0.57, 8.76, 2	0.57, 8.76, 2	1.14, 17.5, 2	0.85, 13.1, 2	0.85, 13.1, 2
DMF [mL]	10	10	20	10	10
Yield [mg, %]	413 mg (95%)	418 mg (96%)	857 mg (99%)	634 mg (97%)	639 mg (98%)

Poly(3-azidooxetane)

Prepared using pTsOx I5-3:

^{1}H NMR (400 MHz, Acetone-d$_6$): δ 3.89–3.45 (m, 5H, CH$_2$ and CH). **^{13}C{^{1}H} NMR** (101 MHz, Acetone-d$_6$): δ 71.5, 61.4. **^{14}N NMR** (29 MHz, Acetone-d$_6$): δ −135.4 (N$_\beta$), −171.4 (N$_\gamma$). **IR** (ATR, cm^{-1}): $\tilde{\nu}$ 2916 (w), 2871 (w), 2086 (vs), 1727 (vw), 1477 (w), 1459 (w), 1320 (m), 1266 (s), 1186 (w), 1112 (s), 1054 (m), 995 (m), 972 (w), 919 (w), 844 (w), 816 (w), 696 (m), 659 (m), 627 (m), 556 (m), 460 (m). **Raman** (1075 nm, 1000 mW, cm^{-1}): $\tilde{\nu}$ 3297 (6), 3069 (75), 2926 (88), 2884 (31), 1600 (75), 1461 (13), 1380 (25), 1175 (100), 1100 (31), 928 (6), 815 (31), 786 (56), 635 (25). **Anal. Calcd** for $(C_3H_5N_3O)_n$: C, 36.36; H, 5.09; N, 42.41. Found: C, 37.62; H, 5.24; N, 39.24. **DSC** (T_{onset}, 5 °C min^{-1}): −56.4 °C (glass transition), 211.1 °C (dec.). **BAM drop hammer**: > 10 J. **Friction test**: > 360 N.

B. Azidation of polymers obtained using triisobutylaluminum–0.7H$_2$O.

Poly(3-tosyloxyoxetane) was dissolved in dimethylformamide while poly(3-mesyloxyoxetane) and poly(epichlorohydrin) gave a suspension upon addition of dimethylformamide. Sodium azide (2 equiv.) was added and the obtained suspensions heated to 100 °C for 36 h using an oil bath. Afterward, the reaction mixture was poured onto water (50 mL) to precipitate the azidated polymers and to dissolve inorganic salts. The obtained emulsions were subject to centrifugation (6000 rpm, 20 minutes) to collect crude poly(3-azidooxetane) which was obtained as yellow to orange honey-like liquid in case of poly(3-tosyloxyoxetane) and as yellowish solid in case of poly(3-mesyloxyoxetane). The supernatant was decanted in both cases. For further purification, poly(3-azidooxetane) obtained from poly(3-tosyloxyoxetane) was dissolved in the minimum amount of acetone, precipitated with an excess of methanol and collected by centrifugation (6000 rpm, 20 minutes) and decanting of the supernatant as described before. Poly(3-azidooxetane) obtained from poly(3-mesyloxyoxetane) was dissolved in the minimum amount of hot dimethylformamide and precipitated using an excess of methanol. Again, centrifugation (6000 rpm, 20 minutes) was performed and the polymer collected by decanting of the supernatant. Both polymers were then transferred to a round bottom flask to remove all volatiles by rotary evaporation. Afterward, additional drying was performed under high vacuum conditions (10^{-2} mbar, 24 h, 70 °C, oil bath) to afford high-molecular-weight poly(3-azidooxetane) in almost quantitative and poly(glycidyl azide) in high yield.

The employed amount of polymer, sodium azide, solvent and the respective yields are summarized in Table S4.

Table 10.4. Employed amounts for the azidation of high-molecular-weight poly(3-tosyloxyoxetane), poly(3-mesyloxyoxetane) and poly(epichlorohydrin).

	pTsOx C10	**pMsOx C10**	**PECH**
Polymer [g]	2.00	2.00	2.00
Sodium azide [g, mmol, equiv.]	1.14, 17.5, 2	1.71, 26.3, 2	2.81, 42.3, 2
DMF [mL]	15	25	15
Yield [mg, %]	851, 98	1251, 96	1.85, 86

Poly(3-azidooxetane)

Prepared using pMsOx C10:

^{1}H NMR (400 MHz, Acetone-d$_6$): δ 4.09–3.19 (m, 5H, CH_2 and CH). **^{13}C{^{1}H} NMR** (101 MHz, Acetone-d$_6$): δ 71.5, 61.4. **^{14}N NMR** (29 MHz, Acetone-d$_6$): δ −134.6 (N_β), −175.5 (N_γ). **IR** (ATR, cm^{-1}): $\tilde{\nu}$ 2911 (w), 2871 (w), 2086 (vs), 1478 (w), 1459 (w), 1320 (m), 1267 (s), 1111 (s), 995 (m), 966 (m), 918 (w), 837 (w), 725 (m), 657 (m), 629 (m), 555 (s), 487 (m). **Raman** (1075 nm, 1000 mW, cm^{-1}): $\tilde{\nu}$ 3262 (25), 3092 (0), 3083 (0), 2923 (100), 2878 (100), 2099 (25), 1933 (25), 1910 (25), 1850 (25), 1617 (0), 1534 (0), 1472 (25), 1268 (25), 1106 (0), 846 (25), 616 (25). **Anal. Calcd** for $(C_3H_5N_3O)_n$: C, 36.36; H, 5.09; N, 42.41. Found: C, 36.93; H, 4.89; N, 41.02. **DSC** (T_{onset}, 5 °C min^{-1}): −47.0 °C (glass transition), 214.8 °C (dec.). **BAM drop hammer**: > 10 J. **Friction test**: > 360 N.

Note: The same data applies to poly(3-azidooxetane) prepared from pTsOx C10. GPC was not performed due to insolubility of the obtained polymers.

Poly(glycidyl azide)

^{1}H NMR (400 MHz, $CDCl_3$): δ 3.87–3.38 (m, 5H, CH_2 and CH). **$^{13}C\{^1H\}$ NMR** (101 MHz, $CDCl_3$): δ 79.7, 70.2, 52.6. **^{14}N NMR** (29 MHz, $CDCl_3$): δ −133.4 (N_β), −174.9 (N_γ). **IR** (ATR, cm^{-1}): $\tilde{\nu}$ 2924 (w), 2873 (w), 2090 (vs), 1442 (w), 1346 (w), 1277 (s), 1107 (s), 1100 (s), 1074 (s), 996 (w), 935 (m), 901 (m), 863 (w), 668 (m), 624 (m), 555 (m), 492 (m), 448 (m), 415 (m). **Raman** (1064 nm, 1074 mW, cm^{-1}): $\tilde{\nu}$ 3852 (20), 3204 (20), 2994 (40), 2932 (100), 2772 (20), 2737 (20), 2697 (20), 2099 (50), 1677 (20), 1449 (40), 1411 (20), 1387 (20), 1279 (20), 1241 (30), 1129 (20), 1025 (20), 849 (20), 813 (20), 691 (20), 647 (20), 448 (20). **Anal. Calcd** for $(C_3H_5N_3O)_n$: C, 36.36; H, 5.09; N, 42.41. Found: C, 36.85; H, 4.67; N, 42.35. **DSC** (T_{onset}, 5 °C min^{-1}): −47.9 °C (glass transition), 218.5 °C (dec.). **BAM drop hammer**: 8 J. **Friction test**: > 360 N.

10.4.1.4 Curing of Poly(3-azidooxetane)

Poly(3-azidooxetane) prepared from pTsOx I5-3 was used.

Poly(3-azidooxetane) (200 mg) was added to a 25 mL Schlenk round bottom flask and thoroughly dried under high vacuum conditions (3 d, 70 °C 10^{-3} mbar) using an oil bath. Subsequently, the flask was vented with protective atmosphere (argon) and the temperature set to 50 °C prior to the addition of 95 wt%. 2,4-toluene diisocyanate (7.2 µL, 8.8 mg, 48 µmol, 1.1 equiv.). After the mixture became homogeneous, dibutyltin dilaurate (2 drops with a 100 µL Hamilton syringe) was added as catalyst. A slight color change of the polymer from orange to bright yellow was observed. The mixture was further stirred (250 rpm) until the stirring stopped due to curing (~12 h). After curing at 50 °C for a total of 48 hours, the rubbery polymer was removed using tweezers.

10.4.2 NMR Spectra

Nitroglycerin (3)

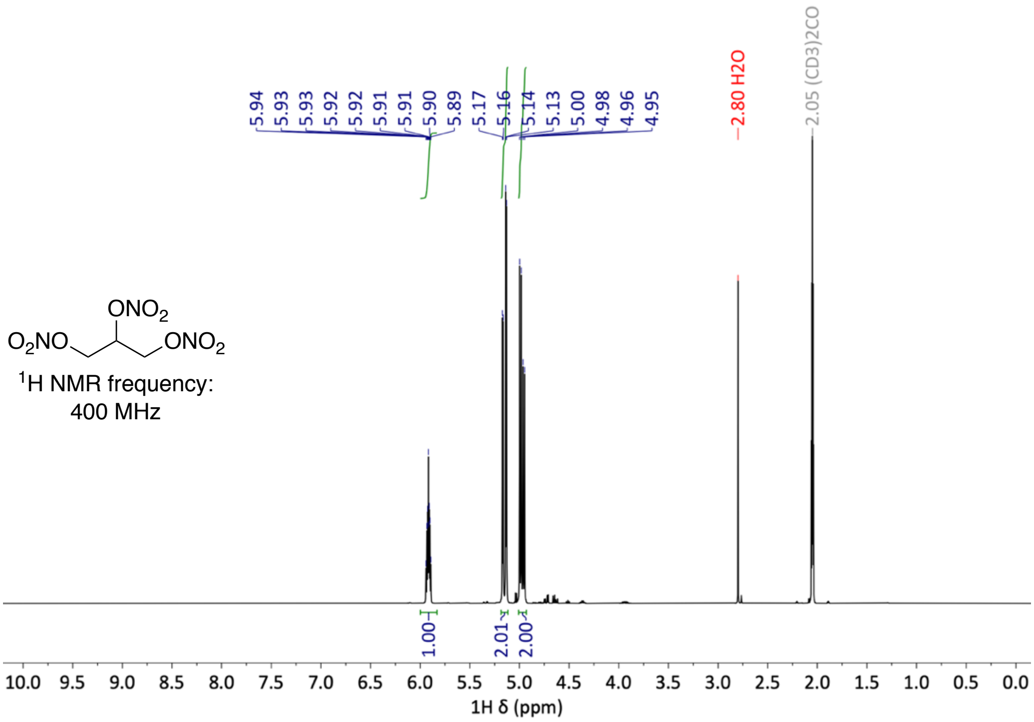

Figure S 10.1. Proton spectrum (^{1}H) of nitroglycerin (**3**).

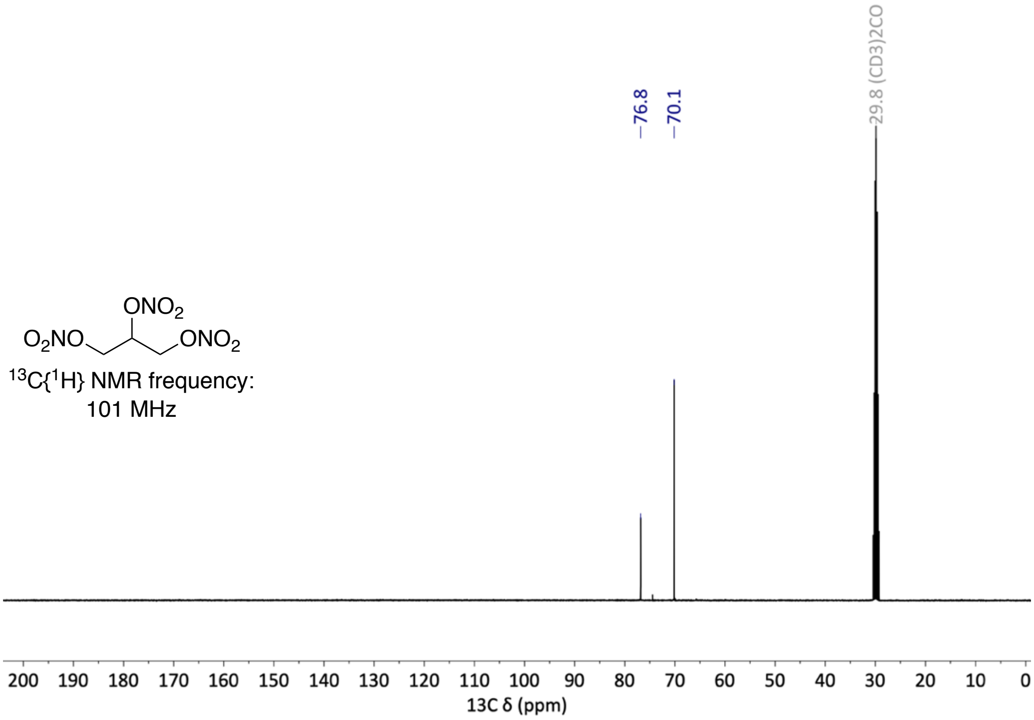

Figure S 10.2. Carbon spectrum (^{13}C) of nitroglycerin (**3**).

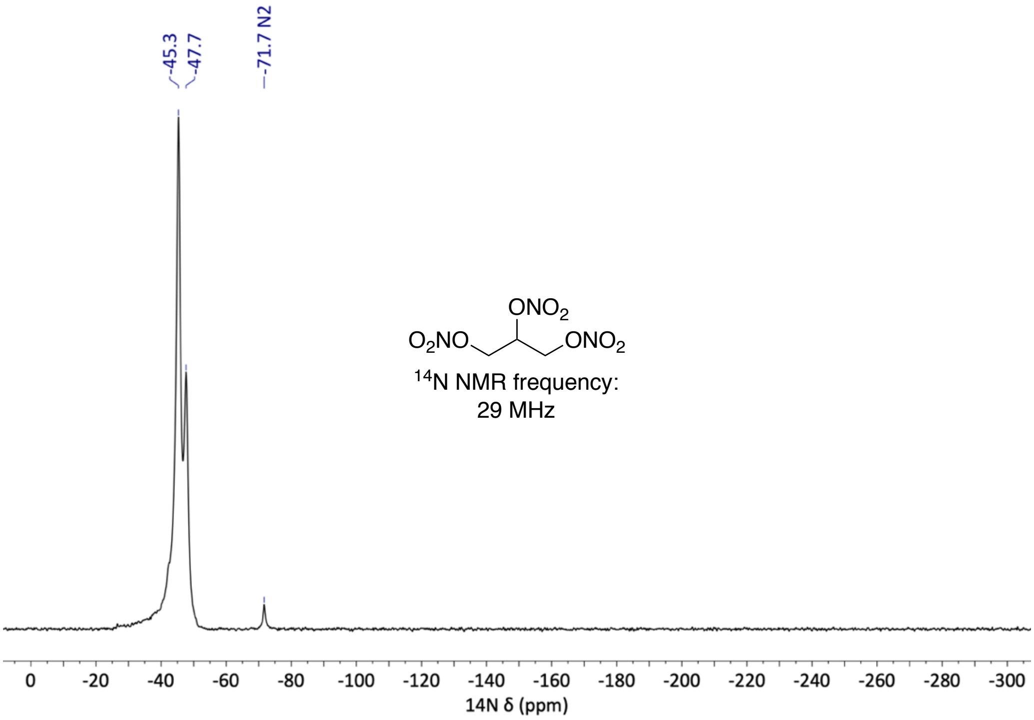

Figure S 10.3. Nitrogen spectrum (^{14}N) of nitroglycerin (**3**).

Ethane-1,2-diyl bis(2-chloroacetate) (4)

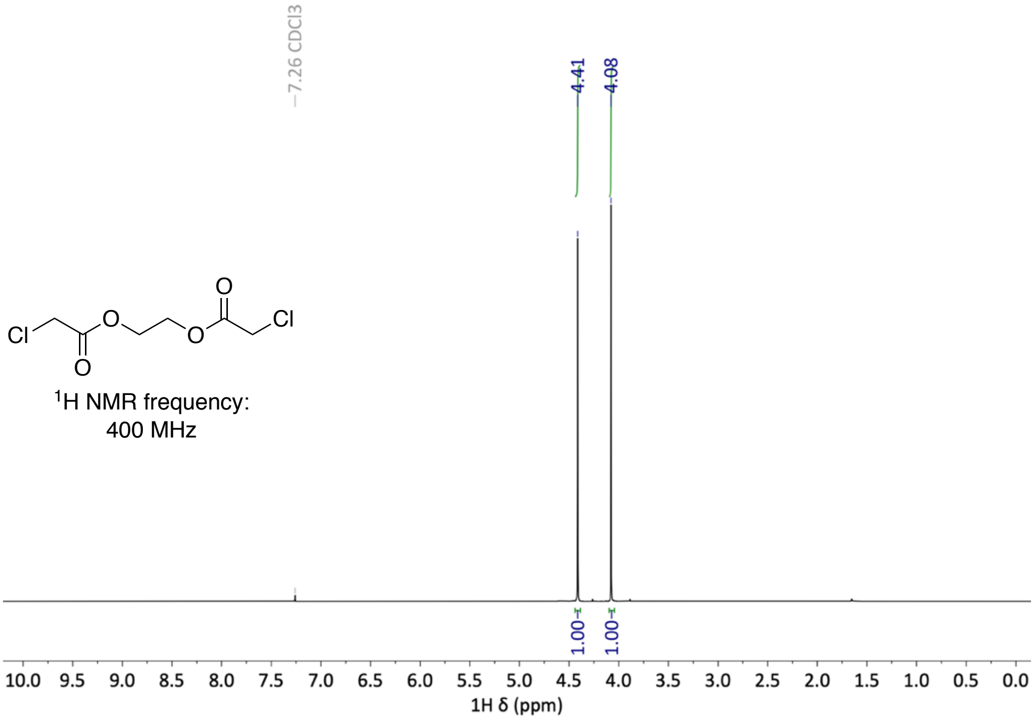

Figure S 10.4. Proton spectrum (^{1}H) of ethane-1,2-diyl bis(2-chloroacetate) (**4**).

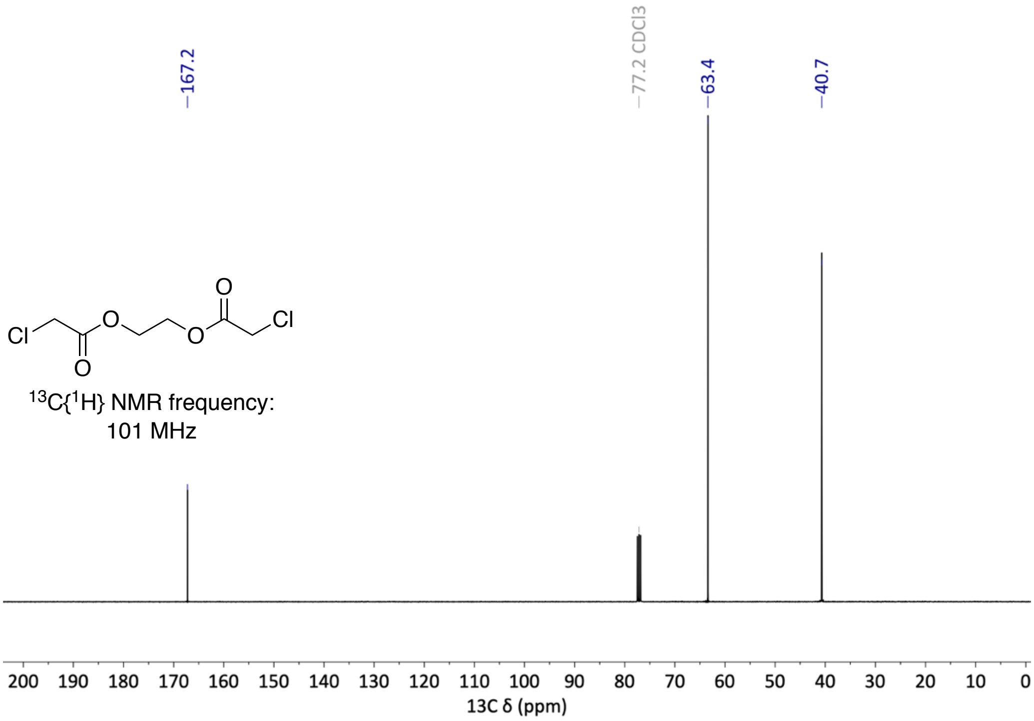

Figure S 10.5. Carbon spectrum (^{13}C) of ethane-1,2-diyl bis(2-chloroacetate) (**4**).

Ethane-1,2-diyl bis(2-azidoacetate) (5)

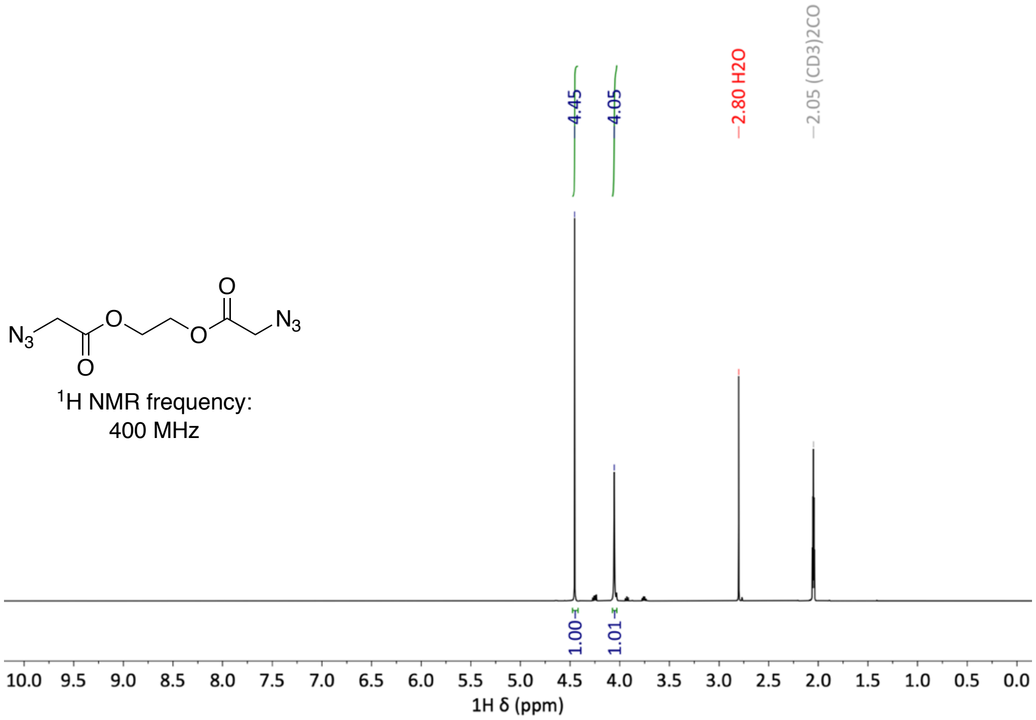

Figure S 10.6. Proton spectrum (^{1}H) of ethane-1,2-diyl bis(2-azidoacetate) (**5**).

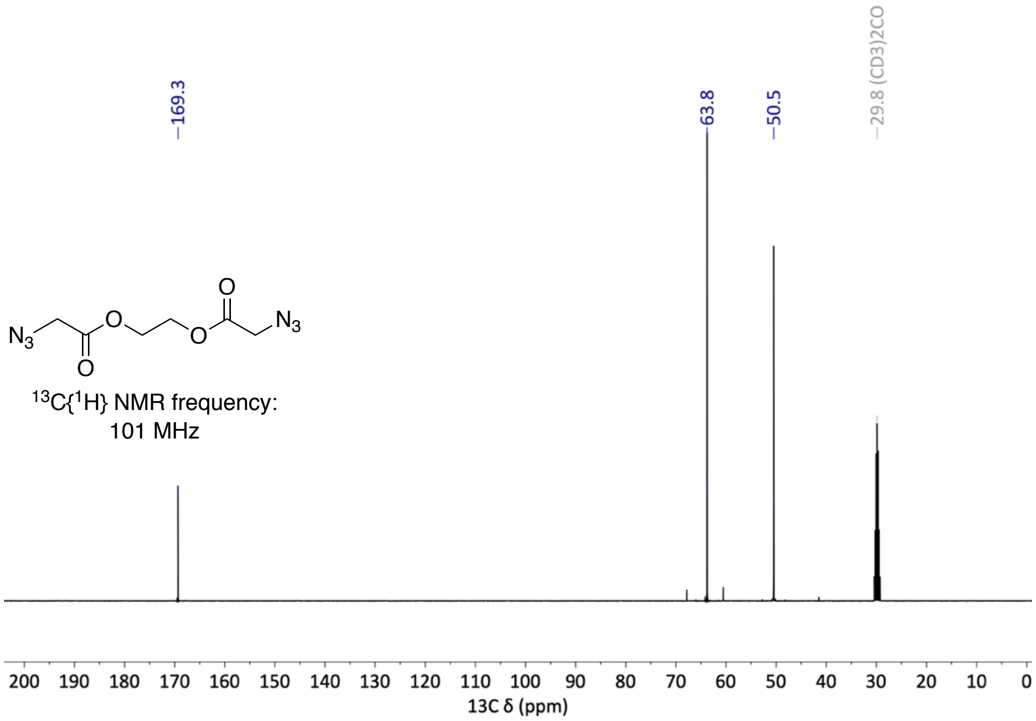

Figure S 10.7. Carbon spectrum (^{13}C) of ethane-1,2-diyl bis(2-azidoacetate) (**5**).

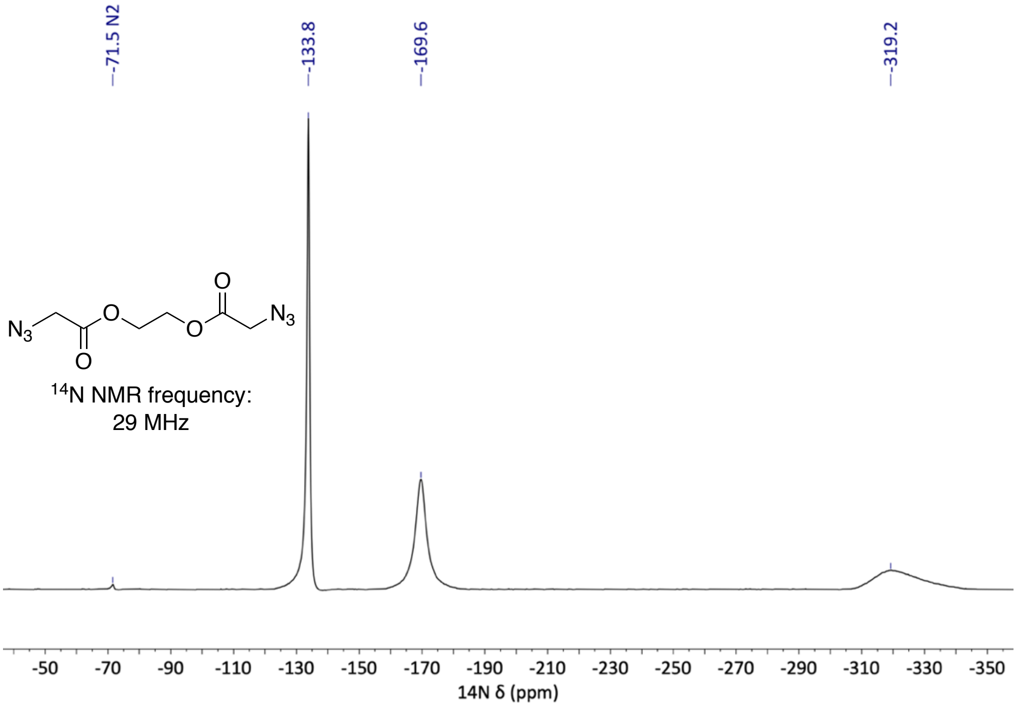

Figure S 10.8. Nitrogen spectrum (^{14}N) of ethane-1,2-diyl bis(2-azidoacetate) (**5**).

Poly(3-tosyloxyoxetane) (pTsOx)

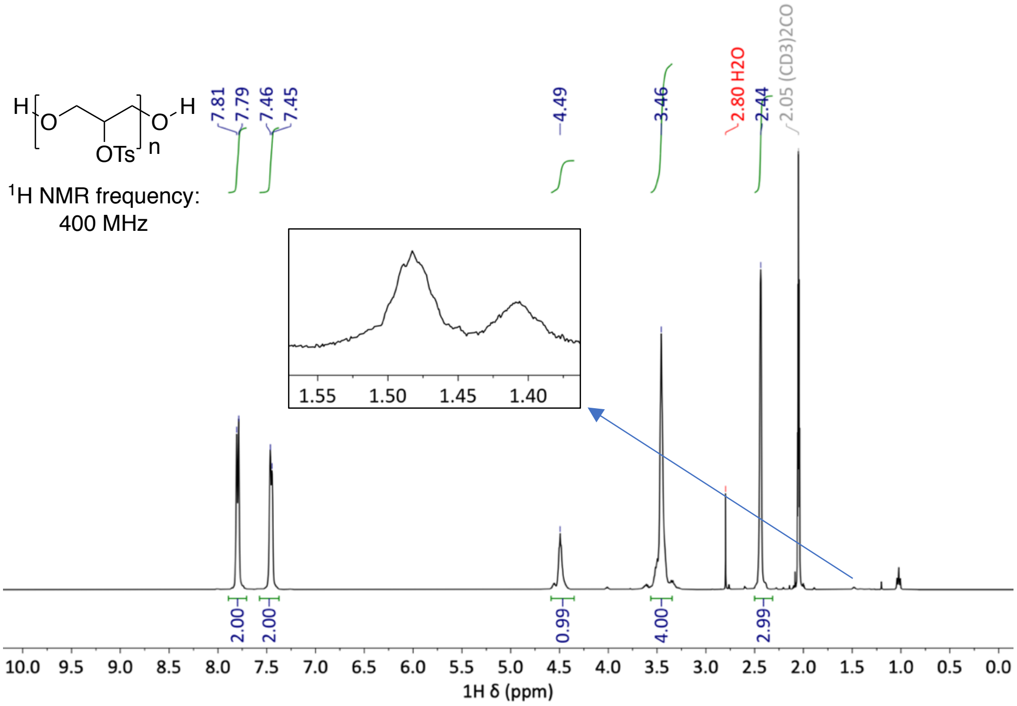

Figure S 10.9. Proton spectrum (^{1}H) of poly(3-tosyloxyoxetane) prepared using 5 mol% initiator (1,4-BDO).

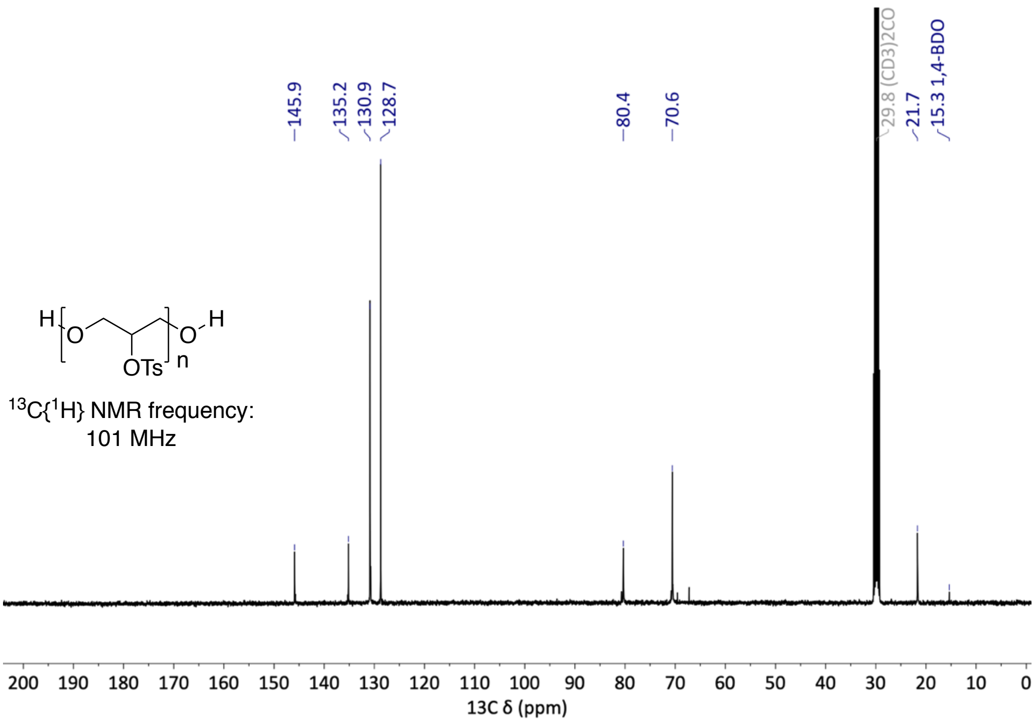

Figure S 10.10. Carbon spectrum (^{13}C) of poly(3-tosyloxyoxetane) prepared using 5 mol% initiator (1,4-BDO).

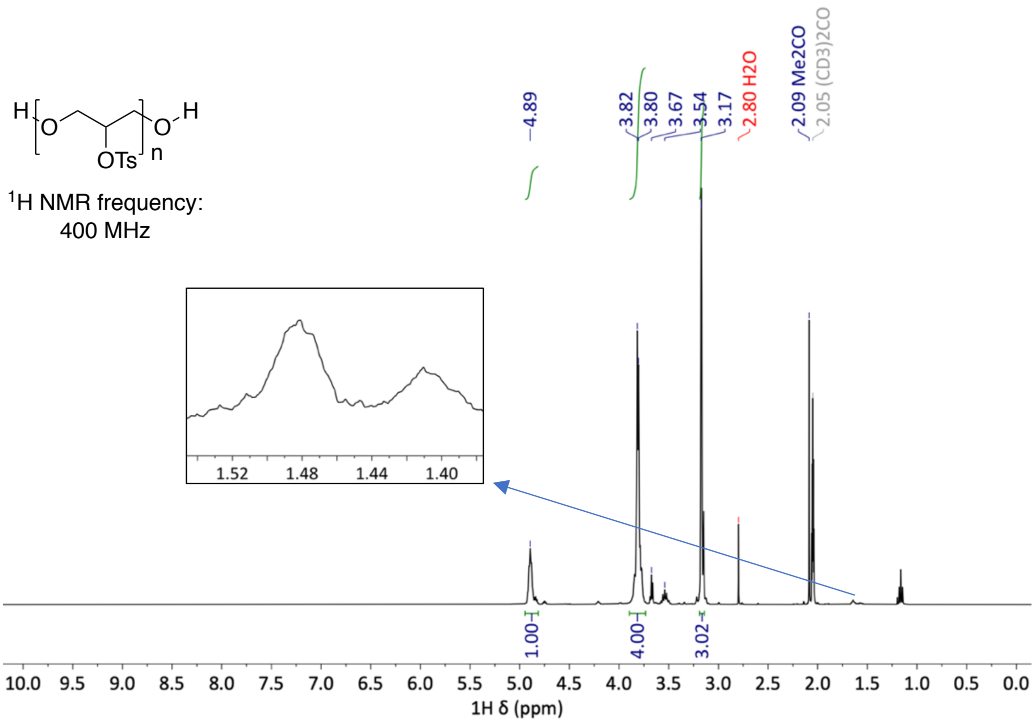

Figure S 10.11. Proton spectrum (^{1}H) of poly(3-tosyloxyoxetane) prepared using 10 mol% initiator (1,4-BDO).

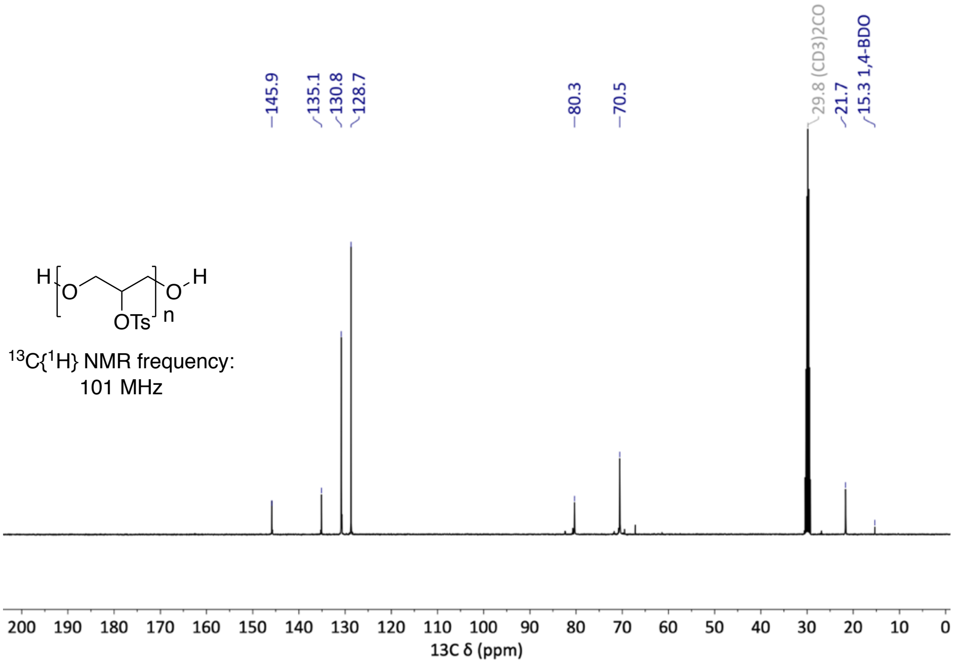

Figure S 10.12. Carbon spectrum (^{13}C) of poly(3-tosyloxyoxetane) prepared using 10 mol% initiator (1,4-BDO).

Poly(3-mesyloxyoxetane) (pMsOx)

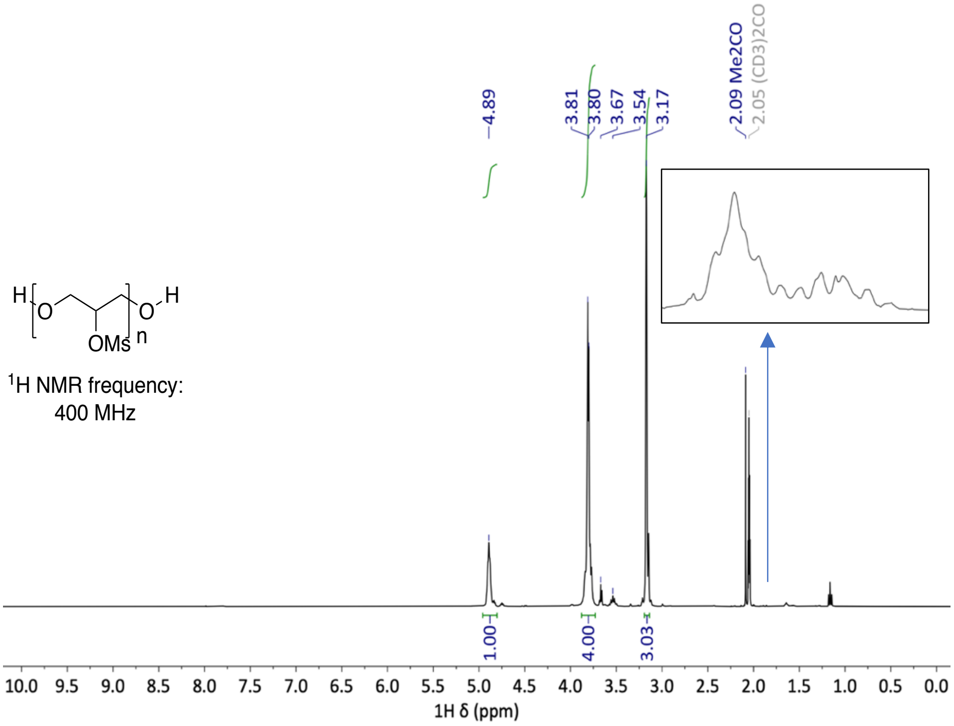

Figure S 10.13. Proton spectrum (^{1}H) of poly(3-mesyloxyoxetane) prepared using 5 mol% initiator (1,4-BDO).

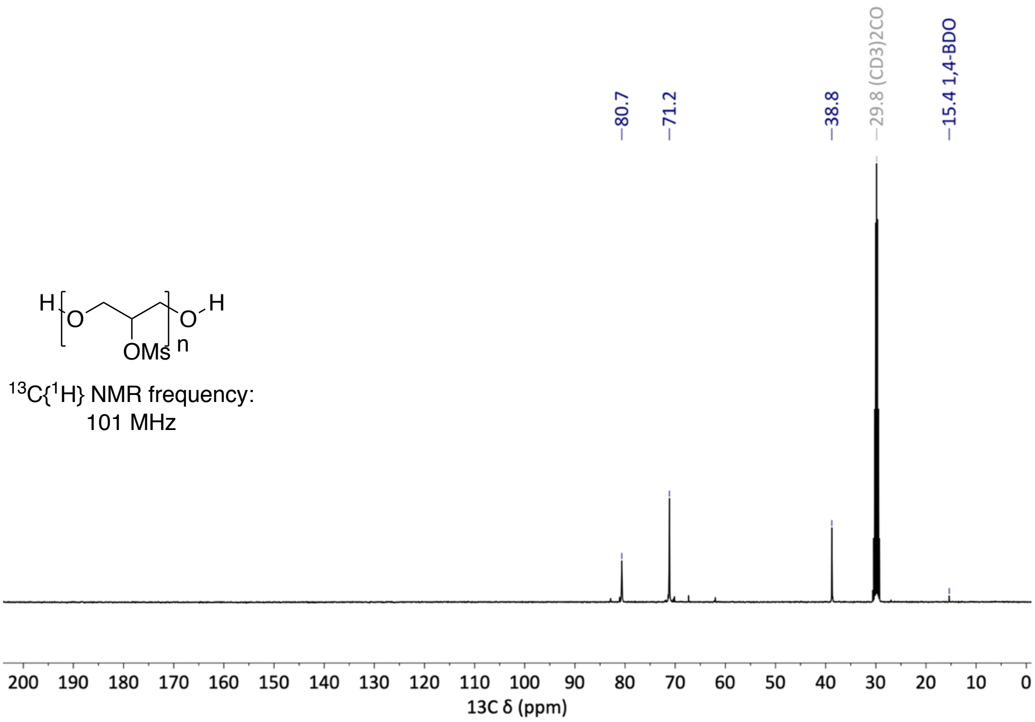

Figure S 10.14. Carbon spectrum (^{13}C) of poly(3-mesyloxyoxetane) prepared using 5 mol% initiator (1,4-BDO).

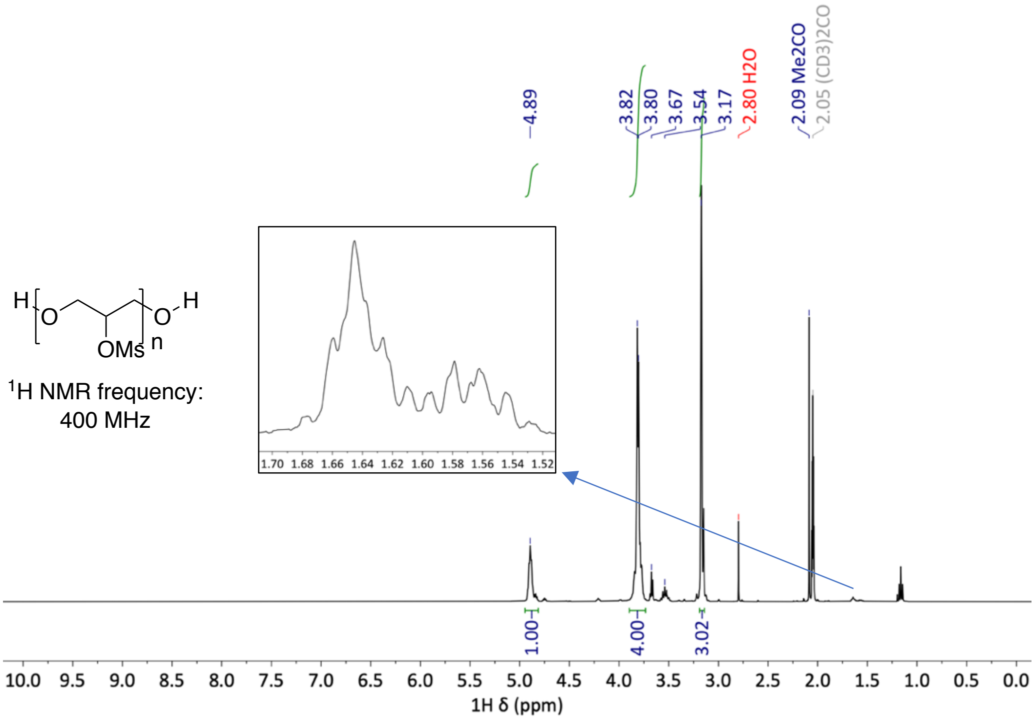

Figure S 10.15. Proton spectrum (^{1}H) of poly(3-mesyloxyoxetane) prepared using 10 mol% initiator (1,4-BDO).

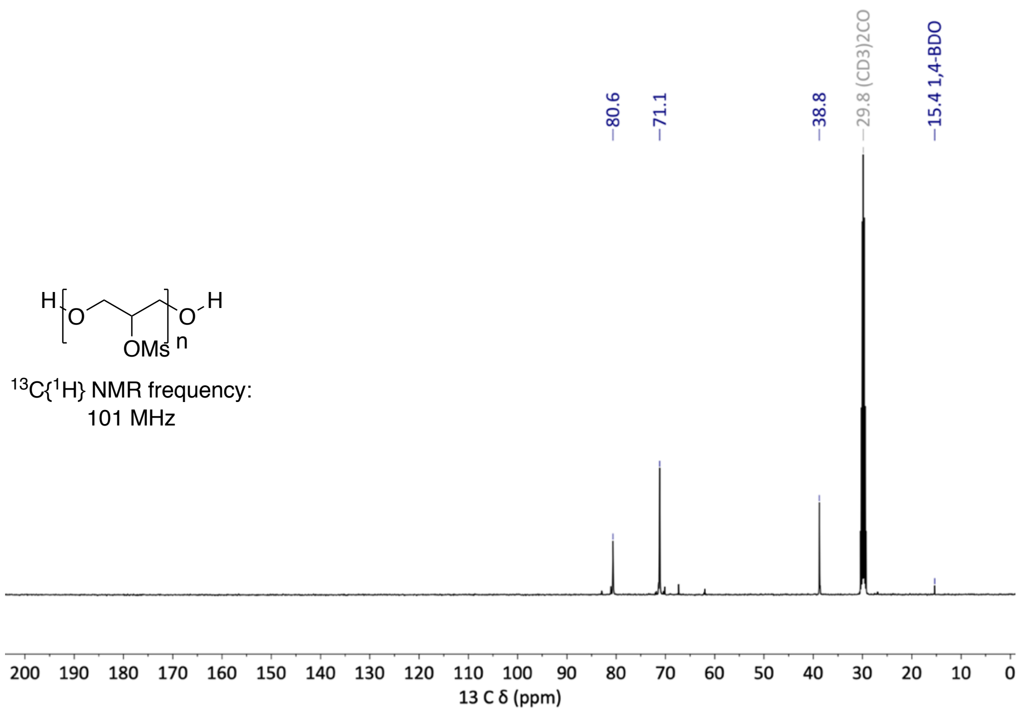

Figure S 10.16. Carbon spectrum (^{13}C) of poly(3-mesyloxyoxetane) prepared using 10 mol% initiator (1,4-BDO).

Poly(3-tosyloxyoxetane) and poly(3-mesyloxyoxetane) (TIBA–0.7H_2O)

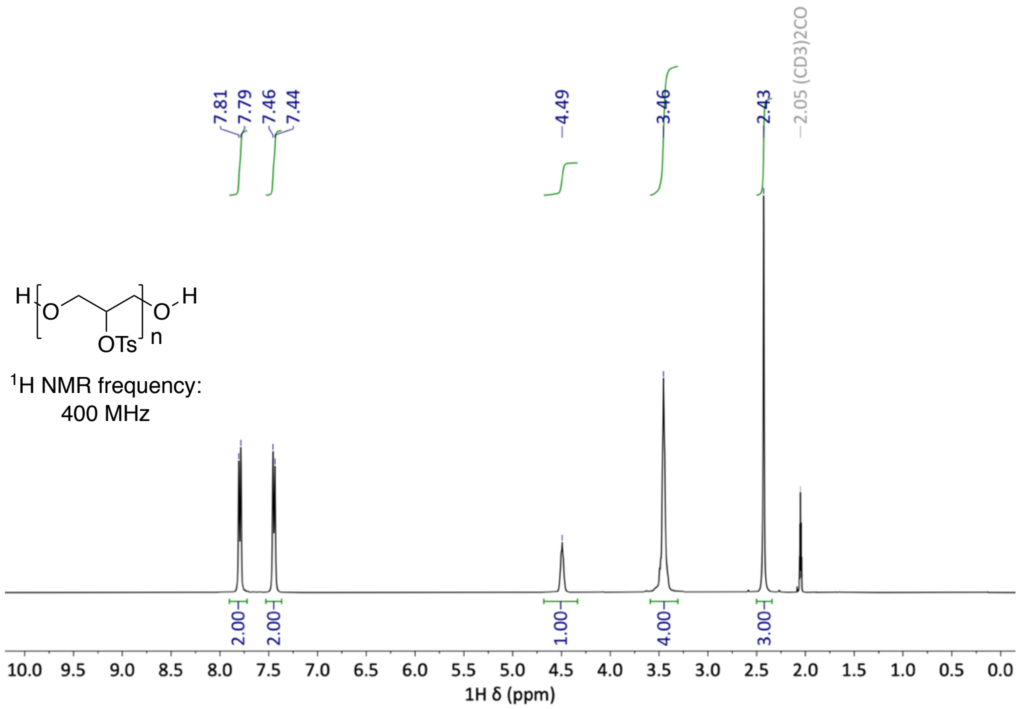

Figure S 10.17. Proton spectrum (^{1}H) of poly(3-tosyloxyoxetane) prepared using TIBA–0.7H_2O.

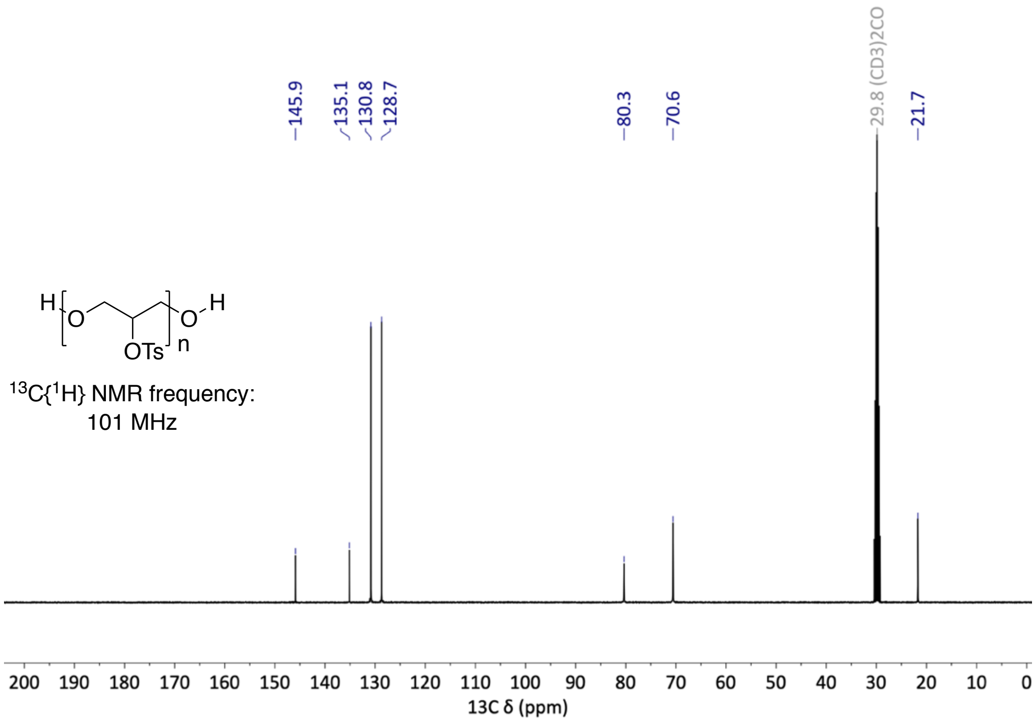

Figure S 10.18. Carbon spectrum (^{13}C) of poly(3-tosyloxyoxetane) prepared using TIBA–0.7H_2O.

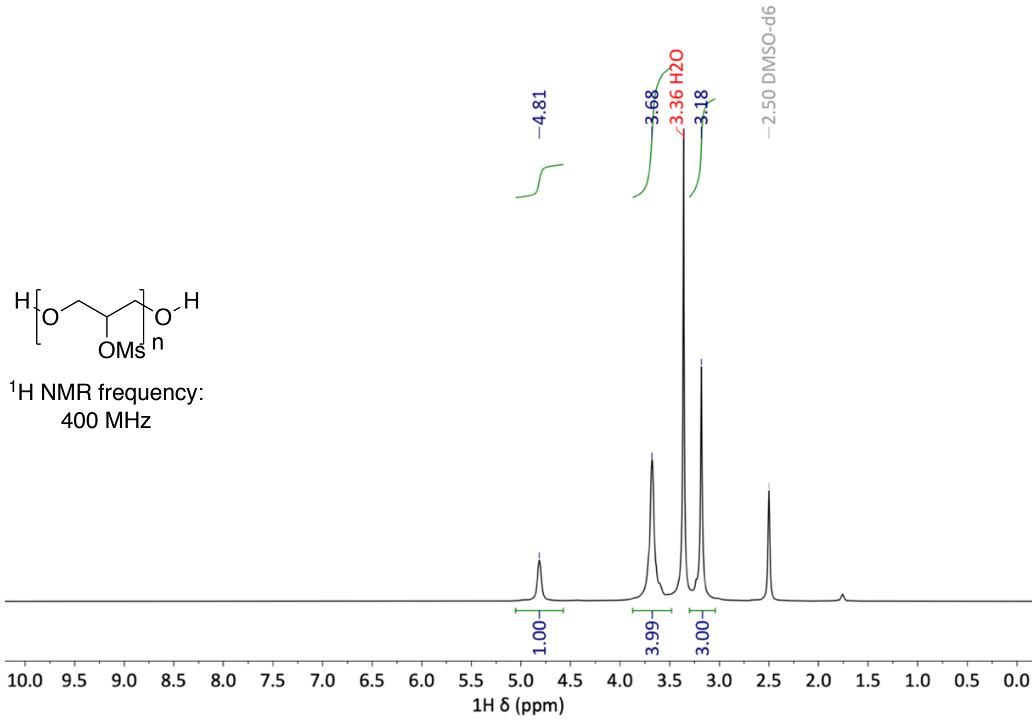

Figure S 10.19. Proton spectrum (^{1}H) of poly(3-mesyloxyoxetane) prepared using TIBA–0.7H_2O.

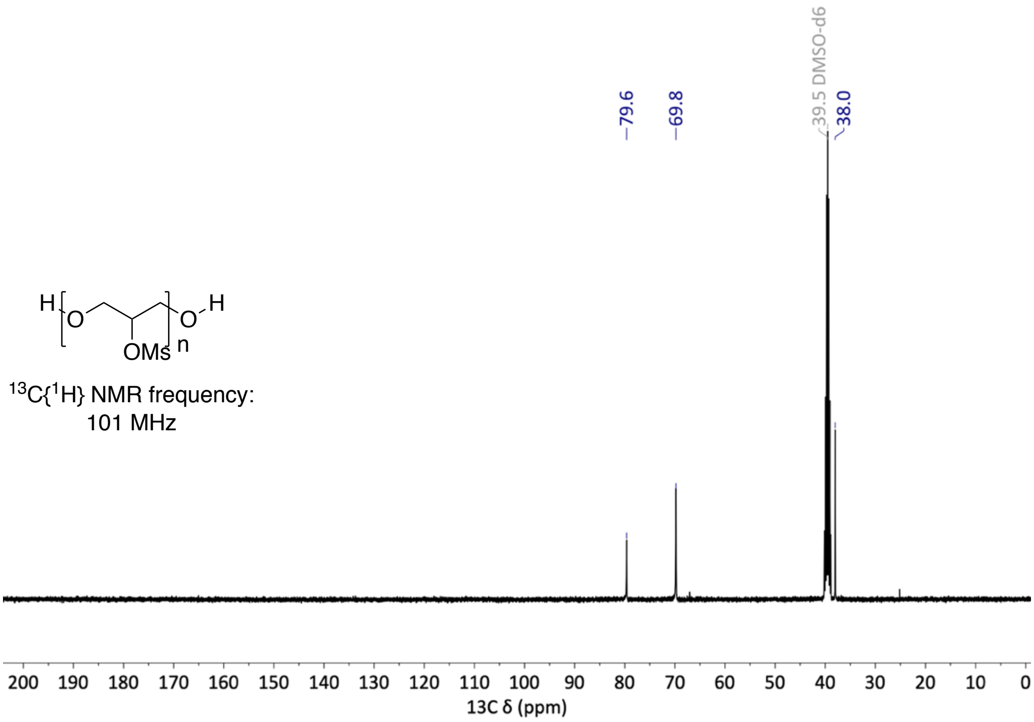

Figure S 10.20. Carbon spectrum (^{13}C) of poly(3-mesyloxyoxetane) prepared using TIBA–0.7H_2O.

Poly(epichlorohydrin) (TIBA–0.7H2O)

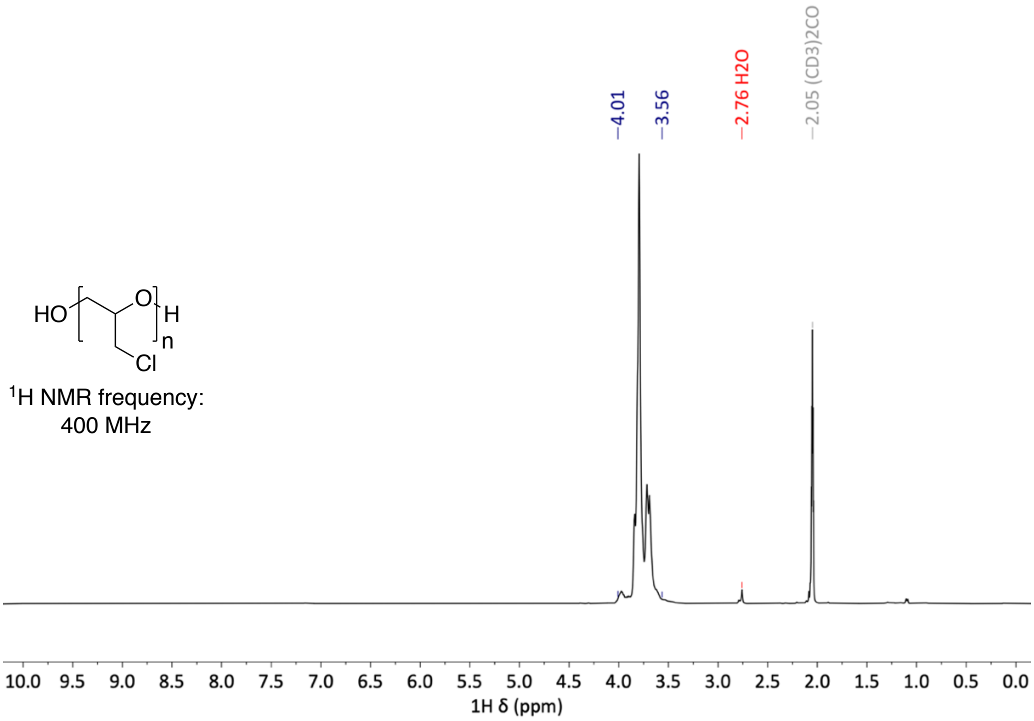

Figure S 10.21. Proton spectrum (^{1}H) of poly(epichlorohydrin) prepared using TIBA–0.7H_2O.

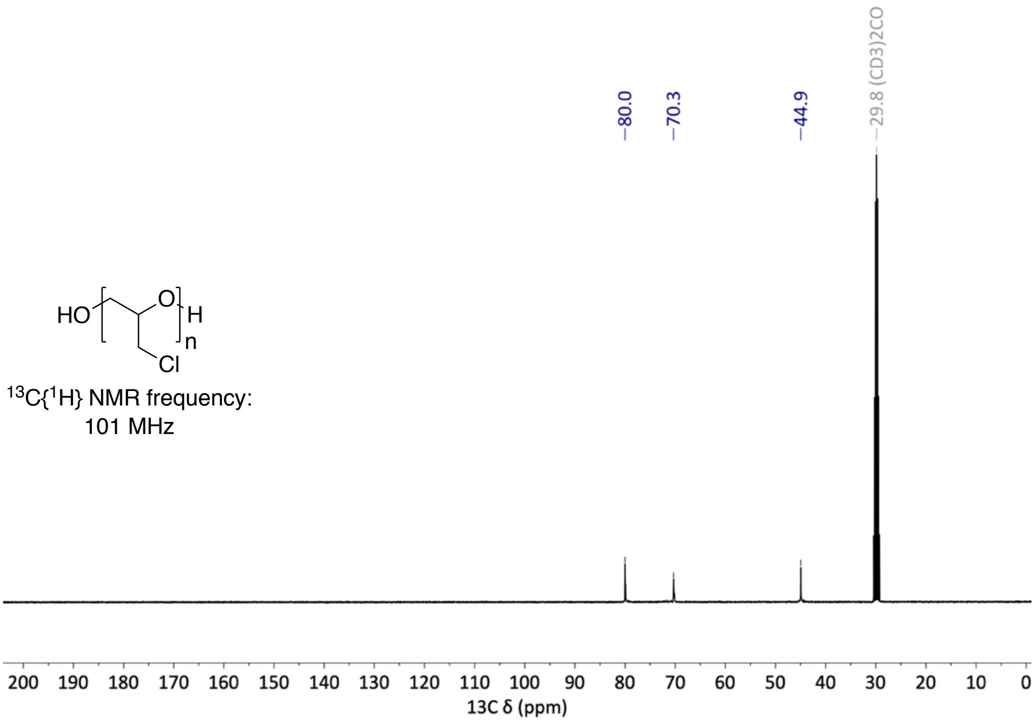

Figure S 10.22. Carbon spectrum (^{13}C) of poly(epichlorohydrin) prepared using TIBA−0.7H_2O.

Poly(3-azidooxetane)

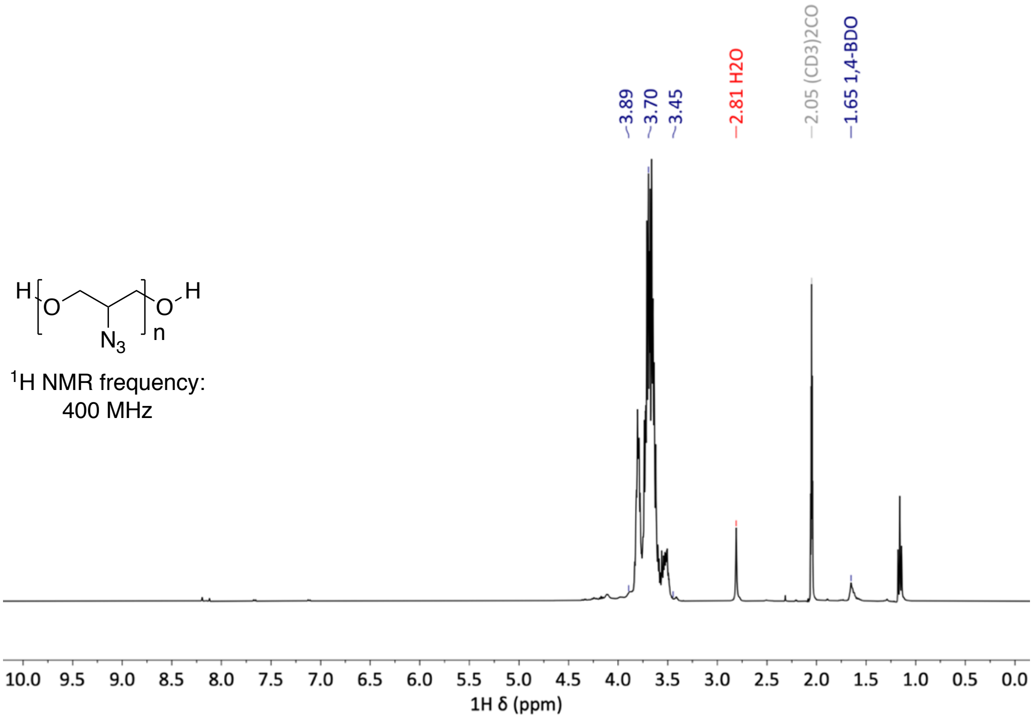

Figure S 10.23. Proton spectrum (^{1}H) of low-molecular-weight poly(3-azidooxetane).

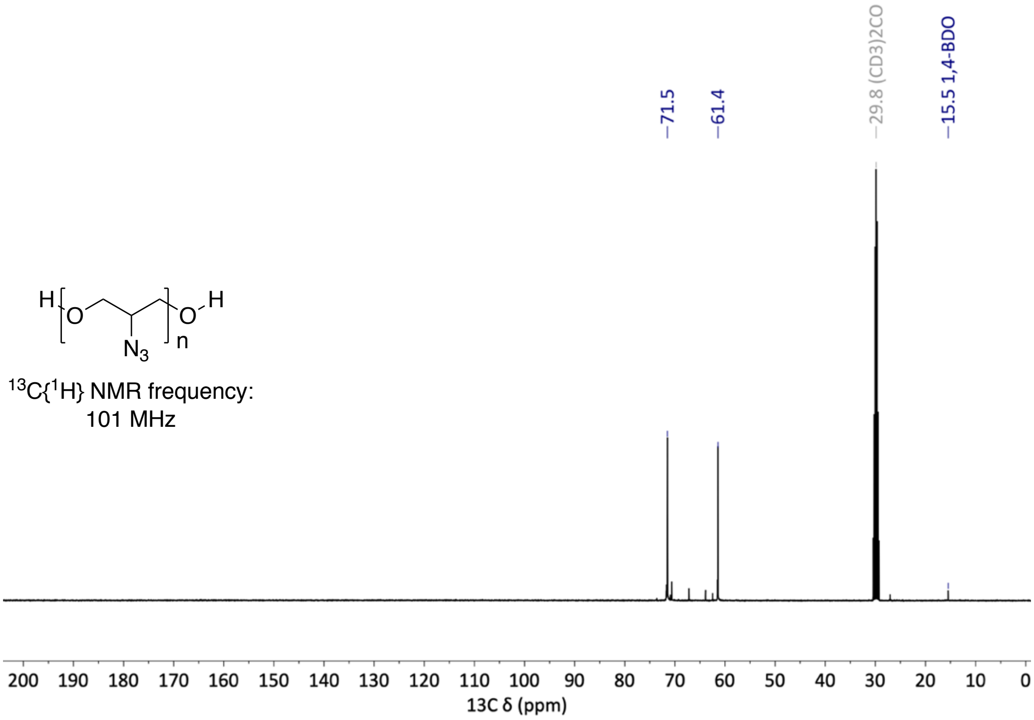

Figure S 10.24. Carbon spectrum (^{13}C) of low-molecular-weight poly(3-azidooxetane).

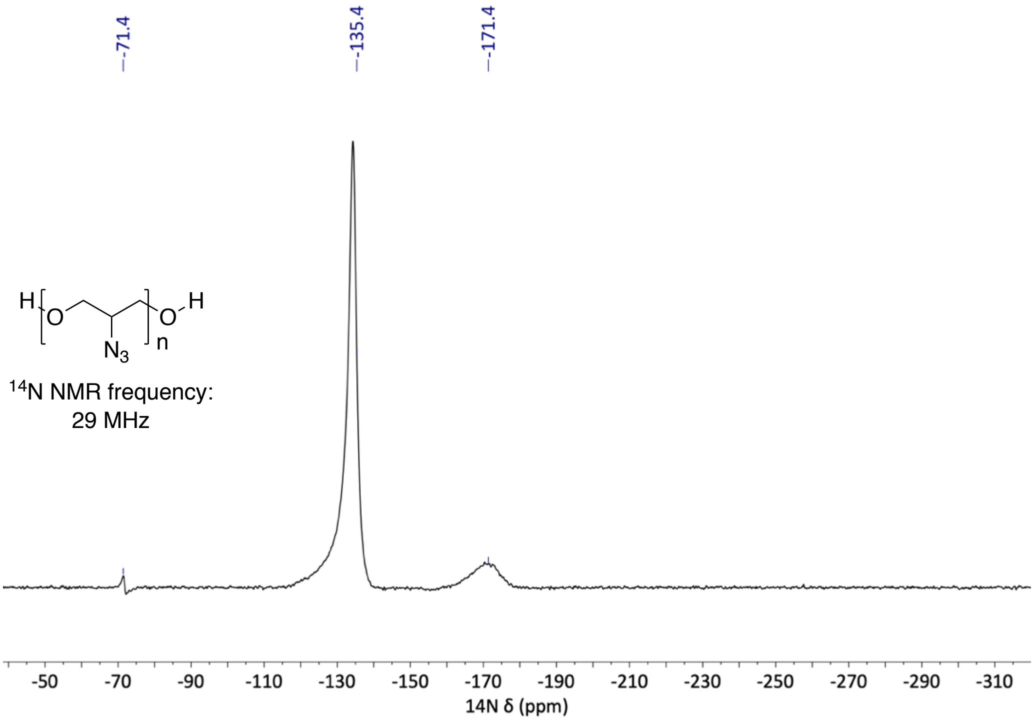

Figure S 10.25. Nitrogen spectrum (^{14}N) of low-molecular-weight poly(3-azidooxetane).

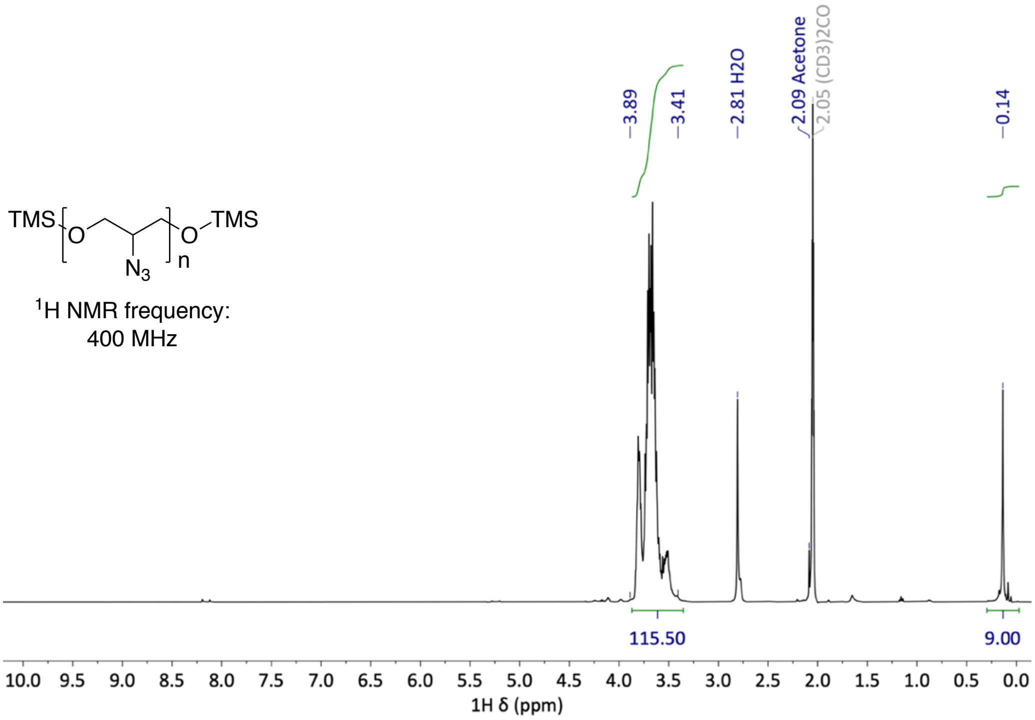

Figure S 10.26. Equivalent weight determination (^1H) of low-molecular-weight poly(3-azidooxetane) using trimethylsilyl groups.

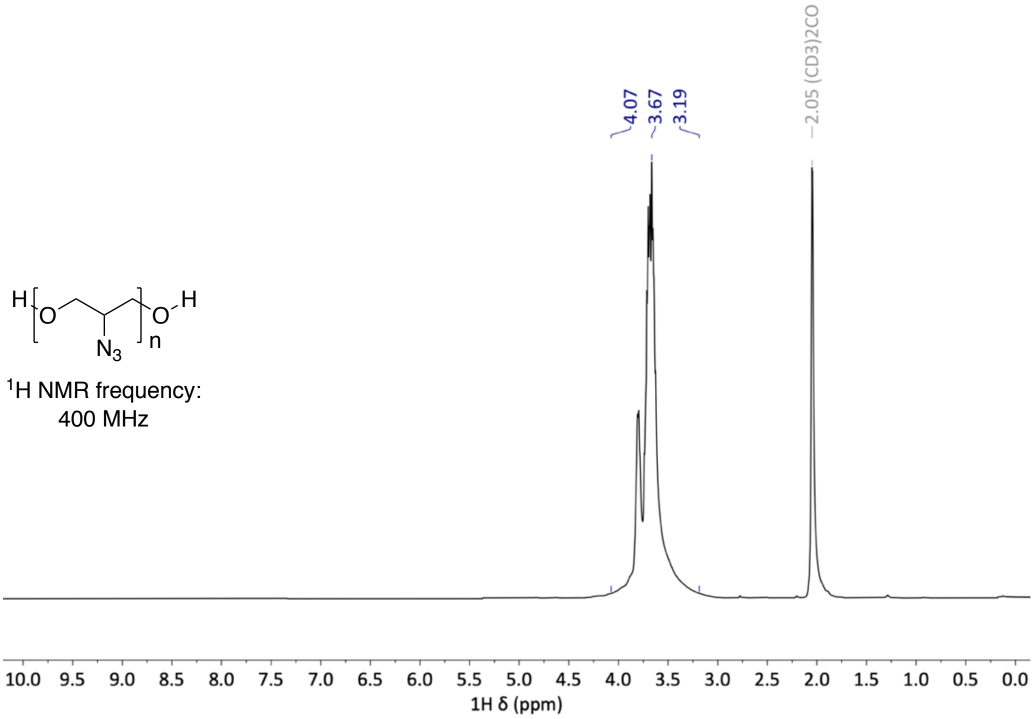

Figure S 10.27. Proton spectrum (^1H) of high-molecular-weight poly(3-azidooxetane) (azidation of pMsOx C10).

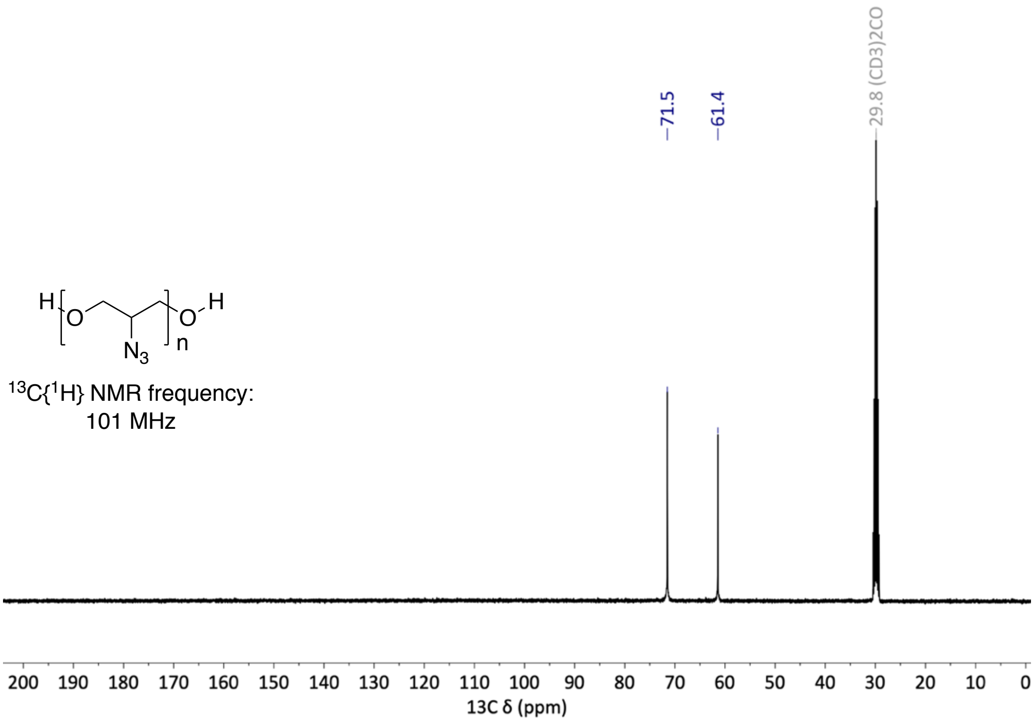

Figure S 10.28. Carbon spectrum (^{13}C) of high-molecular-weight poly(3-azidooxetane).

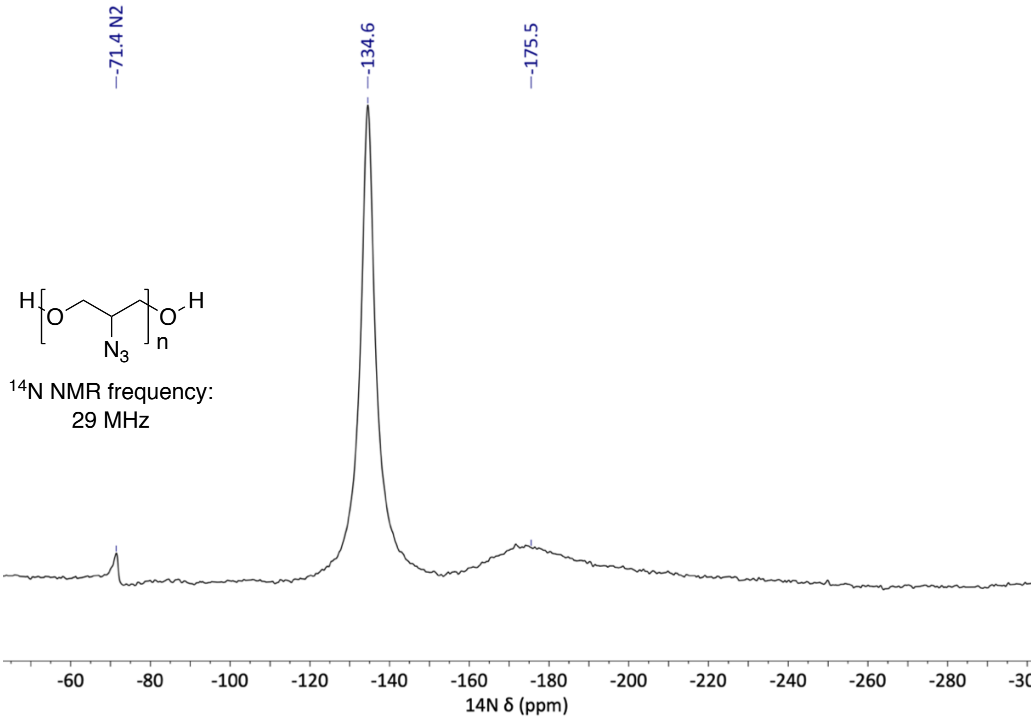

Figure S 10.29. Nitrogen spectrum (^{14}N) of high-molecular-weight poly(3-azidooxetane).

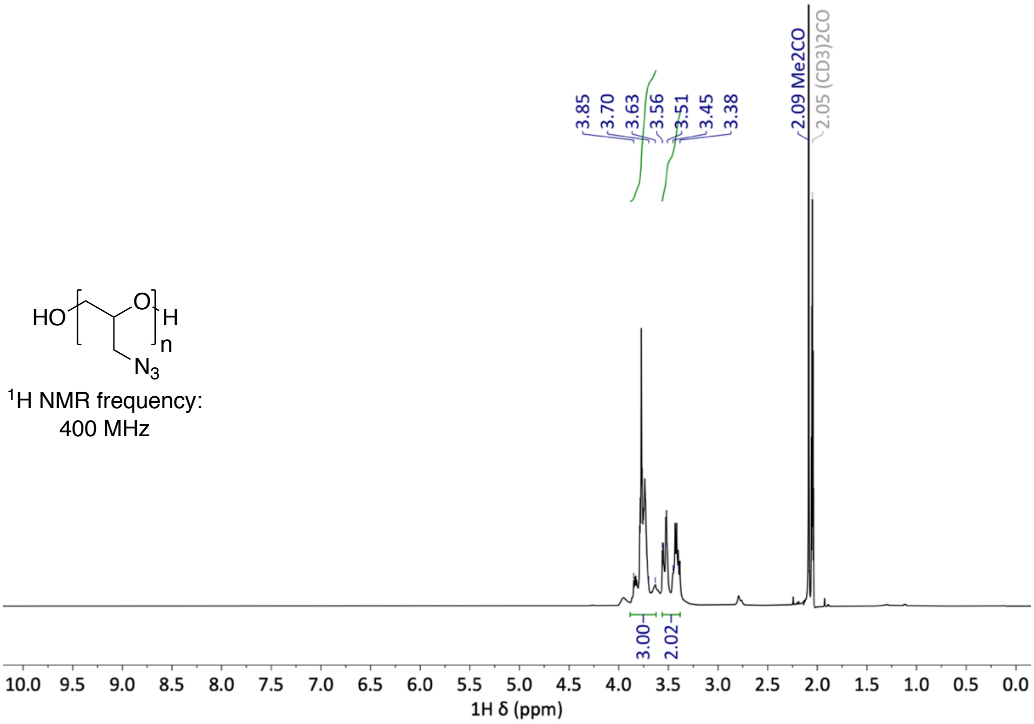

Figure S 10.30. Proton spectrum (^{1}H) of high-molecular-weight GAP (azidation of PECH).

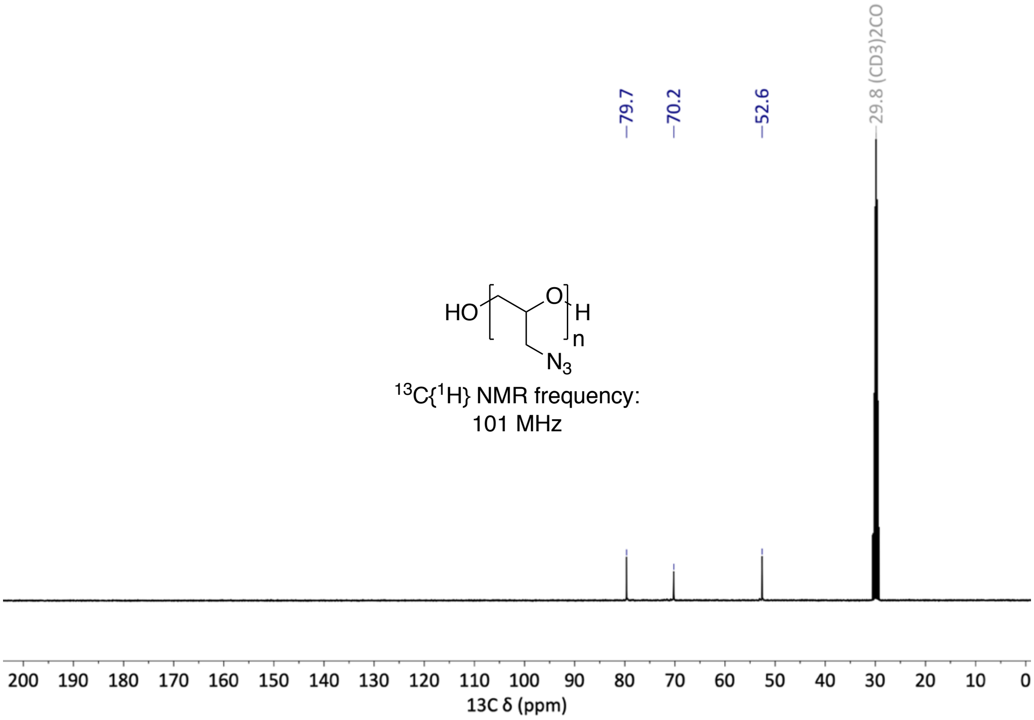

Figure S 10.31. Carbon spectrum (^{13}C) of GAP (glycidyl azide polymer).

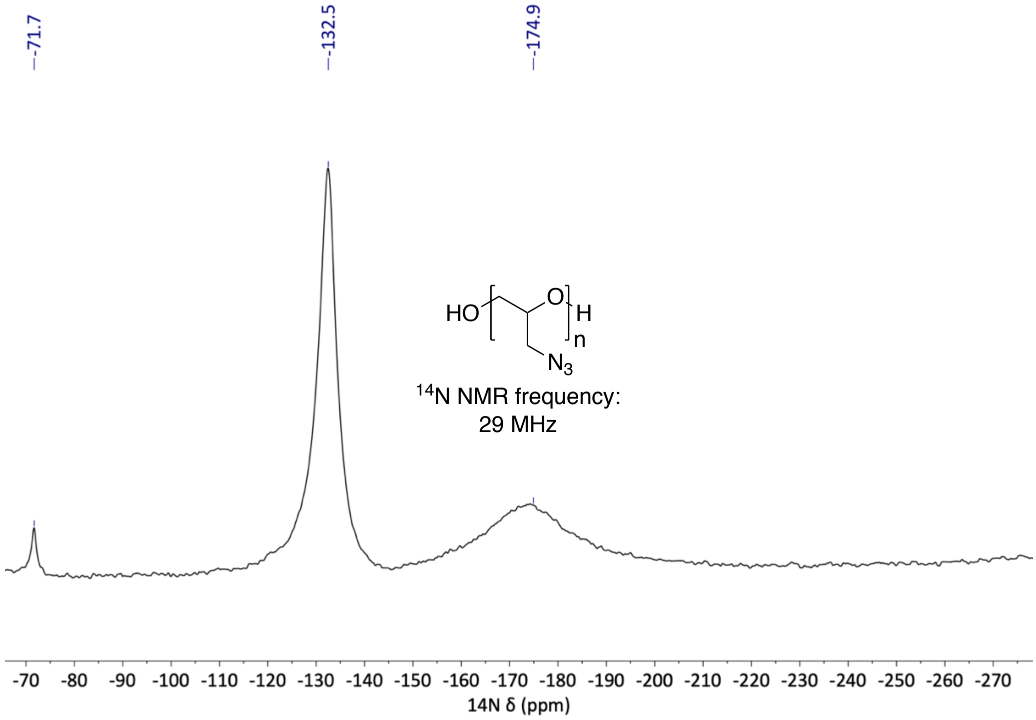

Figure S 10.32. Nitrogen spectrum (^{14}N) of GAP.

10.4.3 Picture Documentation

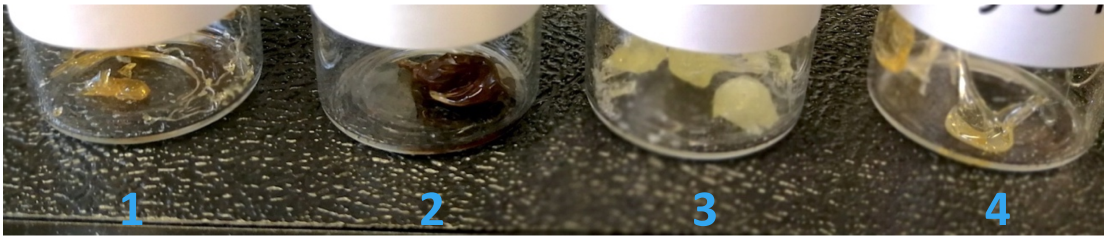

Figure S 10.33. Poly(3-mesyloxyoxetane) (I5-2 (1), I10-2 (2)) and poly(3-tosyloxyoxetane) (I5-2 (3), I10-2 (4)) after high-vacuum drying.

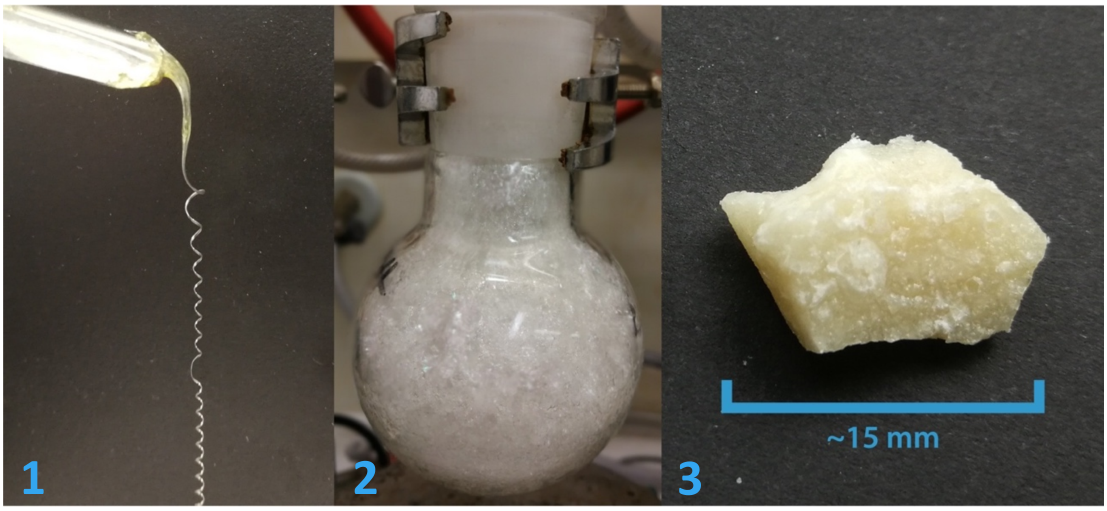

Figure S 10.34. Poly(3-tosyloxyoxetane) I5-2 – behavior above the glass transition temperature at 60 °C (1), drying of the polymer under high-vacuum conditions (2), and large crumbs after rotary evaporation of a 10 g batch (3).

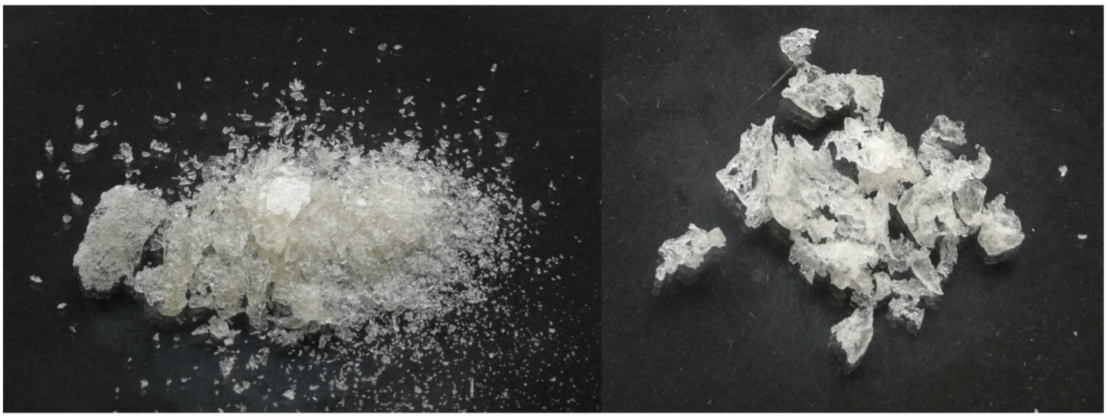

Figure S 10.35. Appearance of poly(3-tosyloxyoxetane) (left) and poly(3-mesyloxyoxetane) (right) using TIBA–0.7H_2O as catalyst.

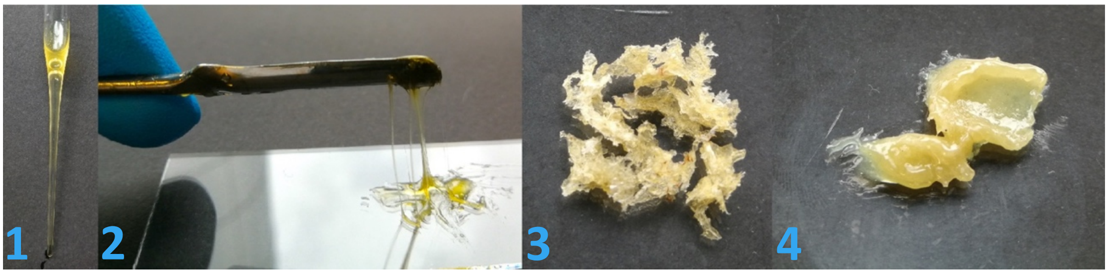

Figure S 10.36. Poly(3-azidooxtane) prepared from low- (1, liquid) and high-molecular-weight poly(3-tosyloxyoxetane) (2) as well as high-molecular-weight poly(3-mesyloxyoxetane) (3) in comparison and glycidyl azide polymer (GAP) prepared from poly(epichlorohydrin) (4).

10.4.4 Bomb Calorimetry

Enthalpies of formation were determined by bomb calorimetry according to literature methods.[8,9] For this purpose, the respective polymer was mixed with benzoic acid and the mixture pressed into tablets. These were placed in the combustion bomb. The combustion bomb was flushed with oxygen and each tablet was burned in pure oxygen atmosphere at a pressure of 35 bar. The change in temperature ΔT was measured and the specific energy of combustion $\Delta_c U$ was calculated using the following equations:

$$\Delta_c U = C \Delta T \tag{1}$$

The calorimeter constant *C* was determined by burning benzoic acid ($\Delta_c U$ = 2514±1.7 cal g^{-1}) as reference. The standard molar enthalpy of combustion is defined as:

$$\Delta_c H_m^0 = \Delta_c U + \Delta n_g RT \tag{2}$$

The change of moles of gas Δn_g can be calculated as follows:

$$\Delta n_g = \Delta n_i(products, g) - \Delta n_i(educts, g) \tag{3}$$

The ideal combustion reaction of CHNO-compounds was assumed for the combustion of the polymers repeating unit:

$$C_a H_b O_c N_d + \left(a + \frac{b}{4} - \frac{c}{2}\right) O_2 \rightarrow a\ CO_2 + \frac{b}{2}\ H_2O + \frac{d}{2}\ N_2 \tag{4}$$

leading to:

$$\Delta n_g = n(CO_2) + n(N_2) - n(O_2) = \frac{1}{2}(d - \frac{b}{2} + c) \tag{5}$$

The respective tablet composition and the corresponding values of $\Delta_c H_m^0$ for poly(3-azidooxetane) and GAP are summarized in Table S 5.

Table S 10.5. Results of the calorimetric combustion experiments.

Sample	Tablet weight [mg]	Polymer weight [mg]	Benzoic acid [mg]	$\Delta_c H_m^0$ / kJ mol^{-1}
		Poly(3-azidooxetane)		
1	631.4	145.7	485.7	−2018.3081
2	601.0	138.7	462.3	−2095.3236
3	616.2	142.2	474.0	−2048.7349
4	639.7	147.6	492.1	−2025.3076
5	599.1	138.2	460.9	−2060.8931
Average	617.5	142.5	475.0	−2049.7135
		GAP		
1	650.8	150.2	500.6	−1841.1435
2	721.4	166.5	554.9	−1927.9377
3	667.8	154.1	513.7	−2095.9554
4	687.1	158.6	528.5	−1833.6621
5	684.2	157.9	526.3	−1853.2958
Average	682.3	157.4	524.8	−1910.3989

The enthalpy of formation $\Delta_f H_m^0(M)$ of polymer M can be calculated by Hess' law:

$$\Delta_f H_m^0(M) = \sum_{j}^{products\ P} \Delta_f H^0(P_j) - \Delta_c H_m^0(M) \tag{6}$$

leading to:

$$\Delta_f H_m^0(M) = a\,\Delta_f H_m^0(CO_2) + \frac{1}{2}\Delta_f H_m^0(H_2O) - \Delta_c H_m^0(M) \tag{7}$$

The following literature values[10] have been used for the calculation:

•$\Delta_f H_m^0(CO_2)$ = −393.52 kJ mol^{-1}
•$\Delta_f H_m^0(H_2O)$ = −241.83 kJ mol^{-1}

The corresponding enthalpies of formation $\Delta_f H_m^0$ arising from $\Delta_c H_m^0$ are shown in Table S 6.

Table S 10.6. Calculated enthalpies of formation of GAP and poly(3-azidooxetane).

	GAP	**Poly(3-azidooxetane)**
$\Delta_f H_m^0$ (kJ mol^{-1})	125.3	264.6

10.4.5 Heat of Formation Calculation and Thermal Analysis

The atomization method was used to determine the heat of formation of **4** and **5** using the atom energies in Table S 7.[11]

$$\Delta_f H°_{(g,\ M,\ 298)} = H_{(molecule,\ 298)} - \Sigma H°_{(atoms,\ 298)} + \Sigma \Delta_f H°_{(atoms,\ 298)}$$

Table S 10.7. CBS-4M electronic enthalpies for atoms C, H, N, and O and their literature values.

	$-H^{298}$ / a.u.	$\Delta_f H°_{gas}$[10]
H	0.500991	217.998
C	37.786156	716.68
N	54.522462	472.68
O	74.991202	249.18

The Gaussian16 program package was used to calculate room temperature enthalpies on the CBS-4M level of theory.[12] In order to obtain the energy of formation for compounds **4** and **5**, Trouton's Rule has to be applied ($\Delta H_{sub} = 90 \cdot T_m$).

Table S 10.8. Heat of formation calculation results for compounds **4** and **5**.

M	$-H^{298}$ [a] [a.u.]	$\Delta_f H°(g, M)$ [b] [kJ mol^{-1}]	$\Delta_{sub} H°(M)$ [c] [kJ mol^{-1}]	$\Delta_f H°(s)$ [d] [kJ mol^{-1}]	Δn	$\Delta_f U(s)$ [e] [kJ k^{-1}]
NG	957.086738	−280.3	40.2975	−320.6	−8.5	−1319.2
EDBAA	861.593329	−18.3	43.2405	−61.6	−9.0	−172.1

[a] CBS-4M electronic enthalpy. [b] Gas phase enthalpy of formation. [c] Sublimation enthalpy. [d] Standard solid state enthalpy of formation. [e] Solid-state energy of formation.

The thermal behavior of compounds **3**–**5** and of both non-energetic and energetic polymers was analyzed by differential scanning calorimetry (DSC) at a heating rate of 5 °C min^{-1}. The obtained thermograms and evaluations are depicted.

10.4.5.1 Precursors and Plasticizers

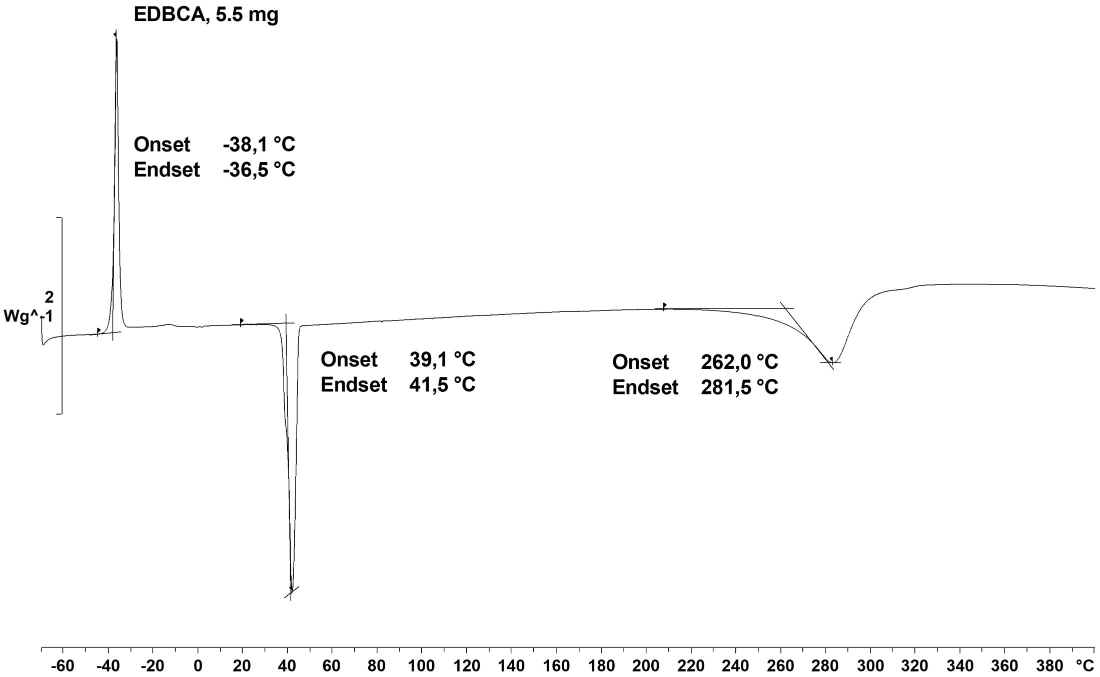

Figure S 10.37. DSC evaluation of ethane-1,2-diyl bis(2-chloroacetate) (**4**).

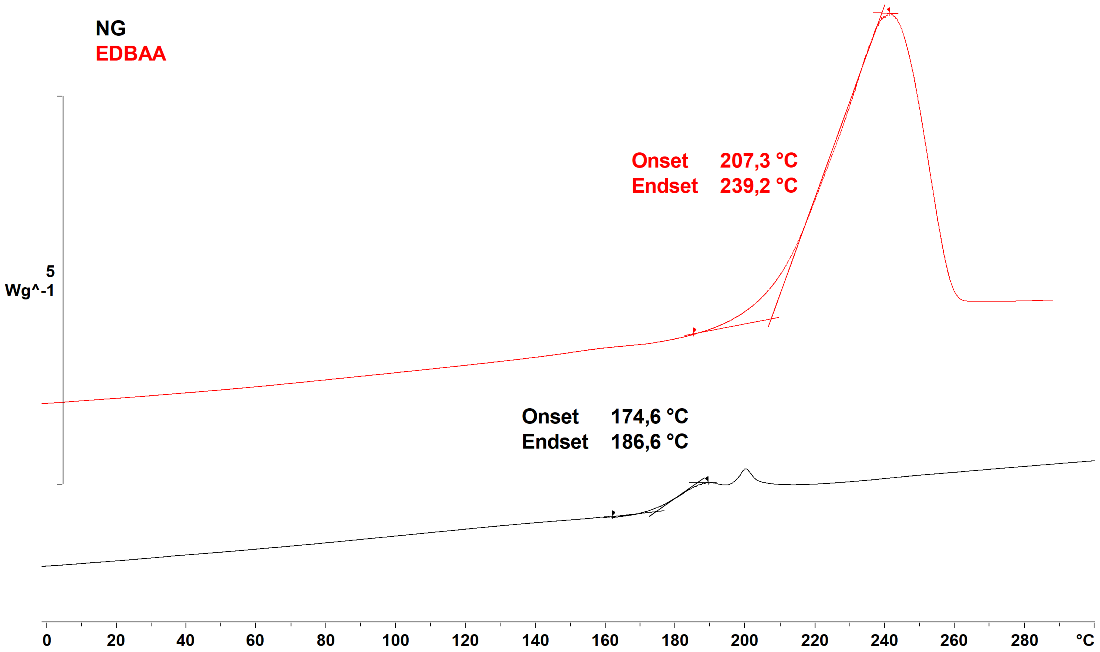

Figure S 10.38. DSC evaluation of nitroglycerin (NG, **3**) and ethane-1,2-diyl bis(2-azidoacetate) (EDBAA, **5**).

10.4.5.2 Non-Energetic Parent Polymers

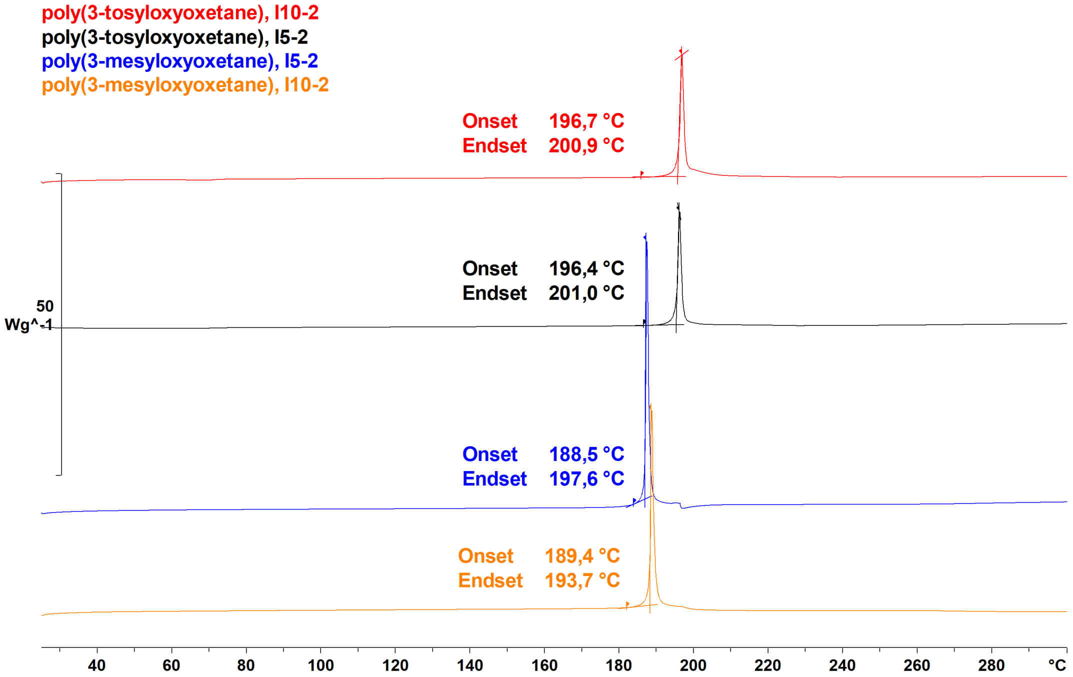

Figure S 10.39. DSC evaluation (exothermic decomposition) of poly(3-tosyloxyoxetane) and poly(3-mesyloxyoxetane) prepared with varying initiator concentrations with regard to butane-1,4-diol.

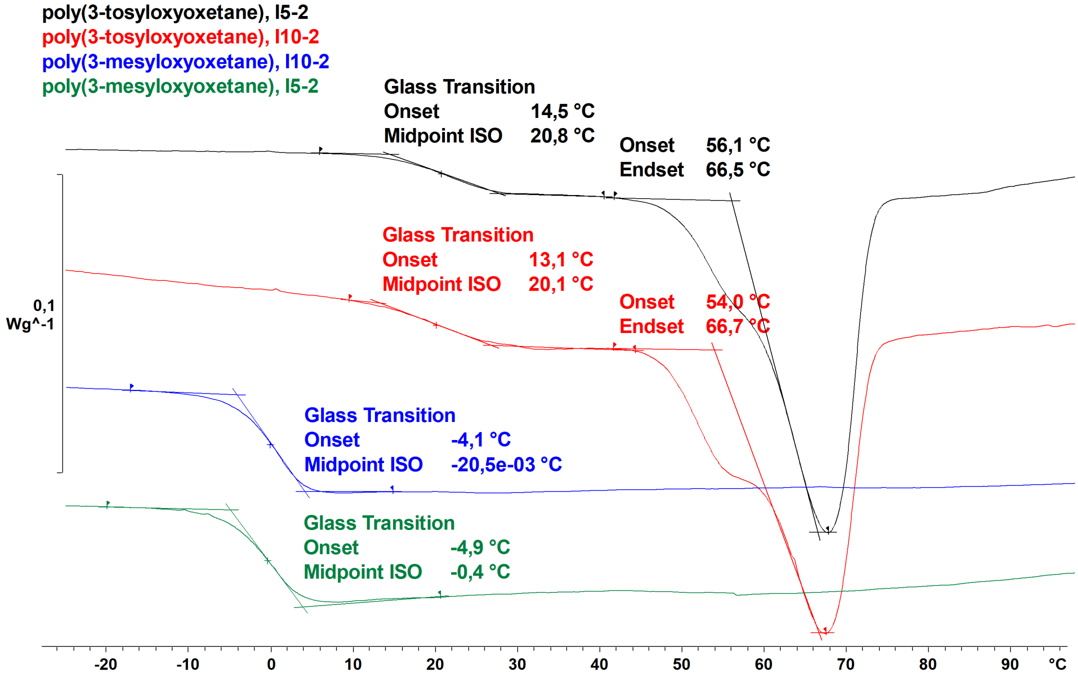

Figure S 10.40. DSC evaluation (glass transition temperature) of poly(3-tosyloxyoxetane) and poly(3-mesyloxyoxetane) prepared with varying initiator concentrations with regard to butane-1,4-diol.

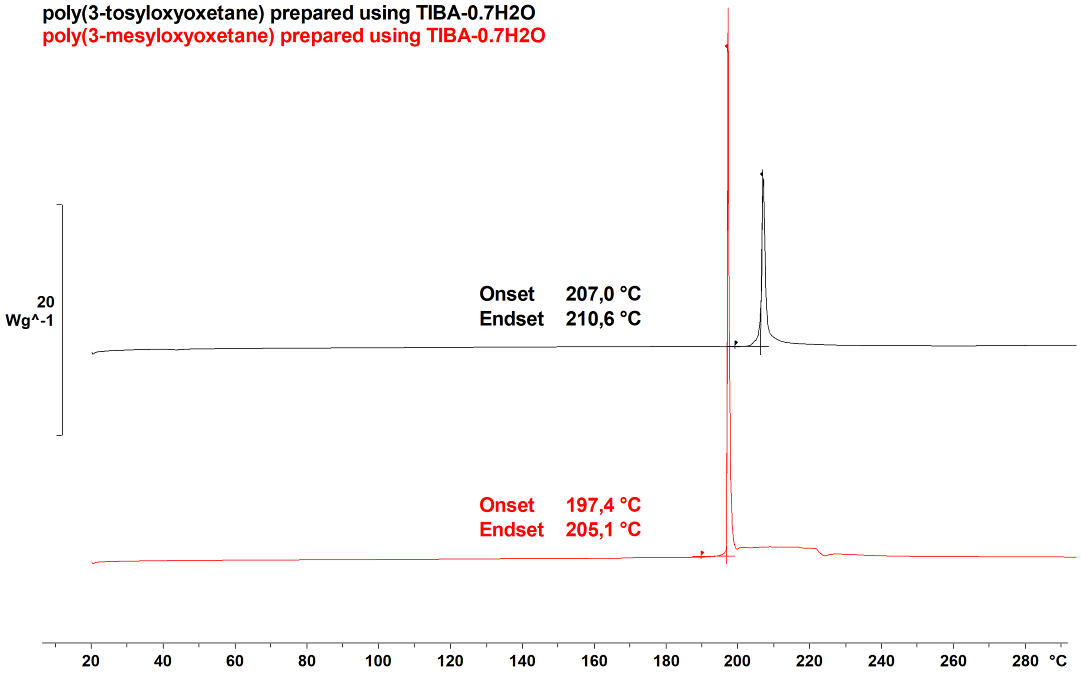

Figure S 10.41. DSC evaluation (decomposition temperature) of poly(3-tosyloxyoxetane) and poly(3-mesyloxyoxetane) prepared using triisobutylaluminum–0.7H_2O as catalyst.

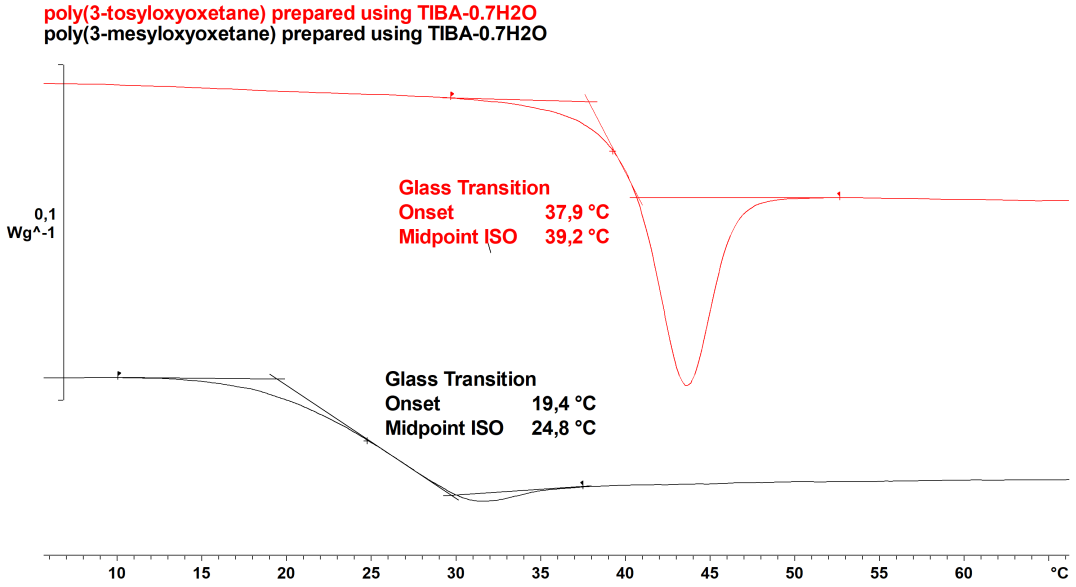

Figure S 10.42. DSC evaluation (glass transition temperature) of poly(3-tosyloxyoxetane) and poly(3-mesyloxyoxetane) prepared using triisobutylaluminum–0.7H_2O as catalyst.

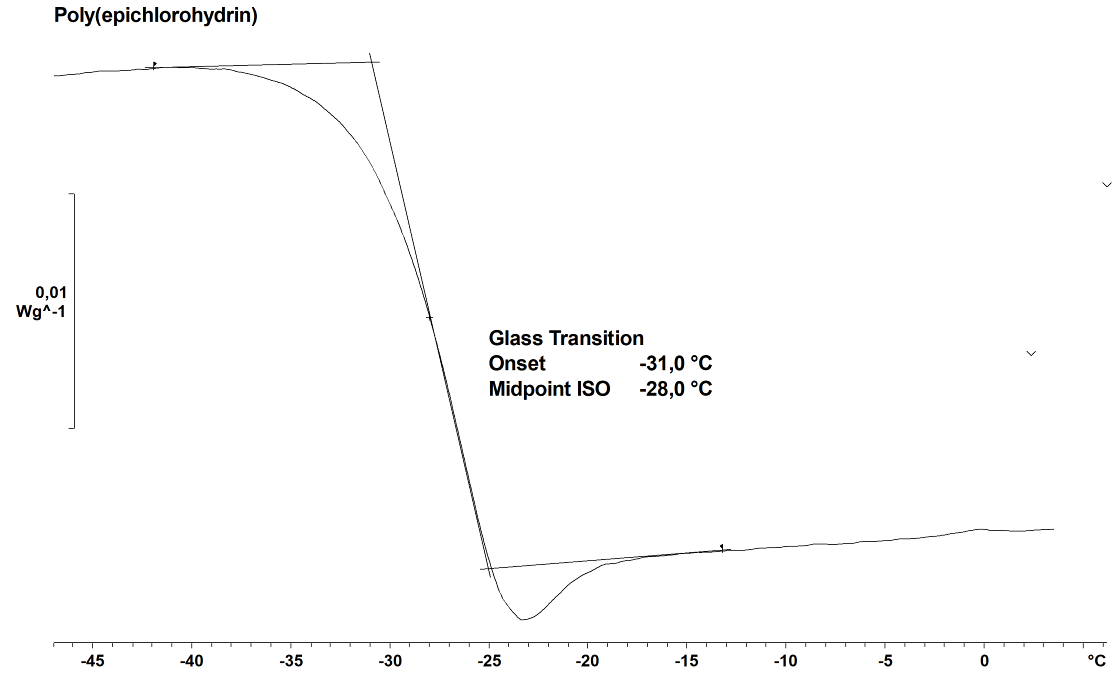

Figure S 10.43. DSC evaluation (glass transition temperature) of poly(epichlorohydrin) prepared using triisobutylaluminum−0.7H_2O as catalyst.

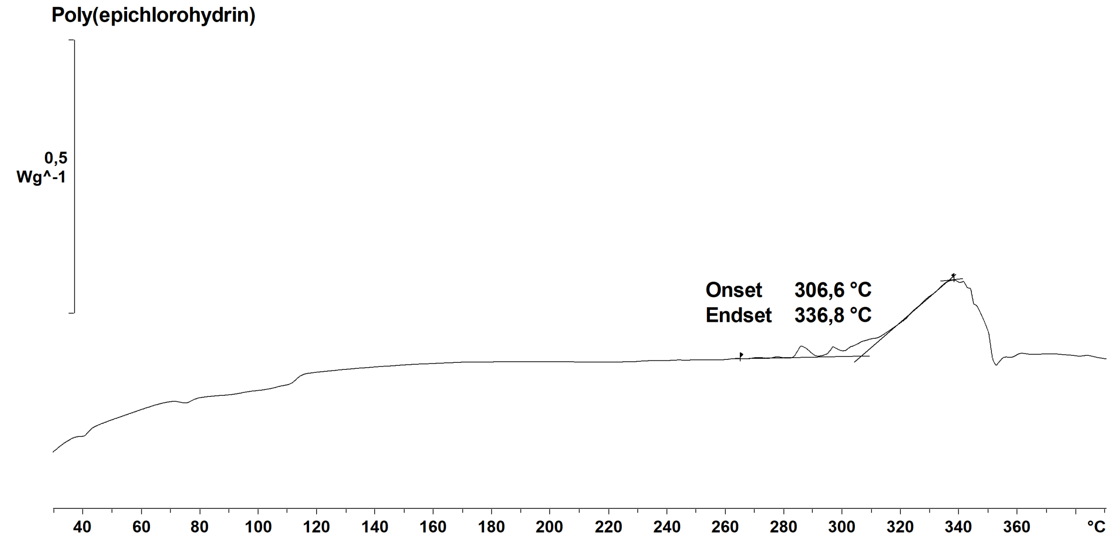

Figure S 10.44. DSC evaluation (decomposition temperature) of poly(epichlorohydrin) prepared using triisobutylaluminum−0.7H_2O as catalyst.

10.4.5.3 Azidated Polymers

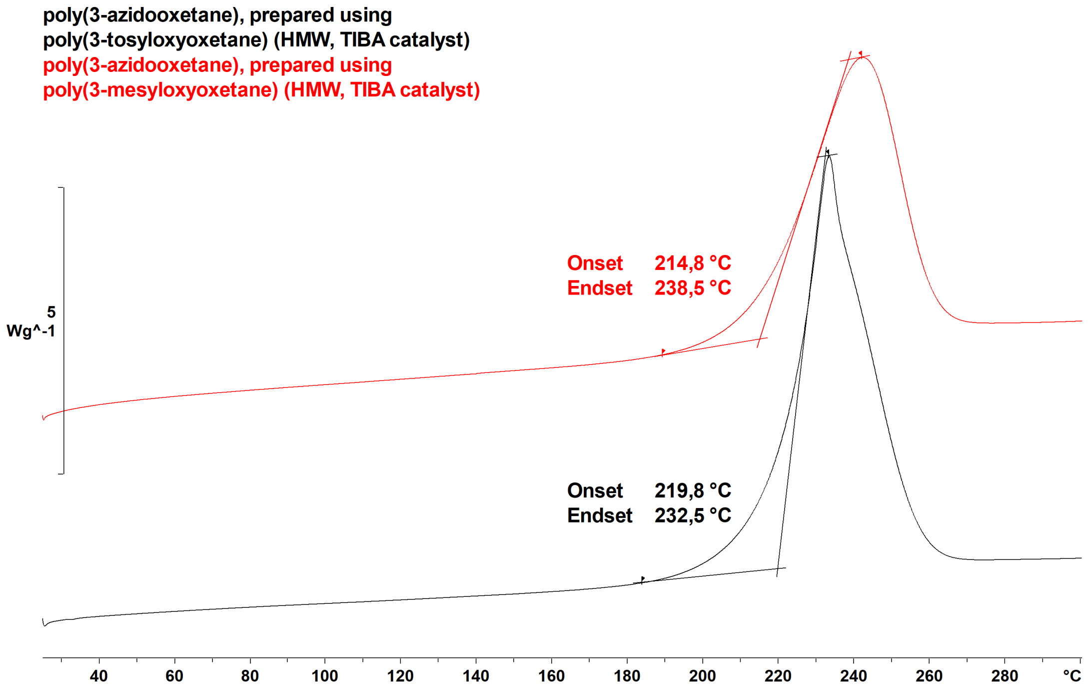

Figure S 10.45. DSC evaluation (exothermic decomposition) of poly(3-azidooxetane) prepared by azidation of the high-molecular-weight species (TIBA catalyst) of poly(3-tosyloxyoxetane) and poly(3-mesyloxyoxetane).

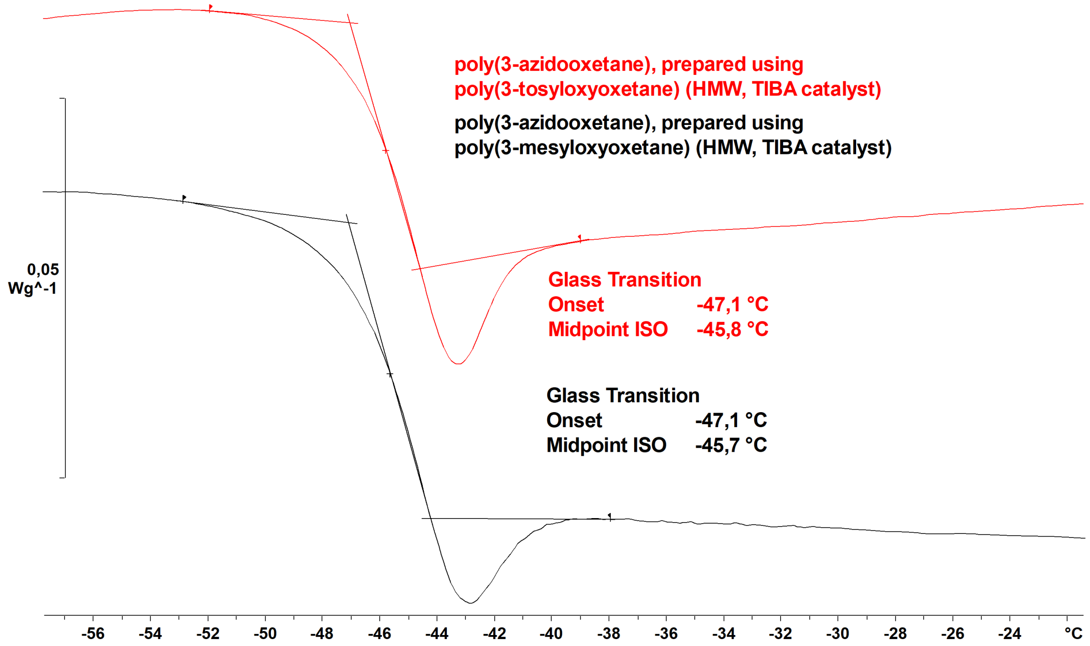

Figure S 10.46. DSC evaluation (glass transition) of poly(3-azidooxetane) prepared from high-molecular-weight (TIBA catalyst) poly(3-tosyloxyoxetane) and poly(3-mesyloxyoxetane).

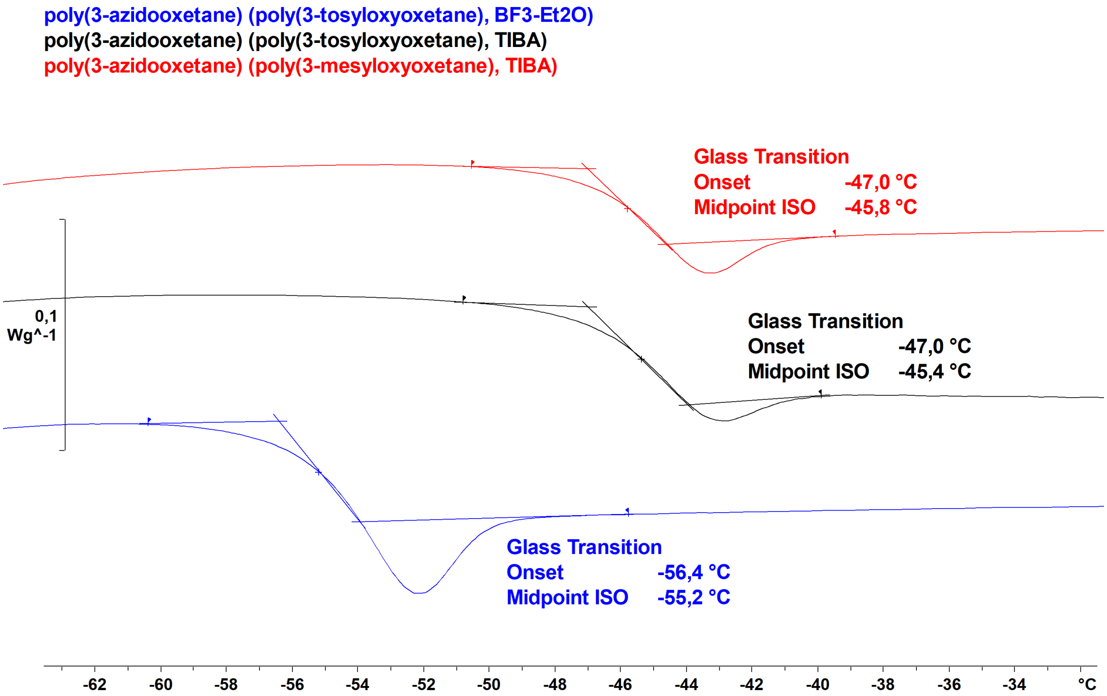

Figure S 10.47. Glass transition temperature comparison for low- and high-molecular-weight poly(3-azidooxetane) prepared from the corresponding tosylate or mesylate prepolymers (pTsOx I5-3, pTsOx C10, pMsOx C10).

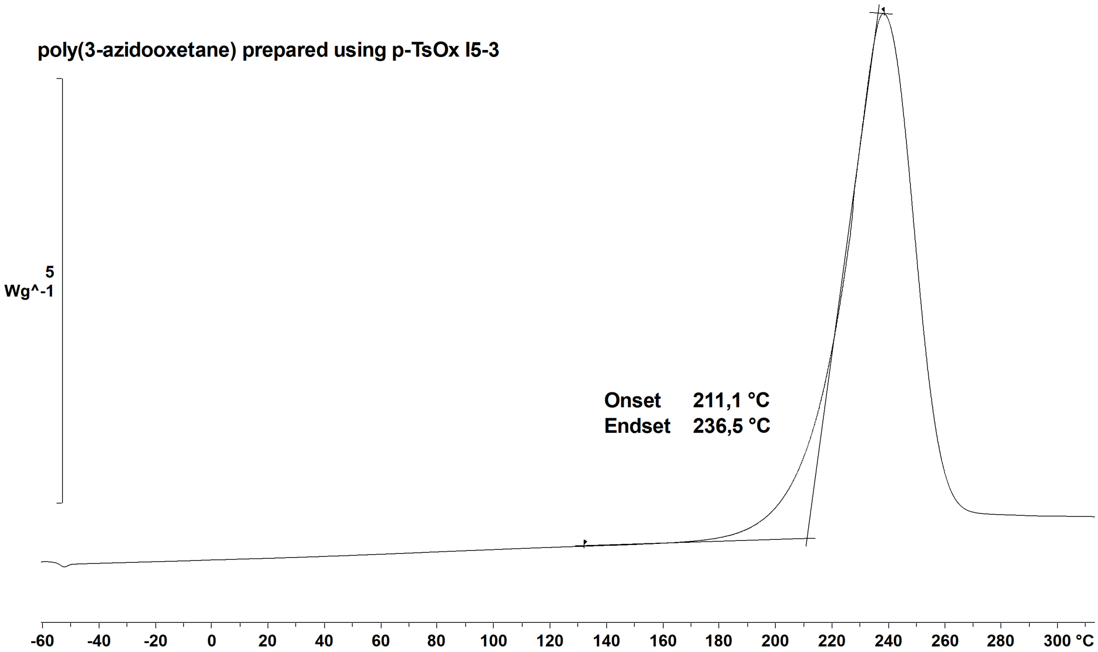

Figure S 10.48. DSC evaluation (exothermic decomposition) of low-molecular-weight poly(3-azido-oxetane) prepared using poly(3-tosyloxyoxetane) (pTsOx I5-3).

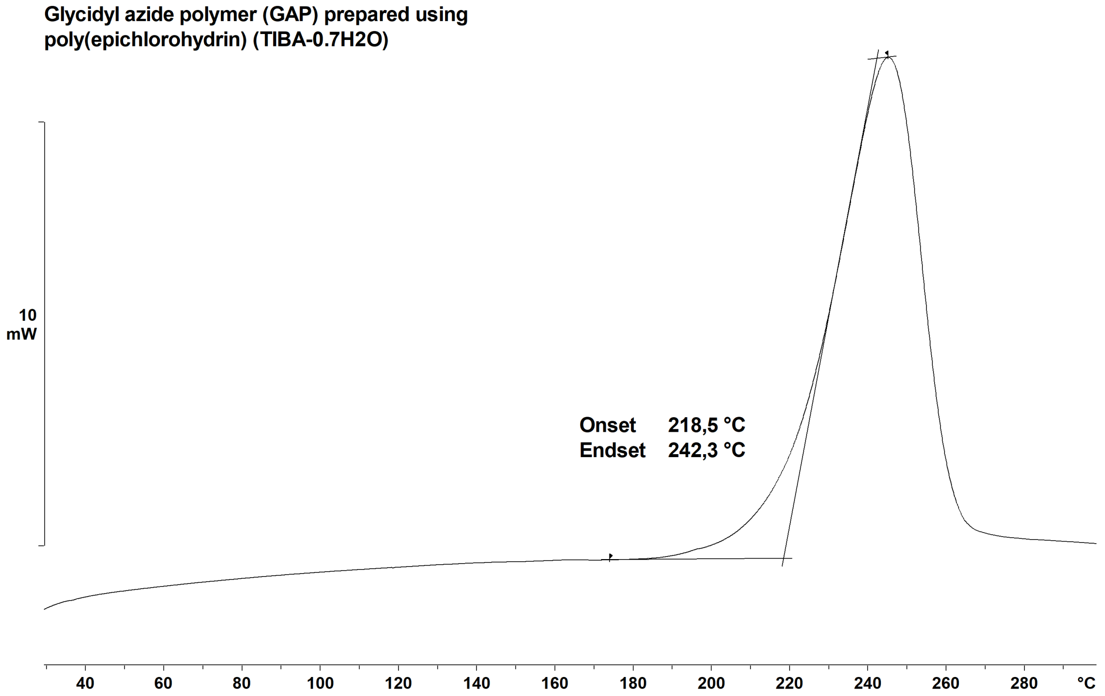

Figure S 10.49. DSC evaluation (exothermic decomposition) of GAP prepared from poly(epichlorohydrin).

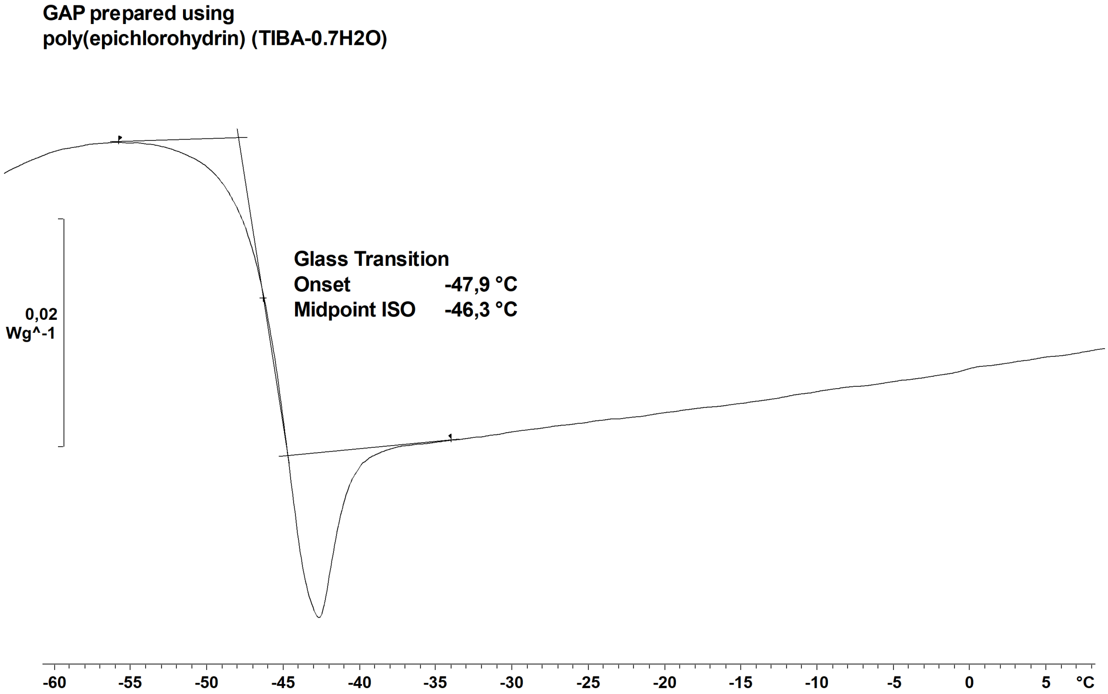

Figure S 10.50. DSC evaluation (glass transition temperature) of GAP prepared from poly(epichlorohydrin).

10.4.5.4 Plasticizer Compatibility of Poly(3-azidooxetane)

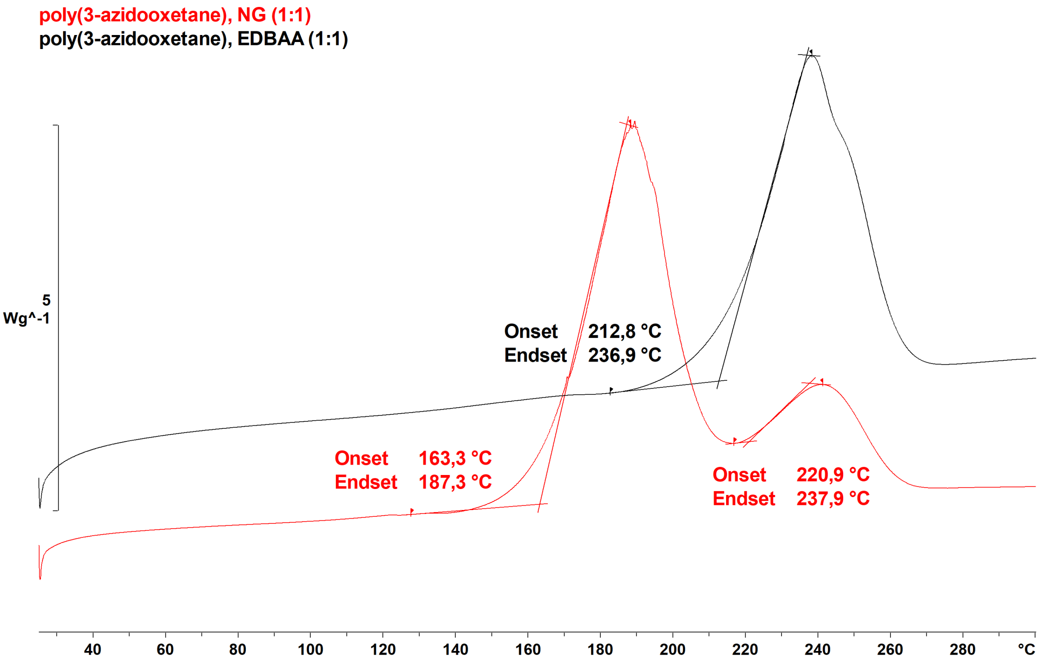

Figure S 10.51. DSC evaluation (exothermic decomposition) of low-molecular-weight poly(3-azidooxetane) mixed with nitroglycerin (NG) or ethane-1,2-diyl bis(2-azidoacetate) (EDBAA) as plasticizer (1:1 mixtures).

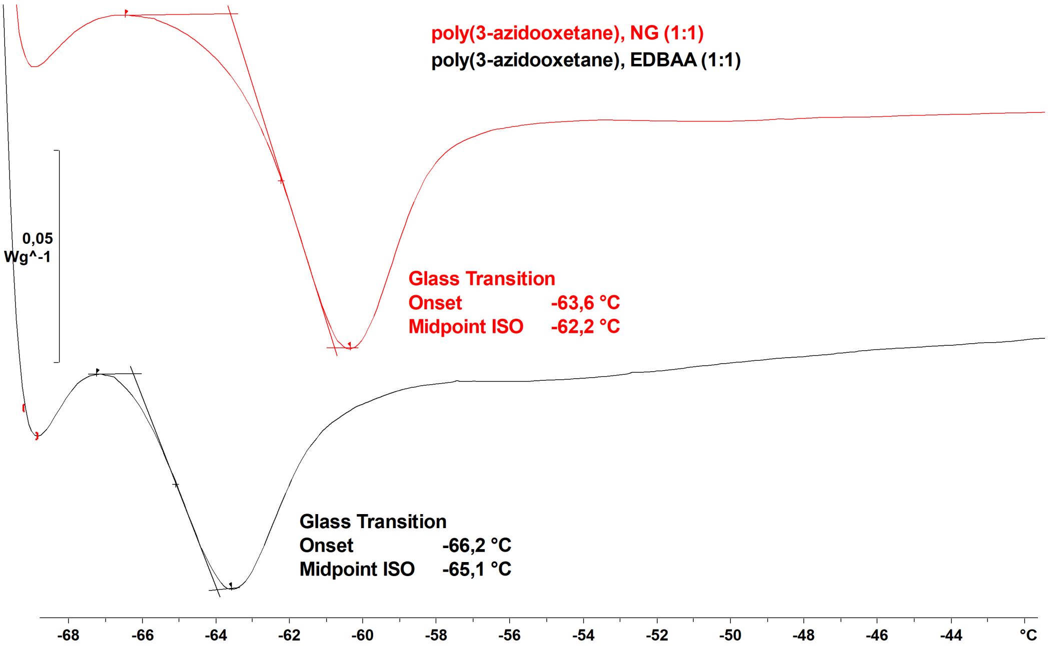

Figure S 10.52. DSC evaluation (lowered glass transition temperature) in case of low-molecular-weight poly(3-azidooxetane) mixed with nitroglycerin (NG) or ethane-1,2-diyl bis(2-azidoacetate) (EDBAA) as plasticizer (1:1 mixtures).

10.4.6 Hot Plate Test

Glycidyl azide polymer (GAP) and poly(3-azidooxetane) were placed on a copper witness plate (50 mg, weighing on aluminum foil) and heated with a Bunsen burner as thermal stress test. A more violent deflagration is observed in the case of poly(3-azidooxetane).

Figure S 10.53. Hot plate test of GAP (50 mg).

Figure S 10.54. Hot plate test of poly(3-azidooxetane) (50 mg) showing a slightly more violent deflagration than in case of GAP.

References

[1] NATO STANAG 4489: *Explosives. Impact Sensitivity Tests*; NATO Standardization Office, Brussels, Belgium, **1999**.

[2] NATO STANAG 4487: *Explosives. Friction Sensitivity Tests*; NATO Standardization Office, Brussels, Belgium, **2002**.

[3] United Nations (UN), UN Recommendations on the Transport of Dangerous Goods, Manual of Tests and Criteria, **2009**.

[4] Born, M.; Karaghiosoff, K.; Klapötke, T. M. A GAP Replacement: Improved Synthesis of 3-Azidooxetane and Its Homopolymer Based on Sulfonic Acid Esters of Oxetan-3-ol. *J. Org. Chem.* **2021**, *86*, 12607-12614.

[5] Härtel, M. Studies towards the gas-phase detection of hazardous materials by vapor pressure measurements with the transpiration method in combination with vacuum outlet GC/MS. Ph. D. Dissertation, Ludwig-Maximilian University (LMU) Munich, Munich, Germany, **2017**.

[6] Bezwada, R. S. Hydrolysable Linkers and Cross-Linkers for Absorbable Polymers. US 8 048 980, **2009**.

[7] Maeno, Z.; Midogochi, K.; Mitsudome, T.; Mizugaki, T.; Jitsukawa, K. Synthesis of glycol diesters through the depolymerization of polyethylene glycols with carboxylic acids using a proton-exchanged montmorillonite catalyst. *Tetrahedron Lett.* **2018**, *59*, 832-835.

[8] Axthammer, Q. J.; Evangelisti, C.; Klapötke, T. M. Characterization, bomb calorimetric measurements and quantum chemical calculations of high energetic dense oxidizers (HEDO). In *44th International Annual Conference of the Fraunhofer ICT, Energetic Materials – Past, Present and Future*, Karlsruhe, Germany, June 25–28, **2013**.

[9] Hafner, S. Internal plasticized glycidyl azide copolymers for energetic solid propellant binders. Ph. D. Dissertation, Ludwig-Maximilian University (LMU) Munich, Munich, Germany, **2019**.

[10] Chase, M. W. NIST-JANAF Thermochemical Tables, Fourth Edition, *J. Phys. Chem. Red. Data, Monograph 9,* **1998**, 1–1951.

[11] Altenburg, T.; Klapötke, Thomas M.; Penger, A.; Stierstorfer, J. Two Outstanding Explosives Based on 1,2-Dinitroguanidine: Ammonium- dinitroguanidine and 1,7-Diamino-1,7-dinitrimino-2,4,6-trinitro-2,4,6-triazaheptane. *Z. Anorg. Allg. Chem.* **2010**, *636*, 463-471.

[12] Frisch, M. J.; Trucks, G. W.; Schlegel, H. B.; Scuseria, G. E.; Robb, M. A.; Cheeseman, J. R.; Scalmani, G.; Barone, V.; Petersson, G. A.; Nakatsuji, H.; Li, X.; Caricato, M.; Marenich, A. V.; Bloino, J.; Janesko, B. G.; Gomperts, R.; Mennucci, B.; Hratchian, H. P.; Ortiz, J. V.; Izmaylov, A. F.; Sonnenberg, J. L.; Williams; Ding, F.; Lipparini, F.; Egidi, F.; Goings, J.; Peng, B.; Petrone, A.; Henderson, T.; Ranasinghe, D.; Zakrzewski, V. G.; Gao, J.; Rega, N.; Zheng, G.; Liang, W.; Hada, M.; Ehara, M.; Toyota, K.; Fukuda, R.; Hasegawa, J.; Ishida, M.; Nakajima, T.; Honda, Y.; Kitao, O.; Nakai, H.; Vreven, T.; Throssell, K.; Montgomery Jr., J. A.; Peralta, J. E.; Ogliaro, F.; Bearpark, M. J.; Heyd, J. J.; Brothers, E. N.; Kudin, K. N.; Staroverov, V. N.; Keith, T. A.; Kobayashi, R.; Normand, J.; Raghavachari, K.; Rendell, A. P.; Burant, J. C.; Iyengar, S. S.; Tomasi, J.; Cossi, M.; Millam, J. M.; Klene, M.; Adamo, C.; Cammi, R.; Ochterski, J. W.; Martin, R. L.; Morokuma, K.; Farkas, O.; Foresman, J. B.; Fox, D. J., Gaussian 16 Rev. C.01, **2016**.

11 Energetic Polymers: A Chance for Lightweight Reactive Structure Materials?

by
Max Born, Jakob Plank, and Thomas M. Klapötke

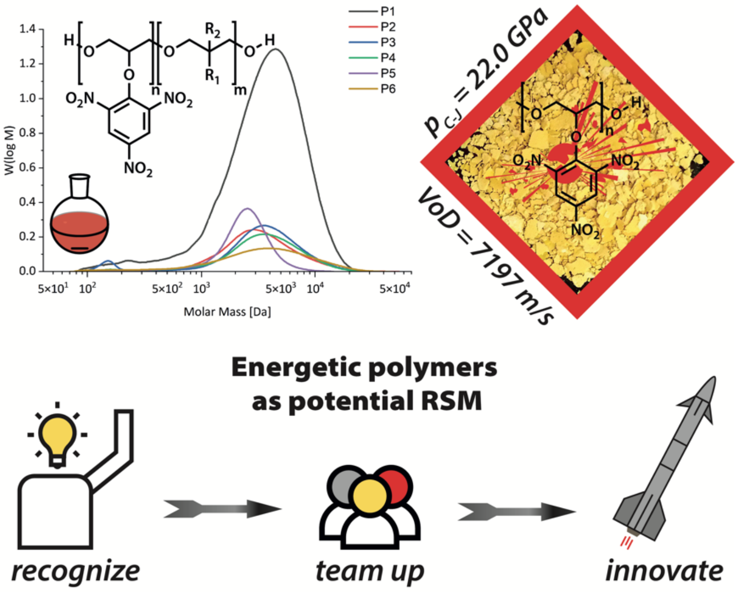

as published in
Propellants, Explosives, Pyrotechnics **2022**, 47, e202100368
(doi:10.1002/prep.202100368)

Abstract

Today's ammunition still consists of about 70 wt% structure-providing materials such as metals providing no energetic contribution. Therefore, reactive structure materials (RSMs) offer tremendous room for improvement. While current research focuses on rather heavy, metal-based materials (e.g., alloys, thermites), energetic polymers appear as an under-recognized opportunity for very lightweight RSMs. Unfortunately, suitable polymers are unavailable as energetic polymer research has almost exclusively focused on elastic binders with the least possible glass transition temperature. An application as RSM, however, requires rigid polymers with a glass transition above operational temperatures. Accordingly, monomers with fundamentally different structures are required. The first step in this particular direction is 3-(2,4,6-trinitrophenoxy)oxetane (TNPO). Herein, we report the synthesis of its homopolymer and investigate its polymerization behavior by copolymerization with prior art energetic oxetanes. All polymers were intensively studied by vibrational and multinuclear (^{1}H, ^{13}C, ^{14}N) NMR spectroscopy, elemental analysis, gel permeation chromatography, and differential scanning calorimetry (DSC). Hereby, DSC revealed the high effect of the TNPO repeating unit on the glass transition temperature. The performance of all polymers was calculated using the EXPLO5 code to evaluate the potential performance range of polymeric RSMs. Further, their shock and friction sensitivity was determined by BAM standard procedures.

Keywords: Energetic polymers, energetic oxetanes, reactive structure material, 3-(2,4,6-trinitrophenoxy)oxetane, TNPO.

11.1 Introduction

Modern ammunitions and effector systems contain only about 30 weight percent of energetic fillers like secondary explosives, while the predominant mass fraction is constituted by structure-providing materials such as metals (e.g., steel, aluminum) that offer no energetic contribution.[1] A potential solution to reduce deadweight is provided by reactive structural materials (RSM), which serve as structural elements and store chemical energy which is released upon a suitable stimulus.[1] Although the first RSMs were composites of polytetrafluoroethylene and aluminum[2,3] which could be viewed as predecessors of polymer-based RSMs, research has almost exclusively focused on metal-based materials such as thermites or alloys, which provide additional energy through redox reactions.[1] However, the underlying chemical reactions are often too slow and require the presence of gaseous oxidizers such as atmospheric oxygen, thereby limiting the scope of application.[1] Therefore, energetic polymers with sufficient performance and mechanical properties appear far more promising as they require no oxidizer, react much faster (deflagration or detonation), and can drastically reduce the effector systems weight due to their lower density compared to metal-based materials. Hence, polymeric RSMs may contribute to a high weight reduction and thereby an increased operational range.[4] Conceptual applications range from structure-providing casings to combustible single components. For this purpose, thermoplastic polymers of low sensitivity, high performance, mechanical strength, and thermostability, together with processability by conventional techniques (e.g., extrusion, 3D printing), appear to be most suitable.[4] However, to provide the necessary stiffness and mechanical strength for the envisioned use, polymeric RSMs ought to be employed below their glass transition temperature (T_G) – similar to technically relevant everyday polymers like polycarbonates (PC), polystyrene (PS), or acrylonitrile-butadiene-styrene (ABS) terpolymers. This is very problematic, as energetic polymer research has focused almost exclusively on binders that are elastic at operational temperatures to absorb mechanical forces acting upon an energetic formulation, thereby reducing the overall sensitivity toward friction and impact.[5,6] Therefore, binder polymers are required to exhibit a T_G as low as possible (e.g., glycidyl azide polymer (GAP): −46 °C).[5,6] As the glass transition temperature correlates with a polymer's chain flexibility, high chain rigidity is needed to achieve high glass transition temperatures.[7] In the case of polyoxetanes, this can be implemented, for instance, by bulky side-groups which impose rigidity to the polymer chains by their steric demand or through interlocking and intermolecular interactions.[7] For example, aromatic or heteroaromatic structures could be employed. Hence, 3-(2,4,6-trinitrophenoxy)-oxetane (TNPO), which was first described by Born et al. in 2019, represents the first monomer of a potentially suitable structure. It is formally a picric acid derivative and can be obtained by a one-pot reaction between picryl chloride and lithium oxetan-3-olate formed *in situ* from lithium hydride and commercially available oxetan-3-ol in THF.[8] Moreover, it combines very low sensitivity with sufficient thermostability and performance comparable to TNT. Herein, we report the preparation of its homopolymer by cationic ring-opening polymerization (CROP) using the well-known boron trifluoride etherate/diol initiator system. In addition, TNPO was copolymerized with various energetic state-of-the-art oxetanes. As these are known to polymerize readily, conclusions about TNPO's polymerization behavior and any adverse effects caused by its steric demand or the relatively low basicity of the oxetane oxygen atom were possible. Besides, copolymerization allowed an evaluation of the glass transition temperature increase caused by a rigid motif like TNPO by comparison with the corresponding parent homopolymers. Next to the thermal behavior, we assessed the heat of formation of all polymers, calculated their energetic performance, and determined their sensitivity toward impact and friction. Although a true polymeric RSM seems currently unfeasible based on the state of research, we hope to give a first impression regarding the general feasibility, as well as the possible advantages and applications of such materials. Beyond, the achievable performance range of energetic polymers – even under non-optimized conditions, was demonstrated.

11.2 Experimental Section

The sensitivities of all described monomers and polymers toward impact and friction were assessed using a BAM (Bundesanstalt für Materialforschung) drop hammer according to STANAG 4489 modified instruction[9] and a BAM friction tester according to STANAG 4487 modified instruction.[10]

11.2.1 Monomer Synthesis

Next to TNPO (**1**), several well-known energetic oxetanes have been synthesized to prepare copolymers. These can be subdivided into two groups – organic azides including 3-azidooxetane (3AO, **2**), 3-azidomethyl-3-methyloxetane (AMMO, **3**) as well as 3,3-bis(azidomethyl)oxetane (BAMO, **4**) and organic nitrates which include 3-nitratomethyl-3-methyloxetane (NIMMO, **5**) and 3-azidomethyl-3-nitratomethyloxetane (AMNMO, **6**). Due to the extent, the synthetic procedures and assessed data for monomers **1**–**6** can be found in the Supporting Information (SI).

11.2.2 Polymer Synthesis

To ensure comparability, all polymers were prepared under the same conditions according to the following, general procedure. Experimental details, yields, and the assessed data can be found in the Supporting Information.

General Procedure:
A Schlenk round bottom flask (25 mL) was closed with a silicone rubber septum and thoroughly dried under a protective atmosphere (argon). An initiating mixture was prepared by the addition of butane-1,4-diol and boron trifluoride etherate (molar ratio 1:2) using a 100 µL Hamilton syringe. The mixture was stirred for 15 minutes and 30% of the total solvent volume (sulfolane-DCM (dry), 9:1) required to achieve a final monomer concentration of 2 mol L^{-1} was added. The residual volume (70%) was used to prepare a solution of TNPO (homopolymer) or an equimolar solution of the respective comonomers. Subsequently, the monomer solution was added using a syringe pump at different feed rates (see SI). The reaction mixture was then stirred for 48 hours at 250 rpm before quenching the polymerization reaction with water (1 mL). The resulting emulsion was vigorously stirred for five minutes and an excess of methanol (~20 mL) was added to precipitate the crude polymer which was allowed to settle. Afterward, the supernatant was decanted and the polymer was dissolved in a minimal amount of acetone and precipitated again using methanol (~20 mL). The polymer was then collected by centrifugation (20 min, 6000 rpm) and the supernatant was removed using a pipette. The purified polymer was transferred to a round bottom flask using acetone and all volatiles were removed by rotary evaporation. Afterward, the polymer was thoroughly dried under high vacuum conditions (0.1 Pa, 24 h) at 70 °C to afford yellow to orange, brittle solids.

11.2.3 Poly(AMNMO)

Since poly(AMNMO) was needed as a reference but is insufficiently described in the literature[11], it was prepared by a modified procedure and characterized in detail.

A Schlenk round bottom flask was closed with a silicone rubber septum and thoroughly dried under a protective atmosphere (argon). Boron trifluoride etherate (98.4 µL, 797 µmol, 0.1 equiv.) and butane-1,4-diol (35.2 µL, 398 µmol, 0.05 equiv.) were added using a 100 µL Hamilton syringe and the mixture was stirred for 15 minutes before the addition of dry dichloromethane (1.12 mL). Afterward, a solution of 3-azidomethyl-3-nitratomethyloxetane (1.50 g, 7.97 mmol) in dry dichloromethane (2.87 mL) was added over three hours using a syringe pump. The colorless reaction mixture was subsequently stirred for 48 hours at 250 rpm. The reaction was then quenched by the addition of water (0.5 mL) and vigorously stirred for five minutes. Afterward, methanol (15 mL) was added to precipitate the crude polymer which settled at the bottom of the flask as a colorless oil. The supernatant was removed using a pipette and the polymer dissolved in a minimal amount of acetone followed by the addition of methanol (15 mL) to precipitate the purified polymer. The supernatant was again removed and the polymer dried under high vacuum conditions (1 Pa, 25 °C, 2 d) to give 0.96 g (64%) of poly(AMNMO) as colorless (opaque), resin-like material.

^{1}H NMR (400 MHz, Acetone-d$_6$, 25 °C): δ = 4.70–4.54 (m, 2H, CH_2ONO_2), 3.70–3.39 (m, 6H, polymer backbone, CH_2N_3). **^{13}C{^{1}H} NMR** (101 MHz, Acetone-d$_6$, 25 °C): δ = 73.1, 70.7, 52.1, 45.3. **^{14}N NMR** (29 MHz, Acetone-d$_6$, 25 °C): δ = −43.3, −133.2. **FT-IR** (ATR, cm^{-1}): $\tilde{\nu}$ 3292 (vw), 3140 (vw), 2890 (w), 2102 (s), 1830 (vw), 1630 (vs), 1456 (m), 1272 (vs), 1100 (vs), 992 (s), 854 (vs), 752 (m), 702 (m), 646 (m), 552 (w). **Raman** (1075 nm, 1000 mW, cm^{-1}): $\tilde{\nu}$ = 2967 (96), 2938 (91), 2880 (100), 2834 (26), 2811 (26), 2109 (39), 1486 (35), 1465 (43), 1453 (43), 1279 (78), 1239 (52), 1044 (22), 942 (26), 928 (22), 869 (52), 653 (22), 622 (22), 614 (22), 604 (22). **EA** calcd. for $C_5H_8N_4O_4$ (188.1430 g mol^{-1}): C 31.92, H 4.29, N 29.78; found: C 33.08, H 4.14, N 27.96. **DSC** (5 °C min^{-1}): −31.0 °C (glass transition), 186.4 °C (dec.). **M$_n$** (calculated, MW (188 g mol^{-1}) · [M]/[I]): 3762 g mol^{-1}. **IS**: 7 J. **FS**: > 360 N.

11.3 Results and Discussion

11.3.1 Monomer Synthesis

All monomers were prepared according to literature, modified literature procedures, or common synthetic strategies (NIMMO) as depicted in Scheme 1.

The key monomer, TNPO (**1**), was prepared by the reaction of lithium oxetan-3-olate (formed *in situ)* with picryl chloride in THF to afford TNPO as yellow solid in 70% yield. If necessary, the crude product can be purified by recrystallization from hot chloroform.[8] Azidation of 3-tosyloxyoxetane using sodium azide in dry DMSO according to our recently published procedure gave 3-azidooxetane (**2**) as yellowish liquid.[12] To achieve purity suitable for polymerization, the crude product was distilled under reduced pressure to afford colorless 3AO in 60% yield. To prepare AMMO (**3**), 3-hydroxymethyl-3-methyloxetane was first mesylated in DCM using mesyl chloride and triethylamine as a base. After liquid-liquid-extraction, the crude product was azidated analogous to literature using sodium azide in water under reflux conditions and tetrabutylammonium bromide (TBAB) as catalyst.[13] To achieve sufficient purity, the crude compound was subject to vacuum distillation to afford 58% of colorless

AMMO. The same reaction conditions were applied for the literature-analogous [13] azidation of 3,3-bis(chloromethyl)oxetane (BCMO) to afford crude BAMO (**4**) in 81% yield as yellow liquid.

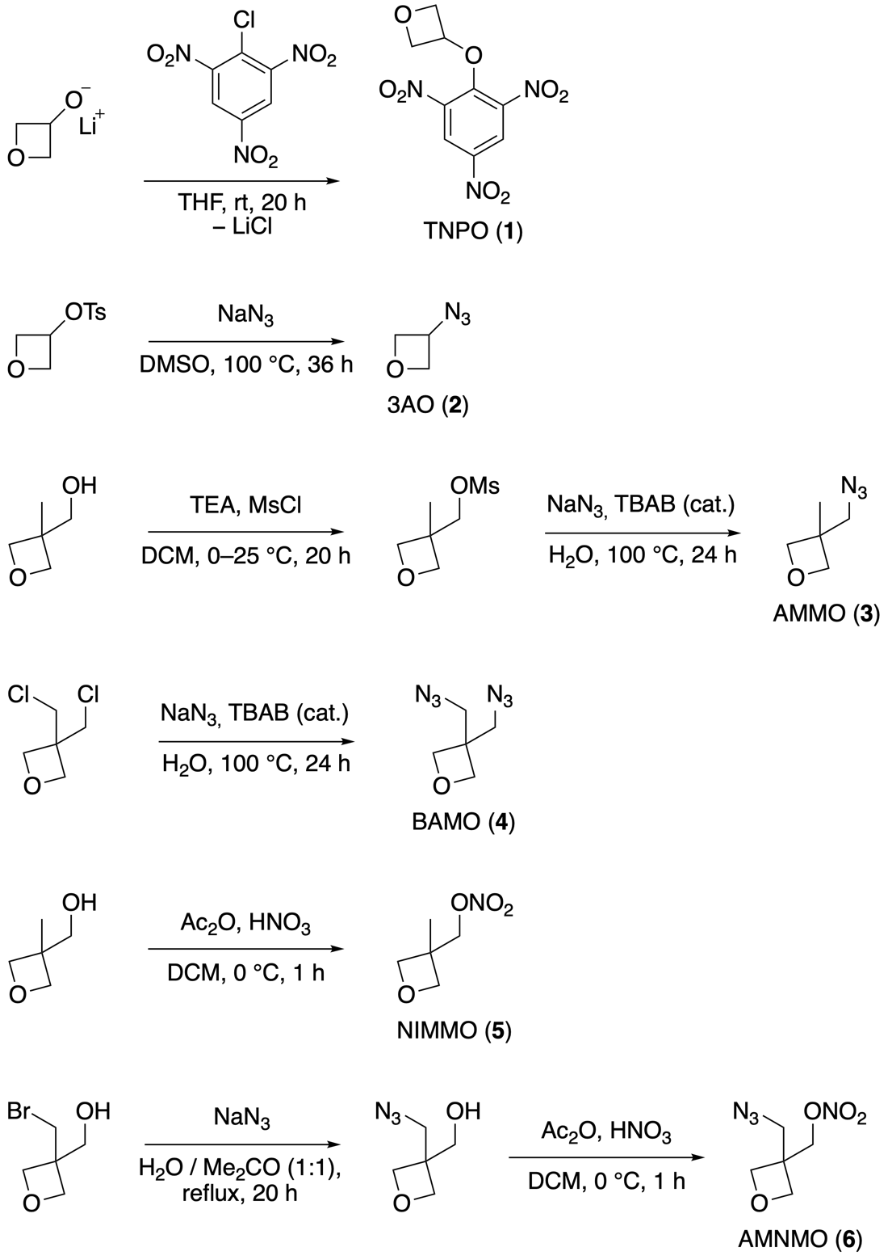

Scheme 11.1. Preparation of monomers **1**–**6**.

As before, the monomer was purified by vacuum distillation to give colorless BAMO with an overall yield of 70%. The organic nitrate NIMMO (**5**) was prepared by nitration of the corresponding alcohol in DCM using acetyl nitrate as a mild, cost-efficient nitrating agent. After liquid-liquid extraction, traces of acid and acetyl nitrate were fully removed using sodium bicarbonate solution to allow a safe purification by vacuum distillation to afford NIMMO as a colorless liquid in 52% yield. AMNMO (**6**) was obtained in a two-step process according to patent literature.[11] First, 3-bromomethyl-3-hydroxymethyloxetane (BMHMO) was azidated under reflux conditions using sodium azide and a 1:1 mixture of water and acetone to provide 3-azidomethyl-3-hydroxymethyloxetane as a yellow liquid. Subsequently, the crude compound was nitrated using acetyl nitrate in DCM. Again, sodium bicarbonate solution was used to ensure that the product is free of acid and acetyl nitrate after liquid-liquid extraction and before vacuum distillation. Ultimately, colorless AMNMO was obtained in 42% yield. Of all monomers purified by distillation, the purifying effect was the lowest in the case of AMNMO. We assume that the compound partially decomposes during vacuum distillation. Hence, the compound may be purified by column chromatography if a higher purity is required.

11.3.2 Polymer Synthesis

A boron trifluoride etherate polyol (butane-1,4-diol) initiating system was used to prepare all polymers by cationic ring-opening polymerization (CROP). This initiator is advantageous, as it allows chain propagation via the activated monomer mechanism (AMM) and thereby lowers the participation of the undesired activated chain end mechanism (ACE). In general, a high AMM participation significantly reduces side reactions such as backbiting or ring elimination. This in turn decreases the proportion of cyclic species to offer an improved end group functionality. Further, the AMM is known to provide improved molecular weight control and polydispersity.[14, 15]

Apart from the initiator system, the choice of solvent turned out to be problematic, as TNPO is sparingly soluble in typical, inert solvents for CROP such as dichloromethane or chlorobenzene. With these solvents, the desired monomer concentration of 2 mol L^{-1} was only achieved by slight heating and application of ultrasound before dosing of the monomer solution. Unfortunately, TNPO showed a high tendency to precipitate partially and thus clogged the feeding needle. As sulfolane is reported to have a rate accelerating effect on the CROP of 2-oxazolines[16], dissolves TNPO well, and may show similar effects in the case of oxetanes, it was chosen as an alternative. As the solvent dryness is of utmost importance for a successful CROP, sulfolane was dried in the molten state (30 °C) using calcium hydride under a protective atmosphere (argon). Afterward, it was distilled under high vacuum conditions (110 °C, 0.1 Pa) onto a molecular sieve using a protective atmosphere (argon). As sulfolane itself tends to solidify at room temperature, 10 vol% of dry dichloromethane was added. To ensure comparability of the reactions and to evaluate TNPO's polymerization behavior, its homo-polymer and all copolymers were prepared under the same conditions (see 2.2, SI). Unfortunately, electron-withdrawing substituents as in the case of TNPO lower the basicity of the oxetane oxygen atom which is crucial for a successful polymerization.[17] Further, we assumed steric hindrance during chain propagation due to the bulky, nitroaromatic motif. Hence, a quite low monomer to initiator ratio ([M]/[I] = 20) was used to ensure proper initiation, and a rather long reaction time of 48 hours was applied.

In the case of poly(TNPO) (Scheme 2), an initiator solution was prepared under dry conditions and a protective atmosphere according to the stated general procedure. Then, the intense yellow monomer solution was dosed uniformly using a syringe pump.

Scheme 11.2. Preparation of poly(TNPO) by cationic ring-opening polymerization.

After several hours, a continuous color change from yellow to orange was observed. After 48 hours, the solution had turned deep red. The polymerization was quenched with water, vigorously stirred for five minutes and the crude polymer was precipitated by the addition of excess methanol. Hereby, the polymer was obtained as a deep orange slurry at the bottom of the flask. The supernatant was removed and the crude polymer dried under high vacuum conditions (70 °C, 0.1 Pa, 24 h). Unfortunately, NMR spectroscopy (^1H) revealed larger traces of sulfolane, butane-1,4-diol (BDO), and TNPO. For further purification, the polymer was dissolved in the minimal amount of hot acetone and precipitated again with a large excess of methanol. A yellow to orange, homogeneous suspension was obtained and the polymer was collected by centrifugation (6000 rpm, 20 min). The supernatant was removed (pipette), and drying under high vacuum conditions (70 °C, 0.1 Pa, 24 h), gave poly (TNPO) (**P1**) as brittle, yellow solid with a satisfying yield of 70%. The copolymers **P2**–**P6** were obtained by copolymerization of TNPO with the azido comonomers 3AO (**P2**), AMMO (**P3**), BAMO (**P4**) as well as the organic nitrates NIMMO (**P5**) and AMNMO (**P6**) using identical conditions and a similar scale (Scheme 3).

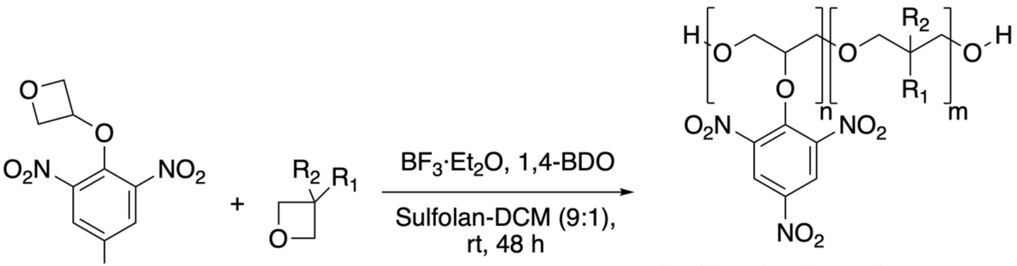

P2 ($R_1 = N_3$, $R_2 = H$)
P3 ($R_1 = CH_2N_3$, $R_2 = CH_3$)
P4 ($R_1 = R_2 = CH_2N_3$)
P5 ($R_1 = CH_2ONO_2$, $R_2 = CH_3$)
P6 ($R_1 = CH_2N_3$, $R_2 = CH_2ONO_2$)

Scheme 11.3. Preparation of copolymers **P2**–**P6** using TNPO and prior art energetic oxetanes as comonomers.

The respective comonomers were used in equimolar amounts to examine whether the stoichiometry is ultimately mirrored by the copolymers as deviations would indicate significantly different monomer reactivities. As in the case of **P1**, a notable color change from initially yellow over dark orange to dark red was observed during the polymerization. After quenching with water and the addition of excess methanol, copolymers **P2**–**P6** were obtained as dark orange slurries, which settled at the bottom of the flask. In each case, the supernatant was removed (pipette) and the crude polymer was analyzed by ^{1}H NMR spectroscopy. Again, an impurification with sulfolane, BDO, and larger quantities of TNPO was found. The latter can be explained by the fact that TNPO partially precipitates together with the polymer, while all other monomers represent liquids that easily migrate into the organic phase for their removal. For this reason, **P2**–**P6** were further purified as performed in the case of **P1**. After centrifugation and removal of the supernatant, the copolymers were transferred to another flask using acetone. Subsequently, the solvent was removed by rotary evaporation, and **P2**–**P6** were dried (70 °C, 0.1 Pa, 24 h) to give essentially orange, brittle solids with yields in the range of 46–83%.

Since we intended to study the influence of the TNPO repeating unit on the glass transition temperature of these copolymers, it was necessary to know the glass transition temperatures of the parent homopolymers. Unfortunately, the corresponding T_G is not literature-known in the case of **P6** as poly(AMNMO) (**P7**) has only been incompletely described in a patent.[11] As the stated polymerization conditions seemed inappropriate regarding monomer feeding and reaction time, we prepared **P7** using modified conditions (Scheme 4).

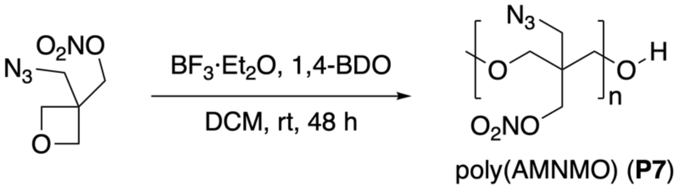

Scheme 11.4. Preparation of poly(AMNMO) using modified literature conditions.

Here, the monomer feeding duration, as well as the reaction time, was increased from 10 minutes and 17 hours to 3 hours and 48 hours, respectively. A monomer concentration of 2 mol L^{-1} instead of roughly 2.7 mol L^{-1}was employed, but the monomer to initiator ratio [M]/[I] of 20 was kept as well as the solvent which dissolves both monomer and polymer well.[11] Contrary to the information disclosed, the polymer was not obtained as colorless oil but rather as an opaque, colorless, and resin-like material with a yield of 64%, which is slightly below the claimed yield of 75%.

11.3.3 Polymer Characterization

11.3.3.1 Gel Permeation Chromatography

The molecular weight distribution of all polymers was assessed by gel permeation chromatography (GPC) using polystyrene standards and a HITACHI L-2350 instrument equipped with a RI and UV detector and a "PSS SDV combination low" column (100–60.000 Da). THF was employed as solvent at a flow rate of 1 mL min^{-1}. The evaluation was performed using the PSS WinGPC software. Subsequently, the experimentally determined average molecular weight M_n was compared to the theoretical average molecular weight (M_n (th.)). The latter was calculated based on the monomer to initiator ratio (20), the molecular weight of the repeating unit (MW_R), and the assumption that BDO (MW = 90.1 g mol^{-1}) acts as an initiator to become incorporated into the polymer chain (M_n (th.) = 20 · MW_R + 90.1 g mol^{-1}). The values of M_n, M_n (th.), the weighted average molecular weight M_W, and the corresponding polydispersities Đ for polymers **P1**–**P6** are summarized in Table 1.

Table 11.1. GPC results in comparison to calculated average molecular weights for polymers **P1**–**P6**.

Polymer	**M_n (th.)**[a]	**M_n**[b]	**M_W**[c]	**Đ**[d]
P1	5703	2008	4548	2.27
P2	7685	1995	4071	2.04
P3	8246	1352	4356	3.22
P4	9066	1768	4388	2.48
P5	8646	1586	2630	1.66
P6	9466	1530	4939	3.23

[a] Theoretical average molecular weight ([M]/[I] + 90.1). [b] Average molecular weight by GPC. [c] Weight average molecular weight by GPC. [d] Polydispersity (M_W/M_n).

Surprisingly, the actual molecular weights are far below expectation and unfortunately reveal the predominant formation of oligomers. Further, the polydispersities are rather high and linked to broad molecular weight distributions as can be seen in the corresponding GPC plots of **P1**–**P6** (Figure 1).

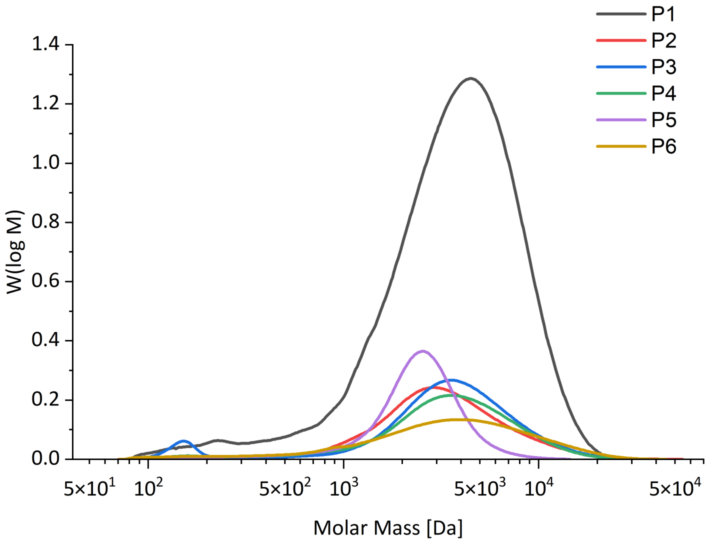

Figure 11.1. GPC analysis of poly(TNPO) (**P1**) and copolymers **P2**–**P6**.

These findings contradict a "living character" of the polymerization reactions and further indicate a high contribution of the ACE mechanism. These results can be largely explained by a very slow polymerization initiation. In this case, the monomers are added considerably faster than they are initiated to result in a propagating chain. Due to overdosing, the monomers are initiated when present in high concentration and cause a large number of chains to grow in parallel. This results in correspondingly short chains and high polydispersities as observed. This assumption was further supported by a brief screening experiment. As the highest molecular weight deviation and polydispersity was observed for **P6**, we dosed the monomer solution at three different feed rates according to Table 2.

Table 11.2. Dependence of molecular weight distribution and polydispersity on monomer addition time (**P6**).

Feed duration [h]	**M_n[a]**	**M_W[b]**	**Đ[c]**
1	972	19591	20.2
2	517	2209	4.28
6	1530	4939	3.23

[a] Average molecular weight by GPC. [b] Weight average molecular weight by GPC. [c] Polydispersity (M_W/M_n).

While a one-hour addition led to an extreme discrepancy of number and weight average molecular weight associated with a broad distribution, it was possible to reduce the polydispersity from 20.2 to 4.3 by doubling the addition time (2 hours). Further, the sixfold addition time (6 hours) resulted in improved convergence of M_n and M_W – but the additional decrease of polydispersity is rather limited. Overall, the data reveals a strong dependence of polydispersity and molecular weight control on the monomer feeding duration. This behavior further proves the initial assumption and can be explained by the existence of a so-called induction period leading to an undesired accumulation of monomers.[14] The effect was described by Kim et al. and is linked to the aggregation of BDO with boron trifluoride at the start of the monomer addition.[14,18] Aggregated initiators are thought to be less reactive[18,19] and can cause an uncontrolled favoring of the ACE mechanism to result in the formation of cyclic oligomers, a high polydispersity, and decreased hydroxy group functionality.[14] The fact that a considerably increased addition time only resulted in a slight improvement (Table 2) is consistent with the assumption of an induction period due to a reduced initiator activity. Ultimately, high participation of the ACE mechanism was confirmed by NMR spectroscopy (^{1}H, ^{13}C). In case of propagation through the AMM, BDO is incorporated into the polymer providing a distinctive signal in the proton spectrum (1.4–1.7 ppm)[20] and the carbon spectrum (~15 ppm). As these signals were not observed (see SI), chain propagation through the ACE mechanism is strongly indicated. However, improved results may be obtained by further adjustment of the polymerization conditions or the use of other initiators.

11.3.3.2 Polymer Constitution

If two monomers M_1 and M_2 shall form a copolymer (**P2**–**P6**), the chain sequence depends on their reactivity described by the corresponding reactivity ratios r_1 and r_2. Several important limiting cases can occur, first described by Mayo and Lewis.[21] If both reactivity ratios (r_1, r_2) are significantly larger than 1, both monomers solely react with themselves to form homopolymers. If both ratios are slightly larger than 1, homopolymerization is preferred (M_1 adds to M_1, M_2 adds to M_2), resulting in a block copolymer. If r_1 is significantly larger than 1, while r_2 is significantly below 1, M_1 adds faster to growing chains already terminated by M_1 to cause an increased M_1 content in the final polymer (composition drift). If r_1 and r_2 are close to 0, M_1 adds M_2 and vice versa to give a perfectly alternating chain. If both ratios are close to 1, a statistical copolymer is formed. Therefore, we analyzed the composition of the copolymers **P2**–**P6** to allow first conclusions to be drawn about the polymerization behavior of TNPO and the reactivity ratio. In this context, the composition was mainly studied via ^{1}H NMR spectroscopy as TNPO provides a very distinctive signal in the aromatic region (~9 ppm) which does not overlap with other signals. Here, the obtained integrals indicated very equal proportions of both monomers in each case with exception of **P5**. Here, the methyl group of NIMMO provided a distinctive signal (0.73–1.66 ppm) with an integral of only 2 indicating a slight composition toward an increased TNPO content. In addition, the copolymers were subject to elemental analysis. Here, the found contents for hydrogen, carbon, and nitrogen essentially matched the calculated compositions for 1:1 copolymers. However, it must be considered that polymers, in general, show higher deviations than monomers, thereby reducing the overall significance of the elemental analysis. Thermal analysis by DSC revealed only one glass transition temperature for **P2**–**P6** contradicting block copolymers. As both NMR spectroscopy (^{1}H) and elemental analysis revealed slight deviations from the ideal comonomer ratio (1:1), statistical copolymers are strongly indicated. Nevertheless, we can conclude that the polymerization behavior of TNPO is very comparable to the literature-known energetic oxetanes. Based on the obtained polymer constitutions, reactivity ratios close to 1 can be anticipated for all employed monomers.

11.3.3.3 Thermal Analysis

The thermal behavior of all polymers was assessed by differential scanning calorimetry at a heating rate of 5 °C min^{-1}. Before the measurement, these were stored at room temperature for three weeks to ensure the same thermal history. The highest decomposition temperature was found for poly(TNPO) which decomposes surprisingly early at 205 °C in comparison to the monomer which decomposes 253 °C. As expected, rather low decomposition temperatures were found for copolymers containing nitrato groups. Here, polymer **P5** decomposes at 185 °C, while **P6** decomposes even earlier at 183 °C. Unfortunately, equally low decomposition temperatures below 200 °C were assessed in the case of the azido-copolymers **P2**–**P4**. The lowest decomposition temperature was observed for **P2** (178 °C), followed by **P3** (184 °C) and **P4** (190 °C). Here, it is notable that **P5** and **P6** decompose at a marginally higher temperature than the corresponding comonomers NIMMO and AMNMO. Contrary to this, the decomposition temperatures of **P2**–**P4** are significantly lower than those of the corresponding comonomers 3AO, AMMO, and BAMO (see SI). Since the decomposition temperature is lowered by more than 4 °C compared to the respective azido-comonomers, a polymer-internal incompatibility of the azido motifs with the nitroaromatic TNPO motif is likely.[22] Further, all polymers have a stepwise, non-uniform decomposition with overlapping exothermic signals in common, while none of the polymers showed an exothermic signal attributable to a crystallization process. Therefore, all polymers are fully amorphous.

Most importantly, the influence of the TNPO repeating unit on the glass transition temperatures (T_G) of copolymers **P2–P6** was examined by comparing these with the glass transition temperatures of the corresponding parent polymers.[5,12,23,24]

Table 11.3. Glass transition temperature of the parent homopolymers (T_{G1}) versus T_G of the copolymers and calculated Gordon-Taylor-constants k.

Homopolymer	**T_{G1} [°C]**	**T_G copolymer**	**ΔT_G**	**k**
Poly(3AO)	−55[12]	25	80	0.73
Poly(AMMO)	−42[5]	1	43	0.31
Poly(BAMO)	−41[23]	23	64	0.94
Poly(NIMMO)	−25[24]	36	61	1.17
Poly(AMNMO)	−31	42	73	2.29

Here, the TNPO repeating unit showed a very dominating effect on the T_G and caused a drastic increase in all cases as desired (Table 3). The smallest shift of +43 °C was observed for poly(TNPO-*stat*-AMMO) (**P3**), while a tremendous shift of +80 °C was observed for poly(TNPO-*stat*-3AO) (**P2**). Very surprisingly, poly(TNPO) itself only shows a T_G of 63 °C, further emphasizing the considerable effect of the slightly bulky TNPO motif on the glass transition in the case of **P2**–**P6**.

As the glass transition temperatures of poly(TNPO) (T_{G2}) and the parent homopolymers of **P2**–**P6** (T_{G1}) are known, the T_G of copolymers with different compositions can be calculated using the Gordon-Taylor equation:[25]

$$T_{G\,\text{copolymer}} = \frac{w_1 T_{G1} + k w_2 T_{G2}}{w_1 + k w_2}$$

Here, w_1 and w_2 represent the mass fractions of the associated parent homopolymers. To determine the dimensionless Gordon-Taylor constant k, the equation was rearranged:

$$k = \frac{w_1 (T_G - T_{G1})}{w_2 (T_{G2} - T_G)} = \frac{MW_1 (T_G - T_{G1})}{MW_2 (T_{G2} - T_G)}$$

As equimolar monomer amounts were employed in the case of **P2**–**P6**, the mass fraction w_1/w_2 can be replaced by the monomer's molecular weight fraction (MW_1/MW_2). For instance, with $k = 0.73$, poly(TNPO-*stat*-3AO) comprising 0.05 mass fractions TNPO (w_2) and 0.95 mass fractions of 3AO (w_1) would roughly show a T_G of −51 °C.

Apart from calculations, our results indicate the feasibility of glass transition temperatures suitable for the envisioned purpose and bulky, energetic side groups will surely take a key role. Therefore, other bulky motifs that impose rigidity to the polymer chains, like energetic heterocycles (e.g., tetrazoles, pyrazoles), are a promising starting point for the development of suitable oxetane monomers. Beyond, an adjustable crosslinking of the chains should be implemented through functional side groups to allow tailoring of both T_G and mechanical properties.

11.3.4 Physicochemical and Energetic Properties

To consider energetic polymers as RSM, a performance at least equal to known, metal-based RSMs is required. Unfortunately, the performance of known energetic polyoxetanes (e.g., poly(AMMO), poly(NIMMO), poly(BAMO)) is very low. Foremost, this is attributed to their low density (1.17–1.25 g cm^{-3})[26] on which detonation velocity and detonation pressure strongly depend.[6] As polymer densities roughly match the monomer densities, TNPO offers a considerable energetic contribution to copolymers **P2**–**P6** with a high density of 1.70 g cm^{-3}. The polymer densities were determined by helium pycnometry on a Micromeritics AccuPyc II 1345 device. As expected, poly(TNPO) offers the highest density (1.62 g cm^{-3}), while the lowest was found for **P3** (1.46 g cm^{-3}). All other polymer densities range between 1.50 and 1.54 g cm^{-3}. Thereby, all densities are notably higher than in the case of the aforementioned polyoxetanes.

To calculate the performance of **P1**–**P6** using the EXPLO5V 6.04 code, the heats of formation were determined by bomb calorimetry using literature methods.[14,27] A Parr 6200 Isoperibol bomb calorimeter was employed and calibrated using benzoic acid (combustion enthalpy 26432±32.7 J g^{-1}).[28] Nitric acid formation was directly factored by the device. Tablets were prepared by dissolving the respective polymer and benzoic acid (ratio 3:10 by mass) in acetone, followed by careful rotary evaporation. The obtained solid was dried (drying cabinet, 48 h, 50 °C) and then ground until homogeneous. Subsequently, tablets were pressed (5 s, 3 tons) and again dried under the aforementioned conditions. Afterward, each tablet was burned in a pure oxygen atmosphere (3.5 MPa) on a platinum crucible. According to Hess' law, the heat of formation (HOF) is obtained as the difference between the HOF of the combustion products (CP) and the measured heat of combustion H_C:

$$\Delta H_f^0(polymer) = \Delta H_f^0(CP) - \Delta H_C(polymer)$$

The heat of formation of carbon dioxide and water is 393.52 kJ mol^{-1} and 241.83 kJ mol^{-1}, respectively.[29] Table 4 summarizes the obtained average values for H_C and the calculated heats of formation for **P1**–**P6**. Further details can be found in the Supporting Information. For all polymers, a positive heat of formation was found. As expected, the lowest HOF was found for **P5**, as it exhibits the least nitrogen content and additional carbon-hydrogen ballast is introduced by the NIMMO monomer. As the nitrato group of **P5** is formally replaced by an azido group, **P3** shows a significantly higher heat of formation (241.2 kJ mol^{-1}), closely followed by poly(TNPO) (281.2 kJ mol^{-1}). The HOF further increases in accordance with expectation from **P2** (426.7 kJ mol^{-1}) to **P6** (703.5 kJ mol^{-1}) and culminates with a value of 906.4 kJ mol^{-1} in case of **P4**, as it represents the by far most nitrogen-rich azido-polymer.

Table 11.4. Heat of combustion as determined by bomb calorimetry and calculated heat of formation for polymers **P1**–**P6**.

Polymer	$-H_C$ [kJ mol^{-1}]	HOF [kJ mol^{-1}]
P1	4669.3	281.2
P2	6599.9	426.7
P3	7685.1	241.2
P4	8229.4	906.4
P5	7452.1	8.2
P6	8026.5	703.5

Ultimately, we calculated the performance of **P1**–**P6** based on the assessed densities and heats of formation. Due to its comparatively low density and HOF, **P3** shows the lowest performance with a detonation velocity of only 6620 ms^{-1} and a detonation pressure of 17.5 GPa. With the most advantageous combination of HOF and density, **P2** and **P6** show the highest performances with detonation velocities of 7417 ms^{-1} and 7498 ms^{-1} next to detonation pressures of 23.5 GPa and 20.2 GPa, respectively. Therefore, with exception of **P3**, all polymers show a calculated performance comparable to (**P5**) or above TNT (EXPLO5 V6.04: $p_{C\text{-}J}$ 18.7 GPa, $D_{C\text{-}J}$ 6809 ms^{-1}) as a secondary explosive (Table 5). Hence, energetic polymers can indeed provide considerable performance and may offer a significant energetic contribution when employed as RSM.

The potential applicability of such materials is further supported by the found sensitivities toward mechanical stimuli such as impact and friction. These are rather low – even when TNPO was copolymerized with very sensitive monomers like BAMO or 3AO. According to the "UN recommendations on the transport of dangerous goods"[30], all polymers are "insensitive" toward friction (FS > 360 N) with exception of **P2** which is "sensitive" (FS < 360 N). Regarding impact sensitivity, poly(TNPO) (**P1**) can be classified as "insensitive", while polymers **P2**, **P3**, **P5,** and **P6** show impact sensitivities between 25 J and 30 J. Thus, they fall slightly short of the classification as "less sensitive" (IS ≥ 35 J) and have to be declared as "sensitive" (IS ≥ 4 J) despite their overall low impact sensitivity. According to expectation, copolymer **P4** shows the highest impact sensitivity (> 7 J) owing to the BAMO repeating unit and needs to be classified as "sensitive". With exception of **P4**, the overall sensitivity of the copolymers seems predominantly influenced by the high insensitivity of the TNPO monomer. This raises hope that a particularly insensitive but still high-performing monomer like TNPO can be copolymerized in high proportions with more performant, maybe more sensitive monomers to only cause a minor sensitivity increase.

Table 11.5. Important physicochemical and energetic properties of homopolymer **P1** and copolymers **P2**–**P6**.

	P1	**P2**	**P3**	**P4**	**P5**	**P6**
Formula	$C_9H_7N_3O_8$	$C_{12}H_{12}N_6O_9$	$C_{14}H_{16}N_6O_9$	$C_{14}H_{15}N_9O_9$	$C_{14}H_{16}N_4O_1$	$C_{14}H_{15}N_7O_1$
FW [$g \cdot mol^{-1}$]	285.17	384.26	412.31	453.33	432.29	473.31
IS[a] [J]	40	25	25	> 7	30	30
FS[b] [N]	> 360	324	> 360	> 360	> 360	> 360
N, O[c] [%]	14.7, 44.9	21.9, 37.5	20.4, 34.9	27.8, 31.8	12.9, 44.4	20.7, 40.6
Ω[d] [%]	−75.7	−28.5	−104.8	−93.5	−88.8	−79.4
T_G[e]/ T_{dec}[f] [°C]	63.0, 204.6	25.2, 177.6	0.7, 183.6	23.4, 190.0	36.0, 185.1	42.4, 183.0
ρ[g] [$g \cdot cm^{-3}$]	1.62	1.54	1.46	1.50	1.51	1.54
ΔH_f°[h] [$kJ \cdot mol^{-1}$]	281.2	426.7	241.1	906.4	8.1	703.5
EXPLO5 V6.04						
$-\Delta_E U^\circ$[i] [$kJ \cdot kg^{-1}$]	5794	4686	4713	5555	5168	6091
$T_{C\text{-}J}$[j] [K]	3907	3373	3147	3607	3362	3800
$p_{C\text{-}J}$[k] [GPa]	22.0	23.5	17.5	19.4	18.4	20.2
$D_{C\text{-}J}$[l] [$m \cdot s^{-1}$]	7197	7417	6620	7056	6817	7498
V_0[m] [$dm^3 \cdot kg^{-1}$]	658	704	701	720	706	728

[a] Impact sensitivity (BAM drop hammer, method 1 of 6). [b] Friction sensitivity (BAM friction apparatus, method 1 of 6). [c] Nitrogen and oxygen content. [d] Oxygen balance based on CO formation. [e] Glass transition temperature (DSC, $\beta = 5\ °C \cdot min^{-1}$). [f] Decomposition temperature (DSC, $\beta = 5\ °C \cdot min^{-1}$). [g] Density at 298 K (helium pycnometry). [h] Standard molar enthalpy of formation. [i] Detonation energy. [j] Detonation temperature. [k] Detonation pressure. [l] Detonation velocity. [m] Volume of detonation gases at standard temperature and pressure.

11.4 Conclusion

As energetic binder research has mainly focused on elastic polymers with the lowest possible glass transition temperature, the development of polymers suitable as RSM is likely to be a long path with major obstacles. This can be attributed to the lack of suitable monomers and not least to the requirements for a viable polymer such as high thermostability and performance, low sensitivity, high glass transition temperature, mechanical strength, and processability by common polymer techniques. Of course, copolymerization of TNPO with prior art monomers unsuitable for the intended purpose cannot meet these requirements. Nevertheless, our results allow interesting conclusions to be drawn. For instance, simple but slightly bulky motifs like TNPO already provide notably high glass transition temperatures. Especially, the equimolar copolymerization of TNPO with prior art monomers designed to provide binders of low glass transition temperature revealed its dominant effect. In the case of **P2**, a tremendous shift of +80 °C was observed in comparison to the parent homopolymer poly(3-azidooxetane). Thus, it can be assumed that bulky monomers similar to TNPO can easily provide the desired, high glass transition temperatures. In particular, energetic heterocycles (e.g., pyrazoles, tetrazoles) may offer a valuable contribution. At first glance, the fact that we only obtained oligomers with also high polydispersity seems very disadvantageous. However, a reduced initiator activity was identified as the main cause. The basic phenomenon is known to literature, and improved results are likely using other polymerization initiators. Nevertheless, as all copolymers essentially reflect the intended 1:1 comonomer ratio, no indication is given that sterically more demanding motifs such as TNPO suffer from a reduced polymerizability. Apart from this, the performance of the investigated polymers appears very promising for the envisioned use of such materials as RSM. In this context, performances in the range of TNT were obtained even under non-optimized conditions. Thus, energetic polymers as reactive structure materials could provide a significant energetic contribution to increasing the blast effect of various ammunitions and effector systems. In addition, the rather high performance was linked to very acceptable sensitivities. Copolymerization of the insensitive TNPO monomer with more sensitive but also more performant monomers led to an almost negligible increase of the friction sensitivity, while the increase in shock sensitivity was found to be more pronounced. Overall, polymer-based RSMs may provide a favorable balance between performance and sensitivity – especially when insensitive but rather powerful monomers such as TNPO partially compensate for the higher sensitivity of higher-performing comonomers. Nevertheless, to achieve any substantial progress in the intended direction, the development of new, suitable monomers is of utmost importance. These should be designed to allow the formation of rigid polymer chains and semi-crystalline polymers. Exhibiting a melting point would allow processing techniques from injection molding to 3D printing. Even though the development of viable polymers appears challenging, we consider their development as reasonable, given the manifold advantages. Among others, these include a high weight reduction compared to metal-based RSMs, a high performance, independence from atmospheric oxygen, broad applicability, and the possibility to obtain energetic, technical components by common processing techniques. Therefore, we hope that the concept will find sufficient appeal to provide an impetus for more focused research in this area.

Abbreviations

DCM, dichloromethane; DMSO, dimethyl sulfoxide; TEA, trimethylamine; THF, tetrahydrofuran; TNT, 2,4,6-trinitrotoluene.

Acknowledgements

Financial support by the Ludwig Maximilian University of Munich (LMU), the Office of Naval Research (ONR) under grant no. ONR N00014-19-1-2078 and the Strategic Environmental Research and Development Program (SERDP) under contract no. W912HQ19C0033 is gratefully acknowledged. Beyond, we want to thank Stefan Huber for the sensitivity testing and Elena Reinhardt for her great efforts regarding bomb calorimetry. Open Access funding enabled and organized by Project DEAL.

References

[1] Hastings, D. L.; Dreizin, E. L. Reactive Structural Materials: Preparation and Characterization. *Adv. Eng. Mater.* **2018**, *20*, 1700631.

[2] Lee, R. J.; Mock, W.; Carney, J. R.; Holt, W. H.; Pangilinan, G. I.; Gamache, R. M.; Boteler, J. M.; Bohl, D. G.; Drotar, J.; Lawrence, G. W. Reactive Materials Studies. *AIP Conference Proceedings* **2006**, *845*, 169-174.

[3] Bogdan, Z. Explosive Properties of the Mg-Al/PTFE Composition. *Chin. J. Energ. Mater.* **2007**,*15*, 592-596.

[4] Born M.; Dosch, D. Energetische Polymere als reaktive Strukturmaterialien zur Verwendung für Waffensysteme, DE 10 2011 118 462 B4, **2011**.

[5] Ang, H. G.; Pisharath, S. *Energetic Polymers: Binders and Plasticizers for Enhancing Performance*; Wiley-VCH: Weinheim, **2012**.

[6] Klapötke, T. M. *Chemistry of High-Energy Materials*; 5th ed.; DeGruyter: Boston, **2019**.

[7] Wang, R.-M.; Zheng, S.-R.; Zheng, Y.-P. In *Polymer Matrix Composites and Technology*; Wang, R.-M., Zheng, S.-R., Zheng, Y.-P., Eds.; Woodhead Publishing: Sawston, UK, **2011**; pp 101-548. DOI 10.1533/9780857092229.1.101

[8] Born, M.; Voggenreiter, M. New energetic oxetane monomers based on nitroaromatic scaffolds. In *Proceedings of the 22th Seminar on New Trends in Research of Energetic Materials (NTREM)*, Pardubice, Czech Republic, April 10–12, **2019**.

[9] NATO STANAG 4489: *Explosives. Impact Sensitivity Tests*; NATO Standardization Office, Brussels, Belgium, **1999**.

[10] NATO STANAG 4487: Explosives. *Friction Sensitivity Tests*; NATO Standardization Office, Brussels, Belgium, **2002**.

[11] Manser, G. E.; Malik, A. A.; Archibald, T. G. 3-Azidomethyl-3-Nitratomethyloxetane, US 5 489 700, **1996**.

[12] Born, M.; Karaghiosoff, K.; Klapötke, T. M. A GAP Replacement: Improved Synthesis of 3-Azidooxetane and Its Homopolymer Based on Sulfonic Acid Esters of Oxetan-3-ol. *J. Org. Chem.* **2021**, *86*, 12607-12614.

[13] Mukhametshin, T. I.; Petrov, A. I.; Kuznetsova, N. V.; Petrov, V. A.; Averianova, N. V.; Garaev, I. K.; Kostochko, A. V.; Gubaidullin, A. T.; Vinogradov, D. B.; Bulatov, P. V. Synthesis and copolymerization of azidomethyl-substituted oxetanes: the morphology of statistical block copolymers. *Chem. Heterocycl. Compd.* **2017**, *53*, 811-821.

[14] Hafner, S. Internal plasticized glycidyl azide copolymers for energetic solid propellant binders, Ph.D. Dissertation, Ludwig-Maximilian University (LMU) Munich, Munich, Germany, **2019**.

[15] Penczek, S. Cationic ring-opening polymerization (CROP) major mechanistic phenomena. *J. Polym. Sci.* **2000**, *38*, 1919-1933.

[16] Vergaelen, M.; Verbraeken, B.; Monnery, B. D.; Hoogenboom, R. Sulfolane as Common Rate Accelerating Solvent for the Cationic Ring-Opening Polymerization of 2-Oxazolines. *ACS Macro Lett.* **2015**, *4*, 825-828.

[17] Dreyfuss, M. P.; Dreyfuss, P. Oxetane Polymers. In *Encyclopedia of Polymer Science and Technology*, (Ed.), John Wiley & Sons: Hoboken, New Jersey, **2011**. DOI 10.1002/0471440264.pst520

[18] J. S. Kim, J. O. Kweon, S. T. Noh, Online monitoring of reaction temperature during cationic ring opening polymerization of epichlorohydrin in presence of BF3 and 1,4-butanediol, *J. Appl. Polym. Sci.* **2014**, *131*, 39912.

[19] Kim, J. S.; Kim, D. K.; Kweon, J. O.; Lee, J. M.; Noh, S. T.; Kim, S. Y. The influence of initiator Diol-BF3 complex solubility and other factors on the induction period in BF3 catalyzed cationic ring opening polymerization of epichlorohydrin. *Macromol. Res.* **2014**, *22*, 436-444.

[20] Barbieri, U.; Keicher, T.; Polacco, G. Homo- and copolymers of 3-tosyloxymethyl-3-methyl oxetane (TMMO) as precursors to energetic azido polymers. *e-Polymers* **2009**, *9*, 565.

[21] Mayo, F. R.; Lewis, F. M. Copolymerization. I. A Basis for Comparing the Behavior of Monomers in Copolymerization; The Copolymerization of Styrene and Methyl Methacrylate. *J. Am. Chem. Soc.* **1944**, *66*, 1594-1601.

[22] NATO STANAG 4147: *Chemical compatibility of ammunition components with explosives (non-nuclear applications)*, NATO Standardization Office, Brussels, Belgium, **2001**.

[23] Cheradame, H.; Andreolety, J. P.; Rousset, E. Synthesis of polymers containing pseudohalide groups by cationic polymerization, 1. Homopolymerization of 3,3-bis(azidomethyl)oxetane and its copolymerization with 3-chloromethyl-3-(2,5,8-trioxadecyl)oxetane. *Makromol. Chem.* **1991**, *192*, 901-918.

[24] Colclough, M. E.; Desai, H.; Millar, R. W.; Paul, N. C.; Stewart, M. J.; Golding, P. Energetic polymers as binders in composite propellants and explosives. *Polym. Adv. Technol.* **1994**, *5*, 554-560.

[25] Gordon, M.; Taylor, J. S. Ideal copolymers and the second-order transitions of synthetic rubbers. i. non-crystalline copolymers. *J. Appl. Chem.* **1952**, *2*, 493-500.

[26] Köhler, J.; Meyer, R.; Homburg, A. *Explosives*; 10th ed.; Wiley-VCH: Weinheim, **2008**.

[27] Axthammer, Q. J.; Evangelisti, C.; Klapötke, T. M. Characterization, bomb calorimetric measurements and quantum chemical calculations of high energetic dense oxidizers (HEDO). In *44th International Annual Conference of the Fraunhofer ICT, Energetic Materials – Past, Present and Future*, Karlsruhe, Germany, June 25–28, **2013**.

[28] Linstrom, P. J.; Mallard, W. G., Eds., *NIST Chemistry WebBook, NIST Standard Reference Database Number 69*; National Institute of Standards and Technology: Gaithersburg MD; https://webbook.nist.gov (accessed 2021-10-01).

[29] Chase, M. W. NIST-JANAF Thermochemical Tables, Fourth Edition, *J. Phys. Chem. Red. Data, Monograph 9,* **1998**, 1–1951.

[30] United Nations (UN), UN Recommendations on the Transport of Dangerous Goods, Manual of Tests and Criteria, **2009**.

11.5 Supporting Information

11.5.1 Experimental Part

General information

Caution! All prepared monomers and polymers are energetic materials with sensitivity toward stimuli like shock, friction, and electric discharge. Therefore, proper security measures (safety glasses, face shield, earthed shoes and equipment, Kevlar gloves, ear plugs) have to be taken while preparing and handling these compounds.

Chemicals and solvents were employed as received (Sigma-Aldrich, Acros, TCI, Fischer Scientific, Spirochem AG). ^{1}H, ^{13}C and ^{14}N spectra were recorded on a Bruker AMX 400 instrument. The chemical shifts refer to tetramethylsilane (^{1}H, ^{13}C) and nitromethane (^{14}N). Decomposition temperatures were determined on a Mettler Toledo DSC822e device at a heating rate of 5 °C min^{-1} using 40 µL aluminum crucibles and nitrogen purge gas at a flow rate of 30 mL min^{-1}. DSC evaluations of thermal behavior were performed using the STARe Software Version 16.20. Infrared (IR) spectra were measured on a Perkin-Elmer Spektrum One FT-IR device. Raman spectra were obtained using a Bruker MultiRam FT spectrometer and a neodymium-doped yttrium aluminum garnet (Nd:YAG) laser (λ = 1064 nm, P = 1074 mW). Elemental analyses were performed with an Elementar Vario el by sample pyrolysis and subsequent gas analysis. Molecular weight distributions were measured by gel permeation chromatography (GPC) using a HITACHI L-2350 device equipped with a RI as well as an UV detector featuring a “PSS SDV combination low” column (100–60.000 Da). THF was used as solvent at a flow rate of 1.0 mL min^{-1}. Polystyrene standards were employed for calibration and evaluation was performed using the PSS WinGPC software. The polymer density was determined by helium pycnometry using a Micromeritics AccuPyc II 1345 device. The sensitivity data was collected by means of a BAM (Bundesanstalt für Materialforschung) drop hammer according to STANAG 4489 modified instruction[1] as well as a BAM friction tester according to STANAG 4487 modified instruction.[2] The classification of the tested compounds is based on the 'UN Recommendations on the Transport of Dangerous Goods'.[3]

11.5.1.1 Monomer synthesis

3-(2,4,6-Trinitrophenoxy)oxetane (TNPO, 1)

TNPO was prepared as described in literature.[4]

Oxetan-3-ol (2.24 g, 30.3 mmol, 1.5 equiv.) was dissolved in tetrahydrofuran (7 mL) and the solution added to a suspension of lithium hydride (241 mg, 30.3 mmol, 1.5 equiv.) in tetrahydrofuran (14 mL). The suspension was stirred for 20 minutes at 0 °C using an ice bath and a solution of picryl chloride (5.00 g, 20.2 mmol, 1.0 equiv.) in tetrahydrofuran (7 mL) was added over a period of five minutes. After 20 minutes, the ice bath was removed and the reaction mixture was stirred overnight at room temperature. Afterward, the mixture was poured onto crushed ice (200 g) which was allowed to melt. The obtained precipitate was collected by suction filtration, washed with cold water and dried in air to give 4.04 g (14.2 mmol, 70%) of 3-(2,4,6-trinitrophenoxy)oxetane as yellow solid.

^{1}H NMR (400 MHz, $CDCl_3$, 25 °C): δ = 8.91 (s, 2H, $CH_{arom.}$), 5.17 (p, *J* = 6.1 Hz, 1H, CH), 4.95 (m, 4H, CH_2). **^{13}C{^{1}H}** NMR (101 MHz, $CDCl_3$, 25 °C): δ = 150.2, 144.7, 142.1, 124.4, 82.3, 78.6. **^{14}N NMR** (29 MHz, $CDCl_3$, 25 °C): δ = −23.0 (NO_2). **FT-IR** (ATR, cm^{-1}): ṽ = 3098 (w), 3000 (w), 2887 (w), 1611 (m), 1600 (s), 1547 (s), 1532 (vs), 1379 (m), 1339 (vs), 1307 (m), 1271 (s), 1090 (s), 1074 (s), 959 (s), 946 (s), 934 (m), 924 (m), 917 (m), 878 (s), 794 (m), 750 (m), 709 (s), 689 (s), 689 (s), 529 (m). **Raman** (1064 nm, 1074 mW, cm^{-1}): ṽ = 2988 (19), 2963 (16), 2924 (12), 2884 (11), 1613 (48), 1549 (52), 1474 (11), 1368 (96), 1343 (100), 1310 (13), 1276 (29), 1177 (12), 1117 (9), 1089 (11),h 1075 (11), 1027 (9), 961 (8), 946 (19), 934 (20), 826 (32), 751 (8). **EA** calcd. for $C_9H_7N_3O_8$ (285.17 g mol^{-1}): C 37.91, H 2.47, N 14.74%; found: C 37.74, H 2.47, N 14.62%. **MS** (EI) m/z: $[M]^+$ calcd. for $C_9H_7N_3O_8$ 285.0233; found 255.0234 $[C_8H_5N_3O_7]^+$, 166.0070 $[C_6H_2N_2O_4]^+$, 120.0132 $[C_6H_2NO_2]^+$, 74.0119 $[C_6H_2]^+$, 57.0257 $[C_3H_5NO]^+$. **DSC** (T_{onset}, 5 °C min^{-1}): 95.1 °C (m.p.), 253.5 °C (dec.). **BAM drop hammer** > 40 J. **Friction test** > 360 N.

3-Azidooxetane (3AO, 2)

3AO was prepared according to our recently published procedure.[5]

Oxetan-3-yl 4-methyl-benzenesulfonate (4.56 g, 20.0 mmol, 1.0 equiv.) and sodium azide (1.95 g, 30.0 mmol, 1.5 equiv.) were suspended in dry DMSO (6 mL) and the reaction heated to 100 °C for 36 hours in a closed (silicone rubber septum) round bottom flask. Afterward, the reaction mixture was poured into saturated sodium chloride solution (75 mL) and the aqueous phase extracted with a 2:1 mixture of diethyl ether and ethyl acetate (5 × 25 mL). The combined organic phases were then washed with saturated sodium chloride solution (3 × 30 mL) and dried over sodium sulfate. The solvent was removed by rotary evaporation to give 1.47 g (14.8 mmol, 74%) of 3-azidooxetane as yellowish liquid. Afterward, the compound was subjected to vacuum distillation (75 °C, 10 mbar) to give 1.19 g (12.01 mmol, 60%) of 3-azidooxetane as colorless liquid.

^{1}H NMR (400 MHz, $CDCl_3$, 25 °C): δ = 4.84 (ddd, *J* = 6.8, 5.8 Hz, 2H, CH_2), 4.62 (ddd, 2H, CH_2), 4.55 (m, 1H, CH). **^{13}C{^{1}H} NMR** (101 MHz, $CDCl_3$, 25 °C): δ = 77.2, 54.6. **^{14}N NMR** (29 MHz, $CDCl_3$, 25 °C): δ = −135.8 (N_β), −164.1 (N_γ), −305.0 (N_α). **FT-IR** (ATR, cm^{-1}): ṽ = 2961 (w), 2880 (w), 2097 (vs), 1359 (m), 1310 (m), 1260 (s), 1062 (w), 1044 (w), 974 (s), 924 (m), 852 (m), 751 (w), 553 (m), 405 (w). **Raman** (1064 nm, 1074 mW, cm^{-1}): ṽ = 2973 (12), 2932 (9), 2886 (15), 2253 (48), 2107 (4), 1482 (4), 1264 (4), 1164 (3), 930 (7), 911 (6), 736 (15), 649 (100). **EA** calcd. for $C_3H_5N_3O$ (99.09 g mol^{-1}): C 36.36, H 5.09, N 42.21%; found: C 36.48, H 4.99, N 43.02%. **MS** (EI) m/z: $[M]^+$

calcd. for $C_3H_5N_3O$ 99.0433; found 57.13 $[C_3H_5O]^+$. **DSC** (T_{onset}, 5 °C min^{-1}): 139.7 °C (b.p.), 189.9 °C (dec.). **BAM drop hammer** 3 J; **Friction test** > 192 N.

3-Azidomethyl-3-methyloxetane (AMMO, 3)

AMMO was prepared step-wise by mesylation of (3-methyloxetan-3-yl)methanol followed by a literature-analogous azidation reaction.[6]

(3-Methyloxetan-3-yl)methanol (6.00 g, 58.8 mmol) was dissolved in dichloromethane (150 mL) and triethylamine (7.14 g, 70.6 mmol, 1.2 equiv.) was added. The solution was cooled to 0 °C by means of an ice bath and methanesulfonyl chloride (7.38 g, 64.4 mmol, 1.1 equiv.) was added portion wise over a period of 10 minutes under vigorous stirring. The formation of a colorless precipitate was observed. The reaction mixture was subsequently stirred overnight at room temperature. The suspension was washed with 2 M hydrochloric acid (3 × 30 mL) and saturated sodium bicarbonate solution (3 × 30 mL). After drying over sodium sulfate, the solvent was evaporated to give 9.41 g (52.2 mmol, 89%) of (3-methyloxetan-3-yl)methyl methanesulfonate as slightly orange liquid which was added to a solution of sodium azide (6.79 g, 104 mmol, 2.0 equiv.) and a catalytic amount of tetrabutylammonium bromide (0.10 g, 0.31 mmol, 0.01 equiv.) in water (100 mL). The reaction mixture was refluxed for 24 hours, allowed to cool to room temperature and extracted with dichloromethane (3 × 30 mL). The combined organic phases were dried over sodium sulfate and the solvent evaporated to give 5.18 g (40.7 mmol, 78%) of crude 3-azidomethyl-3-methyloxetane as yellowish liquid. For purification, the material was distilled under vacuum conditions (10 mbar, 80 °C) to give 3.87 g (30.4 mmol, 58%) of 3-azidomethyl-3-methyloxetane as colorless liquid.

^{1}H NMR (400 MHz, $CDCl_3$, 25 °C): δ = 4.42 (d, J = 6.1 Hz, 2H, CH_2), 4.35 (d, J = 6.1 Hz, 2H, CH_2), 3.51 (s, 2H, CH_2N_3), 1.31 (s, 3H, CH^3). **^{13}C{^{1}H} NMR** (101 MHz, $CDCl_3$, 25 °C): δ = 80.1, 58.5, 40.2, 21.7. **^{14}N NMR** (29 MHz, $CDCl_3$, 25 °C): δ = −133.1 (N_β), −171.8 (N_γ), −315.7 (N_α). **FT-IR** (ATR, cm^{-1}): $\tilde{\nu}$ = 2965 (w), 2934 (w), 2870 (m), 2161 (w), 2152 (w), 2094 (vs), 1454 (w), 1448 (w), 1382 (w), 1345 (w), 1302 (m), 1270 (m), 978 (s), 944 (m), 833 (m), 689 (w), 555 (w), 419 (w). **Raman** (1064 nm, 1074 mW, cm^{-1}): $\tilde{\nu}$ = 2932 (70), 2878 (100), 2745 (3), 2101 (15), 1490 (18), 1451 (14), 1351 (4), 1281 (6), 1254 (6), 1179 (9), 1146 (9), 994 (14), 940 (6), 890 (6), 832 (11), 630 (5), 460 (7). **EA** calcd. for $C_5H_9N_3O$ (127.15 g mol^{-1}): C 47.23, H 7.14, N 33.05%; found: C 47.19, H 7.07, N 32.47%. **MS** (EI) m/z: $[M]^+$ calcd. for $C_5H_9N_3O$ 127.0746; found 98.0599 $[C_3H_4N_3O]^+$, 82.065 $[C_3H_4N_3]^+$, 68.0494 $[C_4H_2N_3]^+$, 56.0494 $[CH_2N_3]^+$. **DSC** (T_{onset}, 5 °C min^{-1}): 177.9 °C (b.p.). **BAM drop hammer** > 40 J. **Friction test** > 360 N.

3,3-Bis(azidomethyl)oxetane (BAMO, 4)

BAMO was prepared according to a modified literature procedure.[6]

Sodium azide (1.89 g, 29.1 mmol, 3.0 equiv.) and a catalytic amount of tetrabutylammonium bromide (50.0 mg, 0.16 mmol, 0.02 equiv.) were dissolved into water (3.6 mL). 3,3-

Bis(chloromethyl)oxetane (1.50 g, 9.68 mmol) was added portion wise under vigorous stirring. Afterward, the reaction mixture was set to reflux overnight. After cooling to room temperature, the solution was extracted with dichloromethane (3 × 30 mL). The combined organic phases were washed with water (3 × 30 mL) and dried over sodium sulfate. The solvent was removed by rotary evaporation to give 1.32 g (7.85 mmol, 81%) as yellowish liquid which was purified by vacuum distillation (1×10^{-2} mbar, 70 °C) to give 1.14 g (6.78 mmol, 70%) of 3,3-bis(azidomethyl)oxetane as colorless liquid.

^{1}H NMR (400 MHz, $CDCl_3$, 25 °C): δ = 4.38 (s, 4H, CH_2), 3.67 (s, 4H, CH_2N_3). **^{13}C{^{1}H} NMR** (101 MHz, $CDCl_3$, 25 °C): δ = 76.4, 54.2, 43.4. **^{14}N NMR** (29 MHz, $CDCl_3$, 25 °C): δ = −133.9 (N_β), −170.8 (N_γ), −319.8 (N_α). **FT-IR** (ATR, cm^{-1}): $\tilde{\nu}$ = 2946 (w), 2877 (w), 2090 (vs), 1448 (m), 1365 (w), 1348 (w), 1276 (s), 1143 (w), 1102 (w), 980 (s), 933 (m), 838 (m), 735 (m), 703 (w), 648 (w), 554 (m), 528 (w), 499 (w). **Raman** (1064 nm, 1074 mW, cm^{-1}): $\tilde{\nu}$ =2986 (48), 2940 (91), 2884 (100), 2107 (43), 1490 (35), 1451 (35), 1349 (13), 1283 (22), 1266 (22), 1252 (17), 1245 (17), 1160 (22), 1144 (22), 994 (26), 971 (22), 940 (13), 915 (22), 836 (17), 705 (17). **EA** calcd. for $C_5H_8N_6O$ (168.16 g mol^{-1}): C 35.71, H 4.80, N 49.98%; found: C 34.59, H 4.65, N 47.62%. **MS** (EI) m/z: $[M]^+$ calcd. for $C_5H_8N_4O_4$ 168.0670; found 70.0451 $[C_4H_6O]^+$, 68.0494 $[C_2H_2N_3]^+$, 56.0494 $[CH_2N_3]^+$. **DSC** (T_{onset}, 5 °C min^{-1}): 207.3 °C (dec.). **BAM drop hammer** > 40 J. **Friction test** > 360 N.

3-Nitratomethyl-3-methyloxetane (NIMMO, 5)

Acetic anhydride (1.32 g, 12.9 mmol, 1.3 equiv.) and white fuming nitric acid (0.74 g, 11.7 mmol, 1.2 equiv.) were added to a round bottom flask while cooling with an ice-salt bath keeping the temperature below 5 °C. The mixture was stirred for 10 minutes prior to the slow addition of a solution of (3-methyloxetan-3-yl)methanol (1.00 g, 9.79 mmol) in dichloromethane (4 mL). The reaction mixture was stirred at 0 °C for one hour. Subsequently, the solution was allowed to reach room temperature and was washed with saturated sodium bicarbonate solution (3 × 30 mL) and saturated sodium chloride solution (30 mL). The organic phase was dried over sodium sulfate and the solvent removed by rotary evaporation. Saturated sodium bicarbonate solution (50 mL) was added to the obtained liquid and the emulsion was vigorously stirred for one hour. The target compound was extracted with dichloromethane (3 × 30 mL) and the combined organic phases were dried over sodium sulfate. The solvent was removed by rotary evaporation to give 0.96 g (6.52 mmol, 67%) of crude product. The yellow liquid was subjected to vacuum distillation (14 mbar, 100 °C) to give 0.75 g (5.10 mmol, 52%) of NIMMO as colorless liquid.

^{1}H NMR (400 MHz, $CDCl_3$, 25 °C): δ = 4.57 (s, 2H, CH_2ONO_2), 4.48 (d, J = 6.3 Hz, 2H, CH_2), 4.39 (d, J = 6.3 Hz, 2H, CH_2), 1.36 (s, 3H, CH_3). **^{13}C{^{1}H} NMR** (101 MHz, $CDCl_3$, 25 °C): δ = 79.3, 77.2, 38.6, 20.9. **^{14}N NMR** (29 MHz, $CDCl_3$, 25 °C): δ = −42.7 (NO_2). **FT-IR** (ATR, cm^{-1}): $\tilde{\nu}$ = 2969 (w), 2941 (w), 2877 (w), 2103 (w), 1735 (vw), 1623 (vs), 1455 (w), 1374 (w), 1280 (s), 1263 (s), 1144 (w), 1021 (w), 1002 (w), 979 (s), 863 (s), 837 (s), 758 (m), 726 (m), 648 (w), 607 (m). **Raman** (1064 nm, 1074 mW, cm^{-1}): $\tilde{\nu}$ = 2953 (66), 2938 (76), 2884 (100), 1630 (7), 1492 (27), 1463 (18), 1351 (7), 1283 (32), 1198 (11), 1164 (10), 1146 (13), 1004 (18), 982 (12), 932 (11), 869 (24), 838 (12), 730 (9), 653 (10), 608 (16), 450 (14). **EA** calcd. for $C_5H_9NO_4$ (147.13 g mol^{-1}): C 40.82, H 6.17, N 9.52%; found: C 40.19, H 6.00, N 9.23%. **MS** (EI) m/z: $[M]^+$ calcd. for $C_5H_9NO_4$ 147.0532; found 65.04 $[C_3H_4O]^+$. **DSC** (T_{onset}, 5 °C min^{-1}): −13.8 °C (m.p.), 170.3 °C (dec.). **BAM drop hammer** > 40 J. **Friction test** > 360 N.

3-Azidomethyl-3-nitratomethyloxetane (AMNMO, 6)

AMNMO was prepared according to a modified literature procedure.[7]

Sodium azide (2.15 g, 33.1 mmol, 1.0 equiv.) was dissolved in a mixture of distilled water (7.5 mL) and acetone (7.5 mL) and 3-bromomethyl-3-hydroxymethyloxetane (6.00 g, 33.1 mmol) was added. The solution was set to reflux overnight and then allowed to cool to ambient temperature. The reaction mixture was extracted with ethyl acetate (3 × 30 mL) and the combined organic phases were washed with water (3 × 30 mL). After drying over sodium sulfate, the solvent was removed by rotary evaporation to give 3.48 g (24.3 mmol, 73%) of 3-azidomethyl-3-hydroxymethyloxetane as yellow liquid. Acetic anhydride (5.56 g, 54.5 mmol, 1.3 equiv.) and white fuming nitric acid (3.17 g, 50.3 mmol, 1.2 equiv.) were added to a round bottom flask at 0 °C using an ice bath. The mixture was stirred for 10 minutes prior to the slow addition of a solution of 3-azidomethyl-3-hydroxymethyloxetane (6.00 g, 41.9 mmol, 1.0 equiv.) in dichloromethane (60 mL). The reaction mixture was stirred at 0 °C for one hour and subsequently washed with saturated sodium bicarbonate solution (3 × 30 mL) as well as saturated sodium chloride solution (30 mL). The organic layer was dried over sodium sulfate and the solvent removed by rotary evaporation. The obtained yellowish liquid was added to sodium bicarbonate solution (50 mL) and the resulting emulsion was vigorously stirred for one hour. The mixture was then extracted with dichloromethane (3 × 30 mL) and the combined organic phases were dried over sodium sulfate. The solvent was removed to give 4.00 g (21.3 mmol, 51%) of crude product. The yellowish liquid was subjected to vacuum distillation (2.3×10^{-2} mbar, 110 °C) to give 3.32 g (17.6 mmol, 42%) of 3-azidomethyl-3-nitratomethyloxetane.

^{1}H NMR (400 MHz, $CDCl_3$, 25 °C): δ = 4.67 (s, 2H, CH_2ONO_2), 4.43 (m, 4H, CH_2), 3.72 (s, 2H, CH_2N_3). **$^{13}C\{^1H\}$ NMR** (101 MHz, $CDCl_3$, 25 °C): δ = 75.6, 73.0, 53.4, 41.9. **^{14}N NMR** (29 MHz, $CDCl_3$, 25 °C): δ = −43.4 (NO_2), −134.3 (N_β), −170.7 (N_γ), −323.0 (N_α). **FT-IR** (ATR, cm^{-1}): $\tilde{\nu}$ = 2960 (w), 2883 (w), 2102 (s), 1627 (vs), 1452 (w), 1382 (w), 1352 (w), 1275 (vs), 1145 (w), 1108 (w), 982 (s), 933 (m), 861 (s), 842 (s), 756 (m), 679 (m), 641 (m), 605 (m), 554 (m), 496 (w). **Raman** (1064 nm, 1074 mW, cm^{-1}): $\tilde{\nu}$ = 3019 (7), 2986 (26), 2957 (42), 2892 (44), 2109 (12), 1492 (16), 1453 (9), 1279 (23), 1173 (9), 1148 (9), 1000 (12), 963 (9), 946 (7), 927 (9), 865 (16), 633 (7), 606 (12). **EA** calcd. for $C_5H_8N_4O_4$ (188.14 g mol^{-1}): C 31.92, H 4.29, N 29.78%; found: C 32.46, H 4.38, N 28.52%. **MS** (EI) m/z: $[M]^+$ calcd. for $C_5H_8N_4O_4$ 188.0546; found 146.09 $[C_5H_8NO_4]^+$, 65.04 $[C_3H_4O]^+$. **DSC** (T_{onset}, 5 °C min^{-1}): −12.4 °C (m.p.), 178.2 °C (dec.). **BAM drop hammer** > 35 J. **Friction test** > 280 N.

11.5.1.2 Polymer Synthesis

Preparation of a dry solvent mixture for polymerization reactions:
A molecular sieve (3 Å, ~50 g) was added to a thoroughly dried Schlenk round bottom flask under protective atmosphere (argon). The flask was then connected to a distillation apparatus equipped with pre-dried Schlenk receiving flask. Sulfolane was added to the round bottom flask (argon counterflow) and distilled under high vacuum conditions (2×10^{-2} mbar, 135 °C). Another Schlenk round bottom flask was closed with a silicone rubber septum and thoroughly dried under protective atmosphere (argon). Distilled sulfolane (72 mL) and dry dichloromethane (8 mL) were added under a protective atmosphere (argon counterflow) to give a dry 9:1 mixture.

Poly(3-(2,4,6-trinitrophenoxy)oxetane) (P1)
A Schlenk round bottom flask was closed with a silicone rubber septum and thoroughly dried under protective atmosphere (argon). Boron trifluoride etherate (74.7 mg, 64.9 µL, 526 µmol, 10 mol%) and butane-1,4-diol (23.7 mg, 23.2 µL, 263 µmol, 5 mol%) were added using a 100 µL Hamilton syringe. After 15 minutes, dry solvent (sulfolane-DCM 9:1, 0.79 mL) was added. A solution of TNPO (1.50 g, 5.26 mmol) in aforementioned solvent (1.84 mL) was added over a period of two hours using a syringe pump and the reaction mixture was stirred at 250 rpm for 48 hours. The polymerization was quenched with water (1 mL) and vigorously stirred for five minutes. Afterward, methanol (~15 mL) was added to precipitate the crude polymer which settled at the bottom of the flask as brownish slurry. Afterward, the supernatant was decanted and the crude polymer dissolved in the minimal amount of boiling acetone. Again, methanol (~15 mL) was added and a pale orange suspension was obtained. The precipitate was collected by centrifugation (6000 rpm, 20 minutes), transferred to a round bottom flask using acetone and all volatiles were removed by rotary evaporation. Then, the polymer was dried under high vacuum conditions (70 °C, 10^{-3} mbar, 24 h) to give 1.05 g (70%) of poly[3-(2,4,6-trinitrophenoxy)oxetane] as yellow solid.

^{1}H NMR (400 MHz, DMSO-d_6, 25 °C): δ = 8.90–9.08, 3.21–3.94. **^{13}C{^{1}H} NMR** (101 MHz, Acetone-d_6, 25 °C): δ = 149.3, 143.5, 141.0, 124.5, 85.9, 70.8. **^{14}N NMR** (29 MHz, Acetone-d_6, 25 °C): δ = −17.3. **FT-IR** (ATR, cm^{-1}): $\tilde{\nu}$ = 1603 (m), 1533 (vs), 1464 (m), 1339 (vs), 1301 (m), 1259 (s), 1146 (m), 1106 (m), 1085 (s), 942 (m), 916 (m), 890 (m), 807 (m), 738 (m), 714 (s), 697 (m), 521 (m), 441 (m). **Raman** (1064 nm, 1074 mW, cm^{-1}): $\tilde{\nu}$ = 3102 (5), 2951 (15), 2882 (11), 2861 (5), 1615 (37), 1546 (31), 1474 (5), 1347 (100), 1270 (20), 1183 (7), 1087 (8), 944 (9), 826 (24), 766 (4), 741 (3), 716 (2), 672 (2), 442 (3). **EA** calcd. for $(C_9H_7N_3O_8)_n$ (285.17 g mol^{-1}): C 37.91, H 2.47, N 14.74%; found: C 38.86, H 2.96, N 13.29%. **DSC** (T_{onset}, 5 °C min^{-1}): 63.0 °C (glass transition), 204.6 °C (dec. 1), 238.7 °C (dec. 2). **BAM drop hammer** > 40 J. **BAM friction test** > 360 N.

Copolymer preparation:

All copolymerization reactions were carried out according to the general procedure stated in the main document on a 1 g scale (3.51 mmol) with regard to TNPO using an overall monomer concentration of 2 mol L^{-1}. Therefore, the solvent volume is the same (3.51 mL) for each batch. The necessary amount of the respective comonomer to achieve an equimolar ratio is stated in Table S1 together with the employed feed rates. Prior to monomer addition, an initiating mixture was prepared from boron trifluoride etherate (99.5 mg, 86.6 µL, 701 µmol) and butane-1,4-diol (31.6 mg, 31.0 µL, 351 µmol).

Table S 11.1. Employed comonomer amounts, feed rates, yields and description of the product appearance.

Monomer	Amount [mg, mmol]	Feed rate [mmol/h]	Product appearance	Yield [g, %]
3AO (2)	347, 3.51	2	Orange solid	1.04, 77
AMMO (3)	446, 3.51	2	Orange solid	0.66, 46
BAMO (4)	590, 3.51	2	Orange solid	1.01, 64
NIMMO (5)	516, 3.51	2	Yellow solid	0.98, 65
AMNMO (6)	660, 3.51	6	Orange solid	1.38, 83

Poly[(3-(2,4,6-trinitrophenoxy)oxetane)-stat-(3-azidooxetane)] (P2)

^{1}H NMR (400 MHz, Acetone-d$_6$, 25 °C): δ = 9.10−8.91, 4.67−3.27. **^{13}C{^{1}H} NMR** (101 MHz, Acetone-d$_6$, 25 °C): δ = 151.1, 145.3, 142.4, 125.2, 86.6, 71.7, 61.4. **^{14}N NMR** (29 MHz, Acetone-d$_6$, 25 °C): δ = −15.9, −134.1, −279.8. **FT-IR** (ATR, cm^{-1}): ṽ = 3097 (w), 2920 (w), 2879 (w), 2097 (m), 1667 (w), 1603 (m), 1534 (vs), 1464 (m), 1415 (w), 1339 (vs), 1305 (m), 1259 (s), 1086 (s), 942 (m), 917 (m), 824 (w), 811 (w), 763 (w), 738 (m), 714 (s), 666 (m), 661 (m), 557 (w), 529 (w), 490 (w), 482 (w). **Raman** (1064 nm, 1074 mW, cm^{-1}): ṽ = 3102 (7), 2967 (10), 2942 (17), 2915 (14), 2876 (14), 1615 (38), 1548 (31), 1480 (7), 1474 (7), 1347 (100), 1310 (14), 1270 (21), 1181 (7), 1087 (7), 1065 (7), 944 (10), 921 (7), 826 (28). **EA** calcd. for $(C_9H_7N_3O_8)_n(C_3H_5N_3O)_m$ (n = m) (384.26 g mol^{-1}): C 37.51, H 3.15, N 21.87%; found: C 38.12, H 3.48, N 18.85%. **DSC** (T_{onset}, 5 °C min^{-1}): 25.2 °C (glass transition), 177.6 °C (dec.). **BAM drop hammer** 25 J. **BAM friction test** 324 N.

Poly[(3-(2,4,6-trinitrophenoxy)oxetane)-*stat*-(3-azidomethyl-3-methyloxetane)] (P3)

^{1}H NMR (400 MHz, Acetone-d$_6$, 25 °C): δ = 9.10−8.82, 4.74−2.92, 1.47−0.63. **^{13}C{^{1}H} NMR** (101 MHz, Acetone-d$_6$, 25 °C): δ = 151.0, 145.2, 142.4, 125.2, 86.7, 74.7, 71.8, 56.1, 41.8, 18.1. **^{14}N NMR** (29 MHz, Acetone-d$_6$, 25 °C): δ = −18.8, −133.0. **FT-IR** (ATR, cm^{-1}): ṽ = 2099 (s), 1611 (m), 1603 (m), 1535 (vs), 1464 (m), 1416 (w), 1339 (vs), 1263 (s), 1086 (s), 942 (m), 916 (m), 890 (m), 824 (w), 807 (w), 762 (w), 738 (m), 714 (s), 697 (m), 554 (w), 527 (m). **Raman** (1064 nm, 1074 mW, cm^{-1}): ṽ = 3106 (6), 3088 (6), 2977 (16), 2930 (22), 2878 (19), 2859 (22), 2822 (6), 1615 (38), 1546

(28), 1480 (6), 1459 (6), 1347 (100), 1270 (22), 1181 (6), 1089 (9), 946 (9), 930 (6), 824 (28), 768 (6). **EA** calcd. for $(C_9H_7N_3O_8)_n(C_5H_9N_3O)_m$ (n = m) (412.31 g mol^{-1}): C 40.78, H 3.91, N 20.38; found: C 40.72, H 3.77, N 18.31. **DSC** (T_{onset}, 5 °C min^{-1}): 0.7 °C (glass transition), 183.3 °C (dec. 1), 222.0 °C (dec. 2). **BAM drop hammer** 25 J. **BAM friction test** > 360 N.

Poly[(3-(2,4,6-trinitrophenoxy)oxetane)-stat-(3,3-bis(azidomethyl)oxetane)] (P4)

^{1}H NMR (400 MHz, Acetone-d$_6$, 25 °C): δ = 9.11–8.91, 4.35–3.14. **^{13}C{^{1}H} NMR** (101 MHz, Acetone-d$_6$, 25 °C): δ = 151.0, 145.2, 142.4, 125.2, 86.5, 72.0, 70.9, 52.5, 45.8. **^{14}N NMR** (29 MHz, Acetone-d$_6$, 25 °C): δ = −17.6, −133.8. **FT-IR** (ATR, cm^{-1}): ṽ = 2096 (s), 1611 (m), 1603 (m), 1537 (vs), 1463 (m), 1450 (m), 1340 (vs), 1300 (s), 1262 (s), 1086 (s), 942 (m), 917 (s), 824 (m), 812 (m), 738 (m), 714 (s), 666 (m), 552 (m), 518 (m), 501 (m), 480 (m), 523 (w). **Raman** (1064 nm, 1074 mW, cm^{-1}): ṽ = 2988 (18), 2967 (27), 2946 (27), 2928 (36), 2876 (27), 2859 (36), 2116 (18), 1615 (45), 1549 (36), 1542 (36), 1451 (9), 1347 (100), 1312 (18), 1303 (18), 1270 (27), 942 (18), 826 (27). **EA** calcd. for $(C_9H_7N_3O_8)_n(C_5H_8N_6O)_m$ (n = m) (453.33 g mol^{-1}): C 37.09, H 3.34, N 27.81%; found: C 37.34, H 3.30, N 26.49%. **DSC** (T_{onset}, 5 °C min^{-1}): 23.4 °C (glass transition), 190.0 °C (dec.). **BAM drop hammer** > 7 J. **BAM friction test** > 360 N.

Poly[(3-(2,4,6-trinitrophenoxy)oxetane)-*stat*-(3-nitratomethyl-3-methyloxetane)] (P5)

^{1}H NMR (400 MHz, Acetone-d$_6$, 25 °C): δ = 9.10–8.84, 4.75–3.11, 1.66–0.73. **^{13}C{^{1}H} NMR** (101 MHz, Acetone-d$_6$, 25 °C): δ = 151.0, 144.3, 141.5, 124.3, 85.8, 75.0, 73.4, 71.0, 40.0, 25.9, 16.4. **^{14}N NMR** (29 MHz, Acetone-d$_6$, 25 °C): δ = −18.1, −39.5. **FT-IR** (ATR, cm^{-1}): ṽ = 1614 (s), 1604 (s), 1538 (vs), 1464 (m), 1416 (w), 1340 (vs), 1306 (m), 1276 (s), 1087 (s), 980 (m), 943 (m), 917 (m), 857 (s), 824 (m), 813 (m), 759 (m), 739 (m), 714 (s), 667 (w), 643 (w), 531 (w), 523 (w). **Raman** (1064 nm, 1074 mW, cm^{-1}): ṽ = 2992 (9), 2965 (18), 2951 (27), 2938 (27), 2928 (27), 2913 (18), 2896 (18), 2884 (27), 2859 (64), 1615 (36), 1546 (27), 1347 (100), 1303 (9), 1272 (18), 1252 (9), 1183 (9), 1090 (9), 942 (18), 826 (27). **EA** calcd. for $(C_9H_7N_3O_8)_n(C_5H_9NO_4)_m$ (n = m) (432.29 g mol^{-1}): C 38.90, H 3.73, N 12.96%; found: C 39.69, H 3.78, N 12.43%. **DSC** (T_{onset}, 5 °C min^{-1}): 36.0 °C (glass transition), 185.1 °C (dec.). **BAM drop hammer** 30 J. **BAM friction test** > 360 N.

Poly[(3-(2,4,6-trinitrophenoxy)oxetane)-*stat*-(3-azidomethyl-3-nitratomethyloxetane)] (P5)

^{1}H NMR (400 MHz, Acetone-d$_6$, 25 °C): δ = 9.11–8.78, 4.76–3.11. **^{13}C{^{1}H} NMR** (101 MHz, Acetone-d$_6$, 25 °C): δ = 151.0, 145.2, 142.4, 125.2, 86.7, 72.9, 71.9, 70.7, 52.0, 45.1. **^{14}N NMR** (29 MHz, Acetone-d$_6$, 25 °C): δ = −17.7, −40.6, −133.6. **FT-IR** (ATR, cm^{-1}): ṽ = 2105 (s), 1631 (s), 1612 (s), 1604 (s), 1537 (vs), 1464 (m), 1341 (vs), 1300 (m), 1275 (vs), 1146 (m), 1105 (s), 1087 (s), 989 (m), 942 (m), 918 (m), 859 (s), 824 (m), 738 (s), 714 (vs), 568 (m), 441 (m), 523 (w). **Raman** (1064 nm, 1074 mW, cm^{-1}): ṽ = 2951 (35), 2884 (27), 2859 (27), 1613 (42), 1548 (35), 1476 (12), 1455 (15), 1349 (100), 1305 (19), 1278 (27), 1270 (27), 1243 (15), 1183 (15), 1090 (12), 1083 (12), 942 (15), 826 (27), 442 (12). **EA** calcd. for $(C_9H_7N_3O_8)_n(C_5H_8N_4O_4)_m$ (n = m) (473.31 g mol^{-1}): C 35.53, H

3.19, N 20.72%; found: C 36.57, H 3.48, N 17.60%. **DSC** (T_{onset}, 5 °C min^{-1}): 42.4 °C (glass transition), 183.0 °C (dec.). **BAM drop hammer** 30 J. **BAM friction test** > 360 N.

11.5.2 NMR Spectra

11.5.2.1 NMR Spectra of Monomers

3-(2,4,6-Trinitrophenoxy)oxetane (TNPO, 1)

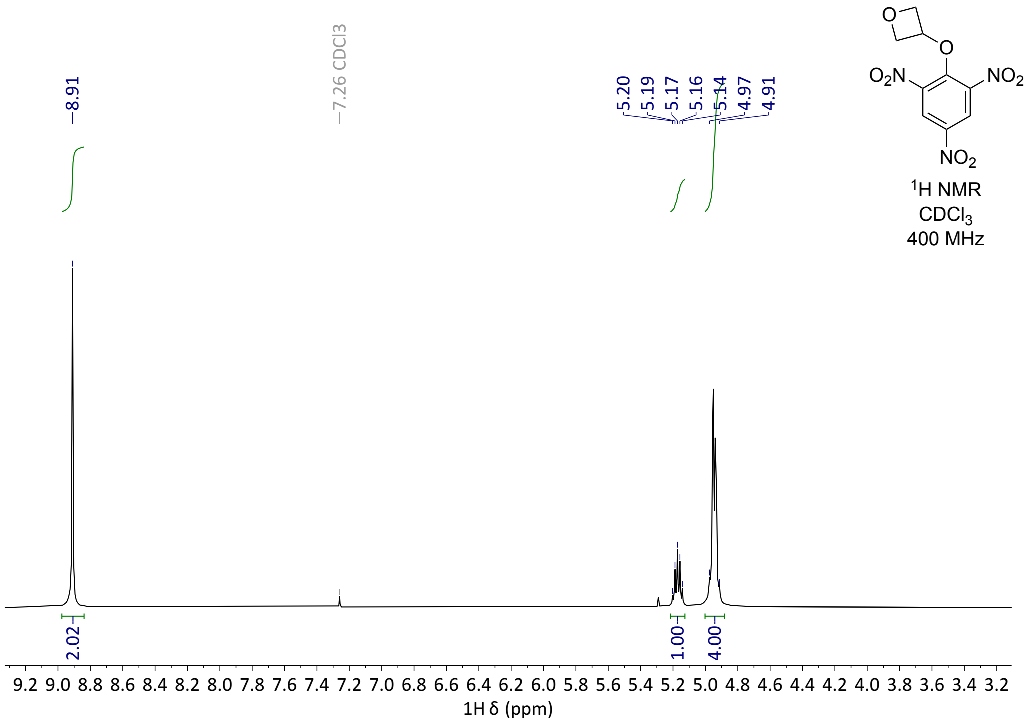

Figure S 11.1. Proton spectrum (^1H) of TNPO.

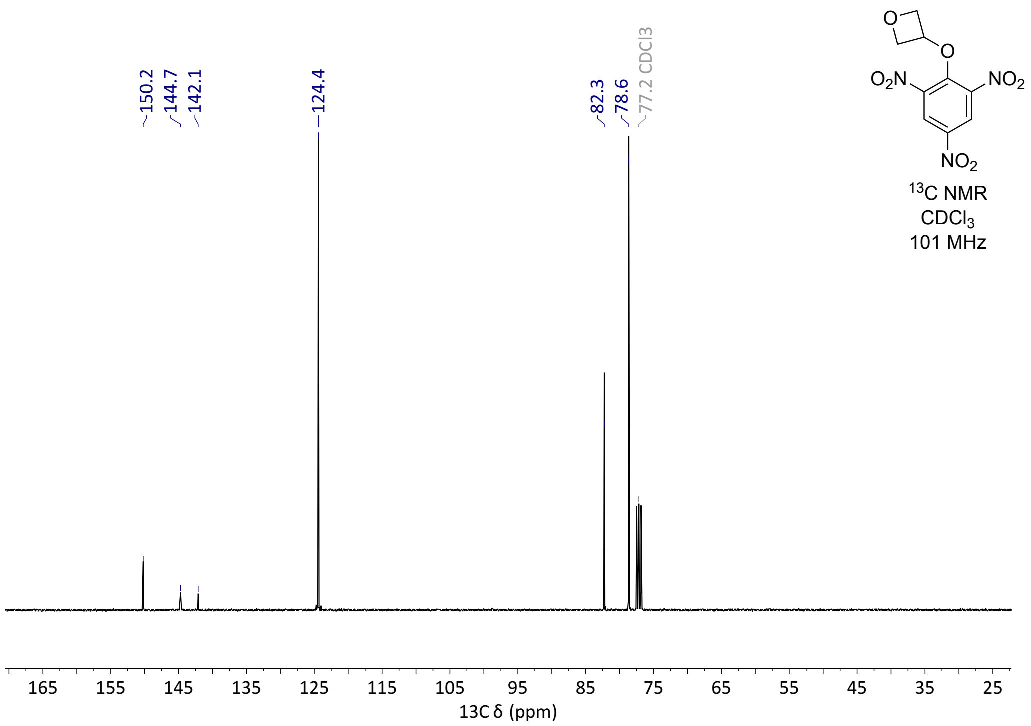

Figure S 11.2. Carbon spectrum (^{13}C) of TNPO.

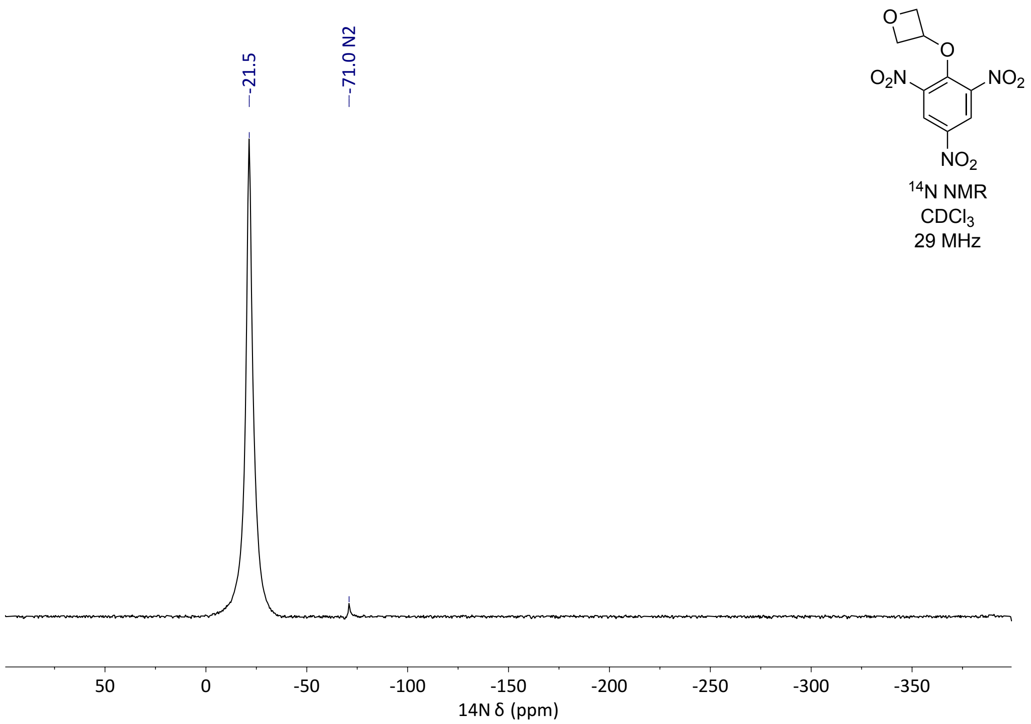

Figure S 11.3. Nitrogen spectrum (^{14}N) of TNPO.

3-Azidooxetane (3AO, 2)

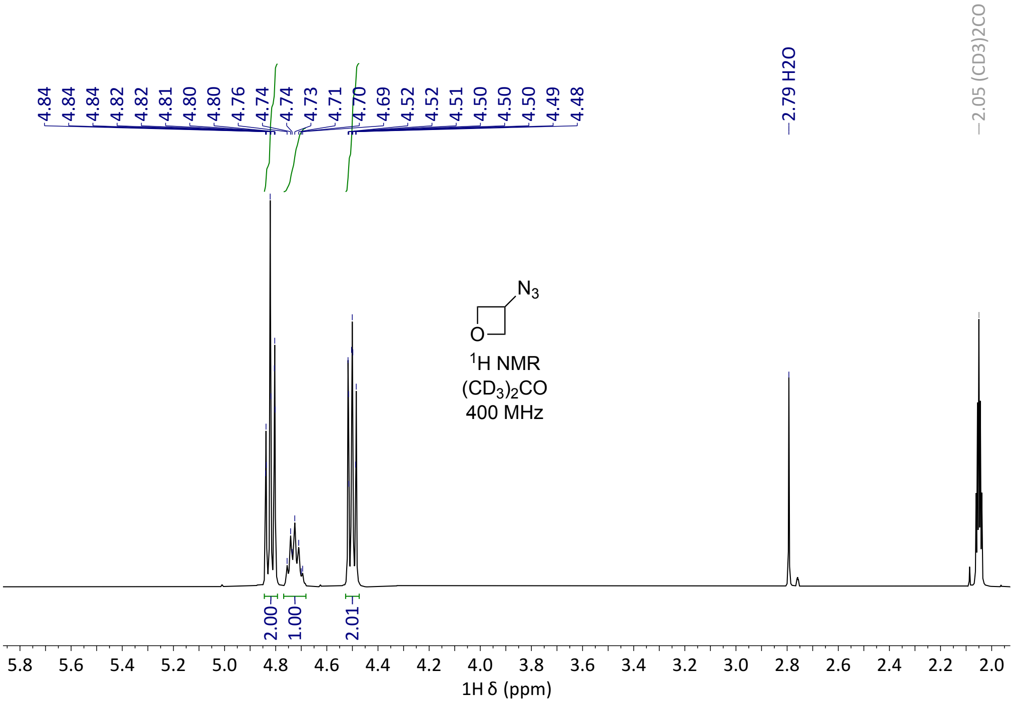

Figure S 11.4. Proton spectrum (^{1}H) of 3-azidooxetane.

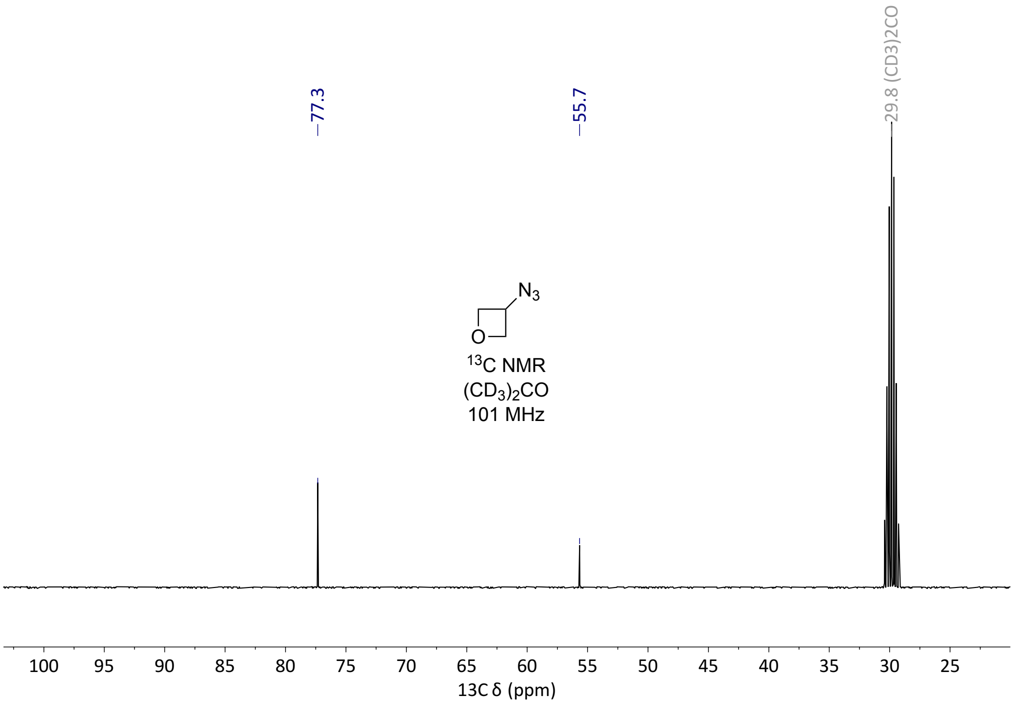

Figure S 11.5. Carbon spectrum (^{13}C) of 3-azidooxetane.

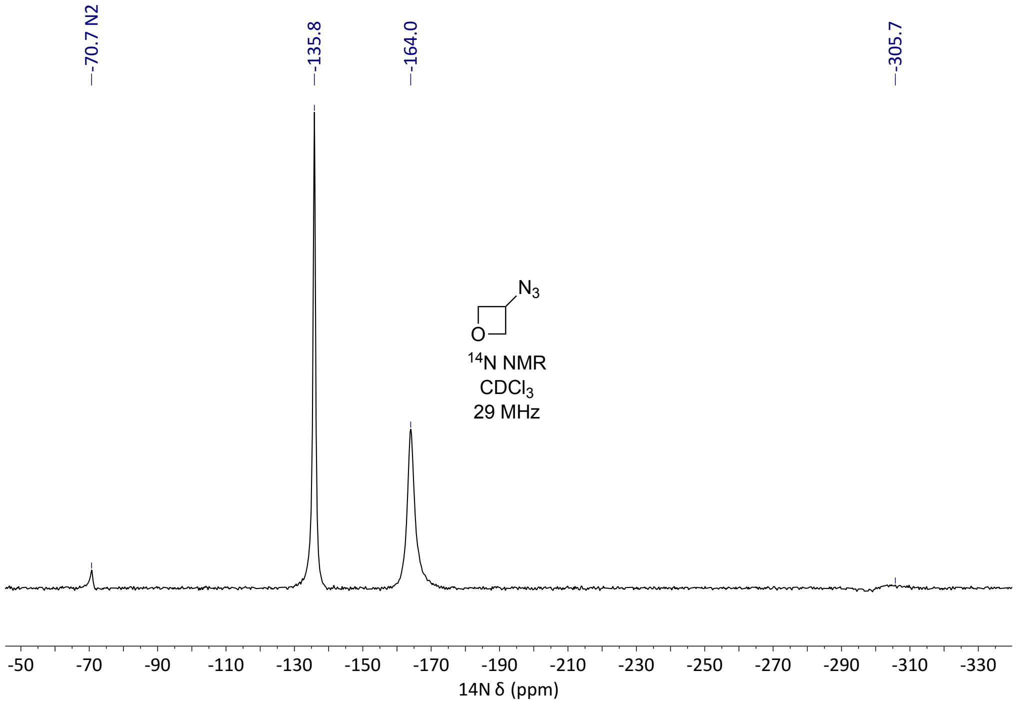

Figure S 11.6. Nitrogen spectrum (^{14}N) of 3-azidooxetane using $CDCl_3$ as solvent.

3-Azidomethyl-3-methyloxetane (AMMO, 3)

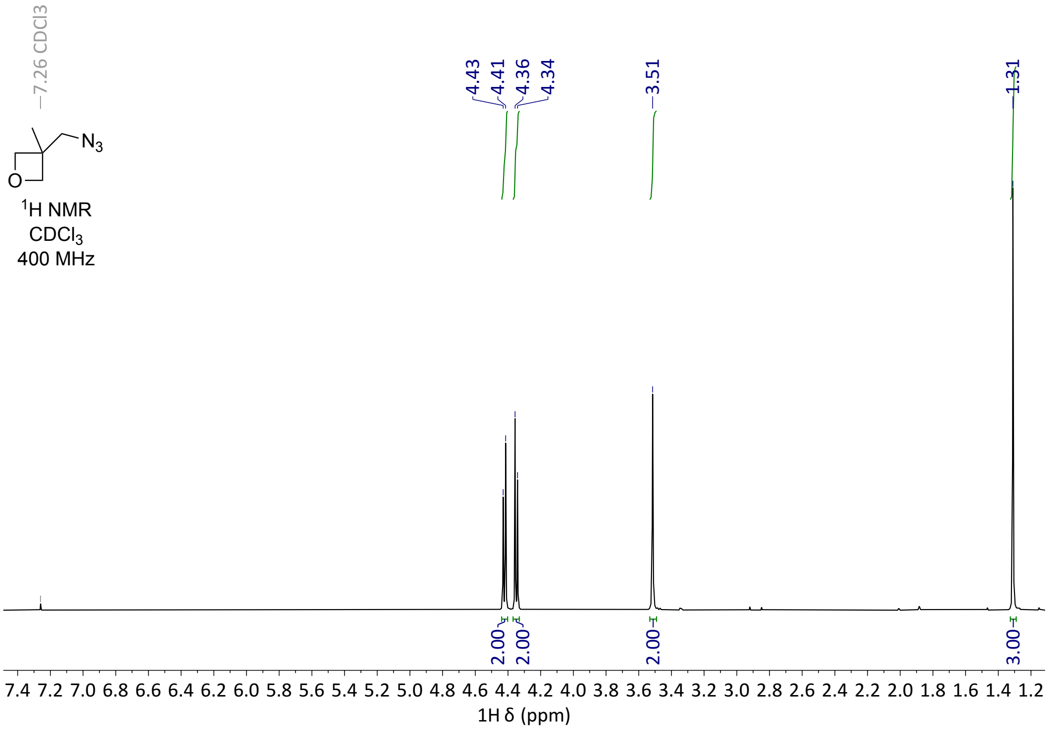

Figure S 11.7. Proton spectrum (^1H) of AMMO.

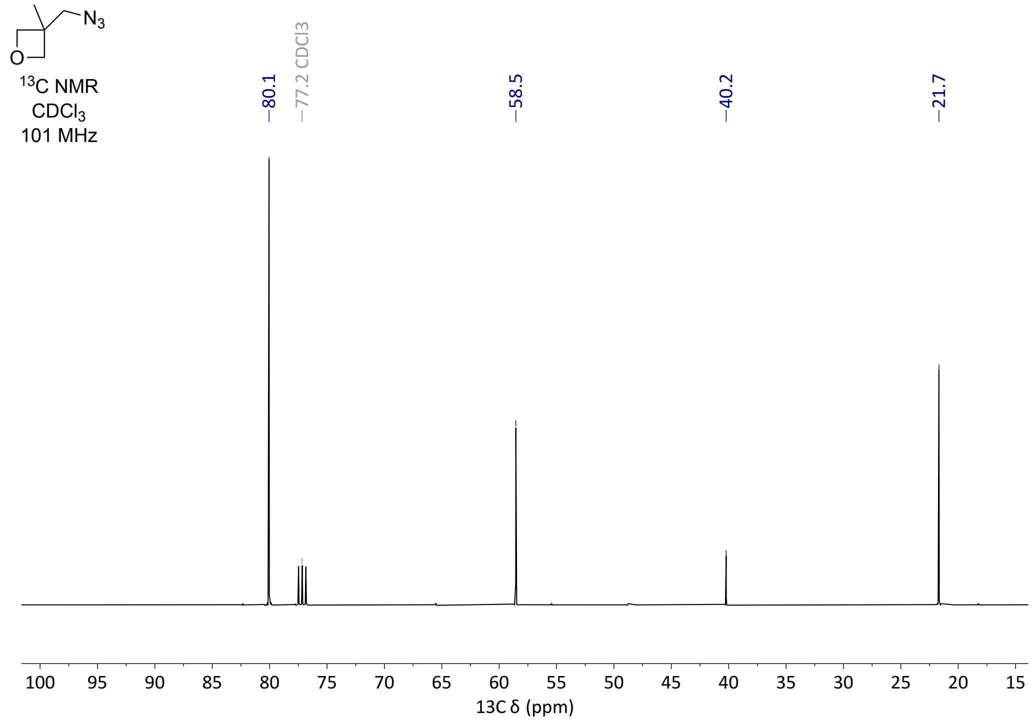

Figure S 11.8. Carbon spectrum (^{13}C) of AMMO.

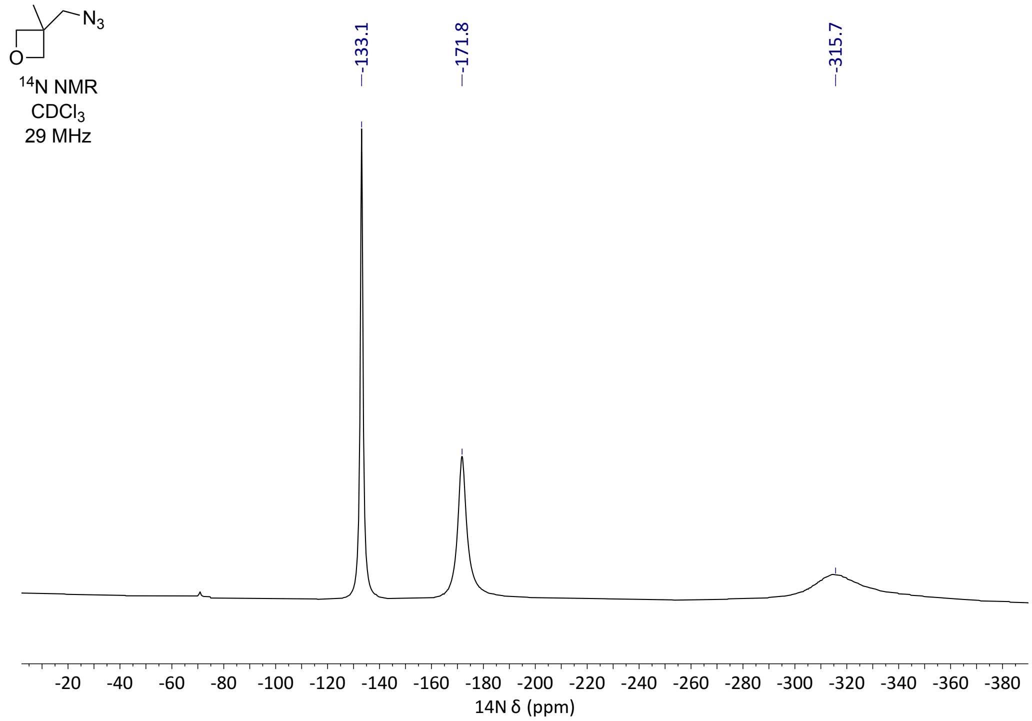

Figure S 11.9. Nitrogen spectrum (^{14}N) of AMMO.

3,3-Bis(azidomethyl)oxetane (BAMO, 4)

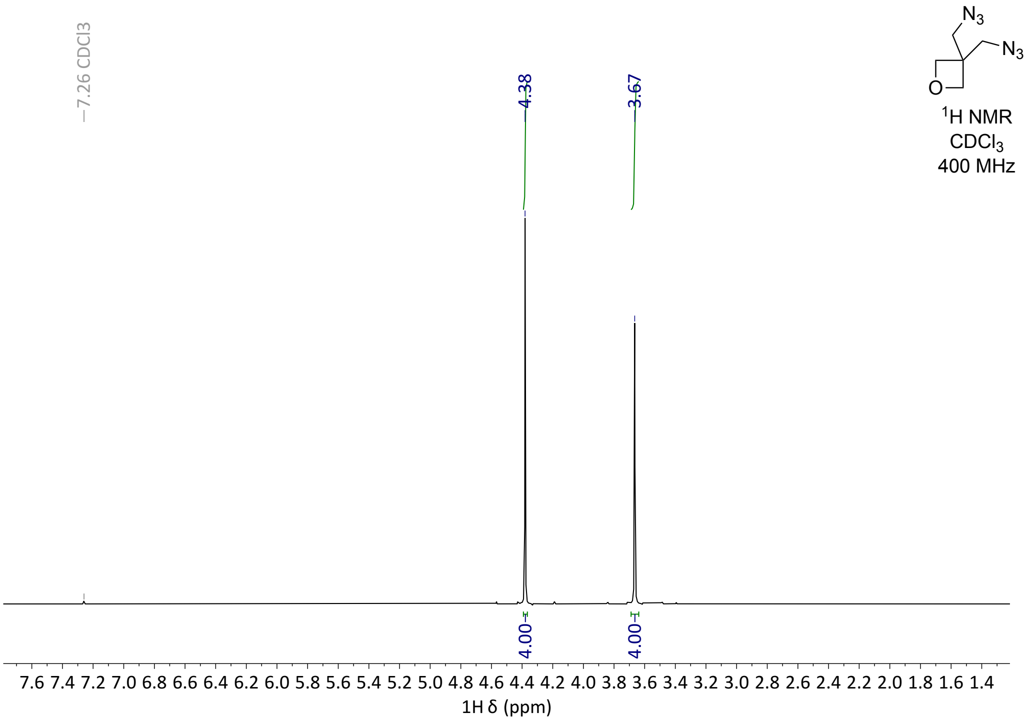

Figure S 11.10. Proton spectrum (^{1}H) of BAMO.

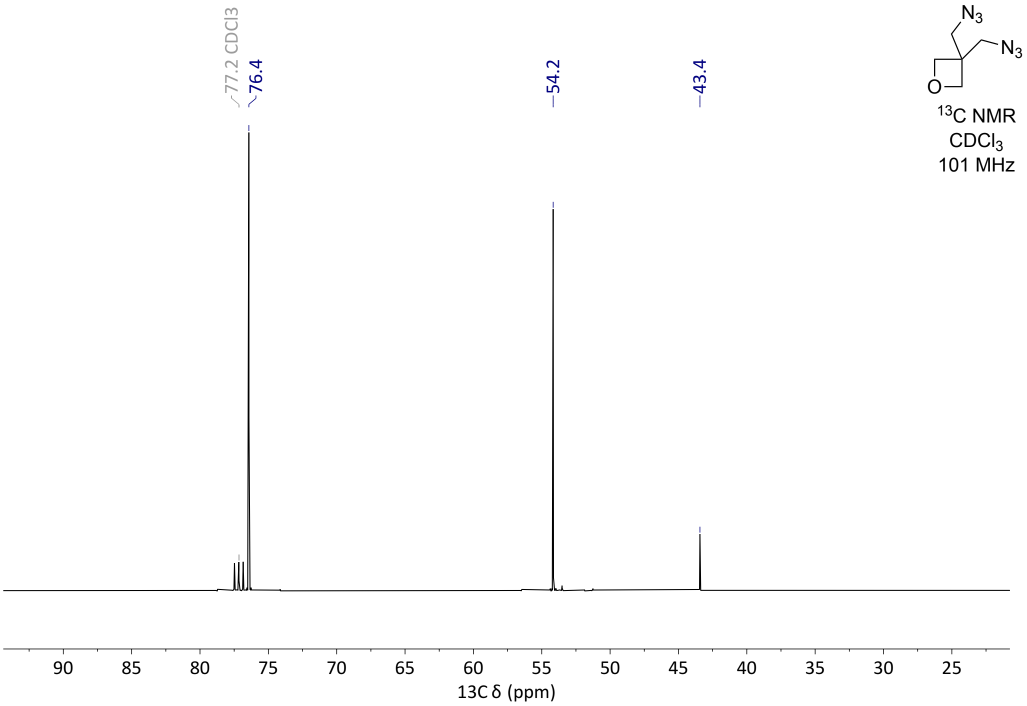

Figure S 11.11. Carbon spectrum (^{13}C) of BAMO.

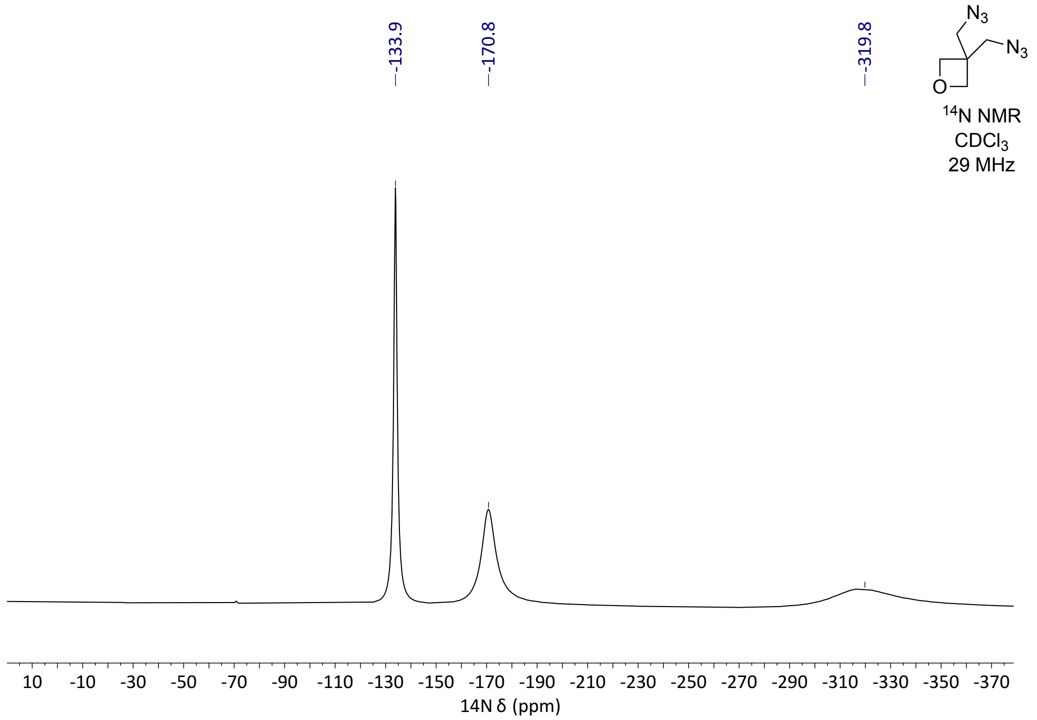

Figure S 11.12. Nitrogen spectrum (^{14}N) of BAMO.

3-Nitratomethyl-3-methyloxetane (NIMMO, 5)

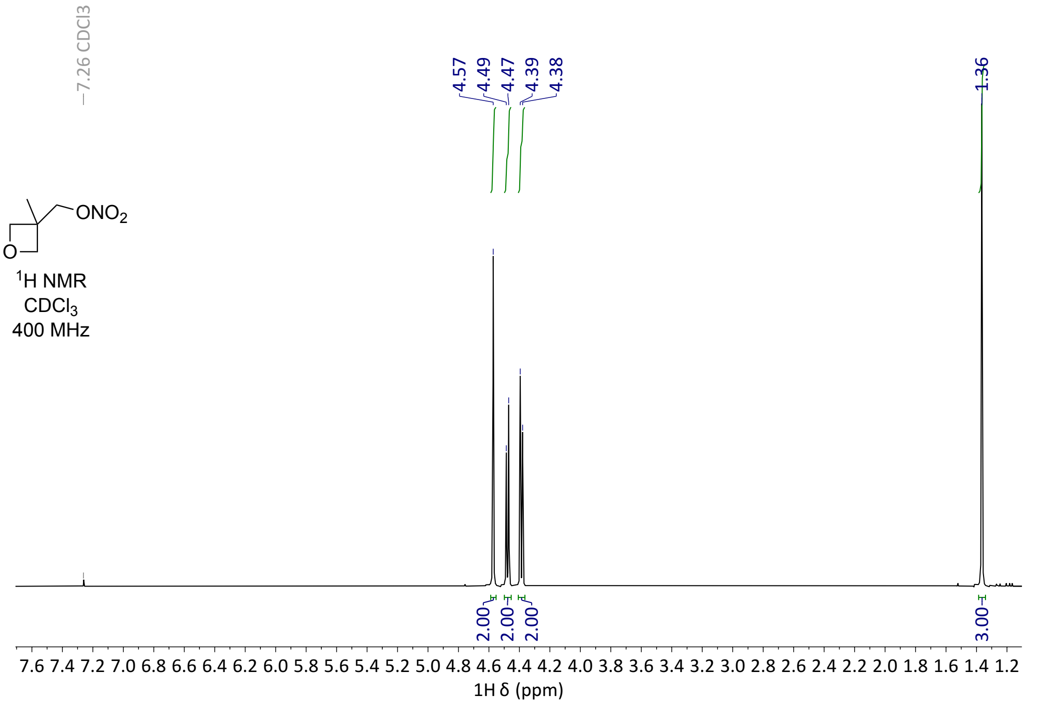

Figure S 11.13. Proton spectrum (^{1}H) of NIMMO.

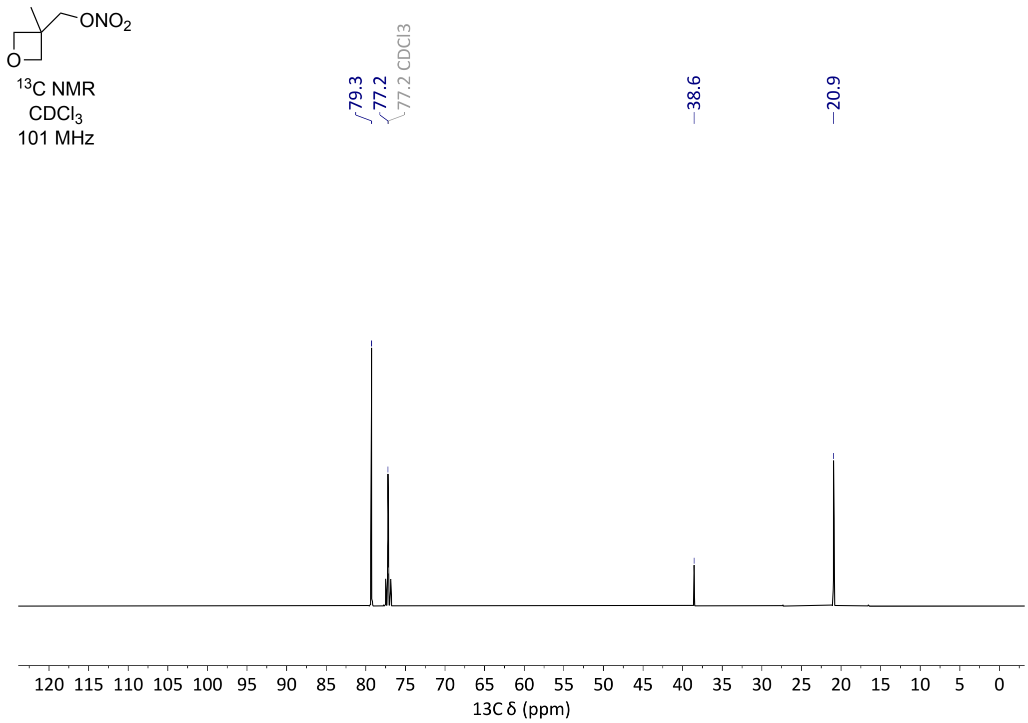

Figure S 11.14. Carbon spectrum (^{13}C) of NIMMO.

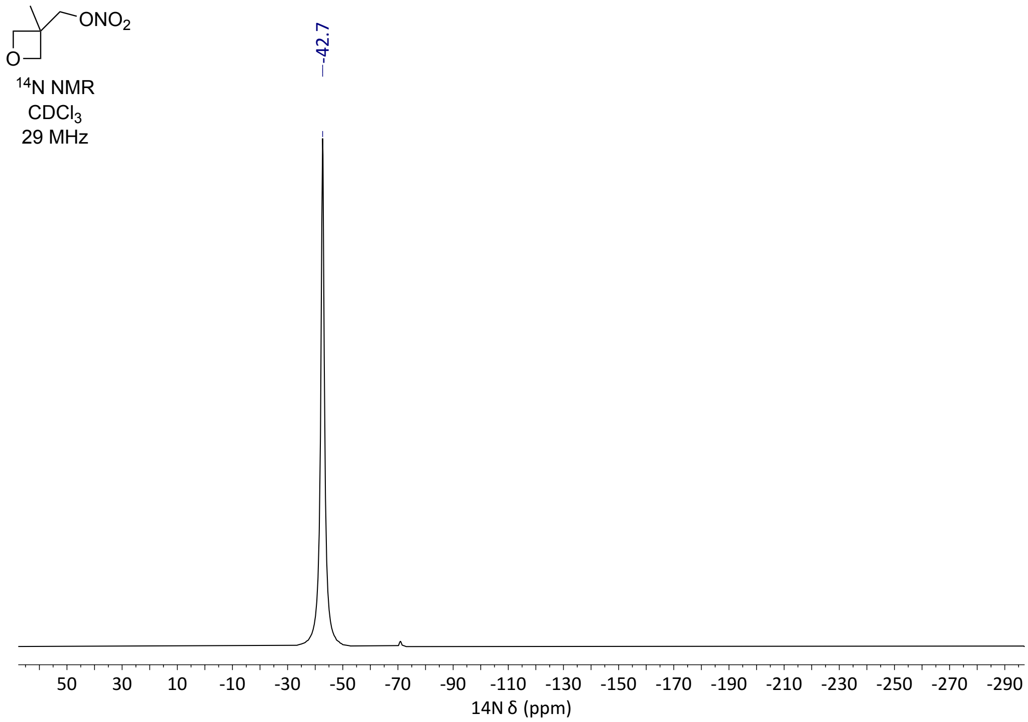

Figure S 11.15. Nitrogen spectrum (^{14}N) of NIMMO.

3-Azidomethyl-3-nitratomethyloxetane (AMNMO, 6)

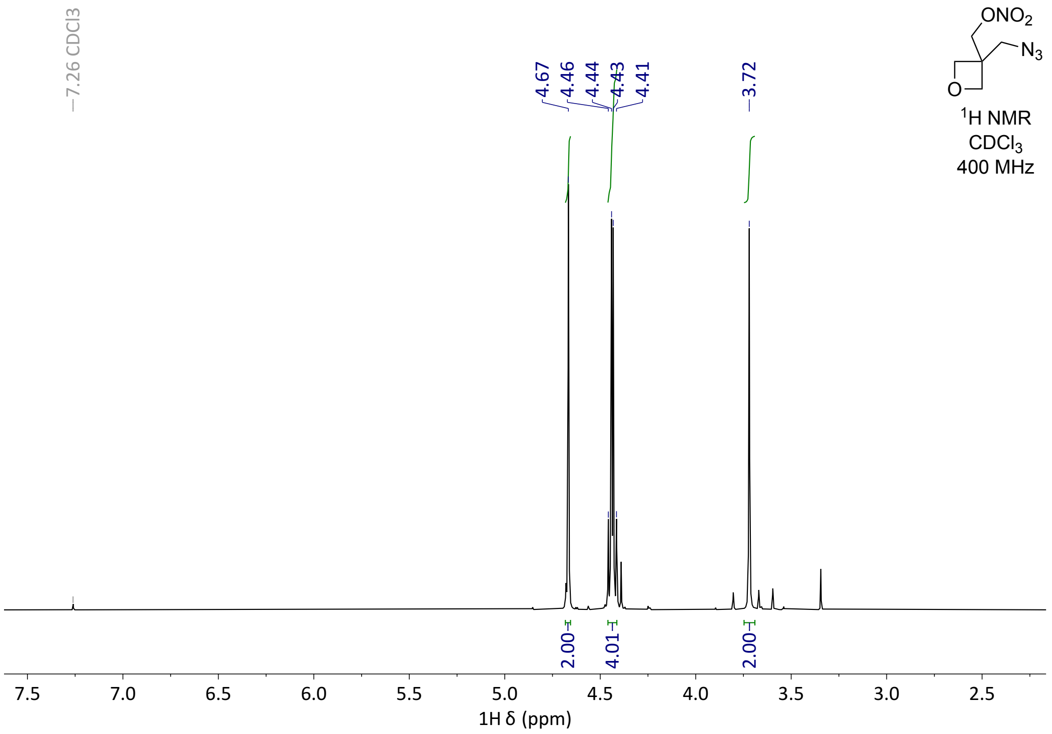

Figure S 11.16. Proton spectrum (^{1}H) of AMNMO.

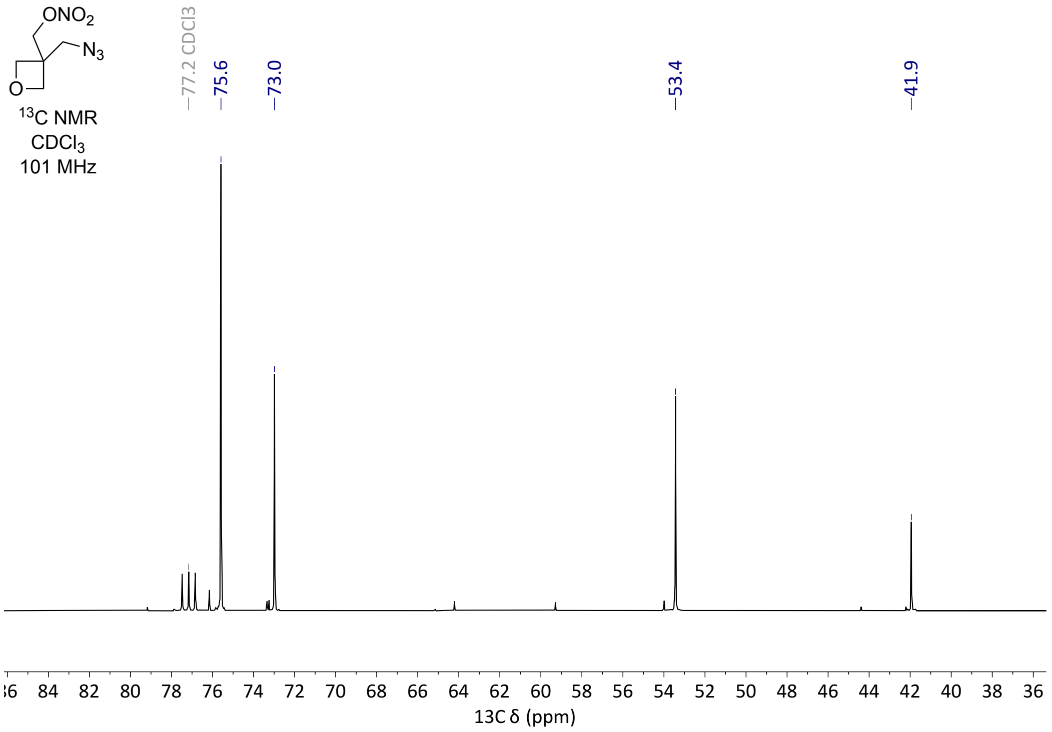

Figure S 11.17. Carbon spectrum (^{13}C) of AMNMO.

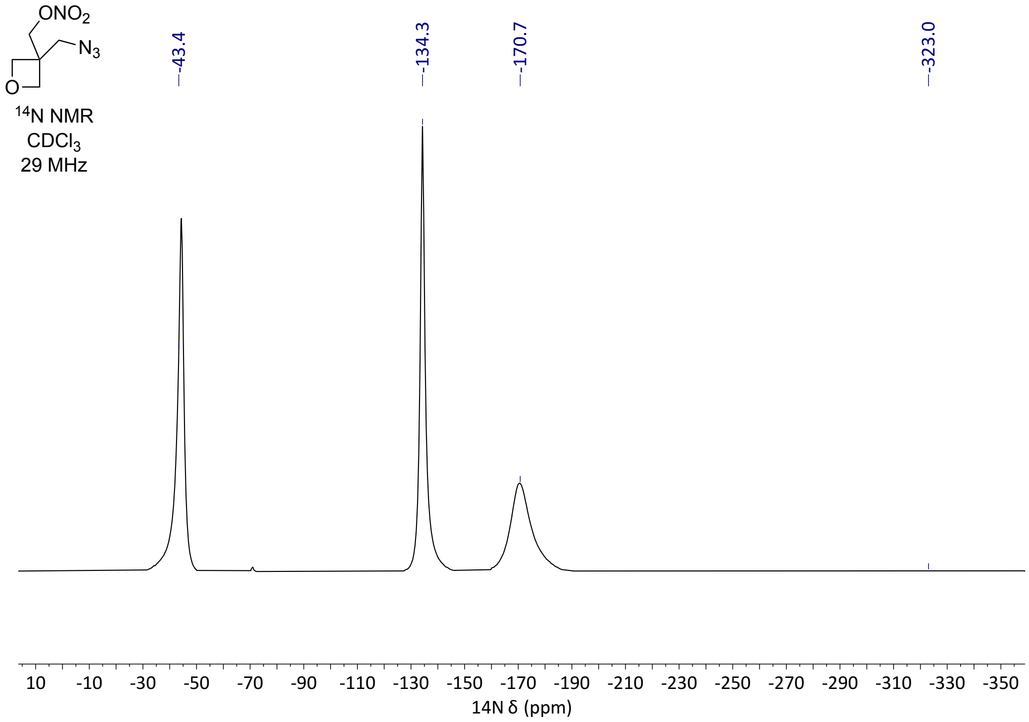

Figure S 11.18. Nitrogen spectrum (^{14}N) of AMNMO.

11.5.2.2 NMR Spectra of Polymers

Poly(3-azidomethyl-3-nitratomethyloxetane) (poly(AMNMO))

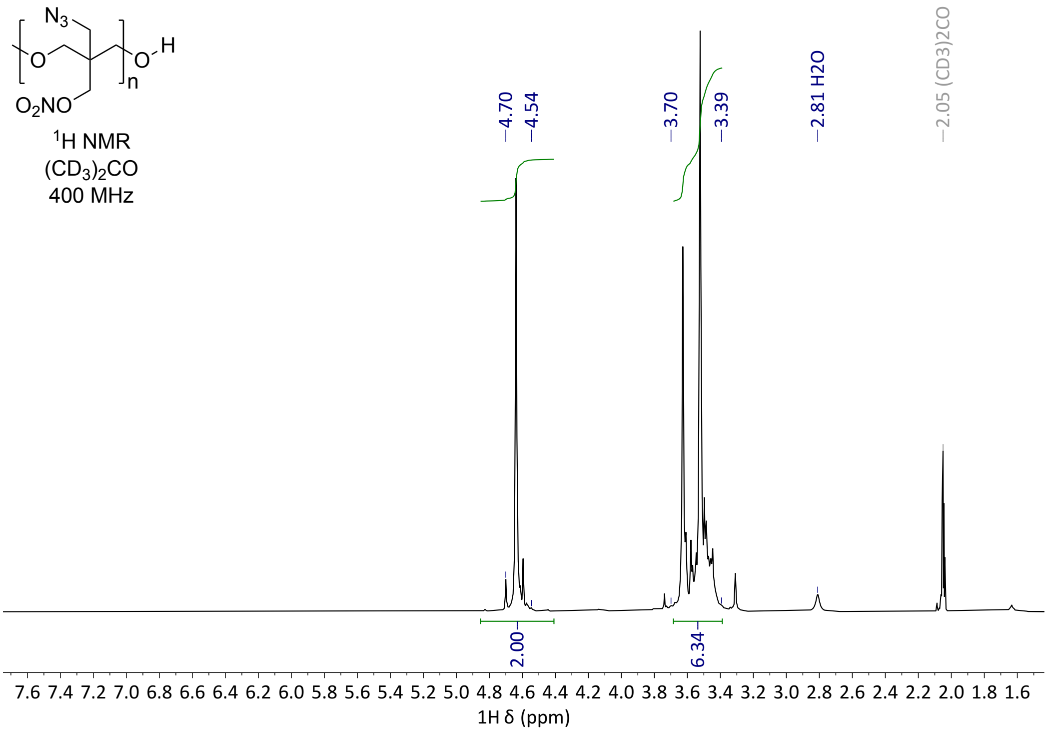

Figure S 11.19. Proton spectrum (^{1}H) of poly(AMNMO).

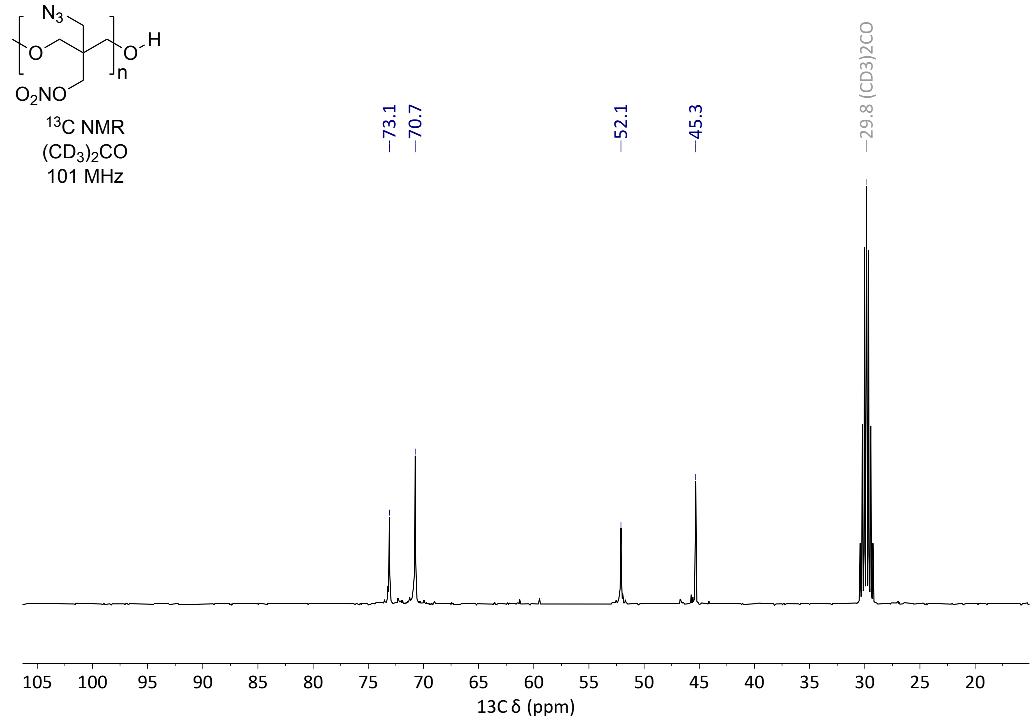

Figure S 11.20. Carbon spectrum (^{13}C) of poly(AMNMO).

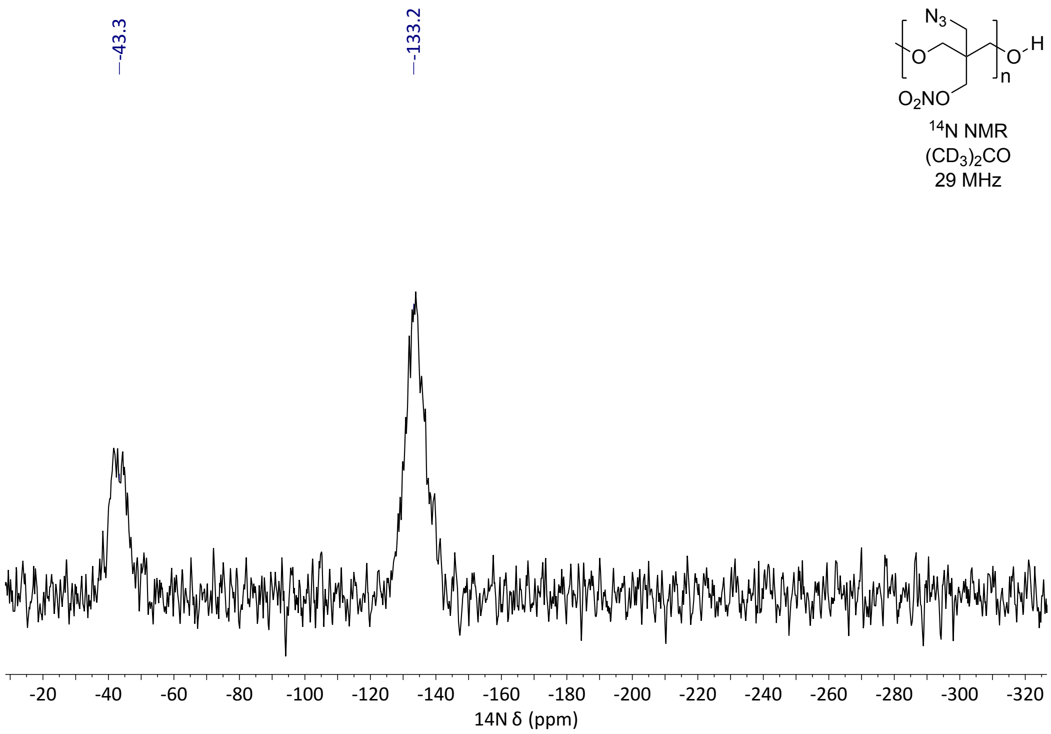

Figure S 11.21. Nitrogen spectrum (^{14}N) of poly(AMNMO).

Poly(3-(2,4,6-trinitrophenoxy)oxetane) (P1)

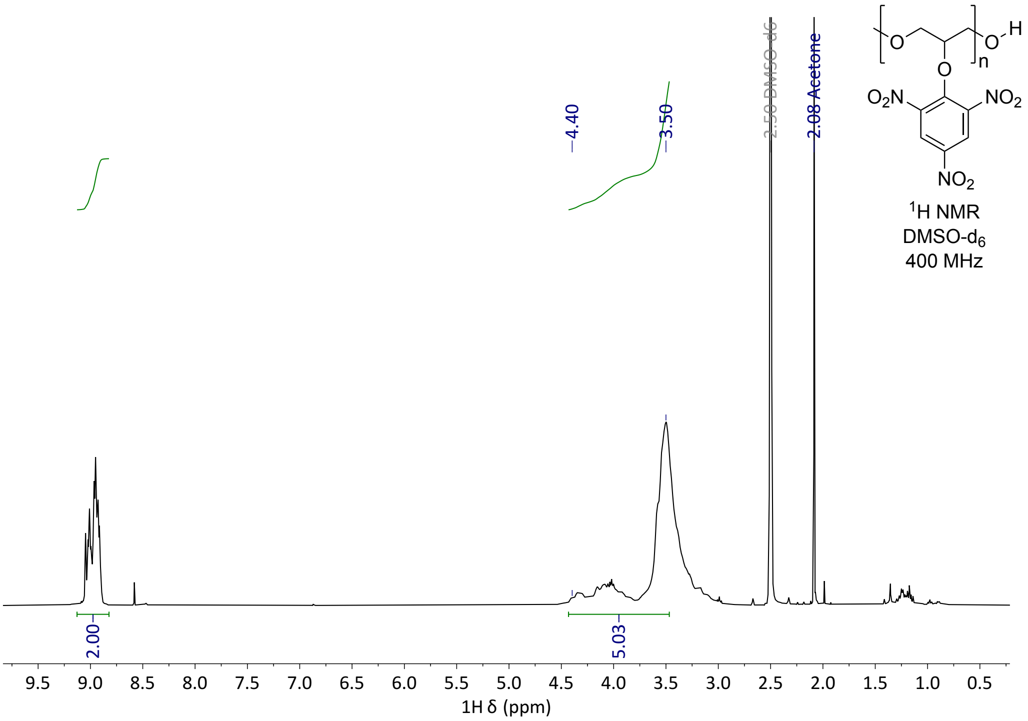

Figure S 11.22. Proton spectrum (^{1}H) of poly(TNPO).

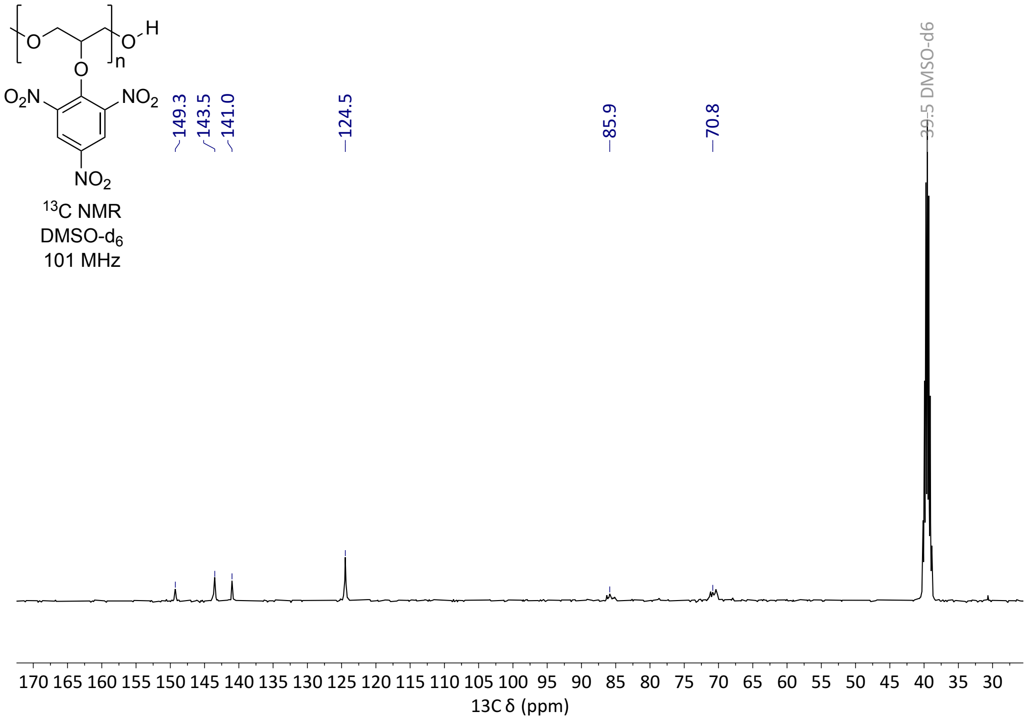

Figure S 11.23. Carbon spectrum (^{13}C) of poly(TNPO).

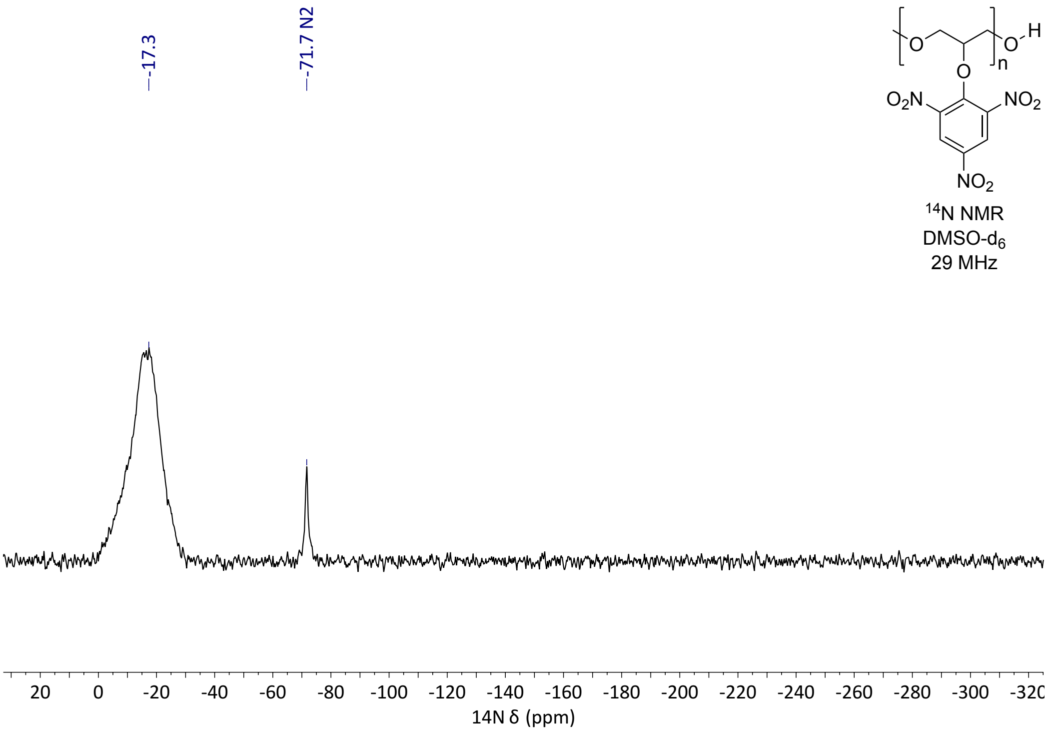

Figure S 11.24. Nitrogen spectrum (^{14}N) of poly(TNPO).

Poly[(3-(2,4,6-trinitrophenoxy)oxetane)-*stat*-(3-azidooxetane)] (P2)

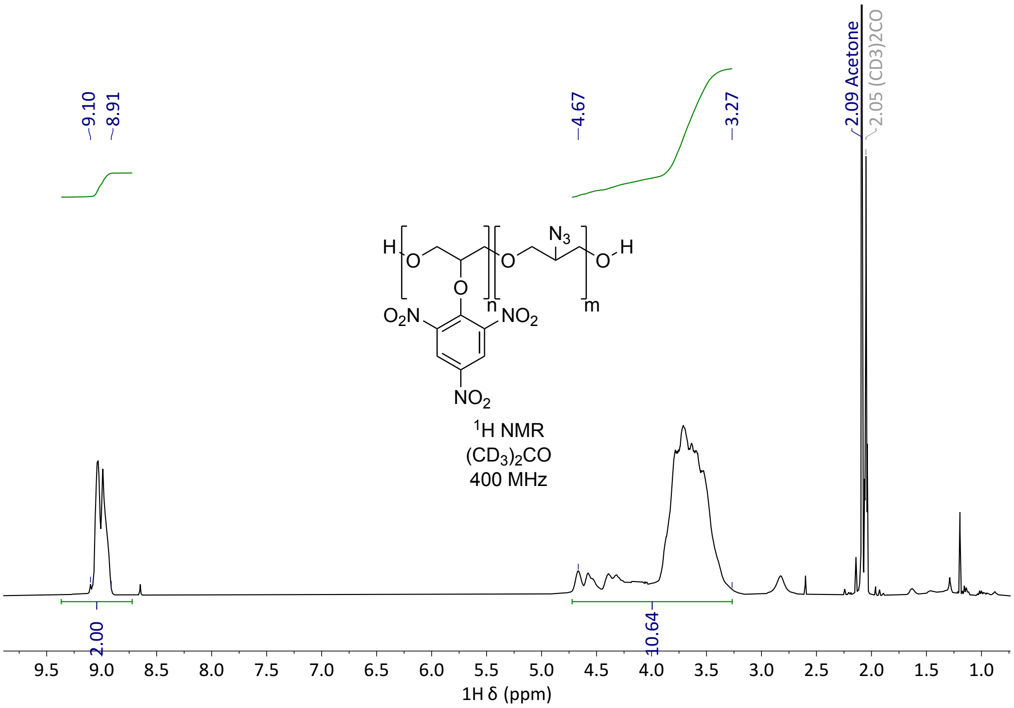

Figure S 11.25. Proton spectrum (^{1}H) of poly(TNPO-*stat*-3AO); n = m.

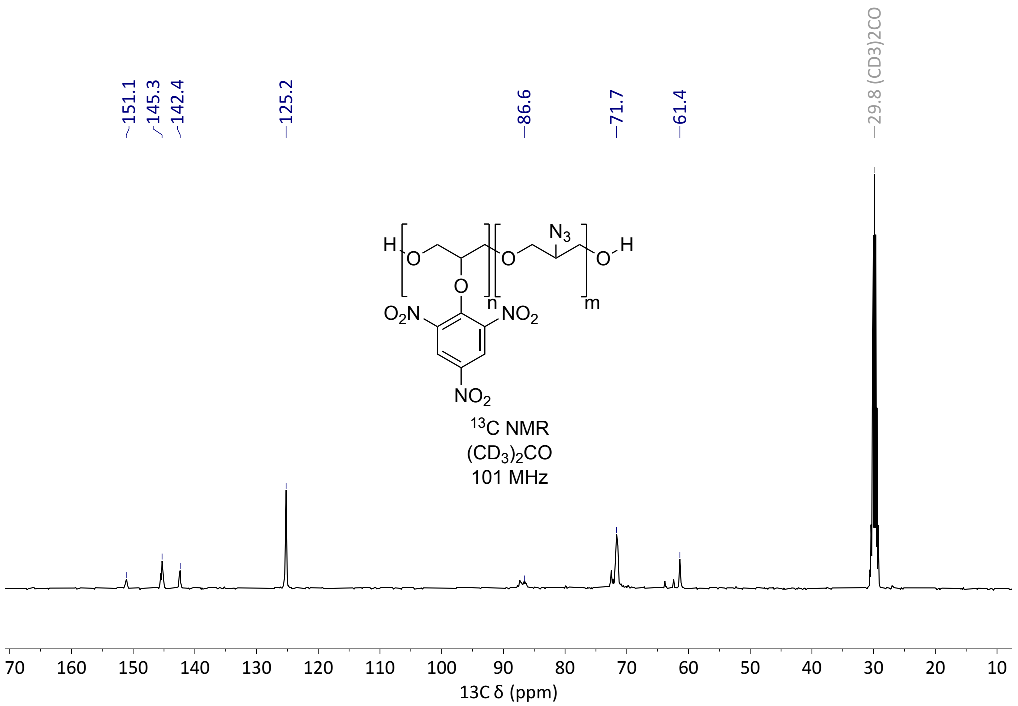

Figure S 11.26. Carbon spectrum (^{13}C) of poly(TNPO-*stat*-3AO); n = m.

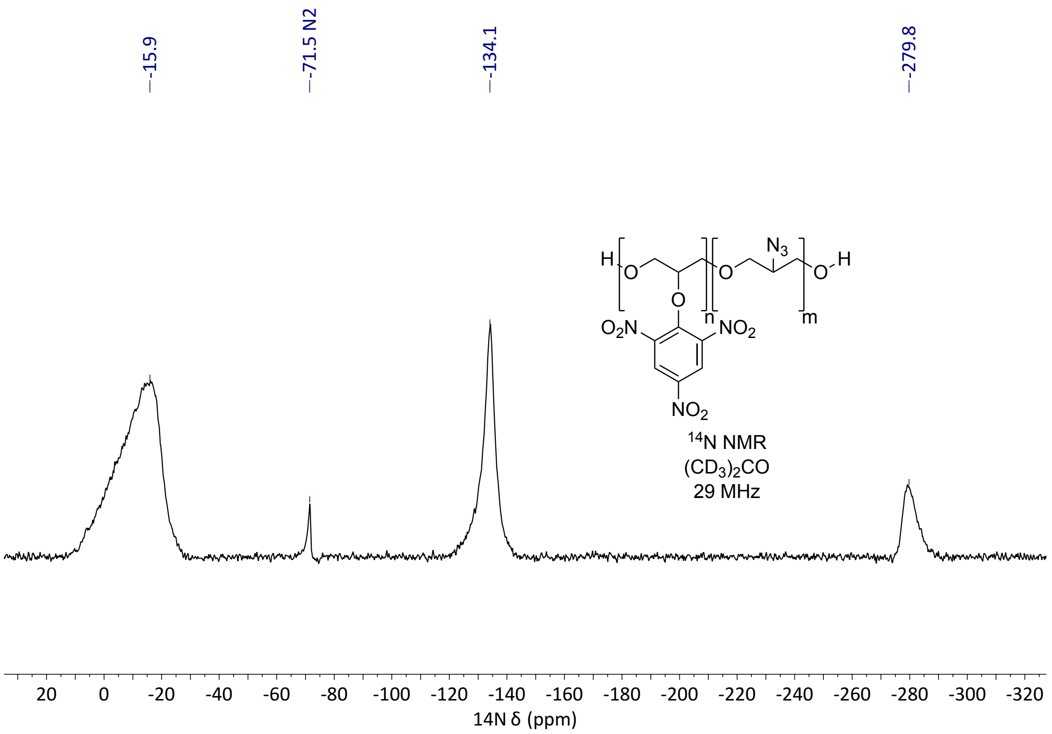

Figure S 11.27. Nitrogen spectrum (^{14}N) of poly(TNPO-*stat*-3AO); n = m.

Poly[(3-(2,4,6-trinitrophenoxy)oxetane)-*stat*-(3-azidomethyl-3-methyloxetane)] (P3)

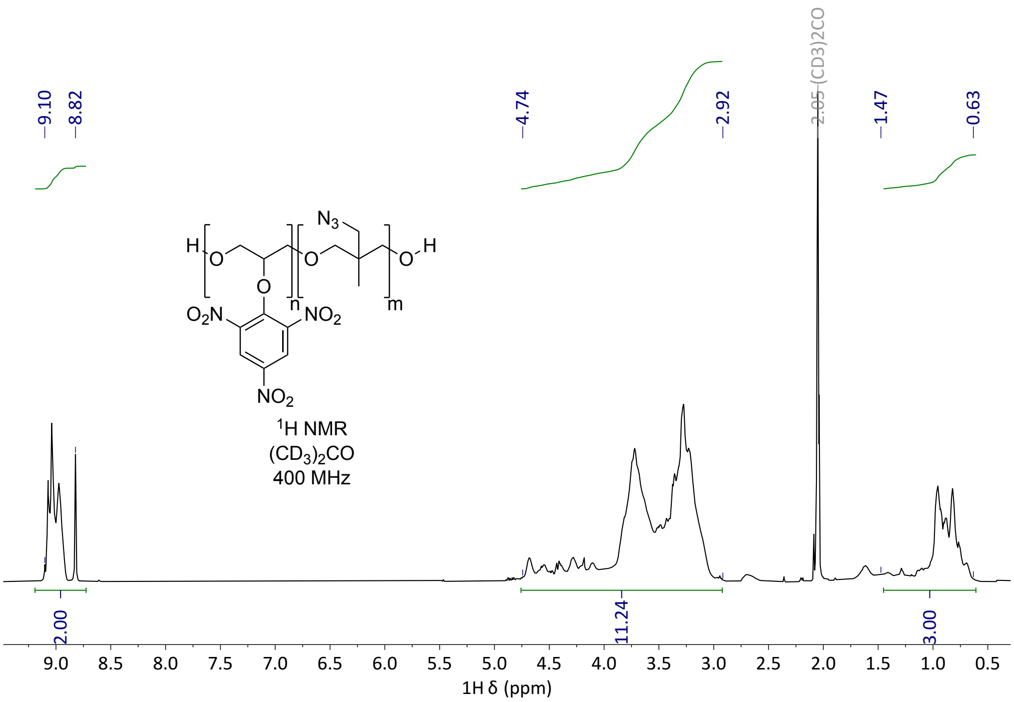

Figure S 11.28. Proton spectrum (^{1}H) of poly(TNPO-*stat*-AMMO); n = m.

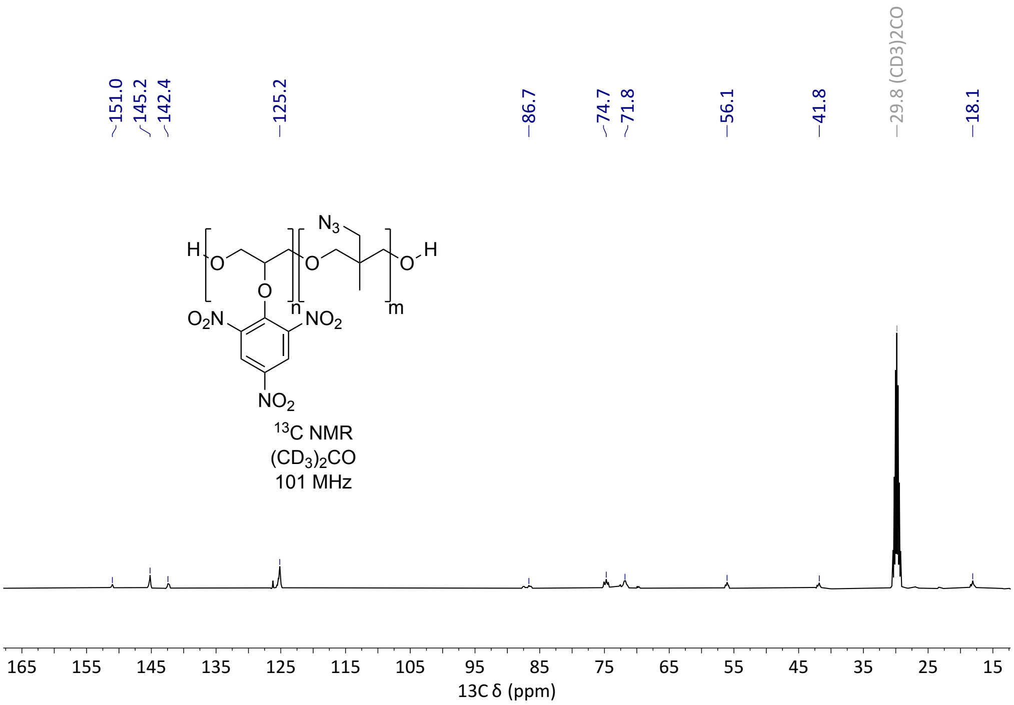

Figure S 11.29. Carbon spectrum (^{13}C) of poly(TNPO-*stat*-AMMO); n = m.

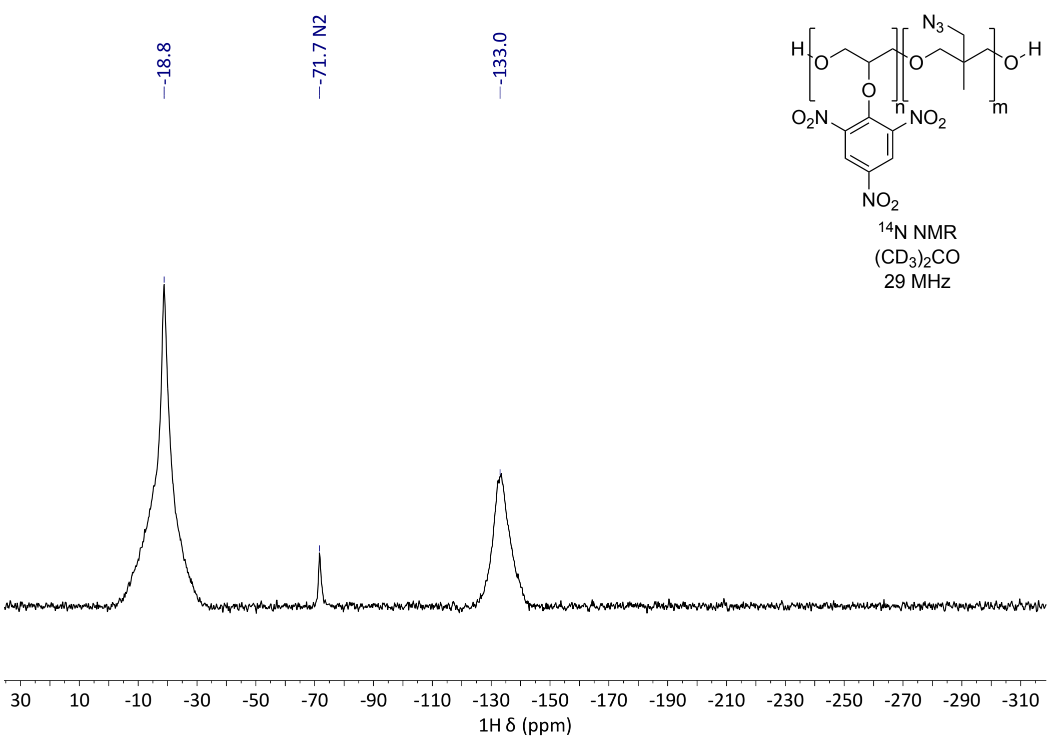

Figure S 11.30. Nitrogen spectrum (^{14}N) of poly(TNPO-*stat*-AMMO); n = m.

Poly[(3-(2,4,6-trinitrophenoxy)oxetane)-stat-(3,3-bis(azidomethyl)oxetane)] (P4)

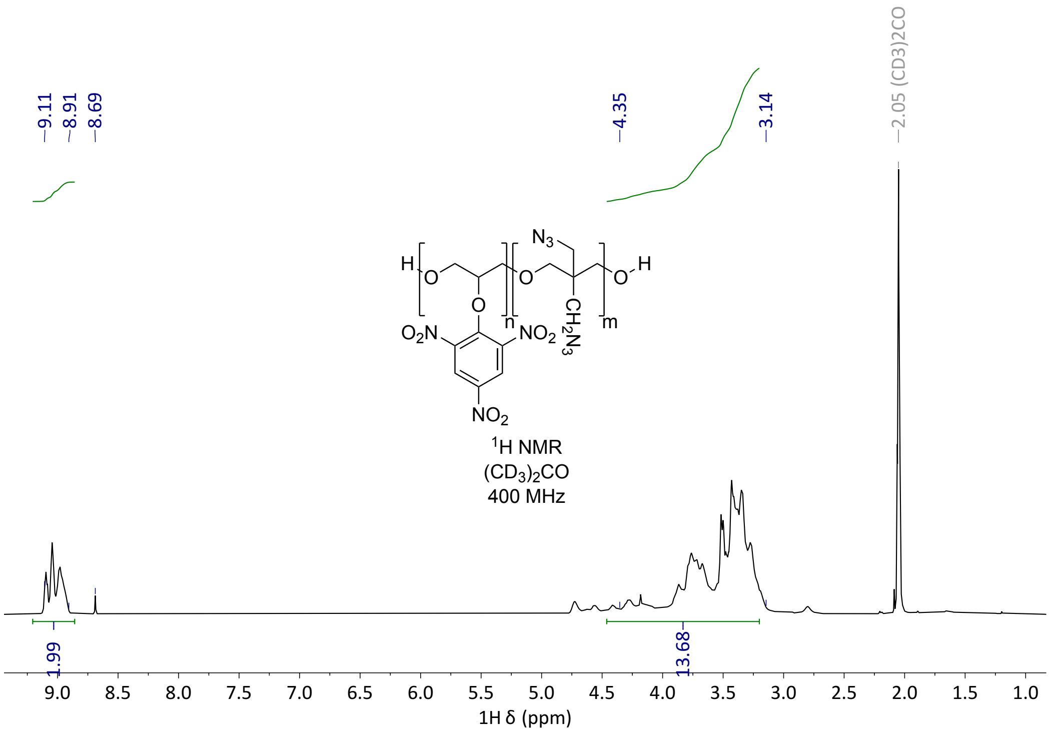

Figure S 11.31. Proton spectrum (^{1}H) of poly(TNPO-*stat*-BAMO); n = m.

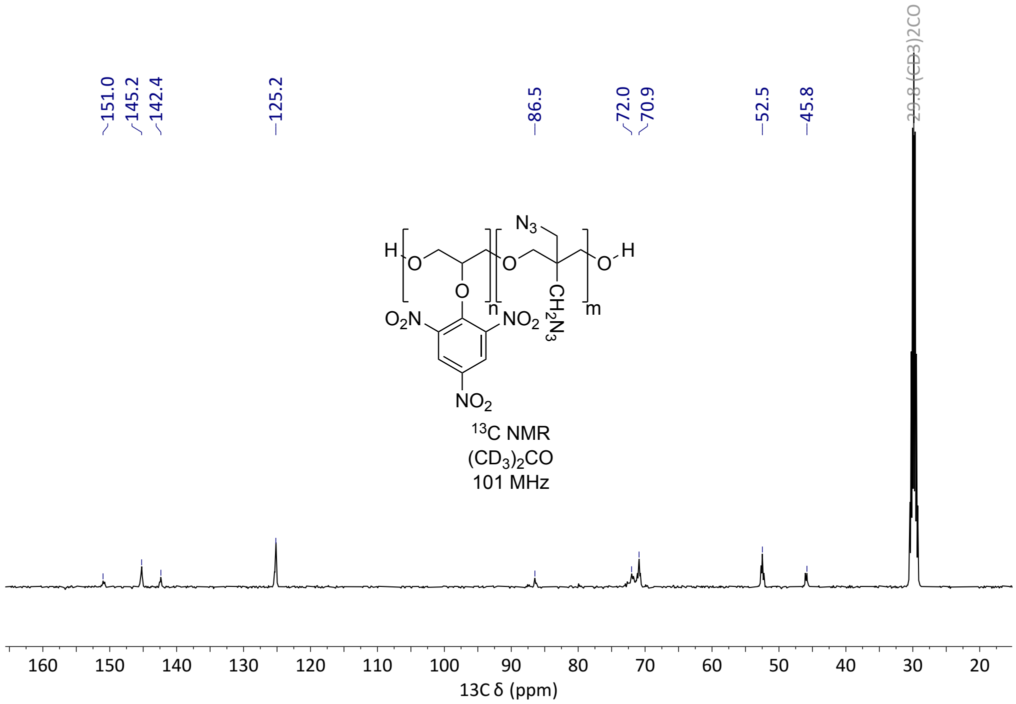

Figure S 11.32. Carbon spectrum (^{13}C) of poly(TNPO-*stat*-BAMO); n = m.

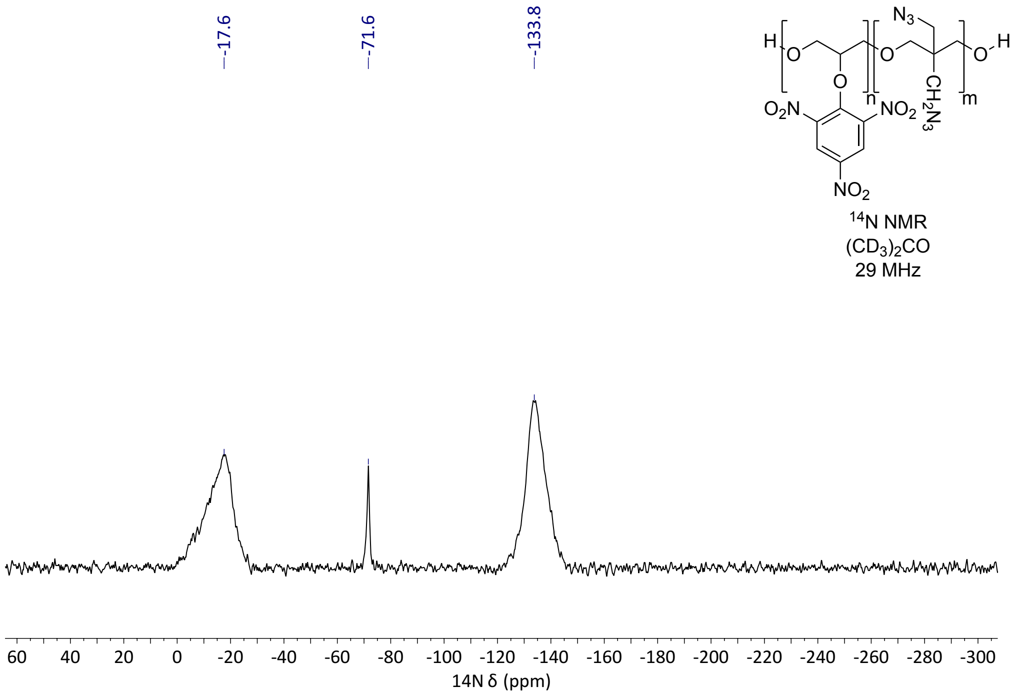

Figure S 11.33. Nitrogen spectrum (^{14}N) of poly(TNPO-*stat*-BAMO); n = m.

Poly[(3-(2,4,6-trinitrophenoxy)oxetane)-*stat*-(3-nitratomethyl-3-methyloxetane)] (P5)

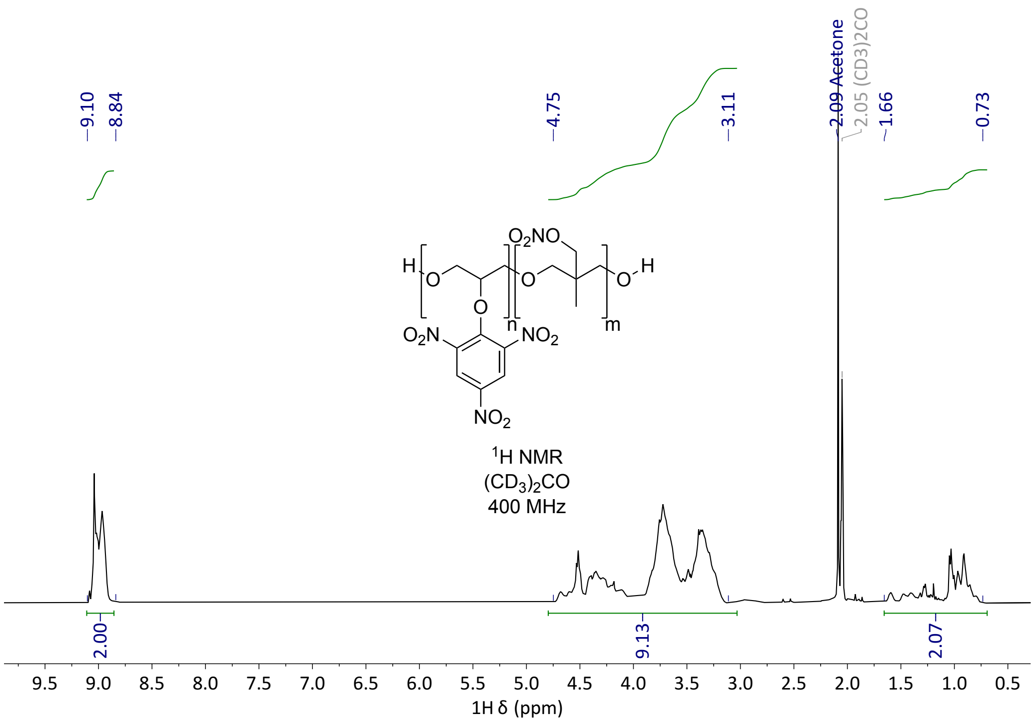

Figure S 11.34. Proton spectrum (^1H) of poly(TNPO-*stat*-NIMMO); n = m.

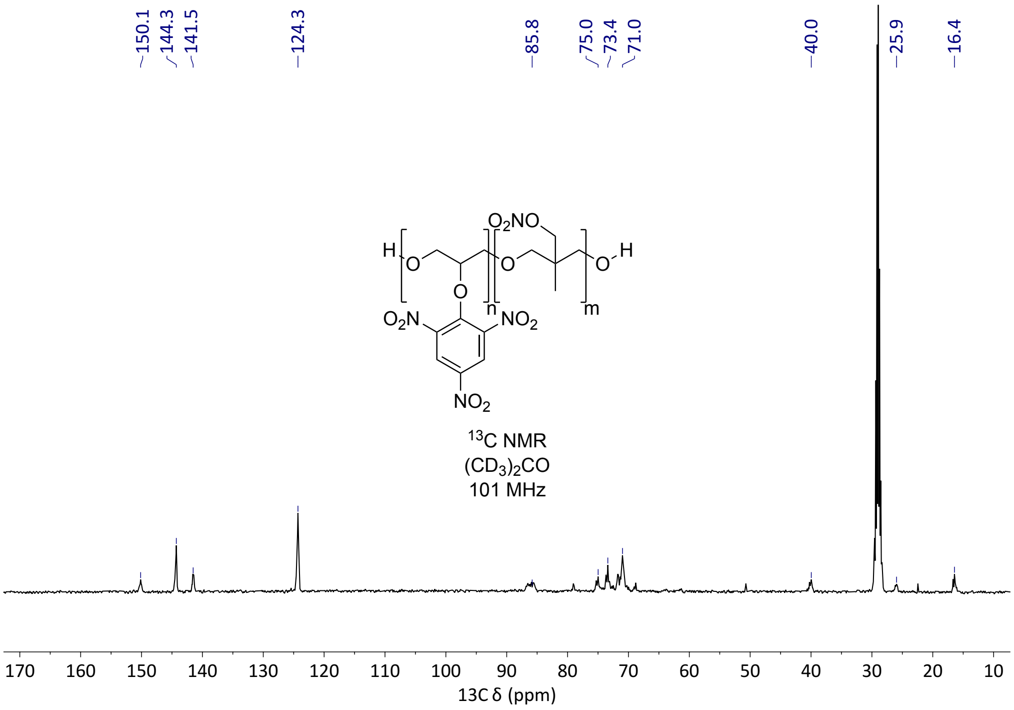

Figure S 11.35. Carbon spectrum (^{13}C) of poly(TNPO-*stat*-NIMMO); n = m.

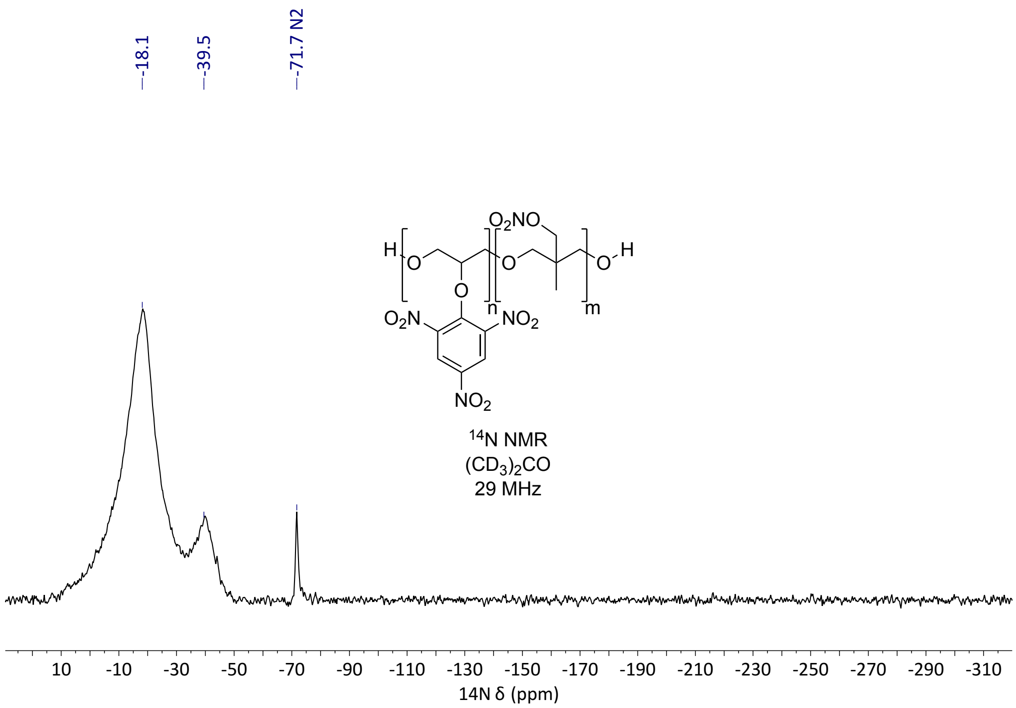

Figure S 11.36. Nitrogen spectrum (^{14}N) of poly(TNPO-*stat*-NIMMO); n = m.

Poly[(3-(2,4,6-trinitrophenoxy)oxetane)-*stat*-(3-azidomethyl-3-nitratomethyloxetane)] (P6)

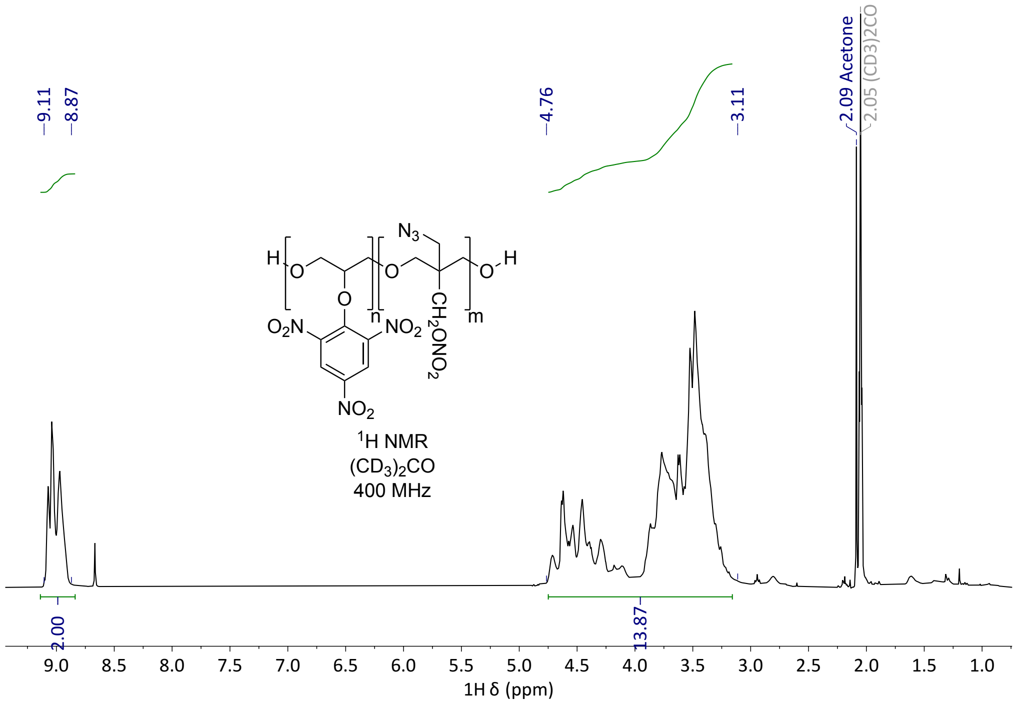

Figure S 11.37. Proton spectrum (^1H) of poly(TNPO-*stat*-AMNMO); n = m.

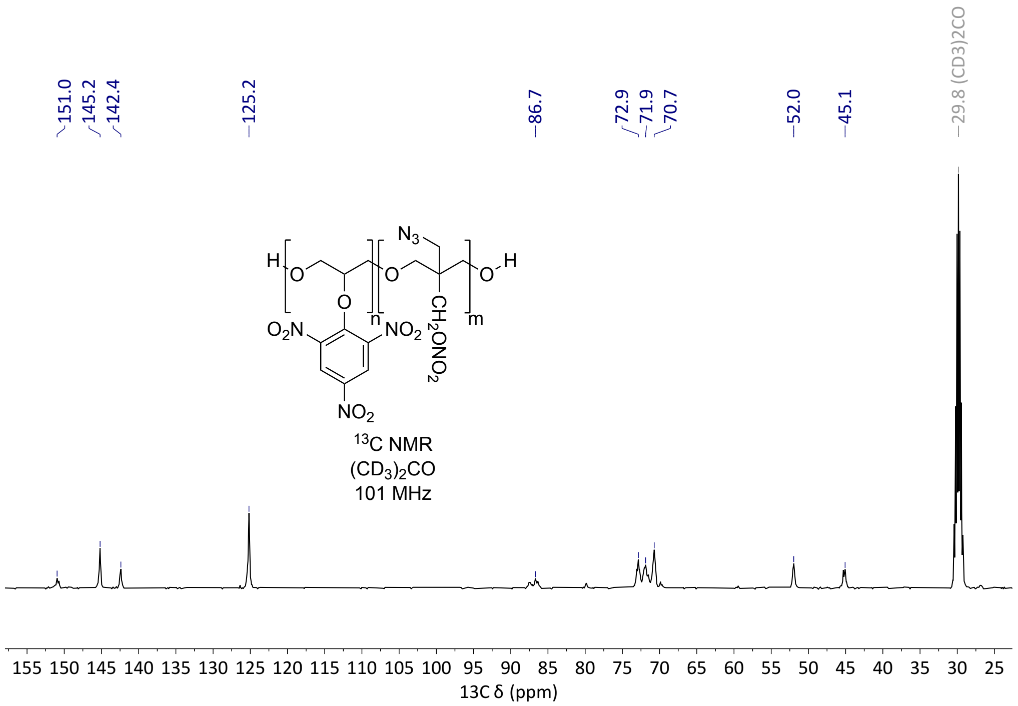

Figure S 11.38. Carbon spectrum (^{13}C) of poly(TNPO-*stat*-AMNMO); n = m.

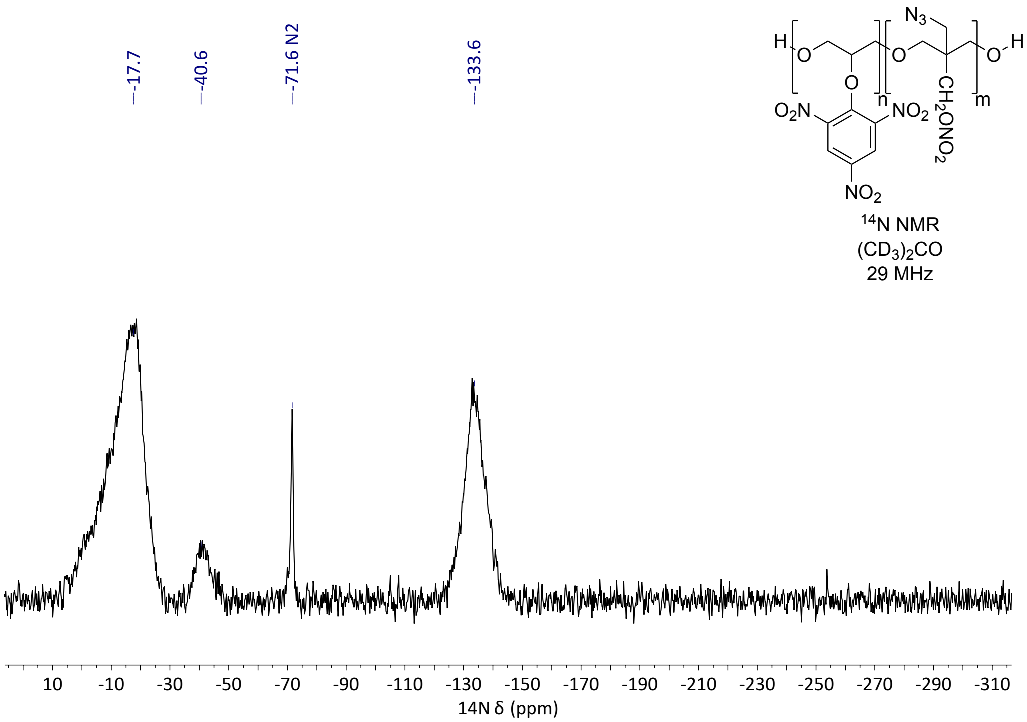

Figure S 11.39. Nitrogen spectrum (^{14}N) of poly(TNPO-*stat*-AMNMO); n = m.

11.5.3 Photo Documentation

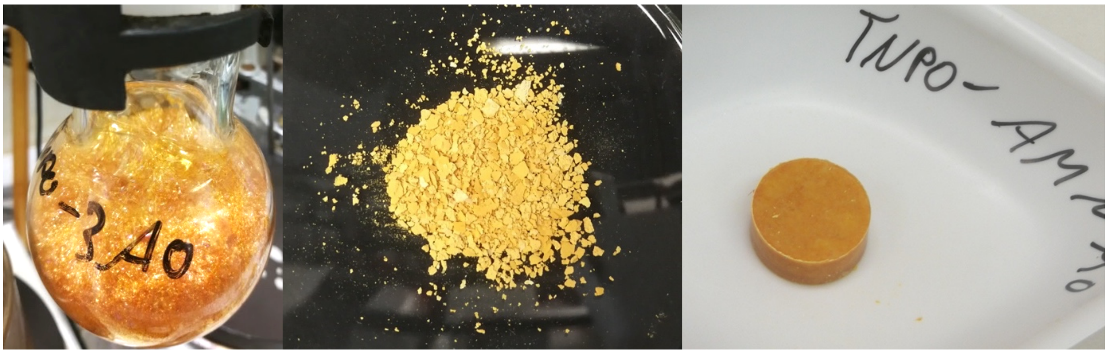

Figure S 11.40. Poly(TNPO-*stat*-3AO) (**P2**) during high vacuum drying (left), poly(TNPO) (**P1**) after isolation (middle), and tablet containing poly(TNPO-*stat*-AMNMO) (**P6**) and benzoic acid for bomb calorimetry (right).

11.5.4 Bomb Calorimetry

Enthalpies of formation were determined by bomb calorimetry according to the literature.[8,9] For this purpose, the polymer was mixed with benzoic acid and the mixture was pressed into pellets, which were placed in the combustion bomb, respectively. The combustion bomb was flushed with oxygen and each pellet was burned in oxygen with a pressure of 35 bar. The change in temperature ΔT was measured and the specific energy of combustion $\Delta_c U$ was calculated using the following equation:

$$\Delta_c U = C \Delta T \tag{1}$$

The calorimeter constant C was determined by burning benzoic acid ($\Delta_c U$ = 2514±1.7 cal g^{-1}) as reference. The standard molar enthalpy of combustion is defined as:

$$\Delta_c H_m^0 = \Delta_c U + \Delta n_g RT \tag{2}$$

With the change of moles of gas Δn_g, which can be calculated by:

$$\Delta n_g = \Delta n_i(products, g) - \Delta n_i(educts, g) \tag{3}$$

the ideal combustion reaction of CHNO-compounds was assumed as follows:

$$C_a H_b O_c N_d + \left(a + \frac{b}{4} - \frac{c}{2}\right) O_2 \rightarrow a\, CO_2 + \frac{b}{2}\, H_2O + \frac{d}{2}\, N_2 \tag{4}$$

leading to:

$$\Delta n_g = n(CO_2) + n(N_2) - n(O_2) = \frac{1}{2}\left(d - \frac{b}{2} + c\right) \quad (5)$$

The tablet composition and calculated values of $\Delta_c H_m^0$ for all polymers are shown in Table S 2.

Table S 11.2. Heat of combustion determination (bomb calorimetry) of copolymers **P2**–**P6** and composition of the prepared tablets.

Sample	Tablet weight [mg]	Polymer weight [mg]	Benzoic acid [mg]	$\Delta_c H_m^0$ [kJ mol^{-1}]
		Poly(TNPO) (P1)		
1	641.2	148.2	493.0	−4593.6335
2	651.1	150.5	500.6	−4680.9783
3	647.0	149.6	497.4	−4733.3284
				Average −4669.3134
		Poly(TNPO-*stat*-3AO) (P2)		
1	659.2	152.1	507.1	−6530.0763
2	659.0	152.1	507.0	−6693.8963
3	662.9	153.0	510.0	−6575.7054
				Average −6599.8927
		Poly(TNPO-*stat*-AMMO) (P3)		
1	653.3	150.6	502.6	−7567.3445
2	659.8	152.1	507.6	−7937.2170
3	567.5	130.9	436.9	−7550.6341
				Average −7685.0652
		Poly(TNPO-*stat*-BAMO) (P4)		
1	643.6	148.5	494.5	−8181.0614
2	658.9	152.1	506.2	−8291.4376
3	655.9	151.4	503.9	−8215.6155
				Average −8229.3715
		Poly(TNPO-*stat*-NIMMO) (P5)		
1	654.6	151.0	503.6	−7195.5568
2	646.5	149.1	497.4	−7617.8683
3	644.5	148.7	495.8	−7542.7775
				Average −7452.0675
		Poly(TNPO-*stat*-AMNMO) (P6)		
1	654.5	150.9	503.6	−8119.0469
2	652.7	150.5	502.2	−7916.2485
3	663.6	153.1	510.5	−8044.2495
				Average −8026.5150

The enthalpy of formation $\Delta_f H_m^0(M)$ of polymer M can be calculated using Hess' law:

$$\Delta_f H_m^0(M) = \sum_{j}^{products\ P} \Delta_f H^0(P_j) - \Delta_c H_m^0(M) \tag{6}$$

leading to:

$$\Delta_f H_m^0(M) = a\,\Delta_f H_m^0(CO_2) + \frac{1}{2}\Delta_f H_m^0(H_2O) - \Delta_c H_m^0(M) \tag{7}$$

Literature values[10] for the heat of formation of water and carbon dioxide have been used for the calculations:

$\Delta_f H_m^0(CO_2)$ = −393.52 kJ mol^{-1}
$\Delta_f H_m^0(H_2O)$ = −241.83 kJ mol^{-1}

The corresponding enthalpies of formation of polymers **P1**–**P6** are shown in Table S 3.

Table S 11.3. Calculated enthalpies of formation of polymers **P1**–**P6**.

Polymer	**P1**	**P2**	**P3**	**P4**	**P5**	**P6**
$\Delta_f H_m^0$ (kJ mol^{-1})	281.2	426.7	241.1	906.4	8.1	703.5

11.5.5 Heat of Formation Calculation and Thermal Analysis

The atomization method was used to determine the heat of formation of monomers **1**–**6** using the atom energies in Table S 4.[11]

$$\Delta_f H^\circ_{(g,\ M,\ 298)} = H_{(molecule,\ 298)} - \Sigma H^\circ_{(atoms,\ 298)} + \Sigma\Delta_f H^\circ_{(atoms,\ 298)}$$

Table S 11.4. CBS-4M electronic enthalpies for atoms C, H, N, and O and their literature values.

	$-H^{298}$ / a.u.	$\Delta_f H^\circ_{gas}$[10]
H	0.500991	217.998
C	37.786156	716.68
N	54.522462	472.68
O	74.991202	249.18

The Gaussian16 program package was used to calculate room temperature enthalpies on the CBS-4M level of theory.[12] In order to obtain the energy of formation for compounds **1**–**6**, Trouton's Rule has to be applied ($\Delta H_{sub} = 90 \cdot T_m$).

Table S 11.5. Heat of formation calculation results for compounds **1**–**6**.

M	$-H^{298}$ [a] [a.u.]	$\Delta_fH°$ (g, M)[b] [kJ mol^{-1}]	$\Delta_{sub}H°$ (M)[c] [kJ mol^{-1}]	$\Delta_fH°$ (s)[d] [kJ mol^{-1}]	Δn	Δ_fU (s)[e] [kJ kg^{-1}]
TNPO (1)	957.086738	−280.3	40.2975	−320.6	−8.5	−1319.2
3AO (2)	356.191018	262.7	41.7735	221.0	−4.5	2342.4
AMMO (3)	434.673464	188.9	40.6215	148.3	−6.5	1293.2
BAMO (4)	598.057987	553.7	43.2405	510.5	−7.5	3146.4
NIMMO (5)	550.685978	−229.0	39.9105	-268.9	−7.0	−1709.7
AMNMO (6)	714.071025	134.4	40.6215	93.8	−8.0	604.0

[a] CBS-4M electronic enthalpy. [b] Gas phase enthalpy of formation. [c] Sublimation enthalpy. [d] Standard solid state enthalpy of formation. [e] Solid state energy of formation.

The thermal behavior of monomers **1**–**6** and polymers **P1**–**P6** as well as poly(AMNMO) was analyzed by DSC at a heating rate of 5 °C min^{-1}.

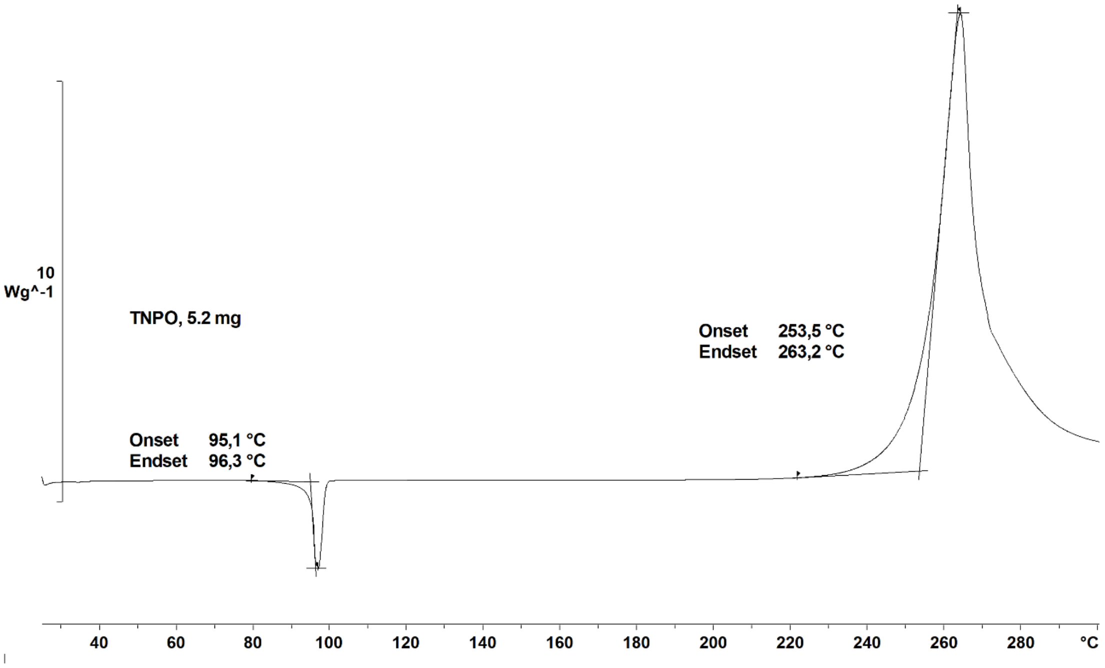

Figure S 11.41. DSC evaluation of TNPO (**1**).

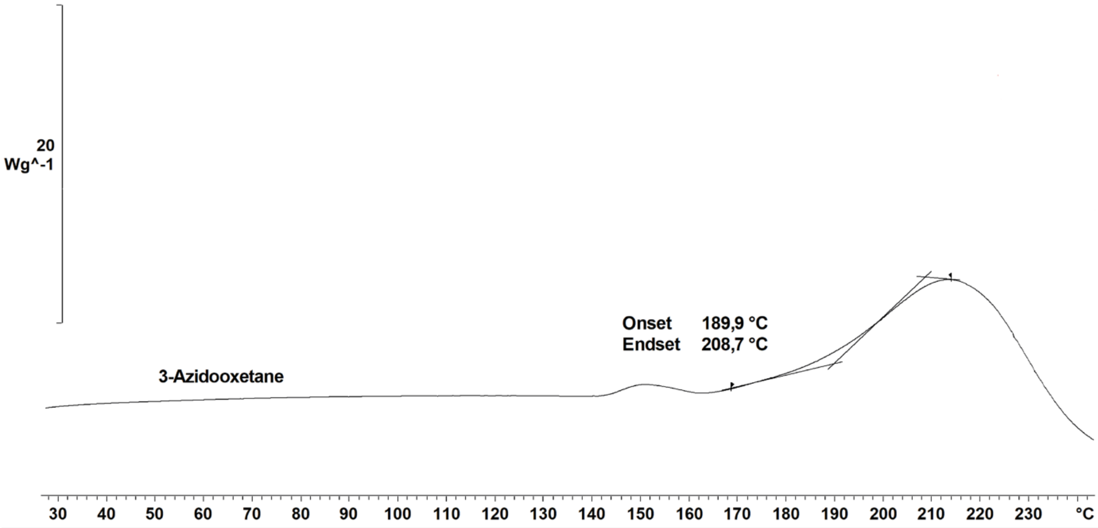

Figure S 11.42. Decomposition temperature evaluation by DSC of 3AO (**2**).

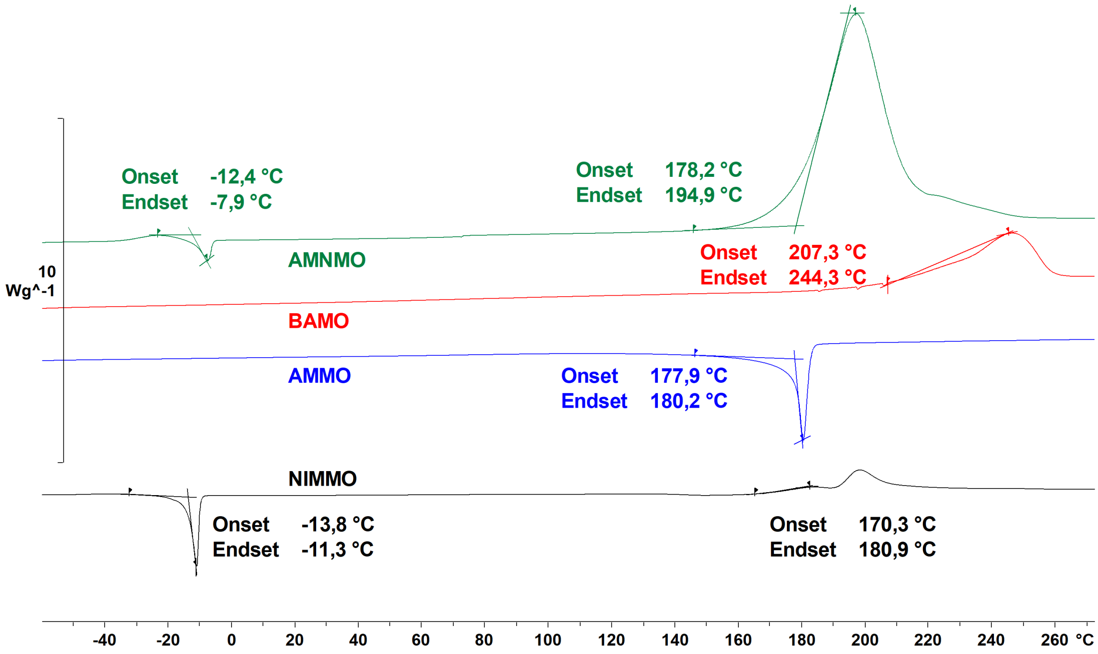

Figure S 11.43. DSC evaluation of the prior art monomers AMMO (**3**), BAMO (**4**), NIMMO (**5**), and AMNMO (**6**).

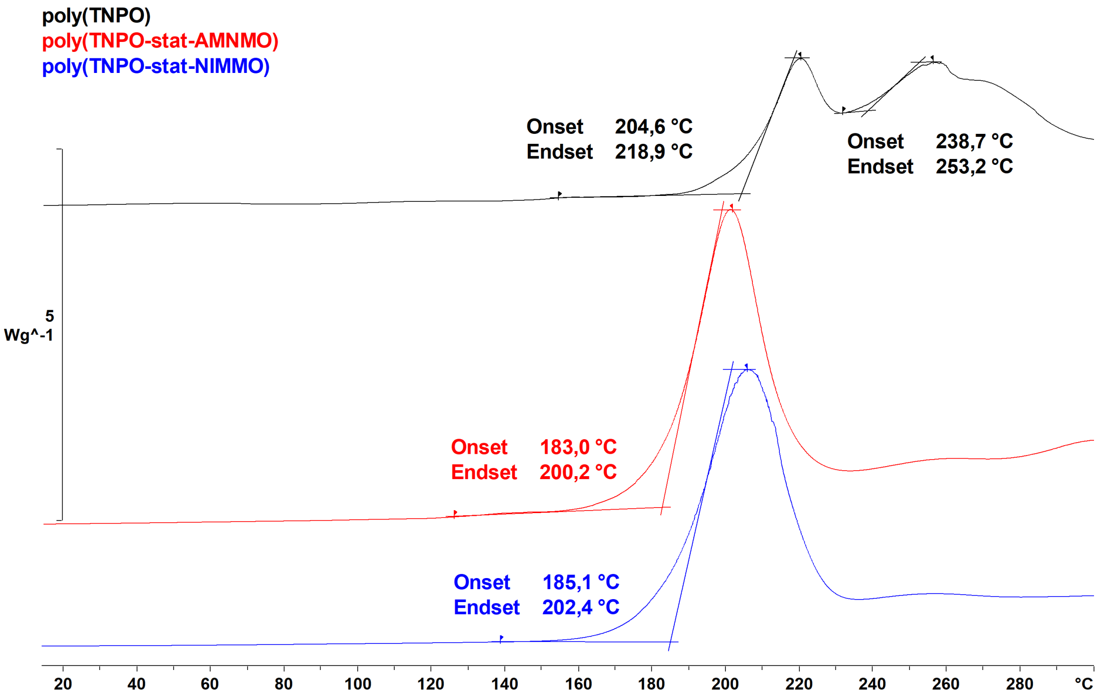

Figure S 11.44. DSC evaluation of **P1** and nitrato-polymers **P5** and **P6** with regard to their decomposition temperature.

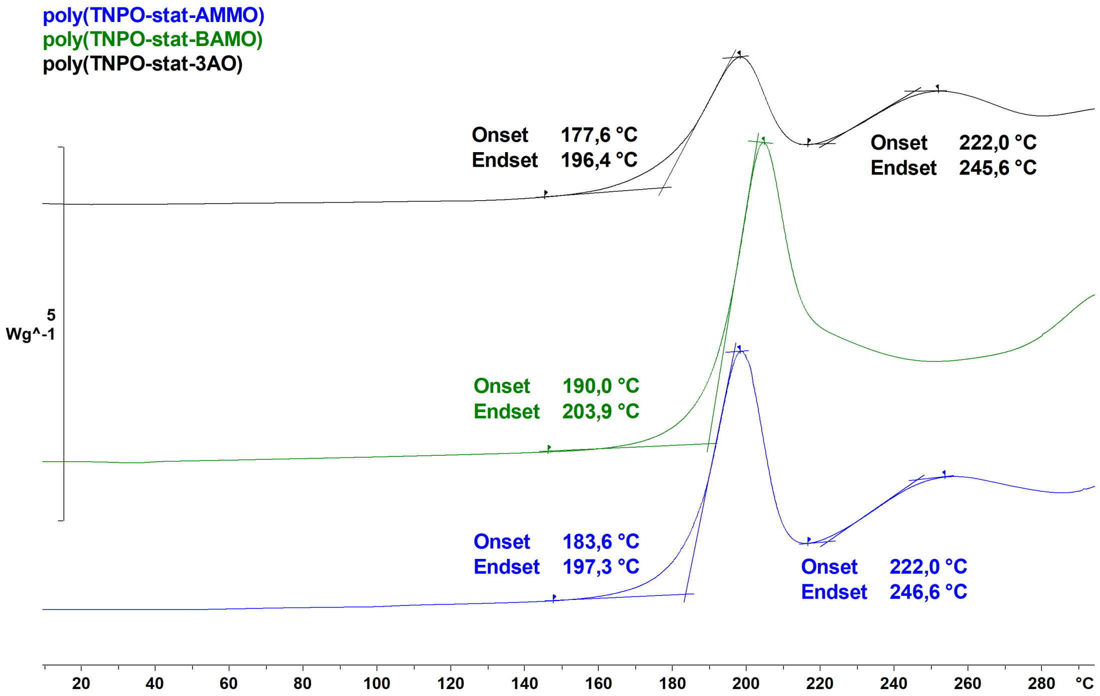

Figure S 11.45. DSC evaluation of azido-polymers **P2**, **P3**, and **P4** with regard to their decomposition temperature.

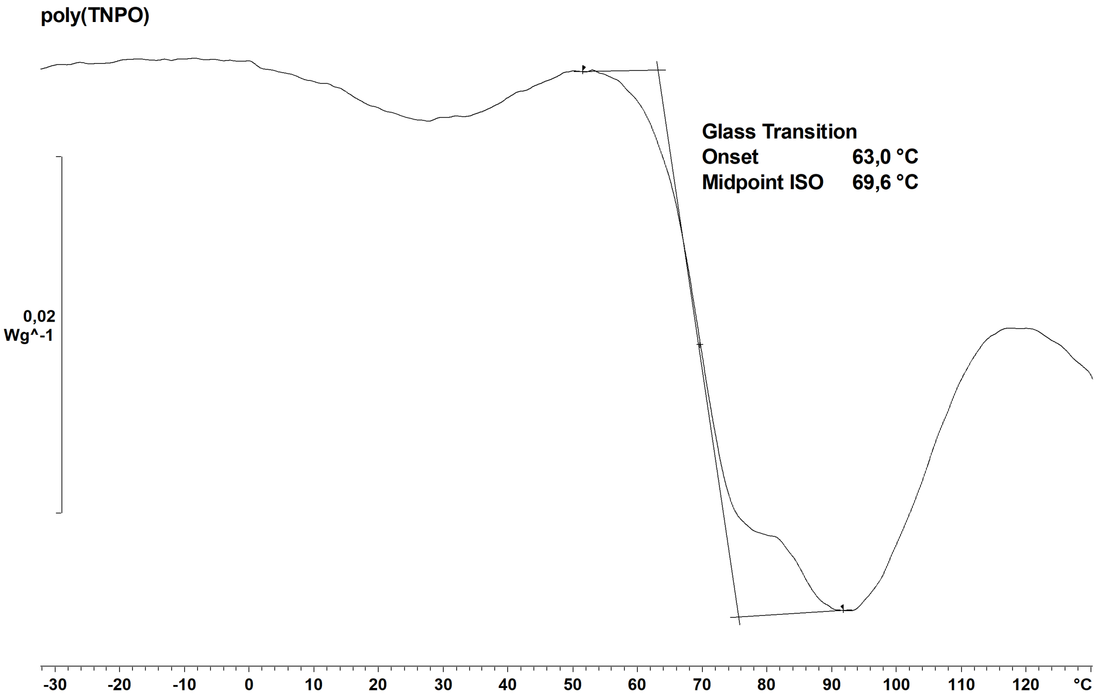

Figure S 11.46. DSC evaluation (glass transition temperature) of **P1**.

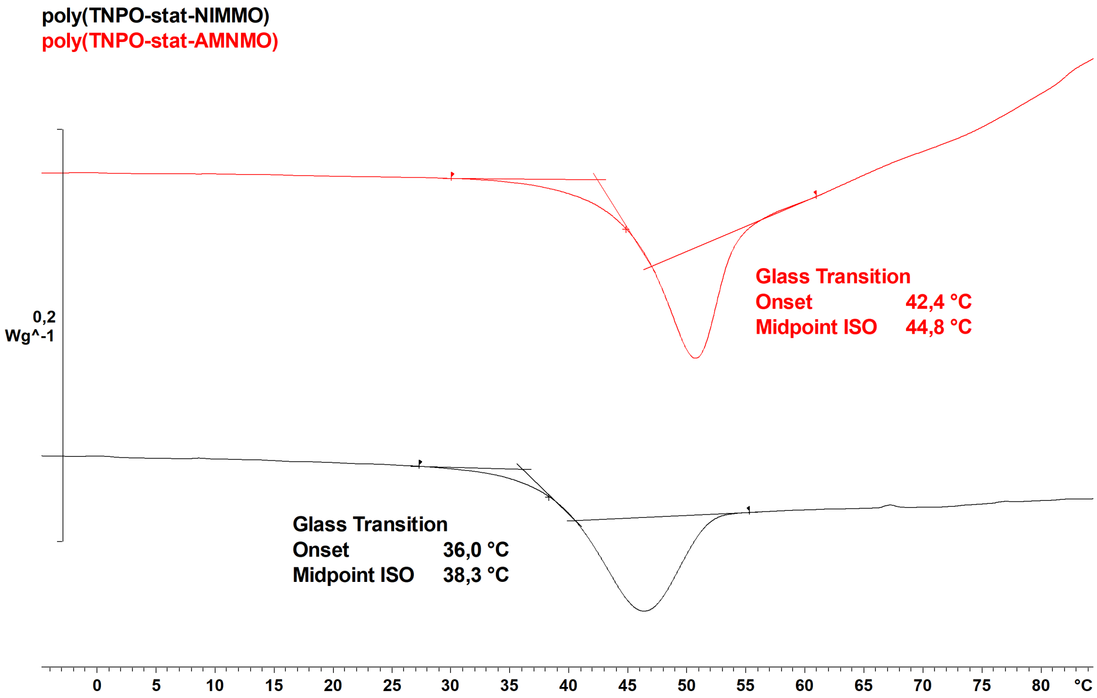

Figure S 11.47. DSC evaluation (glass transition temperature) of nitrato-polymers **P5** and **P6**.

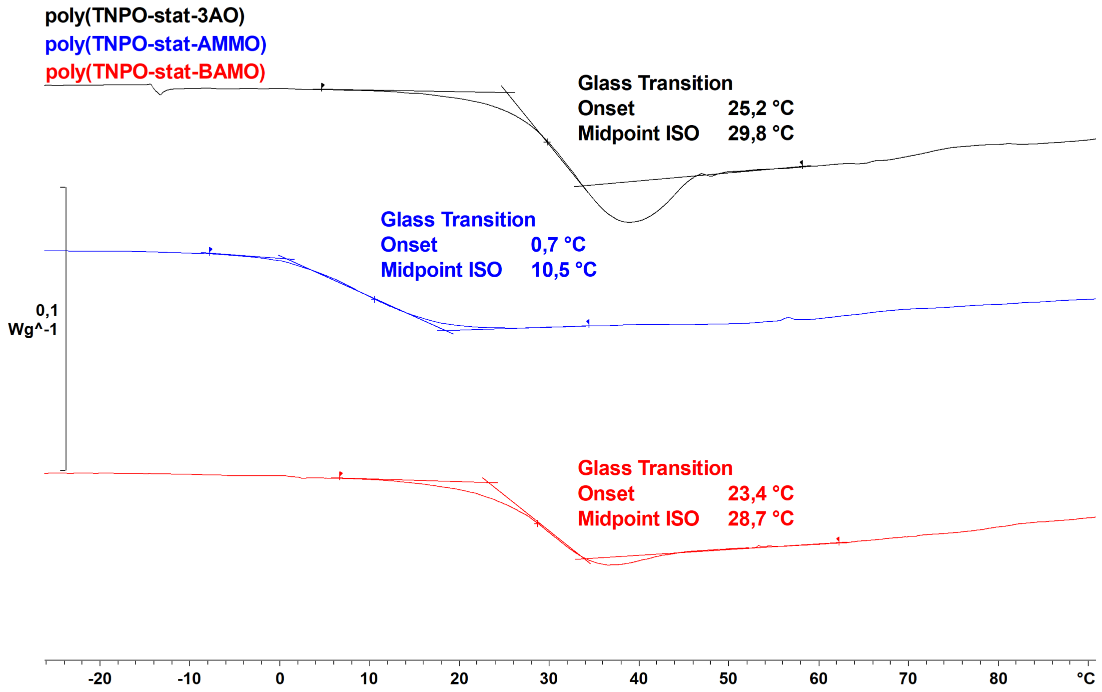

Figure S 11.48. DSC evaluation (glass transition temperature) of azido-polymers **P2**, **P3**, and **P4**.

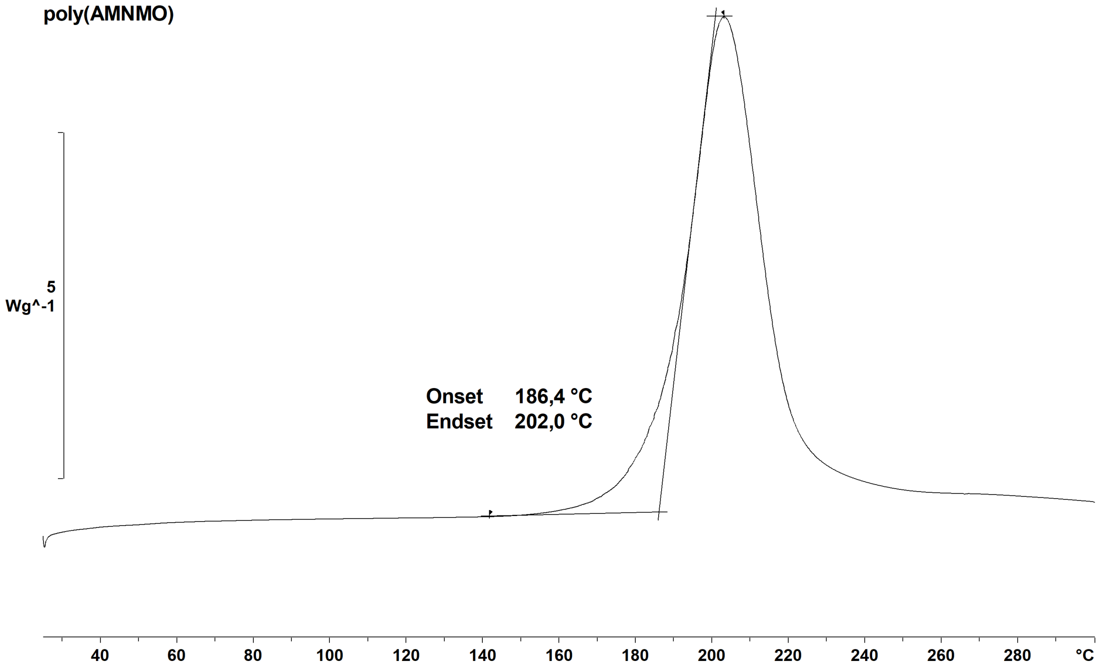

Figure S 11.49. Decomposition temperature evaluation (DSC) of poly(AMNMO).

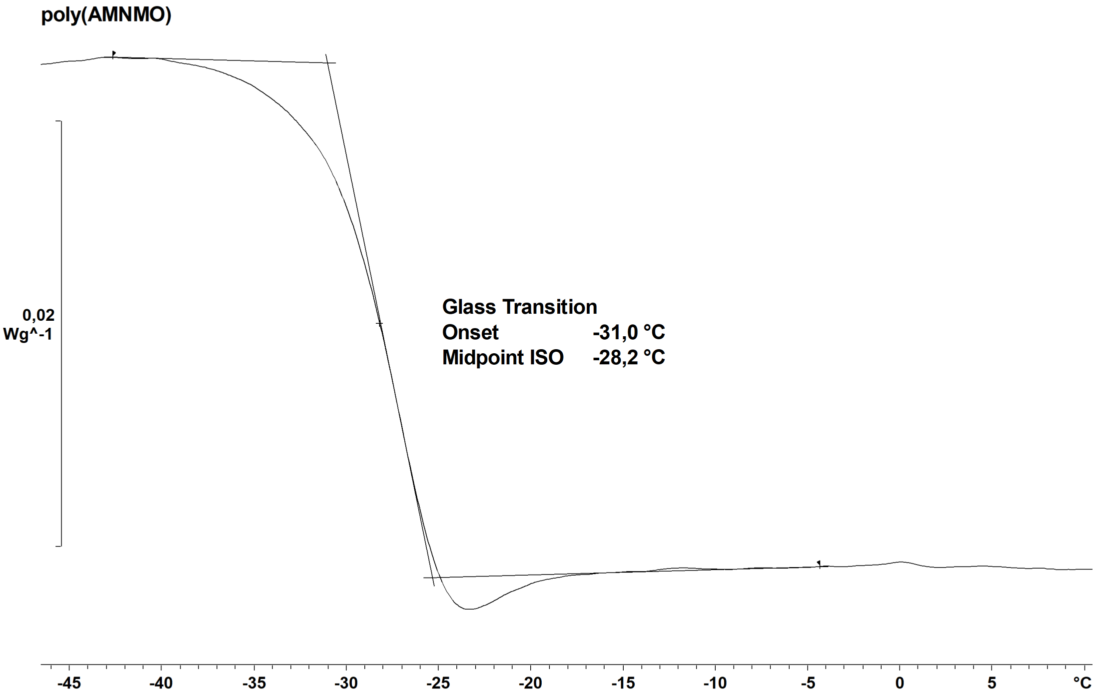

Figure S 11.50. Glass transition temperature evaluation (DSC) of poly(AMNMO).

References

[1] NATO STANAG 4489: *Explosives. Impact Sensitivity Tests*; NATO Standardization Office, Brussels, Belgium, **1999**.

[2] NATO STANAG 4487: *Explosives. Friction Sensitivity Tests*; NATO Standardization Office, Brussels, Belgium, **2002**.

[3] United Nations (UN), UN Recommendations on the Transport of Dangerous Goods, Manual of Tests and Criteria, **2009**.

[4] Born, M.; Voggenreiter, M. New energetic oxetane monomers based on nitroaromatic scaffolds. In *Proceedings of the 22th Seminar on New Trends in Research of Energetic Materials (NTREM)*, Pardubice, Czech Republic, April 10–12, **2019**.

[5] Born, M.; Karaghiosoff, K.; Klapötke, T. M. A GAP Replacement: Improved Synthesis of 3-Azidooxetane and Its Homopolymer Based on Sulfonic Acid Esters of Oxetan-3-ol. *J. Org. Chem.* **2021**, *86*, 12607-12614.

[6] Mukhametshin, T. I.; Petrov, A. I.; Kuznetsova, N. V.; Petrov, V. A.; Averianova, N. V.; Garaev, I. K.; Kostochko, A. V.; Gubaidullin, A. T.; Vinogradov, D. B.; Bulatov, P. V. Synthesis and copolymerization of azidomethyl-substituted oxetanes: the morphology of statistical block copolymers. *Chem. Heterocycl. Compd.* **2017**, *53*, 811-821.

[7] Manser, G. E.; Malik, A. A.; Archibald, T. G. 3-Azidomethyl-3-Nitratomethyloxetane, US 5 489 700, **1996**.

[8] Axthammer, Q. J.; Evangelisti, C.; Klapötke, T. M. Characterization, bomb calorimetric measurements and quantum chemical calculations of high energetic dense oxidizers (HEDO). In *44th International Annual Conference of the Fraunhofer ICT, Energetic Materials – Past, Present and Future*, Karlsruhe, Germany, June 25–28, **2013**.

[9] Hafner, S. Internal plasticized glycidyl azide copolymers for energetic solid propellant binders, Ph.D. Dissertation, Ludwig-Maximilian University (LMU) Munich, Munich, Germany, **2019**.

[10] Chase, M. W. NIST-JANAF Thermochemical Tables, Fourth Edition, *J. Phys. Chem. Red. Data, Monograph 9,* **1998**, 1–1951.

[11] Altenburg, T.; Klapötke, Thomas M.; Penger, A.; Stierstorfer, J. Two Outstanding Explosives Based on 1,2-Dinitroguanidine: Ammonium- dinitroguanidine and 1,7-Diamino-1,7-dinitrimino-2,4,6-trinitro-2,4,6-triazaheptane. *Z. Anorg. Allg. Chem.* **2010**, *636*, 463-471.

[12] Frisch, M. J.; Trucks, G. W.; Schlegel, H. B.; Scuseria, G. E.; Robb, M. A.; Cheeseman, J. R.; Scalmani, G.; Barone, V.; Petersson, G. A.; Nakatsuji, H.; Li, X.; Caricato, M.; Marenich, A. V.; Bloino, J.; Janesko, B. G.; Gomperts, R.; Mennucci, B.; Hratchian, H. P.; Ortiz, J. V.; Izmaylov, A. F.; Sonnenberg, J. L.; Williams; Ding, F.; Lipparini, F.; Egidi, F.; Goings, J.; Peng, B.; Petrone, A.; Henderson, T.; Ranasinghe, D.; Zakrzewski, V. G.; Gao, J.; Rega, N.; Zheng, G.; Liang, W.; Hada, M.; Ehara, M.; Toyota, K.; Fukuda, R.; Hasegawa, J.; Ishida, M.; Nakajima, T.; Honda, Y.; Kitao, O.; Nakai, H.; Vreven, T.; Throssell, K.; Montgomery Jr., J. A.; Peralta, J. E.; Ogliaro, F.; Bearpark, M. J.; Heyd, J. J.; Brothers, E. N.; Kudin, K. N.; Staroverov, V. N.; Keith, T. A.; Kobayashi, R.; Normand, J.; Raghavachari, K.; Rendell, A. P.; Burant, J. C.; Iyengar, S. S.; Tomasi, J.; Cossi, M.; Millam, J. M.; Klene, M.; Adamo, C.; Cammi, R.; Ochterski, J. W.; Martin, R. L.; Morokuma, K.; Farkas, O.; Foresman, J. B.; Fox, D. J., Gaussian 16 Rev. C.01, **2016**.

Appendix

11.6 Acronyms and Abbreviations

1,2-DCE	1,2-Dichloroethane
3AO	3-Azidooxetane
3NO	3-Nitratooxetane
ACE or ACEM	Active chain end mechanism
AMM	Activated monomer mechanism
AMMO	3-Azidomethyl-3-methyloxetane
AMNMO	3-Azidomethyl-3-nitratomethyloxetane
B.p.	Boiling point
BAM	Bundesanstalt für Materialprüfung
BAMO	3,3-Bis(azidomethyl)oxetane
BDO	Butane-1,4-diol
BMHMO	3-Bromomethyl-3-hydroxymethyloxetane
BP	Black powder
BTFE	Boron trifluoride etherate
CL20	2,4,6,8,10,12-Hexanitrohexaazaisowurtzitane
CROP	Cationic ring-opening polymerization
CTPB	Carboxy-terminated polybutadiene
DCM	Dichloromethane
DDT	Deflagration to detonation transition
Dec.	Decomposition
DMF	*N,N*-Dimethylformamide
DMSO	Dimethyl sulfoxide
DNO	3,3-Dinitratooxetane
DRA	Defence Research Agency (GB)
DSC	Differential scanning calorimetry
DTA	Differential thermal analysis
EA	Elemental analysis or ethyl acetate
ECH	Epichlorohydrin

EDBAA	Ethane-1,2-diyl bis(2-azidoacetate)
EI	Electron impact
Eq. or equiv.	Equivalent
ESI	Electrospray ionization
Et_2O	Diethyl ether
EtOAc	Ethyl acetate
ETPE	Energetic thermoplastic elastomer
EW	Equivalent weight
FS	Friction sensitivity
FT-IR	Fourier-Transform-Infrared (spectroscopy)
FW	Formula weight
GA	Glycidyl azide
GAP	Glycidyl azide polymer
GLYN	Glycidyl nitrate
GPC	Gel permeation chromatography
HACl	Hydroxylammonium chloride
HMDS	Hexamethyldisilazane
HMMO	3-Hydroxymethyl-3-methyloxetane
HMPA	Hexamethylphosphoramide
HMW	High-molecular-weight
HMX	Cyclotetramethylentetranitramin
HNS	Hexanitrostilbene
HOF	Heat of formation
HRMS	High resolution mass spectroscopy
HSA	Hirshfeld surface analysis
HTPB	Hydroxy-terminated polybutadiene
IM	Insensitive munition
IS	Impact sensitivity
K_2DNABT	Potassium 1,1'-dinitramino-5,5'-bistetrazolate
LA	Lead azide
LMW	Low-molecular-weight
LOVA	Low vulnerability ammunition

LRMS	Low resolution mass spectroscopy
M.p.	Melting point
mCPBA	*Meta*-chloroperoxybenzoic acid
MeCN	Acetonitrile
MeOH	Methanol
MF	Mercury fulminate
M_n	Number average molecular weight
Mol.% or mol%	Molar percentage
Ms	Methylsulfonyl (mesyl)
M_W	Weight average molecular weight
NATO	North Atlantic Treaty Organization
NC	Nitrocellulose
NG	Nitroglycerine
NIMMO	3-Nitratomethyl-3-methyloxetane
NMO	3-(Nitromethylene)oxetane
NMR	Nuclear magnetic resonance
OCC	Oxetane containing compound
ONC	Octanitrocubane
ONR	Office of Naval Research
***p*-TsCl**	*Para*-toluenesulfonyl chloride
p3AO	Poly(3-azidooxetane)
PAT	Polymer-analogous transformation
PBAA	Polybutadiene-acrylic-acid acrylonitrile
PBAN	Polybutadiene-acrylic-acid
PBX	Polymer-bonded explosive
$p_{C\text{-}J}$	Detonation pressure (at C-J point)
PD(I)	Polydispersity (index); M_W/M_n
PECH	Poly(epichlorohydrin)
PETN	Pentaerythritol tetranitrate
PGN	Poly(glycidyl nitrate)
pMsOx	Poly(3-mesyloxyoxetane)
ppm	Parts per million

pTsOx	Poly(3-tosyloxyoxetane)
RDX	Cyclotrimethylentrinitramin
REACH	Registration, Evaluation, Authorization and Restriction of Chemicals
R_f	Retention factor
RI(D)	Refractive index (detector)
RSM	Reactive structure material
rt	Room temperature
SERDP	Strategic Environmental Research and Development Program
SSRT	Small-scale shock reactivity text
STANAG	Standardization Agreement (NATO)
TATB	1,3,5-Triamino-2,4,6-trinitrobenzene
TBAB	Tetrabutylammonium bromide
$T_{dec.}$	Decomposition temperature
TDI	2,4-Toluenyldiisocyanate
TEA	Triethylamine
Tetryl	*N*-methyl-*N-(*2,4,6-trinitrophenyl)nitramide
T_G	Glass transition temperature
THF	Tetrahydrofurane
TIBA	Triisobutylaluminum
TKX-50	Dihydroxylammonium-5,5'-bitetrazole-1,1'-diolate
TKX-55	Bis(2,4,6-trinitrophenyl)-2,2'-bi(1,3,4-oxadiazole)
TLC	Thin-layer chromatography
TMSCl	Trimethylsilyl chloride
TNM	Tetranitromethane
TNPO	3-(2,4,6-Trinitrophenoxy)oxetane
TNT	2,4,6-Trinitrotoluene
Ts	*Para*-toluenesulfonyl (tosyl)
UN	United Nations
UV	Ultraviolet
VdW	Van der Waals
VoD or $V_{det.}$	Velocity of detonation
Wt.% or wt%	Weight percent

$\Delta_f H^0$	Heat of formation
Ω	Oxygen balance with regard to CO or CO_2

11.7 List of Figures

11.8 List of Schemes

11.9 List of Tables